S-N/99205--076

Groundwater Flow Model of Corrective Action Units 101 and 102: Central and Western Pahute Mesa, Nevada Test Site, Nye County, Nevada

Revision No.: 0

June 2006

Prepared for U.S. Department of Energy under Contract No. DE-AC52-03NA99205.

Approved for public release; further dissemination unlimited.

Uncontrolled When Printed

Available for public sale, in paper, from:

U.S. Department of Commerce
National Technical Information Service
5285 Port Royal Road
Springfield, VA 22161
Phone: 800.553.6847
Fax: 703.605.6900
Email: *orders@ntis.gov*
Online ordering: *http://www.ntis.gov/ordering.htm*

Available electronically at *http://www.osti.gov/bridge*

Available for a processing fee to U.S. Department of Energy and its contractors, in paper, from:

U.S. Department of Energy
Office of Scientific and Technical Information
P.O. Box 62
Oak Ridge, TN 37831-0062
Phone: 865.576.8401
Fax: 865.576.5728
Email: *reports@adonis.osti.gov*

Reference herein to any specific commercial product, process, or service by trade name, trademark, manufacturer, or otherwise, does not necessarily constitute or imply its endorsement, recommendation, or favoring by the United States Government or any agency thereof or its contractors or subcontractors.

Uncontrolled When Printed

S-N/99205--076

GROUNDWATER FLOW MODEL OF CORRECTIVE ACTION UNITS 101 AND 102: CENTRAL AND WESTERN PAHUTE MESA, NEVADA TEST SITE, NYE COUNTY, NEVADA

Contributors:

Stoller-Navarro Joint Venture
Greg Ruskauff
John Ewing
Eric Bhark
Srikanta Mishra
Neil Deeds
Tad Beard
Richard Rondeau
John McCord
Alaa Aly

Los Alamos National Laboratory
Andrew Wolfsberg
Wendy Soll
Zora Dash
Carl Gable

Revision No.: 0

June 2006

Stoller-Navarro Joint Venture
7710 W. Cheyenne, Building 3
Las Vegas, NV 89129

Prepared for U.S. Department of Energy under Contract No. DE-AC52-03NA99205.

Approved for public release; further dissemination unlimited.

Uncontrolled When Printed

**GROUNDWATER FLOW MODEL OF CORRECTIVE ACTION UNITS 101 AND 102:
CENTRAL AND WESTERN PAHUTE MESA,
NEVADA TEST SITE, NYE COUNTY, NEVADA**

Approved by: Approved signature Date: 6-2-06

John McCord, UGTA Project Manager
Stoller-Navarro Joint Venture

Uncontrolled When Printed

TABLE OF CONTENTS

List of Figures xi
List of Tables xxxvii
List of Plates xliv
List of Acronyms and Abbreviations xlv
List of Geological Abbreviations and Symbols xlviii
Acknowledgements li
Executive Summary ES-1

1.0 Introduction 1-1
1.1 Purpose and Scope 1-3
1.2 Project Participants 1-4
1.3 Summary of the Federal Facility Agreement and Consent Order 1-4
1.3.1 Summary of the FFACO UGTA Corrective Action Strategy 1-8
1.4 Pahute Mesa Background 1-8
1.4.1 Underground Nuclear Testing on Pahute Mesa 1-11
1.5 Major Supporting Reports Documenting CAU-Specific Data Analysis and Evaluation 1-13
1.6 Report Organization 1-13

2.0 Framework for Groundwater Flow Modeling of Central and Western Pahute Mesa - Data, Information, and Conceptual Models 2-1
2.1 Summary of the UGTA Regional Model 2-3
2.1.1 UGTA Regional Model Hydrostratigraphic Framework 2-3
2.1.2 Groundwater Occurrence and Movement 2-7
2.2 Pahute Mesa Flow System Hydrostratigraphic Framework Models 2-9
2.2.1 Hydrostratigraphic Framework Model Development 2-10
2.2.2 Base HFM 2-11
2.2.2.1 Structural Features 2-15
2.2.2.2 Stratigraphy 2-15
2.2.3 Silent Canyon Caldera Complex HFM Alternative 2-19
2.2.3.1 Structural Features 2-19
2.2.3.2 Stratigraphy 2-19
2.3 Groundwater Characteristics 2-24
2.3.1 Inflow and Outflow (Lateral Boundary Fluxes) 2-24
2.3.2 Precipitation and Recharge 2-25
2.3.2.1 Precipitation Distribution 2-25
2.3.2.2 Alternative Recharge Models 2-28
2.4 Surface Groundwater Discharge 2-36
2.4.1 Natural Discharge 2-41
2.4.2 Evapotranspiration Summary 2-41
2.4.3 Well Discharge 2-43
2.5 Hydraulic Heads 2-50

Uncontrolled When Printed

TABLE OF CONTENTS (CONTINUED)

2.6 Hydraulic Parameters 2-52
2.6.1 Hydraulic Conductivity Data 2-53
2.7 Groundwater Chemistry 2-62
2.7.1 Conservative Tracers 2-63
2.7.1.1 Conservative Tracer Data 2-63
2.7.1.2 Conservative Tracer Data Evaluation 2-66
2.7.2 Geochemical Modeling 2-72

3.0 Computer Code Selection 3-1

3.1 Code Selection Process 3-1
3.2 Code Attributes 3-1
3.3 Code Testing Criteria 3-8
3.4 Initial Screening of Candidate Codes 3-10
3.5 Description of Selected Candidate Codes 3-13
3.6 Test Problem Used To Evaluate Candidate Codes 3-15
3.7 Results of Code Evaluation 3-23
3.7.1 Evaluation of Code Capabilities 3-23
3.7.2 Comparison of SWIFT-98 and FEHM Relative to the Testing Criteria 3-24
3.7.3 Recommended Code for Use in the Pahute Mesa CAU Flow and Transport Model 3-28
3.8 TYBO-BENHAM Case Study 3-28

4.0 Groundwater Flow Model Construction 4-1

4.1 General Approach 4-1
4.2 Mesh Generation 4-3
4.2.1 Base-Case and SCCC HFMs 4-3
4.2.2 Truncation of Top Surface of Mesh To Represent Water Table 4-9
4.3 Boundary Conditions 4-10
4.3.1 Recharge 4-12
4.3.2 Discharge 4-16
4.3.3 Boundary Heads 4-20
4.3.4 Lateral-Boundary Fluxes 4-20
4.4 Initial Conditions 4-21

5.0 Flow Model Calibration 5-1

5.1 Calibration Approach 5-2
5.2 Calibration Data 5-8
5.3 Boundary Head Adjustments 5-18
5.4 Geologic Model Subdivision 5-22
5.5 Parameter Assignment 5-28
5.6 Base Hydrostratigraphic Framework Model Flow Model Calibration 5-28
5.6.1 No-Depth-Decay, No-Anisotropy Case 5-29

Uncontrolled When Printed

TABLE OF CONTENTS (CONTINUED)

5.6.2 Selected HSU Depth Decay and Anisotropy (SDA) 5-41
5.6.3 All HSU Depth Decay and Anisotropy (ADA) 5-55
5.7 Silent Canyon Caldera Complex Hydrostratigraphic Framework Model Flow Model Calibration 5-68
5.8 Calibration Summary 5-79
5.8.1 Purse Fault Behavior 5-80
5.8.2 Head and Flow Path Comparison Along B-B' and J-J' 5-85
5.8.3 Comparison of Model and Single-Well Test Permeabilities 5-90
5.8.4 Comparison of Model and Estimated Permeabilities 5-93
5.8.5 Water-Balance Summary 5-102
5.8.6 Evaluation of Low-Weight Head Data 5-103
5.8.7 Data Components of Calibration 5-105
5.8.8 Hydrostratigraphic Framework Model Assessment 5-106
5.8.9 Model Limitations 5-106

6.0 Flow Model Sensitivity and Uncertainty Analysis 6-1

6.1 Approach 6-2
6.1.1 Parameter Sensitivity Analysis 6-2
6.1.1.1 Local Sensitivity Analysis 6-2
6.1.1.2 Global Sensitivity Analysis 6-5
6.1.2 Conceptual Model Uncertainty Analysis 6-10
6.2 Parameter Sensitivity Analysis 6-11
6.2.1 Local Parameter Sensitivity and Correlations 6-11
6.2.1.1 Base HFM - Selected HSU Depth-Decay and Anisotropy (BN-MME-SDA) Model Parameter Sensitivity and Correlations 6-12
6.2.1.2 Base HFM - All HSU Depth-Decay and Anisotropy (BN-MME-ADA) Model Parameter Sensitivity and Correlations 6-16
6.2.1.3 SCCC HFM - Selected Depth-Decay and Anisotropy (SCCC-MME-SDA) Model Parameter Sensitivity and Correlations 6-20
6.2.2 Parameter Perturbation Analysis 6-23
6.2.2.1 Base HFM - Selected HSU Depth-Decay and Anisotropy (BN-MME-SDA) Model Parameter Perturbation Analysis 6-24
6.2.2.2 Base HFM - All HSU Depth-Decay and Anisotropy (BN-MME-ADA) Model Parameter Perturbation Analysis 6-30
6.2.2.3 SCCC HFM - Selected Depth-Decay and Anisotropy (SCCC-MME-SDA) Model Parameter Perturbation Analysis 6-36
6.2.3 Global Parameter Sensitivity 6-43

Uncontrolled When Printed

TABLE OF CONTENTS (CONTINUED)

6.2.3.1 Base HFM - Selected HSU Depth-Decay and Anisotropy (BN-MME-SDA) Model 6-44
6.2.3.2 Base HFM - All HSU Depth-Decay and Anisotropy (BN-MME-ADA) 6-54
6.2.3.3 SCCC HFM - Selected HSU Depth Decay and Anisotropy (SCCC-MME-SDA) 6-62
6.2.3.4 Boundary Flux Sensitivity 6-72
6.2.4 Other Model Sensitivities 6-80
6.2.4.1 Sensitivity to Evapotranspiration Extinction Depth in Oasis Valley 6-80
6.2.4.2 Reduced LCCU1 Permeability Alternative 6-80
6.2.4.3 Chimney Permeability Enhancement 6-85
6.2.4.4 Fortymile Canyon Alternative 6-87
6.2.4.5 Selected Hydrostratigraphic Horizontal Anisotropy . . . 6-88
6.2.4.6 Timber Mountain Hydraulic Effects 6-96
6.2.5 Summary of Parameter Sensitivity Analysis 6-103
6.3 HFM Uncertainty Analysis 6-107
6.3.1 Thirsty Canyon Lineament Alternative (TCL-MME-SDA). 6-119
6.3.2 Basement Ridge Model Alternative (RIDGE-MME-SDA) 6-125
6.3.3 Raised Pre-Tertiary Surface Alternative (PZUP-MME-SDA). 6-132
6.3.4 Deeply Rooted Belted Thrust Fault Alternative (DRT-MME-SDA) 6-139
6.3.5 Contiguous Imbricate Thrust Sheet Alternative (SEPZ-MME-SDA) 6-146
6.3.6 HFM Uncertainty Analysis Summary 6-153
6.4 Water-Balance Uncertainty Analysis 6-158
6.4.1 Recharge Uncertainty 6-158
6.4.2 Lateral-Flow Uncertainty 6-159
6.4.3 Base Geologic Model Water-Balance Uncertainty Analysis 6-160
6.4.3.1 DRI Recharge Model. 6-160
6.4.3.2 USGS Recharge Model 6-165
6.4.4 SCCC Geologic Model Water-Balance Uncertainty Analysis. 6-173
6.4.4.1 DRI Recharge Model 6-173
6.4.4.2 USGS Recharge Model 6-176
6.4.5 Summary of Water-Balance Uncertainty Analysis 6-179
6.5 Combining HFM and Water-Balance Uncertainty 6-180
6.5.1 Raised Pre-Tertiary Surface (PZUP) HFM 6-181
6.5.1.1 DRIA Recharge Model 6-181
6.5.1.2 USGSD Recharge Model 6-184
6.5.2 Deeply Rooted Belted Thrust Fault (DRT) HFM. 6-187
6.5.2.1 DRIA Recharge Model 6-187
6.5.2.2 USGSD Recharge Model 6-190
6.5.3 Summary of HFM and Water-Balance Uncertainty Analysis 6-193

Uncontrolled When Printed

TABLE OF CONTENTS (CONTINUED)

7.0 Geochemical Verification 7-1

7.1 Approach 7-1
7.1.1 Review of Verification Target Study Results 7-1
7.1.1.1 Inverse Modeling Method 7-2
7.1.1.2 Results at Boreholes Considered 7-4
7.1.2 Reverse-Particle-Tracking Method 7-8
7.1.3 Recharge and Inflow Zone Definitions 7-10
7.1.4 Method for Comparing Model Results to Targets 7-12
7.1.4.1 Comparison Zones 7-12
7.1.4.2 Explanation of Comparison Plots 7-13
7.2 Geochemical Verification Results for BN-MME-SDA 7-13
7.2.1 UE-18r 7-16
7.2.1.1 Simulated Rainier Mesa Recharge at UE-18r 7-16
7.2.1.2 BN-MME-SDA Reduced LCCU1 Permeability Alternative 7-18
7.2.1.3 UE-18r Summary 7-20
7.2.2 ER-EC-6 7-22
7.2.3 ER-OV-01 7-26
7.2.4 ER-OV-05 7-30
7.2.5 ER-OV-04a 7-30
7.2.6 ER-OV-03a 7-33
7.2.7 ER-OV-03c 7-39
7.2.8 Coffer Windmill Well 7-42
7.3 Geochemical Verification Results: Comparing Alternative Uncertain Models 7-46
7.3.1 UE-18r 7-48
7.3.1.1 Alternative Water-Balance Conditions, BN HFM 7-48
7.3.1.2 SCCC Alternative HFM 7-48
7.3.1.3 PZUP, DRT, RIDGE, TCL, and SEPZ Alternative HFMs 7-49
7.3.1.4 Summary: UE-18r 7-50
7.3.2 ER-EC-6 7-63
7.3.2.1 Alternative Water-Balance Conditions, BN HFM 7-63
7.3.2.2 SCCC Alternative HFM 7-63
7.3.2.3 PZUP, DRT, RIDGE, TCL, and SEPZ Alternative HFMs 7-64
7.3.2.4 Summary: ER-EC-6 7-64
7.3.3 ER-OV-01 7-77
7.3.3.1 Alternative Water-Balance Conditions, BN HFM 7-77
7.3.3.2 SCCC Alternative HFM 7-77
7.3.3.3 PZUP, DRT, RIDGE, TCL, and SEPZ Alternative HFMs 7-77
7.3.3.4 Summary: ER-OV-01 7-78

Uncontrolled When Printed

TABLE OF CONTENTS (CONTINUED)

7.3.4 ER-OV-05 . . . 7-91
7.3.4.1 Alternative Water-Balance Conditions, BN HFM . . . 7-91
7.3.4.2 SCCC Alternative HFM . . . 7-91
7.3.4.3 PZUP, DRT, RIDGE, TCL, and SEPZ Alternative HFMs . . . 7-91
7.3.4.4 Summary: ER-OV-05 . . . 7-91
7.3.5 ER-OV-04a . . . 7-103
7.3.5.1 Alternative Water-Balance Conditions, BN HFM . . . 7-103
7.3.5.2 SCCC Alternative HFM . . . 7-103
7.3.5.3 PZUP, DRT, RIDGE, TCL, and SEPZ Alternative HFMs . . . 7-104
7.3.5.4 Summary: ER-OV-04a . . . 7-104
7.3.6 ER-OV-03a . . . 7-117
7.3.6.1 Alternative Water-Balance Conditions, BN HFM . . . 7-117
7.3.6.2 SCCC Alternative HFM . . . 7-117
7.3.6.3 PZUP, DRT, RIDGE, TCL, and SEPZ Alternative HFMs . . . 7-118
7.3.6.4 Summary: ER-OV-03a . . . 7-119
7.3.7 ER-OV-03c . . . 7-132
7.3.7.1 Alternative Water-Balance Conditions, BN HFM . . . 7-132
7.3.7.2 SCCC Alternative HFM . . . 7-132
7.3.7.3 PZUP, DRT, RIDGE, TCL, and SEPZ Alternative HFMs . . . 7-132
7.3.7.4 Summary: ER-OV-03c . . . 7-133
7.3.8 Coffer Windmill Well . . . 7-146
7.3.8.1 Summary: Coffer Windmill Well . . . 7-146
7.4 Geochemistry Performance of the Fortymile Canyon Alternate . . . 7-159
7.5 Quantitative Analysis and Ranking of Flow Models Based on Geochemistry . . . 7-164
7.5.1 Quantifying the Flow Models . . . 7-164
7.5.2 Ranking the Flow Models . . . 7-169
7.6 Summary . . . 7-170

8.0 Thermal Sensitivity and Verification . . . 8-1

8.1 Introduction . . . 8-1
8.2 Flow Model Verification to Vertical Flow Indicated by Temperature Analysis . . . 8-1
8.2.1 Southwestern Silent Canyon Caldera . . . 8-2
8.2.2 Northeastern Silent Canyon Caldera . . . 8-3
8.2.3 Eastern Timber Mountain Caldera . . . 8-6
8.2.4 Extra Caldera Zone Western Timber Mountain Caldera . . . 8-8
8.2.5 Summary . . . 8-8
8.3 Flow Model Sensitivity to Steady-State Temperature Distribution . . . 8-10

Uncontrolled When Printed

TABLE OF CONTENTS (CONTINUED)

8.3.1 Introduction 8-10
8.3.2 Sensitivity Results 8-11
8.3.3 Summary of Thermal Sensitivity Results 8-11

9.0 Summary and Conclusions 9-1

10.0 References 10-1

Appendix A - Evaluation of Flow and Transport Codes for Application to the Western Pahute Mesa Corrective Action Unit

A.1.0 Introduction A-1

A.2.0 Code Attributes A-2

A.2.1 General Attributes A-2
A.2.2 Groundwater Flow Model Attributes A-4
A.2.3 Transport Model Attributes A-5
A.2.4 Desirable Attributes A-6

A.3.0 Code Identification and Preliminary Selection A-8

A.4.0 Description of the Candidate Codes A-10

A.5.0 Testing Criteria A-12

A.6.0 Test Problem A-14

A.7.0 FRAC3DVS Test A-17

A.7.1 Grid Development A-17
A.7.2 Model Properties A-18
A.7.3 Boundary and Initial Conditions A-18
A.7.4 Simulation Results A-19
A.7.5 Performance Evaluation A-22

A.8.0 SWIFT-98 Test A-24

A.8.1 Model Assumptions A-24
A.8.2 Grid Development A-24
A.8.3 Model Properties A-25
A.8.4 Model Boundary and Initial Conditions A-26
A.8.5 Simulation Results A-27
A.8.6 Nonisothermal Test A-29
A.8.7 Performance Evaluation A-29

A.9.0 FEHM Test A-33

A.9.1 Model Assumptions A-33
A.9.2 Grid Development A-34
A.9.3 Model Properties A-37

Uncontrolled When Printed

TABLE OF CONTENTS (CONTINUED)

A.9.4 Boundary and Initial Conditions A-38
A.9.5 Simulation Results A-38
A.9.6 Nonisothermal Test A-40
A.9.7 Performance Evaluation A-41

A.10.0 Conclusions A-44

A.11.0 References A-49

Appendix B - Investigation of the Influence of Faults on Groundwater Movement in the Pahute Mesa/Oasis Valley Flow Model Domain

B.1.0 Purpose and Scope B-1

B.2.0 Hydrogeologic Setting B-3

B.2.1 Pre-Cenozoic Tectonic, Depositional, and Igneous History B-3
B.2.2 Cenozoic Volcanic and Tectonic History B-5
B.2.3 Description of Major Structural Features B-7
B.2.3.1 Architecture and Mineralization of Faults B-8
B.2.3.2 Alternative Structural Treatments B-9
B.2.3.3 Normal Faults (NF) B-9
B.2.3.4 Caldera Margins (CM) B-15
B.2.3.5 Thrust Faults (TF) B-24
B.2.3.6 Structural Zones (TSZ) B-25
B.2.3.7 Detachment Faults (DFS) B-29
B.2.4 Hydrologic Effects of Major Structural Features Within SWNVF B-29

B.3.0 Evidence of Fault Behavior from Other Areas of the NTS and Vicinity B-31

B.3.1 Evidence of Fault Behavior in Non-Tuffaceous Rocks B-31
B.3.2 Evidence of Fault Characteristics in Tuff from Yucca Mountain B-33

B.4.0 Evidence of Fault Behavior in the PM/OV Flow Domain B-37

B.4.1 Comparison of Structural Feature Map with the Potentiometric Surface Map B-38
B.4.2 Comparison of Structural Feature Map with Dissolved Chloride and Sulfate Distributions B-43
B.4.3 Evidence for Fault Behavior from Permeability Data B-45
B.4.4 Examination of the Role of Feature Orientation, Hydrothermal Alteration, Reactivation, Amount of Hydrostratigraphic Offset, and Feature Type on Feature Hydraulic Properties B-46

B.5.0 Summary and Conclusions B-49

B.6.0 Acknowledgements B-52

B.7.0 References B-53

Uncontrolled When Printed

TABLE OF CONTENTS (CONTINUED)

Appendix C - Development of a Steady-State Thermal Field and Evaluation of the Potential Use of Temperature Data To Constrain Pahute Mesa CAU Groundwater Flow Models

C.1.0 Introduction . . . C-1

C.2.0 Background . . . C-3

C.3.0 Model Overview . . . C-7

C.3.1 Modeling Approach . . . C-7
C.3.2 The PM/OV Heat-Conduction Model . . . C-7

C.4.0 Temperature Observations . . . C-9

C.5.0 Thermal Conductivity Estimates . . . C-21

C.5.1 LCA, LCA3, LCAA, and UCCU . . . C-23
C.5.2 LCCU . . . C-23
C.5.3 Intrusive Confining Units . . . C-24
C.5.4 Volcanic Rocks . . . C-24
C.5.4.1 Extra-Caldera Volcanic Rocks . . . C-25
C.5.4.2 Intra-Caldera Volcanic Rocks . . . C-25
C.5.5 Alluvium . . . C-26
C.5.6 Summary of Thermal Conductivity Estimates . . . C-27

C.6.0 Boundary Condition Estimates . . . C-28

C.6.1 Upper Boundary Condition . . . C-28
C.6.2 Lower Boundary Condition . . . C-35
C.6.2.1 Specified Heat Flux Lower Boundary Conditions . . . C-35
C.6.2.2 Specified Temperature Lower Boundary Conditions . . . C-36
C.6.2.3 Summary of Lower Boundary Conditions . . . C-41

C.7.0 Model Results . . . C-42

C.7.1 Forward Heat Conduction Models . . . C-42
C.7.2 Inverse Modeling To Optimize Grouped Thermal Conductivities and Deep Heat Fluxes . . . C-50
C.7.2.1 Inverse Modeling Background Summary . . . C-50
C.7.2.2 Inverse Models for the PM/OV Flow Domain . . . C-53
C.7.2.2.1 Calibrating Thermal Conductivities of Volcanic HSUs with a Specified Heat Flux of 65 mW/m^2 . . . C-54
C.7.2.2.2 Calibrating Heat Fluxes at the Base of the Model Domain . . . C-56
C.7.2.3 Evaluation of Deep Subregional Heat Flux Estimates . . . C-60
C.7.2.3.1 Subregion (1), North of Black Mountain . . . C-60
C.7.2.3.2 Subregion (2), Silent Canyon Caldera Complex . . . C-60

Uncontrolled When Printed

TABLE OF CONTENTS (CONTINUED)

C.7.2.3.3 Subregion (3), East Timber Mountain Caldera Complex and Black Mountain Caldera C-68
C.7.2.3.4 Subregion (4), West Timber Mountain Caldera Complex C-69
C.7.2.3.5 Subregion (5), Extra-Caldera Area East of the Timber Mountain and Silent Canyon Caldera Complexes C-69
C.7.2.3.6 Subregion (6), Extra-Caldera Areas West of Silent Canyon Caldera Complex and West and South of the Timber Mountain Caldera Complex C-69

C.8.0 Hydrological Significance of Temperature Residuals C-70

C.8.1 Subregion (2) - Silent Canyon Caldera Complex C-71
C.8.2 Subregion (4) - Western Timber Mountain Caldera Complex C-72
C.8.3 Subregion (5) - Extra-Caldera Area East of Timber Mountain and Silent Canyon Caldera Complexes C-73
C.8.4 Subregion (6) - Extra-Caldera Areas West of Silent Canyon Caldera Complex, and West and South of the Timber Mountain Caldera Complex . . . C-74

C.9.0 Summary and Conclusions C-75

C.10.0 References. C-77

Appendix D - Perturbation Sensitivity Analysis Plots

D.1.0 Introduction. D-1

D.2.0 Data Presentation D-2

D.3.0 Access to Data D-3

D.3.1 Base HFM with Depth Decay and Anisotropy with MME Recharge D-3
D.3.2 Base HFM with Selected Depth Decay and Selected Anisotropy with MME Recharge. D-3
D.3.3 Silent Canyon Caldera Complex Selected Depth Decay and Anisotropy with MME Recharge. D-4

Appendix E - CAU Model Permeability Along Geologic Model Cross Sections

E.1.0 CAU Model Permeability Along Geologic Model Cross Sections E-1

Appendix F - Well and Spring Head Calibration Data

F.1.0 Introduction. F-1

F.1.1 Hydraulic Head Summary Data F-1

F.2.0 References. F-13

Uncontrolled When Printed

LIST OF FIGURES

NUMBER	TITLE	PAGE
1-1	Location of the Pahute Mesa Corrective Action Units	1-2
1-2	Map Showing Location of the Pahute Mesa Model Area (Modified from BN, 2002)	1-5
1-3	Process Flow Diagram for the Underground Test Area Corrective Action Units	1-7
1-4	Geophysically Inferred Geologic Features of the Pahute Mesa Area	1-9
1-5	Features of the Nevada Test Site Regional Groundwater Flow System	1-12
2-1	Information Flow into the Pahute Mesa Groundwater Flow Model	2-2
2-2	Three-Dimensional View of the Base Hydrostratigraphic Model of the Pahute Mesa Area, Top at Land Surface (BN, 2002)	2-14
2-3	Comparison of Silent Canyon Caldera Margins: Base HFM Model and SCCC Alternative (Modified from BN, 2002)	2-20
2-4	Typical West-East Cross Section through the Silent Canyon Caldera for the SCCC Model (BN, 2002)	2-22
2-5	Typical West-East Cross Section through the Silent Canyon Caldera for the BN Model (BN, 2002)	2-23
2-6	Precipitation Map for the Nevada Test Site Region	2-26
2-7	UGTA Regional Model Recharge Distribution	2-32
2-8	UGTA Revised Maxey-Eakin Recharge Distribution in the NTS Region	2-33
2-9	USGS Recharge Distribution Model (USGSD), Overland Flow Component Included	2-34
2-10	USGS Recharge Distribution Model (USGSND), No Overland Flow Component	2-35
2-11	DRI Recharge Distribution with Alluvial Mask (Russell and Minor, 2002)	2-37
2-12	DRI Recharge Distribution with Alluvial and Elevation Mask (Russell and Minor, 2002)	2-38
2-13	General Spring Locations and Major Structural Features Controlling Spring Discharge in Oasis Valley, NV (Modified from Reiner et al., 2002)	2-42

Uncontrolled When Printed

LIST OF FIGURES (CONTINUED)

NUMBER	TITLE	PAGE
2-14	Locations of Pumping Wells in the Pahute Mesa Area Used in the Well Discharge Analysis	2-48
2-15	Total Withdrawals from Pumping Wells Located within the Pahute Mesa Area (No Data Available between 1968 and 1982)	2-49
2-16	Map Showing Composite Potentiometric Surface with Elevated Heads in the Northwest and HSUs at the Water Table	2-51
2-17	Map of the Locations of Hydraulic Conductivity Data	2-54
2-18	Geographic Distribution of δD Values for Wells and Springs in the Study Area	2-64
2-19	Geographic Distribution of Dissolved Cl^- Concentrations for Wells and Springs in the Study Area	2-65
2-20	Approximate Flow Paths Determined from Conservative Tracer Analyses	2-71
3-1	Code Evaluation Test Problem Boundaries, Selected Faults, and Locations of SERENA (U20an) and SCOTCH (U19as) Tests	3-17
3-2	3-D Hydrostratigraphic Model Used for the Code Evaluation Test Problem	3-18
3-3	Schematic Representation of a Cross Section Through Test Problem Domain as Viewed from the Southwest	3-19
3-4	Head Distribution for the North Boundary of the Test Problem Domain from the UGTA Regional Model	3-22
4-1	Octree Mesh Refinement Example	4-6
4-2	Example Mesh Refinement in HSUs	4-8
4-3	3-D View Showing Fault Thickness with Depth	4-9
4-4	Fault Numbering Key - Base HFM	4-10
4-5	Base HFM Fault Structure Viewed from the Southwest	4-11
4-6	Base HFM Fault Structure Viewed from the Northeast	4-12
4-7	Closeup View of Faults in Area 19	4-13

Uncontrolled When Printed

LIST OF FIGURES (CONTINUED)

NUMBER	TITLE	PAGE
4-8	Fault Numbering Key - SCCC HFM	4-14
4-9	SCCC HFM Fault Structure Viewed from the Southwest	4-16
4-10	SCCC HFM Fault Structure Viewed from the Northeast	4-17
4-11	Mesh Detail Near Test Chimney	4-18
4-12	USGS Recharge Model (Hevesi et al., 2003), Redistribution Included	4-21
4-13	USGS Recharge Model (Hevesi et al., 2003), Redistribution Not Included	4-22
4-14	MME Recharge	4-23
4-15	DRI Chloride Mass-Balance Recharge (Russell and Minor, 2002) with Alluvial Mask	4-24
4-16	DRI Chloride Mass-Balance Recharge (Russell and Minor, 2002) with Alluvial Mask and Elevation Screen	4-25
4-17	Oasis Valley Discharge Zones	4-26
4-18	CAU Model Boundary Heads Modified from the UGTA Regional Model (SNJV, 2004a)	4-27
4-19	Calibrated Temperature Field	4-28
5-1	General Calibration Protocol	5-4
5-2	Histogram of Head Calibration Weights	5-15
5-3	Calibrated CAU-Model Boundary Heads and Difference from UGTA Regional Model Viewed from the Northeast	5-19
5-4	Calibrated CAU-Model Boundary Heads and Difference from UGTA Regional Model Viewed from the Southwest	5-21
5-5	CAU-Model Pre-Belted Range Composite (PBRCM) Material Zones	5-23
5-6	Map Showing Hydrogeologic Domains in the Pahute Mesa/Oasis Valley Model Area	5-24
5-7	Map Showing LCA Nodes from UGTA Regional Model Zone 1	5-25

Uncontrolled When Printed

LIST OF FIGURES (CONTINUED)

NUMBER	TITLE	PAGE
5-8	Map Showing TMA Nodes Following UGTA Regional Model TMA Subdivision	5-26
5-9	Map Showing TCA Subdivision from UGTA Regional Model Zone 52	5-27
5-10	Observed Versus Simulated Well Head - Base HFM, No Depth Decay, No Anisotropy	5-30
5-11	Observed Versus Simulated Spring Head - Base HFM, No Depth Decay, No Anisotropy	5-31
5-12	Observed Versus Simulated Oasis Valley Discharge - Base HFM, No Depth Decay, No Anisotropy	5-32
5-13	Estimated and Simulated Boundary Flows - Base HFM, No Depth Decay, No Anisotropy	5-33
5-14	Histogram of Weighted Head Residuals - Base HFM, No Depth Decay, No Anisotropy	5-34
5-15	Post Plot of Weighted Well and Spring Head Residuals - Base HFM, No Depth Decay, No Anisotropy	5-35
5-16	Simulated Water Table - Base HFM, No Depth Decay, No Anisotropy	5-37
5-17	Particle Tracks - Base HFM, No Depth Decay, No Anisotropy	5-38
5-18	Hydrostratigraphic Unit Parameters - No Depth Decay, No Anisotropy	5-40
5-19	Observed Versus Simulated Well Head for BN-MME-SDA	5-43
5-20	Observed Versus Simulated Spring Head for BN-MME-SDA	5-44
5-21	Observed Versus Simulated Oasis Valley Discharge for BN-MME-SDA	5-45
5-22	Estimated and Simulated Boundary Flow for BN-MME-SDA	5-46
5-23	Histogram of Weighted Head Residuals for BN-MME-SDA	5-47
5-24	Post Plot of Weighted Well and Spring Head Residuals for BN-MME-SDA	5-48
5-25	Simulated Water Table for BN-MME-SDA	5-50

Uncontrolled When Printed

LIST OF FIGURES (CONTINUED)

NUMBER	TITLE	PAGE
5-26	Particle Tracks for BN-MME-SDA	5-51
5-27	Observed Versus Simulated Well Head for BN-MME-ADA	5-56
5-28	Observed Versus Simulated Spring Head for BN-MME-ADA	5-57
5-29	Observed and Simulated Oasis Valley Discharge for BN-MME-ADA	5-58
5-30	Estimated and Simulated Boundary Flows for BN-MME-ADA	5-59
5-31	Histogram of Weighted Head Residuals for BN-MME-ADA	5-60
5-32	Post Plot of Weighted Well and Spring Head Residuals for BN-MME-ADA	5-61
5-33	Simulated Water Table for BN-MME-ADA	5-63
5-34	Particle Tracks for BN-MME-ADA	5-64
5-35	Observed Versus Simulated Well Head for SCCC-MME-SDA	5-69
5-36	Observed Versus Simulated Spring Head for SCCC-MME-SDA	5-70
5-37	Observed Versus Simulated Oasis Valley Discharge for SCCC-MME-SDA	5-71
5-38	Estimated Versus Simulated Boundary Flows for SCCC-MME-SDA	5-72
5-39	Histogram of Weighted Head Residuals for SCCC-MME-SDA	5-73
5-40	Post Plot of Weighted Well and Spring Head Residuals for SCCC-MME-SDA	5-73
5-41	Simulated Water Table for SCCC-MME-SDA	5-76
5-42	Particle Tracks for SCCC-MME-SDA	5-76
5-43	Groundwater Levels on Pahute Mesa and Vicinity	5-82
5-44	Simulated Heads Near the Purse Fault for BN-MME-SDA	5-83
5-45	Simulated Heads Near the Purse Fault for SCCC-MME-SDA	5-83
5-46	Simulated Head Along B-B' and J-J' with Simulated Flow Path for SCCC-MME-SDA	5-84

Uncontrolled When Printed

LIST OF FIGURES (CONTINUED)

NUMBER	TITLE	PAGE
5-47	Simulated Head Along B-B' and J-J' with Simulated Flow Path for BN-MME-SDA	5-86
5-48	Simulated Head Along B-B' and J-J' with Simulated Flow Path for BN-MME-ADA	5-87
5-49	Permeability Along Section B-B'	5-88
5-50	Permeability Along Section J-J'	5-89
5-51	Comparison of Hydraulic Test and Model Permeability - Newer Well Data	5-91
5-52	Comparison of Hydraulic Test and Model Permeability - Older Well Data	5-92
5-53	Comparison of Model and Permeabilities for TMCM and TMA	5-96
5-54	Comparison of Model and Estimated Permeabilities for PBRCM and YMCFCM	5-97
5-55	Comparison of Model and Estimated Permeabilities for PCM and LCA	5-98
5-56	Comparison of Model and Estimated Permeabilities for BFCU, KA, CFCU, CFCM, IA, CHCU, CHZCM, CHVCM, and CHVTA	5-99
5-57	Comparison of Model and Estimated Permeabilities for TSA, LPCU, PLFA, TCA, UPCU, BA, FCCU, THCM, and THLFA	5-100
5-58	Comparison of Model and Estimated Permeabilities for FCA, FCCM, DVA, DVCM, PVTA, YVCM, AA, UCCU, and LCCU1	5-101
5-59	Observed Versus Simulated Low-Weight Head Data	5-104
6-1	Sample Objective Function for Perturbation Analysis	6-5
6-2	Largest Sensitivity Coefficients from PEST for BN-MME-SDA	6-14
6-3	Composite Observation Sensitivity from PEST for BN-MME-SDA	6-15
6-4	Correlation Coefficients from PEST for BN-MME-SDA	6-16
6-5	Largest Sensitivity Coefficients from PEST for BN-MME-ADA	6-17
6-6	Composite Observation Sensitivity from PEST for BN-MME-ADA	6-18

Uncontrolled When Printed

LIST OF FIGURES (CONTINUED)

NUMBER	TITLE	PAGE
6-7	Correlation Coefficients from PEST for BN-MME-ADA	6-19
6-8	Largest Sensitivity Coefficients from PEST for SCCC-MME-SDA	6-21
6-9	Composite Observation Sensitivity from PEST for SCCC-MME-SDA	6-22
6-10	Correlation Coefficients from PEST for SCCC-MME-SDA	6-22
6-11	Mean Head Difference for BN-MME-SDA	6-25
6-12	Mean Head Difference for Volcanic HSU Depth Decay for BN-MME-SDA	6-25
6-13	Mean Head Difference for Carbonate HSU Depth Decay for BN-MME-SDA	6-26
6-14	Mean Head Difference for Purse Fault Permeability Multipliers for BN-MME-SDA	6-26
6-15	PHI Perturbation Plot for BN-MME-SDA	6-27
6-16	PHI Perturbation Plot for Volcanic HSU Depth Decay for BN-MME-SDA	6-27
6-17	PHI Perturbation Plot for Carbonate HSU Depth Decay for BN-MME-SDA	6-28
6-18	PHI Perturbation Plot for Purse Fault Permeability Multipliers for BN-MME-SDA	6-28
6-19	Mean Head Difference for BN-MME-ADA	6-31
6-20	Mean Head Difference for Depth-Decay Parameters for BN-MME-ADA	6-32
6-21	Mean Head Difference for Purse Fault Permeability Multipliers for BN-MME-ADA	6-32
6-22	PHI Perturbation Plot for BN-MME-ADA	6-33
6-23	PHI Perturbation Plot for Depth Decay for BN-MME-ADA	6-33
6-24	PHI Perturbation Plot for Purse Fault Permeability Multipliers for BN-MME-ADA	6-34
6-25	Mean Head Difference for SCCC-MME-SDA	6-37
6-26	Mean Head Difference for Volcanic HSU Depth Decay for SCCC-MME-SDA	6-37

Uncontrolled When Printed

LIST OF FIGURES (CONTINUED)

NUMBER	TITLE	PAGE
6-27	Mean Head Difference for Carbonate HSU Depth Decay for SCCC-MME-SDA	6-38
6-28	Mean Head Difference for Sensitive Fault Permeability Multipliers for SCCC-MME-SDA	6-38
6-29	PHI Perturbation Plot for SCCC-MME-SDA	6-40
6-30	PHI Perturbation Plot for Volcanic HSU Depth Decay for SCCC-MME-SDA	6-41
6-31	PHI Perturbation Plot for Carbonate HSU Depth Decay for SCCC-MME-SDA	6-41
6-32	PHI Perturbation Plot for Sensitive Fault Permeability Multipliers for SCCC-MME-SDA	6-42
6-33	100 Best Simulations Ranked by PHI for BN-MME-SDA	6-45
6-34	Classification Tree on PHI for BN-MME-SDA	6-46
6-35	Classification Tree on WELL for BN-MME-SDA	6-47
6-36	Classification Tree on SPRING for BN-MME-SDA	6-48
6-37	Classification Tree on FLUX for BN-MME-SDA	6-48
6-38	Classification Tree on ETF for BN-MME-SDA	6-49
6-39	Bubble Plots from Entropy Analysis on PHI for BN-MME-SDA	6-50
6-40	Bubble Plots from Entropy Analysis on WELL for BN-MME-SDA	6-52
6-41	Bubble Plots from Entropy Analysis on FLUX for BN-MME-SDA	6-53
6-42	100 Best Simulations Ranked by PHI for BN-MME-ADA	6-54
6-43	Classification Tree on PHI for BN-MME-ADA	6-56
6-44	Classification Tree on WELL for BN-MME-ADA	6-56
6-45	Classification Tree on SPRING for BN-MME-ADA	6-57
6-46	Classification Tree on FLUX for BN-MME-ADA	6-58
6-47	Classification Tree on ETF for BN-MME-ADA	6-59

Uncontrolled When Printed

LIST OF FIGURES (CONTINUED)

NUMBER	TITLE	PAGE
6-48	Bubble Plots from Entropy Analysis on PHI for BN-MME-ADA	6-60
6-49	Bubble Plots from Entropy Analysis on WELL for BN-MME-ADA	6-61
6-50	Bubble Plots from Entropy Analysis on FLUX for BN-MME-ADA	6-62
6-51	100 Best Simulations Ranked by PHI for SCCC-MME-SDA	6-63
6-52	Classification Tree on PHI for SCCC-MME-SDA	6-64
6-53	Classification Tree on WELL for SCCC-MME-SDA	6-65
6-54	Classification Tree on SPRING for SCCC-MME-SDA	6-66
6-55	Classification Tree on FLUX for SCCC-MME-SDA	6-67
6-56	Classification Tree on ETF for SCCC-MME-SDA	6-67
6-57	Bubble Plots from Entropy Analysis on PHI for SCCC-MME-SDA	6-69
6-58	Bubble Plots from Entropy Analysis on WELL for SCCC-MME-SDA	6-70
6-59	Bubble Plots from Entropy Analysis on FLUX for SCCC-MME-SDA	6-71
6-60	Histogram of Log-Transformed Northern Boundary Flux for BN-MME-SDA	6-73
6-61	Histogram of Log-Transformed Resampled Northern Boundary Flux for BN-MME-SDA	6-74
6-62	Classification Tree for Northern Boundary Flux for BN-MME-SDA	6-74
6-63	Histogram of Log-Transformed Resampled Southern Boundary Flux for BN-MME-SDA	6-76
6-64	Classification Tree for Southern Boundary Flux for BN-MME-SDA	6-76
6-65	Histogram of Log-Transformed Resampled Eastern Boundary Flux for BN-MME-SDA	6-77
6-66	Classification Tree for Eastern Boundary Flux for BN-MME-SDA	6-77
6-67	Histogram of Log-Transformed Resampled Western Boundary Flux for BN-MME-SDA	6-79

Uncontrolled When Printed

LIST OF FIGURES (CONTINUED)

NUMBER	TITLE	PAGE
6-68	Classification Tree for Western Boundary Flux for BN-MME-SDA	6-79
6-69	Observed Versus Simulated Observation Well Head for BN-MME-SDA Reduced LCCU1 Permeability Alternative	6-82
6-70	Observed Versus Simulated Spring Head for BN-MME-SDA Reduced LCCU1 Permeability Alternative	6-82
6-71	Observed and Simulated Oasis Valley Discharge for BN-MME-SDA Reduced LCCU1 Permeability Alternative	6-83
6-72	Observed and Simulated Boundary Flows for BN-MME-SDA Reduced LCCU1 Permeability Alternative	6-83
6-73	Simulated Water Table for BN-MME-SDA Reduced LCCU1 Permeability Alternative	6-84
6-74	Particle Tracks for BN-MME-SDA Reduced LCCU1 Permeability Alternative	6-85
6-75	Particle Tracks for Chimney Permeability Enhancement	6-86
6-76	Post Plot of Weighted Well and Spring Head Residuals for BN-MME-SDA Fortymile Canyon Alternative	6-88
6-77	Particle Tracks for BN-MME-SDA Fortymile Canyon Alternative	6-89
6-78	Observed Versus Simulated Observation Well Head for BN-MME-SDA Reduced LCCU1 Permeability Alternative with 5:1 North-South Anisotropy	6-91
6-79	Observed Versus Simulated Spring Head for BN-MME-SDA Reduced LCCU1 Permeability Alternative with 5:1 North-South Anisotropy	6-91
6-80	Observed and Simulated Oasis Valley Discharge for BN-MME-SDA Reduced LCCU1 Permeability Alternative with 5:1 North-South Anisotropy	6-92
6-81	Observed and Simulated Boundary Flows for BN-MME-SDA Reduced LCCU1 Permeability Alternative with 5:1 North-South Anisotropy	6-92
6-82	Post Plot of Weighted Well and Spring Head Residuals for BN-MME-SDA Reduced LCCU1 Permeability Alternative with 5:1 North-South Anisotropy	6-93
6-83	Simulated Water Table for BN-MME-SDA Reduced LCCU1 Permeability Alternative with 5:1 North-South Anisotropy	6-94

Uncontrolled When Printed

LIST OF FIGURES (CONTINUED)

NUMBER	TITLE	PAGE
6-84	Particle Tracks for BN-MME-SDA Reduced LCCU1 Permeability with 5:1 North-South Anisotropy	6-94
6-85	HSU Permeability Changes for BN-MME Reduced LCCU1 Permeability with 5:1 North-South Anisotropy	6-95
6-86	Observed Versus Simulated Observation Well Head for TMCM-MME-SDA	6-97
6-87	Observed Versus Simulated Spring Head for TMCM-MME-SDA	6-97
6-88	Observed and Simulated Oasis Valley Discharge for TMCM-MME-SDA	6-98
6-89	Observed and Simulated Boundary Flows for TMCM-MME-SDA	6-98
6-90	Post Plots of Weighted Well and Spring Head Residuals for Timber Mountain Dome k_0 10x (Upper) and 100x (Lower)	6-100
6-91	Simulated Water Tables for Timber Mountain Dome k_0 10x (Upper) and 100x (Lower)	6-101
6-92	Particle Tracks for Timber Mountain Dome k_0 10x (Upper) and 100x (Lower)	6-102
6-93	PHI Perturbation Results for Selected HSUs in BN-MME-SDA	6-105
6-94	Observed Versus Simulated Observation Well Head for TCL-MME-SDA	6-120
6-95	Observed Versus Simulated Spring Head for TCL-MME-SDA	6-120
6-96	Observed and Simulated Oasis Valley Discharge for TCL-MME-SDA	6-121
6-97	Observed and Simulated Boundary Flows for TCL-MME-SDA	6-121
6-98	Histogram of Weighted Head Residuals for TCL-MME-SDA	6-122
6-99	Post Plot of Weighted Well and Spring Head Residuals for TCL-MME-SDA	6-123
6-100	Simulated Water Table for TCL-MME-SDA	6-124
6-101	Particle Tracks for TCL-MME-SDA	6-125
6-102	Observed Versus Simulated Observation Well Head for RIDGE-MME-SDA	6-126
6-103	Observed Versus Simulated Spring Head for RIDGE-MME-SDA	6-127

Uncontrolled When Printed

LIST OF FIGURES (CONTINUED)

NUMBER	TITLE	PAGE
6-104	Observed and Simulated Oasis Valley Discharge for RIDGE-MME-SDA	6-127
6-105	Observed and Simulated Boundary Flows for RIDGE-MME-SDA	6-128
6-106	Histogram of Weighted Head Residuals for RIDGE-MME-SDA	6-128
6-107	Post Plot of Weighted Well and Spring Head Residuals for RIDGE-MME-SDA	6-129
6-108	Simulated Water Table for RIDGE-MME-SDA	6-131
6-109	Particle Tracks for RIDGE-MME-SDA	6-131
6-110	Observed Versus Simulated Observation Well Head for PZUP-MME-SDA	6-133
6-111	Observed Versus Simulated Spring Head for PZUP-MME-SDA	6-133
6-112	Observed and Simulated Oasis Valley Discharge for PZUP-MME-SDA	6-134
6-113	Observed and Simulated Boundary Flows for PZUP-MME-SDA	6-134
6-114	Histogram of Weighted Head Residuals for PZUP-MME-SDA	6-135
6-115	Post Plot of Weighted Well and Spring Head Residuals for PZUP-MME-SDA	6-136
6-116	Simulated Water Table for PZUP-MME-SDA	6-138
6-117	Particle Tracks for PZUP-MME-SDA	6-138
6-118	Observed Versus Simulated Observation Well Head for DRT-MME-SDA	6-140
6-119	Observed Versus Simulated Spring Head for DRT-MME-SDA	6-140
6-120	Observed and Simulated Oasis Valley Discharge for DRT-MME-SDA	6-141
6-121	Observed and Simulated Boundary Flows for DRT-MME-SDA	6-141
6-122	Histogram of Weighted Head Residuals for DRT-MME-SDA	6-142
6-123	Post Plot of Weighted Well and Spring Head Residuals for DRT-MME-SDA	6-143
6-124	Simulated Water Table for DRT-MME-SDA	6-144
6-125	Particle Tracks for DRT-MME-SDA	6-145

Uncontrolled When Printed

LIST OF FIGURES (CONTINUED)

NUMBER	TITLE	PAGE
6-126	Observed Versus Simulated Observation Well Head for SEPZ-MME-SDA	6-147
6-127	Observed Versus Simulated Spring Head for SEPZ-MME-SDA	6-147
6-128	Observed and Simulated Oasis Valley Discharge for SEPZ-MME-SDA	6-148
6-129	Observed and Simulated Boundary Flows for SEPZ-MME-SDA	6-148
6-130	Histogram of Weighted Head Residuals for SEPZ-MME-SDA	6-149
6-131	Post Plot of Weighted Well and Spring Head Residuals for SEPZ-MME-SDA	6-149
6-132	Simulated Water Table for SEPZ-MME-SDA	6-151
6-133	Particle Tracks for SEPZ-MME-SDA	6-151
6-134	Normalized Objective Function of Alternative HFMs	6-157
6-135	Posted Weighted Residuals for BN-DRIA-SDA	6-162
6-136	Simulated Water Table for BN-DRIA-SDA	6-162
6-137	Particle Tracks for BN-DRIA-SDA	6-163
6-138	Post Plot of Weighted Well and Spring Head Residuals for BN-DRIA-SDA Reduced LCCU1 Permeability Alternative	6-164
6-139	Simulated Water Table for BN-DRIA-SDA Reduced LCCU1 Permeability Alternative	6-164
6-140	Particle Tracks for BN-DRIA-SDA Reduced LCCU1 Permeability Alternative	6-165
6-141	Post Plot of Weighted Well and Spring Head Residuals for BN-USGSND-SDA	6-167
6-142	Post Plot of Weighted Well and Spring Head Residuals for BN-USGSD-SDA	6-167
6-143	Simulated Water Table for BN-USGSND-SDA	6-168
6-144	Simulated Water Table for BN-USGSD-SDA	6-168
6-145	Particle Tracks for BN-USGSND-SDA	6-170
6-146	Particle Tracks for BN-USGSD-SDA	6-170

Uncontrolled When Printed

LIST OF FIGURES (CONTINUED)

NUMBER	TITLE	PAGE
6-147	Post Plot of Weighted Well and Spring Head Residuals for BN-USGSD-SDA Reduced LCCU1 Permeability Alternative	6-171
6-148	Simulated Water Table for BN-USGSD-SDA Reduced LCCU1 Permeability Alternative	6-172
6-149	Particle Tracks for BN-USGSD-SDA Reduced LCCU1 Permeability Alternative	6-172
6-150	Post Plot of Weighted Well and Spring Head Residuals for SCCC-DRIA-SDA	6-175
6-151	Simulated Water Table for SCCC-DRIA-SDA	6-175
6-152	Particle Tracks for SCCC-DRIA-SDA	6-176
6-153	Post Plot of Weighted Well and Spring Head Residuals for SCCC-USGSD-SDA	6-177
6-154	Simulated Water Table for SCCC-USGSD-SDA	6-178
6-155	Particle Tracks for SCCC-USGSD-SDA	6-178
6-156	Post Plot of Weighted Well and Spring Head Residuals for PZUP-DRIA-SDA	6-183
6-157	Simulated Water Table for PZUP-DRIA-SDA	6-183
6-158	Particle Tracks for PZUP-DRIA-SDA	6-184
6-159	Post Plot of Weighted Well and Spring Head Residuals for PZUP-USGSD-SDA	6-185
6-160	Simulated Water Table for PZUP-USGSD-SDA	6-186
6-161	Particle Tracks for PZUP-USGSD-SDA	6-186
6-162	Post Plot of Weighted Well and Spring Head Residuals for DRT-DRIA-SDA	6-188
6-163	Simulated Water Table for DRT-DRIA-SDA	6-189
6-164	Particle Tracks for DRT-DRIA-SDA	6-189
6-165	Post Plot of Weighted Well and Spring Head Residuals for DRT-USGSD-SDA	6-191

Uncontrolled When Printed

LIST OF FIGURES (CONTINUED)

NUMBER	TITLE	PAGE
6-166	Simulated Water Table for DRT-USGSD-SDA	6-192
6-167	Particle Tracks for DRT-USGSD-SDA	6-192
7-1	Zones Used To Identify Sources of Recharge and Inflow	7-2
7-2	Schematic of Mixing Ratios from Upstream Source Wells Along Path 1 Toward ER-OV-01(from Kwicklis et al., 2005, Figure 13)	7-5
7-3	Schematic of Mixing Ratios from Upstream Source Wells Along Path 4 Toward ER-OV-04a (from Kwicklis et al., 2005, Figure 15)	7-6
7-4	Schematic of Mixing Ratios from Upstream Source Wells Along Path 6 Toward Coffer Windmill Well (from Kwicklis et al., 2005, Figure 13)	7-7
7-5	Flow Paths Estimated by Kwicklis et al. (2005) Based on Mixing Models	7-8
7-6	Locations of Flow Model Calibration Wells (black circles), Geochemical Target Wells (blue circles), and Pathlines for Forward SPTR Particles Originating in Open Screened Intervals of Wells in Model Domain	7-9
7-7	Comparison of Reverse PTRK and SPTR Particle-Tracking Methods for Particles Originating at Well ER-OV-03a	7-11
7-8	Example of Geochemistry Comparison Plot	7-14
7-9	Example of PHREEQC and PTRK Results Comparison	7-15
7-10	Comparison of Flow Model with Geochemical Mixing Targets at UE-18r for BN-MME-SDA	7-17
7-11	Comparison of Flow Model with Geochemical Mixing Targets at UE-18r in the Reduced LCCU1 Permeability Alternative	7-19
7-12	Particle Exit Locations on Model East Face for (a) BN-MME-SDA and (b) for BN-MME-SDA Reduced LCCU1 Permeability Alternative	7-21
7-13	Comparison of Flow Model with Geochemical Mixing Targets at ER-EC-6 for BN-MME-SDA	7-23
7-14	Comparison of Flow Model with Geochemical Mixing Targets at ER-EC-6 in the Reduced LCCU1 Permeability Alternative	7-24

Uncontrolled When Printed

LIST OF FIGURES (CONTINUED)

NUMBER	TITLE	PAGE
7-15	Comparison of Flow Model with Geochemical Mixing Targets at ER-OV-01 for BN-MME-SDA	7-28
7-16	Comparison of Flow Model with Geochemical Mixing Targets at ER-OV-01 in the Reduced LCCU1 Permeability Alternative	7-29
7-17	Comparison of Flow Model with Geochemical Mixing Targets at ER-OV-05 for BN-MME-SDA	7-31
7-18	Comparison of Flow Model with Geochemical Mixing Targets at ER-OV-05 in the Reduced LCCU1 Permeability Alternative	7-32
7-19	Comparison of Flow Model with Geochemical Mixing Targets at ER-OV-04a for BN-MME-SDA	7-34
7-20	Comparison of Flow Model with Geochemical Mixing Targets at ER-OV-04a in the Reduced LCCU1 Permeability Alternative	7-35
7-21	Comparison of Flow Model with Geochemical Mixing Targets at ER-OV-03a for BN-MME-SDA	7-37
7-22	Comparison of Flow Model with Geochemical Mixing Targets at ER-OV-03a in the Reduced LCCU1 Permeability Alternative	7-38
7-23	Comparison of Flow Model with Geochemical Mixing Targets at ER-OV-03c for BN-MME-SDA	7-40
7-24	Comparison of Flow Model with Geochemical Mixing Targets at ER-OV-03c in the Reduced LCCU1 Permeability Alternative	7-41
7-25	PHREEQC Models for Coffer Windmill Well	7-43
7-26	Comparison of Flow Model with Geochemical Mixing Targets at Coffer Windmill Well for BN-MME-SDA	7-44
7-27	Comparison of Flow Model with Geochemical Mixing Targets at Coffer Windmill Well in the Reduced LCCU1 Permeability Alternative	7-45
7-28	Comparison of Flow Model with Geochemical Mixing Targets at UE-18r for BN-USGSD-SDA in the Reduced LCCU1 Permeability Alternative	7-51
7-29	Comparison of Flow Model with Geochemical Mixing Targets for UE-18r for BN-DRIA-SDA in the Reduced LCCU1 Permeability Alternative	7-52

Uncontrolled When Printed

LIST OF FIGURES (CONTINUED)

NUMBER	TITLE	PAGE
7-30	Quantitative Geochemical Comparison at UE-18r for (a) BN-USGSD-SDA and (b) BN-DRIA-SDA	7-53
7-31	Comparison of Flow Model Geochemical Mixing Targets at UE-18r for BN-MME-ADA	7-54
7-32	Comparison of Flow Model with Geochemical Mixing Targets at UE-18r for SCCC-MME-SDA	7-55
7-33	Quantitative Geochemical Comparisons at UE-18r for (a) SCCC-USGSD-SDA and (b) SCCC-DRIA-SDA	7-56
7-34	Quantitative Geochemical Comparisons at UE-18r for (a) PZUP-MME-SDA and (b) DRT-MME-SDA	7-57
7-35	Quantitative Geochemical Comparisons at UE-18r for (a) RIDGE-MME-SDA and (b) TCL-MME-SDA	7-58
7-36	Quantitative Geochemical Comparison at UE-18r for SEPZ-MME-SDA	7-59
7-37	Quantitative Geochemical Comparisons at UE-18r for (a) PZUP-USGSD-SDA and (b) PZUP-DRIA-SDA	7-60
7-38	Quantitative Geochemical Comparisons at UE-18r for(a) DRT-USGSD-SDA and (b) DRT-DRIA-SDA	7-61
7-39	Comparison of Flow Model with Geochemical Mixing Targets at ER-EC-6 for BN-USGSD-SDA in the Reduced LCCU1 Permeability Alternative	7-65
7-40	Comparison of Flow Model with Geochemical Mixing Targets at ER-EC-6 for BN DRIA-SDA in the Reduced LCCU1 Permeability Alternative	7-66
7-41	Quantitative Geochemical Comparison at ER-EC-6 for (a) BN-USGSD-SDA and (b) BN-DRIA-SDA	7-67
7-42	Comparison of Flow Model with Geochemical Mixing Targets at ER-EC-6 for BN-MME-ADA	7-68
7-43	Comparison of Flow Model with Geochemical Mixing Targets at ER-EC-6 for SCCC-MME-SDA	7-69
7-44	Quantitative Geochemical Comparisons at ER-EC-6 for (a) SCCC-USGSD-SDA and (b) SCCC-DRIA-SDA	7-70

Uncontrolled When Printed

LIST OF FIGURES (CONTINUED)

NUMBER	TITLE	PAGE
7-45	Quantitative Geochemical Comparisons at ER-EC-6 for (a) PZUP-MME-SDA and (b) DRT-MME-SDA	7-71
7-46	Quantitative Geochemical Comparison at ER-EC-6 for (a) RIDGE-MME-SDA and (b) TCL-MME-SDA	7-72
7-47	Comparison of Flow Model with Geochemical Mixing Targets at ER-EC-6 for SEPZ-MME-SDA	7-73
7-48	Quantitative Geochemical Comparisons at ER-EC-6 for (a) PZUP-USGSD-SDA and (b) PZUP-DRIA-SDA	7-74
7-49	Quantitative Geochemical Comparisons at ER-EC-6 for (a) DRT-USGSD-SDA and (b) DRT-DRIA-SDA	7-75
7-50	Comparison of Flow Model with Geochemical Mixing Targets at ER-OV-01 for BN-USGSD-SDA in the Reduced LCCU1 Permeability Alternative	7-79
7-51	Comparison of Flow Model with Geochemical Mixing Targets at ER-OV-01 for BN-DRIA-SDA in the Reduced LCCU1 Permeability Alternative	7-80
7-52	Quantitative Geochemical Comparison at ER-OV-01 for (a) BN-USGSD-SDA and (b) BN-DRIA-SDA	7-81
7-53	Comparison of Flow Model with Geochemical Mixing Targets at ER-OV-01 for BN-MME-ADA	7-82
7-54	Comparison of Flow Model with Geochemical Mixing Targets at ER-OV-01 for SCCC-MME-SDA	7-83
7-55	Quantitative Geochemical Comparisons at ER-OV-01 for (a) SCCC-USGSD-SDA and (b) SCCC-DRIA-SDA	7-84
7-56	Quantitative Geochemical Comparison at ER-OV-01 for (a) PZUP-MME-SDA and (b) DRT-MME-SDA	7-85
7-57	Quantitative Geochemical Comparisons at ER-OV-01 for (a) RIDGE-MME-SDA and (b) TCL-MME-SDA	7-86
7-58	Comparison of Flow Model with Geochemical Mixing Targets at ER-OV-01 for SEPZ-MME-SDA	7-87

Uncontrolled When Printed

LIST OF FIGURES (CONTINUED)

NUMBER	TITLE	PAGE
7-59	Quantitative Geochemical Comparisons at ER-OV-01 for (a) PZUP-USGSD-SDA and (b) PZUP-DRIA-SDA	7-88
7-60	Quantitative Geochemical Comparisons at ER-OV-01 for (a) DRT-USGSD-SDA and (b) DRT-DRIA-SDA	7-89
7-61	Comparison of Flow Model with Geochemical Mixing Targets at ER-OV-05 for BN-USGSD-SDA in the Reduced LCCU1 Permeability Alternative	7-92
7-62	Comparison of Flow Model with Geochemical Mixing Targets at ER-OV-05 for BN-DRIA-SDA in the Reduced LCCU1 Permeability Alternative	7-93
7-63	Quantitative Geochemical Comparisons at Well ER-OV-05 for (a) BN-USGSD-SDA and (b) BN-DRIA-SDA	7-94
7-64	Comparison of Flow Model with Geochemical Mixing Targets at ER-OV-05 for BN-MME-ADA	7-95
7-65	Comparison of Flow Model with Geochemical Mixing Targets at ER-OV-05 for SCCC-MME-SDA	7-96
7-66	Quantitative Geochemical Comparisons at ER-OV-05 for (a) SCCC-USGSD-SDA and (b) SCCC-DRIA-SDA	7-97
7-67	Quantitative Geochemical Comparison at ER-OV-05 for (a) PZUP-MME-SDA and (b) DRT-MME-SDA	7-98
7-68	Quantitative Geochemical Comparisons at ER-OV-05 for (a) RIDGE-MME-SDA and (b) TCL-MME-SDA	7-99
7-69	Comparison of Flow Model with Geochemical Mixing Targets at ER-OV-05 for SEPZ-MME-SDA	7-100
7-70	Quantitative Geochemical Comparisons at ER-OV-05 for (a) PZUP-USGSD-SDA and (b) PZUP-DRIA-SDA	7-101
7-71	Quantitative Geochemical Comparisons at ER-OV-05 for (a) DRT-USGSD-SDA and (b) DRT-DRIA-SDA	7-102
7-72	Comparison of Flow Model with Geochemical Mixing Targets at ER-OV-04a for BN-DRIA-SDA in the Reduced LCCU1 Permeability Alternative	7-105

Uncontrolled When Printed

LIST OF FIGURES (CONTINUED)

NUMBER	TITLE	PAGE
7-73	Comparison of Flow Model with Geochemical Mixing Targets at ER-OV-04a for BN-USGSD-SDA in the Reduced LCCU1 Permeability Alternative	7-106
7-74	Quantitative Geochemical Comparison at ER-OV-04a for (a) BN-USGSD-SDA and (b) BN-DRIA-SDA	7-107
7-75	Comparison of Flow Model with Geochemical Mixing Targets at ER-OV-04a for BN-MME-ADA	7-108
7-76	Comparison of Flow Model with Geochemical Mixing Targets at ER-OV-04a for SCCC-MME-SDA	7-109
7-77	Quantitative Geochemical Comparisons at ER-OV-04a for (a) SCCC-USGSD-SDA and (b) SCCC-DRIA-SDA	7-110
7-78	Quantitative Geochemical Comparisons at ER-OV-04a for (a) PZUP-MME-SDA and (b) DRT-MME-SDA	7-111
7-79	Quantitative Geochemical Comparisons at ER-OV-04a for (a) RIDGE-MME-SDA and (b) TCL-MME-SDA	7-112
7-80	Comparison of Flow Model with Geochemical Mixing Targets at ER-OV-04a for SEPZ-MME-SDA	7-113
7-81	Quantitative Geochemical Comparisons at ER-OV-04a for (a) PZUP-USGSD-SDA and (b) PZUP-DRIA-SDA	7-114
7-82	Quantitative Geochemical Comparisons at ER-OV-04a for (a) DRT-USGSD-SDA and (b) DRT-DRIA-SDA	7-115
7-83	Comparison of Flow Model with Geochemical Mixing Targets at ER-OV-03a for BN-USGSD-SDA in the Reduced LCCU1 Permeability Alternative	7-120
7-84	Comparison of Flow Model with Geochemical Mixing Targets at ER-OV-03a for BN-DRIA-SDA in the Reduced LCCU1 Permeability Alternative	7-121
7-85	Quantitative Geochemical Comparisons at ER-OV-03a for (a) BN-USGSD-SDA and (b) BN-DRIA-SDA	7-122
7-86	Comparison of Flow Model with Geochemical Mixing Targets at ER-OV-03a for BN-MME-ADA	7-123

Uncontrolled When Printed

LIST OF FIGURES (CONTINUED)

NUMBER	TITLE	PAGE
7-87	Comparison of Flow Model with Geochemical Mixing Targets at ER-OV-03a for SCCC-MME-SDA	7-124
7-88	Quantitative Geochemical Comparisons at ER-OV-03a for (a) SCCC-USGSD-SDA and (b) SCCC-DRIA-SDA	7-125
7-89	Quantitative Geochemical Comparisons at ER-OV-03a for (a) PZUP-MME-SDA and (b) DRT-MME-SDA	7-126
7-90	Quantitative Geochemical Comparisons at ER-OV-03a for (a) RIDGE-MME-SDA and (b) TCL-MME-SDA	7-127
7-91	Comparison of Flow Model with Geochemical Mixing Targets at ER-OV-03a for SEPZ-MME-SDA	7-128
7-92	Quantitative Geochemical Comparisons at ER-OV-03a for (a) PZUP-USGSD-SDA and (b) PZUP-DRIA-SDA	7-129
7-93	Quantitative Geochemical Comparisons at ER-OV-03a for (a) DRT-USGSD-SDA and (b) DRT-DRIA-SDA	7-130
7-94	Comparison of Flow Model with Geochemical Mixing Targets at ER-OV-03c for BN-USGSD-SDA in the Reduced LCCU1 Permeability Alternative	7-134
7-95	Comparison of Flow Model with Geochemical Mixing Targets at ER-OV-03c for BN-DRIA-SDA in the Reduced LCCU1 Permeability Alternative	7-135
7-96	Quantitative Geochemical Comparisons at ER-OV-03c for (a) BN-USGSD-SDA and (b) BN-DRIA-SDA	7-136
7-97	Comparison of Flow Model with Geochemical Mixing Targets at ER-OV-03c for BN-MME-ADA	7-137
7-98	Comparison of Flow Model with Geochemical Mixing Targets at ER-OV-03c for SCCC-MME-SDA	7-138
7-99	Quantitative Geochemical Comparisons at ER-OV-03c for (a) SCCC-USGSD-SDA and (b) SCCC-DRIA-SDA	7-139
7-100	Quantitative Geochemical Comparisons at ER-OV-03c for (a) PZUP-MME-SDA and (b) DRT-MME-SDA	7-140

Uncontrolled When Printed

LIST OF FIGURES (CONTINUED)

NUMBER	TITLE	PAGE
7-101	Quantitative Geochemical Comparisons at ER-OV-03c for (a) RIDGE-MME-SDA and (b) TCL-MME-SDA	7-141
7-102	Comparison of Flow Model with Geochemical Mixing Targets at ER-OV-03c for SEPZ-MME-SDA	7-142
7-103	Quantitative Geochemical Comparisons at ER-OV-03c for (a) PZUP-USGSD-SDA and (b) PZUP-DRIA-SDA	7-143
7-104	Quantitative Geochemical Comparisons at ER-OV-03c for (a) DRT-USGSD-SDA and (b) DRT-DRIA-SDA	7-144
7-105	Comparison of Flow Model with Geochemical Mixing Targets at Coffer Windmill Well for BN-USGSD-SDA in the Reduced LCCU1 Permeability Alternative	7-147
7-106	Comparison of Flow Model with Geochemical Mixing Targets at Coffer Windmill Well for BN-DRIA-SDA in the Reduced LCCU1 Permeability Alternative	7-148
7-107	Quantitative Geochemical Comparisons at Coffer Windmill Well for (a) BN-USGSD-SDA and (b) BN-DRIA-SDA	7-149
7-108	Comparison of Flow Model with Geochemical Mixing Targets at Coffer Windmill Well for BN-MME-ADA	7-150
7-109	Comparison of Flow Model with Geochemical Mixing Targets at Coffer Windmill Well for SCCC-MME-SDA	7-151
7-110	Quantitative Geochemical Comparisons at Coffer Windmill Well for (a) SCCC-USGSD-SDA and (b) SCCC-DRIA-SDA	7-152
7-111	Quantitative Geochemical Comparisons at Coffer Windmill Well for (a) PZUP-MME-SDA and (b) DRT-MME-SDA	7-153
7-112	Quantitative Geochemical Comparisons at Coffer Windmill Well for (a) RIDGE-MME-SDA and (b) TCL-MME-SDA	7-154
7-113	Comparison of Flow Model with Geochemical Mixing Targets at Coffer Windmill Well for SEPZ-MME-SDA	7-155
7-114	Quantitative Geochemical Comparisons at Coffer Windmill Well for (a) PZUP-USGSD-SDA and (b) PZUP-DRIA-SDA	7-156

Uncontrolled When Printed

LIST OF FIGURES (CONTINUED)

NUMBER	TITLE	PAGE
7-115	Quantitative Geochemical Comparisons at Coffer Windmill Well for (a) DRT-USGSD-SDA and (b) DRT-DRIA-SDA	7-157
7-116	Paths of Particles Released in Wells for BN-USGSD-FMC Calibrated Flow Model	7-160
7-117	Comparison of Flow Model with Geochemical Mixing Targets for UE-18r with the BN-USGSD-FMC Flow Model	7-161
7-118	Comparison of Flow Model with Geochemical Mixing Targets for ER-OV-04a with the FMC-USGSD-SDA Flow Model	7-161
7-119	Comparison of Flow Model with Geochemical Mixing Targets for ER-OV-03a with the FMC-USGSD-SDA Flow Model	7-162
7-120	Comparison of Flow Model with Geochemical Mixing Targets for ER-OV-03c with the FMC-USGSD-SDA Flow Model	7-162
7-121	Comparison of Flow Model with Geochemical Mixing Targets for Coffer Windmill Well with the FMC-USGSD-SDA Flow Model	7-163
7-122	Geochemical Residual Means for Each Cluster	7-166
7-123	Components of the Total Geochemical Residual for Each Model	7-167
7-124	Flow Model Calibration Objective Functions, Sorted To Compare with Geochemical Residuals in Figure 7-123	7-168
8-1	Reverse-Particle Paths Originating in Inlet Aquifer Below ER-20-5 #3 Simulated for the BN-MME-SDA Reduced LCCU1 Permeability Alternative Flow Model	8-4
8-2	Reverse-Particle Paths Originating in UE-19e for BN-MME-SDA Reduced LCCU1 Permeability Alternative Flow Model	8-5
8-3	Reverse-Particle Paths Originating in the Fault Breccia Lithologic Subunit of the Timber Mountain Composite Unit at UE-18r for BN-MME-SDA Reduced LCCU1 Permeability Alternative Flow Model	8-7
8-4	Reverse-Particle Paths Originating in the LCA Below ER-EC-4 for BN-MME-SDA Reduced LCCU1 Permeability Alternative Flow Model	8-9

Uncontrolled When Printed

LIST OF FIGURES (CONTINUED)

NUMBER	TITLE	PAGE
8-5	Comparison of Flow Model Objective Functions for Different Thermal Fields	8-12
8-6	Comparison of Forward Flow Paths (Grey) and Reverse-Particle Exits from ER-OV-04a	8-13
A.11-1	Code Evaluation Test Problem Boundaries, Selected Faults, and Locations of SERENA (U20an) and SCOTCH (U19as) Tests	A-52
A.11-2	Schematic Representation of the Three-Dimensional Hydrogeologic Model Used for the Code Evaluation Test Problem as Viewed from the Southwest Corner of the Test Problem Area	A-53
A.11-3	Schematic Representation of a Cross Section Through Test Problem Domain as Viewed from the Southwest	A-54
B.7-1	Map Showing Structural Features and Model Boundaries for the PM/OV Flow Model	B-66
B.7-2	Map Showing Hydraulic Head Measurements and Contours, Including Structural Features in the Vicinity of the PM/OV Flow Model	B-67
B.7-3	Map Showing Hydraulic Heads Measurements and Contours with Structural Features in the Vicinity of NTS Areas 19 and 20	B-68
B.7-4	Map Showing Groundwater Chloride Concentrations, Hydraulic Head Contours, and Structural Features in the PM/OV Flow Domain	B-69
B.7-5	Map Showing Groundwater Chloride Concentrations, Hydraulic Head Contours, and Structural Features in the Vicinity of NTS Areas 19 and 20	B-70
B.7-6	Map Showing Groundwater Sulfate Concentrations, Hydraulic Head Contours, and Structural Features in the PM/OV Flow Domain	B-71
B.7-7	Map Showing Groundwater Sulfate Concentrations, Hydraulic Head Contours, and Structural Features in the Vicinity of NTS Areas 19 and 20	B-72
B.7-8	Figure Showing Hydraulic Conductivities as a Function of Hydrostratigraphic Unit and Depth in the PM/OV Flow Domain and Surrounding Areas	B-73
C.2-1	Simulated (a) Temperature and (b) Heat Flux Profiles in Homogenous Rock Simulated (c) Temperature and (d) Heat Flux Profiles in Layered Rock	C-4
C.4-1	Location of Boreholes Used in Study	C-10

Uncontrolled When Printed

LIST OF FIGURES (CONTINUED)

NUMBER	TITLE	PAGE
C.4-2	Location of Structural Zones Used in Study	C-20
C.6-1	Contour Map of Water Table Temperatures (°C) Used as Upper Boundary Conditions.	C-29
C.7-1	Simulated Temperature (°C) at the Lower Boundary for a Uniform Heat Flux of 85 mW/m^2	C-44
C.7-2	Simulated Temperatures (°C) for a Specified Lower Heat Flux of 85 mW/m^2 at Four Elevations (a) z = -3,200 m, (b) z = -2,000, (c) z = 0 m, and (d) z = 1,000 m.	C-45
C.7-3	East-West Transects for Uniform 85 mW/m2 Lower Boundary Flux Simulation at (a) y = 4,127,000 m, (b) y = 4,110,000 m, and (c) y = 4,097,500 m, Corresponding Approximately to Transects C-C', E-E', and B-B' (BN, 2002)	C-46
C.7-4	North-South Transects for Uniform 85 mW/m^2 Lower Boundary Flux Simulation at (a) x = 532,000 m, (b) x = 548,000 m, and (c) x = 564,000 m, Corresponding Approximately to Transects G-G', H-H', and I-I' (BN, 2002)	C-47
C.7-5	Results from Forward Model with a Uniform Lower Heat Flux of 85 mW/m^2 and Base-Case Thermal Conductivities for all 46 HSUs Listed in Table C.5-1	C-48
C.7-6	Simulated Versus Measured Temperatures for Uniform Lower Heat Flux of 65 mW/m^2 and Base-Case Thermal Conductivities for all 46 HSUs Listed in Table C.5-1	C-50
C.7-7	Simulated Versus Measured Temperatures for Uniform Lower Heat Flux of 45 mW/m^2 and Base-Case Thermal Conductivities for all 46 HSUs Listed in Table C.5-1	C-51
C.7-8	Average Residual Temperature (°C) in Deep Saturated Boreholes Simulations Use Specified Uniform Temperature at Lower Boundary of 160°C	C-52
C.7-9	Simulated Versus Measured Temperatures for Specified Lower Heat Flux of 65 mW/m^2 and Calibrated Thermal Conductivities for Volcanic HSU Groupings 6, 7, and 8 Listed in Table C.7-1	C-56
C.7-10	Calibrated Heat Fluxes at Base of Model.	C-58
C.7-11	Results from Inverse Model with Calibrated Heat Fluxes in Multiple Zones and Thermal Conductivities Assigned for all 46 HSUs Listed in Table C.5-1	C-59

Uncontrolled When Printed

LIST OF FIGURES (CONTINUED)

NUMBER	TITLE	PAGE
C.7-12	Simulated Temperatures (°C) at 5 Elevations for Calibrated Thermal Fluxes in 6 Zones on Lower Boundary: (a) -3,200 m, (b) -2,000 m, (c) 0 m, (d) 500 m, and (e) 1,000 m	C-61
C.7-13	East-West Transects for Calibrated Six-Zone Heat-Flux Model at (a) y = 4,127,000 m, (b) y = 4,110,000 m, and (c) y = 4,097,500 m, Corresponding Approximately to Transects C-C', E-E', and B-B' (BN, 2002)	C-62
C.7-14	North-South Transects for Calibrated Six-Zone Heat-Flux Model at (a) x = 532,000 m, (b) x = 548,000 m, and (c) x = 564,500 m, Corresponding Approximately to Transects G-G', H-H', and I-I' (BN, 2002)	C-63
E.1-1	Geologic Cross-Section Key	E-1

Uncontrolled When Printed

LIST OF TABLES

NUMBER	TITLE	PAGE
1-1	Major Supporting Documents	1-14
2-1	Hydrogeologic Units of the UGTA Regional Model	2-4
2-2	Hydrostratigraphic Units of the Pahute Mesa Area Included in the UGTA Regional HFM	2-5
2-3	Range of Hydraulic Parameters for Major Aquifers	2-7
2-4	Estimated Steady-State Groundwater Budget for the Regional Groundwater Flow System	2-9
2-5	Summary of Alternative HFMs Considered in the Pahute Mesa Flow Model	2-12
2-6	Correlation of Hydrostratigraphic Units of the Pahute Mesa Base HFM and Earlier Models	2-16
2-7	Correlation of Hydrostratigraphic Units Between the Silent Canyon Caldera Complex HFM and the Base HFM	2-21
2-8	Summary of Net Boundary Flux Ranges (m^3/d)	2-25
2-9	Precipitation Station Data	2-27
2-10	Comparison of Calculated Precipitation Volumes to Published Values by Hydrographic Area	2-29
2-11	Recharge Volumes for Hydrographic Areas for all Recharge Models	2-39
2-12	Description of Springs Occurring in Oasis Valley	2-43
2-13	ET Units Determined from Spectral Analysis of Satellite Imagery Data (June 13, 1992), Oasis Valley Discharge Area, Nevada	2-44
2-14	Estimated Mean Annual ET and Groundwater ET by ET Unit from Oasis Valley Discharge Area, Nevada	2-46
2-15	Summary Statistics of Simulated Annual ET from 1,000 Monte Carlo Realizations for the Oasis Valley Discharge Area	2-47
2-16	Statistics of Laboratory-Scale Hydraulic Conductivity Data	2-55
2-17	Statistics of Slug-Test-Scale Hydraulic Conductivity Data	2-56

Uncontrolled When Printed

LIST OF TABLES (CONTINUED)

NUMBER	TITLE	PAGE
2-18	Statistics of Constant-Rate-Scale Hydraulic Conductivity Data as Compared to Statistics of Slug-Test-Scale and Laboratory-Scale Data	2-57
2-19	Hydraulic Conductivity Distributions of Hydrostratigraphic Units of the Pahute Mesa Hydrostratigraphic Framework Model	2-58
2-20	Statistical Summary of Representative Conservative Tracer Data	2-67
2-21	Description of Plausible Groundwater Flow Paths in the Pahute Mesa Flow System (SNJV, 2004a)	2-69
2-22	Summary of Geochemical Flow Path Model Results for the Pahute Mesa Flow System (SNJV, 2004a)	2-73
3-1	Required Hydrologic Code Attributes	3-2
3-2	Comparison of Candidate Codes by Attribute	3-11
3-3	Summary of HSU/Fault Parameter Values Used in the Test Model	3-21
4-1	Hydrostratigraphic Unit Abbreviations and Names	4-4
4-2	Base HFM Fault Indices and Names	4-15
4-3	SCCC HFM Fault Indices and Names	4-18
4-4	Base and SCCC Mesh Statistics	4-20
4-5	Mass Flows for USGS, MME, and DRI Recharge Maps	4-25
5-1	Calibration Components and Implementation	5-5
5-2	Head and Spring Calibration Weights	5-10
5-3	Corrected Spring Locations	5-16
5-4	Oasis Valley Zone Discharge	5-16
5-5	Interpolated Regional Model Boundary Flows	5-18
5-6	Calibration Summary Statistics - Base HFM, No Depth Decay, No Anisotropy	5-36
5-7	Contribution to Model Goodness of Fit by Data Type for Base HFM Selected HSU Depth Decay and Anisotropy	5-36

Uncontrolled When Printed

LIST OF TABLES (CONTINUED)

NUMBER	TITLE	PAGE
5-8	Hydrostratigraphic Units with Depth Decay and Anisotropy	5-42
5-9	Calibration Summary Statistics for BN-MME-SDA	5-49
5-10	Contribution to Model Goodness of Fit by Data Type for BN-MME-SDA	5-49
5-11	Hydrostratigraphic Unit Parameters for BN-MME-SDA	5-51
5-12	Fault Permeability Multiplier for BN-MME-SDA	5-53
5-13	Calibration Summary Statistics for BN-MME-ADA	5-62
5-14	Contribution to Model Goodness of Fit by Data Type for BN-MME-ADA	5-62
5-15	Hydrostratigraphic Unit Parameters for BN-MME-ADA	5-65
5-16	Fault Permeability Multiplier for BN-MME-ADA	5-67
5-17	Calibration Summary Statistics for SCCC-MME-SDA	5-74
5-18	Contribution to Model Goodness of Fit by Data Type for SCCC-MME-SDA	5-75
5-19	Hydrostratigraphic Unit Parameters for SCCC-MME-SDA	5-77
5-20	Fault Permeability Multipliers for SCCC-MME-SDA	5-78
5-21	Water-Balance Components (kg/s)	5-102
6-1	Recharge, Boundary, and HFM Uncertainty Matrix	6-11
6-2	Spearman Rank Correlation Matrix for BN-MME-SDA	6-45
6-3	Results of Entropy Analysis on PHI for BN-MME-SDA	6-50
6-4	Results of Entropy Analysis on WELL for BN-MME-SDA	6-52
6-5	Results of Entropy Analysis for FLUX for BN-MME-SDA	6-53
6-6	Spearman Rank Correlation Matrix for BN-MME-ADA	6-55
6-7	Results of Entropy Analysis on PHI for BN-MME-ADA	6-60
6-8	Results of Entropy Analysis on WELL for BN-MME-ADA	6-61

Uncontrolled When Printed

LIST OF TABLES (CONTINUED)

NUMBER	TITLE	PAGE
6-9	Results of Entropy Analysis on FLUX for BN-MME-ADA	6-62
6-10	Spearman Rank Correlation Matrix for SCCC-MME-SDA	6-64
6-11	Results of Entropy Analysis on PHI for SCCC-MME-SDA	6-69
6-12	Results of Entropy Analysis on WELL for SCCC-MME-SDA	6-70
6-13	Results of Entropy Analysis on FLUX for SCCC-MME-SDA	6-71
6-14	Calibration Summary Statistics for BN-MME-SDA Reduced LCCU1 Permeability Alternative	6-84
6-15	Calibration Summary Statistics for Chimney Permeability Enhancement	6-86
6-16	Calibration Summary Statistics for BN-MME-SDA Fortymile Canyon Alternative	6-87
6-17	Calibration Summary Statistics for LCCU1-MME-SDA with Selected HSU Horizontal Anisotropy of 5:1	6-93
6-18	Calibration Summary Statistics for Timber Mountain Dome Sensitivity	6-99
6-19	Summary of Key Sensitivity Analysis Findings	6-104
6-20	Abridged List of Alternative Scenarios for the Pahute Mesa/Oasis Valley 3-D Hydrostratigraphic Model	6-109
6-21	Calibration Summary Statistics for TCL-MME-SDA	6-123
6-22	Contribution to Model Goodness of Fit by Data Type for TCL-MME-SDA	6-124
6-23	Selected Node Changes for TCL HFM Alternative	6-125
6-24	Calibration Summary Statistics for RIDGE-MME-SDA	6-130
6-25	Contribution to Model Goodness of Fit by Data Type for RIDGE-MME-SDA	6-130
6-26	Selected Node Changes for RIDGE HFM Alternative	6-132
6-27	Calibration Summary Statistics for PZUP-MME-SDA	6-137
6-28	Contribution to Model Goodness of Fit by Data Type for PZUP-MME-SDA	6-137

Uncontrolled When Printed

LIST OF TABLES (CONTINUED)

NUMBER	TITLE	PAGE
6-29	Selected Node Changes for PZUP HFM Alternative	6-139
6-30	Calibration Summary Statistics for DRT-MME-SDA	6-143
6-31	Contribution to Model Goodness of Fit by Data Type for DRT-MME-SDA	6-144
6-32	Selected Node Changes for DRT HFM Alternative	6-145
6-33	Calibration Summary Statistics for SEPZ-MME-SDA	6-150
6-34	Contribution to Model Goodness of Fit by Data Type for SEPZ-MME-SDA	6-150
6-35	Selected Node Changes for SEPZ HFM Alternative	6-152
6-36	Calibrated HSU Parameters for All Five HFMs	6-154
6-37	Summary of Flow Model Results for HFM Uncertainty Analysis	6-156
6-38	Calibration Summary Statistics for BN-DRIAE-SDA	6-160
6-39	Calibration Summary Statistics for BN-DRIA-SDA	6-161
6-40	Calibration Summary Statistics for BN-DRIA-SDA Reduced LCCU1 Permeability Alternative	6-163
6-41	Calibration Summary Statistics for BN-USGSND-SDA	6-166
6-42	Calibration Summary Statistics for BN-USGSD-SDA	6-166
6-43	Calibration Summary Statistics for BN-USGSD-SDA Reduced LCCU1 Permeability Alternative	6-171
6-44	Calibration Summary Statistics for SCCC-DRIA-SDA	6-173
6-45	Calibration Summary Statistics for SCCC-USGSD-SDA	6-177
6-46	Summary of Flow Model Results for Water-Balance Uncertainty	6-180
6-47	Calibration Summary Statistics for PZUP-DRIA-SDA	6-182
6-48	Calibration Summary Statistics for PZUP-USGSD-SDA	6-185
6-49	Calibration Summary Statistics for DRT-DRIA-SDA	6-188

Uncontrolled When Printed

LIST OF TABLES (CONTINUED)

NUMBER	TITLE	PAGE
6-50	Calibration Summary Statistics for DRT-USGSD-SDA	6-190
6-51	Summary of Flow Model Results for HFM and Water-Balance Uncertainty	6-194
7-1	Spatial Association of Geochemistry Source Wells	7-12
7-2	Fractions of Groundwater from Various Upgradient Wells Present in Groundwater at Well UE-18r	7-18
7-3	Fractions of Groundwater from Various Upgradient Wells Present in Groundwater at Well ER-EC-6	7-25
7-4	Fractions of Groundwater from Various Upgradient Wells Present in Groundwater at Well ER-OV-01	7-27
7-5	Fractions of Groundwater from Various Upgradient Wells Present in Groundwater at Well ER-OV-05	7-30
7-6	Fractions of Groundwater from Various Upgradient Wells Present in Groundwater at Well ER-OV-04a	7-33
7-7	Fractions of Groundwater from Various Upgradient Wells Present in Groundwater at Well ER-OV-03a	7-36
7-8	Fractions of Groundwater from Various Upgradient Wells Present in Groundwater at Well ER-OV-03c, Including Sources for Groundwater at ER-EC-5	7-39
7-9	Fractions of Groundwater from Various Upgradient Wells Present in Groundwater at the Coffer Windmill Well	7-42
7-10	Hydrostratigraphic Models and Water-Balance Conditions Evaluated with Respect to Chemical Mixing Targets	7-47
7-11	Comparison of Alternative Models at UE-18r	7-62
7-12	Comparison of Alternative Models at ER-EC-6	7-76
7-13	Comparison of Alternative Models at ER-OV-01	7-90
7-14	Comparison of Alternative Models at ER-OV-04a	7-116
7-15	Comparison of Alternative Models at ER-OV-03a	7-131

Uncontrolled When Printed

LIST OF TABLES (CONTINUED)

NUMBER	TITLE	PAGE
7-16	Comparison of Alternative Models at ER-OV-03c	7-145
7-17	Comparison of Alternative Models at Coffer Windmill Well	7-158
7-18	k-Means Clusters of Flow Models Based on Geochemical Residuals	7-165
A.11-1	Comparison of Candidate Codes by Attribute	A-55
A.11-2	CPU Times in Minutes for SWIFT-98 Test Problem Simulations	A-58
A.11-3	CPU Times in Minutes for FEHM Test Problem Simulations	A-59
B.7-1	Structures of the Pahute Mesa/Oasis Valley Model Area	B-61
B.7-2	Hydrothermal Alteration Associated with Calderas of the SWNVF	B-65
C.4-1	Borehole Names and Locations (see Figure C.4-1)	C-11
C.4-2	Observed Temperature and Elevation in Boreholes that Correlate with Elevation in Model Simulations	C-14
C.5-1	Range of SZ Thermal Conductivity Estimates for Rock Types in HSU	C-21
C.6-1	Depth and Elevation Range, Hydrostratigraphic Unit, and Temperature of Borehole Composite Water Levels	C-30
C.6-2	Temperature Estimates at the Base of the PM/OV Model (3.5 km Below Sea Level)	C-38
C.6-3	Temperature Estimates in ER-19-1 from Base of the PM/OV Model (3.5 km Below Sea Level)	C-40
C.7-1	Optimal Thermal Conductivity Estimates and Fixed Thermal Conductivities Used with a Heat Flux of 65 mW/m^2	C-54
C.7-2	Subregional Lower Boundary Heat Flux Estimates	C-64
F.1-1	Summary of Hydraulic Heads at Selected Sites within the Pahute Mesa/Oasis Valley Area and Vicinity	F-2

Uncontrolled When Printed

LIST OF PLATES

NUMBER **TITLE**

Plate 1: Pahute Mesa Model Area Showing Topography, Selected Geographic Features, and Wells and Springs Used in Calibration of the Flow Model . . . . . .Pocket

Uncontrolled When Printed

LIST OF ACRONYMS AND ABBREVIATIONS

ac-ft	Acre-foot
ac-ft/yr	Acre-feet per year
Am	Americium
amsl	Above mean sea level
ASTM	American Society for Testing and Materials
bmsl	Below mean sea level
BN	Bechtel Nevada
°C	Degrees Celsius
CADD	Corrective Action Decision Document
CAI	Corrective Action Investigation
CAIP	Corrective Action Investigation Plan
CAP	Corrective Action Plan
CAS	Corrective Action Site
CAU	Corrective Action Unit
Cl^-	Chloride
cm	Centimeter
cm/yr	Centimeters per year
CP	Control Point
CR	Closure Report
CRWMS M&O	Civilian Radioactive Waste Management System Management and Operating Contractor
DOE	U.S. Department of Energy
DRI	Desert Research Institute
ERP	Environmental Restoration Program
ET	Evapotranspiration
EV	EarthVision®
°F	Degrees Fahrenheit
FEHM	Finite element heat-mass
FFACO	*Federal Facility Agreement and Consent Order*
FGE	Forced-Gradient Experiment
ft	Foot
ft/d	Feet per day
GB	Gigabyte

Uncontrolled When Printed

LIST OF ACRONYMS AND ABBREVIATIONS (CONTINUED)

GHz	Gigahertz
HST	Hydrologic Source Term
HTH	Hydrologic Test Hole
in.	Inch
in./yr	Inches per year
IT	IT Corporation
°/km	Degrees per kilometer
K	Hydraulic conductivity
k	Intrinsic permeability
k_0	Reference permeability
K_d	Distribution coefficient
kg/s	Kilograms per second
km	Kilometer
km^2	Square kilometer
LaGriT	Los Alamos Grid Toolbox
LANL	Los Alamos National Laboratory
LLNL	Lawrence Livermore National Laboratory
m	Meter
m/d	Meters per day
m^2	Square meter
m^3	Cubic meter
m^3/d	Cubic meters per day
m^3/yr	Cubic meters per year
ME	Mean error
mg/L	Milligrams per liter
mi	Mile
mi^2	Square mile
moles/kg	Moles per kilogram
moles/L	Moles per liter
mW/m^2	Milliwatts per square meter
N/A	Not applicable
NAD	North American Datum
NDEP	Nevada Division of Environmental Protection

Uncontrolled When Printed

LIST OF ACRONYMS AND ABBREVIATIONS (CONTINUED)

NNSA/NSO	U.S. Department of Energy, National Nuclear Security Administration Nevada Site Office
NTS	Nevada Test Site
OMR	Ochtree mesh refinement
PC	Personal computer
PEST	Parameter Estimation Software
PM/OV	Pahute Mesa/Oasis Valley
PTRK	Residence time transfer function particle-tracking method
Pu	Plutonium
QA	Quality Assurance
RAM	Random access memory
S	Storativity
SD	Standard deviation of error
SDWA	*Safe Drinking Water Act*
s/kg	Seconds per kilogram
SNJV	Stoller-Navarro Joint Venture
SO_4^{2-}	Sulfate
SPTR	Streamline-particle-tracking method
Sr	Strontium
SWIFT	Sandia Waste Isolation Fractured Transport
SWIP	Survey Waste Injection Program
T	Transmissivity
TTR	Tonopah Test Range
TW	Test Well
TWG	Technical Working Group
UGTA	Underground Test Area
USGS	U.S. Geological Survey
UTM	Universal Transverse Mercator
WW	Water Well
YMP	Yucca Mountain Project
3-D	Three-dimensional
δD	Delta deuterium
$\delta^{13}C$	Delta carbon-13
$\delta^{18}O$	Delta oxygen-18

Uncontrolled When Printed

LIST OF GEOLOGICAL ABBREVIATIONS AND SYMBOLS

AA	Alluvial Aquifer
ADA	All HSU Depth Decay and Anisotropy
ATICU	Ammonia Tanks Intrusive Confining Unit
BA	Benham Aquifer
BAQ	Basal Aquifer
BCU	Basal Confining Unit
BFCU	Bullfrog Confining Unit
BMICU	Black Mountain Intrusive Confining Unit
BRA	Belted Range Aquifer
CA	Carbonate Aquifer
CCICU	Claim Canyon Intrusive Confining Unit
CCU	Clastic Confining Unit
CFCM	Crater Flat Composite Unit
CFCU	Crater Flat Confining Unit
CHCU	Calico Hills Confining Unit
CHICU	Calico Hills Intrusive Confining Unit
CHVCM	Calico Hills Vitric Composite Unit
CHVTA	Calico Hills Vitric-Tuff Aquifer
CHZCM	Calico Hills Zeolitic Composite Unit
DRIA	Desert Research Institute Chloride Mass-Balance Alluvial and No Elevation Screen Recharge Model
DRIAE	Desert Research Institute Chloride Mass-Balance Alluvial and Elevation Screen Recharge Model
DRT	Deeply Rooted Belted Range Thrust Fault
DVA	Detached Volcanic Aquifer
DVCM	Detached Volcanic Composite Unit
DVRFM	Death Valley Regional Flow Model
DVRFS	Death Valley Regional Flow System
FCA	Fortymile Canyon Aquifer
FCCM	Fortymile Canyon Composite Unit
FCCU	Fluorspar Canyon Confining Unit
HFM	Hydrostratigraphic Framework Model
HGU	Hydrologic Unit
HST	Hydrologic Source Term

Uncontrolled When Printed

LIST OF GEOLOGICAL ABBREVIATIONS AND SYMBOLS (CONTINUED)

HSU	Hydrostratigraphic Unit
I	Intrusives
IA	Inlet Aquifer
ICU	Intrusive Confining Unit
KA	Kearsarge Aquifer
LCA	Lower Carbonate Aquifer
LCA1	Lower Carbonate Aquifer-Thrust Plate
LCA3	Lower Carbonate Aquifer-Thrust Plate
LCCU	Lower Clastic Confining Unit
LCCU1	Lower Clastic Confining Unit-Thrust Plate
LFA	Lava-Flow Aquifer
LPCU	Lower Paintbrush Confining Unit
MGCU	Mesozoic Granite Confining Unit
MME	Modified Maxey-Eakin Recharge Model
PBRCM	Pre-Belted Range Composite Unit
PCM	Paintbrush Composite Unit
PLFA	Paintbrush Lava-Flow Aquifer
PM/OV	Pahute Mesa/Oasis Valley
PVTA	Paintbrush Vitric-Tuff Aquifer
PreT	Pre-Tertiary
PZUP	Raised Pre-Tertiary Surface
RIDGE	Basement Ridge Model
RMICU	Rainier Mesa Intrusive Confining Unit
SCCC	Silent Canyon Caldera Complex
SCICU	Silent Canyon Intrusive Confining Unit
SCVCU	Subcaldera Volcanic Confining Unit
SDA	Selected HSU Depth Decay and Anisotropy
SEPZ	Contiguous Imbricate Thrust Sheet
SWNVF	Southwestern Nevada Volcanic Field
TC	Tuff Cone
TCA	Tiva Canyon Aquifer
TCL	Thirsty Canyon Lineament
TCU	Tuff Confining Unit

Uncontrolled When Printed

LIST OF GEOLOGICAL ABBREVIATIONS AND SYMBOLS (CONTINUED)

TCVA	Thirsty Canyon Volcanic Aquifer
THCM	Tannenbaum Hill Composite Unit
THLFA	Tannenbaum Hill Lava-Flow Aquifer
TM	Timber Mountain
TMA	Timber Mountain Aquifer
TMCM	Timber Mountain Composite Unit
TSA	Topopah Spring Aquifer
UCCU	Upper Clastic Confining Unit
UPCU	Upper Paintbrush Confining Unit
USGSD	U.S. Geological Survey Redistribution Recharge Model
USGSND	U.S. Geological Survey No Redistribution Recharge Model
VA	Volcanic Aquifer
VCU	Volcanic Confining Unit
VTA	Vitric-Tuff Aquifer
VU	Volcanics Undifferentiated
WTA	Welded-Tuff Aquifer
WWA	Windy Wash Aquifer
YMCFCM	Yucca Mountain Crater Flat Composite Unit
YVCM	Younger Volcanic Composite Unit

Uncontrolled When Printed

ACKNOWLEDGEMENTS

The Pahute Mesa CAU flow model report is a very large and complicated document, and many people in addition to the authors aided in its production. In particular, the project team acknowledges the efforts of Janice Rose, Barbara Deshler, Yvonne Lewis, Ellen Cook, Shirley Murray, Afief Fadil, Caroline Gilbert, and John Flinn. We also thank the following individuals for their contributions and review of this report: John McCord, Bill Fryer, John Pickens, and Van Kelley.

We also gratefully acknowledge the advice of Sig Drellack and Lance Protho, the supporting analyses from Edward Kwicklis, and the code enhancement of Sharad Kelkar.

Uncontrolled When Printed

EXECUTIVE SUMMARY

This Executive Summary is a synopsis of the report entitled *Groundwater Flow Models of CAUs 101 and 102: Central and Western Pahute Mesa, Nye County, Nevada*, prepared for the U.S. Department of Energy (DOE). A steady-state groundwater flow model of the Pahute Mesa Corrective Action Unit (CAU) has been constructed using a suite of hydrostratigraphic frameworks, recharge distributions, and hydraulic parameter assignment conceptualizations. Model calibration and sensitivity analyses, and geochemical verification were conducted and documented.

INTRODUCTION

The DOE, National Nuclear Security Administration Nevada Site Office (NNSA/NSO) initiated the Underground Test Area (UGTA) Project to assess and evaluate the effects of the underground nuclear weapons tests on groundwater on the Nevada Test Site (NTS) and vicinity through the *Federal Facility Agreement and Consent Order* (FFACO) (1996). The processes that will be used to complete UGTA corrective actions are described in the "Corrective Action Strategy" in the FFACO Appendix VI, Rev. 1 (December 7, 2000). The objective of the strategy is to analyze and evaluate each UGTA CAU through a combination of data and information collection and evaluation, and modeling groundwater flow and contaminant transport, including uncertainty. The FFACO corrective action process for the Central and Western Pahute Mesa CAUs was initiated with the Corrective Action Investigation Plan (CAIP) (DOE/NV, 1999). This CAIP identified a three-step model development process to evaluate the impact of testing on groundwater and simulate a contaminant boundary. The first step is the compilation and evaluation of existing and new data for use in the flow model and is documented in a series of data compilation and analysis reports, including *Hydrologic Data for Groundwater Flow and Contaminant Transport Model of Corrective Action Units 101 and 102: Central and Western Pahute Mesa, Nye County, Nevada* (SNJV, 2004a). The second step is the development of the groundwater flow model, documented in this report. The third step is the development of the transport model to assess the migration of radionuclides away from underground nuclear test cavities on Pahute Mesa.

Underground nuclear tests conducted at Pahute Mesa that are of interest to the UGTA Project are those detonated in deep vertical shafts, or drilled into volcanic rock near or below the water table.

Uncontrolled When Printed

A total of 82 such underground nuclear tests were conducted in Pahute Mesa. Sixty-four of these tests were detonated on Central Pahute Mesa (CAU 101), and 18 tests were detonated in Western Pahute Mesa (CAU 102) (DOE/NV, 2000). Transport in groundwater is the primary mechanism of migration for the subsurface contamination away from Pahute Mesa underground nuclear tests.

Pahute Mesa is located in the northwestern part of the NTS. Pahute Mesa is an elevated plateau of about 500 square kilometers (km^2) (200 square miles [mi^2]). The area of interest for the Pahute Mesa flow model is defined by the potentially affected portion of the regional groundwater flow system, which includes a region stretching from the northern side of Pahute Mesa south and southwestward to Oasis Valley. Pahute Mesa geology is dominated by the deposition of rock units from volcanic eruptions from nested calderas of the Southwestern Nevada Volcanic Field. The Silent Canyon Caldera is the oldest series of calderas and consists of at least two nested calderas, the Area 20 Caldera and the older Grouse Canyon Caldera. Both calderas were formed, and subsequently filled, by voluminous eruptions of tuff and lava of generally rhyolitic composition. The youngest caldera complex of hydrologic significance is the Timber Mountain Caldera. This caldera collapse and its filling with volcanic materials affect the southern portion of the Pahute Mesa CAU.

Groundwater beneath Pahute Mesa generally flows in a southwest direction, primarily through fractures in the lava-flow and tuff aquifers. Zeolitized bedded and nonwelded tuffs act as confining units that inhibit the flow of groundwater. The spatial distribution of permeable aquifers relative to the confining units is not well understood. Thickness variations of aquifers and confining units and their connectivity across faults or caldera boundaries are important hydrostratigraphic relationships that are also not well understood. A number of wells provide water-level information in the areas of Pahute Mesa and Oasis Valley, but water levels in the area between Pahute Mesa and Oasis Valley are less well defined. However, what data are available suggest that groundwater elevations generally gently mimic the topography. Some groundwater discharges to the surface within the Oasis Valley discharge area in the form of springs. Groundwater recharge occurs locally from precipitation and by underflow from areas located to the north of Pahute Mesa. Groundwater then flows south southwestward to the Oasis Valley and Death Valley to the southwest.

Uncontrolled When Printed

Specific objectives of the Central and Western Pahute Mesa (referred to hereafter as simply Pahute Mesa) groundwater flow model are to:

- Develop a three-dimensional (3-D), numerical flow model that incorporates the important physical features of the flow system and honors CAU-specific data and information.
- Simulate the groundwater flow system to determine the direction and magnitude of groundwater fluxes based on calibration to Pahute Mesa hydrogeologic data and boundary flux data determined from the UGTA regional flow model.
- Quantify the uncertainty in the direction and magnitude of groundwater flow due to uncertainty in parameter values and alternative component conceptual models (e.g., hydrostratigraphic framework, boundary flux, and recharge).

FRAMEWORK FOR GROUNDWATER FLOW MODELING OF CENTRAL AND WESTERN PAHUTE MESA - DATA, INFORMATION, AND CONCEPTUAL MODELS

The data, information, and conceptual models used to develop the Pahute Mesa flow model represent a large body of work and are described in detail in the integrating report *Hydrologic Data for the Groundwater Flow and Contaminant Transport Model of Corrective Action Units 101 and 102: Central and Western Pahute Mesa, Nye County, Nevada* (SNJV 2004a). The regional and site-specific elements that are integrated into the Pahute Mesa flow model include:

- Regional data and information that provide the hydrogeologic context for the CAU-specific flow model.
- CAU-specific geologic data and information that establish the local hydrostratigraphic framework (BN, 2002).
- Alternative CAU-specific data that address uncertainty in hydrostratigraphy, lateral boundary flux and heads, and recharge (BN, 2002).
- CAU-specific hydrologic parameters, including their uncertainty.

An overview of the data, information, and conceptual models is presented below.

Uncontrolled When Printed

Hydrostratigraphic Framework Models (HFMs)

HFM Development. The Pahute Mesa area HFMs were constructed using EarthVision®, a 3-D geologic model building and visualization software package. Input data included drill-hole data, digital elevation model data, and outcrop and fault data from surface geologic maps. The 3-D HFM area encompasses over 2,700 km^2 (1,042 mi^2). The HFM has a north-south length of 53.4 kilometers (km) (33.2 miles [mi]) and an east-west length of 50.8 km (31.6 mi), and includes geologic units as deep as 7 km (4.3 mi) below mean sea level (bmsl).

All rocks of the NTS and vicinity can be classified as one of eight hydrogeologic units (HGUs), which include the alluvial aquifer (AA), four volcanic HGUs, an intrusive HGU, and two HGUs that represent the pre-Tertiary sedimentary and metasedimentary rocks. Hydrostratigraphic units (HSUs) are groupings of contiguous stratigraphic units that have a particular hydrogeologic character, such as an aquifer or a confining unit. An HSU may contain several HGUs but is defined so that a single general type of HGU dominates (for example, mostly welded-tuff and vitric-tuff aquifers, or mostly tuff confining units).

Following the completion of the preliminary base HFM, a number of alternative HFM conceptual models were considered. The main criterion for selecting alternative HFMs for full grid development was the potential impact of the alternative interpretation on groundwater flow and the transport of contaminants in groundwater. The results using the above criterion showed that only the Silent Canyon Caldera Complex (SCCC) alternative produced results that were clearly different from those produced by the base HFM (SNJV, 2004a). Therefore, only distinct meshes were developed for the base HFM and the SCCC alternative. An additional five HFM alternatives are evaluated by varying the hydraulic parameters within the base HFM mesh.

Base HFM. The base HFM includes a total of 47 structural elements that are either faults or calderas. Only faults that were considered to be significant were included in the model. These include the larger ones and the ones that seem to form significant structural boundaries. Six calderas have been identified in the Pahute Mesa model area, two of which are buried. The base HFM for the area also includes 20 faults and structural zones in addition to the caldera-forming faults. Thirteen of these 20 structural features are basin-and-range type faults mapped at the surface that are extended to the bottom of the model. There are a total of 46 HSUs included in the base HFM.

Uncontrolled When Printed

SCCC HFM Alternative. The alternative SCCC model is based on the same HGUs as the base HFM. Differences between the two models relate to the structural model used and the categorizing of HGUs into HSUs. The alternative structural model of the SCCC is more simplified than the base HFM, as is the hydrostratigraphy. The SCCC HFM includes an elliptical ring-fracture fault system elongated to the north-northeast. Major structural differences with the base HFM include the margins of this caldera complex, locations of caldera-forming faults, and the number and depth of the faults considered. The SCCC HFM includes the single caldera ring-fracture system, and only 11 of the basin-and-range faults mapped at the surface. Another key difference is that the faults in the SCCC HFM end at shallower depths than in the base HFM.

Hydrostratigraphic differences between the two HFMs of the Pahute Mesa area are the number of HSUs, their definition, and their distribution. In the base HFM, the Pahute Mesa area includes 25 HSUs; only 12 are included in the SCCC alternative model. Six post-Paintbrush HSUs are lumped together in the SCCC alternative model. Significant differences also exist in the configuration of the HSU surfaces. The surfaces of the HSUs are less rugged in the SCCC HFM than in the base HFM. The upper surfaces of HSUs in the SCCC HFM are generally bowl-shaped and dip more gently than those in the base HFM. Upper surfaces of HSUs in the SCCC HFM are also higher along the down-thrown sides of faults, and lower along the up-thrown sides. The differences in the locations of caldera margins and in structure result in differences in HSU thicknesses. Generally, the thicknesses of HSUs located within the Pahute Mesa area vary to a greater degree in the base HFM. In comparison, in the SCCC HFM, the HSUs are generally lens-shaped. These lenses are thick in the middle and thin out towards the margins of the SCCC. The hydrogeologic importance of the Calico Hills Formation in the SCCC area is recognized in both the base and SCCC HFMs. It is, however, handled differently in the two models. In the base HFM, the Calico Hills Formation is subdivided into four HSUs based on differences in lithologic composition and alteration effects, whereas it is treated as a single composite unit in the SCCC HFM.

Groundwater Flow System Characteristics

Lateral Boundary Fluxes. A set of boundary fluxes to be used with the CAU flow model was developed based on results generated for eight alternate regional-scale flow models using the UGTA regional model. The eight models represent combinations of different flow system conceptual

Uncontrolled When Printed

models (HFMs described above) and recharge models. The recharge models represent different methods of approximating recharge for the NTS area. The alternate flux boundary conditions can be used to help evaluate the uncertainty in the CAU flow model associated with the choice of flow system conceptual model (and associated HFM) and recharge model. The approach used to calculate these fluxes does not specify the locations on the boundary where the flux occurs, just quantifies bounds on the total amount of flow through the CAU-model lateral edges.

Recharge. Three basic approaches have been used to develop alternative recharge models for the NTS area. These are: Maxey-Eakin empirical approach, net-infiltration recharge model from watershed distributed parameter modeling by the U.S. Geological Survey (USGS), and chloride mass-balance modeling by the Desert Research Institute (DRI).

Natural Discharge. Within the Pahute Mesa area and vicinity, most groundwater discharge to the surface occurs naturally in the form of evapotranspiration (ET) and springs at the Oasis Valley discharge area. The area of interest to this activity includes the Pahute Mesa area and all of the Oasis Valley hydrographic area because the discharge area extends outside of the Pahute Mesa CAU area boundary. The majority of the groundwater discharged by springs is effectively lost from the groundwater system through ET within the discharge area. The net natural groundwater discharge to the surface is best approximated by an estimate of ET.

Well Discharge. Wells of interest include nine NTS water supply wells, one Beatty water supply well, and two mine wells. The well discharge volume represents only 15 percent of the ET estimate. Transient well-related effects are very localized and likely not representative of conditions over a majority of the model area. Thus, discharge from pumping wells is not included in the model.

Hydraulic Heads. Observed hydraulic heads are derived from depth-to-water measurements and well information. Hydraulic heads may also be approximated by the land surface elevations of regional springs. The results of the water-level data analysis were used to identify hydraulic head values that are most representative of steady state, predevelopment conditions at specific boreholes and well locations. Each temporal subset of measurements that represents steady-state conditions was reduced statistically to a mean, standard deviation, and variance of the mean. The hydraulic head data derived from the water-level data were supplemented with land surface elevations of the selected regional springs.

Uncontrolled When Printed

Hydraulic Conductivity Data. Analysis of hydraulic conductivity data included evaluations of measurement scale (laboratory-scale, slug-test-scale, and constant-rate-scale data), scaling and spatial variability, vertical anisotropy, and the alteration of hydraulic conductivity in test cavities. Approximately 300 hydraulic conductivity values were obtained from analyses of constant-rate test data from the NTS area. These tests sample a larger volume of the tested formation than either laboratory or slug-scale tests. For the purposes of the Pahute Mesa CAU flow model, the constant-rate-scale data are the most appropriate. No HSU-specific hydraulic conductivity data are available for 21 of the 46 HSUs. For these HSUs, mean and standard deviation of hydraulic conductivity is determined from units with similar lithology for which data are available.

Groundwater Chemistry. Groundwater geochemistry data are considered during the evaluation of the groundwater flow system because they provide a means for determining the origin, pathway, and timescale of groundwater flow that is independent of estimates based on conventional hydraulic data. Groundwater geochemistry evaluations were performed for the Central and Western Pahute Mesa CAUs that address groundwater flow path, water budget, and travel-time evaluations. These geochemical evaluations were performed on representative Pahute Mesa data in order to identify and assess viable flow paths and groundwater mixing models. The comparison of flow model results and geochemical evaluations was performed as a verification step after model calibration using hydraulic information (heads and fluxes) only.

COMPUTER CODE SELECTION

The Pahute Mesa CAIP (DOE/NV, 1999) identified a process for the identification and selection of the numerical code for use in Pahute Mesa flow and transport modeling. The process identified three objectives for the numerical code used in the CAU model. The first objective requires the CAU model to have the ability to represent the important physical and chemical features of the CAU groundwater flow system. The features include faulting, stratigraphy, sources and sinks of water, the distribution of contaminants and their rates of introduction into the groundwater flow system, and other physical or chemical features unique to the CAU. The second objective requires the CAU model to simulate the movement of a variety of contaminants for which their distribution and abundance serve to define the contaminant boundary. The third objective requires flexibility in the CAU model to allow grid changes, placement of additional wells, and boundary condition variations.

Uncontrolled When Printed

The Pahute Mesa CAIP (DOE/NV, 1999) identified 14 numerical codes as possible candidates for Pahute Mesa CAU modeling. Three codes were evaluated further. The features of the test problem used to evaluate the three candidates codes were chosen to represent conditions expected in the Pahute Mesa model area. The features included in the test problem were: complex caldera geology, such as lithologic and structural features; temperature-dependent flow; radionuclide migration from a cavity; and matrix diffusion. Code testing criteria were used to represent the CAU hydrogeology, portability, quality assurance evaluation, ease of use, and speed of simulation. The code testing and evaluation of relative rankings of the tested codes was completed in 1999, and the finite element heat-mass (FEHM) code was selected as the flow and transport simulator for the Pahute Mesa CAU model.

GROUNDWATER FLOW MODEL CONSTRUCTION

The overall goal of the approach for construction of the Pahute Mesa flow model is the transformation of the conceptual model into a mathematical model for simulating groundwater flow in and around Pahute Mesa. Development and implementation of the CAU flow model involves the following activities:

- Defining the CAU numerical model boundaries
- Mesh generation
- Establishing boundary and initial conditions

CAU Numerical Model Boundaries. The numerical model boundaries were chosen such that they coincide with perceived geologic and hydrologic domains to the extent possible, contain the contaminant source areas and discharge points with some buffer, and are within practical constraints. The CAU model lies within the geologic model domain with lower-left plan coordinates of 519,125 and 4,085,000 meters (m) Universal Transverse Mercator (UTM) (UTM Zone 11 North American Datum 27) and upper-right plan coordinates of 569,000 and 4,138,000 m. The model is aligned north-south, with no rotation. The numerical model extends from the estimated water table to a depth of -3,500 m bmsl. The hydrologic model area encompasses more than 2,700 km^2 (1,042 mi^2). This area incorporates both the Pahute Mesa CAUs, including Timber Mountain; the eastern edge of Oasis Valley; the northern part of Fortymile Canyon; and the northern portion of Yucca Mountain. The area has a north-south length of 53.4 km (33.2 mi) and an east-west length of 50.8 km (31.6 mi).

Uncontrolled When Printed

Contained within these boundaries are the well data within the Pahute Mesa area, and the springs and regional discharge area at Oasis Valley.

Mesh Generation. The model construction involved building finite-element meshes for use with the FEHM code to capture the complex HSU geometries, faults, and test chimneys for the two primary HFMs: the base and SCCC cases. In general, the criteria for grid generation are as follows (DOE/NV, 1999):

- The external boundary of the CAU model will correspond to appropriate cell boundaries within the UGTA regional groundwater flow model. Because the regional model is rotated with respect to the coordinate system and the CAU model is not, interpolation procedures were developed to account for the non-coincidence of CAU and regional model nodes.
- Nodes will be placed as close as practical at each underground test location and at specific well locations.
- Nodes will be placed along faults that are identified as being important to the distribution of HSUs.
- The node density will be greatest in the vicinity of the underground tests and at other points of interest, and will decrease in density towards the CAU-model boundaries.
- Nodes will be preferentially placed along HSU contacts to more precisely incorporate the geologic model structure in the simulations. The nodes will form a pattern representative of the CAU-scale geology.
- The node spacing will vary from small in the vicinity of test cavities and wells to nearly as large as the regional groundwater flow model grid at the CAU boundary.

The mesh node spacing ranged from 67.5 m to 1 km, with refinement in thinner HSUs and faults, around tests, and estimated flow paths from Areas 19 and 20 to Oasis Valley. Two FEHM computational meshes were produced. One represents the base HFM; the other, the SCCC alternative HFM. The base HFM has 45 HSU surfaces (the Windy Wash Aquifer was omitted due to nearly negligible saturated extent) and 37 faults. The SCCC HFM model has 40 HSU surfaces and 25 faults. The list of HSUs is identical with the exception of the Calico Hills HSUs, which are lumped into a single HSU in the SCCC HFM. This resulted in two meshes with approximately 1.4 million and 1.3 million nodes for the base and SCCC HFMs, respectively.

Uncontrolled When Printed

Boundary Conditions. The solution of the groundwater flow equations requires specification of head and/or flow at the edges of the numerical model. The Pahute Mesa CAU model must account for regional inflow and outflow across all four lateral edges, internal flow from precipitation recharge, and internal discharge from springs and ET at Oasis Valley.

There are three categories of recharge estimates for consideration in the CAU model: Maxey-Eakin elevation-based approach as described in the UGTA regional model evaluation and modified to reflect an updated base precipitation map (case MME), USGS distributed-parameter watershed model, and DRI chloride mass-balance estimate. Two subsets of the USGS and DRI recharge maps were also considered. For the USGS map, the recharge with (case USGSD) and without runoff or run-on (redistribution) (case USGSND) was used. For the DRI map, the recharge with (case DRIAE) and without an elevation (case DRIA) mask at 1,237 m was also used. Recharge is implemented in the CAU model as a specified flux condition. Recharge flux is considered to be constant over time but varies over the domain. The MME recharge distribution is chosen as the base recharge model for use in groundwater flow modeling because, in general, the method yields recharge volumes that are within the ranges of the other models. The other alternative recharge models are incorporated into the Pahute Mesa flow model to evaluate uncertainty associated with recharge.

The only internal discharge represented in the Pahute Mesa CAU model is Oasis Valley springs and ET outflow. Discharge from pumping wells is not included in the model. Spring and ET discharge are represented in a similar manner with FEHM as with the regional flow model with “drain” boundary conditions.

The FEHM simulations utilize a confined aquifer approximation in which the water table defines the top of the model domain location and is estimated as a potentiometric surface in the simulations. An estimate of the water table, approximated by contouring observed heads from wells with relatively shallow sampling intervals, provides a guide for setting the upper confining surface in the grid. The approach does not include an unsaturated zone or moving water table and, therefore, solves a simplified and computationally more efficient numerical model.

Boundary heads interpolated from the UGTA regional model analysis were initially assigned to the edge nodes of the FEHM CAU model as boundary conditions. These heads represent a mass conservative calibrated solution to the groundwater flow equation from the UGTA regional model

Uncontrolled When Printed

(DOE/NV, 1997). During the calibration process, these heads were reviewed, and in spots, revised based on further examination of measured heads and heads determined from the UGTA regional model.

Part of the CAU flow modeling strategy is to use the UGTA regional model as a mass conservative integrating model that allows evaluation of water-balance uncertainty around the lateral edges of the CAU model. In this analysis, the flows are not directly specified on all edges; heads are specified, and FEHM computes and reports the lateral boundary flows, which are used as calibration targets.

Initial Conditions. Initial conditions are those applied at the start of a simulation. Theoretically, for steady-state flow, the initial conditions are not important. Practically, the iterative solvers employed in large numerical models gain efficiency if the starting conditions are as consistent as possible with the properties and boundary conditions used in calibration. The initial conditions were determined from interpolation of the UGTA regional model results onto the FEHM nodes in the CAU domain. However, once converged CAU steady-state model results were obtained, they became the new initial conditions for the continuation of model calibration.

Within the model domain, temperature varies enough that it should be considered in the calculation of flow. A 3-D steady-state heat-conduction model was developed for the model domain in order to provide a 3-D temperature distribution for the steady-state flow model calibration. The calibrated thermal fields from the heat-conduction model were used to specify the temperature distribution as a fixed condition; that is, thermal transport was not simulated, but the effect of the variable temperature field was included.

Uncontrolled When Printed

FLOW MODEL CALIBRATION

The purpose of the CAU flow model calibration is to use observed head data, discharge estimates from Oasis Valley, boundary flow estimates from the UGTA regional model, and estimated hydraulic properties for HSUs to develop a numerical model representation of the groundwater flow system in the Pahute Mesa CAU area. The Pahute Mesa CAU flow model considered seven HFMs and five recharge models. The following naming convention was used to identify the various flow models that were calibrated. The first part of the name is the HFM and the second is the water-balance condition. An additional naming modification is applied to denote the permeability parameterization approach: denoted SDA and ADA, for selected HSU depth decay and anisotropy, and for all HSU depth decay and anisotropy, respectively. In addition to the base and SCCC alternative HFMs, there are five other HFMs that were investigated using the base HFM grid: PZUP - Raised pre-Tertiary Surface, DRT - Deeply Rooted Belted Range Thrust Fault, RIDGE - Basement Ridge Model, TCL - Thirsty Canyon Lineament, and SEPZ - Contiguous Imbricate Thrust Sheet.

Calibration Approach. Flow model calibration followed a generally accepted protocol in which model parameter sensitivities to calibration were evaluated and interpreted in light of the conceptual model of the system. An automated approach for groundwater flow model calibration was adopted where the model response to parameter changes is systematically evaluated and the more important parameters that improve calibration identified. The parameter-estimation (PEST) code was used for this purpose (Watermark, 2004). The PEST code also includes a variety of statistical analyses that help develop understanding of the model. These features include sensitivity and correlation coefficients, parameter confidence limits, and eigenvalue and eigenvector analysis. The sensitivity and correlation coefficients describe how much the model calibration changes relative to a parameter's change, and how parameters may influence one another. This is useful in testing the conceptual model as to what parameters are believed to control model behavior, and what parameters may act similarly on model results. In addition, parameters that may be important to model calibration can be quantitatively identified and considered in more detail. The confidence limits and eigenvalue and eigenvector analysis are useful in understanding how well the observation data support the model parameters and how many parameters should be considered for calibration.

Uncontrolled When Printed

Several approaches for evaluating the agreement between a flow model and modeled system were utilized. These procedures were used in calibrating the Pahute Mesa flow model, and include qualitative and quantitative comparisons between model results and the following: measured heads at wells and springs, water-balance information (Oasis Valley discharge flux and model boundary flows), flow-direction information, and estimated values of HFM hydraulic parameters from characterization data.

The goal of model calibration is to make the model agree with reality by adjusting, within their ranges of variation, model parameters and boundary conditions. Achieving the best calibration is not the sole objective of model calibration. The reasonableness of the flow directions was also assessed qualitatively during the calibration phase via streamline particle tracking and quantitatively via geochemical analysis (as a verification step subsequent to head and flux calibration). Finally, it is important to recognize that no matter the procedure, the goal of model calibration is a set of model parameters that best (or at least reasonably) represents the hydrogeologic system. A further constraint was the desire to honor, within the range of uncertainty, the estimated hydraulic properties for the HSUs.

Calibration Data. Considering different types of data, especially flows, enhances the goodness of the flow model. In particular, matching both head and flow in Oasis Valley increases confidence that the model behavior is correct in this area. Four data types, or targets, were used for calibration of the Pahute Mesa flow model as follows:

- Hydraulic head from wells
- Estimated spring head in and near Oasis Valley
- Oasis Valley discharge
- Lateral boundary flows on CAU model estimated from regional flow model

Because an automated procedure was used to aid calibration, multiplicative weight factors were developed and assigned to data with different levels of accuracy and measurement units. The standard deviations of reference point uncertainty, head value uncertainty, and heterogeneity were summed and the initial weights for PEST computed. However, an alternate empirical approach was also adopted in which the weights are assigned by considering accuracy along with judgment to give the desired contribution to the calibration for selected data types. Mathematically, Oasis Valley

Uncontrolled When Printed

discharge is important to constraining the flow model because it is well known that a steady-state model with constant head boundaries calibrated only to head is not unique.

Boundary Head Adjustments. The starting point for the CAU model specified-head boundary conditions was the UGTA regional model results interpolated onto the mesh edges. Changes were made during calibration to address inconsistencies to measured heads in the following areas: western part of the northern boundary, the north-central model edge near UE-20p and PM-2, southern edge of the model east of Oasis Valley, and eastern boundary near TW-1. Also, the northwest corner of the model (both north and west faces) was converted to a no-flow in conjunction with correction of heads north of PM-2 and UE-20p.

Base HFM Flow Model Calibration. A variety of permeability parameterization approaches have been used to simulate groundwater flow in the NTS area (e.g., the UGTA regional model [DOE/NV, 1997], the USGS flow model of D'Agnese et al. [1997], and the Yucca Mountain Project [YMP] saturated-zone model [DOE/ORD, 2004]). For the base HFM, the viability of four different parameterization approaches was tested:

- No anisotropy and no depth decay of HSU permeability
- Depth decay applied to selected HSUs
- Anisotropy and depth decay applied to selected HSUs
- Anisotropy and depth decay applied to all HSUs

The same calibration data and model structure was used in each case; only the approach to assigning parameters was changed. The first approach is a limiting case of simplicity; the second and third approaches reflect parts of the 1997 USGS regional model (D'Agnese et al., 1997), the Death Valley regional flow model (DVRFM) (Belcher et al., 2004), and the YMP saturated zone models (DOE/ORD, 2004); and the fourth approach reflects the same approach used in the UGTA regional model (DOE/NV, 1997).

Flow model calibration was conducted with the four approaches above. The no-anisotropy and no-depth-decay case was rejected as a reasonable approach because flow paths from Pahute Mesa tended to dive deep below Oasis Valley, reflecting the poor match to Oasis Valley discharge data. It also required systematically low permeabilities relative to the expected values and ranges as described in the Pahute Mesa hydrologic data document (SNJV, 2004a). The selected HSU depth

Uncontrolled When Printed

decay with no anisotropy was investigated briefly, but completely neglecting anisotropy was deemed unreasonable, and it was discarded. The application of anisotropy and depth decay to selected HSUs and to all HSUs cases was carried to final calibrations. Both models could represent the flow system reasonably well, as defined by matching the head and flow calibration targets.

The selected HSU depth-decay and anisotropy parameterization approach began by assessing the effect of permeability depth decay only, and its effects were found to be quite pronounced in terms of not requiring consistently low permeabilities as in the case described in the no-depth-decay, no-anisotropy case. Depth decay applied to regionally contiguous units existing at a wide variety of depths along with horizontal-to-vertical anisotropy of 10:1 in selected units provided reasonable results.

SCCC HFM Flow Model Calibration. This model has fewer HSUs than the base HFM, and does not have as deep or extensive of a fault system. In particular, the Calico Hills formation is reduced from four separate HSUs to one that is several hundred meters thick. The calibration of the SCCC alternative began with the calibrated parameters from the selected HSU depth decay and anisotropy base HFM for both HSUs (where still present) and faults (where still present). However, because of the lumped nature of the Calico Hills unit, its anisotropy was increased to 50:1 because many dissimilar types of units were combined. In addition, the Benham Aquifer (BA) also incorporates the Lower Paintbrush Confining Unit in the SCCC HFM. The BA was assigned anisotropy of 20:1. The units selected to have permeability depth decay and anisotropy are the same as presented for base HFM selected depth decay and anisotropy. The SCCC HFM did not calibrate as well as the SDA and ADA models using the base HFM.

Calibration Summary. Three calibrations for the base and SCCC HFMs were carried to completion: base HFM with selected HSU depth decay and anisotropy with MME recharge, base HFM with all HSU depth decay and anisotropy with MME recharge, and SCCC HFM with selected HSU depth decay and anisotropy with MME recharge. Key behaviors and observations of the model calibrations are summarized below:

1. **Purse Fault Behavior**. A striking difference between the base and SCCC HFMs is the area along the Purse Fault. An area of "hydraulic discontinuity" exists coincident with the Purse Fault that shows about 100-m head difference (west to east) across the fault with flow directed sub-parallel to the fault (e.g., the fault may act as an approximate no-flow barrier). In order to

Uncontrolled When Printed

match the head in Wells PM-3, PM-2, UE-20p, UE-20j, and U-20m in the base HFM on the western side of the Purse Fault and wells in southwestern Area 20, the Purse Fault permeability had to be reduced by a factor of 10,000 relative to the surrounding HSUs in order to maintain the 100 m or so difference between the two areas. In contrast, the SCCC HFM does not have a Purse Fault geometry that allowed fault continuity along its length or goes as deep (the base HFM has faults projected to the bottom of the model). Thus, simulated head at PM-3 was too low and head in southwestern Area 20 too high because the fault did not separate the two areas sufficiently. The SCCC does incorporate juxtaposition across the caldera margins, so HSU juxtaposition alone seems insufficient to replicate the observed behavior. Whether or not the Purse Fault alone is the source of the observed discontinuity is unclear, but its configuration in the base HFM does allow the observed head to be reproduced, whereas HSU juxtaposition alone does not.

2. **Comparison of Model and Estimated HSU Permeabilities**. Estimates of mean hydraulic properties and their uncertainty were made before beginning model calibration. These estimates were used as a guideline during calibration. The model-calibrated permeabilities were compared to the estimated values for all HSUs. The comparisons suggest that the flow model has been reasonably parameterized for the three calibrated models with respect to the expected values of HSU permeability.

3. **Water-Balance Summary**. An additional check on the CAU water balance is the comparison of flow along the northern edge of the Yucca Mountain saturated zone model, which lies entirely within the Pahute Mesa CAU flow model. The YMP saturated zone model (DOE/ORD, 2004) gives a value of 196 kilograms per second (kg/s) inflow. The calibrated base HFM with MME recharge and selected and all depth decay of 250 and 300 kg/s for the SCCC with MME recharge. The DVRFM (Belcher et al., 2004) boundary flows were also estimated for the Pahute Mesa CAU flow model boundaries, and found to be in reasonable agreement with estimates developed from the UGTA regional model (DOE/NV, 1997). Thus, the Pahute Mesa CAU model is in reasonable agreement with other independent water-balance analyses in the area.

4. **Data Components of Calibration**. Four categories of data, representing two types (head and flow), were used to calibrate the Pahute Mesa CAU flow model: observation well head, spring head, Oasis Valley ET discharge, and net model boundary flow. An evaluation of the contribution of each data type to the model goodness of fit shows that observation well heads comprised the bulk (between about 50 to 60 percent) of the objective function, followed by Oasis Valley discharge (about 25 percent), estimated regional boundary flow (about 15 percent), and spring head (5 to 10 percent). Clearly, observation well data must be given strong consideration in model calibration because they define the direction and magnitude of the hydraulic gradient, which is directly related to the velocity field that will be used to simulate radionuclide transport. Oasis Valley discharge is the only internal flow constraint for the model, and as such is a major control on the effective permeability. Oasis Valley is also the nearest access point for radionuclides that might leave Pahute Mesa, and matching its discharge ensures that the potential for such migration is properly captured in the flow model. In addition, matching the spring data also helps ensure that the heads in Oasis

Uncontrolled When Printed

Valley are reasonably matched, and that the combination of head and flow that results is plausible.

5. **HFM Assessment**. Two HFMs, the base and SCCC alternative, were considered during model calibration. The SCCC does not perform as well in matching observed heads along the Purse Fault, and, in general, does not calibrate as well as the base HFM. The parameter set or model that reduces the value of the objective function is considered superior to those that give higher values because it improves the model fit according to the criterion embedded in the objective function itself. Thus, from purely the standpoint of flow model calibration goodness, the SCCC HFM is not as likely as the base HFM.

6. **Model Limitations**. The Pahute Mesa CAU flow model covers a plan area of approximately 2,000 km^2 and has a saturated thickness of nearly 5 km, for a total volume of about 10,000 cubic kilometers. A total of 191 calibration targets of head and flow were used in calibration. The overall density of the data versus the size of the model suggests that the calibration data are somewhat sparse. Not all of the uncertainty is likely to be important; for instance, it is almost certain that flow in the intrusive confining units is very slow, if not nil, which has no effect on the shallower part of the flow system. However, many types of analysis such as head mapping and geochemistry tend to give a similar broad picture of flow from Pahute Mesa southwest to Oasis Valley, and while there may be further refinements in understanding if more data are collected, the key point of migration to Oasis Valley is unlikely to change.

The CAU flow model was calibrated to estimated steady-state conditions and is not currently configured for transient flow analysis. The flow model also assumes regional steady state in the CAU area, and any future change in hydrologic conditions could affect this assumption.

Flow Model Sensitivity and Uncertainty Analysis

Approach. The Pahute Mesa CAU flow model has a large number of parameters that can be changed in order to calibrate the model to observations of hydraulic heads, spring heads, lateral boundary flows, and ET flows. It is necessary to identify those parameters to which the model outputs are most sensitive, and how they relate to the conceptual model. The results of sensitivity analyses are presented for three models: base HFM with selected HSU depth decay and anisotropy with MME recharge, base HFM with all HSU depth decay and anisotropy with MME recharge, and SCCC HFM with selected HSU depth decay and anisotropy with MME recharge. While sensitivity analyses are formally presented below, such analyses were also carried out as an integral part of the calibration process. In addition, alternative HFMs and alternative recharge models and boundary flows have been considered in the CAU flow model sensitivity and uncertainty analysis.

Uncontrolled When Printed

Additional sensitivity and uncertainty analyses were conducted after model calibration. The sensitivity analysis used local techniques (all parameters are perturbed slightly or one at a time over their range of uncertainty) and global techniques (considered effects of joint parameter uncertainty over full range of uncertainty) to identify and evaluate key parameters in the Pahute Mesa CAU groundwater model. The local sensitivity analysis techniques include PEST sensitivity analysis and perturbation analysis. The PEST code calculates a sensitivity coefficient for each parameter with respect to all weighted observations.

This analysis is termed "local" because only slight changes are made that investigate parameter values near the base value. The second local approach involves perturbing each of the parameters, one at a time, from a reference value and computing the corresponding change in the model output.

The global sensitivity analysis techniques include classification tree analysis and entropy analysis. Global sensitivity analysis techniques are used for investigating input-output sensitivities that are valid over the entire range of possible parameter variations and not just at or near the reference point.

To address HFM and water-balance uncertainty seven HFMs, five recharge models, and five sets of lateral boundary flows were considered. If all combinations were considered, this would result in 175 calibrated flow models. However, it is neither necessary nor reasonable to investigate all combinations. The approach taken was to use a given recharge model in the Pahute Mesa CAU flow model with the regional model boundary flows derived from the same recharge model in the regional model. The strategy is to combine HFMs with recharge models and corresponding lateral boundary flows in order to at least bound uncertainty associated with each model component.

Summary of Parameter Sensitivity Analyses. Parameter sensitivity analysis was performed on the two major HFMs in the Pahute Mesa CAU-scale groundwater model using a complementary suite of techniques.

The local approach used PEST to identify sensitive model parameters and parameter correlations. This analysis led to the following findings:

- The Paintbrush Composite Unit (PCU), Lower Clastic Confining Unit-Thrust Plate (LCCU1), Yucca Mountain Crater Flat Composite Unit (YMCFCM), Detached Volcanic Composite

Uncontrolled When Printed

Unit (DVCM), and Claim Canyon Caldera Structural Margin fault were sensitive in controlling heads in the base and SCCC HFMs.

- Reference permeability and depth decay have a nearly perfect correlation, which considering the formulation of depth decay is expected.
- Over their range of uncertainty, the reference permeability of HSUs with depth decay was more sensitive than the depth-decay parameter itself. It is important to note that this was recognized during calibration, and depth-decay coefficients as estimated for each type of HSU (e.g., volcanics and carbonates) were fixed and reference permeability calibrated.

The perturbation analysis varied properties of HSUs and faults over their range of uncertainty, providing a comprehensive picture of model behavior (although without considering compensating effects). Major faults often showed a one-sided sensitivity behavior, where fault permeability multiplier ceased to have a noticeable effect below a certain value.

Global sensitivity analysis was conducted by generating 1,000 uncorrelated parameter samples using Latin Hypercube sampling, computing flow models for these samples, and recording the model results for the two calibrated versions of the base HFM (all and selected HSU depth decay and anisotropy) and SCCC HFM. This approach was taken to attempt to identify whether there were parameter combinations that were as good as or better in calibrating the model than the chosen sets over the range of parameter uncertainty, and whether there were systematic effects of some model parameters. The results were analyzed using Spearman rank correlations, classification and regression trees, and entropy statistics. Similar sets of sensitive variables were identified as in the local and perturbation analyses.

The local and global sensitivity analyses confirmed what was observed during flow model calibration: that the major controls on the groundwater flow system are not necessarily all the HSUs on Pahute Mesa. For instance, while it appears that the Pre-Belted Range Composite Unit, and to a lesser extent the Belted Range Aquifer, have a noticeable role in calibration, the fact that the DVCM, PCM, YMCFCM, and LCCU1 dominate calibration (and that the Timber Mountain Confining Unit had any role at all) was unexpected. The underground nuclear tests were all conducted in Areas 19 and 20; hence, the observation well data tend to be clustered there, and the base HFM is also relatively complex in this area.

Uncontrolled When Printed

The Pahute Mesa HFMs, base and SCCC, incorporate a number of faults and other structural features. The Purse and Boxcar Fault systems have been previously identified as having sealing properties. Many others though, are unknown. The sensitivity analysis revealed the Claim Canyon Caldera Structural Margin as a consistently sensitive feature due to its location on the southern edge of the model. Perturbation analysis showed the Hogback and the Rainier Mesa Caldera Structural Margin have a strong effect at a permeability multiplier of 100 (the response between 10 and 100 appears very nonlinear and shows little effect at 10). The Ribbon Cliff Structural Zone that runs east-west between Black Mountain and the Purse Fault is strongly sensitive at low values because it can restrict flow through the area; the North Timber Mountain Moat Structural Zone (Moat Fault), Rainier Mesa Caldera Structural Margin, and Ammonia Tanks Caldera Structural Margin are sensitive for the same reason. Fault sensitivity tends to be one-sided; only lower values have any impact. Conceptually, this is sensible because a low- (or high-) permeability feature located in line with a flow path would have little obvious effect; the faults noted above all tend to lay across groundwater flow paths.

HFM Uncertainty Analysis. The complexity of the geology in the area, and the resulting uncertainty in geologic interpretation, was addressed in the development of the geologic models by including five additional alternatives beyond the base and SCCC HFMs. The additional HFM alternatives were addressed using the mesh developed for the base HFM. The selected HSU depth-decay and anisotropy approach was used in parameterizing the models beginning with the calibrated parameters. The flow model was calibrated with each of these alternative HFMs utilizing the MME recharge and boundary flow targets. Thus, the uncertainty in geologic structure was further addressed.

Calibrations were performed for all five alternative HFMs. Of the five alternatives, three required no additional effort over the base HFM to recalibrate, although the calibrations and simulated flow paths did show some differences. In the case of TCL, RIDGE, and SEPZ alternatives, parameters are identical to those used for the base HFM with selected HSU depth decay and anisotropy because the effects of the HSU changes required minimal parameter adjustment. Two alternatives (DRT and PZUP), both involving raising or otherwise increasing the amount of low-permeability rocks in the domain, required extensive effort to recalibrate. The calibration process resulted in metrics similar to the base HFM calibration, with some modest changes in simulated flow paths.

Uncontrolled When Printed

A summary understanding can be developed of the relative HFM performance by considering the goodness of the respective calibrations. The objective function of each alternative HFM, normalized by the results presented for base HFM with MME recharge and selected depth decay and anisotropy was compared. The alternative SEPZ HFM actually performed slightly better than the base HFM, with all of the improvement coming from a better agreement to the observation well data. The TCL alternative was nearly identical to the base HFM. The RIDGE case was mildly worse than the base HFM, primarily from increased misfit with the wells, although Oasis Valley flow was also noticeably undersimulated. The RIDGE alternative truncated the extent of volcanic aquifers (Benham Aquifer, Tiva Canyon Aquifer, and Topopah Spring Aquifer) in southern Area 20 with older, lower permeability units. This results in more scatter in the model agreement with the observation well data, as shown by the increased error standard deviation. The PZUP and DRT alternatives give the most different results in comparison to the base HFM calibration, which relative to the degree of HFM changes is not unreasonable. The DRT alternative has significant misfit on the boundary flows because the large section of low-permeability LCCU1 extending westward and northward into the model greatly reduces transmissivity along the northern boundary.

Water-Balance Uncertainty Analysis. Recalibrating the base and SCCC HFMs to a suite of recharge models and boundary flows addresses the water-balance component of flow model uncertainty. A total of eight combinations of recharge model, boundary flow, and HFM were considered. The boundary flows developed from the UGTA regional model analysis for the corresponding recharge models were used in conjunction with each respective recharge model. The base HFM with anisotropy and depth decay applied to selected HSUs was recalibrated using the two USGS and two DRI recharge models. The results were very similar between the pairs of models (e.g., USGS with and without runoff). The USGS recharge model with run-on and runoff (USGSD) is conceptually more reasonable, so it was retained for further analysis for the SCCC HFM. Likewise, the DRI recharge model with alluvial screen (DRIA) was retained because it has the highest flux rates and should bound the upper end of flow through the system. Thus, the SCCC HFM was tested with the DRIA and USGSD recharge models only. The USGSD recharge model provided some of the best calibrations, with the DRIA recharge giving results similar to or worse than the MME recharge model. The most noticeable effect was that flow paths in the SCCC HFM changed with the different recharge models such that more paths were directed down Fortymile Canyon.

Uncontrolled When Printed

In general, all the combinations of HFMs, recharge models, and boundary flows could be as well calibrated as with the MME recharge and boundary flow. This recalibration, however, can result in a few marginal parameter values. In general, reducing recharge via the USGS recharge model had the effect of dropping permeability, with the converse resulting from the DRI recharge model. This is expected behavior in a steady-state model. Some of the downward changes, notably the Inlet Aquifer for the USGS recharge model cases, are to the lower limit of estimated parameter uncertainty range. The poorest-performing HFM considered under all recharge models was the SCCC alternative. The lack of deep faults, particularly along the Purse Fault, limits the key degrees of freedom necessary to give a reasonable calibration. The SCCC HFM also showed the greatest sensitivity of simulated flow paths to recharge model, with significantly more flow paths down Fortymile Canyon for the DRIA and the USGSD recharges than for the MME recharge, as compared to any other HFM and recharge combination. The particle paths, with the notable exception of the SCCC HFM, tend to behave similarly across all recharge alternatives, suggesting that HFM uncertainty plays a greater role than recharge uncertainty.

Combining HFM and Water-Balance Uncertainty. Another type of uncertainty analysis was to combine HFM and water-balance uncertainty. Two of the alternative HFMs that are most distinctly different than the base HFM (i.e., the DRT and PZUP cases) were combined with the DRIA and USGSD recharge models to further bound flow system uncertainty. Both the DRT and PZUP HFMs have increased volumes of low permeability rock, although as a consequence of the different conceptual models. Not surprisingly, both these alternatives do not perform well in matching boundary flows with the high volume (relative to the USGS and MME recharge models) DRIA recharge model simply because they do not have sufficient system transmissivity to move enough water across the boundaries. The simulated Oasis Valley flows tend to be on the high side, but not unreasonably so, and the heads are matched with a slight oversimulation bias. With respect to the boundary flows, these HFMs do perform reasonably with the USGSD recharge model, which is a direct consequence of the larger amount of lower permeability rocks in each HFM. However, there is a bias, modest for DRT and severe for PZUP, to undersimulate observation well head.

The PZUP HFM with the USGSD recharge model has a bias on the order of 20 m to undersimulate head on Pahute Mesa, but qualitatively the flow paths still appear reasonable. This is because the bias is ubiquitous; thus, the flow direction is maintained. The DRT HFM, in all cases, simulates a focused

Uncontrolled When Printed

flow path that seems counterintuitive to the conceptual model of flow from Pahute Mesa to Oasis Valley, but still can match Oasis Valley discharge. With changing recharge models the main simulated flow paths do not change in the DRT HFM, but at the highest recharge (DRIA) distinctly more paths exit in Oasis Valley than with the lowest recharge (USGSD). Thus, the large changes in flow paths from the DRT HFM are generated by the HFM itself, not the variation in recharge models. Conversely, the goodness of the calibrations varies in the PZUP case, but the flow paths show relatively minor variations. In both cases it appears that the HFM uncertainty dominates over the recharge model uncertainty.

Other Sensitivity Analyses. A set of discrete sensitivity analyses was also considered including the following: testing the effects of permeability enhancement of test chimneys, evaluating two additional rooting depths for Oasis Valley discharge, assessing the effect of the reduced LCCU1 permeability alternative (suggested by the sensitivity analysis), and testing the consequences of trying to enhance flow down Fortymile Canyon. The effects of test chimneys was found to be negligible, the extinction depth is not a greatly sensitive parameter, the model could still be calibrated well with lower LCCU1 permeability alternative, and enhancing flow down Fortymile Canyon does not look feasible.

GEOCHEMICAL VERIFICATION

Geochemical signatures of various groundwaters in the area were used to generate mixing targets at key points in the model domain for model verification purposes as described in the Pahute Mesa CAIP (DOE/NV, 1999). Nineteen of the calibrated flow models are evaluated with respect to independently developed groundwater mixing targets determined from geochemical analyses. The purpose of these comparisons is to determine whether the sources of groundwater at eight target wells within the domain, as modeled, are consistent with the geochemical interpretation. In the comparisons, the sources of groundwater in the models are determined with reverse-particle simulations. The top of the model has been discretized into nine separate recharge zones and the side boundaries have been discretized into seven separate inflow zones for a total of 16 unique source zones associated with specific groundwater chemical signatures. With this method, the fraction of water from each of the recharge and boundary inflow zones that is present in the groundwater at the

Uncontrolled When Printed

mixing target wells is computed. These fractions are compared with the mixing ratios estimated by interpreting geochemical compositions.

Comparison of calibrated flow models, via reverse-particle tracking, with geochemistry mixing targets was performed as a blind evaluation. The mixing targets were developed independently of the flow model calibration and were only considered after calibration was complete. However, absolute acceptance or rejection of flow models cannot be determined based upon the geochemistry comparisons alone. If flow models are to be either weighted or rejected for subsequent use in transport modeling, then such evaluation would have to be conducted with simultaneous consideration of the following: (a) the quality of the calibration, (b) the likelihood and/or reasonableness of the alternative stratigraphic model, (c) the specific water-balance condition considered, and (d) the results of the geochemistry comparison. Many of the discrepancies between calibrated flow models and geochemistry-mixing targets are local in nature and due to small-scale processes, forcing flow paths slightly away from intended targets. A primary source of such discrepancies is related to the independently developed recharge maps used in the models. A large component of local recharge serves to force flow paths from upgradient sources away, but only slightly for certain target wells. Other large-scale issues involve the magnitude of flow into the model from side boundaries. The impacts of such model differences can be seen tens of kilometers away from the source. The target wells at the higher parts of the flow system were more difficult to match because there is less distance for mixing to occur, and very complex flow paths (at ER-EC-6, for instance) produce poor comparisons because of narrow flow-path deviations. Thus, the various discrepancies identified should not be weighted equally in quantitative evaluation of the calibrated flow models advanced in this study. In general, the trends are captured.

Cluster analysis of the geochemical verification results was used to group the combinations of calibrated HFM and recharge models. The best cluster of models with respect to the geochemical verification included DRT-MME-SDA, DRT-DRIA-SDA, PZUP-MME-SDA, SCCC-MME-SDA, BN-MME-SDA with reduced LCCU1 permeability, and BN-USGSD-SDA with reduced LCCU1 permeability.

Uncontrolled When Printed

THERMAL SENSITIVITY AND VERIFICATION

Thermal analysis identified specific locations where pure vertical conduction of heat did not adequately explain thermal anomalies observed in borehole temperature profiles. Such locations were identified during the development of the calibrated steady-state heat-conduction model. Several of these locations qualitatively suggested areas where flow of cooler water downward could explain the temperature anomalies.

Four locations within the CAU model, identified as being affected by downward-groundwater flow, were investigated. Following these identifications, reverse-particle-tracking simulations (with the particles released in deeper zones) were conducted to investigate whether shallow groundwater sources were feasible at the depths indicated in the heat-conduction study. The BN-MME-SDA reduced LCCU1 permeability alternative is evaluated with respect to vertical flow indicated by analysis of temperature data. For two locations within the Silent Canyon Caldera, one within the Timber Mountain Caldera and one to the west of the Timber Mountain Caldera, the results were positive with the simulations verifying that the flow model could qualitatively capture the convective components identified.

The sensitivity of the calibrated base HFM with MME recharge and selected depth decay and anisotropy was evaluated with respect to changes in the prescribed steady-state temperature profiles. Starting with the calibrated parameters for the BN-MME-SDA flow model, the temperature distribution is changed to reflect the low and high linear geothermal gradients. The flow model is not recalibrated, and forward simulations are compared with the base-case model. Here, as part of an assessment of model sensitivity to temperature, two different temperature distributions based on linear thermal gradients and extrapolation from a high-quality measurement are considered. It is not surprising that the model objective function increases with the two sensitivity runs, because these fields are different than that determined from the calibrated conduction model. Increased temperature at depth results in larger hydraulic conductivities for the same permeability developed in the calibrated base model. Thus, it is likely that the objective function could be reduced through recalibration. It is possible that reasonable calibrated permeability fields could be achieved with the linear thermal gradients. To offset the higher viscosities, lower rock permeabilities would be needed.

Uncontrolled When Printed

However, it is unlikely that linear thermal gradients would lead to as good or better results than those achieved with the calibrated thermal field, which captures non-linear distributions of rock properties

The pathlines and reverse-particle-tracking simulations are nearly identical for the base model and the two thermal sensitivity runs. This is likely due to the fact that the models are most similar at the shallower depths where the forward particles are introduced. Recharge also enters the model at the shallower depths and is the same for each of the model runs. Thus, the reverse particles are likely to exit at the locations where recharge occurs.

Uncontrolled When Printed

1.0 INTRODUCTION

The U.S. Department of Energy (DOE), National Nuclear Security Administration Nevada Site Office (NNSA/NSO) initiated the Underground Test Area (UGTA) Project to assess and evaluate the effects of the underground nuclear weapons tests on groundwater on the Nevada Test Site (NTS) and vicinity. The framework for this evaluation is provided in Appendix VI, Revision No. 1 (December 7, 2000) of the *Federal Facility Agreement and Consent Order* (FFACO) (1996). Appendix VI of the FFACO, "Corrective Action Strategy," describes the processes that will be used to complete corrective actions, including those in the UGTA Project. The objective of the strategy is to analyze and evaluate each UGTA corrective action unit (CAU) (Figure 1-1) through a combination of data and information collection and evaluation, and modeling groundwater flow and contaminant transport. Section 1.3 of this report provides a summary of the FFACO corrective action process and the UGTA corrective action strategy.

The FFACO corrective action process for Central and Western Pahute Mesa was initiated with the Corrective Action Investigation Plan (CAIP) (DOE/NV, 1999). This Pahute Mesa CAIP identified a three-step model development process to evaluate the impact of underground nuclear testing on groundwater and simulate a contaminant boundary (DOE/NV, 1999, Section 5.1.1). The first step is the data analysis task to compile and evaluate existing and new data for use in the model. The second step is the development of the groundwater flow model. The third step is the development of the transport model.

The first step has been completed and is documented in a series of data compilation and analysis reports, including the *Hydrologic Data for Groundwater Flow and Contaminant Transport Model of Corrective Action Units 101 and 102: Central and Western Pahute Mesa, Nye County, Nevada* (SNJV, 2004a). A listing and summary of these supporting reports is provided in Section 1.5.

This report completes the second step and documents the development of the groundwater flow model to assess the migration of radionuclides away from underground nuclear test cavities on Pahute

Uncontrolled When Printed

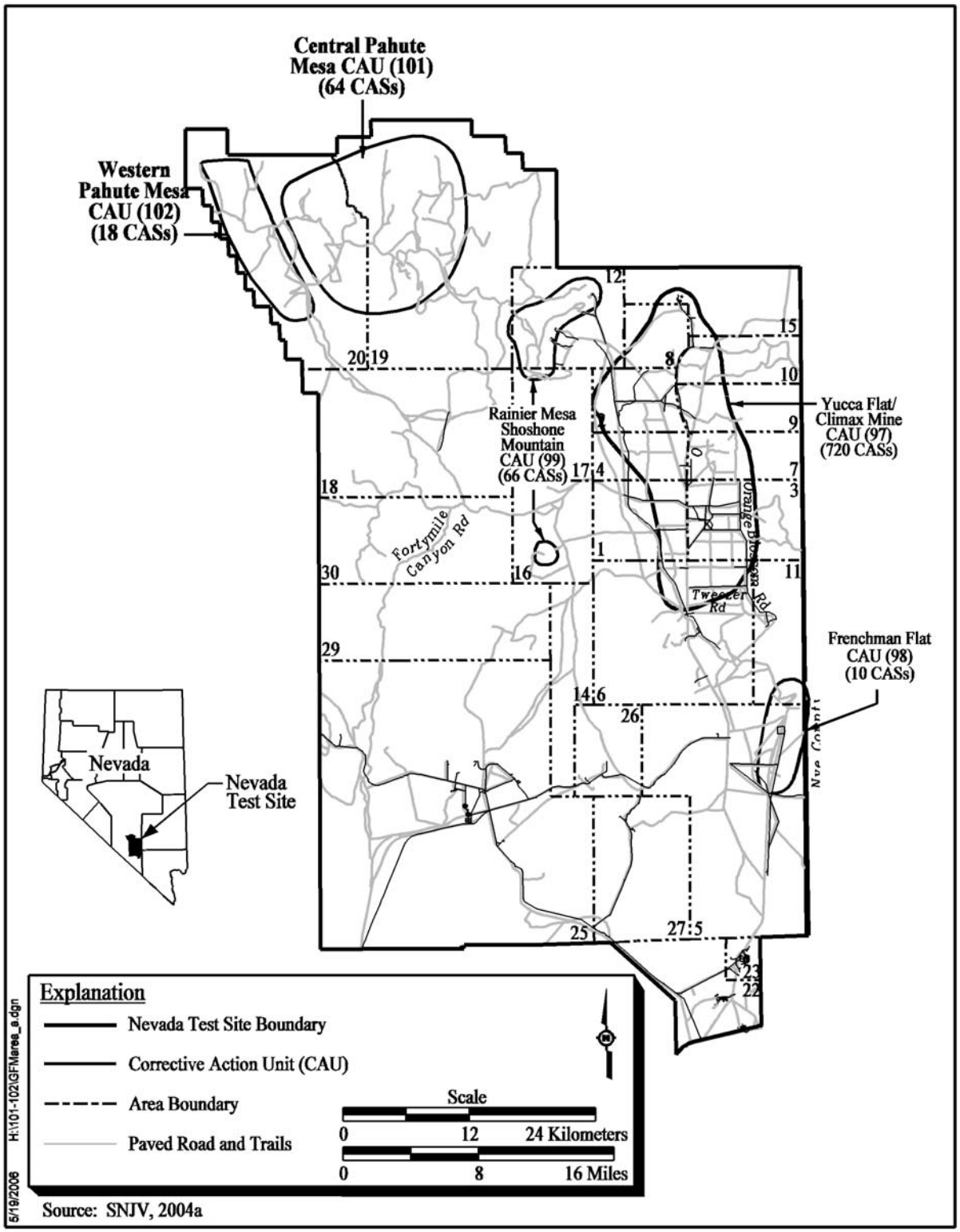

Figure 1-1
Location of the Pahute Mesa Corrective Action Units

Mesa. The third step, the development of the contaminant transport model, will be documented in a future report.

1.1 Purpose and Scope

The Pahute Mesa groundwater flow model supports the FFACO UGTA corrective action strategy objective of providing an estimate of the vertical and horizontal extent of contaminant migration for each CAU in order to predict contaminant boundaries. A contaminant boundary is the model-predicted perimeter that defines the extent of radionuclide-contaminated groundwater from underground nuclear testing above background conditions exceeding *Safe Drinking Water Act* (SDWA) standards. The contaminant boundary will be composed of both a perimeter boundary and a lower hydrostratigraphic unit (HSU) boundary. Additional results showing contaminant concentrations and the location of the contaminant boundary at selected times will also be presented. These times may include the verification period, the end of the five-year proof-of-concept period, as well as other times that are of specific interest.

The FFACO (1996) requires that the contaminant transport model predict the contaminant boundary at 1,000 years and "at a 95% level of confidence." The Pahute Mesa Phase I flow model described in this report provides, through the flow fields derived from alternative hydrostratigraphic framework models (HFMs) and recharge models, one part of the data required to compute the contaminant boundary. Other components include the simplified source term model, which incorporates uncertainty and variability in the factors that control radionuclide release from an underground nuclear test (SNJV, 2004a), and the transport model with the concomitant parameter uncertainty as described in Shaw (2003). The uncertainty in all the above model components will be evaluated to produce the final contaminant boundary.

This report documents the development of the groundwater flow model for the Central and Western Pahute Mesa CAUs.

Specific objectives of the Central and Western Pahute Mesa flow model are to:

- Develop a three-dimensional (3-D), mathematical flow model that incorporates the important physical features of the flow system and honors CAU-specific data and information.

Uncontrolled When Printed

- Simulate the groundwater flow system to determine the direction and magnitude of groundwater fluxes based on calibration to Pahute Mesa hydrogeologic data.
- Quantify the uncertainty in the direction and magnitude of groundwater flow due to uncertainty in parameter values and alternative component conceptual models (e.g., geology, boundary flux, and recharge).

Figure 1-2 shows the hydrologic model area that encompasses the Pahute Mesa CAUs, including Timber Mountain, the eastern edge of Oasis Valley, the northern part of Fortymile Canyon, and the northern portion of Yucca Mountain (DOE/NV, 1999). This area was selected to better define the regional groundwater flow system of the Lower Carbonate Aquifer (LCA) in the vicinity of Pahute Mesa.

1.2 Project Participants

The UGTA Project is a component of the NNSA/NSO Environmental Restoration Program (ERP). The UGTA Project Corrective Action Investigations (CAIs) are managed by the NNSA/NSO UGTA Project Manager. A Technical Working Group (TWG) has been established to assist the NNSA/NSO UGTA Project Manager with technical management issues. Tasks assigned to the TWG include providing expert technical support to plan, guide, and monitor UGTA technical work and serve as internal peer reviewers of UGTA products. The TWG consists of representatives from the participating organizations, which are: Bechtel Nevada (BN), Desert Research Institute (DRI), Lawrence Livermore National Laboratory (LLNL), Los Alamos National Laboratory (LANL), Stoller-Navarro Joint Venture (SNJV), and the U.S. Geological Survey (USGS).

1.3 Summary of the Federal Facility Agreement and Consent Order

Since 1996, the Nevada Division of Environmental Protection (NDEP) has regulated the NNSA/NSO corrective actions through the FFACO (1996). The individual locations covered by the agreement are known as corrective action sites (CASs), and they are grouped into CAUs. The UGTA CAUs are Frenchman Flat, Central and Western Pahute Mesa, Yucca Flat, and Rainier Mesa/Shoshone Mountain (Figure 1-1). Central Pahute Mesa (CAU 101) and Western Pahute Mesa (CAU 102) are addressed together due to their adjacent locations and common groundwater regime as well as similarities in testing practices, geology, and hydrology (SNJV, 2004a).

Uncontrolled When Printed

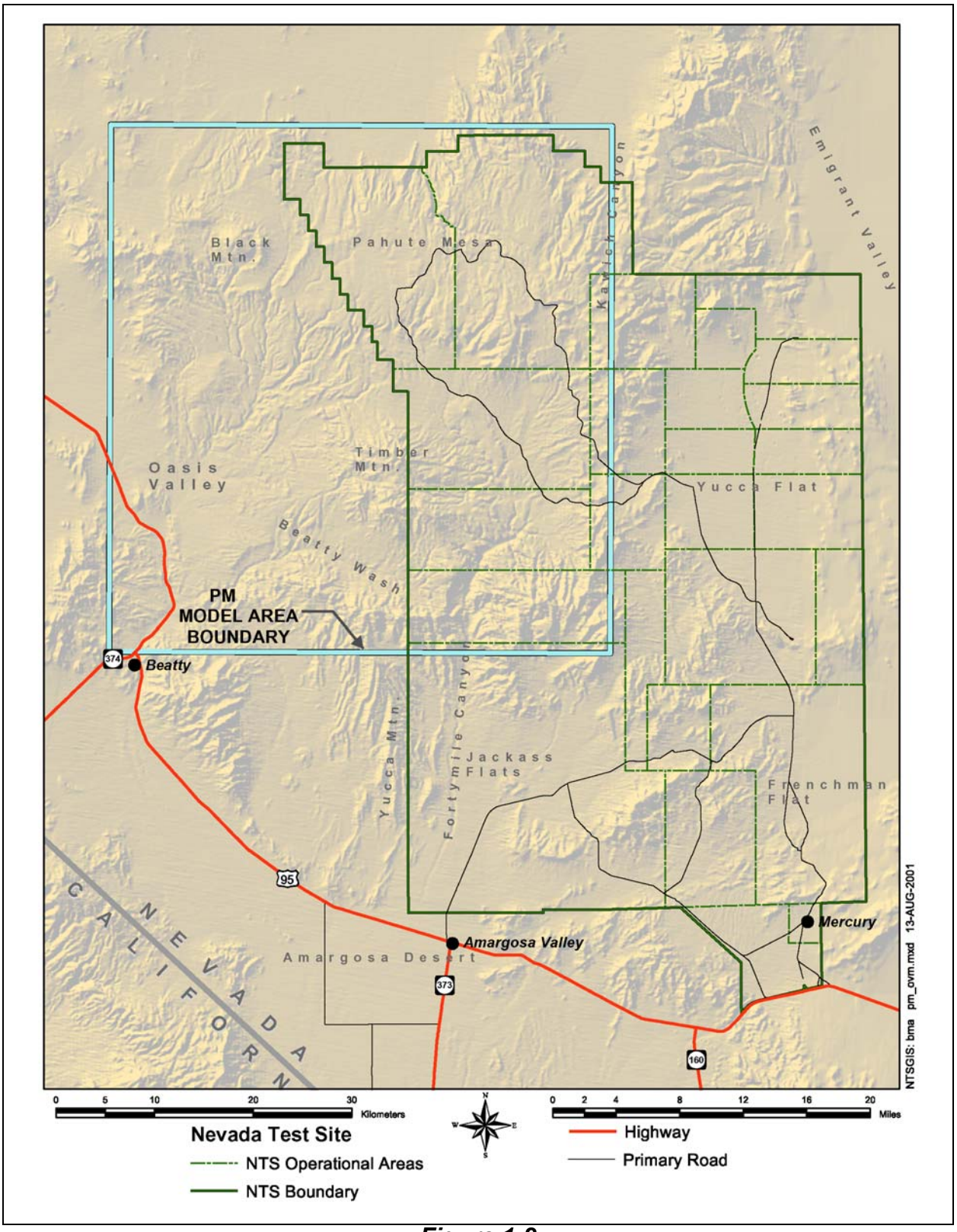

Figure 1-2
Map Showing Location of the Pahute Mesa Model Area
(Modified from BN, 2002)

Uncontrolled When Printed

Appendix VI, Revision No. 1 (December 7, 2000) of the FFACO (1996), "Corrective Action Strategy," describes the processes that will be used to complete corrective actions, including those in the UGTA Project. The UGTA corrective action strategy, described in Section 3.0 of the FFACO, provides the current regulatory guidance on the UGTA corrective action strategy and is incorporated into this document. All references to the FFACO or its appendices in this document will refer to the FFACO as a whole (i.e., FFACO, 1996) because it is the official document that incorporates the Appendix VI, December 2000 revision.

The CAU-specific corrective action process includes six major components: CAIP, CAI, Corrective Action Decision Document (CADD), Corrective Action Plan (CAP), Closure Report (CR), and long-term monitoring. The purpose or contents of these documents are summarized as follows:

- The CAI planning is documented in the CAIP, an FFACO-required document that provides or references all specific information for planning investigation activities associated with CAUs or sites.
- The CAI includes the collection of new data, the evaluation of new and existing data, and the development and use of CAU-specific groundwater flow and transport model(s).
- The CADD is an FFACO-required report that documents the CAI. It describes the results of the CAI, the corrective action alternatives considered, the results of their comparative evaluation, the selected corrective action, and the rationale for its selection.
- The CAP is an FFACO-required document describing how the selected remedial alternative is to be implemented. The CAP will contain the engineering design and all necessary specifications to implement the selected remedial alternative.
- The UGTA strategy has provisions for CAU closure only if the long-term-monitoring alternative is selected. Closure activities include the preparation of a CR, a review of the CR by NDEP, and long-term closure monitoring by NNSA/NSO.
- The long-term, post-closure monitoring is designed to ensure the compliance boundary is not violated (SNJV, 2004a).

Figure 1-3 presents the decision process used to achieve the strategy for the Pahute Mesa CAU groundwater flow model. The shaded portion of the diagram illustrates the portion of the process that has been completed as part of the Pahute Mesa CAI.

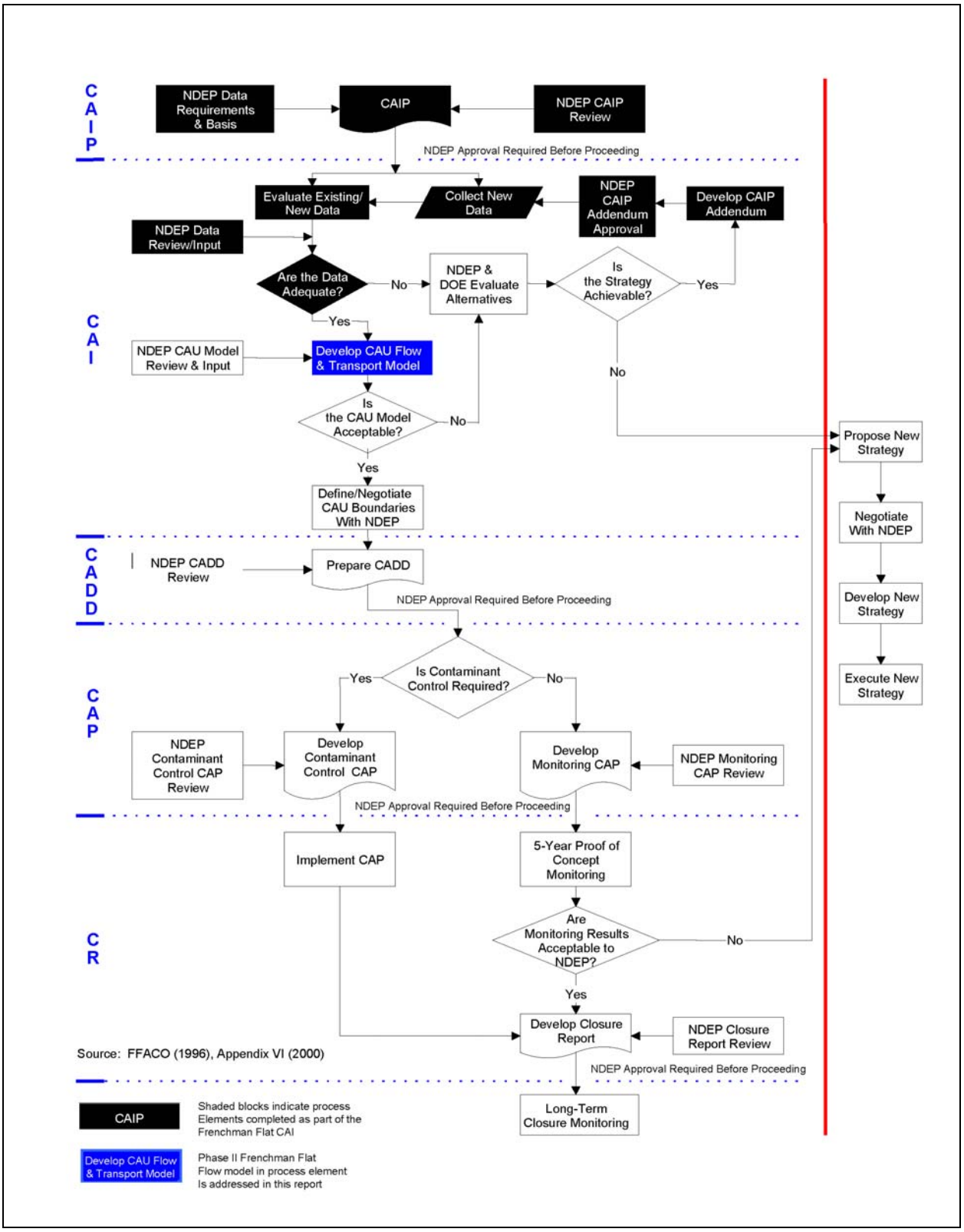

Figure 1-3
Process Flow Diagram for the Underground Test Area Corrective Action Units

Uncontrolled When Printed

1.3.1 Summary of the FFACO UGTA Corrective Action Strategy

The UGTA corrective action strategy consists of two major phases: development of a regional flow model for use in evaluation and coordination for all the UGTA CAUs, and a corrective action process for each of the CAUs. A model of regional flow encompassing the NTS and the groundwater flow systems extending to downgradient discharge has been completed and is documented in *Regional Groundwater Flow and Tritium Transport Modeling and Risk Assessment of the Underground Test Area, Nevada Test Site, Nevada* (DOE/NV, 1997). Regional modeling is a cross-cutting activity, supporting the entire UGTA Project, which provides the initial basis for assessing flow paths from CAUs, determining potential receptors, evaluating isolation or interaction of CAUs, and creating a consistent hydrogeologic framework across all the CAUs. Regional transport modeling provided the initial basis for determining the magnitude of risk from the source to potential receptors and for scaling individual CAU work (FFACO, 1996).

The second phase of the CAI process focuses on developing CAU-specific models that include CAU-specific data. The CAU-specific modeling objectives are to determine boundaries that encompass the extent of contamination, as defined in the FFACO (1996). Thus, this second phase is the basis for the analysis of relevant hydrologic data, and the development of the Pahute Mesa groundwater flow and transport model. The development of the groundwater flow model is presented in this report.

1.4 Pahute Mesa Background

Pahute Mesa is located in the northwestern part of the NTS. It includes NTS Areas 19 and 20 (Figure 1-1). Pahute Mesa is an elevated plateau of about 500 square kilometers (km^2) (200 square miles [mi^2]) at an altitude that ranges from 1,676 meters (m) (5,500 feet [ft]) on the western edge to over 2,134 m (7,000 ft) above mean sea level (amsl) throughout the eastern range (Blankennagel and Weir, 1973). The area of interest for the Pahute Mesa CAU is defined by the potentially affected portion of the regional groundwater flow system, which includes a region stretching from the northern side of Pahute Mesa south and southwestward to Oasis Valley (Figure 1-2).

Pahute Mesa geology is dominated by deposition of rock units from volcanic eruptions from nested calderas of the Southwestern Nevada Volcanic Field (SWNVF) (Figure 1-4). All rocks known to

Uncontrolled When Printed

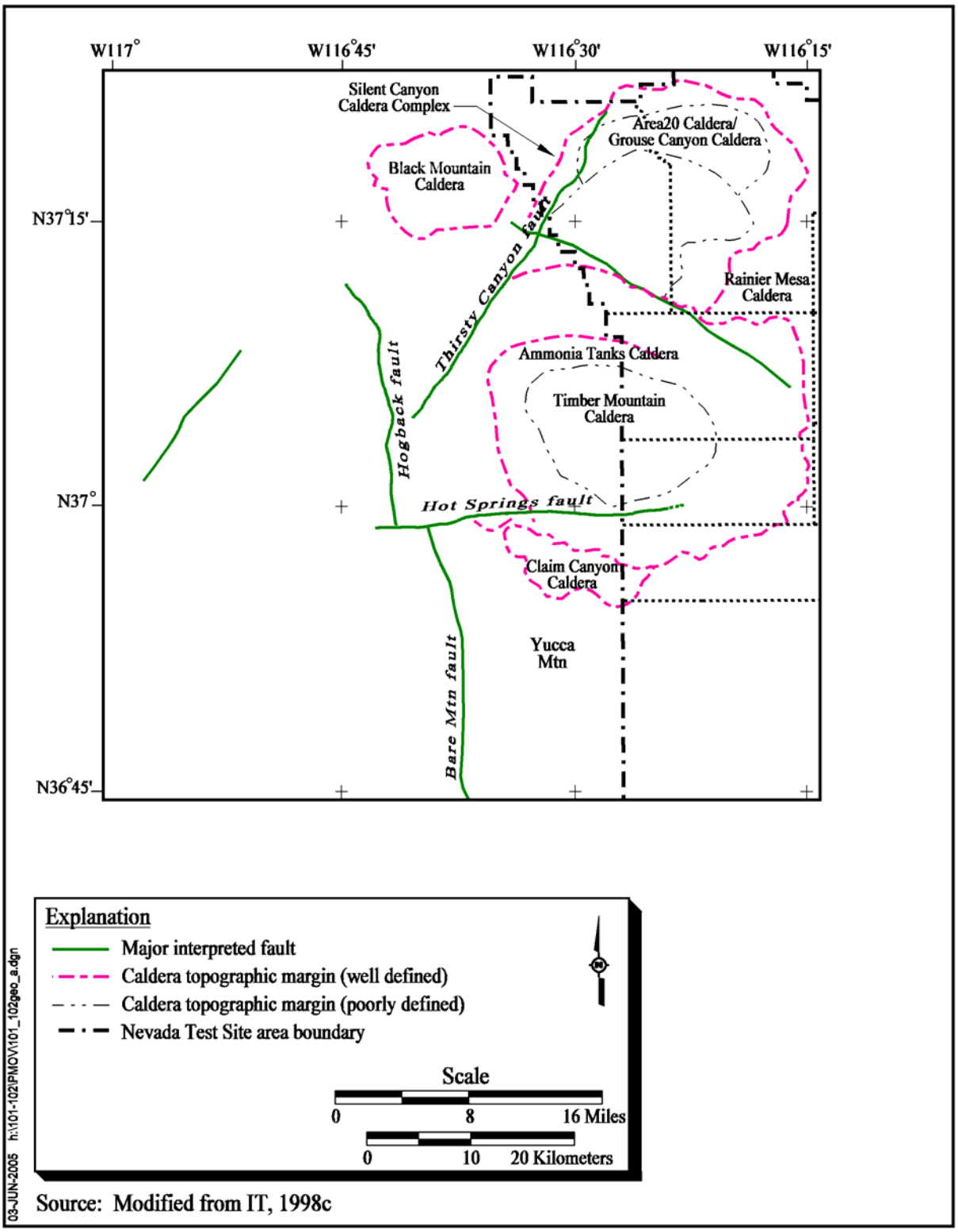

Figure 1-4
Geophysically Inferred Geologic Features of the Pahute Mesa Area

Uncontrolled When Printed

underlie Pahute Mesa are volcanic. The younger caldera complex of hydrologic significance is the Timber Mountain Caldera. This caldera collapse and its filling with volcanic materials affect the southern portion of the Western Pahute Mesa CAU. The Timber Mountain Caldera erupted volcanic ash flows that covered much of Pahute Mesa to the north.

On Pahute Mesa, the rocks from Timber Mountain Caldera cover an older series of calderas that make up the Silent Canyon Caldera Complex (SCCC). This caldera complex consists of at least two nested calderas, the Area 20 Caldera and the older Grouse Canyon Caldera (Sawyer and Sargent, 1989). Both calderas were formed and subsequently filled by voluminous eruptions of tuff and lava of generally rhyolitic composition. Total thickness of volcanic rocks beneath Pahute Mesa approaches 5 kilometers (km) (Ferguson et al., 1994).

The volcanic rocks that control groundwater flow beneath Pahute Mesa can be grouped into four volcanic hydrogeologic units (HGUs) based mainly on lithology and secondary alteration. These units are lava-flow aquifers (LFAs), welded-tuff aquifers (WTAs), vitric-tuff aquifers (VTAs), and tuff confining units (TCUs).

Groundwater beneath Pahute Mesa generally flows in a southwest direction, primarily through fractures in the lava-flow and tuff aquifers. Zeolitized bedded and nonwelded tuffs act as confining units that inhibit the flow of groundwater. The spatial distribution of permeable aquifers relative to the confining units is not well understood. Thickness variations of aquifers and confining units and their connectivity across faults or caldera boundaries are important hydrostratigraphic relationships that are also not well understood outside Pahute Mesa.

Groundwater-elevation data in the area of interest are sparse. A number of wells provide water-level information in the area of Pahute Mesa and Oasis Valley, but water levels in the area between Pahute Mesa and Oasis Valley are less well defined. However, what data are available suggest that groundwater elevations generally mimic the topography. Groundwater elevations are highest beneath northern Pahute Mesa, ranging in elevation from approximately 1,280 to nearly 1,500 m (4,200 to 4,900 ft). Groundwater elevations drop off gradually to the south and west, ranging from 1,100 to 1,250 m (3,600 to 4,100 ft) in Oasis Valley. Some groundwater discharges to the surface within the Oasis Valley discharge area in the form of springs. Figure 1-4 shows the regional topography, and

Figure 1-5 shows the generalized groundwater flow directions for the regional groundwater flow system.

Groundwater recharge occurs locally from precipitation and by underflow from areas located to the north of Pahute Mesa. Groundwater then flows south-southwestward to the Oasis Valley and Death Valley to the southwest. Several factors are believed to account for the flow around Timber Mountain. Due to its elevation, Timber Mountain receives excess precipitation compared to surrounding areas of lower elevation, which leads to additional groundwater recharge beneath Timber Mountain. In addition, extensive zeolitization and clay alteration of the tuffs within the Timber Mountain Caldera causes these volcanic units to behave more like confining units than aquifers. Both of these factors are expected to lead to a mounding of the groundwater levels beneath the mountain, which affects groundwater flow path from Pahute Mesa such that they go around both sides of Timber Mountain.

The bulk of the groundwater flow from Pahute Mesa to Oasis Valley occurs around the northwest side of Timber Mountain. However, a significant portion flows south along the east side of Timber Mountain and makes an abrupt turn to the west to converge with the remaining flow at Oasis Valley (Figure 1-5). This westerly turn appears to be caused by a structural high of the Lower Clastic Confining Unit (LCCU) associated with the Belted Range thrust system, which forces the groundwater to turn west at this point and flow towards the discharge areas. Pathlines from underground nuclear tests on Pahute Mesa generally move downgradient in volcanic aquifers above the LCA before discharging in Oasis Valley.

The east-west striking boundary of the Timber Mountain and Claim Canyon Calderas may line up with a geophysically inferred east-west structure (Hot Springs Fault) (Grauch et al., 1997) (Figure 1-4). The combination of these structures may inhibit southerly flow of groundwater in the vicinity, and impart an east-west gradient to groundwater flow south of Timber Mountain (IT, 1998c).

1.4.1 Underground Nuclear Testing on Pahute Mesa

Pahute Mesa was used as an underground nuclear testing area of the NTS for 27 years. Underground nuclear testing on Pahute Mesa began with Operation Whetstone in 1965 and ended with Operation Julin in 1992 (DOE/NV, 2000). Underground nuclear tests conducted at Pahute Mesa that are of

Uncontrolled When Printed

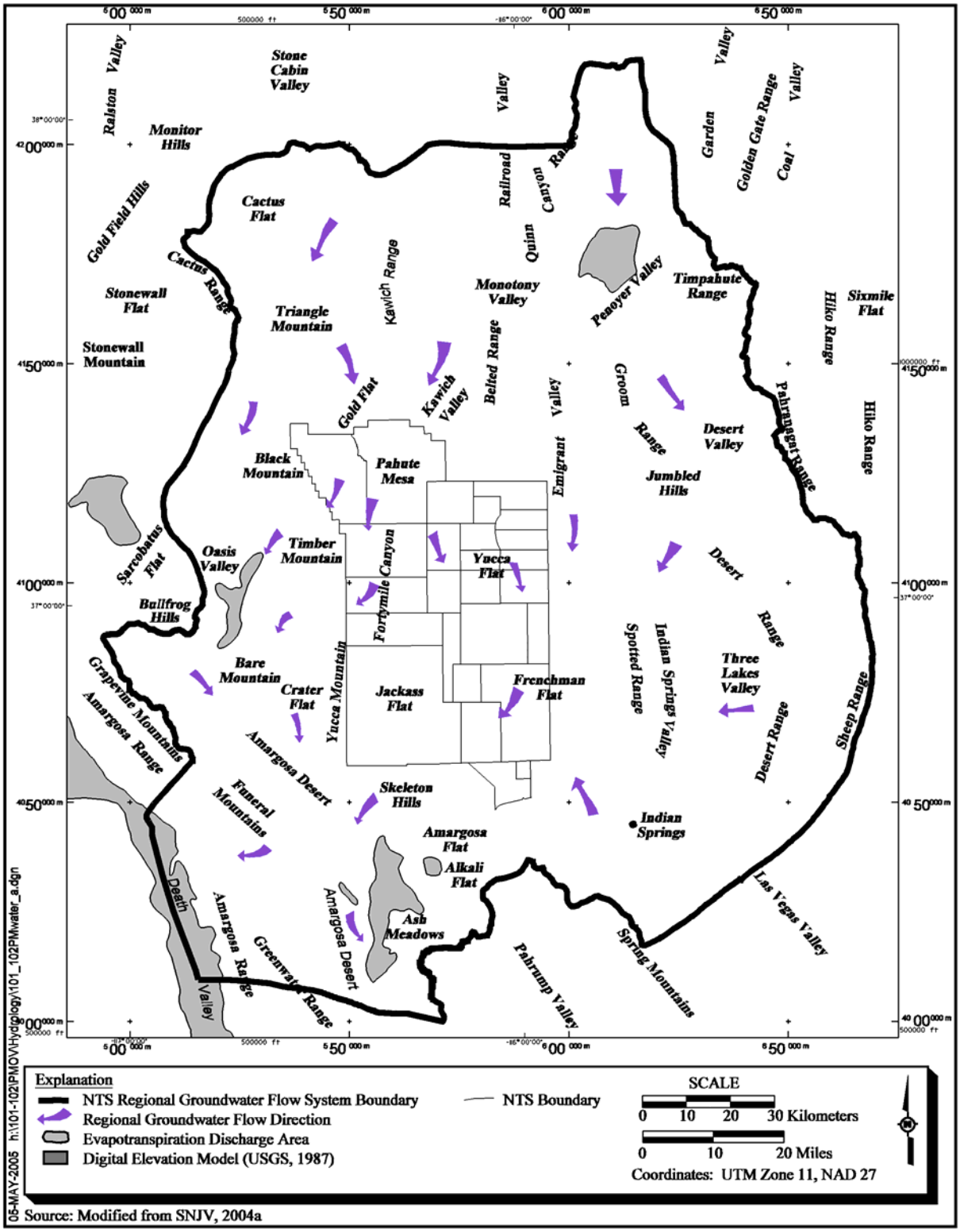

Figure 1-5
Features of the Nevada Test Site Regional Groundwater Flow System

Uncontrolled When Printed

interest to the UGTA Project are those detonated in deep vertical shafts, drilled into volcanic rock near or below the water table. A total of 82 such underground nuclear tests were conducted in Pahute Mesa. Sixty-four of these tests were detonated on Central Pahute Mesa (CAU 101), and 18 tests were detonated in Western Pahute Mesa (CAU 102) (DOE/NV, 1999). Media contaminated by the underground nuclear tests on Pahute Mesa are geologic formations within the unsaturated and saturated zones. Transport in groundwater is the primary mechanism of migration for the subsurface contamination away from the Pahute Mesa underground nuclear tests.

1.5 Major Supporting Reports Documenting CAU-Specific Data Analysis and Evaluation

The Pahute Mesa CAUs 101 and 102 groundwater flow model is supported by a number of major reports that describe a series of data analysis and modeling tasks. Table 1-1 summarizes these reports and identifies their contribution to the development of the Pahute Mesa flow model.

1.6 Report Organization

This report is organized into the following sections:

Section 1.0 presents an introduction to the document.

Section 2.0 presents the stratigraphic framework and alternative conceptual models of the geologic framework and groundwater flow that represent the information base for the CAU flow system; the numerical models of groundwater flow are constructed to replicate these conceptual geologic and flow system models.

Section 3.0 presents the computer code selection and code description.

Section 4.0 is the groundwater flow model construction that explains and demonstrates how the model was converted into its numerical representation.

Section 5.0 presents the flow model calibration and describes the purpose of calibration, the calibration protocol, use of parameter estimation (PEST), and how parameter sensitivities and constraint of flow paths were utilized.

Uncontrolled When Printed

Table 1-1
Major Supporting Documents
(Page 1 of 3)

Report	Report Synopsis	Contribution to Flow Model
Summary of Hydrogeologic Controls on Ground-Water Flow at the Nevada Test Site, Nye County, Nevada (Laczniak et al., 1996)	This report summarizes what is known and inferred about groundwater flow throughout the NTS region. As such, major controls on groundwater flow are identified, some uncertainties about groundwater flow are highlighted, and technical needs are prioritized and identified relative to the ERP.	• Conceptual model
Regional Groundwater Flow and Tritium Transport Modeling and Risk Assessment of the Underground Test Area, Nevada Test Site, Nevada (DOE/NV, 1997)	This report provided the initial rationale to determine the magnitude of risk from various underground nuclear tests on the NTS to potential downgradient receptors, such as the public and the environment from possible groundwater contamination. The regional evaluation consisted of data analysis, model development, and model predictions. Results of the regional evaluation of groundwater flow, tritium migration, and risk assessment performed for the underground test areas are presented in this report. As such, the regional evaluation was used during the planning of the Pahute Mesa CAI and is the basis for the development of the CAU conceptual model.	• Conceptual model • Regional model framework • Boundary fluxes
Corrective Action Investigation Plan for Corrective Action Units 101 and 102: Central and Western Pahute Mesa, Nevada Test Site, Nevada (DOE/NV, 1999)	This report is a requirement of the FFACO (1996) that summarizes the site-specific historic data for the Pahute Mesa CAUs and describes the characterization activities implemented to evaluate the extent of contamination in groundwater due to the underground nuclear testing, and the development of a groundwater flow model to predict the contaminant boundary.	• Summary of historic data • Background information • CAU model approach
Quality Assurance and Analysis of Water Levels in Wells on Pahute Mesa and Vicinity, Nevada Test Site, Nye County, Nevada (Fenelon, 2000)	This report states that accurate water-level measurements are essential to determine groundwater flow paths that may contain contaminants from underground nuclear tests conducted on Pahute Mesa. As such, quality-assured data can be utilized to construct flow maps, calibrate steady-state and transient groundwater flow models, locate sites for future remedial monitoring, and identify existing trends that can be used as a means to understand the factors that influence the groundwater flow system.	• Supplement water-level targets for flow model calibration
A Hydrostratigraphic Model and Alternatives for the Groundwater Flow and Contaminant Transport Model of Corrective Action Units 101 and 102: Central and Western Pahute Mesa, Nye County, Nevada (BN, 2002)	This report presents the evaluation of geologic data and the resulting 3-D HFM. The framework was built utilizing a collection of stratigraphic, lithologic, and alteration data; a structural model; and results of geophysical, geological, and hydrological studies to formulate the hydrostratigraphic system.	• HFM • Alternative HFMs • HSU definition and description

Uncontrolled When Printed

Table 1-1
Major Supporting Documents
(Page 2 of 3)

Report	Report Synopsis	Contribution to Flow Model
Evaluation of the Hydrologic Source Term from Underground Nuclear Tests on Pahute Mesa at the Nevada Test Site: The CHESHIRE Test (Pawloski et al., 2001)	This report develops, summarizes, and interprets a series of detailed, unclassified simulations to forecast the nature and extent of radionuclide release and near-field migration in groundwater away from the CHESHIRE test over 1,000 years. The results are referred to as the CHESHIRE Hydrologic Source Term (HST).	• Background • Input into conceptual flow model
Geochemical and Isotopic Interpretations of Groundwater Flow in the Oasis Valley Flow System, Southern Nevada (Thomas et al., 2002)	This report summarizes the findings of a geochemical investigation of the Pahute Mesa/Oasis Valley (PM/OV) groundwater flow system in support of the flow and contaminant transport modeling for the Western Pahute Mesa CAU.	• Flow paths derived from geochemical analysis used to qualitatively assess flow model
Ground-Water Discharge Determined from Measurements of Evapotranspiration, Other Available Hydrologic Components, and Shallow Water-Level Changes, Oasis Valley, Nye County, Nevada (Reiner et al., 2002)	This report describes the natural groundwater discharge in the Oasis Valley, an area within the groundwater flow system of the Death Valley region and California. An estimate of groundwater discharge from the Oasis Valley was examined in numerous studies. As a result of these studies, this report refined the estimated groundwater discharge from Oasis Valley by quantifying evapotranspiration (ET), compiling groundwater withdrawal data, and estimating subsurface outflow.	• Flow system discharge from ET used as calibration data
*TYBO/BENHAM: Model Analysis of Groundwater Flow and Radionuclide Migration from Underground Nuclear Tests in Southwestern Pahute Mesa, Nevad*a (Wolfsberg et al., 2002)	This report provides a description of an integrated modeling approach used to simulate groundwater flow, radionuclide release, and radionuclide transport near the TYBO and BENHAM underground nuclear test sites.	• Test case for finite element heat-mass (FEHM) transfer code model • Results used to help parameterize CAU model
Reconnaissance Estimates of Recharge Based on an Elevation-Dependent Chloride Mass-Balance Approach (Russell and Minor, 2002)	This study describes the DRI evaluation of net infiltration and determination of recharge via the development of recharge models for data gathered from 17 springs located in the Sheep Range, Spring Mountains, and on the NTS. The objective was to improve an existing aquifer-response method based on the chloride mass-balance approach. Results of the recharge estimates are reported.	• Recharge models
Simulation of Net Infiltration and Potential and Potential Recharge Using a Distributed Parameter Watershed Model for the Death Valley Region, Nevada and California (Hevesi et al., 2003)	This study reports the development and application of a distributed parameter watershed model to estimate the temporal and spatial distribution of net infiltration for the Death Valley region. As stated, because of uncertainty relative to the input parameters, “averaging results from multiple realizations is more likely to provide a more robust estimate of current climate potential recharge.”	• Recharge models

Uncontrolled When Printed

Table 1-1
Major Supporting Documents
(Page 3 of 3)

Report	Report Synopsis	Contribution to Flow Model
Evaluation of Groundwater Flow in the Pahute Mesa - Oasis Valley Flow System Using Groundwater Chemical and Isotopic Data (Kwicklis et al., 2005)	This report documents the utilization of groundwater geochemical and isotopic data from the vicinity of the PM/OV flow system to interpret groundwater flow patterns as well as to independently evaluate the groundwater flow model that is currently being developed. A combination of graphical methods and inverse geochemical models form the basis for the PM/OV model area.	• Flow paths derived from geochemical analysis • Geochemical verification dataset
Hydrologic Data for the Groundwater Flow and Contaminant Transport Model of Corrective Action Units 101 and 102: Central and Western Pahute Mesa, Nye County, Nevada (SNJV, 2004a)	This report describes an assessment of hydrologic data and information in support of the CAU groundwater flow model. Relevant information, existing data, and newly-acquired data were analyzed for the hydrologic components of the groundwater flow system of Pahute Mesa and vicinity.	• Hydraulic head data for calibration • Hydraulic properties data • Discharge due to pumping • Boundary fluxes • Recharge models • Flow paths derived from geochemical analysis
Modeling Approach/Strategy for Corrective Action Units 101 and 102, Central and Western Pahute Mesa (SNJV, 2004b)	This report summarizes the data and information that are the technical basis for the groundwater flow model. Two approaches are described that propose developing the models to forecast how the hydrogeologic system, which includes the underground nuclear test cavities, will behave over time. One approach is the development of numerical process models to represent the processes that influence flow and transport. The other approach shows how simplified representations of the process models are utilized to assess the interactions between model and parameter uncertainty.	• Numerical code selection • Overall approach

Uncontrolled When Printed

Section 6.0 is the flow model sensitivity and uncertainty analysis.

Section 7.0 presents the geochemical verification.

Section 8.0 presents the thermal verification.

Section 9.0 is the summary and conclusions.

Section 10.0 contains the reference list.

Appendix A provides the 1999 letter report documenting the evaluation of flow and transport codes for application to the Pahute Mesa CAUs.

Appendix B is the LANL fault study.

Appendix C is the LANL thermal field analysis.

Appendix D presents the perturbation sensitivity analysis plots.

Appendix E presents permeabilities on cross sections A through J of the geologic model for several HFMs.

Appendix F presents the well and spring head calibration data.

2.0 FRAMEWORK FOR GROUNDWATER FLOW MODELING OF CENTRAL AND WESTERN PAHUTE MESA - DATA, INFORMATION, AND CONCEPTUAL MODELS

The development of a CAU-scale groundwater flow model for Central and Western Mesa Pahute Mesa is a key element of the FFACO corrective action strategy. The framework for this flow model incorporates data and information related to multiple component models of the Pahute Mesa hydrogeologic system. Each of these component models is characterized by uncertainties in both the data and information that characterize the processes described by the component model, and in the conceptual models that incorporate the data and information.

Figure 2-1 summarizes the regional and site-specific elements that are integrated into the Pahute Mesa flow model. These elements include:

- Regional data and information that provide the hydrogeologic context for the CAU-specific flow model.
- CAU-specific geologic data and information that establish the local hydrostratigraphic framework within which groundwater flows.
- Component models that integrate the regional hydrogeology into the CAU-specific hydrogeology.
- Alternative CAU-specific models to address uncertainty in hydrostratigraphy, lateral boundary flux and heads, and recharge.
- CAU-specific hydrologic parameters (including their uncertainty).

This section provides an overview of the data, information, and conceptual models that are incorporated into the Pahute Mesa flow model. The data, information, and conceptual models presented in this overview represent a large body of work (Table 1-1) and are described in more detail in the integrating report *Hydrologic Data for the Groundwater Flow and Contaminant Transport*

Uncontrolled When Printed

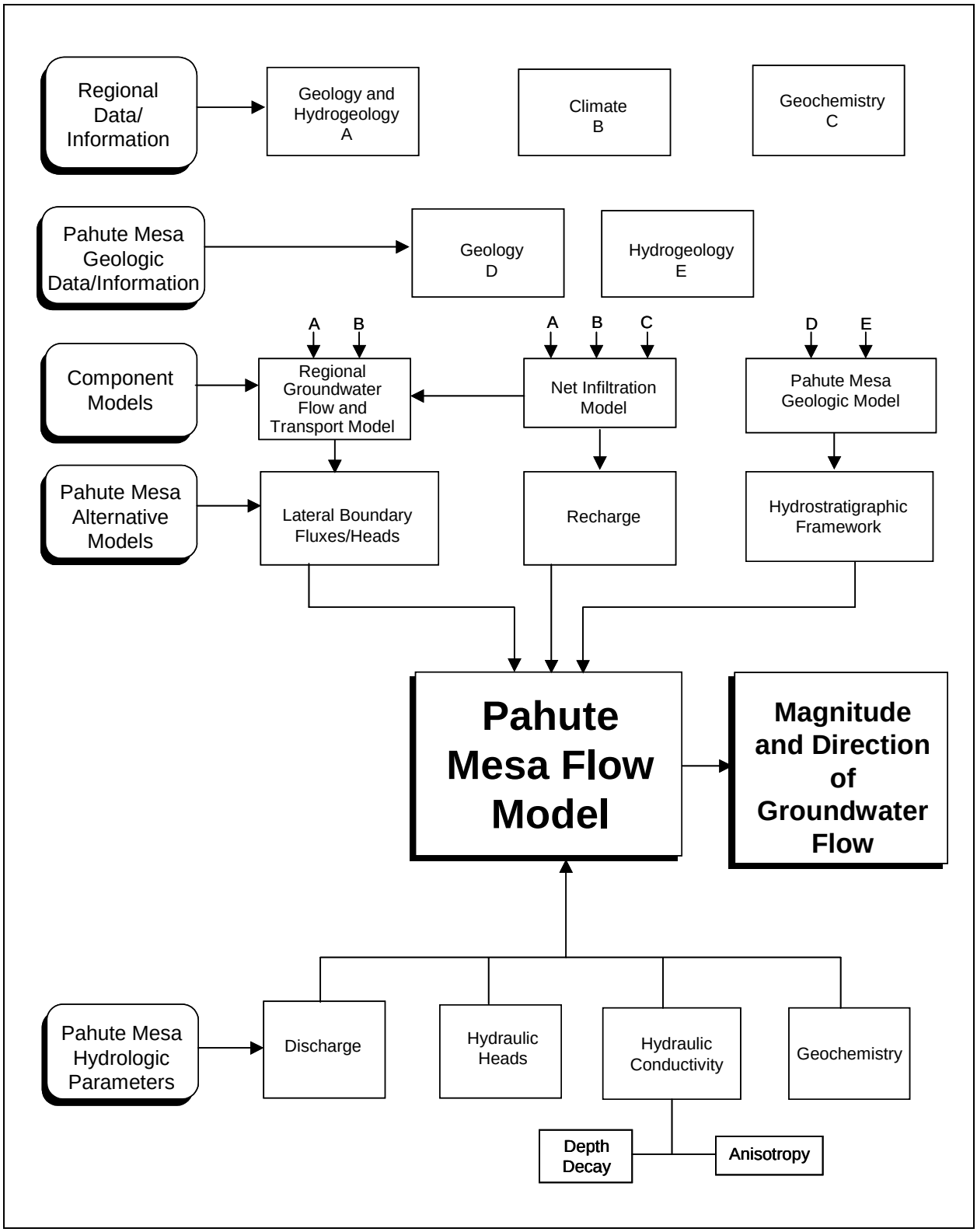

Figure 2-1
Information Flow into the Pahute Mesa Groundwater Flow Model

Uncontrolled When Printed

Model of Corrective Action Units 101 and 102: Central and Western Pahute Mesa, Nye County, Nevada (SNJV 2004a).

2.1 Summary of the UGTA Regional Model

A model of the regional groundwater flow through the NTS extending to downgradient discharge areas was developed during the regional evaluation (DOE/NV, 1997). The Pahute Mesa flow system model area is part of the NTS regional flow system model area (Figure 1-2), which is part of the Death Valley regional flow system (DVRFS) (Faunt et al., 2004; Hevesi et al., 2003). The following sections provide an overview of this regional model.

Belcher et al. (2004) published a revised regional model, the Death Valley regional flow model (DVRFM), in early 2005, after the Pahute Mesa flow model analysis was largely complete. It is DOE policy not to use work products that are unpublished. Thus, it was not possible to include the newer results in any comprehensive way.

2.1.1 UGTA Regional Model Hydrostratigraphic Framework

The hydrogeologic framework used in the UGTA regional groundwater flow model is based on the conceptual hydrologic system established for the NTS area by Winograd and Thordarson (1975) and Blankennagel and Weir (1973). This early work was summarized and updated by Laczniak et al. (1996) and was further developed by UGTA (IT, 1996d).

All rocks of the NTS and vicinity can be classified as one of eight HGUs, which include the alluvial aquifer (AA), four volcanic HGUs, an intrusive HGU, and two HGUs that represent the pre-Tertiary sedimentary and metasedimentary rocks. Table 2-1 summarizes the HGUs of the UGTA regional model.

Hydrostratigraphic units are groupings of contiguous stratigraphic units that have a particular hydrogeologic character, such as aquifer (unit through which water moves readily) or confining unit (unit that generally impedes water movement). An HSU may contain several HGUs but is defined so that a single general type of HGU dominates (for example, mostly WTAs and VTAs, or mostly TCUs). Twenty HSUs were defined in the UGTA regional HFM (IT, 1996d).

Uncontrolled When Printed

Table 2-1
Hydrogeologic Units of the UGTA Regional Model

Hydrogeologic Unit	Typical Lithologies	Hydrologic Significance
Alluvial Aquifer (AA) (AA is also an HSU in hydrogeologic models.)	Unconsolidated to partially consolidated gravelly sand, aeolian sand, and colluvium; thin, basalt flows of limited extent	Has characteristics of a highly conductive aquifer, but less so where lenses of clay-rich paleocolluvium or playa deposits are present.
Welded-Tuff Aquifer (WTA)	Welded ash-flow tuff; vitric to devitrified	Degree of welding greatly affects interstitial porosity (less porosity as degree of welding increases) and permeability (greater fracture permeability as degree of welding increases).
Vitric-Tuff Aquifer (VTA)	Bedded tuff; ash-fall and reworked tuff; vitric	Constitutes a volumetrically minor HGU; generally does not extend far below the static water level due to tendency of tuffs to become zeolitic (which drastically reduces permeability) under saturated conditions; significant interstitial porosity (20 to 40 percent); generally insignificant fracture permeability.
Lava-Flow Aquifer (LFA)	Rhyolite lava flows; includes flow breccias (commonly at base) and pumiceous zones (commonly at top)	Generally a caldera-filling unit; hydrologically complex, wide range of transmissivities, fracture density and interstitial porosity differ with lithologic variations.
Tuff Confining Unit (TCU)	Zeolitic bedded tuff with interbedded, but less significant, zeolitic, nonwelded to partially welded ash-flow tuff	May be saturated but measured transmissivities are very low; may cause accumulation of perched and/or semi-perched water in overlying units.
Intrusive Confining Unit (ICU)	Granodiorite, quartz monzonite	Relatively impermeable; forms local bulbous stocks, north of Rainier Mesa, Yucca Flat, and scattered elsewhere in the UGTA regional model area; may contain perched water.
Clastic Confining Unit (CCU)	Argillite, siltstone, quartzite	Clay-rich rocks are relatively impermeable; more siliceous rocks are fractured, but with fracture porosity generally sealed due to secondary mineralization.
Carbonate Aquifer (CA)	Dolomite, limestone	Transmissivity values vary greatly and are directly dependent on fracture frequency.

Source: Modified from SNJV, 2004a

In the Pahute Mesa-Timber Mountain caldera complex area, the rocks were divided into six Tertiary volcanic HSUs, one intrusive HSU, and five pre-Tertiary HSUs. The volcanic rocks west of the Timber Mountain-Oasis Valley caldera complex were not subdivided and are represented by a single HSU, volcanics undifferentiated (VU). The HSUs defined for the UGTA regional HFM that are within the Pahute Mesa model area are listed in Table 2-2. These units are listed in approximate order from surface to basement, although some are laterally rather than vertically contiguous, and not all units are present in all parts of the model area.

Uncontrolled When Printed

Table 2-2
Hydrostratigraphic Units of the Pahute Mesa Area Included in the UGTA Regional HFM
(Page 1 of 2)

Model HSU Number[a]	Hydrostratigraphic Unit (Symbol)	Dominant Hydrogeologic Unit(s)[b]	Stratigraphic Unit Map Symbols[c]	General Description
20	Alluvial Aquifer (AA) (this term is also used to designate a hydrogeologic unit)	AA	Qay, QTc, Qs, Qam, QTa, QTu, Qb, Tgy, Tgc, Tgm, Tgyx, Tt	Consists mainly of alluvium that fills extensional basins such as Crater Flat. Also includes generally older Tertiary gravels, tuffaceous sediments, and nonwelded tuffs (where thin) that partially fill other basins such as Oasis Valley and the moat of the Timber Mountain caldera complex.
19	Timber Mountain Aquifer (TMA)	Mostly WTA, minor VTA; TCU within the Tm caldera complex	Tt, Tf, Tm	"The uppermost welded tuffs" in the Pahute Mesa model area. Consists mainly of extra-caldera welded ash-flow tuffs (aquifer-like lithologies). However, the altered intra-caldera equivalent rocks within the Timber Mountain caldera are modeled as confining units.
18	Tuff Cone (TC)	LFA, TCU	Tp, Th (formerly Ta), Tc	Complex three-dimensional distribution of rhyolite lava and zeolitic nonwelded tuff of the Paintbrush Group, Calico Hills Formation or Crater Flat Group. Present in the northern portion of the Pahute Mesa model area beneath most of eastern and central Area 20.
17	Bullfrog Confining Unit (BFCU)	TCU	Tcb	Major confining unit differentiated within the NTS caldera complex area. Unit consists of thick intra-caldera, zeolitic, mostly nonwelded tuff of the Bullfrog Formation.
16	Belted Range Aquifer (BRA)	LFA and WTA, with lesser TCU	Tub, Tcbs, Tr	Consists of welded ash-flow tuff and lava of the Belted Range Group (Tb) above the Grouse Canyon Tuff (Tbg), but may also include the lava-flow lithofacies of the commendite of Split Ridge (Tbgs) and the commendite of Quartet Dome (Tbq) where present. Differentiated within the NTS caldera complex area.
15	Basal Confining Unit (BCU)	TCU	Tn, Tub, To, Tr, Tq	Mostly zeolitized nonwelded tuffs differentiated in the NTS caldera complex area.
14	Basal Aquifer (BAQ)	WTA	To, Tlt, Tqm	Mostly aquifer-like older volcanic rocks. Differentiated within the NTS caldera complex area.
11	Volcanics Undifferentiated (VU)	WTA, TCU, lesser LFA	Potentially includes all Tertiary volcanic units	All Quaternary and Tertiary volcanic units outside the NTS proper and the proximal NTS caldera complex.
8	Upper Clastic Confining Unit (UCCU)	CCU	MDc, MDe	Late Devonian through Mississippian siliciclastic rocks. Present in the eastern third of the Pahute Mesa model area.
7	Lower Carbonate Aquifer (LCA)	CA	Dg through Cc	Cambrian through Devonian mostly limestone and dolomite. Widespread throughout the Pahute Mesa area.

Uncontrolled When Printed

Table 2-2
Hydrostratigraphic Units of the Pahute Mesa Area Included in the UGTA Regional HFM
(Page 2 of 2)

Model HSU Number[a]	Hydrostratigraphic Unit (Symbol)	Dominant Hydrogeologic Unit(s)[b]	Stratigraphic Unit Map Symbols[c]	General Description
6	Lower Clastic Confining Unit (LCCU)	CCU	Cc, Cz, Czw, Zs, Zj	Late Proterozoic through Early Cambrian siliciclastic rocks. Widespread throughout the Pahute Mesa area.
5	Lower Carbonate Aquifer - Thrust Plate (LCA1)	CA	Dg through Cc	Cambrian through Devonian, mostly limestone and dolomite, rocks that occur in the hanging wall of the Belted Range thrust fault.
4	Lower Clastic Confining Unit - Thrust Plate (LCCU1)	CCU	Cc, Cz, Czw, Zs	Late Proterozoic to Early Cambrian siliciclastic rocks that occur within the hanging wall of the Belted Range thrust fault.
1	Intrusives (I)	ICU	Ti, Kg	Consists of granitic rocks that comprise the Gold Meadows stock along the northeastern margin of the Pahute Mesa area and intrusives greater than 2 km in size elsewhere in the UGTA regional HFM.

[a]UGTA regional model (IT, 1996d; DOE/NV, 1997)
[b]See Table 2-1 for definitions of HGUs.
[c]Refer to Slate et al. (1999) and Ferguson et al. (1994) for definitions of stratigraphic unit map symbols.

Source: Modified from SNJV, 2004a

Uncontrolled When Printed

Based on data used in the UGTA regional model (IT, 1996b; DOE/NV, 1997), hydraulic conductivity ranges for the main aquifers are as summarized in Table 2-3. The mean hydraulic conductivity of the AA is smaller than that of carbonate aquifers (CAs), but higher than that of the volcanic aquifers (VAs). The ranges extend over orders of magnitude. For example, within the LCA, the range of hydraulic conductivity is estimated to be between 0.0008 and 1,570 meters per day (m/d) (0.003 and 5,150 feet per day [ft/d]), representing interstitial and fracture porosity, respectively. This large range suggests that at the local scale, large variability in hydraulic conductivity can be expected. At the larger scales, the degree of fracturing controls the heterogeneity. It was also found that a linear trend exists, showing a decrease in hydraulic conductivity with increased depth. The data, however, displayed a significant level of scatter (SNJV, 2004a).

Table 2-3
Range of Hydraulic Parameters for Major Aquifers

Aquifer	Hydraulic Conductivity	
	Mean (m/d)	**Range** (m/d)
Alluvial Aquifer	8.44	0.00005-83
Volcanic Aquifers	1.18	0.0003-12
Carbonate Aquifer	31.71	0.0008-1,570

Source: Modified from DOE/NV, 1997

2.1.2 Groundwater Occurrence and Movement

Within the NTS region, groundwater occurs in alluvial, volcanic, and carbonate materials. Saturated alluvial materials are present in central and southern Yucca Flat, Frenchman Flat, and Jackass Flats on the NTS and in the basins located throughout the flow system. Saturated Tertiary volcanics are present in the western section of the region. The distribution and thickness of alluvial and volcanic aquifers are highly variable throughout the region and are not interpreted to be continuous. In most instances, an AA is confined to a basin by surrounding mountain ranges. In some basins, AAs are discontinuous due to structural controls elevating the bottom of the alluvium above the water table. In general, alluvial and volcanic aquifers are considered depositional elements overlying the regional flow system and only influence regional flow in localized areas. The underlying LCA is the principal aquifer of the UGTA regional flow system. The LCA forms a nearly continuous aquifer across the

Uncontrolled When Printed

region except where interrupted by calderas, truncated by structural controls, or penetrated by intrusive rocks.

Based on the water-level dataset compiled during the regional evaluation (IT, 1996c; DOE/NV, 1997), depths to groundwater beneath the NTS and surrounding region vary greatly. Groundwater depths in the southern NTS range from about 23 m (75 ft) beneath upper Fortymile Wash to over 213 m (700 ft) beneath Frenchman Flat, compared to more than 610 m (2,000 ft) beneath Pahute Mesa in the northern NTS (IT, 1996c; DOE/NV, 1997). Perched groundwater is found locally throughout the NTS and occurs within the TCUs and, to some extent, overlying units. In the highlands, springs emerge from perched groundwater lenses. Spring discharge rates are low and this water is used only by wildlife.

The general direction of groundwater flow in the regional flow system is from north to south and east to southwest (Figure 1-5). The direction of groundwater flow is locally influenced in areas where structural and geologic conditions have controlled the distribution and thickness of the LCA. In some areas of the regional flow system, groundwater encounters structural and geologic conditions, such as structural highs of the LCCU, that promote an upward flow component. The upward flow component brings water to discharge at the surface in the form of a wet playa or springs. Groundwater flow between basins occurs in the form of subsurface inflow and outflow.

Horizontal hydraulic gradients are very low to the east and west of the NTS (see Figure 2-16). In other areas, the prevailing flow direction and hydraulic gradients may locally be influenced by the structural position of geologic units with significantly lower transmissivity than that of the LCA. If the low transmissive units are structurally oriented so that they are perpendicular to flow, flow might be significantly altered, causing large hydraulic gradients. If their structural orientation is parallel to the prevailing flow direction, their effect may be insignificant. Structural uplifts of the LCCU and the distribution of the UCCU have caused several of the observed steep gradients within the flow system. Low-permeability sediments along the Funeral Mountains, such as the Tertiary Death Valley section sediments, also cause a steep hydraulic gradient between Amargosa Desert and Death Valley.

Groundwater recharge results from precipitation at higher elevations, and infiltration along stream courses and in playas. Recharge rates and distribution may be estimated. The estimates are, however,

Uncontrolled When Printed

uncertain. The recharge model used in the regional flow model was based on a modification of the Maxey-Eakin method (Maxey and Eakin, 1949; IT, 1996a).

Groundwater discharges to the surface in the form of springs, seeps, and ET in several areas. Major areas of natural groundwater discharge include Oasis Valley, Ash Meadows, Alkali Flat, Death Valley, and Penoyer Valley. Estimates of ET have recently been updated by the USGS for the first four areas listed above (Laczniak et al., 2001). Within the NTS region, artificial discharge occurs as groundwater pumpage from drinking water supply wells (public and domestic), agricultural wells, and industrial wells. Public, domestic, and industrial water supply wells for the NTS produce water from the carbonate, volcanic, and valley-fill aquifers. South of the NTS, private and public water supply wells are completed in the valley-fill aquifer.

An estimate of the regional, steady-state, groundwater budget is provided in Table 2-4.

Table 2-4
Estimated Steady-State Groundwater Budget for the Regional Groundwater Flow System

Recharge	
Recharge from precipitation	177,484 - 289,410 m^3/d
Subsurface inflow	5,405 - 70,100 m^3/d
Total Natural Recharge	**182,889 - 359,510 m^3/d**
Discharge	
Surface discharge (ET)	135,340 - 300,700 m^3/d
Subsurface outflow	850 - 5,100 m^3/d
Total Natural Discharge	**136,190 - 305,800 m^3/d**

Source: SNJV, 2004a

m^3/d = Cubic meters per day

2.2 Pahute Mesa Flow System Hydrostratigraphic Framework Models

The Pahute Mesa area HFMs were constructed using EarthVision® (EV) (Version 5.1, by Dynamic Graphics [2002]), a 3-D geologic model building and visualization software package. Input data included drill-hole data, digital elevation model data, and outcrop and fault data from surface geologic maps. Where deemed necessary, the data were supplemented with interpretations in the form of "pseudo drill holes," cross sections, and structure-contour maps. A "pseudo drill hole" is an

Uncontrolled When Printed

assumed data point used to facilitate the automated contouring of data. The data for the pseudo drill hole are obtained from surficial geology maps and/or geologist's interpretations.

The 3-D HFM area encompasses more than 2,700 km^2 (1,678 mi^2) of southern Nye County, Nevada (Figure 1-2). The model has a north-south length of 53.4 km (33.2 miles [mi]) and an east-west length of 50.8 km (31.6 mi), and includes geologic units as deep as 7 km (4.3 mi) below mean sea level (bmsl) (BN, 2002).

The processes of HFM development and screening are summarized in this section along with the geologic models retained for use in the CAU groundwater flow and transport model. The details may be found in the HFM report (BN, 2002).

2.2.1 Hydrostratigraphic Framework Model Development

A preliminary base HFM was constructed based on the conceptual model of the UGTA hydrologic system described by Winograd and Thordarson (1975). Further developments made by Laczniak et al. (1996), IT Corporation (IT) (1996a, b, and c), and Drellack and Prothro (1997) were also used to develop the Pahute Mesa CAU base HFM. A revised structural block model for the SWNVF (Warren et al., 2003) and an alternative 3-D model of the SCCC (McKee et al., 1999 and 2001) were incorporated into the information used for development of the base HFM. The hydrologic and geologic information developed for the USGS Death Valley region groundwater flow model was also included (D'Agnese et al., 1997; Faunt, 1997). Finally, information from the Yucca Mountain Project (YMP) hydrogeologic and flow model was incorporated in assessments of the southern part of the Western Pahute Mesa CAU.

Following the completion of the preliminary base HFM, a number of alternative HSU conceptual models were considered. These alternatives were screened for impact on groundwater flow and then evaluated and organized into four groups as follows:

- Group A - Alternatives of this group were developed using EV to improve the base HFM.
- Group B - Alternative HFMs were further developed in EV.
- Group C - These alternatives could be addressed by varying hydrologic parameters during the analysis and evaluation of the Pahute Mesa flow model.

Uncontrolled When Printed

- Group D - These alternatives were identified as low priority or not necessary to model.

The main criterion for selecting alternative HFMs for full development was the potential impact of the alternative interpretation on groundwater flow and the transport of contaminants in groundwater. Following this evaluation of the alternative HFMs, the base HFM was updated using the Group A alternatives, and the alternatives placed under Group B were further developed into EV models. Table 2-5 summarizes the Group B alternative HSUs.

For details on the base HFM and the alternative HSUs models, see *A Hydrostratigraphic Model for the Groundwater Flow and Contaminant Transport Model of Corrective Action Units 101 and 102: Central and Western Pahute Mesa, Nye County, Nevada* (BN, 2002).

After the development of all alternative HFMs, screening groundwater flow models were used to evaluate the impact of each alternative on contaminant transport (SNJV, 2004a). These models were developed using the Finite Element Heat-Mass (FEHM) Transfer Computer Code (Zyvoloski et al., 1997a and b) (see Section 3.0). The "particle-tracking" capability of FEHM was used to approximate the transport of radionuclides in groundwater using the base HFM and the six alternatives. None of these flow models were calibrated.

Except for the SCCC alternative, the results of the "particle-tracking" analyses for the other five alternatives were statistically similar to those of the base HFM. The results of the SCCC alternative produced results that were clearly different from those produced by the base HFM. Based on the screening results, only the base HFM and the SCCC alternative are used to develop alternative CAU flow models. The other five HFM alternatives are evaluated by varying the hydrologic parameters of the base HFM.

2.2.2 Base HFM

The structural features, HGUs, and HSUs of the base HFM developed for the Pahute Mesa area are summarized in this section. A 3-D view of this model is shown in Figure 2-2. A west-east cross section along C-C' (as shown in Figure 2-3) is shown in Figure 2-4 (BN 2002).

Table 2-5
Summary of Alternative HFMs Considered in the Pahute Mesa Flow Model
(Page 1 of 2)

Alternative HFM	Key Difference(s) Compared to Base HFM	Potential Impacts on Flow Model
Silent Canyon Caldera Complex (SCCC)	The SCCC alternative is stratigraphically and structurally less complex than the base HFM in the vicinity of the Silent Canyon caldera. The SCCC has a reduced number of HSUs, faults, and structural zones. In addition, the eastern and western margins of the SCCC area are different.	• Simplifications may impact flow directions and magnitudes in this area of the flow model. Comparisons between flow model results for this HFM and the base HFM will support an evaluation of the impact of faults on groundwater flow.
Basement Ridge Model (RIDGE)	The RIDGE alternative focuses on the bench area between the Timber Mountain caldera and SCCC. For this alternative, the southward distribution of important aquifer units (BA, TCA, TSA, and CFCM) pinch out or truncate against older, less conductive units that, for this HFM, are assumed to form the gravity-high ridge.	• Alternate HSU geometries may impact flow through the bench area between the Timber Mountain caldera and SCCC.
Thirsty Canyon Lineament (TCL)	The TCL alternative treats the north-northeast trending linear feature extending from just west of Well ER-EC-8 northeastward beneath western Pahute Mesa east of the Black Mountain caldera to the southern edge of Gold Flat as a continuous structural feature. The base HFM treats this feature as a continuous zone of en echelon faults 2 to 3 km wide.	• Treating the TCL as a continuous feature (interpreted in this HFM as a normal fault, down to the east) will help explore whether this feature on the west side of the ridge between the Timber Mountain caldera and SCCC acts as a potential hydraulic connection or barrier to groundwater flow.
Raised Pre-Tertiary Surface (PZUP)	The PZUP alternative raises the pre-Tertiary basement surface to its highest geologically permissible elevation (or least possible depth) and raises the basement inside the calderas. Paleozoic rock tops were raised over the entire domain. Under parts of Area 19 and 20 the SCICU was raised 750 m.	• This alternative examines the impact on groundwater flow from the reduction of the thickness of the transmissive units that results from maximizing the elevation of the basement.
Contiguous Imbricate Thrust Sheet (SEPZ)	The SEPZ alternative models the isolated surface exposure of Paleozoic carbonate rocks that are mapped in the southeast corner of the model area, east of the Belted Range thrust fault, as part of a more extensive imbricate fault. The base HFM considers this outcrop as a small erosional remnant of the hanging wall of an imbricate fault.	• This alternative tests the impact of the Paleozoic carbonate rock on the direction of groundwater flow around the east side of Timber Mountain.

Uncontrolled When Printed

Table 2-5
Summary of Alternative HFMs Considered in the Pahute Mesa Flow Model
(Page 2 of 2)

Alternative HFM	Key Difference(s) Compared to Base HFM	Potential Impacts on Flow Model
Deeply Rooted Belted Range Thrust Fault (DRT)	The DRT alternative considers the Belted Range thrust fault to be more deeply rooted than the base HFM resulting in a very thick thrust sheet over most of the model area.	• This alternative results in the LCA not being a continuous, coherent sheet across the model area. The uppermost pre-Tertiary rock immediately downgradient of Pahute Mesa is the nonconductive LCCU1 rather than the conductive LCA.

BA = Benham Aquifer
CFCM = Crater Flat Composite Unit
LCA = Lower Carbonate Aquifer
LCCU1 = Lower Clastic Confining Unit-Thrust Plate
SCICU = Silent Canyon Intrusive Confining Unit
TCA = Tiva Canyon Aquifer
TSA = Topopah Spring Aquifer

Uncontrolled When Printed

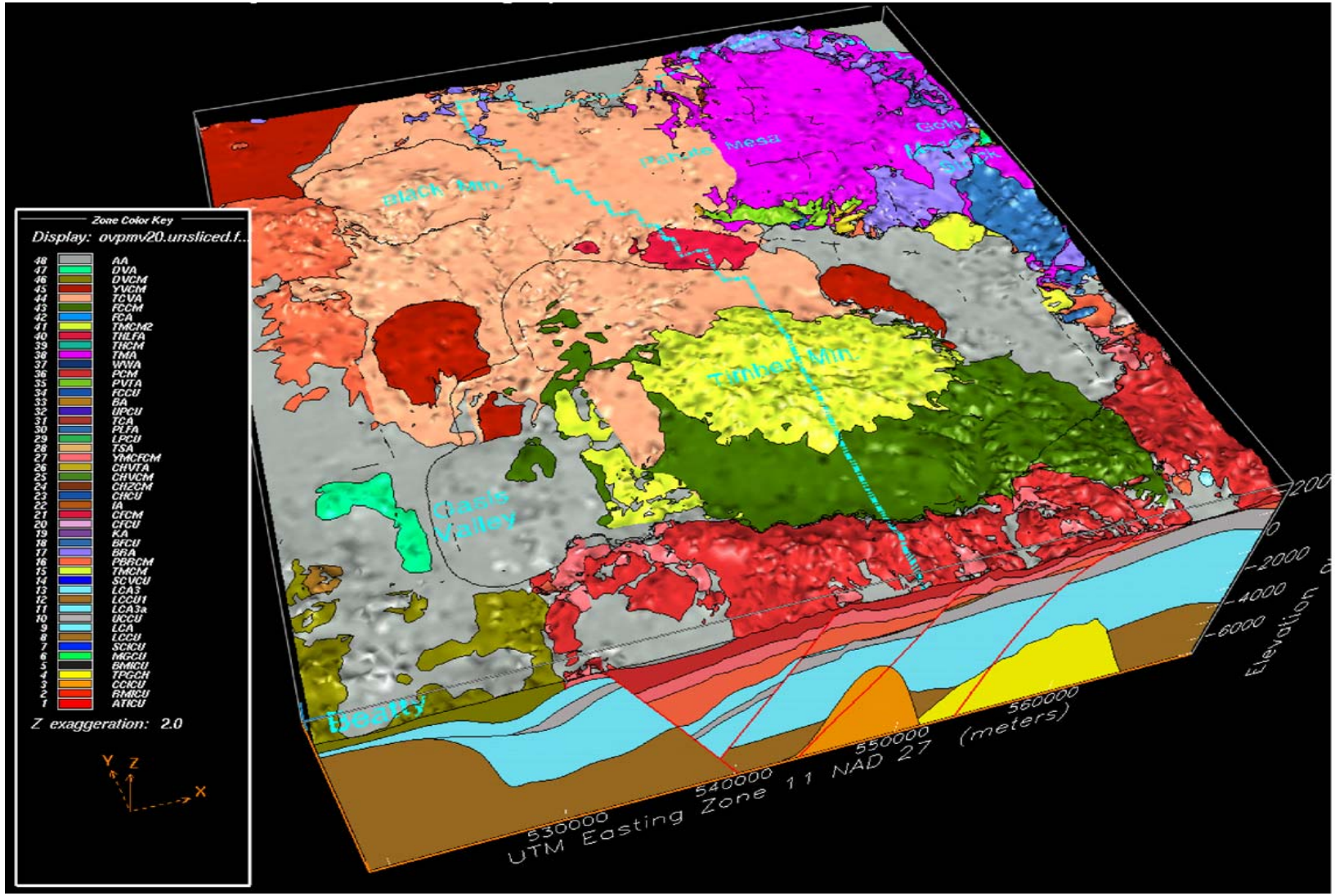

Source: Adapted from SNJV, 2004a

Figure 2-2
Three-Dimensional View of the Base Hydrostratigraphic Model of the Pahute Mesa Area, Top at Land Surface (BN, 2002)

Uncontrolled When Printed

2.2.2.1 Structural Features

The base HFM includes a total of 47 structural elements that are either faults or calderas. Only faults that were considered to be significant were included in the model. These include the larger ones and the ones that seem to form significant structural boundaries. Thus, only faults with significant displacement were included in the model. Six calderas have been identified in the Pahute Mesa model area, two of which are buried. Of particular interest is the SCCC. As stated previously, an alternative scenario was developed to evaluate the effect of caldera shape (see following subsection).

In the base HFM, the SCCC includes two calderas: the Grouse Canyon and Area 20 calderas. The base HFM for the SCCC area also includes 20 faults and structural zones in addition to the caldera-forming faults. Thirteen of these 20 structural features are basin-and-range type faults mapped at the surface.

2.2.2.2 Stratigraphy

As described in Section 2.1.1, the rocks of the NTS have been classified for hydrologic modeling using a two-level classification scheme in which HGUs are grouped to form HSUs (IT, 1996d). New units and additional detail have been added to the basic framework definition, but the systems developed by these early workers remain the best way to understand the groundwater of the NTS region.

Table 2-6 shows the correlation of Pahute Mesa HSUs with HSUs from earlier hydrostratigraphic models for this region. They are listed in approximate order from surface to basement, although some are laterally rather than vertically contiguous, and not all units are present in all parts of the model area.

As can be seen from the information presented in this section, the Pahute Mesa HFM (BN, 2002) includes considerable structural detail and stratigraphic enhancement over the UGTA regional HFM (IT, 1996d). The total number of HSUs increased from 20 to 46; most of the increase affected the Tertiary volcanic section. The six Tertiary volcanic HSUs in the Pahute Mesa and Timber Mountain caldera complex and the single volcanics undifferentiated outside the caldera complex (of the UGTA regional HFM) were subdivided into 40 HSUs for the Pahute Mesa model. Except for geometry details, the five pre-Tertiary HSUs remain as initially defined.

Uncontrolled When Printed

Table 2-6
Correlation of Hydrostratigraphic Units of the Pahute Mesa Base HFM and Earlier Models[a]
(Page 1 of 3)

HSU Layer No.[b]	Hydrostratigraphic Unit	Symbol This Report[b]	Correlation with PM-300 Model[c]	Correlation with UGTA Phase I[d]	Correlation with YMP[e] (Lithostratigraphic Units)
46	Alluvial Aquifer	AA	TMA	AA	QAL, TPAL, TLIM
45	Younger Volcanic Composite Unit	YVCM	NP[f]	VU	B
44	Thirsty Canyon Volcanic Aquifer	TCVA	TMA	TMA, VU	NP
43	Detached Volcanic Aquifer	DVA	NP	VU	
42	Detached Volcanic Composite Unit	DVCM			NR[g]
41	Fortymile Canyon Composite Unit	FCCM	TMA	TMA, VA	NP
40	Fortymile Canyon Aquifer	FCA	NP	VU	
39	Timber Mountain Composite Unit	TMCM	TMCU	TMA	
38	Tannenbaum Hill Lava-Flow Aquifer	THLFA	TMA		
37	Tannenbaum Hill Composite Unit	THCM			
36	Timber Mountain Aquifer	TMA		TMA, VA	UVA
35	Subcaldera Volcanic Confining Unit	SCVCU	Pre-T	BCU	NR
34	Fluorspar Canyon Confining Unit	FCCU	TMA	TMA, VA	NP
33	Windy Wash Aquifer	WWA	WWA	TMA	
32	Paintbrush Composite Unit	PCM	NP	TMA, VA, TC	UVA
31	Paintbrush Vitric-Tuff Aquifer	PVTA	PVTA	TMA, TC, VA	
30	Benham Aquifer	BA	BA	TC	NP
29	Upper Paintbrush Confining Unit	UPCU	UPCU		NR
28	Tiva Canyon Aquifer	TCA	TCA	TMA, TC, VA	UVA
27	Paintbrush Lava-Flow Aquifer	PLFA	PLFA	TC	NP
26	Lower Paintbrush Confining Unit	LPCU	LPCU	TC	NR
25	Topopah Spring Aquifer	TSA	TSA	TC, VA	UVA

Uncontrolled When Printed

Table 2-6
Correlation of Hydrostratigraphic Units of the Pahute Mesa Base HFM and Earlier Models[a]
(Page 2 of 3)

HSU Layer No.[b]	Hydrostratigraphic Unit	Symbol This Report[b]	Correlation with PM-300 Model[c]	Correlation with UGTA Phase I[d]	Correlation with YMP[e] (Lithostratigraphic Units)
24	Yucca Mountain Crater Flat Composite Unit	YMCFCM	NP	VA, VU	UVCU, MVA
23	Calico Hills Vitric-Tuff Aquifer	CHVTA	CHVTA	TC	MVA
22	Calico Hills Vitric Composite Unit	CHVCM	CHVCM		
21	Calico Hills Zeolitic Composite Unit	CHZCM	CHZCM		
20	Calico Hills Confining Unit	CHCU	CHCU	TC	NR
19	Inlet Aquifer	IA	IA	TC, VA	NP
18	Crater Flat Composite Unit	CFCM	CFCM	TC, VU	MVA
17	Crater Flat Confining Unit	CFCU	CFCU		NR
16	Kearsarge Aquifer	KA	KA	TC	NP
15	Bullfrog Confining Unit	BFCU	BFCU	TCB	
14	Belted Range Aquifer	BRA	BRA	TBA	NR
13	Pre-Belted Range Composite Unit	PBRCM	PBRCM	BAQ, BCU	MVCU, LVA, LVCU, LCU
12	Black Mountain Intrusive Confining Unit	BMICU	NP	VU	NP
11	Ammonia Tanks Intrusive Confining Unit	ATICU	TMCM	TMA	
10	Rainier Mesa Intrusive Confining Unit	RMICU			
9	Claim Canyon Intrusive Confining Unit	CCICU	NP	VA	NR
8	Calico Hills Intrusive Confining Unit	CHICU		I	NP
7	Silent Canyon Intrusive Confining Unit	SCICU	PreT	LCCU	
6	Mesozoic Granite Confining Unit	MGCU		I	
5	Lower Carbonate Aquifer-Thrust Plate	LCA3	NP	LCA3	NR
4	Lower Clastic Confining Unit-Thrust Plate	LCCU1	PreT	LCCU1	
3	Upper Clastic Confining Unit	UCCU	NP	UCCU	ECU

Uncontrolled When Printed

Table 2-6
Correlation of Hydrostratigraphic Units of the Pahute Mesa Base HFM and Earlier Models[a]
(Page 3 of 3)

HSU Layer No.[b]	Hydrostratigraphic Unit	Symbol This Report[b]	Correlation with PM-300 Model[c]	Correlation with UGTA Phase I[d]	Correlation with YMP[e] (Lithostratigraphic Units)
2	Lower Carbonate Aquifer	LCA	PreT	LCA	LCA
1	Lower Clastic Confining Unit	LCCU		LCCU	QCU

Source: Modified from SNJV, 2004a

[a]If correlative to more than one HSU, all HSUs are listed.
[b]See BN (2002) and SNJV (2004a) model HSU nomenclature.
[c]See Drellack and Prothro (1997) for explanation of PM-300 HSU nomenclature.
[d]See IT (1996d) for explanation of the UGTA Phase I HSU nomenclature.
[e]See CRWMS M&O (1997 and 2000) for explanation of the YMP lithostratigraphic unit nomenclature.
[f]Not present.
[g]Not recognized as a separate HSU.

Uncontrolled When Printed

2.2.3 Silent Canyon Caldera Complex HFM Alternative

The alternative SCCC model is based on the same HGUs as the base HFM. Despite the considerable differences in basic concepts such as style of caldera formation and number and activity of faults, as well as in scale and level of detail, both models honor the available drill-hole and outcrop data. Differences between the two models relate to the structural model used and the categorizing of HGUs into HSUs. Descriptions of these features are summarized from the HFM report (BN, 2002).

2.2.3.1 Structural Features

The alternative structural model of the SCCC is more simplified than the base HFM. Figure 2-3 shows a comparison of structural features and caldera margins for the base HFM model and the SCCC alternative. This structural model is based on previous models of calderas of the Pahute Mesa region developed by Noble et al. (1968) and Orkild et al. (1969), and analogies with other calderas of the world.

The SCCC HFM includes an elliptical ring-fracture fault system elongated to the north-northeast (Figure 2-3). Major structural differences with the base HFM include the margins of this caldera complex, locations of caldera-forming faults, and the number and depth of the faults considered.

The number of faults is different. The SCCC HFM includes the single caldera ring-fracture system, and only 11 of the basin-and-range faults mapped at the surface. Another difference is that the faults in the SCCC HFM end at shallower depths than in the base HFM.

2.2.3.2 Stratigraphy

Hydrostratigraphic differences between the two models of the SCCC area are the number of HSUs, their definition, and their distribution (BN, 2002).

Whereas in the base HFM, the SCCC area includes 25 HSUs, it includes only 12 in the SCCC alternative model (Table 2-7). Six post-Paintbrush HSUs are lumped together in the alternative model. This simplification may not be important because these units are mostly unsaturated, but other simplifications such as the lumping of the four Calico Hills HSUs may be important (BN, 2002).

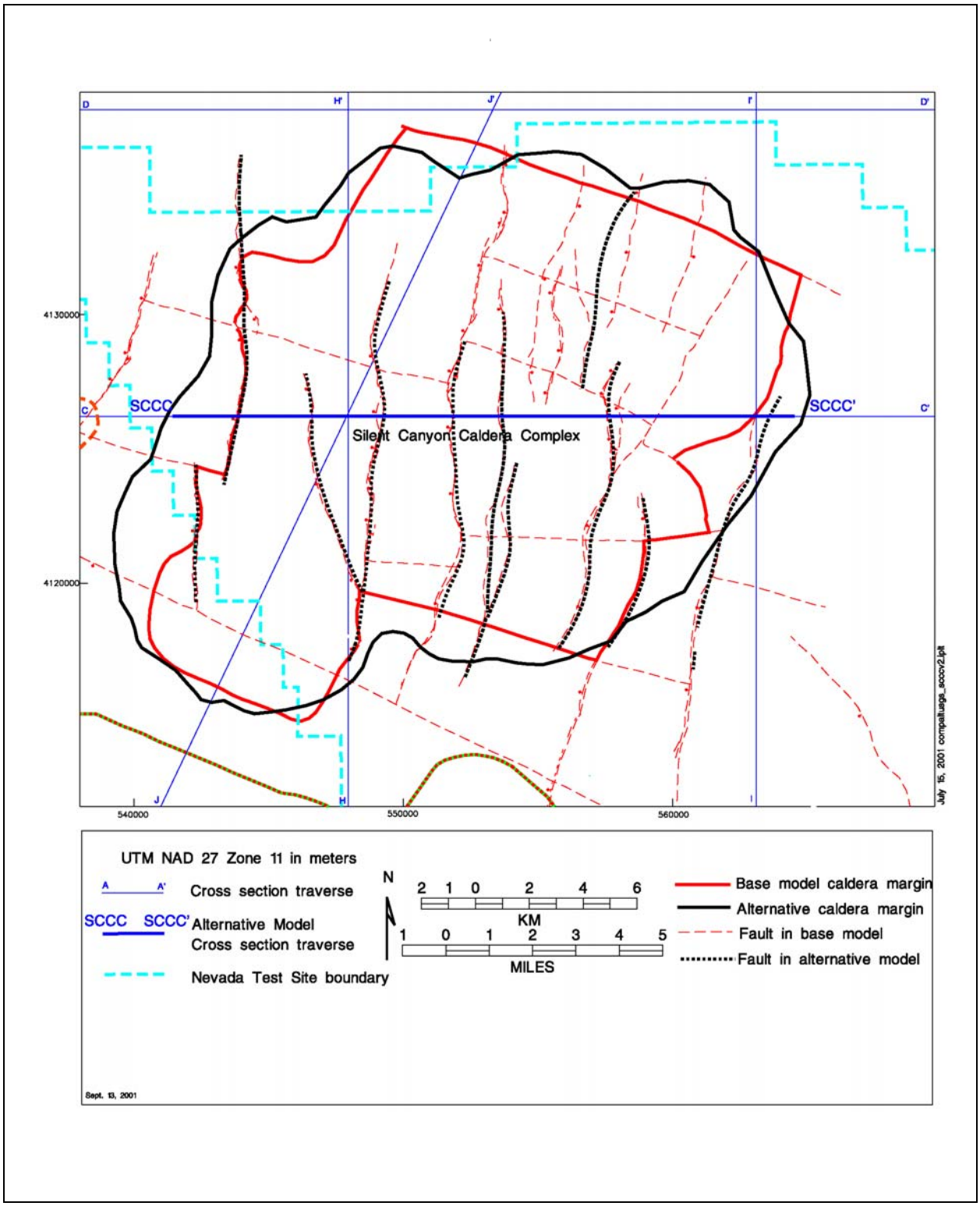

Figure 2-3
Comparison of Silent Canyon Caldera Margins:
Base HFM Model and SCCC Alternative (Modified from BN, 2002)

Table 2-7
Correlation of Hydrostratigraphic Units Between the Silent Canyon Caldera Complex HFM and the Base HFM

UGTA Base Model HSUs	Alternative SCCC Model HSUs
Thirsty Canyon Volcanic Aquifer	Silent Canyon Timber Mountain Composite Unit
Tannenbaum Hill Lava-Flow Aquifer	
Tannenbaum Hill Composite Unit	
Timber Mountain Aquifer	
Fluorspar Canyon Confining Unit	
Windy Wash Aquifer	
Paintbrush Vitric-Tuff Aquifer	
Benham Aquifer	Silent Canyon Benham Aquifer
Upper Paintbrush Confining Unit	
Tiva Canyon Aquifer	Silent Canyon Tiva Canyon Aquifer
Paintbrush Lava-Flow Aquifer	Silent Canyon Lower Paintbrush Confining Unit
Lower Paintbrush Confining Unit	
Topopah Spring Aquifer	Silent Canyon Topopah Spring Aquifer
Calico Hills Vitric-Tuff Aquifer	Silent Canyon Calico Hills Composite Unit
Calico Hills Vitric Composite Unit	
Calico Hills Zeolitic Composite Unit	
Calico Hills Confining Unit	
Inlet Aquifer	Silent Canyon Inlet Aquifer
Crater Flat Composite Unit	Silent Canyon Crater Flat Composite Unit
Crater Flat Confining Unit	
Kearsarge Aquifer	
Bullfrog Confining Unit	Silent Canyon Bullfrog Confining Unit
Belted Range Aquifer	Silent Canyon Belted Range Aquifer
Pre-Belted Range Composite Unit	Silent Canyon Pre-Belted Range Composite Unit
Silent Canyon Intrusive Confining Unit	Silent Canyon Intrusive Confining Unit

Source: Modified from SNJV, 2004a

Note: The HSU names used in the alternative model were modified by adding the prefix "Silent Canyon" for differentiation purposes.

Significant differences also exist in the configuration of the HSU surfaces. The surfaces of the HSUs are less rugged in the SCCC model than in the base HFM. Within the SCCC area, the upper surfaces of HSUs in the SCCC HFM (Figure 2-4) are generally bowl-shaped, and dip more gently than those in the base HFM (Figure 2-5). Upper surfaces of HSUs in the SCCC HFM are also higher along the down-thrown sides of faults, and lower along the up-thrown sides (BN [2002] and McKee et al. [1999 and 2001] show the same section line through the BN HFM).

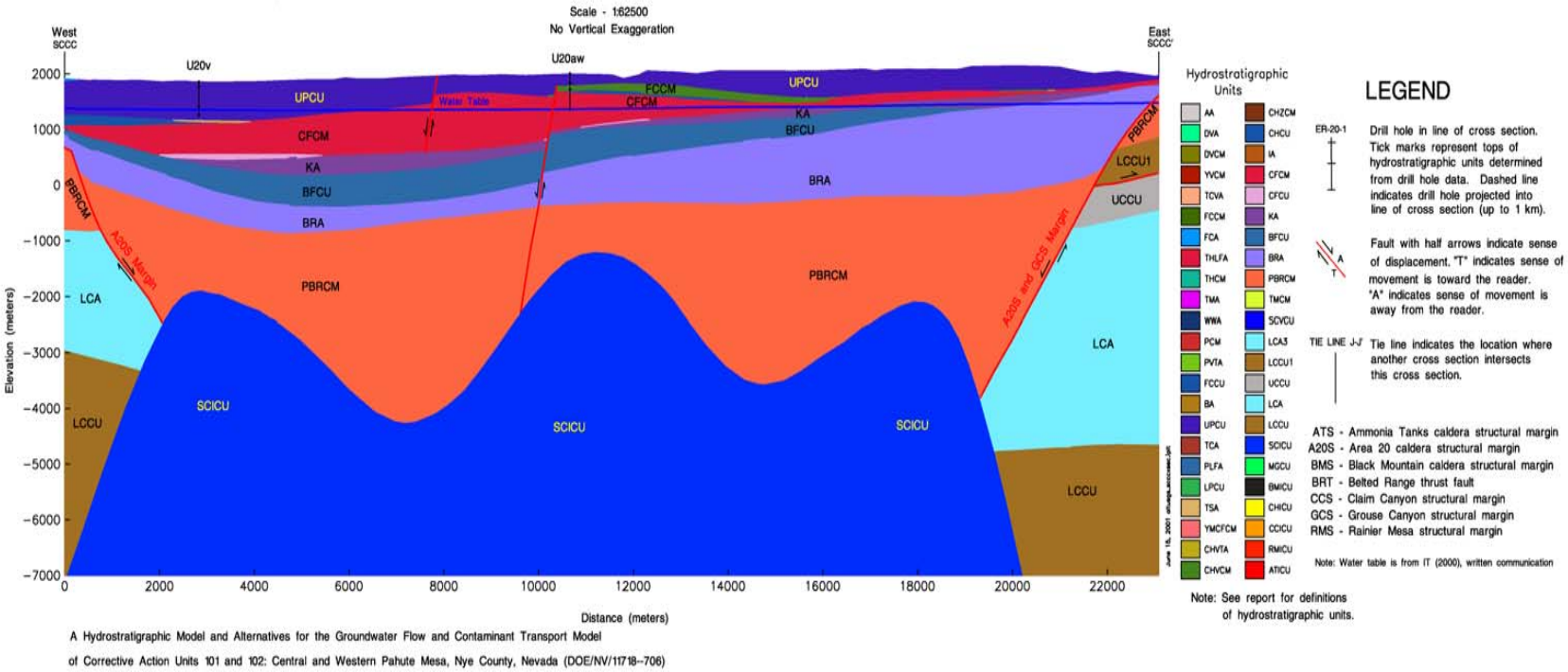

Figure 2-4
Typical West-East Cross Section through the Silent Canyon Caldera for the SCCC Model (BN, 2002)
Cross-section location shown in Figure 2-2.

Uncontrolled When Printed

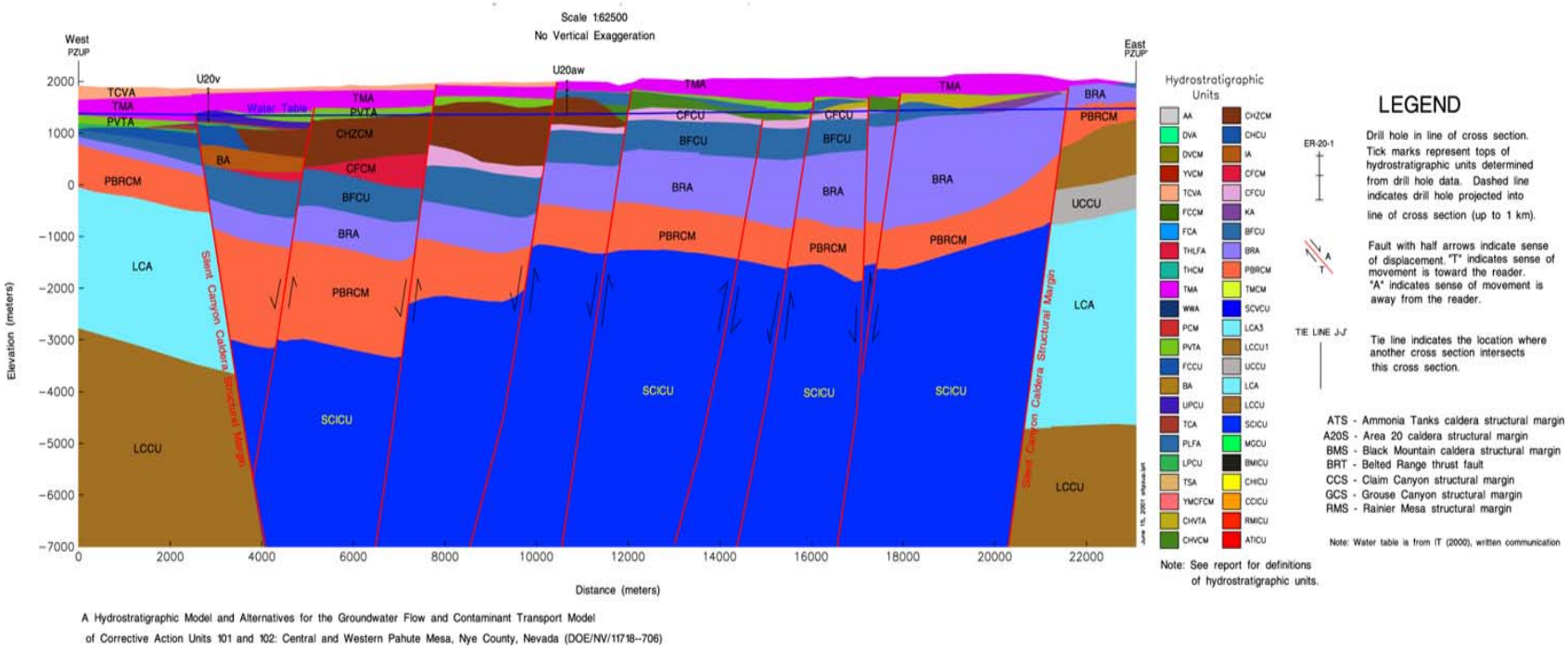

Figure 2-5
Typical West-East Cross Section through the Silent Canyon Caldera for the BN Model (BN, 2002)
Cross-section location shown in Figure 2-2.

Uncontrolled When Printed

The differences in the locations of caldera margins and in structure result in differences in HSU thicknesses. Generally, the thicknesses of HSUs located within the SCCC vary to a greater degree in the base HFM. In comparison, in the SCCC HFM, the HSUs are generally lens-shaped. These lenses are thick in the middle and thin out towards the margins of the SCCC (BN, 2002).

The hydrogeologic importance of the Calico Hills Formation in the SCCC area is recognized in both the base and SCCC HFMs. It is, however, handled differently in the two models. In the base HFM, the Calico Hills Formation is subdivided into four HSUs based on differences in lithologic composition and alteration effects, whereas it is treated as a single composite unit in the SCCC HFM (Table 2-7). A more detailed discussion of the SCCC HFM may be found in the HFM report (BN, 2002).

2.3 Groundwater Characteristics

This section summarizes data, information, and alternative component models that characterize the groundwater budget and general flow directions in the Pahute Mesa flow domain.

2.3.1 Inflow and Outflow (Lateral Boundary Fluxes)

A set of boundary fluxes to be used with the CAU flow model have been developed based on results generated for eight alternate regional-scale flow models using the UGTA regional model (DOE/NV, 1997). The eight models represent combinations of different flow system conceptual models and recharge models. Hydrostratigraphic models reflecting the different conceptual models were chosen from a larger set of conceptual models based on the difference in the flow field (and associated radionuclide transport) they generate. The recharge models represent different methods of approximating recharge for the NTS area (see Section 2.3.2). The alternate flux boundary conditions can be used to help evaluate the uncertainty in the CAU flow model associated with the choice of a flow system conceptual model (and associated HFM) and recharge model. A more detailed discussion of the development of boundary fluxes is provided in SNJV (2004a, Section 9.0). The range in net boundary flux across each of the CAU model boundaries is summarized in Table 2-8. These fluxes are rounded to the nearest 100 m^3/d for presentation. The approach used to calculate these fluxes does not specify the location or locations on the boundary where the flux occurs, just

Uncontrolled When Printed

Table 2-8
Summary of Net Boundary Flux Ranges (m^3/d)

Model Boundary	Range in Net Inflow	Range in Net Outflow
Northern	14,000 to 28,000	100 to 6,700
Southern	200 to 3,500	26,000 to 54,000
Eastern	5,600 to 17,000	300 to 5,000
Western	1,700 to 17,000	2,400 to 17,000

Source: SNJV, 2004a

bounds on the total amount of flow. More specific ranges were developed for the CAU model using the interpolation approach and tools developed by LANL (Gable and Cherry, 2001) (see Section 5.2).

2.3.2 Precipitation and Recharge

The groundwater flow system of the Pahute Mesa area is replenished by areal recharge from precipitation and inflow into the Pahute Mesa area. Inflow is summarized in Section 2.3.1.

In the arid environment of the NTS region, quantification of precipitation recharge is an important aspect of the groundwater flow system. This section provides a summary of precipitation distribution for the NTS area and recharge estimates from this precipitation for six alternative recharge models.

2.3.2.1 Precipitation Distribution

The distribution of mean annual precipitation is shown on Figure 2-6. Figure 2-6 was generated from the precipitation station data only. Table 2-9 summarizes the precipitation stations used in this evaluation. As indicated by Figure 2-6, the precipitation depth increases with increasing land surface elevation and follows the general topography. On the NTS, precipitation ranges from a high of approximately 32.4 centimeters per year (cm/yr) (12.76 inches per year [in./yr]) at the Area 12 Mesa Station to a low of 12.7 cm/yr (5.0 in./yr) at the Well 5B Station.

Table 2-10 compares precipitation totals calculated for hydrographic areas. The total precipitation calculated from the precipitation distribution (column 3) only includes the precipitation within the UGTA groundwater flow system boundary. Any precipitation outside the groundwater flow system boundary is not included in the total for the hydrographic area. Total precipitation from Scott et al.

Uncontrolled When Printed

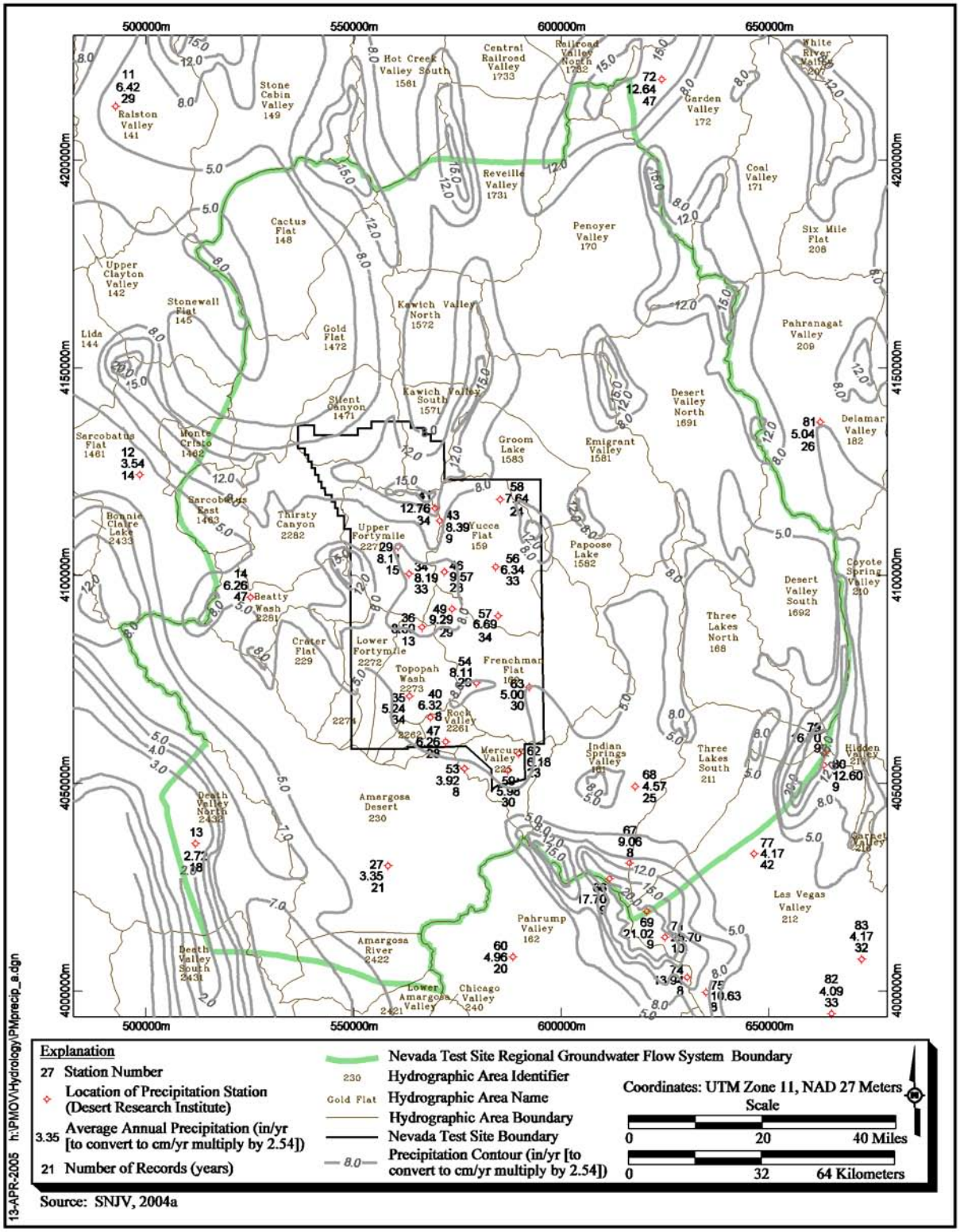

Figure 2-6
Precipitation Map for the Nevada Test Site Region

Table 2-9
Precipitation Station Data
(Page 1 of 2)

Station Number	Station Name	UTM Zone 11, NAD 27		Land Surface Elevation (m)	Average Annual Precipitation	
		Easting (m)	Northing (m)		Depth cm/yr (in./yr)	Years Record
11	Tonopah Airport	492,689	4,213,009	1,655	16.3 (6.42)	29
12	Sarcobatus	498,522	4,124,251	1,225	9.0 (3.54)	14
13	Death Valley	511,946	4,035,517	-52	6.9 (2.72)	18
14	Beatty	525,210	4,094,706	1,082	15.9 (6.26)	47
27	Lathrop Wells	558,275	4,030,159	664	8.5 (3.35)	21
29	Little Feller 2	560,698	4,106,882	1,573	20.6 (8.11)	15
34	40 MN	563,341	4,100,364	1,469	20.8 (8.19)	33
35	4JA	563,445	4,071,032	1,043	13.3 (5.24)	34
36	Shoshone Basin	566,464	4,087,547	1,725	21.6 (8.50)	13
40	Skull Mountain Pass	568,500	4,065,887	1,186	16.1 (6.32)	8
41	Area 12 Mesa	569,624	4,116,171	2,283	32.4 (12.76)	34
43	Stockade Pass	570,759	4,113,178	2,053	21.3 (8.39)	9
46	Tippipah Spring 2	571,887	4,100,851	1,518	24.3 (9.57)	28
47	RV-1	572,151	4,060,050	1,036	15.9 (6.26)	28
49	Mid Valley	573,701	4,091,914	1,420	23.6 (9.29)	29
53	RV-Wash	576,721	4,053,568	866	10.0 (3.92)	8
54	Cane Springs	579,583	4,074,185	1,219	20.6 (8.11)	29
56	BJY	584,209	4,102,022	1,241	16.1 (6.34)	33
57	Yucca	584,791	4,090,231	1,195	17.0 (6.69)	34
58	PHS Farm	585,301	4,118,280	1,391	19.4 (7.64)	24
59	Desert Rock	587,122	4,053,108	1,005	15.2 (5.98)	30
60	Pahrump	588,385	4,008,227	823	12.6 (4.96)	20
62	Mercury	589,740	4,057,169	1,149	15.7 (6.18)	23
63	Well 5B	592,263	4,073,193	939	12.7 (5.00)	30
66	Trough Spring	610,107	4,026,349	2,512	45.0 (17.70)	9
67	Cold Creek	613,563	4,030,708	1,862	23.0 (9.06)	8
68	Indian Springs	617,793	4,049,256	951	11.6 (4.57)	25
69	Lee Canyon	619,087	4,018,516	2,594	53.4 (21.02)	9
71	Kyle Canyon	623,466	4,012,260	2,365	67.8 (26.70)	10
72	Adaven	624,188	4,219,501	1,905	32.1 (12.64)	47
74	Roberts Ranch	627,418	4,003,163	1,862	35.4 (13.94)	8
75	Red Rock Summit	631,972	3,999,532	1,984	27.0 (10.63)	8
79	Hayford Peak	660,932	4,058,248	2,999	42.4 (16.70)	9

Uncontrolled When Printed

Table 2-9
Precipitation Station Data
(Page 2 of 2)

Station Number	Station Name	UTM Zone 11, NAD 27		Land Surface Elevation (m)	Average Annual Precipitation	
		Easting (m)	Northing (m)		Depth cm/yr (in./yr)	Years Record
80	Hidden Forest	660,934	4,055,504	2,304	32.0 (12.60)	9
81	Alamo	662,347	4,136,921	1,049	12.8 (5.04)	26
82	Las Vegas Airport	665,072	3,994,546	661	10.4 (4.09)	33
83	Sunrise Manor	672,321	4,007,633	555	10.6 (4.17)	32

Source: SNJV, 2004a

(1971) is included in the table for comparison (columns 4 and 5). The footnoted totals in column 4 were prorated based on the area within the flow system boundary using the following equation: (published precipitation total) x ([area within flow system boundary] ÷ [total area of hydrographic area]).

In general, the comparison between the calculated precipitation and published precipitation is reasonably good; the difference between the two totals is 118,343 m^3/d. For each, the maximum precipitation is found in the Tikaboo and Emigrant Valley hydrographic areas. The precipitation totals for those hydrographic areas including testing areas (Gold Flat, Yucca Flat, and Frenchman Flat) are similar to the published data. The hydrographic areas with the largest discrepancy between totals are the Las Vegas Valley and Amargosa Desert. These hydrographic areas lend very little, if any, recharge to the UGTA groundwater flow system and should not affect the modeling results.

2.3.2.2 Alternative Recharge Models

Three basic approaches have been used to develop alternative recharge models for the NTS area (including the Pahute Mesa flow model area). These are:

- Maxey-Eakin estimation techniques
- Net infiltration-recharge distributed parameter modeling
- Chloride mass-balance modeling

Uncontrolled When Printed

Table 2-10
Comparison of Calculated Precipitation Volumes to Published Values by Hydrographic Area
(Page 1 of 2)

Hydrographic Area		Total Precipitation Calculated from Distribution (m^3/d)	Published Precipitation Data (Scott et al., 1971)	
Hydrographic Area No.	Hydrographic Area Name		Total Precipitation within Flow System (m^3/d)	Total Precipitation in Hydrographic Area (m^3/d)
145	Stonewall Flat	2,546	4,878	371,737
146	Sarcobatus Flat	202,290	311,556	642,091
147	Gold Flat	889,195	844,856	844,856
148	Cactus Flat	491,956	439,325	439,325
149	Stone Cabin Valley	1,471	2,402	1,182,799
156	Hot Creek Valley	1,846	2,544	1,317,976
157	Kawich Valley	622,296	506,914	506,914
158	Emigrant Valley	1,164,236	959,757	959,757
159	Yucca Flat	461,941	337,942	337,942
160	Frenchman Flat	511,223	506,914	506,914
161	Indian Springs Valley	728,691	912,445	912,445
162	Pahrump Valley	1,531	5,397	1,419,358
168	Three Lakes Valley North	276,120	371,737	371,737
169	Tikaboo Valley	1,260,641	1,284,181	1,284,181
170	Penoyer Valley	1,127,129	912,445	912,445
171	Coal Valley	835	1,249	574,502
172	Garden Valley	68,283	115,092	777,268
173	Railroad Valley South	681,245	844,856	844,856
209	Pahranagat Valley	1,446	3,564	912,445
210	Coyote Spring Valley	13,005	18,106	743,473
211	Three Lakes Valley South	359,289	439,325	439,325
212	Las Vegas Valley	248,265	613,223	2,230,420
225	Mercury Valley	104,576	128,418	128,418
226	Rock Valley	85,759	87,865	87,865
227	Fortymile Canyon	715,443	669,126	669,126
228	Oasis Valley	660,013	506,914	506,914
229	Crater Flat	153,895	206,145	206,145
230	Amargosa Desert	1,131,415	811,062	811,062

Uncontrolled When Printed

Table 2-10
Comparison of Calculated Precipitation Volumes to Published Values by Hydrographic Area
(Page 2 of 2)

Hydrographic Area		Total Precipitation Calculated from Distribution (m^3/d)	Published Precipitation Data (Scott et al., 1971)	
Hydrographic Area No.	Hydrographic Area Name		Total Precipitation within Flow System (m^3/d)	Total Precipitation in Hydrographic Area (m^3/d)
242	Amargosa River	117,067	117,067[a]	--
243	Death Valley	398,318	398,318[a]	--
	Total Precipitation:	**12,481,966**	**12,363,623**	--

Source: SNJV, 2004a

[a]Calculated hydrographic area total is included in published precipitation total. Published data for this hydrographic area are not available at time of printing.

The Maxey-Eakin approach is an empirically-derived method relating recharge to precipitation zones from a base precipitation map. Several modified versions of this approach are analyzed, including a model from the UGTA regional groundwater flow modeling results and a revised Maxey-Eakin model using a revised base precipitation map.

Maxey and Eakin (1949) first described a method of estimating recharge to groundwater from precipitation in a report on groundwater in White River Valley, Nevada. In this method recharge is estimated from precipitation by assuming that a set percentage of precipitation recharge occurs for specific ranges of precipitation. The initial percentages (Maxey-Eakin coefficients) were: 0 percent recharge for precipitation less than 20.3 centimeters (cm); 3 percent recharge when precipitation ranges between 20.3 to 30.5 cm; 7 percent recharge when precipitation ranges between 30.5 to 38 cm; 15 percent recharge when precipitation ranges between 38 to 50.8 cm; and 25 percent recharge when precipitation is greater than 50.8 cm. These Maxey-Eakin coefficients were determined by trial and error by balancing of recharge with estimates of groundwater discharge for 13 valleys in east-central Nevada (Maxey and Eakin, 1949).

Uncontrolled When Printed

The recharge distribution used in the UGTA regional groundwater flow model (DOE/NV, 1997) was constructed using a modification of the Maxey-Eakin method (1949). This modification incorporated:

- An updated precipitation map using new and existing data
- The calculation of recharge using modified Maxey-Eakin coefficients
- The calculation of total recharge volumes for individual hydrographic areas
- The redistribution of a percentage of the total recharge within selected subareas to stream channels

Figure 2-7 shows the Maxey-Eakin recharge distribution for the UGTA Regional Model. This recharge distribution model is designated as the UGTA Regional Model recharge alternative (SNJV, 2004a).

Subsequent to the development of the UGTA regional flow model (DOE/NV, 1997) a revised recharge distribution was generated for the NTS area by updating the original UGTA recharge model. The update included the redigitization and recontouring of the precipitation map, and the redigitization of the hydrographic areas using larger-scale maps. Following the update, a comparison to other recharge models was conducted. This updated recharge distribution model is designated as the UGTA Revised Maxey-Eakin recharge alternative. Figure 2-8 shows the UGTA Revised Maxey-Eakin recharge distribution in the NTS area.

Two alternative recharge models are taken from the USGS net infiltration/recharge model (Hevesi et al., 2003). The USGS net infiltration/recharge model is a distributed parameter watershed model to estimate temporal and spacial distribution of net infiltration for the Death Valley region. The major components of this model include infiltration of rain, snowmelt, or surface water into the soil or bedrock, with subsequent bare-soil evaporation and transpiration from the root zone. All water percolating past the root zone is considered net infiltration. The two alternative USGS recharge models include the recharge model that includes a runoff/run-on component (USGSD) and the recharge model that does not include the runoff/run-on component (USGSND). Figures 2-9 and 2-10 show the recharge distribution for these two alternative models.

Uncontrolled When Printed

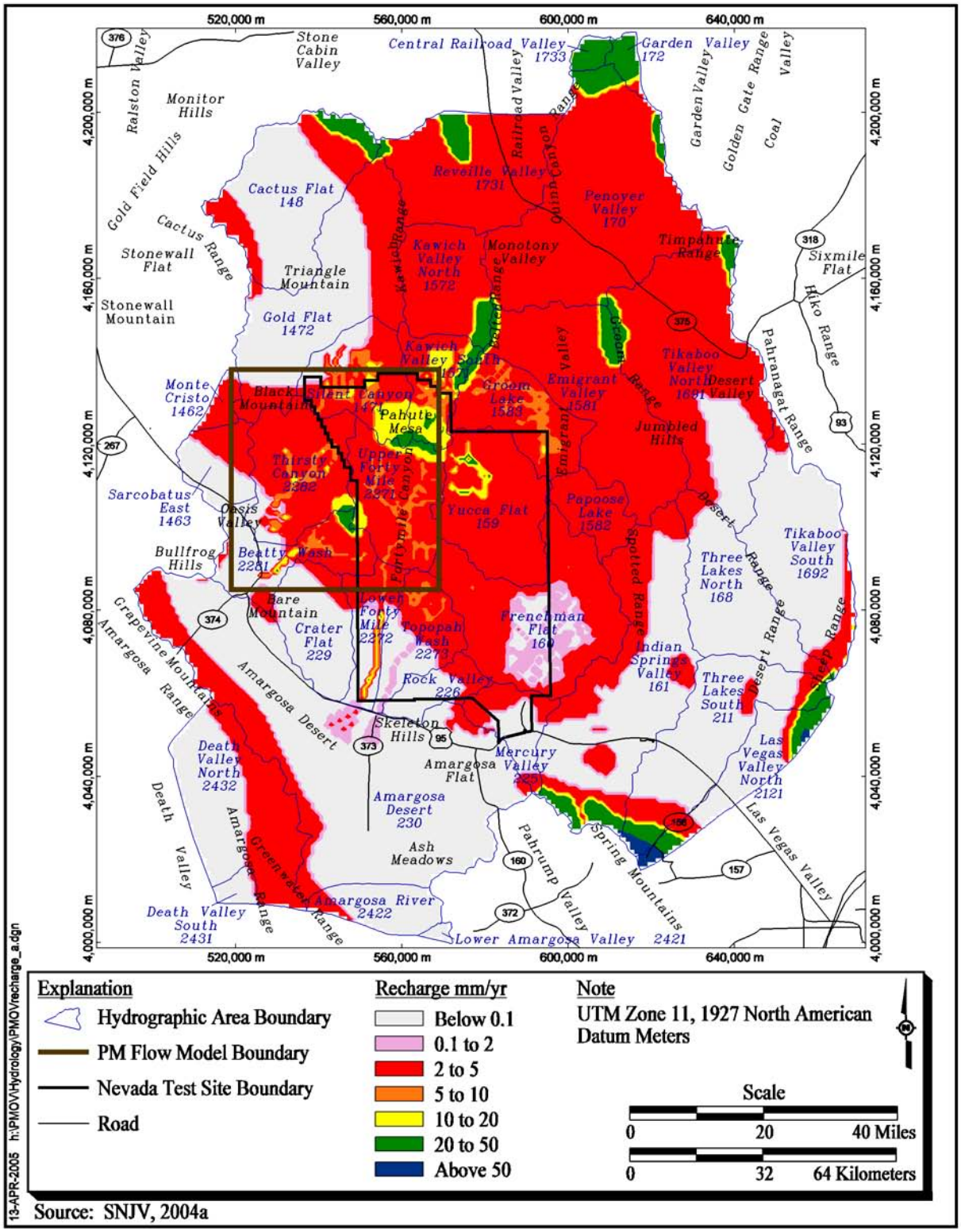

Figure 2-7
UGTA Regional Model Recharge Distribution

Uncontrolled When Printed

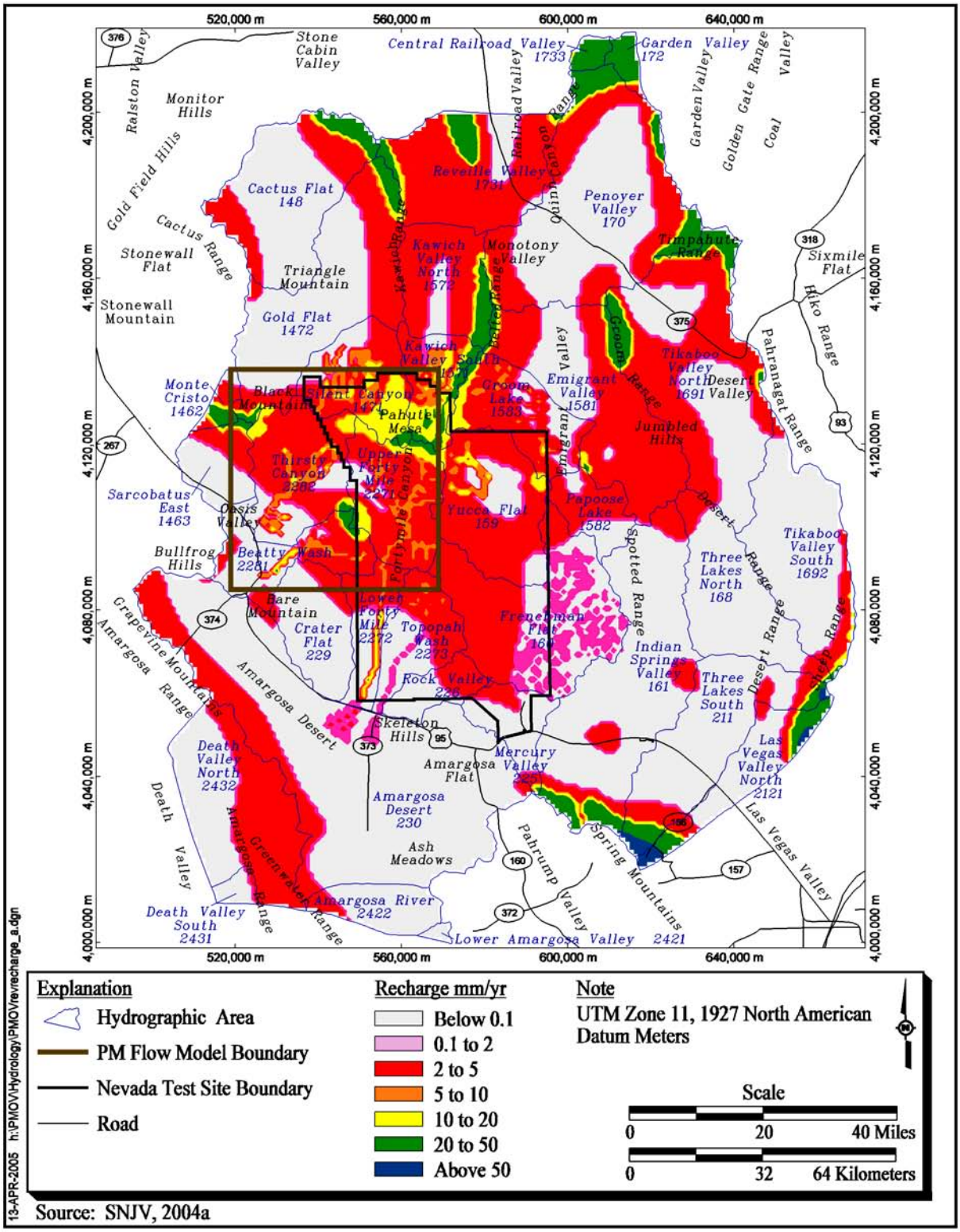

Figure 2-8
UGTA Revised Maxey-Eakin Recharge Distribution in the NTS Region

Uncontrolled When Printed

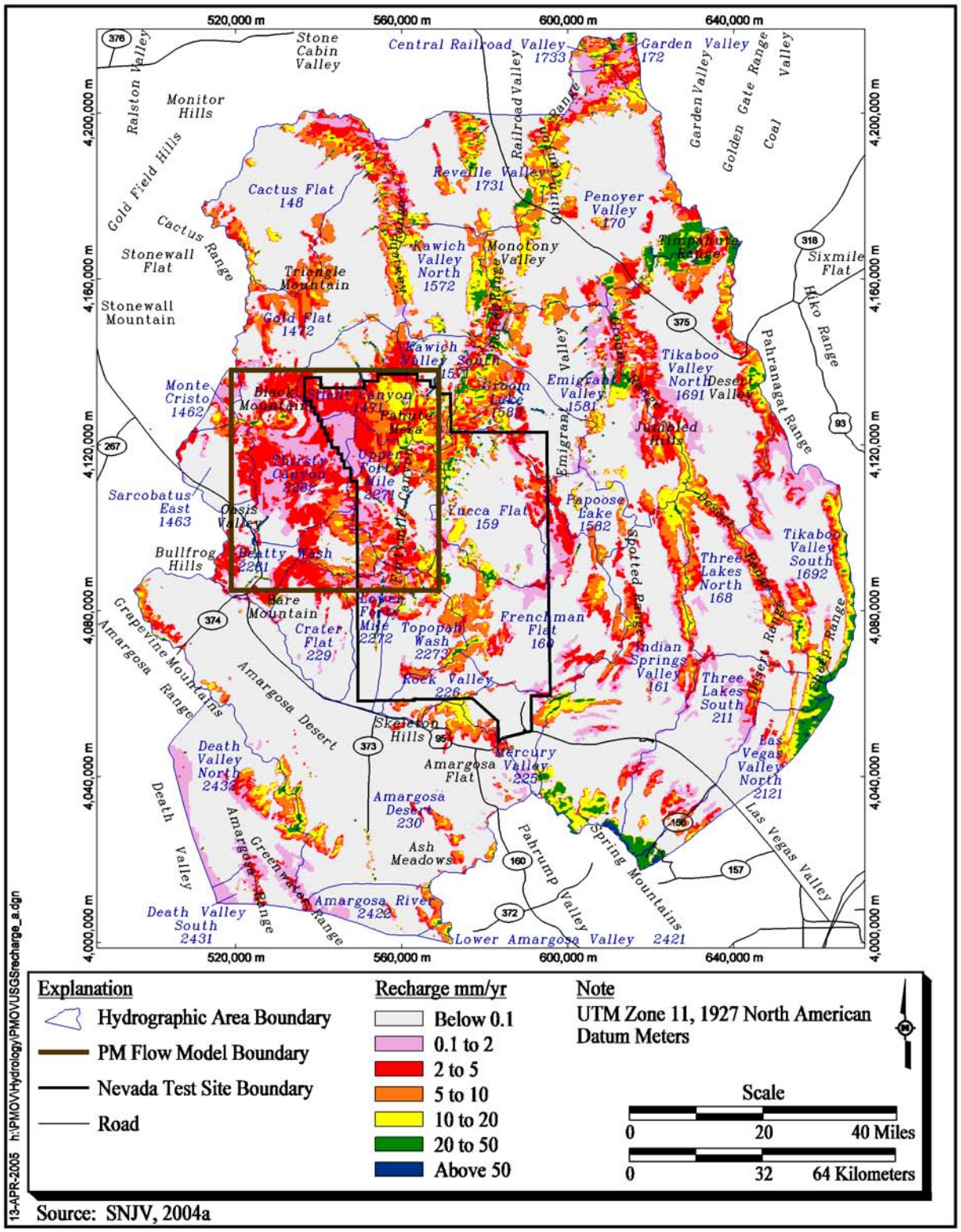

Figure 2-9
USGS Recharge Distribution Model (USGSD), Overland Flow Component Included

Uncontrolled When Printed

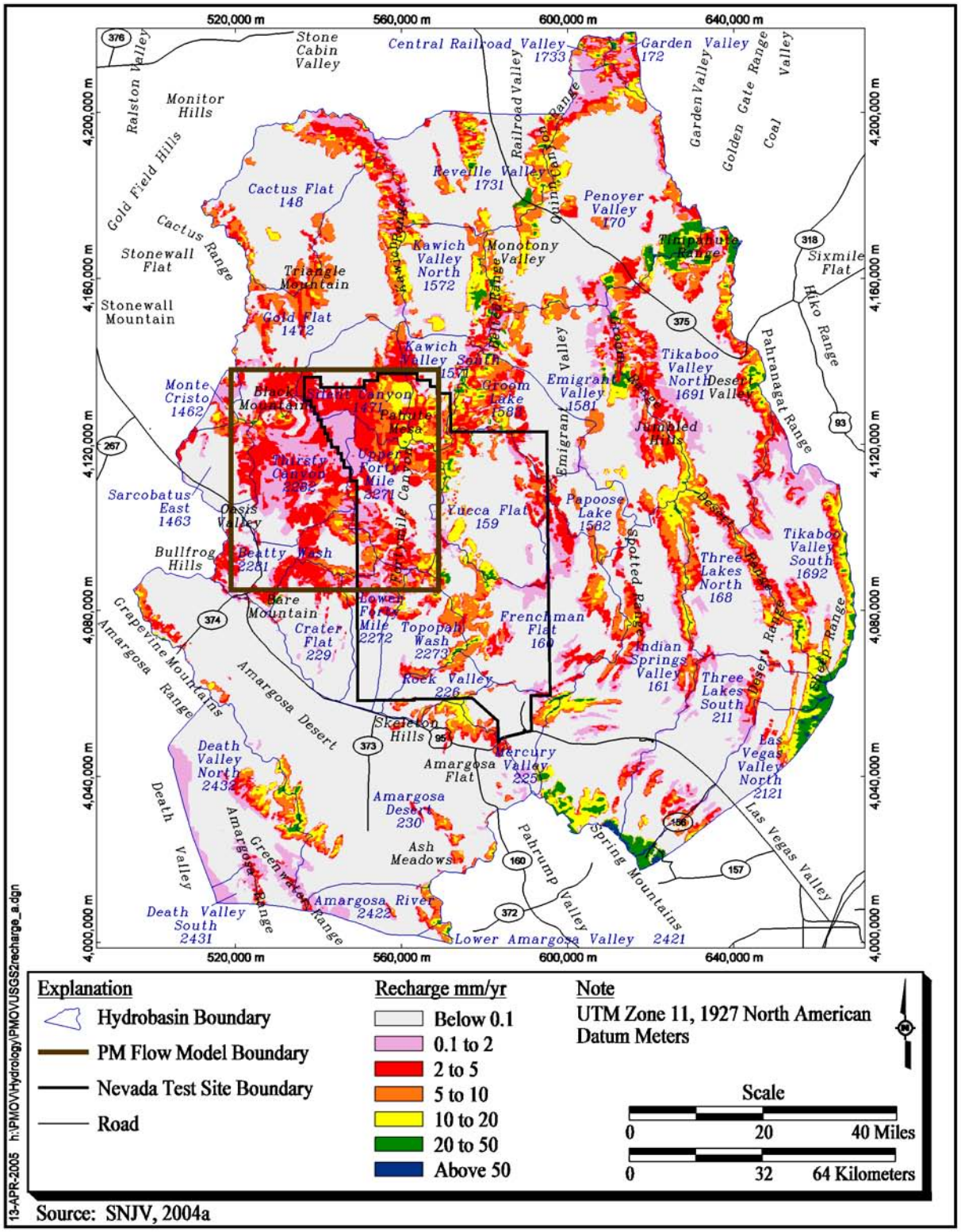

Figure 2-10
USGS Recharge Distribution Model (USGSND), No Overland Flow Component

Uncontrolled When Printed

Two alternative recharge models have been developed by DRI for the NTS area using an elevation-dependent chloride mass-balance approach (Russell and Minor, 2002). The DRI chloride mass-balance approach estimates recharge by analyzing the chloride ratios of precipitation and groundwater. Higher chloride concentrations in groundwater discharged from springs result from ET of precipitation that contains low amounts of conservative atmospheric chloride ion, thus providing a relative gauge of recharge. This information, in conjunction with soil chloride profiles in differing recharge locales (wash versus non-wash), allowed DRI to estimate recharge and associated confidence intervals. The alternative recharge models included one model for no recharge in the alluvial areas (DRI alluvial mask alternative) and one model for no recharge in the alluvial areas and no recharge below an elevation of 1,237 m (DRI alluvial and elevation mask alternative). The data for each model were compiled in a geographic information system and used in a Monte Carlo analysis to determine recharge in the study area. Results of the analysis yielded estimates of the mean and standard deviation of recharge. The resultant recharge distributions for the entire UGTA regional model area for the alluvial mask alternative 50th percentile is shown in Figure 2-11. The recharge distribution for the alluvial and elevation mask, alternative 50th percentile distribution is shown in Figure 2-12 (SNJV, 2004a).

Comparison of recharge volumes in the NTS area for all alternative recharge models are summarized in Table 2-11. The recharge volumes for both UGTA-based recharge distributions differ from the original values found in the UGTA regional flow model report (DOE/NV, 1997) because of the changes to the definitions of the hydrographic areas. The UGTA Revised Maxey-Eakin recharge distribution model was chosen as the base recharge model for use in groundwater flow modeling because, in general, the method yields recharge volumes that are within the ranges of the other models. The other alternative recharge models are incorporated into the Pahute Mesa flow model to evaluate uncertainty associated with recharge.

2.4 Surface Groundwater Discharge

Within the Pahute Mesa area and vicinity, most groundwater discharge to the surface occurs naturally in the form of ET and springs at the Oasis Valley discharge area. Some groundwater is also withdrawn from the flow system by wells. The area of interest to this activity includes the Pahute Mesa area and all of the Oasis Valley hydrographic area because the discharge area extends outside of

Uncontrolled When Printed

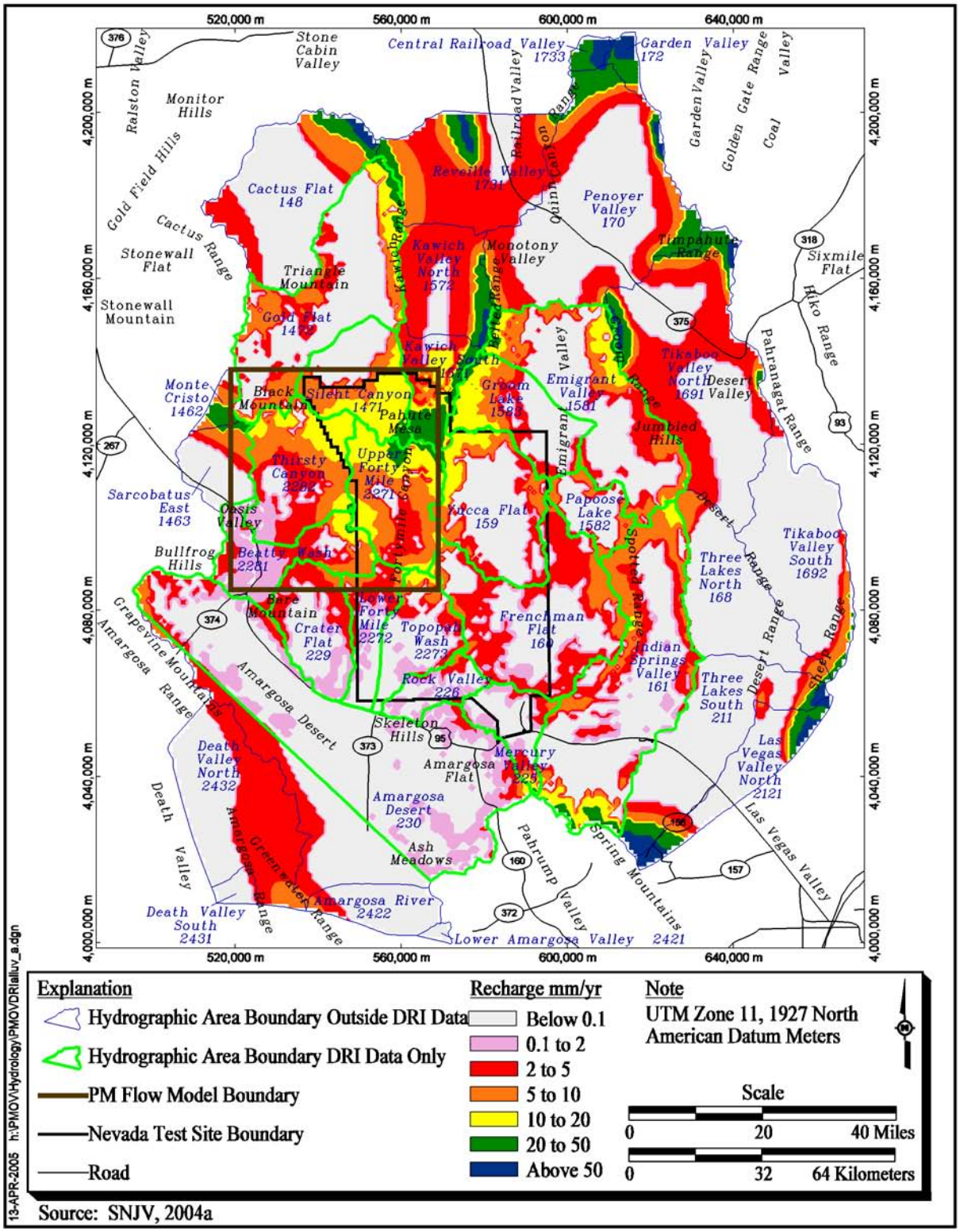

Figure 2-11
DRI Recharge Distribution with Alluvial Mask
(Russell and Minor, 2002)

Uncontrolled When Printed

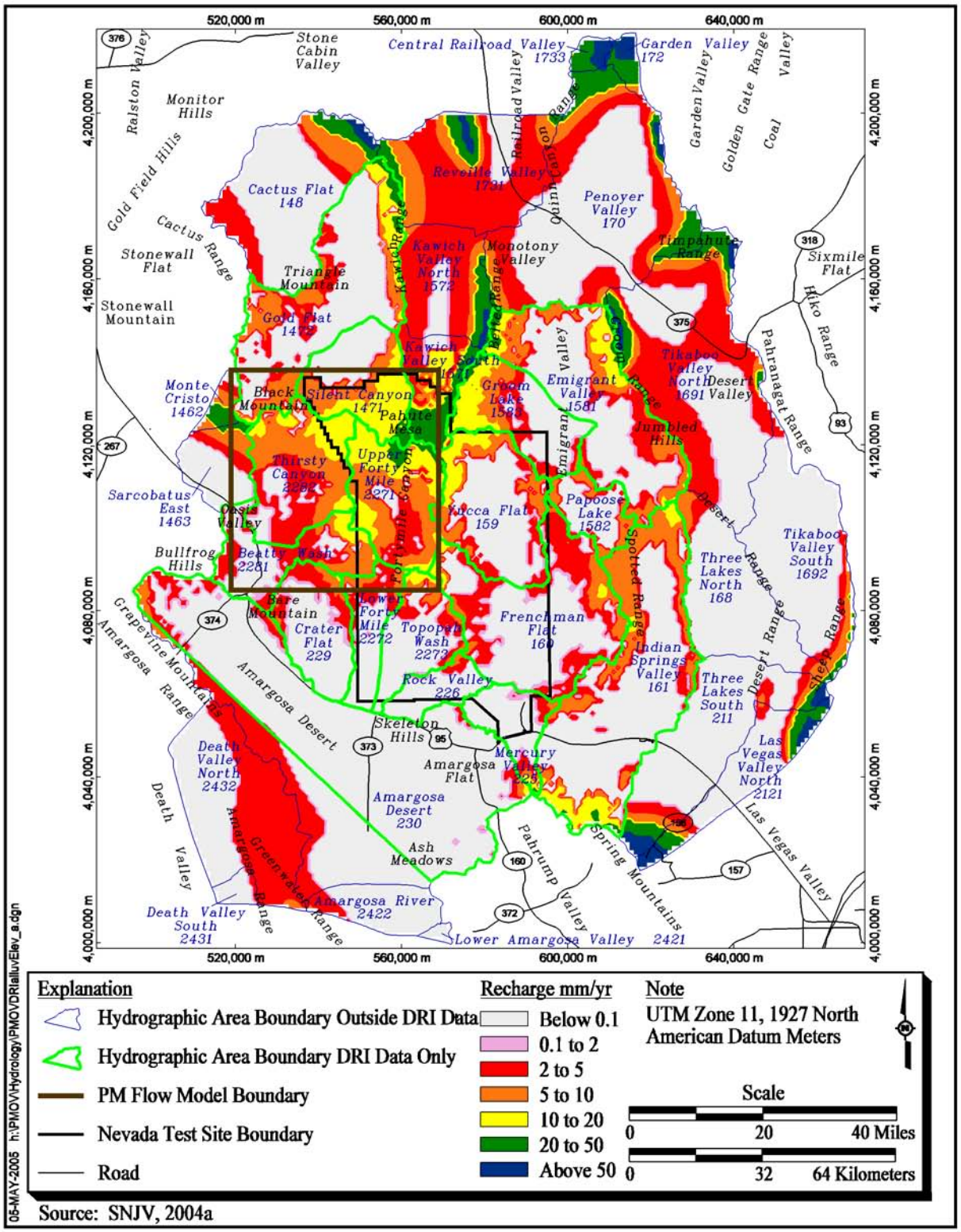

Figure 2-12
DRI Recharge Distribution with Alluvial and Elevation Mask
(Russell and Minor, 2002)

Uncontrolled When Printed

Table 2-11
Recharge Volumes for Hydrographic Areas for all Recharge Models
(Page 1 of 2)

Subarea Number	Area Name	Secondary Name	UGTA	UGTA	USGS	USGS	DRI-Alluvial Mask Only			DRI-Alluvial and Elevation Mask		
			Regional Model Phase I (m^3/yr)	Revised Maxey-Eakin Based (m^3/yr)	Model 1 (m^3/yr)	Model 2 (m^3/yr)	5% (m^3/yr)	50% (m^3/yr)	95% (m^3/yr)	5% (m^3/yr)	50% (m^3/yr)	95% (m^3/yr)
1462	Sarcobatus Flat-2	Monte Cristo	324,700	794,500	162,400	153,300		1,277,000			1,196,000	
1463	Sarcobatus Flat-3	Sarcobatus East	420,300	568,900	297,400	280,800		922,300			861,700	
1471	Gold Flat-1 & 2	Silent Canyon	4,739,000	6,389,000	5,269,000	4,052,000	3,889,000	8,350,000	12,810,000	3,889,000	8,350,000	12,810,000
148	Cactus Flat		3,147,000	3,304,000	1,653,000	1,326,000		4,814,000			4,643,000	
1571	Kawich Valley-1 & 2	Kawich Valley South	6,952,000	7,456,000	4,372,000	2,923,000	2,063,000	5,176,000	8,289,000	2,063,000	5,176,000	8,289,000
1582	Emigrant Valley-2	Papoose Lake	887,800	466,900	412,600	305,300	352,800	552,800	752,700	352,800	552,800	752,700
1581	Emigrant Valley-1 & 3[a]	Emigrant Valley	7,891,000	5,982,000	6,897,000	4,510,000	3,805,000	7,375,000	10,950,000	3,805,000	7,375,000	10,950,000
159	Yucca Flat		2,589,000	2,040,000	1,950,000	1,508,000	1,467,000	2,465,000	3,463,000	1,459,000	2,456,000	3,453,000
160	Frenchman Flat		2,542,000	1,466,000	2,340,000	2,183,000	1,560,000	2,506,000	3,452,000	1,404,000	2,224,000	3,044,000
161	Indian Springs Valley		4,741,000	3,655,000	4,376,000	4,210,000	2,842,000	5,013,000	7,184,000	2,610,000	4,772,000	6,934,000
168	Three Lakes Valley North		300,600	319,000	1,824,000	1,819,000		521,900			486,400	
1691	Tikaboo Valley-1	Tikaboo Valley North	5,997,000	6,452,000	4,595,000	4,241,000		8,182,000			8,254,000	
1692	Tikaboo Valley-2	Tikaboo Valley South	606,700	760,400	2,401,000	2,402,000		1,224,000			1,146,000	
170	Penoyer Valley		8,382,000	6,487,000	6,289,000	5,175,000		8,213,000			8,291,000	
172	Garden Valley		1,859,000	2,476,000	587,500	478,600		3,731,000			3,562,000	
1731	Railroad Valley South-1	Reveille Valley	5,416,000	5,464,000	2,696,000	2,266,000		7,253,000			7,207,000	
1733	Railroad Valley South-3	Central Railroad Valley	1,914,000	1,920,000	373,500	290,000		2,957,000			2,805,000	

Uncontrolled When Printed

Table 2-11
Recharge Volumes for Hydrographic Areas for all Recharge Models
(Page 2 of 2)

Subarea Number	Area Name	Secondary Name	UGTA	UGTA	USGS	USGS	DRI-Alluvial Mask Only			DRI-Alluvial and Elevation Mask		
			Regional Model Phase I (m^3/yr)	Revised Maxey-Eakin Based (m^3/yr)	Model 1 (m^3/yr)	Model 2 (m^3/yr)	5% (m^3/yr)	50% (m^3/yr)	95% (m^3/yr)	5% (m^3/yr)	50% (m^3/yr)	95% (m^3/yr)
211	Three Lakes Valley South		4,221,000	4,220,000	2,143,000	2,117,000		5,916,000			5,775,000	
2121	Las Vegas Valley-1		5,063,000	5,083,000	2,412,000	2,382,000		6,863,000			6,781,000	
225	Mercury Valley		424,800	229,300	475,000	446,400	307,600	480,600	653,700	236,500	370,700	504,900
226	Rock Valley		176,700	239,200	385,200	374,600	103,300	193,200	283,000	58,500	94,940	131,400
2271	Fortymile Canyon-1	Upper Fortymile	3,477,000	3,679,000	2,545,000	1,709,000	3,241,000	5,951,000	8,662,000	3,241,000	5,951,000	8,662,000
2272	Fortymile Canyon-2 & 3	Lower Fortymile	1,129,300	1,018,800	1,932,900	1,146,300	916,000	1,426,000	1,936,000	832,700	1,303,000	1,772,000
2281	Oasis Valley-1 & 2	Beatty Wash	4,022,000	4,138,000	3,041,000	2,380,800	3,866,000	6,149,000	8,432,000	3,642,000	5,860,000	8,078,000
229	Crater Flat		179,800	187,800	347,500	327,500	395,500	661,400	927,300	335,400	540,300	745,200
230	Amargosa Desert		1,457,000	1,456,000	1,893,000	1,730,000		2,548,000			1,958,000	
2421	Amargosa River-1	Lower Amargosa Valley	0	0	17,920	17,600		0			0	
2422	Amargosa River-2	Amargosa River	105,000	103,700	279,900	257,300		171,000			159,000	
2431	Death Valley Central-1	Death Valley South	15,870	23,980	41,670	37,180		39,670			36,850	
2432	Death Valley Central-2	Death Valley North	1,348,000	1,559,000	1,216,000	1,195,000		2,435,000			2,300,000	

Source: SNJV, 2004a

[a]The reported recharge volume is only for the Emigrant Valley-3 basin.

m^3/yr = Cubic meters per year

Uncontrolled When Printed

the Pahute Mesa CAU area boundary. A more detailed discussion of the evaluation of surface groundwater discharge is provided in SNJV (2004a, Section 7.0).

2.4.1 Natural Discharge

Natural discharge to the surface from the Pahute Mesa area and vicinity occurs in the form of springs and ET in the Oasis Valley discharge area. However, because of the processes involved, these two forms of discharge are not independent. In Oasis Valley, most groundwater discharged from springs does not leave the valley by surface flow. Surface water flow out of the valley occurs mostly through the Amargosa River on an intermittent basis. Spring water either re-infiltrates into the flow system or evaporates. Thus, the majority of the groundwater discharged by springs is effectively lost from the groundwater system through ET within the discharge area. In addition, ET estimates include water that moves up from the underlying regional flow system into the shallow flow system. Total spring discharge could provide a lower bound for ET estimates; however, spring flow rates are difficult to measure at the numerous seeps and at spring locations that are inaccessible. The net natural groundwater discharge to the surface is, therefore, best approximated by an estimate of ET.

2.4.2 Evapotranspiration Summary

Figure 2-13 and Table 2-12 summarize the locations and descriptions of Oasis Valley springs. Two reports provide the basis for estimates of natural discharge to the surface in the Pahute Mesa flow model area. Reiner et al. (2002) documents a comprehensive study on groundwater discharge in Oasis Valley. This study estimated groundwater discharge by quantifying ET, estimating subsurface outflow, and compiling groundwater withdrawal data. Laczniak et al. (2001) documents estimates of annual ET from discharge areas located within the Death Valley flow system, including Oasis Valley. The estimates of mean annual Oasis Valley ET from these two studies are slightly different due to differences in data interpretation. These studies are discussed in detail in SNJV (2004a, Section 7.5) and summarized below.

Evapotranspiration rates and volumes as derived by Reiner et al. (2002) and Laczniak et al. (2001) were determined for 10 different ET units in the Oasis Valley discharge area. Table 2-13 identifies these ET units. Table 2-14 compares the estimated mean annual ET for these Oasis Valley ET units from these two studies.

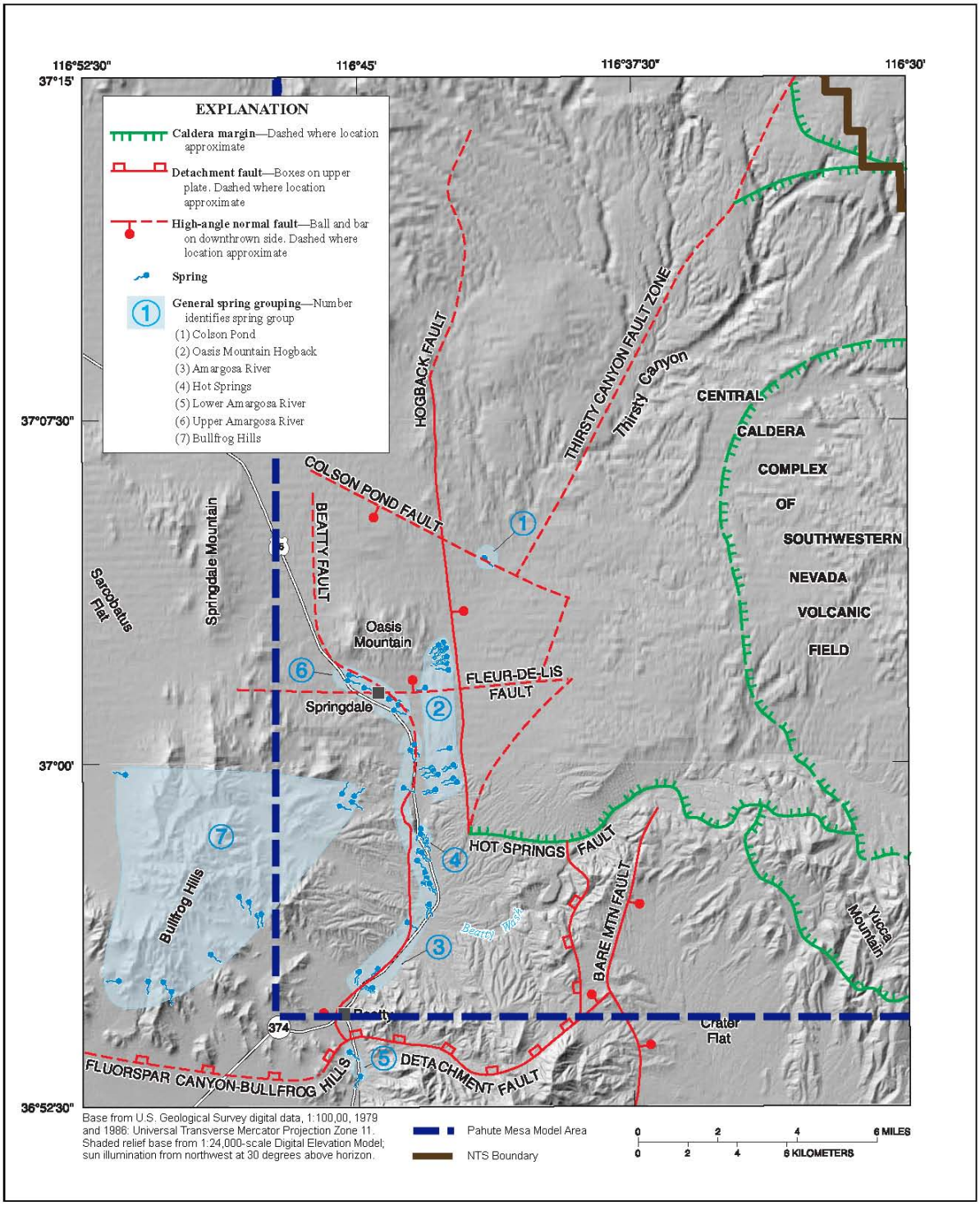

Figure 2-13
General Spring Locations and Major Structural Features Controlling Spring Discharge in Oasis Valley, NV (Modified from Reiner et al., 2002)

Uncontrolled When Printed

Table 2-12
Description of Springs Occurring in Oasis Valley

Group Number	Group Name	Probable Cause	Source
1	Colson Pond Group	Transmissivity change across the Colson Pond Fault	Likely fed by groundwater flowing from the north and northeast
2	Oasis Mountain Hogback Group	Abrupt westward thinning of the welded-tuff aquifer across the Hogback Fault	Likely fed by groundwater flowing from Pahute Mesa
3	Amargosa River Group	Transmissivity change and disruption in aquifer continuity across the Beatty Fault	Likely fed by a mixture of the groundwater flowing into Oasis Valley from the east, west, and north
4	Hot Springs Group	Upward flow along the fault (elevated water temperatures [about 105°F])	Likely fed by groundwater flow from the east and north, possibly Timber Mountain and/or Pahute Mesa
5	Lower Amargosa River Group	--	Probably fed primarily by groundwater flowing from the north through Oasis Valley
6	Upper Amargosa River Group	Transmissivity change and disruption in aquifer continuity across the Beatty Fault	Likely fed by groundwater inflow from the north and northwest (White, 1979)
7	Bullfrog Hills Group	Permeability changes within the welded-tuff aquifer caused by hydrothermal alteration	Likely fed by local recharge to nearby highlands and therefore perched

Source: SNJV, 2004a

See Figure 2-13 for locations.

In addition to mean annual ET, Laczniak et al. (2001) assessed uncertainty in annual ET using Monte Carlo simulations. Table 2-15 provides the summary statistics from this uncertainty analysis. Section 5.2 documents how these data were used in the Pahute Mesa flow model calibration.

2.4.3 Well Discharge

Wells of interest to this activity are only those that were pumped or have been pumping for longer than a year. Discharge data collected during short-term pumping such as during well testing were not included. The locations of pumping wells located within the Pahute Mesa modeling area and vicinity are shown in Figure 2-14. These include nine NTS water supply wells, one Beatty water supply well, and two mine wells (Gexa Well 4 and nearby PW-2). Well PW-2 is located within 500 m of Gexa Well 4 and was used as a substitute pumping well for Gexa Well 4 during 1997 and 1998.

Uncontrolled When Printed

Table 2-13
ET Units Determined from Spectral Analysis of Satellite Imagery Data (June 13, 1992), Oasis Valley Discharge Area, Nevada
(Page 1 of 2)

Laczniak et al. (2001)			Reiner et al. (2002)		
ET-Unit Number	ET-Unit Area (m^2)	General Description of ET Unit	ET-Unit Identifier	ET-Unit Area (m^2)	General Description of ET Unit
0	0	Area of no significant ET from groundwater source (unclassified); water table typically greater than 50 ft below land surface	UCL	0	Area of no substantial ET from ground-water source (unclassified); water table typically greater than 20 ft below land surface; soil very dry
1	4,047	Area of open water, primarily reservoir or large spring pool	OWB	4,047	Area of open water, primarily spring pool or pond
2	20,234	Area of submerged aquatic vegetation; includes sparse emergent vegetation and shallow part of open water areas; perennially loaded; water at surface	SAV	16,187	Area of submerged and sparse emergent aquatic vegetation; includes primarily shallow part of open water areas; perennially flooded; water at surface
3	161,874	Area dominated by dense wetland vegetation, primarily tall reedy and rushy marsh plants, typically tule, cattail, or giant reed; perennially flooded; water at surface	DWV	161,874	Area dominated by dense wetland vegetation, primarily tall reedy and rushy marsh plants, typically tule, cattail, or giant reed; perennially flooded; water at surface
4	3,767,627	Area dominated by dense meadow and forested vegetation, primarily trees, meadow grasses, or mixed trees, shrubs, and grasses; trees include saltcedar, mesquite, or desert willow; water table typically ranges from a few feet to about 20 ft below land surface; soil moist to dry	DMV	3,366,988	Area dominated by dense meadow and woodland vegetation, primarily trees, meadow and marsh grasses, or mixed trees, shrubs, and grasses; trees include desert ash and cottonwood, with some desert willow and mesquite; water table typically ranges from above land surface to about 20 ft below land surface; soil wet to dry
5	2,610,225	Area dominated by dense to moderately dense grassland vegetation, primarily saltgrass, and/or short rushes with an occasional tree or shrub; intermittently flooded; water table typically less than 5 ft below land surface; soil wet to moist	DGV	1,375,932	Area dominated by moderately dense to dense grassland vegetation, primarily saltgrass, and/or short rushes with an occasional tree or shrub; intermittently flooded; water table typically less than 10 ft below land surface; soil wet to moist

Uncontrolled When Printed

Table 2-13
ET Units Determined from Spectral Analysis of Satellite Imagery Data (June 13, 1992), Oasis Valley Discharge Area, Nevada
(Page 2 of 2)

Laczniak et al. (2001)			Reiner et al. (2002)		
ET-Unit Number	ET-Unit Area (m^2)	General Description of ET Unit	ET-Unit Identifier	ET-Unit Area (m^2)	General Description of ET Unit
6	3,893,079	Area dominated by sparse grassland vegetation, primarily salt and bunch grasses but also includes areas of very low density shrubs (mesquite); water table typically ranges from a few feet to about 12 ft below land surface; soil dry	SGV	4,916,935	Area dominated by sparse to moderately dense grassland vegetation, primarily salt and bunch grasses with occasional tree or shrub; water table typically ranges from a few feet below land surface to about 10 ft below land surface; soil damp to dry
7	327,796	Area dominated by moist bare soil; vegetation very sparse, primarily grasses; intermittently flooded, water table typically near land surface throughout most of the year but in some areas declines to a maximum depth of about 5 ft below land surface during late summer and early fall; soil typically moist	MBS	412,780	Area dominated by moist bare soil; vegetation very sparse, primarily grasses; intermittently flooded, water table typically near land surface throughout most of the year but in some areas declines to a maximum depth of about 5 ft below land surface during late summer and early fall; soil wet to moist
8	3,265,816	Area dominated by sparse to moderately dense shrub land vegetation, primarily greasewood, rabbitbrush, wolfberry, and seepweed; water table typically ranges from about 5 ft to about 20 ft below land surface; soil dry	SSV	3,609,799	Area dominated by sparse to moderately dense shrubland vegetation, primarily greasewood, rabbitbrush, and wolfberry; water table typically ranges from about 5 ft below land surface to about 20 ft below land surface; soil damp to dry
9	N/A	Area dominated by sparse woodland vegetation, primarily mesquite; water table typically ranges from about 10 to 40 ft below land surface; soil dry	N/A	N/A	N/A
10	4,047	Area dominated by open playa, primarily bare soil, often encrusted with salts; water table ranges from about 5 to 40 ft below land surface; soil typically dry but can be moist for short periods after intermittent flooding	N/A	N/A	N/A

Source: Modified from SNJV, 2004a

m^2 = Square meter N/A = Not applicable

Uncontrolled When Printed

Table 2-14
Estimated Mean Annual ET and Groundwater ET by ET Unit from Oasis Valley Discharge Area, Nevada

Laczniak et al., 2001						Reiner et al., 2002					
ET-Unit Identification	**Area (m^2)**	**ET Rate (m/d)**	**Annual ET (m^3)**	**Mean ET Rate (m/d)[a]**	**Mean Annual ET (m^3)**	**ET-Unit Identification**	**Area (m^2)**	**ET Rate (m/d)**	**Annual ET (m^3)**	**Mean ET Rate (m/d)[a]**	**Mean Annual ET (m^3)**
1	4,047	7.182×10^{-3}	11,101	6.764×10^{-3}	9,868	OWB	4,047	7.182×10^{-3}	10,608	6.764×10^{-3}	9,991
2	20,234	7.098×10^{-3}	51,806	6.681×10^{-3}	49,339	SAV	16,187	7.182×10^{-3}	41,938	6.764×10^{-3}	39,471
3	161,874	3.507×10^{-3}	209,692	3.090×10^{-3}	185,022	DWV	161,874	3.257×10^{-3}	197,357	2.839×10^{-3}	172,687
4	3,767,627	2.589×10^{-3}	3,577,092	2.171×10^{-3}	2,960,352	DMV	3,366,988	2.756×10^{-3}	3,330,396	2.338×10^{-3}	2,837,004
5	2,610,225	2.589×10^{-3}	2,466,960	2.171×10^{-3}	2,096,916	DGV	1,375,932	2.672×10^{-3}	1,356,828	2.255×10^{-3}	1,134,802
6	3,893,079	1.002×10^{-3}	1,480,176	5.845×10^{-4}	826,432	SGV	4,916,935	1.670×10^{-3}	2,960,352	1.253×10^{-3}	2,220,264
7	327,796	2.255×10^{-3}	271,366	1.837×10^{-3}	222,026	MBS	412,780	2.171×10^{-3}	333,040	1.754×10^{-3}	259,031
8	3,265,816	1.587×10^{-3}	1,850,220	1.169×10^{-3}	1,356,828	SSV	3,609,799	1.002×10^{-3}	1,356,828	5.845×10^{-4}	764,758
9	--	--	--	--	--	--	--	--	--	--	--
10	4,047	4.175×10^{-4}	1,233	8.351×10^{-6}	--	--	--	--	--	--	--
Total	14,054,745	1.921×10^{-3}	9,867,840	1.503×10^{-3}	7,647,576	--	13,864,542	1.921×10^{-3}	9,621,144	1.420×10^{-3}	7,400,880

Source: Modified from SNJV, 2004a

[a]Subtract precipitation rate from ET rate (Precipitation rate = 4.175×10^{-4} m/d)

Uncontrolled When Printed

Table 2-15
Summary Statistics of Simulated Annual ET from 1,000 Monte Carlo Realizations for the Oasis Valley Discharge Area

Statistic	Value	Unit
Mean	7,754,889	m^3
Median	7,758,589	m^3
Minimum	5,142,378	m^3
Maximum	11,005,109	m^3
Standard Deviation	953,480	m^3
5% Confidence Bound	6,185,950	m^3
95% Confidence Bound	9,325,180	m^3
Coefficient of Variability	0.12	unitless

Source: SNJV, 2004a

Note: Added 95% confidence range as mean minus 2 standard deviations and mean plus 2 standard deviations.

The total yearly water withdrawals for wells located within the boundaries of the Pahute Mesa area are shown in Figure 2-15. Only NTS water supply wells that contributed to the total pumpage from 1963 to 1993 are included in this figure. In 1995 and 1996, the totals include contributions from Beatty Well No. 1. For the remainder of the years, the totals also include the mine wells. The total yearly volumes are based on available data only and are, therefore, an underestimation of the actual volumes pumped. Records for NTS water supply wells are not available from 1972 to 1982. For the area of interest, the gap in the dataset is from 1968 to 1982, as shown on the graph (Figure 2-15). The graph shows a general increase in pumping from 1983 to 1989. The peak annual production of 1,154,700 cubic meters (m^3) occurred in 1989. All water was pumped from U-20 WW (cased), UE-19c WW, and WW-8 at that time. A decreasing trend started in 1990 and ended in 1993. A marked drop in pumping occurred from 1992 to 1993. This drop coincides with the end of underground nuclear testing in 1992.

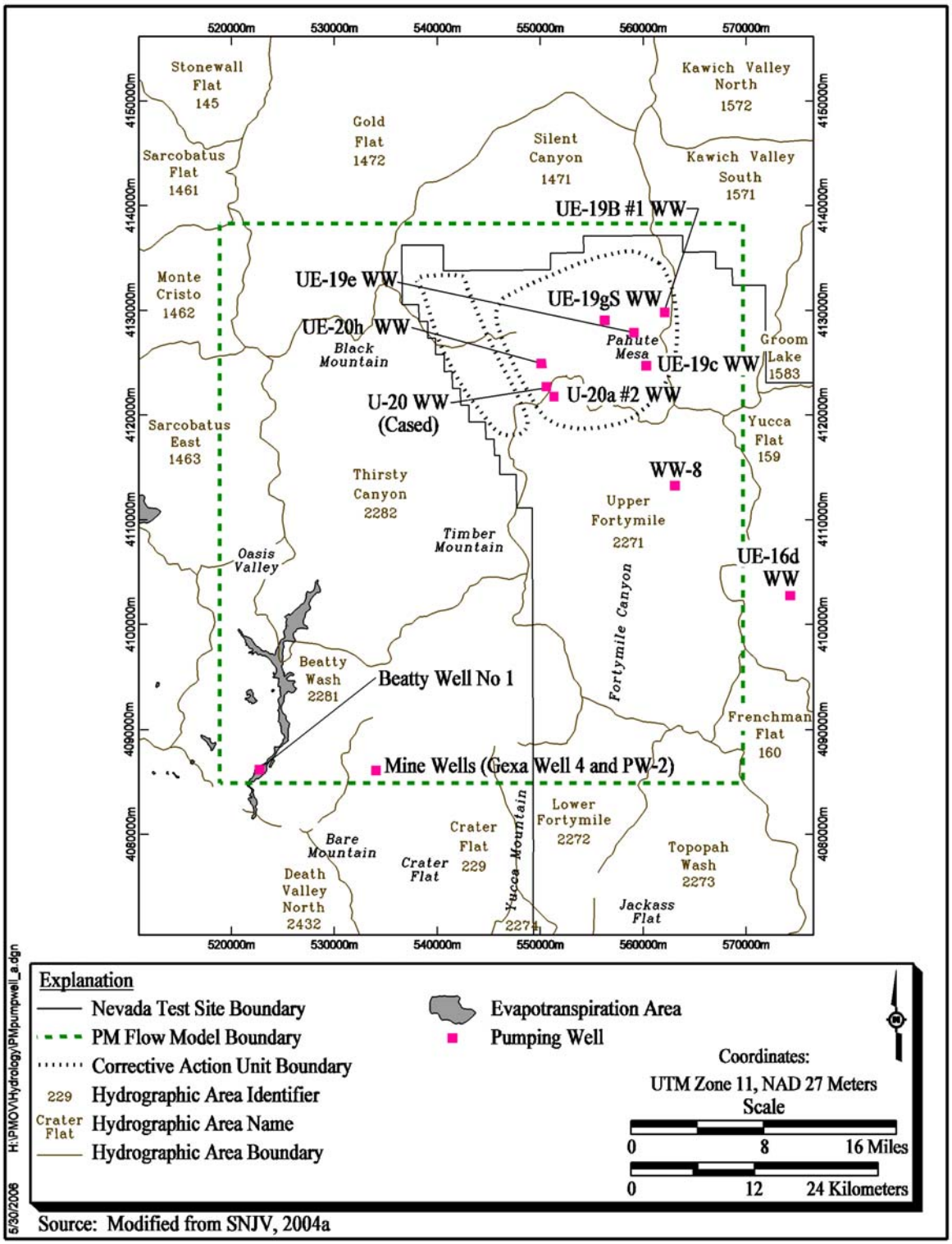

Figure 2-14
Locations of Pumping Wells in the Pahute Mesa Area Used in the Well Discharge Analysis

Uncontrolled When Printed

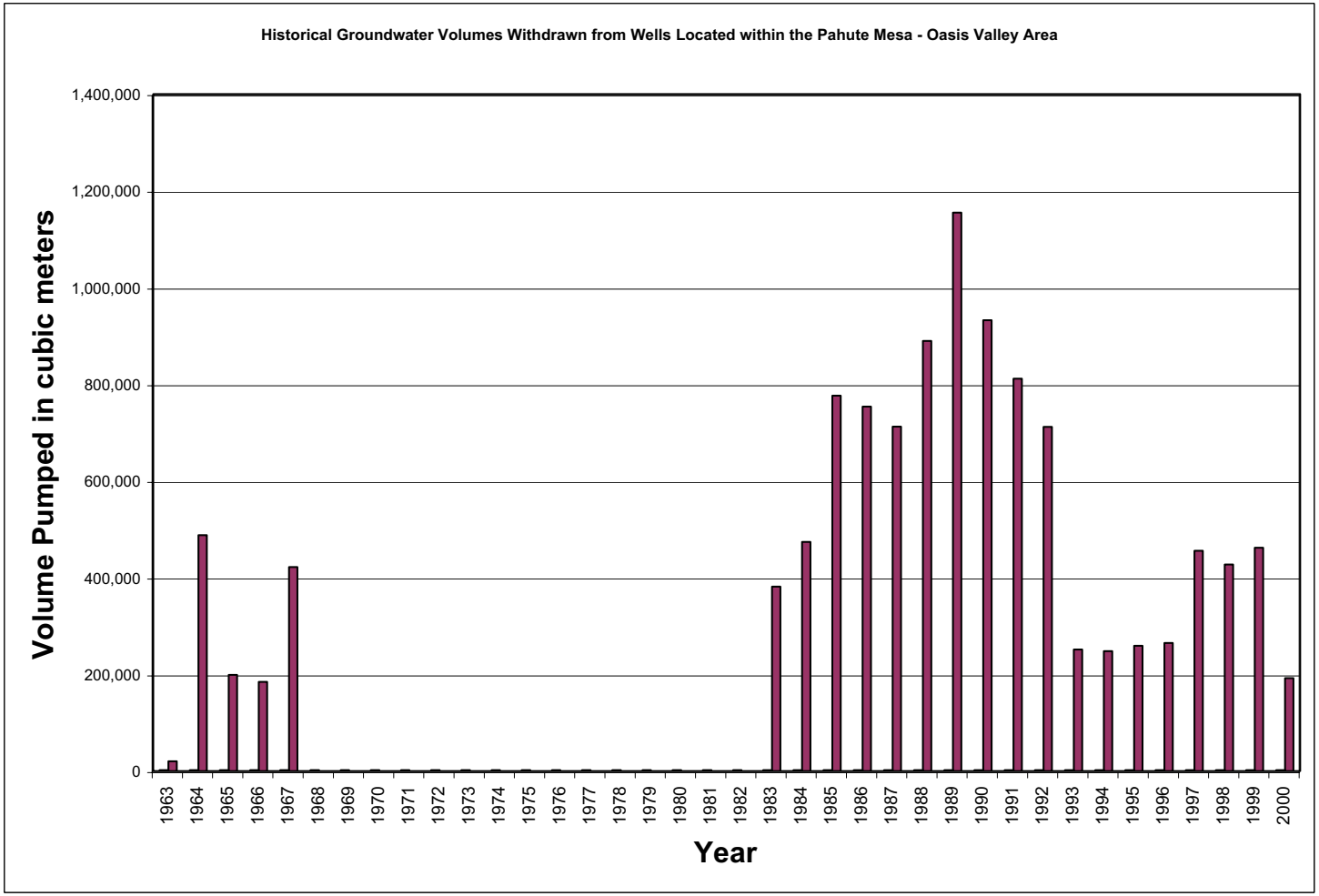

Figure 2-15
Total Withdrawals from Pumping Wells Located within the Pahute Mesa Area
(No Data Available between 1968 and 1982)
Source: Modified from SNJV, 2004a

Uncontrolled When Printed

2.5 Hydraulic Heads

Observed hydraulic heads are derived from depth-to-water measurements and well information. Hydraulic heads may also be approximated by the land surface elevations of regional springs. This section provides a summary of the evaluation of hydraulic head data in the Pahute Mesa area. A more detailed description of this evaluation is provided in SNJV (2004a, Section 8.0).

The results of the water-level data analysis were used to identify hydraulic head values that are most representative of steady-state, predevelopment conditions at specific boreholes and well locations. Each temporal subset of measurements that represents steady-state conditions was reduced statistically to a mean, standard deviation, and variance of the mean. The hydraulic head data derived from the water-level data were supplemented with land surface elevations of the selected regional springs.

The uncertainty associated with each of the hydraulic head values was estimated in several different ways depending on the case. The uncertainty associated with hydraulic heads derived from multiple water-level measurements is represented by the total variance. In this case, a given steady-state hydraulic head variance was calculated as the sum of the variance of the mean hydraulic head and the variance of the land surface elevation derived from the accuracy estimates provided in SNJV (2004a). The uncertainty associated with hydraulic heads derived from land surface elevations at spring locations was equated to the variance of the land surface elevation derived from the accuracy estimates also provided in SNJV (2004a). It was not possible to quantify the measurement variance for many of the wells due to a lack of information. No estimates of uncertainty have been made for these cases. As part of the modeling analysis, weights will be derived and assigned to the hydraulic heads as described in Section 5.2.

A potentiometric contour map was prepared using composite water-level data to provide a general understanding of the hydraulic gradient and direction of groundwater flow. Figure 2-16 shows the potentiometric surface and the HSUs at the water table. The wells and hydraulic heads used in the calibration of the Pahute Mesa flow model are summarized in Table 5-2.

Vertical flow analysis was performed with the aid of the EV software program (Version 5.1 by Dynamic Graphics, 2002) to produce an isocontour model. The amount of information available on

Uncontrolled When Printed

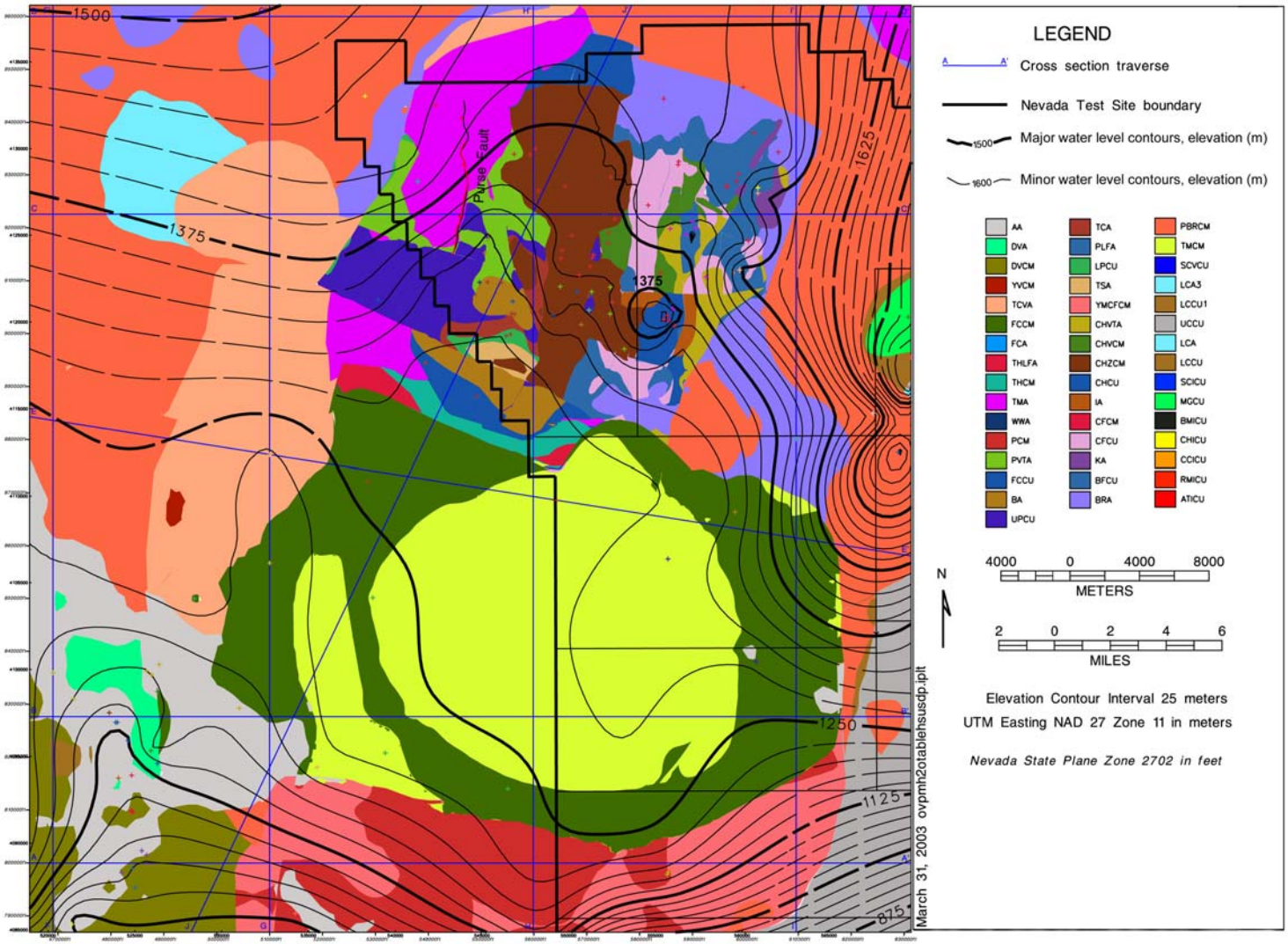

Figure 2-16
Map Showing Composite Potentiometric Surface with Elevated Heads in the Northwest and HSUs at the Water Table
Source: SNJV, 2004a

Uncontrolled When Printed

the vertical distribution of hydraulic heads in the region is sparse. The EV model was, therefore, only used to evaluate regions with sufficient data. In wells with multiple screened intervals, the vertical gradient was calculated as the difference in hydraulic heads divided by the difference in vertical distance between open intervals. The vertical gradient was then applied to the midpoint between effective open intervals.

An analysis of vertical flows indicated:

- A strong downward vertical gradient occurs near the water table in the Rainier Mesa region with a slight upward gradient at depth.
- A moderate downward gradient occurs in the area of Beatty Wash.
- There is a slight upward gradient at intermediate depths throughout the central portions of NTS Area 19 and Area 20.
- The Oasis Valley region contains a mixture of vertical gradients. Near the surface, there is a very weak upward gradient as well as areas of localized downward gradients.

As described in Section 2.4, 10 pumping wells have been historically used to withdraw groundwater from the Pahute Mesa area; eight of them are NTS water supply wells located in Pahute Mesa. The two other wells are Beatty Well No. 1 and Gexa Well 4, located outside of the NTS. In 1989, the maximum volume of 1,154,700 m^3 was pumped. This volume represents only 15 percent of the ET estimate. The three largest producing wells are WW 8, UE-19c WW, and U-20 WW. The effects of pumping at U-20 WW were observed as drawdown at several wells located up to 5.9 km away (Fenelon, 2000). As reported by Fenelon (2000), the correlation of monthly withdrawal rates and drawdown is hindered because of relatively long periods of no pumping interspersed with periods of pumping. In conclusion, transient well-related effects are very localized and likely not representative of conditions over a majority of the model area.

2.6 Hydraulic Parameters

Hydraulic parameters are required to simulate groundwater movement. The following sections summarize the assessment of hydraulic parameter data presented in SNJV (2004a.)

2.6.1 Hydraulic Conductivity Data

Analysis of hydraulic conductivity data included evaluations of measurement scale (laboratory-scale data, slug-test-scale data, constant-rate-scale data), scaling and spatial variability, vertical anisotropy, and the alteration of hydraulic conductivity in test cavities (SNJV 2004a). Hydraulic conductivity parameters for each HSU are presented at the end of this section. All hydraulic conductivities are in m/d. Figure 2-17 shows the locations where the hydraulic conductivity data were obtained.

Approximately 1,200 laboratory-scale data measurements are available for 44 locations, nearly all of which are outside the Pahute Mesa model boundary. Laboratory data have been subdivided on the basis of the regional model HSUs including the AA, LCA, LCCU, VCU, VA, and VU. Table 2-16 provides the statistics of laboratory-scale hydraulic conductivity data.

More than 200 hydraulic conductivity values were obtained by methods that have been lumped into the general category of slug tests. The types of tests in this category include bailing recovery, drill-stem test, falling-head slug test, packer-injection test, pressure-injection test, slug-injection test, slug-withdrawal test, and swabbing-recovery test. Each of these test types are of relatively short duration, involving the movement of smaller volumes of water through the formation than would be typical for a constant-rate test. Therefore, hydraulic conductivity values derived from slug tests represent a smaller volume of the tested formation than either single-well or multi-well constant-rate aquifer tests. Table 2-17 provides the statistics of the slug-test-scale hydraulic conductivity data. Plots of slug-test hydraulic conductivity versus depth from SNJV (2004a, Section 5.5.4, Figures 5-9 and 5-10) suggest that there is a trend of decreasing hydraulic conductivity with increasing depth.

Approximately 300 hydraulic conductivity values were obtained from analyses of constant-rate test data. The data classified as constant-rate-scale represent tests in which water was injected or withdrawn at a constant rate for several hours to several days. As a result, these tests sampled a larger volume of the tested formation than either laboratory-scale or slug-scale tests. This group of data contains results from both single- and multi-well aquifer tests. Table 2-18 summarizes the statistics for these analyses.

Uncontrolled When Printed

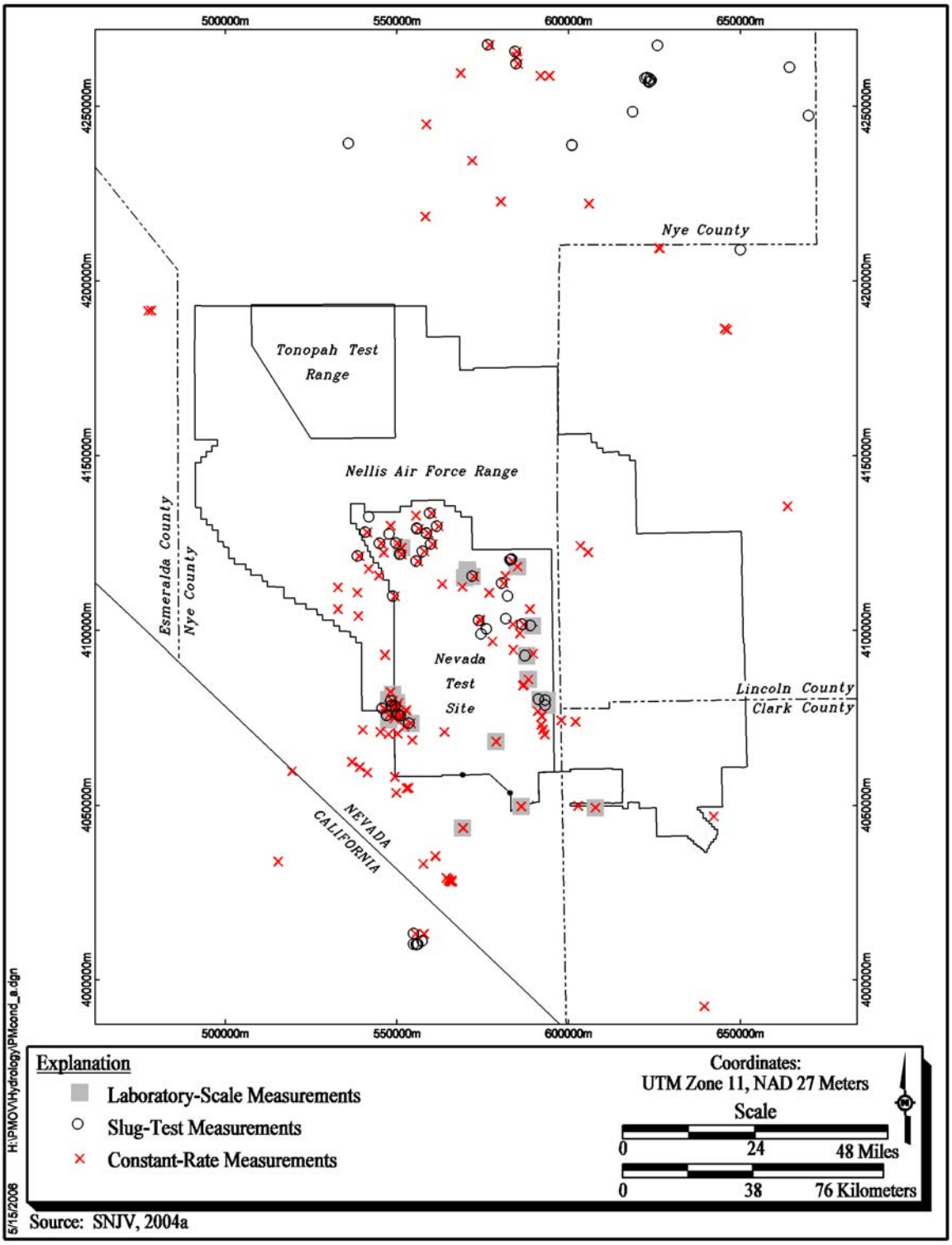

Figure 2-17
Map of the Locations of Hydraulic Conductivity Data

Uncontrolled When Printed

Table 2-16
Statistics of Laboratory-Scale Hydraulic Conductivity[a] Data

Hydrostratigraphic Unit[b]	Number of Data Points	Log 10 Mean of Hydraulic Conductivity	Log 10 Standard Deviation of Hydraulic Conductivity	Accept Log Normality at the 5% Level
Alluvial Aquifer (AA)	66	-0.4	0.8	Yes
Lower Carbonate Aquifer (LCA)	33	-4.2	1.6	Yes
Lower Clastic Confining Unit (LCCU)	30	-6.6	0.7	Yes
Volcanic Aquifer (VA)	400	-3.8	2.2	No
Volcanic Confining Unit (VCU)	639	-4.4	1.5	No
Volcanic Aquifer (VA)	19	-3.0	2.0	Yes

Source: SNJV, 2004a

[a]Hydraulic conductivity is in m/d.
[b]See Table 2-6 for HSU descriptions.

Plots of constant-rate-test hydraulic conductivity versus depth from SNJV (2004a, Section 5.5.5, Figure 5-22) show a strong trend of decreasing hydraulic conductivity with increasing depth. The treatment of hydraulic conductivity depth decay is described in SNJV (2004a, Section 5.5.6).

For the purposes of the Pahute Mesa CAU flow model, the constant-rate-scale data are the most appropriate. Slug tests are judged less reliable because they are strongly affected by near-well mechanical disturbance (Butler, 1997).

In the general case, hydraulic conductivity is not a scalar value, but a second rank tensor, where hydraulic conductivity at a point in space is a function of direction. The measurement of horizontal anisotropy requires multiple observation wells during aquifer testing. Anisotropy in the vertical direction can be determined from oriented core, or observation wells set at depths that differ from the pumped well. Data to define anisotropy are limited. Laboratory data are not appropriate for large-scale model parameters such as those needed for the Pahute Mesa CAU model. Careful testing at the C-well complex at Yucca Mountain yielded a range of anisotropy values (defined as vertical/horizontal hydraulic conductivity) from 0.025 to as large as 2.0. Because the dataset is limited, it is not possible to provide anisotropy values for each HSU. Vertical anisotropy is treated in the Pahute Mesa flow model (see SNJV, 2004a, Section 5.5.8). Horizontal anisotropy is not considered.

Uncontrolled When Printed

Table 2-17
Statistics of Slug-Test-Scale Hydraulic Conductivity[a] Data

Hydrostratigraphic Unit[b]	Number of Data Points	Log 10 Mean Hydraulic Conductivity	Log 10 Standard Deviation of Hydraulic Conductivity	Accept Log Normality at the 5% Level
Alluvial Aquifer (AA)	15	-1.0	1.4	Yes
Lower Carbonate Aquifer (LCA)	32	-1.2	1.0	Yes
Bullfrog Confining Unit (BFCU)	19	-3.3	0.6	Yes
Belted Range Aquifer (BRA)	76	-2.9	0.9	Yes
Crater Flat Composite Unit (CFCM)	5	-3.1	0.3	Yes
Crater Flat Confining Unit (CFCU)	2	-2.6	1.3	N/A
Calico Hills Confining Unit (CHCU)	2	-2.8	0.6	N/A
Calico Hills Zeolitic Composite Unit (CHZCM)	29	-2.7	0.8	Yes
Inlet Aquifer (IA)	8	-2.4	0.9	Yes
Pre-Belted Range Composite Unit (PBRCM)	16	-3.7	1.1	Yes
Timber Mountain Composite Unit (TMCM)	16	-2.5	1.1	Yes
Upper Paintbrush Confining Unit (UPCU)	3	-3.2	0.3	N/A

Source: SNJV, 2004a

[a]Hydraulic conductivity is in m/d.
[b]See Table 2-6 for HSU descriptions.

The detonation of underground nuclear tests creates underground cavities and collapsed chimneys (Pawloski et al., 2001). The melt glass that forms at the bottom of the cavity is generally accepted to be of very low permeability, as is the crushed zone beneath the cavity. However, the chimney region, because of its rubblized nature, may be more permeable than the surrounding host rock. In their study of flow and transport from an underground nuclear test cavity, Pawloski et al. (2001) used chimney hydraulic conductivity values that were at least 70 times larger than in the native rock. As Pawloski et al. (2001) note, these values were estimated using the scant data available from underground nuclear tests, insights gained from calibration of flow and transport models, and understanding of the phenomenology of underground nuclear tests. The scale of these effects should be small with respect to the size of the Pahute Mesa flow model domain. However, this assumption on increased chimney

Table 2-18
Statistics of Constant-Rate-Scale Hydraulic Conductivity[a] Data as Compared to Statistics of Slug-Test-Scale and Laboratory-Scale Data

Hydrostratigraphic Unit[b]	Number of Data Points	Log 10 Mean of Hydraulic Conductivity	Log 10 Standard Deviation of Hydraulic Conductivity	Accept Log Normality at the 5% Level	Slug-Test-Scale Log 10 Mean of Hydraulic Conductivity	Slug-Test-Scale Log 10 Standard Deviation of Hydraulic Conductivity	Laboratory-Scale Log 10 Mean of Hydraulic Conductivity	Laboratory-Scale Log 10 Standard Deviation of Hydraulic Conductivity
Alluvial Aquifer (AA)	38	0.7	0.7	Yes	-1.0	1.4	-0.4	0.8
Lower Carbonate Aquifer (LCA)	49	-0.3	1.2	Yes	-1.2	1.0	-4.2	1.6
Intrusives (I)	1	-2.5	N/A	N/A				
Upper Clastic Confining Unit (UCCU)	2	-2.2	1.3	N/A				
Lower Clastic Confining Unit (LCCU)	3	-0.5	1.5	N/A			-6.6	0.7
Volcanic Confining Unit (VCU)	101	-1.0	1.4	Yes			-4.4	1.5
Volcanic Aquifer (VA)	35	0.1	0.9	Yes			-3.8	2.2
Volcanics Undifferentiated (VU)	7	-1.3	1.2	Yes			-3.0	2.0
Benham Aquifer (BA)	6	0.6	0.8	N/A				
Belted Range Aquifer (BRA)	15	-0.1	0.9	Yes	-2.9	1.0		
Bullfrog Confining Unit (BFCU)	1	-0.3	N/A	N/A	-2.3	1.0		
Inlet Aquifer (IA)	3	-1.0	1.6	N/A	-2.0	0.9		
Calico Hills Zeolitic Composite Unit (CHZCM)	6	-0.2	0.5	N/A	-1.9	0.9		
Fortymile Canyon Composite Unit (FCCM)	11	-0.1	1.1	Yes				
Pre-Belted Range Composite Unit (PBRCM)	2	-0.7	0	N/A	-2.8	1.5		
Thirsty Canyon Volcanic Aquifer (TCVA)	4	1.8	0.4	N/A				
Timber Mountain Composite Unit (TMCM)	13	0.4	1.1	Yes	-2.1	1.0		
Upper Paintbrush Confining Unit (UPCU)	3	-0.9	0.9	N/A				

Source: SNJV, 2004a

[a]Hydraulic conductivity is in m/d.
[b]See Table 2-6 for HSU descriptions.

Uncontrolled When Printed

hydraulic conductivity was addressed in the sensitivity analysis of the Pahute Mesa flow model (see Section 6.2).

Table 2-19 summarizes the hydraulic conductivity parameters determined for each HSU. The table contains the HSU number and identifier, the log 10 mean and standard deviation, and a description of where the chosen mean and standard deviation were obtained. The given distributions were applied to the model at the start of calibration (see Section 5.2).

Table 2-19
Hydraulic Conductivity[a] Distributions of Hydrostratigraphic Units of the Pahute Mesa Hydrostratigraphic Framework Model
(Page 1 of 5)

HFM Layer Number[a]	Hydrostratigraphic Unit (Symbol)	Dominant Hydrogeologic Unit(s)[b]	Mean Hydraulic Conductivity Log 10 (m/d)	Mean Intrinsic Permeability (m^2)	Log 10 Hydraulic Conductivity Standard Deviation	Source of the Parameters
45	Alluvial Aquifer (AA) (this term is also used to designate a hydrogeologic unit)	AA	0.7	5.9×10^{-12}	0.7	Values obtained from the constant-rate-scale data in Table 2-18.
44	Younger Volcanic Composite Unit (YVCM)	LFA, WTA, VTA	1.8	7.4×10^{-11}	0.4	No data were available for this unit. Used values from the TCVA in Table 2-18 because of lithologic similarity. This minor unsaturated unit is not expected to influence the flow model.
43	Thirsty Canyon Volcanic Aquifer (TCVA)	WTA, LFA, lesser VTA	1.8	7.4×10^{-11}	0.4	Values obtained from the constant-rate-scale data in Table 2-18.
42	Detached Volcanics Composite Unit (DVCM)	WTA, LFA, TCU	-1.0	1.2×10^{-13}	1.4	No data were available for this unit. Used value from the VCU in Table 2-18 because it provides a distribution that spans nearly the full range of observed values. It is expected that composite units have a larger range of values because of the varied lithologies.
41	Detached Volcanics Aquifer (DVA)	WTA, LFA	0.1	1.5×10^{-12}	0.9	No data were available for this unit. Used value from the VA in Table 2-18 because it provides a distribution that spans nearly the full range of observed values for an aquifer lithology.
40	Fortymile Canyon Composite Unit (FCCM)	LFA, TCU, lesser WTA	-0.1	9.4×10^{-13}	1.1	Values obtained from the constant-rate-scale data in Table 2-18.
39	Fortymile Canyon Aquifer (FCA)	WTA, LFA	0.1	1.5×10^{-12}	0.9	No data were available for this unit. Used value from the VA in Table 2-18 because it provides a distribution that spans nearly the full range of observed values for an aquifer lithology.

Uncontrolled When Printed

Table 2-19
Hydraulic Conductivity[a] Distributions of Hydrostratigraphic Units of the Pahute Mesa Hydrostratigraphic Framework Model
(Page 2 of 5)

HFM Layer Number[a]	Hydrostratigraphic Unit (Symbol)	Dominant Hydrogeologic Unit(s)[b]	Mean Hydraulic Conductivity Log 10 (m/d)	Mean Intrinsic Permeability (m^2)	Log 10 Hydraulic Conductivity Standard Deviation	Source of the Parameters
38	Timber Mountain Composite Unit (TMCM)	TCU (altered tuffs, lavas) and unaltered WTA and lesser LFA	0.4	3.0×10^{-12}	1.1	Values obtained from the constant-rate-scale data in Table 2-18.
37	Tannenbaum Hill Lava-Flow Aquifer (THLFA)	LFA	0.1	1.5×10^{-12}	0.9	No data were available for this unit. Used value from the VA in Table 2-18 because it provides a distribution that spans nearly the full range of observed values for an aquifer lithology.
36	Tannenbaum Hill Composite Unit (THCM)	Mostly TCU, lesser WTA	-1.0	1.2×10^{-13}	1.4	No data were available for this unit. Used value from the VCU in Table 2-18 because it provides a distribution that spans nearly the full range of observed values. It is expected that composite units have a larger range of values because of the varied lithologies.
35	Timber Mountain Aquifer (TMA)	Mostly WTA, minor VTA	0.1	1.5×10^{-13}	0.9	No data were available for this unit. Used value from the VA in Table 2-18 because it provides a distribution that spans nearly the full range of observed values for an aquifer lithology.
34	Subcaldera Volcanic Confining Unit (SCVCU)	TCU	-4.4	4.7×10^{-17}	1.5	No data were available for this unit. Used value from the VCU in Table 2-18 because it is expected that this unit will be of low permeability.
33	Fluorspar Canyon Confining Unit (FCCU)	TCU	-1.0	1.2×10^{-13}	1.4	No data were available for this unit. Used value from the VCU in Table 2-18 because it provides a distribution that spans nearly the full range of observed values.
32	Paintbrush Composite Unit (PCM)	WTA, LFA, TCU	-1.0	1.2×10^{-13}	1.4	No data were available for this unit. Used value from the VCU in Table 2-18 because it provides a distribution that spans nearly the full range of observed values. It is expected that composite units have a larger range of values because of the varied lithologies.
31	Paintbrush Vitric-Tuff Aquifer (PVTA)	VTA	0.1	1.5×10^{-12}	0.9	No data were available for this unit. Used value from the VA in Table 2-18 because it provides a distribution that spans nearly the full range of observed values for an aquifer lithology.
30	Benham Aquifer (BA)	LFA	0.6	4.7×10^{-12}	0.8	Values obtained from the constant-rate-scale data in Table 2-18.
29	Upper Paintbrush Confining Unit (UPCU)	TCU	-0.9	1.5×10^{-13}	0.9	Values obtained from the constant-rate-scale data in Table 2-18.

Uncontrolled When Printed

Table 2-19
Hydraulic Conductivity[a] Distributions of Hydrostratigraphic Units of the Pahute Mesa Hydrostratigraphic Framework Model
(Page 3 of 5)

HFM Layer Number[a]	Hydrostratigraphic Unit (Symbol)	Dominant Hydrogeologic Unit(s)[b]	Mean Hydraulic Conductivity Log 10 (m/d)	Mean Intrinsic Permeability (m^2)	Log 10 Hydraulic Conductivity Standard Deviation	Source of the Parameters
28	Tiva Canyon Aquifer (TCA)	WTA	0.1	1.5×10^{-12}	0.9	No data were available for this unit. Used value from the VA in Table 2-18 because it provides a distribution that spans nearly the full range of observed values for an aquifer lithology.
27	Paintbrush Lava-Flow Aquifer (PLFA)	LFA	0.1	1.5×10^{-12}	0.9	No data were available for this unit. Used value from the VA in Table 2-18 because it provides a distribution that spans nearly the full range of observed values for an aquifer lithology.
26	Lower Paintbrush Confining Unit (LPCU)	TCU	-0.9	1.5×10^{-13}	0.9	No data were available for this unit. Used values from the UPCU in Table 2-18 because of lithologic similarity.
25	Topopah Spring Aquifer (TSA)	WTA	0.1	1.5×10^{-12}	0.9	No data were available for this unit. Used value from the VA in Table 2-18 because it provides a distribution that spans nearly the full range of observed values for an aquifer lithology.
24	Yucca Mountain Crater Flat Composite Unit (YMCFCM)	LFA, WTA, TCU	-1.0	1.2×10^{-13}	1.4	No data were available for this unit. Used value from the VCU in Table 2-18 because it provides a distribution that spans nearly the full range of observed values. It is expected that composite units have a larger range of values because of the varied lithologies.
23	Calico Hills Vitric-Tuff Aquifer (CHVTA)	VTA	0.1	1.5×10^{-12}	0.9	No data were available for this unit. Used value from the VA in Table 2-18 because it provides a distribution that spans nearly the full range of observed values for an aquifer lithology.
22	Calico Hills Vitric Composite Unit (CHVCM)	VTA, LFA	-1.0	1.2×10^{-13}	1.4	No data were available for this unit. Used value from the VCU in Table 2-18 because it provides a distribution that spans nearly the full range of observed values. It is expected that composite units have a larger range of values because of the varied lithologies.
21	Calico Hills Zeolitic Composite Unit (CHZCM)	LFA, TCU	-0.2	7.4×10^{-13}	0.5	Values obtained from the constant-rate-scale data in Table 2-18.
20	Calico Hills Confining Unit (CHCU)	Mostly TCU, minor LFA	-0.9	1.5×10^{-13}	0.9	No data were available for this unit. Used values from the UPCU in Table 2-18 because of lithologic similarity.
19	Inlet Aquifer (IA)	LFA	-1.0	1.2×10^{-13}	1.6	Values obtained from the constant-rate-scale data in Table 2-18.

Uncontrolled When Printed

Table 2-19
Hydraulic Conductivity[a] Distributions of Hydrostratigraphic Units of the Pahute Mesa Hydrostratigraphic Framework Model
(Page 4 of 5)

HFM Layer Number[a]	Hydrostratigraphic Unit (Symbol)	Dominant Hydrogeologic Unit(s)[b]	Mean Hydraulic Conductivity Log 10 (m/d)	Mean Intrinsic Permeability (m^2)	Log 10 Hydraulic Conductivity Standard Deviation	Source of the Parameters
18	Crater Flat Composite Unit (CFCM)	Mostly LFA, intercalated with TCU	-1.4	4.7×10^{-14}	0.9	Values obtained from the slug-scale data in Table 2-18. The magnitude of the mean was increased one order of magnitude to account for observed differences between the slug and constant-rate-scale.
17	Crater Flat Confining Unit (CFCU)	TCU	-0.9	1.5×10^{-13}	0.9	No data were available for this unit. Used values from the UPCU in Table 2-18 because of lithologic similarity.
16	Kearsarge Aquifer (KA)	LFA	0.1	1.5×10^{-12}	0.9	No data were available for this unit. Used value from the VA in Table 2-18 because it provides a distribution that spans nearly the full range of observed values for an aquifer lithology.
15	Bullfrog Confining Unit (BFCU)	TCU	-1.3	5.9×10^{-14}	1.0	Values obtained from the slug-scale data in Table 2-18. The magnitude of the mean was increased one order of magnitude to account for observed differences between the slug and constant-rate-scale.
14	Belted Range Aquifer (BRA)	LFA and WTA, with lesser TCU	-0.1	9.4×10^{-13}	0.9	Values obtained from the constant-rate-scale data in Table 2-18.
13	Pre-Belted Range Composite Unit (PBRCM)	TCU, WTA, LFA	-0.7	2.4×10^{-13}	1.5	Mean Value obtained from the constant-rate-scale data in Table 2-18. The standard deviation was taken from the slug-scale data in Table 2-17.
12	Black Mountain Intrusive Confining Unit (BMICU)	IICU	-2.5	3.7×10^{-15}		Mean Value obtained from the Intrusive (I) in the constant-rate-scale data in Table 2-18. No standard deviation was calculated.
11	Ammonia Tanks Intrusive Confining Unit (ATICU)	IICU	-2.5	3.7×10^{-15}		
10	Rainier Mesa Intrusive Confining Unit (RMICU)	IICU	-2.5	3.7×10^{-15}		
9	Claim Canyon Intrusive Confining Unit (CCICU)	IICU	-2.5	3.7×10^{-15}		
8	Calico Hills Intrusive Confining Unit (CHICU)	IICU	-2.5	3.7×10^{-15}		

Uncontrolled When Printed

Table 2-19
Hydraulic Conductivity[a] Distributions of Hydrostratigraphic Units of the Pahute Mesa Hydrostratigraphic Framework Model
(Page 5 of 5)

HFM Layer Number[a]	Hydrostratigraphic Unit (Symbol)	Dominant Hydrogeologic Unit(s)[b]	Mean Hydraulic Conductivity Log 10 (m/d)	Mean Intrinsic Permeability (m^2)	Log 10 Hydraulic Conductivity Standard Deviation	Source of the Parameters
7	Silent Canyon Intrusive Confining Unit (SCICU)	IICU	-2.5	3.7×10^{-15}		Mean Value obtained from the Intrusive (I) in the constant-rate-scale data in Table 2-18. No standard deviation was calculated.
6	Mesozoic Granite Confining Unit (MGCU)	GCU	-2.5	3.7×10^{-15}		Mean Value obtained from the Intrusive (I) in the constant-rate-scale data in Table 2-18. No standard deviation was calculated.
5	Lower Carbonate Aquifer - Thrust Plate (LCA3)	CA	-0.3	5.9×10^{-13}	1.2	Values obtained from the constant-rate-scale data in Table 2-18 for the LCA.
4	Lower Clastic Confining Unit - Thrust Plate (LCCU1)	CCU	-0.5	3.7×10^{-13}	1.5	Values obtained from the constant-rate-scale data in Table 2-18. This unit may be broken up and have a larger permeability than when at depth.
3	Upper Clastic Confining Unit (UCCU)	CCU	-2.2	7.4×10^{-15}	1.3	Values obtained from the constant-rate-scale data in Table 2-18.
2	Lower Carbonate Aquifer (LCA)	CA	-0.3	5.9×10^{-13}	1.2	Values obtained from the constant-rate-scale data in Table 2-18 for the LCA.
1	Lower Clastic Confining Unit (LCCU)	CCU	-6.6	3.0×10^{-19}	0.7	Values taken from the laboratory-scale data in Table 2-16 because this unit is expected to be very impermeable.

Source: Modified from SNJV, 2004a

[a]PM 3-D Hydrostratigraphic Framework model (BN, 2002)
[b]See Table 2-1 for HGU descriptions.

2.7 Groundwater Chemistry

Groundwater geochemistry data are considered during the evaluation of the groundwater flow system because they provide a means for determining the origin, pathway, and timescale of groundwater flow that is independent of estimates based on conventional hydraulic data. Geochemical and hydraulic data reflect distinct but complimentary aspects of a groundwater flow system, and must be considered in unison in order to develop a consistent, comprehensive, and defensible flow system assessment. For example, geochemical data may identify flow paths and source areas that would otherwise not be recognized on the basis of hydraulic information alone; however, these flow paths must be consistent with potentiometric data in order to be valid.

Uncontrolled When Printed

A detailed discussion of groundwater geochemistry is provided in SNJV (2004a, Section 10.0). This section provides a summary of groundwater geochemistry evaluations for the Central and Western Pahute Mesa CAUs that address groundwater flow path, water budget, and travel time evaluations. These geochemical evaluations were performed on representative Pahute Mesa-CAU data in order to identify and assess viable flow paths and groundwater mixing models and included the evaluation of both conservative tracers and of non-conservative tracers. In addition, the NETPATH computer program (Plummer et al., 1994) was used as part of the evaluation process to calculate the net geochemical mass-balance reactions, groundwater mixing ratios, and apparent groundwater travel times along viable flow paths (SNJV, 2004a).

More than 1,200 sampling events, conducted before 1992, generated data from 220 individual locations for more than 280 different parameters within the area of interest (oldest recorded sample date within the area of interest is February 22, 1956). Note that only 95 of the total number of individual parameters measured before 1992 were analyzed 10 or more times. Since 1992 (and the initiation of the ERP), more than 600 sample events have generated data from 138 individual well, spring, and seep locations within the same area of interest for more than 500 different parameters. Note that only 307 of the total number of individual parameters measured since 1992 were analyzed 10 or more times. There are 54 locations that have been sampled both before and since 1992.

2.7.1 Conservative Tracers

Conservative tracers are geochemical species that move with groundwater, exhibiting little or no change in concentration caused by reactive processes. Conservative tracers can be used to support the identification of groundwater flow paths, mixing ratios, and timescales of environmental processes (Cook and Bohlke, 2000). The chloride (Cl^-) and often sulfate (SO_4^{2-}) ions, and the stable isotopes of hydrogen and oxygen are considered conservative tracers. These parameters provide the fundamental basis for the flow path identification and mixing model estimates reported in SNJV (2004a).

2.7.1.1 Conservative Tracer Data

Figures 2-18 and 2-19 illustrate the geographic variations in groundwater delta deuterium (δD) values and Cl^- concentrations, respectively, in the Pahute Mesa flow system. Deuterium is a heavy stable isotope of hydrogen that can substitute for hydrogen in water (hence “heavy water”); the

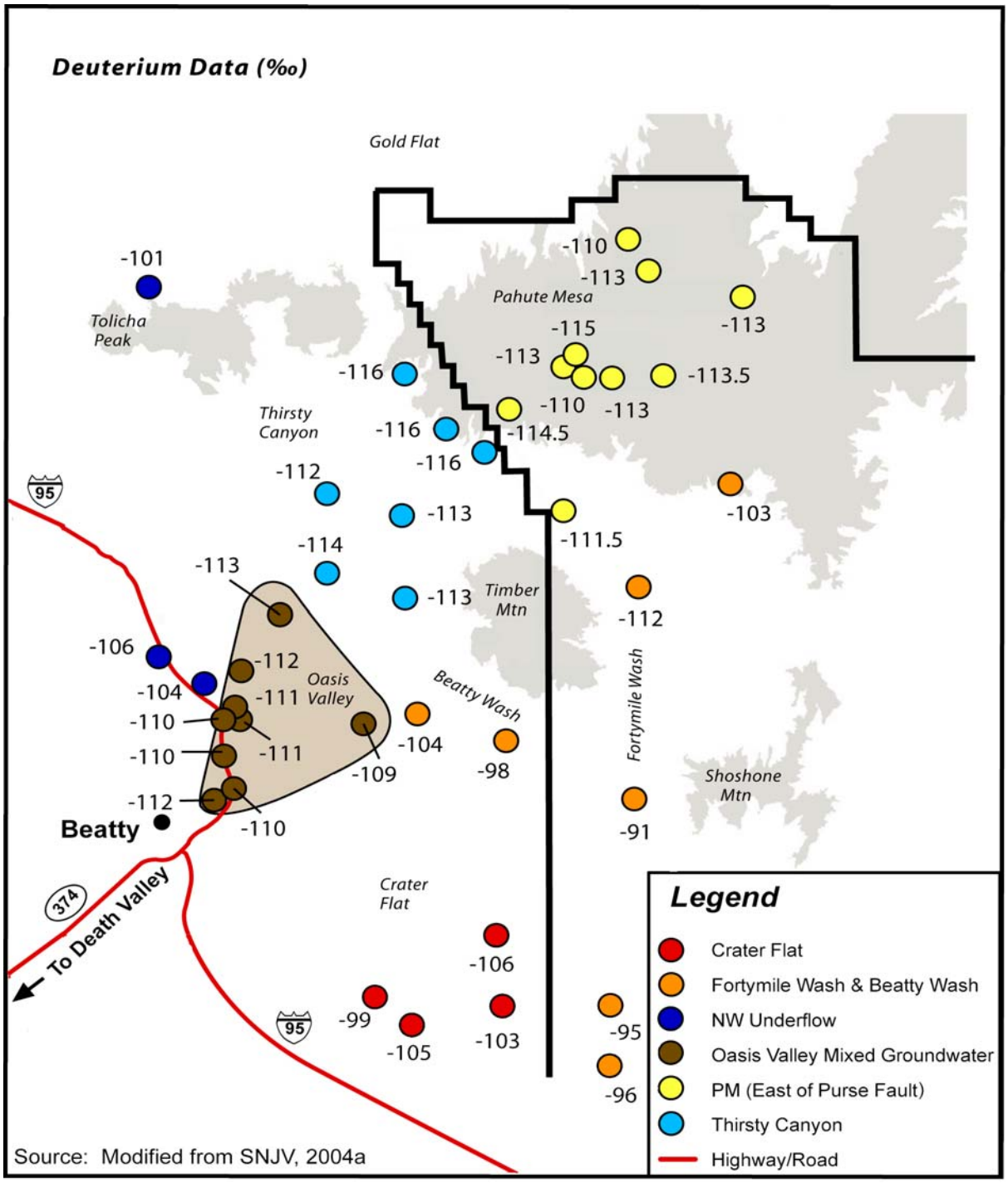

Figure 2-18
Geographic Distribution of δD Values for Wells and Springs in the Study Area

Uncontrolled When Printed

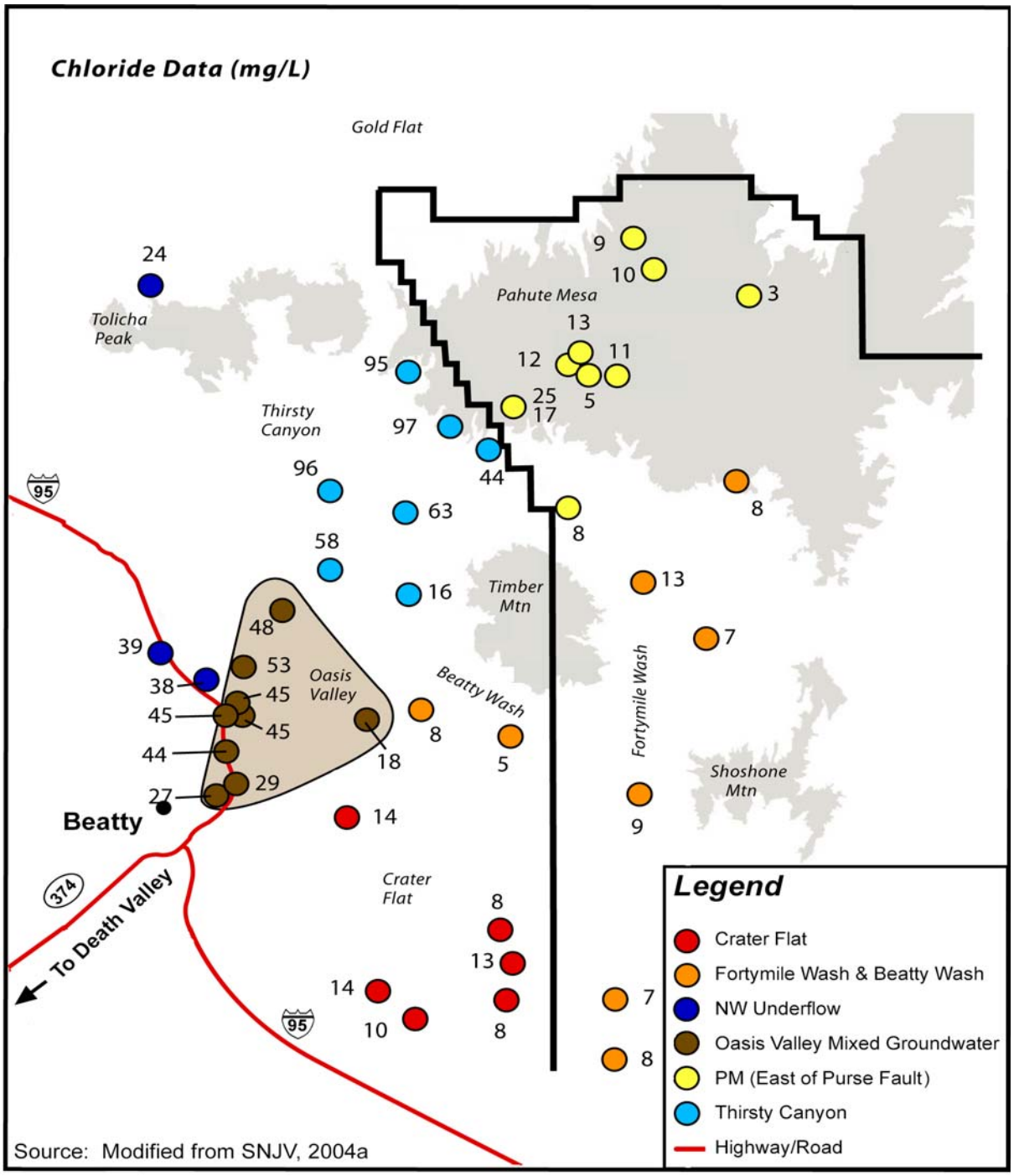

Figure 2-19
Geographic Distribution of Dissolved Cl^- Concentrations for Wells and Springs in the Study Area

Uncontrolled When Printed

concentration of deuterium is expressed as a change, or "delta," from a global standard. Reactions occur more slowly with heavy water. Thus, precipitation condensed at higher altitudes and lower temperatures is lighter, or depleted with respect to deuterium. This information allows inferences about recharge areas and groundwater flow paths. These figures illustrate that groundwater in upper Thirsty Canyon, west of the Purse Fault, has relatively light δD values (as light as -116 per mil) and high Cl^- concentrations (up to 97 milligrams per liter [mg/L]) that are distinct from Pahute Mesa groundwater immediately to the east. In the Pahute Mesa area east of the Purse Fault, the δD values ranged from -110 to -115 per mil and the Cl^- values ranged from 5 to 25 mg/L. The Purse Fault is spatially associated with a major discontinuity in regional water levels, in the western part of Area 20 (O'Hagan and Laczniak, 1996; Laczniak et al., 1996). According to SNJV (2004a), the difference in the conservative tracer compositions of groundwater on either side of the Purse Fault indicates that two distinct water masses are present in that area. Downgradient from this water level discontinuity, changes in δD and Cl^- values indicate that mixing of these two water masses occurs in the area downgradient from ER-EC-1 and PM-3 toward the Oasis Valley discharge area (SNJV, 2004a).

2.7.1.2 Conservative Tracer Data Evaluation

Representative well sites were selected for the conservative tracer modeling effort. The following section describes the criteria reported by SNJV (2004a) in the selection process to define representative data for use in the conservative tracer modeling. Conservative tracer data for a number of well locations within the Pahute Mesa flow system are summarized in Table 2-20. The range in reported values is indicated for those sites that have been sampled on more than one occasion. The "n" value after each record indicates the number of independent analyses. The data in Table 2-20 have been subdivided into three categories (Pahute Mesa - West of Purse Fault, Pahute Mesa - East of Purse Fault, and "Local" Recharge) to represent the end-member mixing components that are present in the flow system. These components are inferred to mix within the flow system and contribute to groundwater discharge in central Oasis Valley. Conservative tracer data are also presented for the Oasis Valley groundwater discharge area.

Stoller-Navarro Joint Venture (2004a) used various combinations of the conservative tracer data to identify six plausible paths for groundwater flow from Pahute Mesa. These flow paths, and the wells/source areas considered as contributory sources, are described in Table 2-21. The location of

Table 2-20
Statistical Summary of Representative Conservative Tracer Data
(Page 1 of 2)

Site ID	δ D	n	δ ^{18}O	n	Cl^- (mg/L)	n	SO_4^{2-} (mg/L)	n
Pahute Mesa - West of Purse Fault								
ER-EC-1	-116	2	-14.8	2	92 - 97	4	120 - 145	4
ER-EC-2A	-113 / -116	2	-14.9	2	59 - 63	3	87 - 99	3
ER-EC-4	-112 / -115	2	-14.6	2	78 - 95.7	5	110 - 130	5
ER-EC-6	-116	2	-15.0	2	44 - 52	4	56 - 79	4
Pahute Mesa #3 (PM-3)	-116	1	-14.8	1	84.2 - 95.2	2	92.3 - 114	2
Range	-112 / -116	9	-14.6 / -15.0	9	44 - 97	18	56 - 145	18
Mean	-115.2	5	-14.82	5	76.1	5	102.7	5
Median	-116	5	-14.8	5	85.5	5	103.2	5
Pahute Mesa - East of Purse Fault								
ER-20-5 #3 (TYBO)	-114	3	-15.0 / -15.1	4	17.0 - 18.9	4	33.3 - 35.3	4
ER-20-6 #3 (BULLION)	-114 / -115	3	-15.0 / -15.1	4	11.9 - 15.3	4	30.5 - 34.0	4
U-19ba #1	---	---	---	---	40.9	1	10.2	1
U-19q PS#1d (CAMEMBERT)	-113	1	-14.6	1	10.4	1	29.7	1
U-20 Water Well	-113	1	-14.7	1	11 - 12.1	2	31 - 31.5	2
U-20a #2 Water Well	-114	1	-14.75	1	9.5 - 11.2	3	28 - 38.4	3
U-20al (EGMONT)	---	---	---	---	30.5 - 32.8	2	68 - 77.6	2
U-20n PS #1 DDH (CHESHIRE)	-113	3	-14.6 / -15.0	9	11.1 - 14.1	7	26.5 - 35.3	7
UE-18r	-110 / -112	2	-14.6 / -14.7	2	6.3 - 12	4	18 - 24	3
UE-19c Water Well	---	---	-15.0	1	2.4	2	5.8 - 6.2	2
UE-19gs	-113.5	1	-14.5	1	9.9	1	75 - 100	2
UE-19h	-110 / -112	2	-14.4 / -14.8	2	8.5 - 9.7	2	38.2	1
UE-20bh #1	-109 / -112	3	-14.7 / -14.8	3	3.5 - 4.7	3	8.3 - 14	2
Range	-109 / -115	20	-14.4 / -15.1	29	2.4 - 40.9	36	8.3 - 100	34
Mean	-112.8	10	-14.77	11	14.0	13	33.6	13
Median	-113	10	-14.73	11	10.4	13	31.3	13
"Local" Recharge								
NTS Springs	-88 / -101	5	-11.0 / -12.7	5	4.7 - 11	4	7.7 - 33.2	4
Rainier Mesa Tunnel Seeps	-90 / -101	80	-11.9 / -14.2	80	6 - 12	17	7.9 - 28.8	17
NTS Surface Runoff	-82.3 / -88.1	2	-11.3 / -12.4	2	3.2 - 4.3	2	8.3 - 9.0	2
UE-29a Wells	-91	2	-12.6	2	7.7 to 9.0	6	15 - 16.5	6

Uncontrolled When Printed

Table 2-20
Statistical Summary of Representative Conservative Tracer Data
(Page 2 of 2)

Site ID	δ D	n	δ ^{18}O	n	Cl^- (mg/L)	n	SO_4^{2-} (mg/L)	n
Range	-82.3 / -101	89	-11.0 / -14.2	89	3.2 - 12	29	7.7 - 33.2	29
Mean	-91.3	4	-12.39	4	7.1	4	14.8	4
Median	-92	4	-12.28	4	7.7	4	16.1	4
Central Oasis Valley Discharge								
Bailey's Hot Spring	-108 / -110	2	-14.6	2	39.5 - 43.5	7	111 - 119	7
ER-OV-02	-112	1	-14.7	1	49.2 - 53.1	2	86 - 90.2	2
ER-OV-03a	-111	1	-14.7	1	41.6 - 44.6	2	76 - 76.1	2
ER-OV-04a	-109	1	-14.8	1	27.6 - 28.8	3	58.7 - 61	3
Goss Spring	-110 / -112	2	-14.7	2	41.9 - 44.8	3	76 - 77	3
Mullen Spring	-111	1	-14.7	1	42.5 - 45.1	2	76 - 76.7	2
Range	-108 / -112	8	-14.6 / -14.8	8	27.6 - 53.1	19	58.7 - 119	19
Mean	-110.3	6	-14.7	6	41.8	6	82.1	6
Median	-110.5	6	-14.7	6	43.1	6	76.6	6

Source: SNJV, 2004a

Cl^- = Chloride
mg/L = Milligrams per liter
n = Number of independent analyses
SO_4^{2-} = Sulfate
δD = Delta deuterium
$\delta^{18}O$ = Delta oxygen-18

these flow paths are shown in Figure 2-20. Relatively abundant data from the well characterized flow path directly between Pahute Mesa and Oasis Valley (Flow Path 1) suggest that central Oasis Valley discharge consists of 29 to 47 percent groundwater from west of the Purse Fault, 45 to 57 percent groundwater from east of the Purse Fault, with 0 to 16 percent local recharge. Several other potential flow paths for groundwater movement away from Pahute Mesa are also identified by SNJV (2004a) using conservative tracers. While these other flow paths are plausible based on existing data, they exhibit greater uncertainties with respect to contributory water sources because of data limitations (scarcity of wells or lack of diagnostic parameters in key areas).

Uncontrolled When Printed

Table 2-21
Description of Plausible Groundwater Flow Paths in the Pahute Mesa Flow System (SNJV, 2004a)
(Page 1 of 2)

Groundwater and/or recharge source end-member groups (with list of individual well and/or spring locations used in flow-path modeling																							
	Pahute Mesa Groundwater from East of the Purse Fault			**Pahute Mesa Groundwater from West of the Purse Fault**					**Gold Flat/Tonopah Test Range (TTR)**				**NW Groundwater Inflow**	**Timber Mountain Area**		**Local Recharge**	**Oasis Valley**					**Amargosa Valley**	**Crater Flat**
Flow path designation and description	U-20 WW	UE-19h	WW-8	ER-EC-1	ER-EC-2a	ER-EC-4	ER-EC-6	ER-EC-8	Cedar Pass	Sandia #6	Roller Coaster	Rose Spring	Tolicha Peak	ER-EC-7	Coffers Windmill	UE-29a#2	ER-OV-01	ER-OV-03a	ER-OV-04a	ER-OV-05	Springdale	J-12	USW-VH-1
Flow Path 1[a]	Pahute Mesa groundwater + local recharge → Oasis Valley groundwater																						
	M1	M1	M1	M1	M1	M1	M1	M1								R	T	T	T	T	T		
Flow Path 2[b]	Pahute Mesa groundwater + Gold Flat/TTR groundwater + local recharge → Oasis Valley groundwater																						
	M1	M1	M1	M1	M1	M1	M1	M1	M2	M2	M2	M2				R	T	T	T	T	T		
Flow Path 3[c]	Tolicha Peak +/- Pahute Mesa groundwater +/- Gold Flat/TTR groundwater +/- local recharge → Oasis Valley groundwater																						
	M1	M1	M1	M1	M1	M1	M1	M1	M2	M2	M2	M2	M3			R	T	T	T	T	T		
Flow Path 4[d]	Pahute Mesa groundwater + local recharge (in Timber Mountain area) → Beatty Wash to Oasis Valley discharge area																						
	M1	M1	M1	M1	M1	M1	M1	M1						R	R		T	T	T	T	T		
Flow Path 5[e]	Pahute Mesa groundwater + local recharge → flow down Fortymile Wash toward the Amargosa Valley																						
	M1	M1	M1	M1	M1	M1	M1	M1								R						T	
Flow Path 6[f]	Pahute Mesa groundwater + local recharge → Crater Flat																						
	M1	M1	M1	M1	M1	M1	M1	M1						R	R	R							T

Uncontrolled When Printed

Table 2-21
Description of Plausible Groundwater Flow Paths in the Pahute Mesa Flow System (SNJV, 2004a)
(Page 2 of 2)

Table Footnotes:

Source: Modified from SNJV, 2004a

Groundwater mixing components	M1- Pahute Mesa Groundwater, M2- Gold Flat/TTR Groundwater, M3- NW Groundwater Inflow
Recharge components	R- Timber Mountain Area or Local Recharge
Mixing target	T- Mixing target in Oasis Valley, Amargosa Valley, or Crater Flat

[a]This flow path considers mixing of Pahute Mesa groundwater with local recharge to yield central Oasis Valley discharge. Reasonable models for this flow path can be derived using three end-member compositions: (1) Pahute Mesa groundwater from wells east of the Purse Fault, (2) Thirsty Canyon groundwater from wells west of the Purse Fault, and (3) local recharge.
[b]Flow Path 2 represents groundwater from north of Pahute Mesa (Cactus Flat area) mixing with Pahute Mesa groundwater and local recharge and then flowing to Oasis Valley.
[c]Flow Path 3 represents groundwater flow from north of Oasis Valley into Northwest Oasis Valley. Potential mixing sources of inflow to northwest Oasis Valley include groundwater from the Tolicha Peak area, groundwater from the Cactus Flat area north of Oasis Valley, and groundwater from Pahute Mesa. Groundwater in wells ER-OV-05 and Springdale Upper have deuterium values that are significantly different than wells and springs in the rest of the Oasis Valley area, therefore justifying an attempt to identify potential sources for that water.
[d]Flow Path 4 represents groundwater flow from Pahute Mesa to southern Oasis Valley through the Timber Mountain-Beatty Wash area. Local recharge along this flow path may include Timber Mountain recharge (represented by ER-EC-7) and/or recharge from surface water flow in Beatty Wash (represented by UE-29a #1). Well ER-OV-04a is used to represent southern Oasis Valley groundwater because it has the lowest carbon-14 value of the three samples in this area and does not appear to have interacted with shallow local groundwater or been subjected to exchange with soil-zone gases (Thomas et al., 2002).
[e]Flow Path 5 represents groundwater flow from Pahute Mesa down Fortymile Wash toward Amargosa Valley combining with local recharge. Thomas et al. (2002) developed models for groundwater from Wells WW-8 and UE-29a#1 mixing to produce the water chemistry observed at Well J-13.
[f]Flow Path 6 represents groundwater from Pahute Mesa mixing with local recharge and flowing south toward Crater Flat.

Uncontrolled When Printed

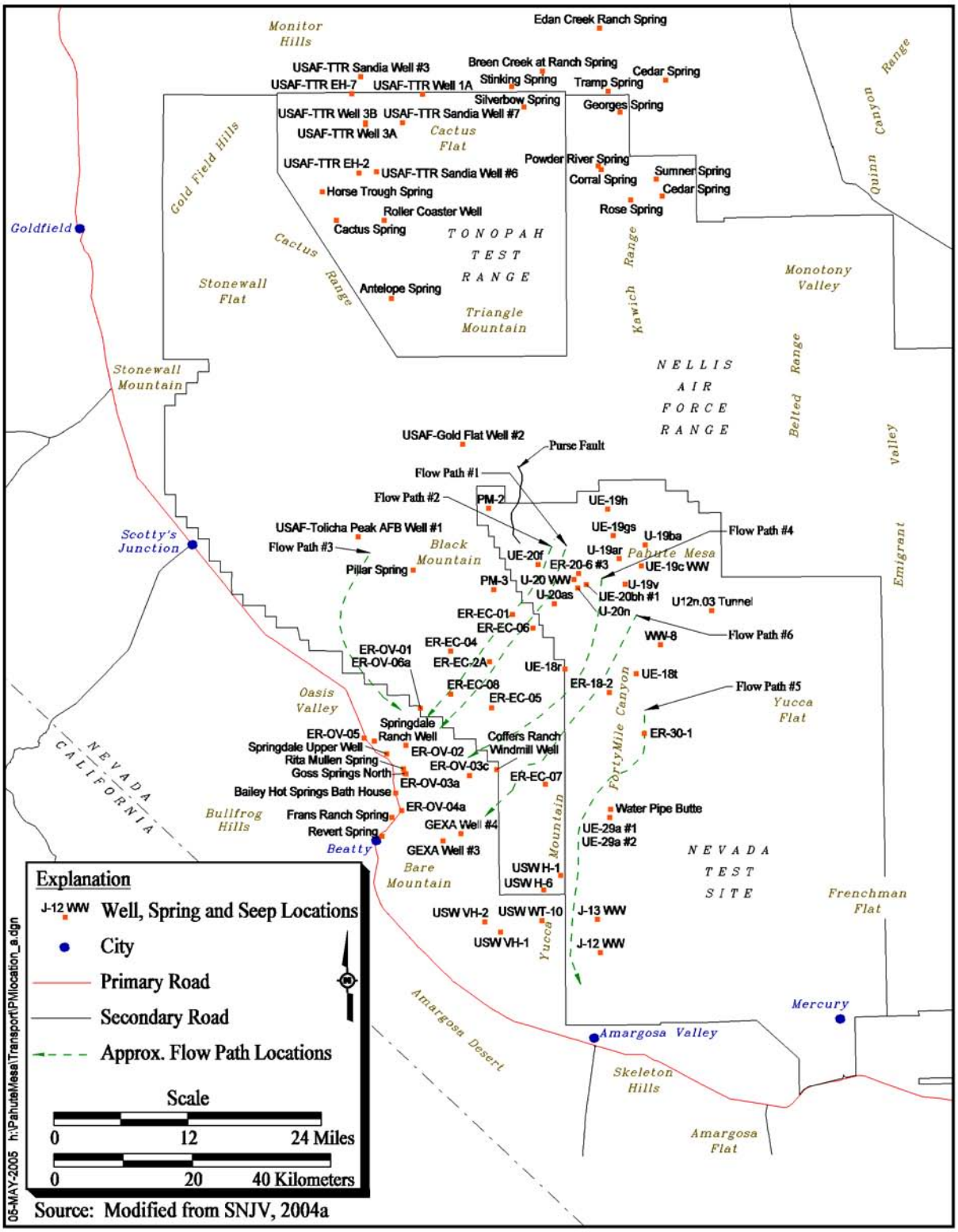

Figure 2-20
Approximate Flow Paths Determined from Conservative Tracer Analyses

Uncontrolled When Printed

2.7.2 Geochemical Modeling

Flow paths defined by SNJV (2004a) based on conservative mixing models were further evaluated using the NETPATH geochemical computer code (Plummer et al., 1994). The NETPATH modeling performed by SNJV (2004a) incorporates data for the ER-EC wells and builds on previous NETPATH modeling done in the Pahute Mesa flow system by Thomas et al. (2002). The geochemical calculations performed using NETPATH were conducted in accordance with procedures described in Plummer et al. (1994) and summarized in SNJV (2004a) and Thomas et al. (2002).

The results of NETPATH geochemical models for the six conceptual flow paths identified by SNJV (2004a), and described in Table 2-21, are summarized (along with the results from the conservative tracer modeling) in Table 2-22. These flow paths are illustrated in Figure 2-20.

The NETPATH program calculates the changes in major ion chemistry that occur along a flow path and determines groundwater-mixing ratios on the basis of chemical mass-balance relationships. The models generated by SNJV (2004a), incorporating new data from the ER-EC wells, provide generally consistent results using both NETPATH and the conservative tracer models presented in Section 2.7.1.2. The variation between results generated by these two methodologies is considered (SNJV, 2004a) to reflect differences in the approach of the two modeling techniques. This variation is also consistent with the natural variability in water chemistry within the system. Whereas the wells used as mixing "end-members" in the respective models are specific in composition, the groundwater compositions within each end-member sub-region or source area of the flow system are more variable, and cannot be completely described using specific individual wells.

Five of six potential groundwater flow paths identified by SNJV (2004a) using conservative tracers also had valid NETPATH models. Valid NETPATH models were not obtained for Flow Path 6, which considered southerly groundwater flow from Pahute Mesa to the Crater Flat area. It was concluded in SNJV (2004a) that insufficient data are available at this time to adequately determine the viability of this flow path. Groundwater travel time estimates generated using delta carbon-13 ($\delta^{13}C$) mass-balance calculations in NETPATH for Flow Paths 1 through 5 range from modern (fewer than 1,000 years) to 3,900 years.

Additional geochemical modeling addressing the evaluation of potential geochemical flow paths is provided in Section 7.0 of this report.

Uncontrolled When Printed

Table 2-22
Summary of Geochemical Flow Path Model Results for the Pahute Mesa Flow System (SNJV, 2004a)
(Page 1 of 2)

Flow Path Designation and Description	Groundwater and/or recharge source and contributory fraction (with flow-path target)								Apparent Travel Time (yrs)
	Pahute Mesa Groundwater from East of the Purse Fault	Pahute Mesa Groundwater from West of the Purse Fault	Gold Flat/Tonopah Test Range (TTR)/Tolicha Peak	Timber Mountain Area	Local Recharge	Oasis Valley	Amargosa Valley	Crater Flat	
Flow Path 1 Pahute Mesa groundwater + local recharge = Oasis Valley groundwater									
Conservative Tracers	0.45 - 0.56	0.39 - 0.42			0.02 - 0.16	Target			
NETPATH	0.39 - 0.57	0.29 - 0.56			0.05 - 0.14	Target			modern (> 1,000) to 3,900
Flow Path 2 Pahute Mesa groundwater + Gold Flat/TTR groundwater + local recharge = Oasis Valley groundwater									
Conservative Tracers	0.09 - 0.12	0.24 - 0.50	0.34 - 0.60		0.33 - 0.42	Target			
NETPATH	0.10 - 0.83	0.10 - 0.40	0.17 - 0.72			Target			modern (> 1,000) to 2,300
Flow Path 3 Tolicha Peak +/- Pahute Mesa groundwater +/- Gold Flat/TTR groundwater +/- local recharge = Oasis Valley groundwater									
Conservative Tracers		0.23 - 0.27	0.73 - 0.77			Target			
NETPATH			1			Target			modern (<1,000) to 1,500
Flow Path 4 Pahute Mesa groundwater + local recharge (in Timber Mountain area) = Beatty Wash to Oasis Valley discharge area									
Conservative Tracers	0.47 - 0.53	0.22 - 0.23		0.24 - 0.31		Target			
NETPATH	0.00 - 0.76			0.24 - 1.0		Target			modern (> 1,000) to 1,600

Uncontrolled When Printed

Table 2-22
Summary of Geochemical Flow Path Model Results for the Pahute Mesa Flow System (SNJV, 2004a)
(Page 2 of 2)

Flow Path Designation and Description	Groundwater and/or recharge source and contributory fraction (with flow-path target)								Apparent Travel Time (yrs)
	Pahute Mesa Groundwater from East of the Purse Fault	Pahute Mesa Groundwater from West of the Purse Fault	Gold Flat/Tonopah Test Range (TTR)/Tolicha Peak	Timber Mountain Area	Local Recharge	Oasis Valley	Amargosa Valley	Crater Flat	
Flow Path 5 Pahute Mesa groundwater + local recharge = flow down Fortymile Wash toward the Amargosa Valley									
Conservative Tracers	0.13 - 0.39			0.05 - 0.29	0.56 - 0.57		Target		
NETPATH	0.08 - 0.37			0.32 - 0.65	0.14 - 0.54		Target		1,000 to 3,800
Flow Path 6 Pahute Mesa groundwater + local recharge = Crater Flat[a]									
Conservative Tracers	0.44 - 0.57	0.00 - 0.02		0.20 - 0.54	0.00 - 0.22			Target	
NETPATH								Target	no valid model

Source: Modified from SNJV, 2004a

[a]No valid NETPATH models were obtained for Flow Path 6; for discussion, see SNJV, 2004a.

Uncontrolled When Printed

3.0 COMPUTER CODE SELECTION

The *Corrective Action Investigation Plan for Corrective Action Units 101 and 102: Central and Western Pahute Mesa, Nevada Test Site Nevada* (DOE/NV, 1999) identified a process for the identification and selection of a numerical code for use in Pahute Mesa flow and transport modeling. This process was completed in 1999, and the FEHM code (Zyvoloski et al., 1997b) was selected as the flow and transport simulator for the Pahute Mesa CAU model. This section provides an overview of the code selection process that supported the selection of the FEHM code. Appendix A provides the 1999 Letter Report that documents the evaluation of flow and transport codes for application to the Pahute Mesa CAUs.

3.1 Code Selection Process

The code selection process was identified in the Pahute Mesa CAIP (DOE/NV, 1999, Section 5.1.2). This process included:

- Identifying a set of desired code attributes.
- Developing a preliminary list of potentially viable codes.
- Evaluating a short list of codes that incorporate key code attributes using a test problem.

The ultimate objective of this code-selection process was to provide a recommendation for the numerical code to use for Pahute Mesa CAU modeling.

3.2 Code Attributes

The Pahute Mesa CAIP (DOE/NV, 1999) identified three objectives for the numerical code used in the CAU model. The first objective requires the CAU model to have the ability to represent the important physical and chemical features of the CAU groundwater flow system. The features include faulting, stratigraphy, sources and sinks of water, the distribution of contaminants and their rates of introduction into the groundwater flow system, and other physical or chemical features unique to the CAU. The second objective requires the CAU model to simulate the movement of a variety of

Uncontrolled When Printed

contaminants for which their distribution and abundance serve to define the contaminant boundary. The third objective requires flexibility in the CAU model to allow grid changes, placement of additional wells, and boundary condition variations.

The required code attributes that were defined to meet these modeling objectives were categorized under "general," "flow model," and "transport model." Table 3-1 summarizes these attributes.

Table 3-1
Required Hydrologic Code Attributes[a]

General Attributes	Flow Model Attributes	Transport Model Attributes
Fully three-dimensional	Saturated groundwater flow	Advection, dispersion, sorption, and matrix diffusion
Large number of nodes (500,000 or more) capability	Heterogeneous and anisotropic hydraulic conductivity	Radioactive decay
Transient capability	Point and distributed sources and sinks of water	Transport of colloids
Multiple boundary condition options	Temperature dependence	
Efficient solver	Simulate complex geology	
Acceptable numerical accuracy		
Minimal numerical dispersion		
Acceptable verification and validation		
Access to source code		

Source: Modified from DOE/NV, 1999

[a]Order of attributes does not indicate order of importance.

In addition, other desirable code attributes were identified including:

- Finite element formulation
- Steady-state capability
- Double-porosity/double-permeability formulation
- Multiple solutes
- Daughter products
- Established pre- and post-processors

The following discussion provides a brief description of these attributes.

Uncontrolled When Printed

General Attributes

The general attributes are defined with the goal of using a code that can closely represent a large modeling domain, in addition to being flexible, user-friendly and efficient.

Fully Three-Dimensional

The groundwater flow system is controlled by the distribution of geologic units as well as the location of sources and sinks of water. Additionally, transport properties including source location and strength, porosity, and diffusion may vary in space. The 3-D nature of the groundwater flow system requires that the CAU model will need to be 3-D to adequately simulate migration of the potential contaminants within the CAU-model area.

Large Numbers of Nodes Capability

For a given formulation, the greater the number of nodes in the CAU model, the greater the detail that can be included. Given the large geographic area of the Pahute Mesa CAU model, the ability of the CAU model to simulate many nodes will control the amount of detail that can be included. In general, each of the selected codes will only be limited by the capacity of the hardware, not by the software used.

Transient Capability

The flow simulations for the CAU model will be steady state. The contaminant transport simulations will all be performed under transient concentration conditions.

Multiple Boundary Condition Options

Options for specified pressure and specified flux boundary conditions for fluids, as well as specified temperature or specified heat flow, may be required in implementing the CAU model.

Efficient Solver

To simulate in sufficient detail, the CAU model will require a large number of nodes as mentioned above. To make a large model practical, the codes must run efficiently. Generally, a code has a selection of solvers available. The solvers must be efficient enough to allow for reasonable simulation times.

Uncontrolled When Printed

Acceptable Numerical Accuracy

The numerical solution of the transport equation is typically more difficult than the solution of the flow equation. This attribute requires the results of the code for a given test problem to have been checked against analytical solutions and also against the results of other numerical codes for the same problem. Documentation of this quality assurance (QA) checking must be available.

Minimal Numerical Dispersion

Under certain circumstances, the error in the numerical approximation of concentration can become as large as the value itself. When this occurs, the numerical solution combines an exclusively numerical dispersion with the real hydrodynamic dispersion, producing an overestimate of the actual dispersion. Solution techniques that minimize numerical dispersion are required.

Acceptable Verification and Validation

The degree of computer code verification and validation varies widely depending on the code being considered. The extent to which this process has been documented for a particular code varies even more. Thoroughly documented testing is required to ensure that the code satisfies requirements specified for its options and features.

Access to Source Code

Computer codes are initially written in a high-level language, such as FORTRAN, and then translated into machine language for execution on the computer. The high-level version of the code is called the "source code," and can be read and modified. The machine-language version is called the "executable code," and can be deciphered only by the computer. Many distributors of computer codes provide only the executable version of the code to the user. During the course of the development or application of the CAU model, it may be necessary to examine or modify the step-by-step procedure implemented in the computer code. To accomplish this, access to the source code will be required.

Groundwater Flow Model Attributes

The attributes for the groundwater flow model are defined with the goal of simulating the flow paths and fluxes.

Uncontrolled When Printed

Saturated Groundwater Flow

The codes must be able to simulate saturated groundwater flow.

Heterogeneous and Anisotropic Hydraulic Conductivity

Aquifer heterogeneity reflects the natural variability in the subsurface. The CAU model must be capable of simulating flow through aquifers in which the hydraulic conductivity may vary from location to location. Anisotropy is a directional dependence of the hydraulic conductivity. In fractured aquifers, it is common for hydraulic conductivity to be larger in a direction parallel to fracturing and smaller perpendicular to fracturing.

Point and Distributed Sources and Sinks of Water

Recharge may occur over a large spatial area due to precipitation or may be concentrated into washes or craters. Discharge may occur at wells or individual springs, or may occur over larger areas such as playas. The CAU model should have the capability to simulate these various cases.

Temperature Dependence

The flow of groundwater may be influenced by water temperature variations. Warm water is more buoyant than colder water and tends to rise. Additionally, warm water is less viscous and tends to move more easily than cold water. These processes may be important in some portions of the CAU where naturally occurring sources of heat have caused elevated groundwater temperatures. An additional source of warm water may be the underground test cavities. It may be important to account for these temperature effects in the simulations.

Simulate Complex Geology

The geology of the Pahute Mesa area is complex. It consists of multiple stratigraphic units, some of which are truncated by faults and other structural features. Even within units, changes in facies result in spatial variations in material properties. The flow of groundwater (amount and direction) is governed, in large part, by the distribution of geologic units. The code must be able to include important features of the geology such as lateral and vertical changes in material properties. Much of this attribute is similar to earlier general attributes related to the number of grid nodes and simulation

Uncontrolled When Printed

speed. The greater the number of nodes, the more detail that can be incorporated into the CAU model.

Transport Model Attributes

The contaminant transport model portion defines the attributes that will be necessary to simulate the migration of potential contaminants including radionuclides and lead.

Advection, Dispersion, Sorption, and Matrix Diffusion

The primary processes of interest in Pahute Mesa that are expected to influence the concentration of radioncludes in groundwater are listed here. The regional contaminant transport model (IT, 1996e) simulations and the Value of Information Analysis (IT, 1998b) showed that advection (via the groundwater flux) and matrix diffusion were the primary factors influencing tritium transport. It is expected that sorption will also be important for reactive contaminants, but this may not be the dominant contributor to the location of contaminant boundary. Dispersion was not shown to be of primary importance in the regional simulations, but is included here because it may be more important at smaller scales.

Radioactive Decay

Most, but not all, of the potential contaminants of interest are radionuclides. The activity per volume of radionuclides decreases via the process of radioactive decay.

Transport of Colloids

The movement of colloids may enhance the movement of otherwise immobile contaminants. Colloids are submicron size particles to which radionuclides or other solutes sorb. The colloids are then transported via the groundwater flow, and the sorbed solutes move with the colloids. Currently, no known contaminant transport codes explicitly simulate the transport of colloids. Thus, this attribute will only be considered if codes that simulate colloid transport are available at the time of the code selection.

Uncontrolled When Printed

Desirable Attributes

Other attributes that were identified during the code selection process address both technical capabilities and code characteristics.

Finite Element Formulation

A finite element formulation allows much more flexibility in representing the geology being modeled. Grids can be developed to represent complex structures such as faults, pinchouts and layer truncations. In addition, grid refinement allows the grid to be modified to provide more resolution in the area of interest.

Steady-State Capability

Some of the codes do not include a steady flow option, but rather reach steady-state by leaving parameters fixed in time and performing transient simulations over large periods of time until steady state is reached. This approach is adequate, but somewhat slower than if a true steady-state option were available.

Double-Porosity/Double-Permeability Formulation

The double-porosity/double-permeability method is similar to the dual-porosity method in that it allows for communication between fractures and matrix material. This feature allows for the modeling of matrix diffusion. The double-porosity/double-permeability method differs in that it allows matrix cells that communicate with fractures to also communicate with other matrix cells. While this method provides a more realistic simulation, its use is more important for unsaturated flow problems.

Multiple Solutes

Many codes are designed to provide a simulation of the migration of a single solute in a given run. Using a code with the ability to model transport for multiple solutes in a single run may be more efficient.

Uncontrolled When Printed

Daughter Products

A radionuclide may decay into another radionuclide (called a daughter product) or into a stable isotope. More accurate estimates of dose can be obtained if the code is capable of simulating the ingrowth and transport of a radionuclide and daughter product(s).

Established Pre- and Post-Processors

The task of creating the input datasets for any model is simplified by having pre-processors take data and put them into a form that is required by the model. Post-processors take model output and typically create graphic images of some simulated parameter such as water level or solute concentration. Pre- and post-processors generally speed up the modeling task. If the processors are not available, then the appropriate processors would be developed.

3.3 Code Testing Criteria

The criteria used to assess the codes were defined in the CAIP for Pahute Mesa (DOE/NV, 1999). These criteria range from a somewhat subjective assessment of ease of use to more quantifiable assessments such as the run time for a sample problem. The testing criteria are as follows:

Ability To Represent the CAU Hydrogeology

The primary geologic features that control flow need to be represented in the CAU model. These features include the hydrostratigraphy, physical boundaries, and structural features such as faults. In addition, the ability to model physical processes of concern (e.g., advection, dispersion, matrix diffusion, adsorption, and radioactive decay) is also important. The criteria also include an assessment of the ability of the model to include sufficient detail and stay within the memory limitations of the computer platform chosen for simulation.

Portability

The CAU model may be sent to independent reviewers as well as the State of Nevada. Each of these stakeholders may want to run the code themselves. This requires that the code, when complete, should require minimal special equipment or software in order to make it usable. Additionally, the CAU model will likely need to be run on a classified computer at the NNSA/NSO or another approved secure location to produce a final estimate of the contaminant boundary (results based on

Uncontrolled When Printed

classified data will be reported in a classified report). The code and associated pre- and post-processors must be portable to the selected secure location to allow for efficient classified simulations.

Quality Assurance Evaluation

The chosen code must have been appropriately verified to ensure the output is accurate. The QA evaluation refers to the level of documentation and testing for a code. The ability of the code to simulate the processes of interest is a function of the formulation of the equations and the quality of the programming. A code meets the QA requirements if its results have been verified against those of other codes as well as compared with analytical solutions. These comparisons must be documented before a code will be used for the Pahute Mesa model.

Ease of Use

The ease of use is a subjective judgment that assesses the modeler's degree of difficulty in getting the model running. This is, by necessity, a value judgment of the modeler and reflects the modeler's experience and background. A great deal of work will be spent calibrating the CAU model and setting up sensitivity and uncertainty analyses. A code that is difficult to use makes the job of calibration more difficult and reduces the code's portability. Ease of use includes factors such as the structure of the input datasets used in the model and the flexibility of pre- and post-processors.

Speed of Simulation

The time required for a solution is also of importance to the evaluation of the codes. The faster the code, the shorter the time to complete each model run. As calibration normally requires many (often greater than 500) model runs, the simulation time becomes a problem if it is too long. To enhance calibration performance, simulation times should be as short as possible. In addition, the ability to carry out model runs in parallel by distributing them across a network can greatly enhance calibration efficiency.

Uncontrolled When Printed

3.4 Initial Screening of Candidate Codes

The Pahute Mesa CAIP (DOE/NV, 1999) identified 14 numerical codes as possible candidates for Pahute Mesa CAU modeling. These codes were:

- AQUA3D (Vatnaskil Consulting Engineers, 1988)
- BIOF&T-3D (Katyal, 1995)
- CFEST (Gupta, 1996)
- FEHM (Zyvoloski et al., 1996)
- FRAC3DVS (Waterloo Hydrogeologic Inc., 1998)
- HST3D (Kipp, 1986)
- MODFLOWT (Duffield et al., 1996)
- MT3D96 (Scientific Software Group, 1998)
- NUFT (Nitao, 1998)
- PARFLOW (Ashby, et al., 1996)
- PORMC (Westinghouse Hanford Co., 1991)
- SWIFT-98 (HSI GeoTrans, 1998). Note this version of SWIFT was identified as a newer version than SWIFT III (HSI GeoTrans, 1990)
- TOUGH2 (Pruess, 1991)
- 3DFEMFAT (Scientific Software Group, 1998)

An initial screening of the codes was performed with respect to the attributes. The results of the comparison are presented in Table 3-2.

Uncontrolled When Printed

Table 3-2
Comparison of Candidate Codes by Attribute
(Page 1 of 2)

Code Attribute	AQUA3D	BIOF&T-3D	CFEST	FEHM	FRAC3DVS	HST3D	MODFLOWT	MT3D96	NUFT	PARFLOW	PORMC	SWIFT-98	TOUGH2	3DFEMFAT
GENERAL														
Fully three-dimensional	Y[a]	Y	Y	Y	Y	Y	Y	Y	Y	Y	Y	Y	Y	Y
Large number (500,000) of nodes	?[b]	Y	Y	Y	Y	?	Y	Y	Y	Y	Y	Y	Y	Y
Transient capability	Y	Y	Y	Y	Y	Y	Y	Y	Y	Y	Y	Y	Y	Y
Multiple boundary condition options	Y	Y	Y	Y	Y	Y	Y	Y	Y	Y	Y	Y	Y	Y
Efficient solver	Y	Y	Y	Y	Y	?	Y	Y	Y	Y	Y	Y	Y	Y
Acceptable numerical accuracy	Y	Y	Y	Y	Y	?	Y	Y	Y	Y	Y	Y	Y	Y
Minimal numerical dispersion	Y	Y	Y	Y	Y	?	Y	Y	Y	Y	Y	Y	Y	Y
Acceptable verification and validation	Y	Y	Y	Y	Y	?	Y	Y	Y	Y	N	Y	Y	Y
Access to source code	N[c]	N	N	Y	Y	Y	Y	Y	N	Y	Y	Y	Y	N
FLOW MODEL														
Saturated groundwater flow	Y	Y	Y	Y	Y	Y	Y	N	Y	Y	Y	Y	Y	Y
Heterogeneous hydraulic conductivity	Y	Y	Y	Y	Y	?	Y	N	Y	Y	Y	Y	Y	Y
Anisotropic hydraulic conductivity	Y	Y	Y	Y	Y	?	Y	N	Y	Y	Y	Y	Y	Y
Point/distributed sources/sinks of water	Y	Y	Y	Y	Y	Y	Y	N	Y	Y	Y	Y	Y	Y
Temperature dependence	Y	N	Y	Y	N	Y	N	N	Y	N	Y	Y	Y	N
Ability to simulate complex geology	Y	Y	Y	Y	Y	?	Y	Y	Y	Y	Y	Y	Y	Y
TRANSPORT MODEL[d]														
Advection	Y	Y	Y	Y	Y	Y	Y	Y	Y	N	Y	Y	Y	Y
Dispersion	Y	Y	Y	Y	Y	Y	Y	Y	N	N	Y	Y	N	Y
Sorption	Y	Y	Y	Y	Y	Y	Y	Y	Y	N	Y	Y	N	Y
Matrix diffusion	Y	Y	N	Y	Y	N	Y	N	Y	N	N	Y	N	N
Radioactive decay	Y	Y	Y	Y	Y	Y	Y	Y	Y	N	Y	Y	Y	Y

Uncontrolled When Printed

Table 3-2
Comparison of Candidate Codes by Attribute
(Page 2 of 2)

Code Attribute	AQUA3D	BIOF&T-3D	CFEST	FEHM	FRAC3DVS	HST3D	MODFLOWT	MT3D96	NUFT	PARFLOW	PORMC	SWIFT-98	TOUGH2	3DFEMFAT
OTHER DESIRABLE ATTRIBUTES														
Finite element formulation	Y	Y	Y	Y	Y	N	N	N	N	N	N	N	N	Y
Steady-state capability	N	N	N	Y	Y	?	Y	Y	N	N	Y	Y	N	N
Double-porosity/double-permeability	N	N	N	Y	N	N	N	N	Y	N	N	N	Y	N
Multiple solutes	N	Y	?	Y	Y	N	N	N	Y	N	N	N	N	N
Daughter products	N	Y	N	Y	Y	N	Y	Y	Y	N	N	Y	N	N
Established pre- and post-processors	Y	Y	Y	Y	Y	?	Y	Y	Y	Y	Y	Y	Y	Y

Source: Modified from DOE/NV, 1999

[a]Y = Yes
[b]? = No data
[c]N = No
[d]The transport of colloids was not considered during the code selection process.

Uncontrolled When Printed

Of this list, 10 codes were eliminated from further consideration. Seven codes (CFEST, HST3D, MT3D96, PARFLOW, PORMC, TOUGH2, and 3DFEMFAT) were eliminated because they do not have the ability to simulate matrix diffusion explicitly. The BIOF&T-3D and AQUA3D codes were eliminated because access to the source codes was not available. The NUFT code was eliminated because current documentation (Nitao, 1998) indicated that hydrodynamic dispersion was not implemented in the code.

Of the remaining four codes, only FEHM and SWIFT-98 have all of the required attributes. The FRAC3DVS and MODFLOWT codes lacked only the ability to simulate thermal effects. The FRAC3DVS code was ranked above MODFLOWT and retained for testing because its finite element formulation would allow a more accurate representation of the complex geology. Therefore, the three codes that were retained for further evaluation are FEHM, FRAC3DVS, and SWIFT-98.

3.5 Description of Selected Candidate Codes

Features of the three codes identified as possible candidates for use in the Pahute Mesa CAU model are described below.

FEHM

The FEHM code (Zyvoloski et al., 1997b) was developed by LANL. The FEHM code simulates 3-D, time-dependent, multiphase, nonisothermal flow, and multicomponent reactive groundwater transport through porous and fractured media. The FEHM finite-element formulation allows for representation of complex 3-D geologic media and structures and their effects on subsurface flow and transport. The hydrologic source term, recharge, lateral boundary conditions, and parameter values are inputs to FEHM. The FEHM output consists of spatial distribution of head and concentration at specified times and concentration with time through specified boundaries and planes. The transport processes of interest include advection, dispersion, sorption, matrix diffusion, radioactive decay, colloid-facilitated transport, and daughter product ingrowth. Specific capabilities include:

- Three-dimensional
- Flow of gas, water, oil, and heat
- Flow of air, water, and heat
- Multiple chemically reactive and sorbing tracers
- Colloid transport

Uncontrolled When Printed

- Finite element/finite volume formulation
- Coupled stress module
- Saturated and unsaturated media
- Preconditioned conjugate gradient solution of coupled nonlinear equations
- Double-porosity and double-porosity/double-permeability capabilities
- Complex geometries with unstructured grids

A number of documents supporting the FEHM code are readily available from LANL. In addition to the user's manual (Zyvoloski, et al., 1997a), these documents include a description of the mathematical models and numerical methods used by FEHM (Zyvoloski, et al., 1997b); documentation of the functional and performance requirements for FEHM; description of the FEHM software, the verification and validation plan; and description of the verification and validation activities (Dash et al., 1997; Dash, 2000 and 2001).

FRAC3DVS

FRAC3DVS (Waterloo Hydrologic, Inc., 1998) is a 3-D, finite element code for simulating steady-state or transient, variably-saturated groundwater flow, and advective-dispersive solute transport in porous or discretely-fractured porous media. The code was developed by E.A. Sudicky at the Waterloo Centre for Groundwater Research and R. Thierren at Laval University. Specific capabilities of this code include:

- Three-dimensional
- Flow of water
- Multi-species transport of either straight or branching decay chains
- Sorption according to a linear or Freundlich isotherm
- Control-volume finite element, Galerkin finite element, or finite difference formulation
- Saturated and unsaturated media
- Conjugate-gradient-like solver
- Dual-porosity and discrete fracture capabilities
- Irregular, layered grids composed of blocks or prisms

SWIFT

The Sandia Waste Isolation Flow and Transport (SWIFT) computer code (Reeves et al., 1986; Ward et al., 1984; HSI GeoTrans, 1990) is a 3-D groundwater flow and transport model that simulates the movement of solutes, including radionuclides, in groundwater. The code is finite-difference and includes fluid flow, heat transfer, and brine transport in saturated porous media.

Uncontrolled When Printed

The SWIFT code evolved from the USGS Survey Waste Injection Program (SWIP) Code (Intercomp, 1976) and has undergone several modifications since its inception. The version of the SWIFT code used in this code comparison is SWIFT-98 (HSI GeoTrans, 1998). Specific capabilities include:

- Simulation of advective-dispersive transport with adsorption and decay
- Simulation of transport in fractured media via a dual-porosity/dual-permeability conceptualization
- Simulation of brine and heat transport in porous or fractured formations
- Inclusion of variable fluid density and variable fluid viscosity
- Accounts for leaching of waste
- Includes a wellbore submodel that simulates energy losses in and surrounding a borehole
- Simulation of planar or spherical matrix block geometry
- Specification of longitudinal, transverse, and vertical dispersivities
- Variable decay rates, retardation factors, and porosities available for transport simulations
- Radioactive decay and simultaneous simulation of up to three daughter products
- Transient and steady-state flow and transport options available
- Can choose time-stepping either as centered in time or backward in time
- A direct or two-line successive, over-relaxation method of solving the governing equation

3.6 Test Problem Used To Evaluate Candidate Codes

The features of the test problem used to evaluate the three candidates codes were chosen to represent conditions expected in the Pahute Mesa model area. The features included in the test problem were: complex caldera geology such as lithologic and structural features, temperature-dependent flow, radionuclide migration from a cavity, and matrix diffusion.

The test problem was designed to represent the expected level of complexity anticipated for Pahute Mesa. The Pahute Mesa hydrostratigraphic model (Drellack and Prothro, 1997) provided the definition and distribution of HSUs for the test problem. A portion of the model area was selected for

Uncontrolled When Printed

the test problem as representative of the complex geology of the Pahute Mesa CAU. The test problem model area was approximately 21 km (13.1 mi) by 19.5 km (12.1 mi) by 5,500 m (18,045 ft) in depth. The locations of the test problem boundaries are shown in Figure 3-1. The 3-D hydrostratigraphic model is shown in Figure 3-2 as viewed from the southwest corner of the test problem area. A cross-section of the test area (Figure 3-3) shows the complexity of the hydrostratigraphic layering and the occurrence of non-vertical faults.

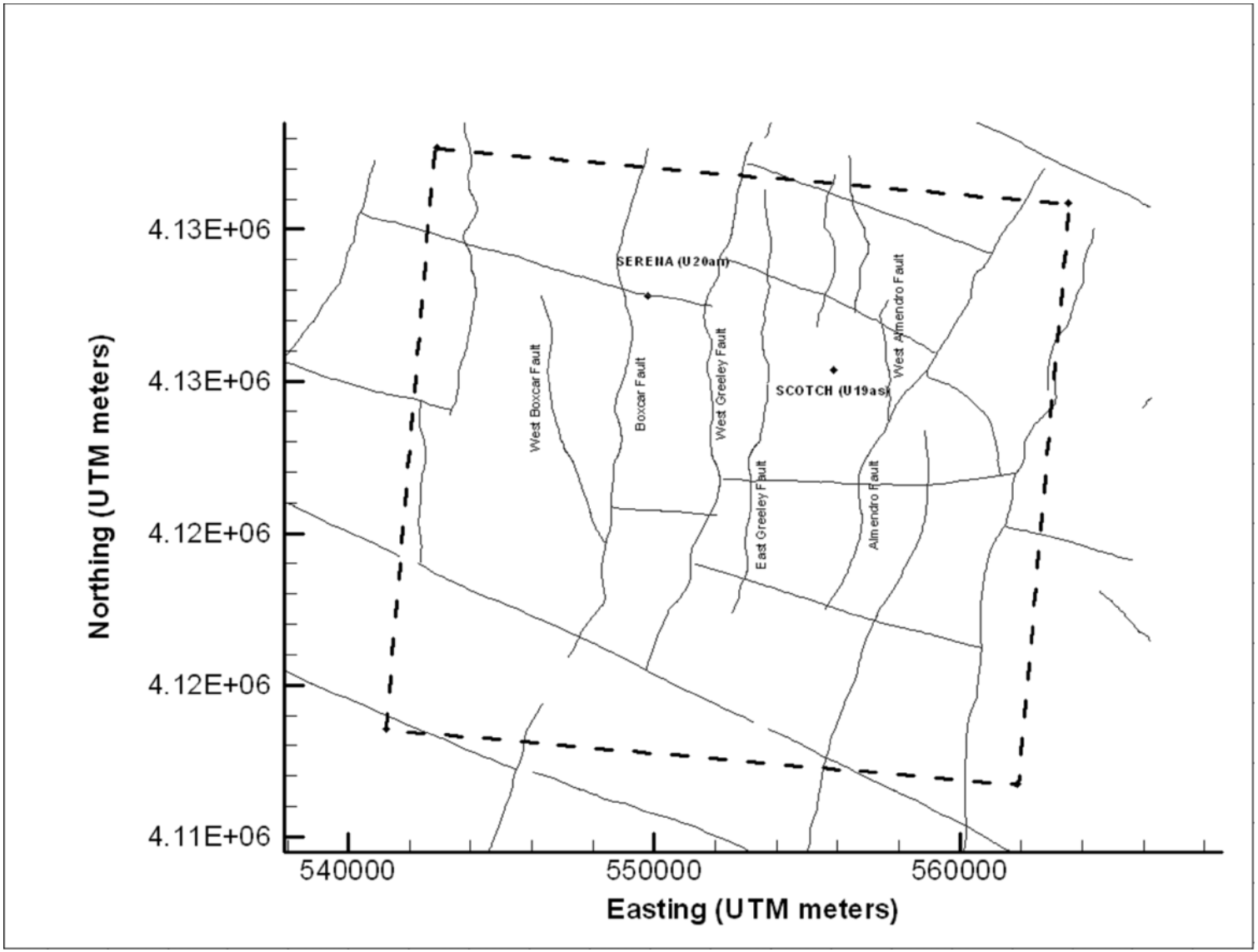

Figure 3-1
Code Evaluation Test Problem Boundaries, Selected Faults, and Locations of SERENA (U20an) and SCOTCH (U19as) Tests

Uncontrolled When Printed

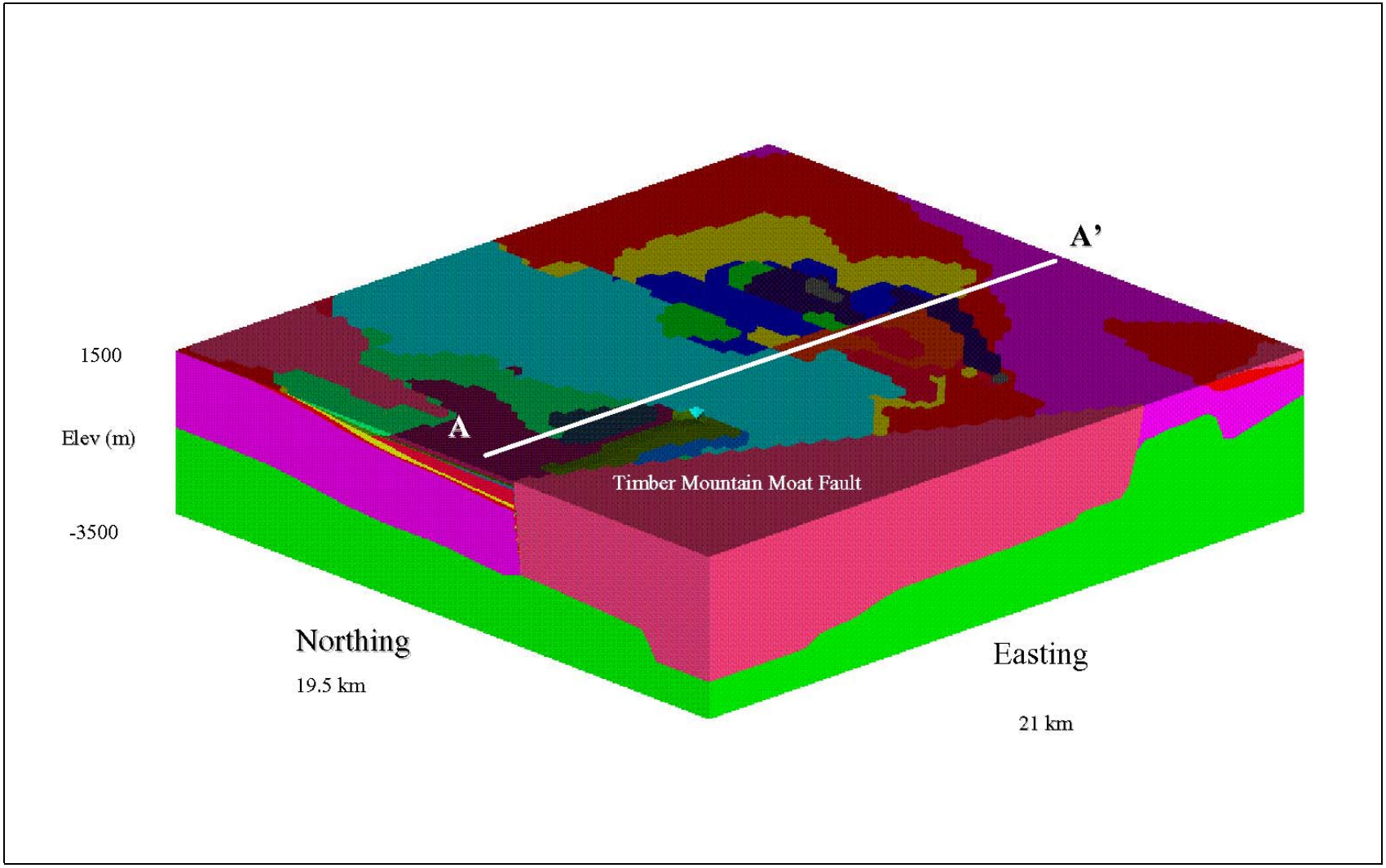

Figure 3-2
3-D Hydrostratigraphic Model Used for the Code Evaluation Test Problem
View is from the southwest.

Uncontrolled When Printed

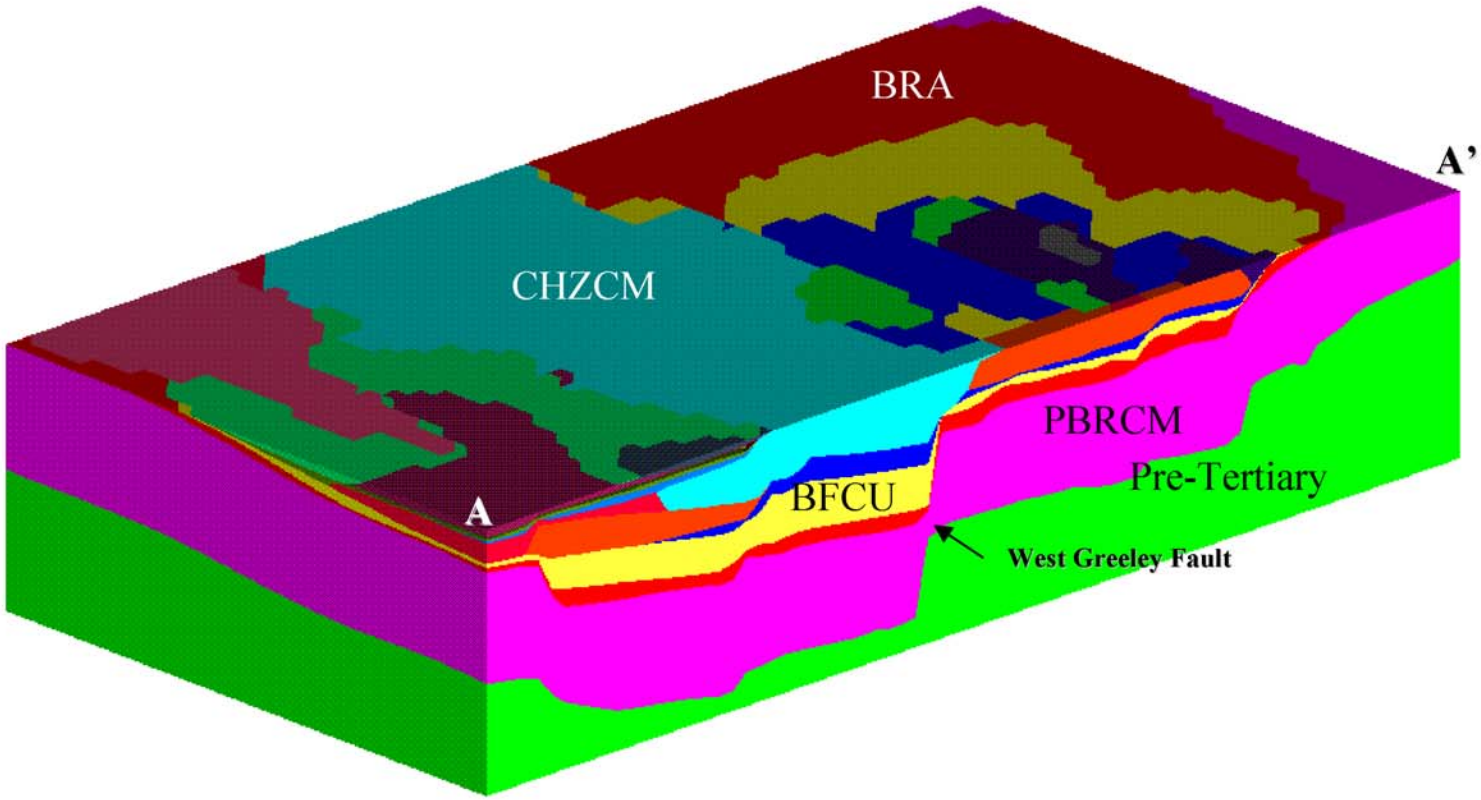

Figure 3-3
Schematic Representation of a Cross Section Through Test Problem Domain as Viewed from the Southwest
Units identified are BFCU, BRA, CHZCM, PBRCM, and Pre-Tertiary rocks.

Uncontrolled When Printed

The hydrogeologic model for the test problem included many of the hydrostratigraphic layers and faults in the Pahute Mesa hydrogeologic model. When using finite-element codes, the grid flexibility is used to attempt to reproduce the stratigraphic contacts and fault contacts. Finite-difference codes do not offer this flexibility; several identical horizontal and uniform grids must be stacked vertically to represent the model layers. As a result of this limitation, faults must be represented as vertical. The present Pahute Mesa geologic model explicitly accounts for dipping faults. As such, the location of a fault shifts, in plan view, for various layers. Thus, to use the finite-difference grid in the test problem, the faults will be approximated as vertical.

Each of the HSUs was assigned a hydraulic conductivity, porosity, and fracture volume fraction consistent with current best estimates of these properties. Parameter values used for the test problem are shown in Table 3-3.

Boundary conditions for the test problem were obtained from the UGTA regional flow model (DOE/NV, 1997). The process used was to average the properties of the Pahute Mesa hydrogeologic model to the same resolution as the regional model. The HSUs from the Pahute Mesa hydrogeologic model were then added to the regional model. A visualization application, EV, was used to examine the correspondence between the CAU-scale model and the regional model. All layers were checked for inversions of layers and that a constant elevation of at least 1 m vertically was maintained in the hydrogeologic model layering. Using this modified regional hydrogeologic model, the UGTA regional flow model (DOE/NV, 1997) was run, without recalibration, to obtain the heads along the boundaries of the test problem. Figure 3-4 shows the head distribution for the northern boundary of the test problem.

Two underground nuclear tests were chosen for consideration as sources in the test problem, SERENA (U20an) and SCOTCH (U19as). The locations of these tests are shown in Figure 3-1. SERENA was chosen because of its location on a fault, and SCOTCH was chosen because of the depth of the working point and the absence of faults in the immediate vicinity in the Pahute Mesa hydrogeologic model. Because the location of SCOTCH is within the BFCU, very little transport was expected. To provide a better test for the codes, additional simulations considered the source to be translated vertically upward to the location of the CHVTA.

Uncontrolled When Printed

Table 3-3
Summary of HSU/Fault Parameter Values Used in the Test Model

HSU or Fault	HSU[a]	Permeability Range (m/d)[a]	Permeability (m/d) (PM Test Problem)	Fracture Volume Fraction	Matrix Porosity
Timber Mountain Aquifer	TMA	1.0-30	1.000	0.001	0.1
Timber Mountain Composite Unit	TMCM	0.001-0.5	0.014	0.01	0.1
Windy Wash Aquifer	WWA	1.0-20	1.000	0.01	0.1
Paintbrush Vitric-Tuff Aquifer	PVTA	0.1-1	0.100	0.01	0.3
Benham Aquifer	BA	1.0-20	1.000	0.01	0.1
Upper Paintbrush Confining Unit	UPCU	0.001-0.5	0.007	0.01	0.3
Tiva Canyon Aquifer	TCA	0.5-0.1	0.500	0.001	0.1
Paintbrush Lava-Flow Aquifer	PLFA	1.0-20	1.000	0.01	0.1
Lower-Paintbrush Confining Unit	LPCU	0.001-0.5	0.011	0.01	0.3
Topopah Spring Aquifer	TSA	5.0-30	30.000	0.001	0.1
Calico Hills Vitric-Tuff Aquifer	CHVTA	0.1-1	0.100	0.01	0.3
Calico Hills Vitric Composite Unit	CHVCM	0.1-20	0.100	0.005	0.2
Calico Hills Zeolitized Composite Unit	CHZCM	0.001-15	0.003	0.01	0.3
Calico Hills Confining Unit	CHCU	0.001-0.5	0.001	0.01	0.3
Inlet Aquifer	IA	0.1-5	2.010	0.01	0.1
Crater Flat Composite Unit	CFCM	0.001-5	5.000	0.01	0.2
Crater Flat Confining Unit	CFCU	0.001-0.5	0.001	0.01	0.3
Kearsarge Aquifer	KA	0.1-5	2.000	0.01	0.1
Bullfrog Confining Unit	BFCU	0.001-0.5	0.001	0.01	0.3
Belted Range Aquifer	BRA	0.5-15	0.500	0.005	0.1
Pre-Belted Range Composite Unit	PBRCM	0.001-0.01	0.001	0.005	0.2
Pre-Tertiary	PreT	-	0.000085	-	-
Moat Fault	N/A	0.0000075-75	75		
South Boxcar Fault	N/A	0.0000075-75	75		
West Boxcar Fault	N/A	0.0000075-75	75		
East Boxcar Fault	N/A	0.0000075-75	75		

[a]Drellack and Prothro, 1997

Uncontrolled When Printed

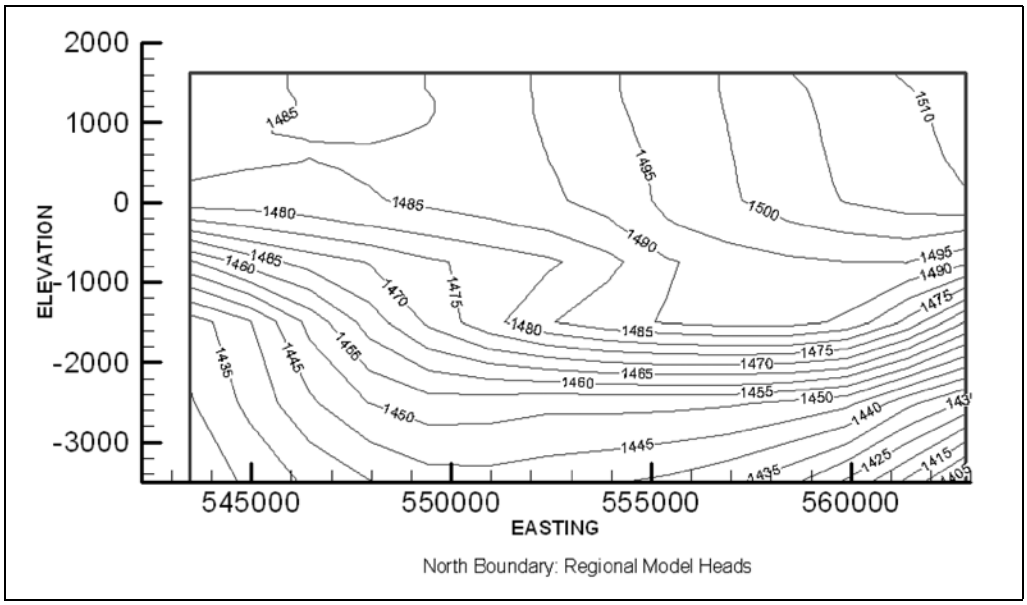

Figure 3-4
Head Distribution for the North Boundary of the Test Problem Domain from the UGTA Regional Model

The unclassified hydrologic source term used for these sources in the test problem was developed by Tompson et al. (1999) for CAMBRIC. Four radionuclides were considered: tritium, strontium (Sr)-90, plutonium (Pu)-239, and americium (Am)-241. A total of 2.04 moles of tritium were introduced instantaneously as a pulse. The other radionuclides entered the flow system as a time-varying flux as determined by Tompson et al. (1999). Tritium and Sr-90 were treated as non-sorbing. Plutonium-239 and Am-241 were assigned distribution coefficient (K_d) values of 50 and 100 liters and kilograms, respectively. These values are consistent with the Frenchman Flat CAU model (IT, 1999, Table 9-1). Analysis of the BULLION Forced-Gradient Experiment (FGE) (IT, 1998a) suggested values of dispersivities of 10, 3, and 2 m for longitudinal, transverse, and vertical directions, respectively. Because this experiment involved transport on the scale of 100 m, dispersivities were increased to 50 and 5 m for longitudinal and transverse directions for the Frenchman Flat CAU model. Consistent with the Frenchman Flat CAU model, dispersivities used for the Pahute Mesa test problem were 50 and 5 m.

The local geothermal gradient was included in the test problem for the two codes that account for temperature dependence. The value of the selected geothermal gradient was 0.0257 degrees Centigrade per meter.

Uncontrolled When Printed

The test problem was simulated without calibration, in some cases using extreme values of properties and hydrologic source terms in order to test the capability of the codes. With this in mind, it is important to note that the results of test problem simulations should not in any way be interpreted as accurately representing the magnitudes of flow and transport processes associated with the Pahute Mesa CAU.

3.7 Results of Code Evaluation

Flow and transport models of the defined test problem were developed and implemented using FRAC3DVS, SWIFT-98, and FEHM. The experience gained in developing these models and the assessment of output from each model provided the information that was used in the code evaluation process. This evaluation process included:

- Evaluation of the capabilities of each code to successfully model the test problem.
- Comparison of SWIFT-98 and FEHM models relative to the testing criteria detailed in Section 3.3.
- Identification of the recommended code for use in Pahute Mesa CAU flow and transport modeling.

3.7.1 Evaluation of Code Capabilities

During the evaluation of the FRAC3DVS transport model output, problems were identified in the simulation of non-decaying, non-sorbing tracers. The model output was characterized by alternating bands of positive and negative concentrations, and solute mass-balance errors as high as 10 percent when the sources were modeled at their working points. When the source was translated upward to the aquifer unit, mass-balance errors were as large as 100 percent due to the model simulating movement of the tracer into the unsaturated zone. In addition, the tested version of FRAC3DVS did not support specification of solute flux at nodes in the interior of the model domain and could not simulate thermal effects. Based on these issues, FRAC3DVS was eliminated from further consideration.

The evaluation of the flow and transport model output results for SWIFT-98 and FEHM simulations were satisfactory and demonstrated the required code capabilities.

Uncontrolled When Printed

3.7.2 Comparison of SWIFT-98 and FEHM Relative to the Testing Criteria

Ability To Represent CAU Hydrogeology

A major difference between FEHM and SWIFT-98 was how the hydrogeologic model was represented by the computational grid. The SWIFT-98 code is a finite-difference program and, as such, is not as flexible as a finite-element model at capturing the geometric shape of the individual HSUs. The FEHM code is a finite-element code that can more accurately represent complex hydrostratigraphy.

The rectangular prism-type blocks used for the SWIFT-98 grid can be defined by rows, columns, and horizontal layers, or in a stair-step fashion by rows and columns with the top elevation of the uppermost block. The latter method allows for flexibility in defining the layering of a system, but not the discretization in the plan view. In plan view, all blocks along a column or a row must have the same width. In the SWIFT-98 test simulations, a simpler horizontal layering scheme was utilized. The change of hydrologic properties with depth as defined by HSUs was implicitly considered in block properties by averaging all of the different HSU properties contained in each finite difference block. When a block contained material from more than one HSU a composite property was generated using a pre-processor. The pre-processor also considers the influence of faults and fault zones by combining fault properties with the porous media properties generated from the hydrogeologic model. Fault properties are combined in parallel to porous-media block properties in the direction of the faults and in series perpendicular to the fault. The trace of all faults is assumed to follow a path from block center to block center parallel (or perpendicular to the block faces). The block structure of the grid does not allow for non-vertical faults.

The grid generation tools interfaced with the FEHM code allowed for the accurate representation of the complexities of the hydrogeologic model for Pahute Mesa. The hydrostratigraphic structure as provided by the hydrogeologic model was captured in the finite-element grid. This included units of variable thickness and units that pinch out. Faults were included through a method that creates fault planes from surface maps of faults. With this method the specific offset across a fault was only as accurate as the resolution of the geologic model. While faults for the test problem were vertical, faults may be specified as non-vertical. Higher resolution of the grid was provided in source and

Uncontrolled When Printed

down gradient regions. The exact specification of HSUs eliminates the need to use composite properties in the model.

For this testing criteria element, FEHM was ranked above SWIFT-98 because it more accurately represented the CAU hydrostratigraphy.

Portability

The SWIFT-98 code was designed to run on personal computer (PC)-based Pentium processors and was specifically designed for use in conjunction with the Lahey LF90 Fortran compiler. The associated pre- and post- processors are also designed to run on Pentium processors. The only restriction on these codes involves GEO2MOD, which generates a binary input file for SWIFT-98 and required the Lahey LF90 Fortran compiler for compatibility if recompilation was necessary. All the other pre- and post-processors could be compiled with any Fortran compiler. Results of the simulations were saved in ASCII map files which could be converted to a format that could be used in any standard contouring package. For the test problem, EXCEL® macro programs were used to plot the results of simulations.

Computational mesh generation tools used with FEHM included the Los Alamos Grid Toolbox (LaGriT) (George, 1997) suite of grid meshing tools. LaGriT is a library of user callable tools that provide mesh generation, mesh optimization and dynamic mesh maintenance in 3-D for a variety of applications. LaGriT and associated applications required a UNIX-based platform. The software, user's manuals, and examples were available at no cost from LANL. However, considerable training is required to use these tools effectively. The FEHM code was available for a number of platforms, including PC. However, the application of FEHM to the test problem was conducted on a workstation computer with twin 400 megahertz Pentium II Xeon processors and 1 gigabyte of physical memory. A post-processor that runs on a PC was available to convert FEHM output files into a format readable by visualization software such as TECPLOT®.

For this testing criteria element, SWIFT-98 was ranked above FEHM because it required less specialized hardware and software.

Uncontrolled When Printed

Quality Assurance Evaluation

The SWIFT genre of codes had undergone verification and field comparison (validation) testing during their development and maintenance by Sandia National Laboratories (Ward et. al., 1984). The SWIFT-98 code, which was maintained by HSI GeoTrans, Inc., had also undergone the same testing procedure as described in Ward et al. (1984). Additionally, all changes made to the code have been tested. The testing was concluded March 1998. All test problems were included on the compact disc release of the code.

The FEHM code was subjected to an extensive verification and validation effort and is maintained in a formal software configuration management system. The verification and validation plan were provided in detail by Dash et al. (1997). The objective of the verification was to test the options and features of the code. This was accomplished by comparing the results of simulations with published analytical solutions and results from other codes. Every time a modification is made to the code, it is tested with a suite of verification problems to ensure no errors were introduced or capabilities eliminated. The tests considered in the verification effort were described in detail by Dash et al. (1997), and test results were discussed. A number of additional documents supporting FEHM were readily available from LANL. These documents included the user's manual (Zyvoloski, et al., 1997a), and a description of the mathematical models and numerical methods used by FEHM (Zyvoloski, et al., 1997b).

For this testing criteria element, FEHM was ranked above SWIFT-98 because it was maintained under a formal LANL software configuration management system.

Ease of Use

The SWIFT-98 code was judged as a difficult code to use, relative to standard groundwater flow and solute transport codes such as MODFLOW/MODFLOWT. The major difficulties were associated with the rigorous nature of the code, which allowed the user to couple density-dependent heat and brine transport with the groundwater flow model. In addition, the user's manual was sometimes unclear as to input needed, but the documented sample problems helped (Ward, et al., 1984). Still, for a fully coupled model, the code was considered average in difficulty of usage.

Because the FEHM test was conducted by an evaluator with only limited previous exposure to FEHM, the model development was completed with technical support from LANL by telephone. With the availability of LANL technical support, all the test model simulations were completed in seven weeks. The user's manual for FEHM was clearly written describing in detail all the data files, input data, and output files, and included examples for many of the macro control statements. Combining the available documentation with some training and telephone access to an experienced user, FEHM was easy to use.

For this testing criteria element, FEHM was ranked above SWIFT-98 primarily because its documentation was more comprehensive.

Speed of Simulation

The time required for simulation of a steady-state flow field with the presence of faults, FEHM required 15 minutes and SWIFT-98, 23 minutes. Transport simulations were consistently faster for SWIFT-98 than for FEHM. The time required to simulate 200 years of tritium transport with faults for sources located at the working points of SCOTCH and SERENA was 64 minutes for SWIFT-98 and 77 minutes for FEHM. When the source was moved up to the CHVTA, SWIFT-98 required 58 minutes and FEHM, 103 minutes. For the simulations with time-varying fluxes the times for simulation of individual radionuclides required by SWIFT-98 must be added for comparison to the multi-species FEHM simulations. Total times required to simulate 1,000 years of transport for Am-241, Pu-239, and Sr-90 with faults for sources located at the working points were 106 minutes for SWIFT-98 and 142 minutes for FEHM. When the source was moved up to the CHVTA, simulation times were 120 minutes for SWIFT-98 and 153 minutes for FEHM.

While the transport simulation times for SWIFT-98 were somewhat faster than for FEHM, an additional characteristic of the SWIFT-98 code must be considered when evaluating the speed of simulation for the CAU modeling effort. The SWIFT-98 code requires that most of the solute transport parameters required for radionuclide transport in a steady-state flow field be input into the steady-state flow simulation dataset. As a result, if a change is desired in the transport parameters, the flow field must be simulated again. This makes it difficult to perform multiple transport simulations based on a single steady-state flow simulation. The FEHM code does not have this limitation.

Uncontrolled When Printed

For this testing criteria element, FEHM was ranked above SWIFT-98 based on the SWIFT-98 requirement to re-simulate the steady-state flow field whenever the transport parameter input files were updated.

3.7.3 Recommended Code for Use in the Pahute Mesa CAU Flow and Transport Model

Based on the relative rankings of SWIFT-98 and FEHM for the five measures discussed in Section 3.7.2, FEHM was the code recommended for the Pahute Mesa CAU flow and transport model.

3.8 TYBO-BENHAM Case Study

Subsequent to completing the code selection process, a sub-CAU-scale model and a site-scale model were developed using FEHM. This summary of the TYBO-BENHAM case study (Wolfsberg et al., 2002) documents the successful application of the FEHM code in UGTA flow and transport models.

The TYBO-BENHAM FEHM models were developed as part of an integrated field, laboratory, and modeling analysis and evaluation of radionuclide transport in the Pahute Mesa groundwater (Wolfsberg et al., 2002). This study was motivated by the discovery of plutonium and other radionuclides in two groundwater observation wells 1.3 km from the BENHAM site located in Area 20 of the NTS on Pahute Mesa (Kersting et al., 1999).

The sub-CAU-scale flow model that was developed used FEHM to model flow with depth-dependent thermal properties. The model domain, approximately 10 km on a side, was discretized using an unstructured finite-element grid that represented the 22 distinct deterministic HSUs in the area. Faults were included as discrete features. The HSU permeabilities were calibrated and the model was used to provide boundary conditions for a site-scale flow model located within the domain of the sub-CAU-scale model.

The site-scale flow model developed using FEHM provided steady-state flow in the BENHAM and TYBO vicinity. This model was developed using a structured high-resolution grid and represented a domain 3.2 by 2.6 km. Boundary conditions were provided by the sub-CAU-scale flow model. The

Uncontrolled When Printed

site-scale flow model was run using the CAU deterministic hydrostratigraphy and 30 geostatistical attribute fields.

A 3-D source model was developed for this study using FEHM. The processes modeled included coupled nonisothermal transient flow, glass dissolution, and particle transport in the BENHAM cavity/chimney system. This model provided mass flux of sorbing and nonsorbing radionuclides into the local aquifers. Linear sorption of radionuclides in the chimney is included in the model. The modeling also considered multiple chimney material properties and thermal conditions in a sensitivity analysis. This model did not include aqueous speciation, rock-water reactions, or pH variations.

Two site-scale transport models were developed using FEHM, a particle transport model and a reactive transport model. Reactive, dual-porosity transport in steady-state, 3-D flow fields were modeled using the particle-tracking approach. This model was very computationally efficient, allowing multiple realizations to be run for sensitivity of source term, flow field, and transport parameters. In addition, the CAU deterministic hydrostratigraphy and 30 heterogeneous realizations were run.

The site-scale reactive transport model included more detailed chemical processes. As this model was significantly more complex, only a single heterogeneous realization was run. Processes modeled were reactive, dual-porosity, solute, and colloid-facilitated plutonium transport along steady-state streamtubes in a 3-D flow field.

These component models were combined with others in a system of models to: (1) simulate complex flow in layered, faulted, and fractured volcanic tuff; (2) investigate temperature-dependent processes associated with radionuclide release from melt glass and cavity-chimney systems; and (3) simulate radionuclide transport in fractured media, addressing fracture properties, diffusion, groundwater chemistry, colloids, fracture mineral exposure, and heterogeneity.

The observed features of the TYBO-BENHAM sub-CAU-scale flow system captured by the calibrated model included steep gradients across faults, downward vertical gradients in the shallow units, and upward vertical gradients in the deep units (Wolfsberg et al., 2002). With respect to the TYBO-BENHAM study, Wolfsberg et al. (2002) concluded:

"With these results, we are confident that we have generally captured the complex processes of source release and site scale migration."

Uncontrolled When Printed

4.0 GROUNDWATER FLOW MODEL CONSTRUCTION

This section describes the approach and results of construction of the Pahute Mesa flow model. The overall goal of this process is the transformation of the conceptual model described in Section 2.0 into a mathematical model for simulating groundwater flow in and around the Pahute Mesa CAUs. For more general information on this subject, refer to American Society for Testing and Materials (ASTM) Standard Guide D 5447-93 (ASTM, 1993a), which summarizes various aspects of this process, including spatial dimensionality and discretization, boundary and initial condition specification, and initial assignment of properties. In addition, ASTM Standard Guides D 5609-94 (ASTM, 1994a) and D 5610-94 (ASTM, 1994b) describe in more detail the process of defining initial and boundary conditions, respectively. Specific elements in the model construction are described in the following subsections.

4.1 General Approach

The Pahute Mesa modeling approach/strategy report (SNJV, 2004b) reviewed the conceptual model of flow and transport, and defined the following needs in implementing the CAU process model relevant to this section:

- Defining the geologic model boundaries
- Defining the CAU numerical model boundary
- Defining multiple alternative conceptual models
- Grid generation
- Establishing boundary conditions and initial condition

The geologic model boundaries are defined in BN (2002) and were chosen such that they coincide with perceived geologic and hydrologic domains to the extent possible, contain the contaminant source areas and discharge points with some buffer, and are within practical constraints. The CAU numerical model lies within the geologic model domain with lower-left plan coordinates of 519,125 and 4,085,000 m Universal Transverse Mercator (UTM) (UTM Zone 11) and upper-right plan coordinates of 569,000 and 4,138,000 m. The model is aligned north-south, with no rotation. The

Uncontrolled When Printed

numerical model extends from the estimated water table to a depth of -3,500 m bmsl. The hydrologic model area encompasses more than 2,700 km^2 (1,042 mi^2) of southern Nye County, Nevada (Figure 1-2). This area incorporates the Pahute Mesa CAUs, including Timber Mountain, the eastern edge of Oasis Valley, the northern part of Fortymile Canyon, and the northern portion of Yucca Mountain. The area has a north-south length of 53.4 km (33.2 mi) and an east-west length of 50.8 km (31.6 mi). The numerical model boundary is approximately the same as the study area boundary shown in Figure 5-2 in the modeling approach/strategy (SNJV, 2004b). Contained within these boundaries are the well data within the Pahute Mesa area, and the springs and regional discharge area at Oasis Valley. The horizontal boundaries of the numerical model do not, because of the great extent of the flow system, coincide with natural hydrologic and geologic boundaries. Thus, the boundaries are, to some degree, arbitrary and must be determined from well data and other regional information. Development of boundary conditions is discussed in Section 4.3.

The UGTA modeling strategy (SNJV, 2004b) includes development of multiple models based on HFMs, each of which must be represented on the model mesh. The alternative HFMs were developed and documented by BN (2002). More detail is provided in Section 4.2 on grid generation and the multiple HFMs. In general, the criteria for grid generation are as follows (DOE/NV, 1999; SNJV, 2004b):

- The external boundary of the CAU model will correspond to appropriate cell boundaries within the regional groundwater flow model. However, the regional model is rotated with respect to the coordinate system, and the CAU model is not. Therefore, interpolation procedures were developed to account for the non-coincidence of CAU and regional model nodes, and are described in Section 5.2.

- Nodes will be placed as close as practical to each underground nuclear test location as well as at specific well locations.

- Nodes will be placed along faults that are identified as being important to the distribution of HSUs.

- The node density will be greatest in the vicinity of the underground nuclear tests and at other points of interest such as discharge wells, and will decrease in density towards the CAU model boundaries.

Uncontrolled When Printed

- Nodes will be preferentially placed along HSU contacts to more precisely incorporate the geologic model structure in the simulations. The nodes will not be layered in the finite-difference sense, but rather will form a pattern representative of the CAU-scale geology.
- The node spacing will vary from small in the vicinity of test cavities and wells to nearly as large as the regional groundwater flow model grid at the CAU boundary.

4.2 Mesh Generation

A set of criteria, outlined below, were developed that produce a mesh that is suitable for flow and transport calculations using FEHM. The resultant mesh should have sufficient resolution to represent features such as hydrostratigraphy, faults, contaminant source zone, wells and the water table, yet not be too large to make computations impractical. In general, it is easy to define criteria that lead to increased refinement in certain volumes of the mesh. The more difficult process is designing criteria that limit the refined volume so that the mesh size (number of nodes) does not grow beyond practical limits. The process of developing these criteria is iterative. During the iterative process, mesh-refinement criteria are defined; control files for the LaGriT (George, 1997) mesh-generation package are written to implement the criteria; mesh-generation calculations are performed; checking is done to ensure the implementation is correct; and the resulting mesh is analyzed to determine whether goals have been met. As stated in the Pahute Mesa modeling strategy (SNJV, 2004b) contaminant boundary calculations will be done with a particle-based method that is not susceptible to numerical dispersion, and grid refinement for transport may yet be undertaken.

4.2.1 Base-Case and SCCC HFMs

Two FEHM computational meshes were produced. One represents the base (or BN) HFM; the other, the SCCC alternative HFM. The EV representation of each geologic model has the same format, a set of surfaces, z(x,y) on uniformly spaced 50-m intervals, defining HSU interfaces, and another set of surfaces defining faults. However, the details of the models are different. The initial base HFM has 45 HSU surfaces and 37 faults. Table 4-1 shows the base HSU abbreviations and names. The SCCC HFM model has 40 HSU surfaces and 25 faults. The list of HSUs is identical with the exception of the Calico Hills HSUs, which are lumped into a single HSU in the SCCC HFM. In both cases, similar criteria are used to decide upon the strategy and logic used to control mesh construction algorithms. Building of the base HFM mesh was done first, so the process involved more iterations. The SCCC

Uncontrolled When Printed

Table 4-1
Hydrostratigraphic Unit Abbreviations and Names
(Page 1 of 2)

HSU Abbreviation	Name
LCCU	Lower Clastic Confining Unit
LCA	Lower Carbonate Aquifer
UCCU	Upper Clastic Confining Unit
LCCU1	Lower Clastic Confining Unit 1 – thrusted LCCU
LCA3	Lower Carbonate Aquifer 3 – thrusted LCA
MGCU	Mesozoic Granite Confining Unit (aka Gold Meadows Stock)
SCICU	Silent Canyon Intrusive Confining Unit
CHICU	Calico Hills Intrusive Confining Unit
CCICU	Claim Canyon Intrusive Confining Unit
RMICU	Rainier Mesa Intrusive Confining Unit
ATICU	Ammonia Tanks Intrusive Confining Unit
BMICU	Black Mountain Intrusive Confining Unit
PBRCM	Pre-Belted Range Composite
BRA	Belted Range Aquifer
BFCU	Bullfrog Confining Unit
KA	Kearsarge Aquifer
CFCU	Crater Flats Confining Unit
CFCM	Crater Flats Composite Unit
IA	Inlet Aquifer
CHCU	Calico Hills Confining Unit
CHZCM	Calico Hills Zeolitized Composite Unit
CHVCM	Calico Hills Vitric Composite Unit
CHVTA	Calico Hills Vitric-Tuff Aquifer
YMCFCM	Yucca Mountain Crater Flat Composite unit
TSA	Topopah Springs Aquifer
LPCU	Lower Paintbrush Confining Unit
PLFA	Paintbrush Lava-Flow Aquifer
TCA	Tiva Canyon Aquifer
UPCU	Upper Paintbrush Confining Unit
BA	Benham Aquifer
PVTA	Paintbrush Vitric-Tuff Aquifer
PCM	Paintbrush Composite Unit
LCA3A	Lower Carbonate Aquifer 3 – thrusted LCA subdivision under Oasis Valley
FCCU	Fluorspar Canyon Confining Unit
SCVCU	Subcaldera Volcanic Confining Unit
TMA	Timber Mountain Aquifer
THCM	Tannenbaum Hill Composite Unit
THLFA	Tannenbaum Hill Lava-Flow Aquifer
TMCM	Timber Mountain Composite Unit
FCA	Fortymile Canyon Aquifer
FCCM	Fortymile Canyon Composite Unit

Uncontrolled When Printed

Table 4-1
Hydrostratigraphic Unit Abbreviations and Names
(Page 2 of 2)

HSU Abbreviation	Name
DVA	Detached Volcanic Aquifer
DVCM	Detached Volcanic Composite Unit
TCVA	Thirsty Canyon Volcanic Aquifer
YVCM	Younger Volcanics Composite Unit
AA	Alluvial Aquifer
LCAr1	Lower Carbonate Aquifer – subdivision from UGTA regional model LCA Zone 1
TCVAr6	Thirsty Canyon Volcanic Aquifer - subdivision from UGTA regional model TCVA Zone 6
TMAr6	Timber Mountain Aquifer - subdivision from UGTA regional model TMA Zone 6
PBRCM Zone 80	Pre-Belted Range Composite – material 80 (see Figure 5-5)
PBRCM Zone 81	Pre-Belted Range Composite – material 81 (see Figure 5-5)
PBRCM Zone 82	Pre-Belted Range Composite – material 82 (see Figure 5-5)
PBRCM Zone 83	Pre-Belted Range Composite – material 83 (see Figure 5-5)
PBRCM Zone 84	Pre-Belted Range Composite – material 84 (see Figure 5-5)
PBRCM Zone 87	Pre-Belted Range Composite – material 87 (see Figure 5-5)
TMCM-ERM	Timber Mountain Composite – East Rainier Mesa sub domain (see Figure 5-6)
TMCM-ATCW	Timber Mountain Composite – Ammonia Tanks sub domain west of 560,000 m (see Figure 5-6)
TMCM-ATCE	Timber Mountain Composite – East Rainier Mesa sub domain east of 560,000 m (see Figure 5-6)
TMCM-THS	Timber Mountain Composite – Tannenbaum Hill sub domain (see Figure 5-6)
TMCM-OV	Timber Mountain Composite – Oasis Valley sub domain (see Figure 5-6)
TMCM-TMD	Timber Mountain Composite – Timber Mountain Dome sub domain (see Figure 5-6)
TMCM-NTMW	Timber Mountain Composite – Northern Timber Mountain sub domain west of 560,000 m (see Figure 5-6)
TMCM-NTME	Timber Mountain Composite – Northern Timber Mountain sub domain east of 560,000 m (see Figure 5-6)

alternative HFM mesh construction also required iteration, but the overall process was more direct because experience from building the base HFM mesh was utilized.

The method of octree mesh refinement (OMR) is used to generate finite element meshes to represent HSUs, structural features such as faults, and engineered features such as wells with spatially variable resolution so as to provide high resolution where needed and allow coarse resolution where it is sufficient. The OMR method helps to achieve the two conflicting goals of providing high resolution and minimizing the number of nodes in the model.

Figure 4-1 shows a simple example of the OMR technique. Octree mesh refinement is used to provide increased resolution in limited volumes of the model volume while maintaining coarse

Uncontrolled When Printed

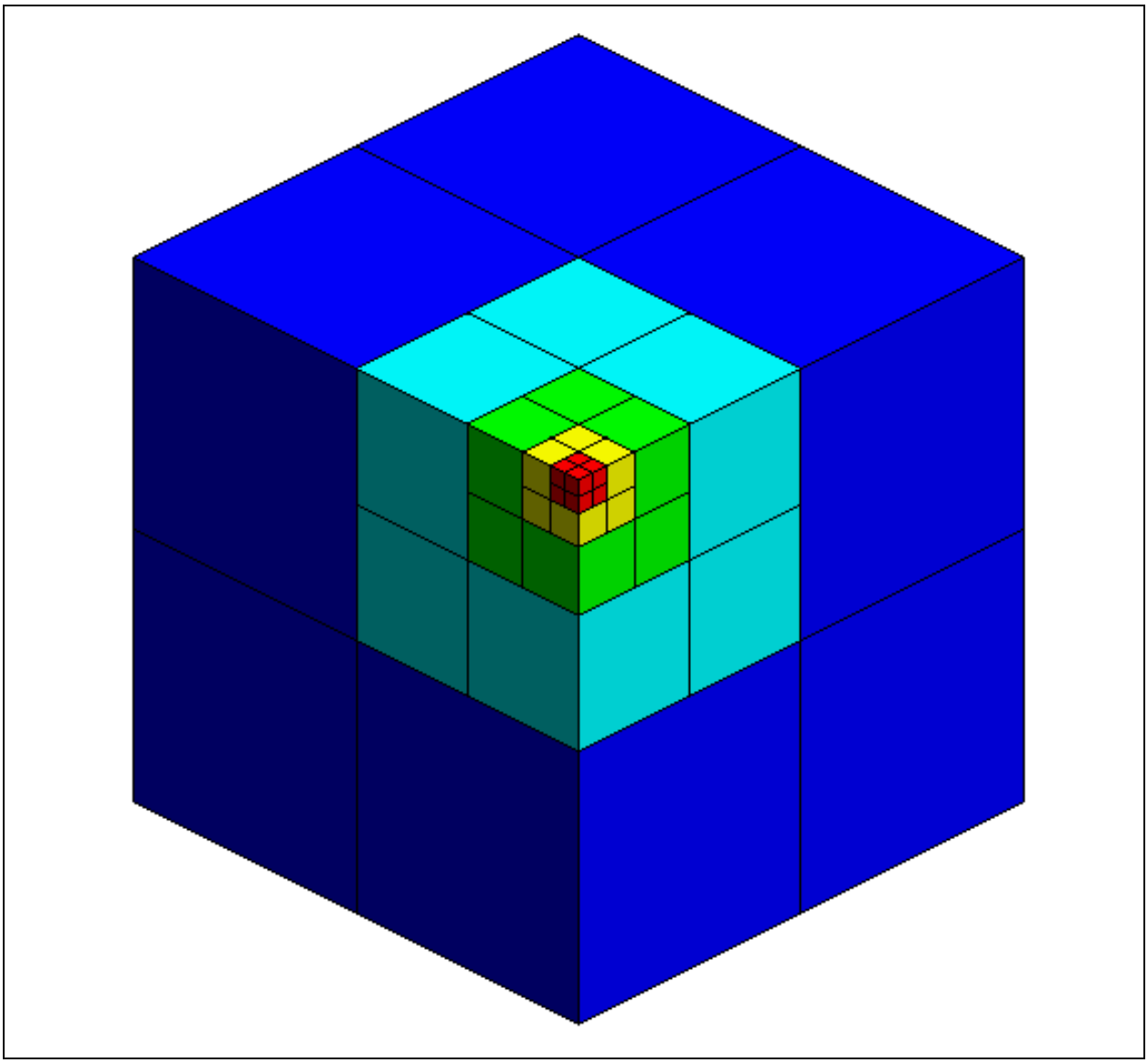

Figure 4-1
Octree Mesh Refinement Example

resolution in other volumes. The process of building an octree mesh begins with an orthogonal uniform mesh. Then the mesh is progressively refined until features of interest are adequately resolved (Figure 4-1). For both the base HFM and SCCC alternative HFM, the coarsest elements are uniform in the X and Y directions with 1,000-m spacing between nodes. The vertical spacing is variable with nodes at -3,500 m, -2,500 m, -1,500 m, -750 m, 0 m, 750 m and 1,500 m. Each time a hexahedral element is refined, eight new elements are formed with the space between nodes cut in

half in each of the coordinate directions. The horizontal spacing of the mesh at different levels of refinement is 1,000 m, 500 m, 250 m, and 125 m, and the highest level of refinement used is 67.5 m.

Octree mesh refinement creates a balanced mesh. This means neighbors to any element are either of the same refinement level or at most one level higher or lower. As a result, progressive refinement of one element may result in the propagation of some refinement of neighboring elements.

The criteria used to determine which elements are refined and to what level they are refined involves tradeoffs. Even using the octree method, if all elements intersecting faults are refined to 67.5 m, the size of the mesh is too large for practical flow and transport calculations. Therefore, criteria are developed to prioritize where mesh refinement occurs and allow the mesh to remain coarse wherever possible.

To represent HSU geometry, criteria are developed to refine thin or steeply dipping portions of an HSU to higher levels and represent thick portions of an HSU with coarser elements. Figure 4-2 illustrates the variable grid resolution that results as HSUs change thickness.

To represent faults, criteria are developed to refine cells that are intersected by fault surfaces. The level of refinement is a function of depth. Elements intersecting fault surfaces at elevations higher than 0 m are refined to 125 m, between 0 m and -1,000 m to 250 m, and below -1,000 to 500 m. In addition, only a subset of the faults is refined to 125 m. As a result, the representation of faults is broader at depth and narrower near the top of the model (Figure 4-3). In all cases, continuity of fault surfaces is maintained and the FEHM computational mesh, which uses node based properties, has a region at least two nodes wide labeled as fault (Figure 4-4). Figures 4-5 through 4-8 show the faults in the base HFM. Table 4-2 shows the fault IDs and associated names for the base HFM. Figures 4-9 and 4-10 show the fault IDs in the SCCC alternative HFM. Figure 4-11 shows the mesh detail near the test chimney. Table 4-3 shows the SCCC fault IDs and names for the SCCC alternative HFM.

Particle paths originating at the Pahute Mesa tests (as shown in the Pahute Mesa hydrologic data document [SNJV, 2004a]) for both BN and SCCC HFMs are used to define 3-D polyhedra for additional refinement for transport paths. If elements are outside that polyhedra, refinement is limited to 125 m; however, inside that polyhedra, thin HSUs may be refined to 67.5 m.

Uncontrolled When Printed

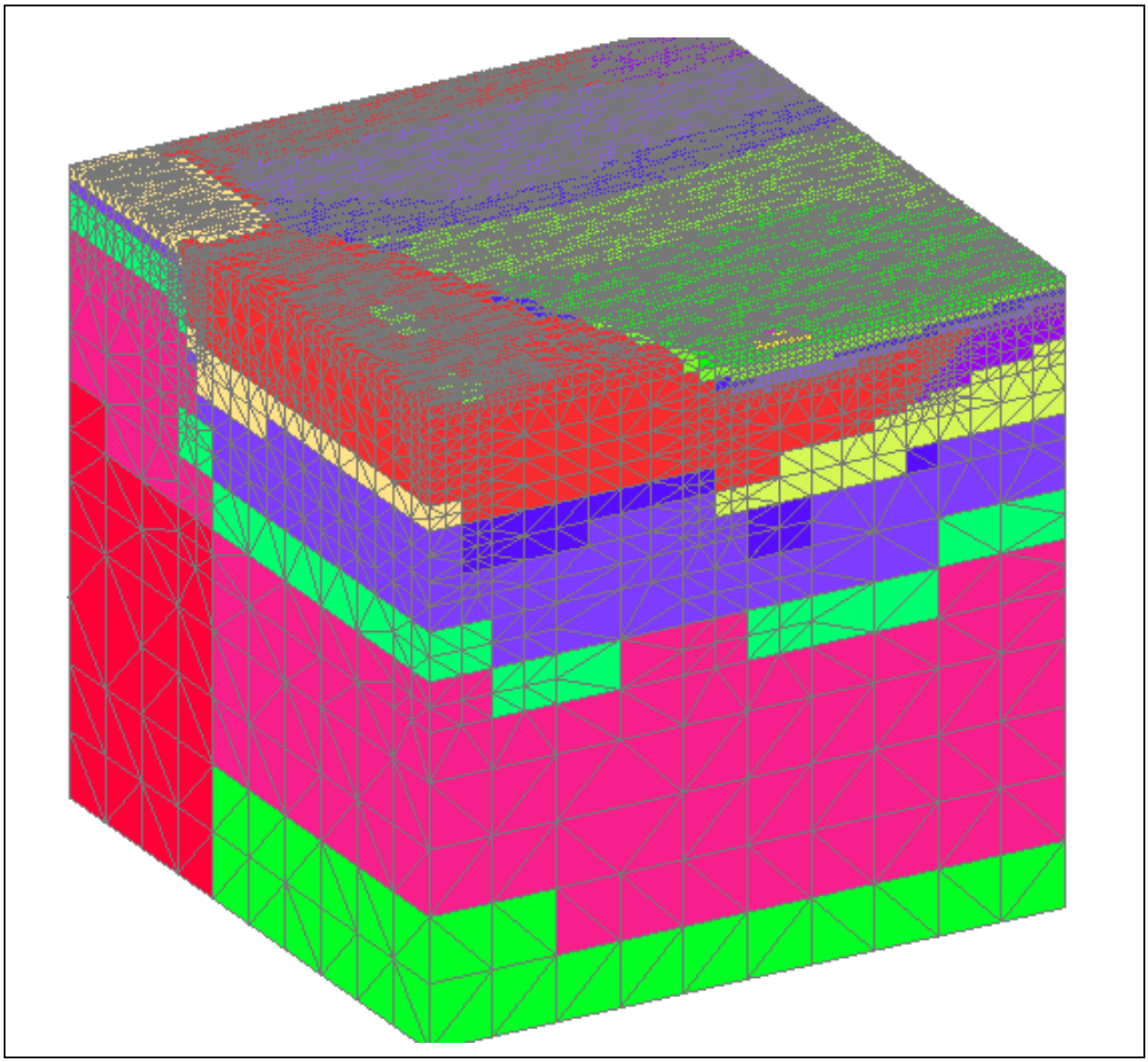

Figure 4-2
Example Mesh Refinement in HSUs

To represent volumes where potential source locations exist, vertical columns of elements are refined to 67.5 m starting just below the coordinate where each are defined. The refined elements continue up to the surface of the model. In addition, all elements that are adjacent to the vertical column are refined to 67.5 m. This ensures that the FEHM control volumes in potential contaminant source locations are uniform. Figure 4-11 shows an example of such refinement.

Vertical columns of elements are refined to 67.5 m if the open interval of one of the 152 wells intersects the mesh. As with the source terms, this ensures that the FEHM control volumes

Uncontrolled When Printed

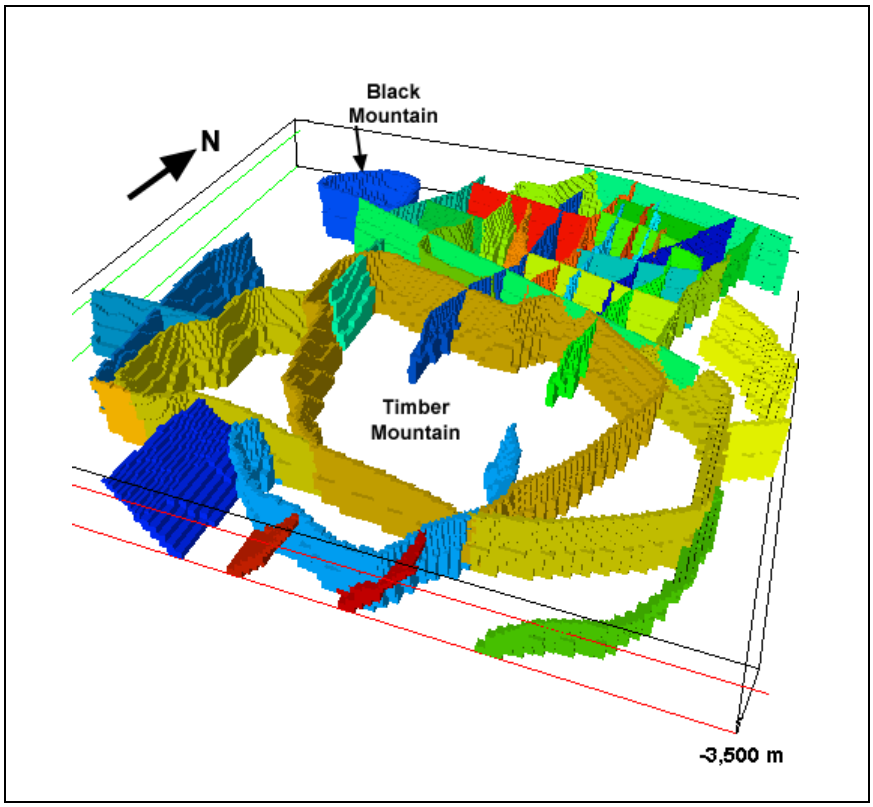

Figure 4-3
3-D View Showing Fault Thickness with Depth

surrounding a well interval are uniform. Table 4-4 summarizes the mesh statistics for the base and SCCC HFMs.

4.2.2 Truncation of Top Surface of Mesh To Represent Water Table

The FEHM simulations utilize a confined aquifer approximation. The estimated water table defines the top of the model domain. The approach does not include an unsaturated zone or moving water table and, therefore, solves a simplified but computationally more efficient numerical model. An estimate of the water table, approximated by contouring observed heads in wells with relatively shallow sampling intervals, provides a guide for setting the upper confining surface in the grid. However, it is impossible to represent continuously the contoured surface without utilizing an impractically large number of grid nodes discretized very finely. Therefore, the contoured surface is approximated with a method that specifies discrete elevations that are consistent with the OMR vertical coordinates. The highest elevation of the contoured water table is 1,500 m, which defines the highest nodal elevation in the grid. Discretization steps of either 125 m or 250 m are used down to

Uncontrolled When Printed

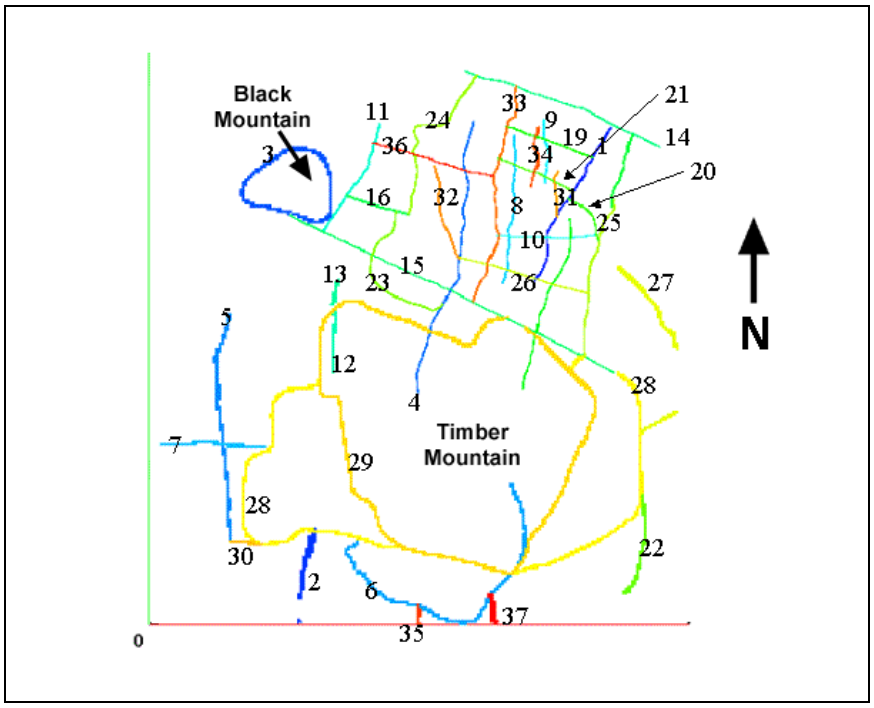

Figure 4-4
Fault Numbering Key - Base HFM

the lowest contoured water-table elevation. The differences are minimized along the primary flow pathway, with errors incurred in the northwest and southeast.

In the numerical model, the top surface has boundary conditions of applied recharge flux. Because none of the fluid or rock properties depend on head, no changes to the true solution occur other than forcing the bookkeeping in FEHM to assume fully saturated conditions. The potential negative side of this approach is that the top surface of the numerical model corresponds to the estimated water-table surface and may be inconsistent with the model-derived water-table surface. This discrepancy could affect the flux through the model. The error is small because the flowing cross-sectional area is proportional to the thickness of the model in the north-south direction, and the average error between the calibrated and field data is small compared to a model thickness of approximately 5,000 m.

4.3 Boundary Conditions

The solution of the groundwater flow equations requires specification of head and/or flow at the edges and at internal discharge points (e.g., springs in Oasis Valley) of the numerical model. This is

Uncontrolled When Printed

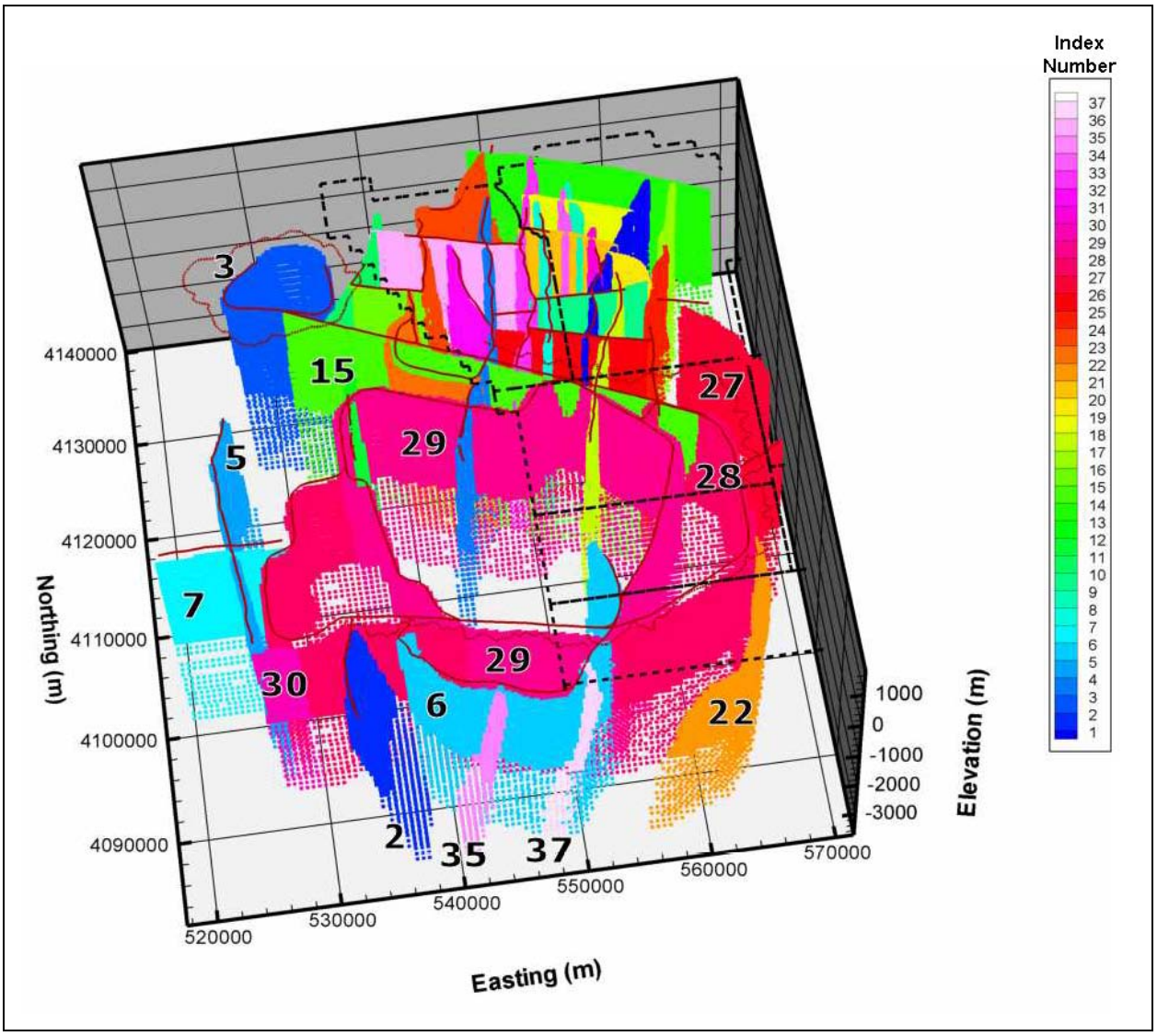

Figure 4-5
Base HFM Fault Structure Viewed from the Southwest

particularly important for the Pahute Mesa CAU model because the model boundaries do not coincide with natural hydrologic boundaries. The Pahute Mesa CAU model must account for regional inflow and outflow across all four lateral edges, internal flow from precipitation recharge, and internal discharge at Oasis Valley. The following sections describe the implementation of these conditions in the Pahute Mesa CAU flow model.

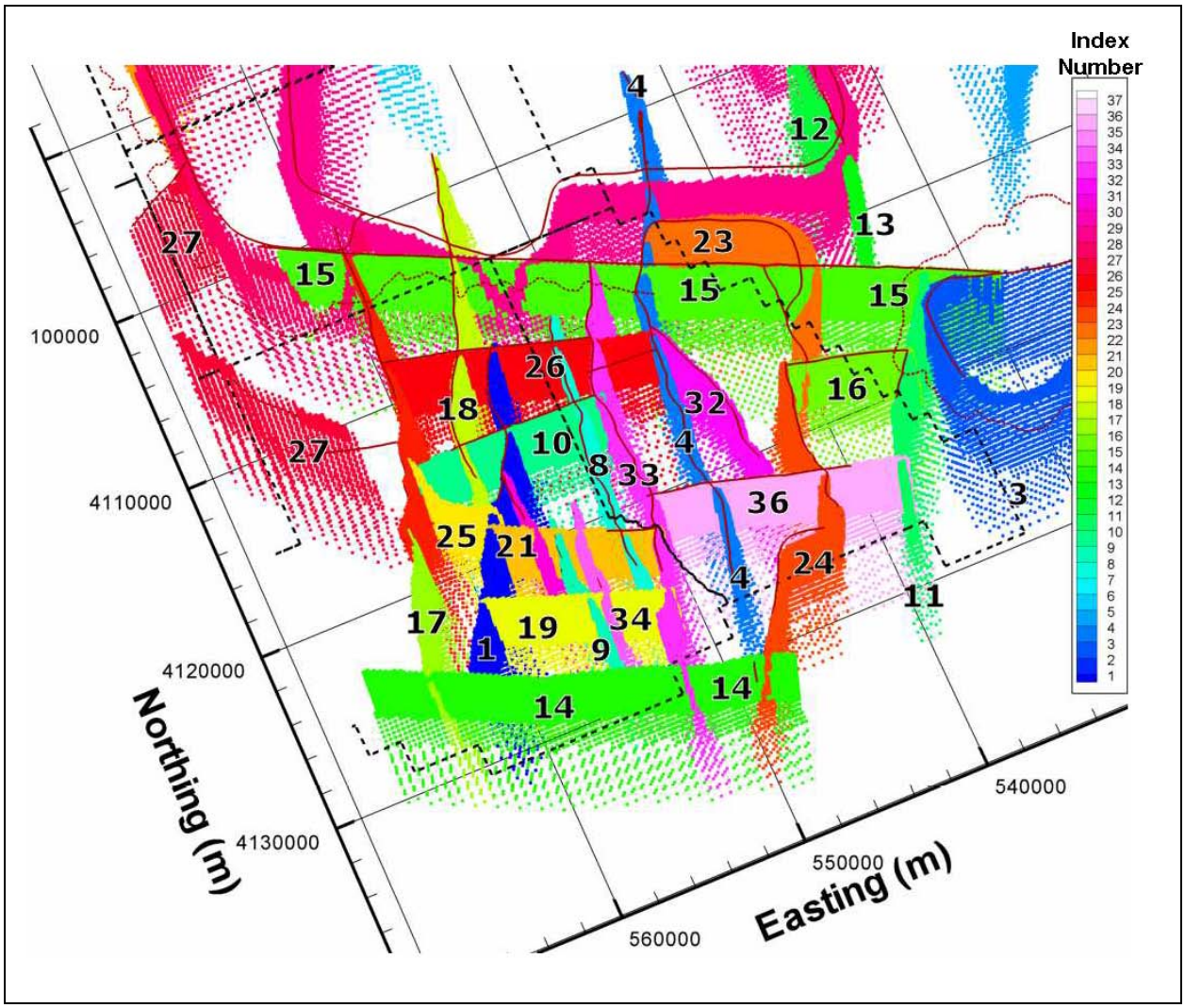

Figure 4-6
Base HFM Fault Structure Viewed from the Northeast

4.3.1 Recharge

As discussed in the conceptual model (Section 2.3.2.2), there are three categories of recharge estimates for consideration in the CAU model as follows: the USGS distributed-parameter watershed model of Hevesi et al. (2003); a Maxey-Eakin elevation-based approach as described in the UGTA regional model evaluation (DOE/NV, 1997; IT, 1996a) and modified to reflect an updated base precipitation map; and the DRI chloride mass-balance estimate of Russell and Minor (2002). Two subsets of the USGS and DRI recharge maps were also considered. For the USGS map, the recharge with (case USGSD) and without runoff or run on (redistribution) (case USGSND) was used. For the

Uncontrolled When Printed

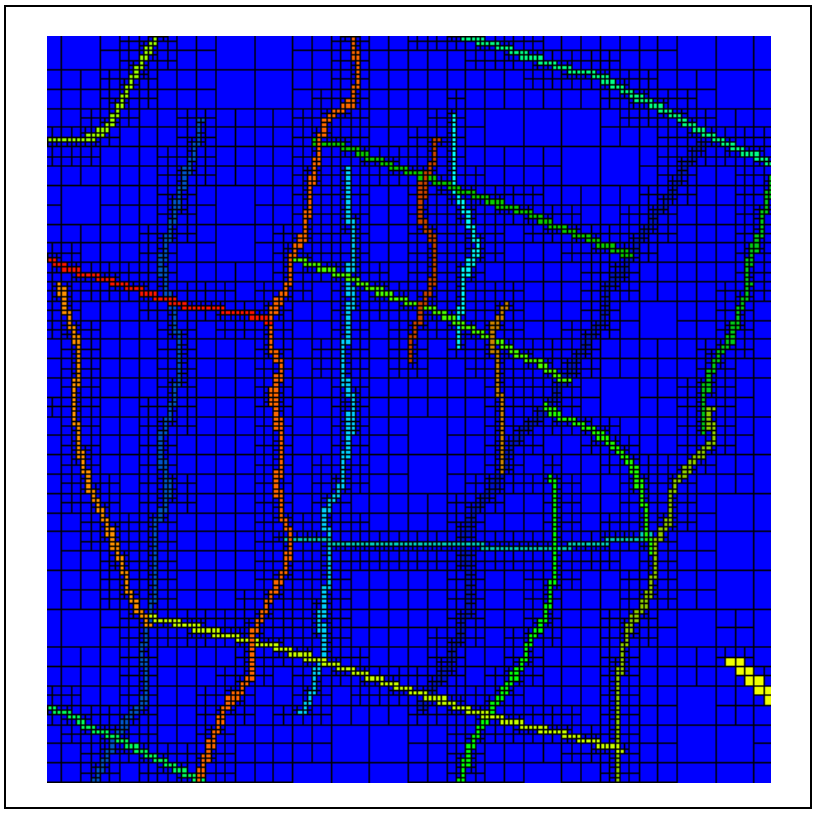

Figure 4-7
Closeup View of Faults in Area 19

DRI map, the recharge with (case DRIAE) and without an elevation (case DRIA) mask at 1,237 m was also used. Section 2.3.2.2 provides more discussion on these alternative recharge models.

Recharge is implemented in the CAU model as a specified flux condition, where a given volume (mass) of water is applied based on the above recharge models. Recharge flux is considered to be constant over time, but varies over the domain as a function of altitude, soil and vegetation types, etc. The recharge flows for FEHM were calculated by averaging a fine grid (30 m) over the contributing area of each node at the top of the FEHM model to obtain the required input in mass per time. Figures 4-12 through 4-16 show the recharge for the USGSD, USGSND, modified Maxey-Eakin (MME), DRIA and DRIAE cases, respectively, as implemented for FEHM input. Table 4-5 summarizes the total mass flows over the numerical model area for each recharge model considered.

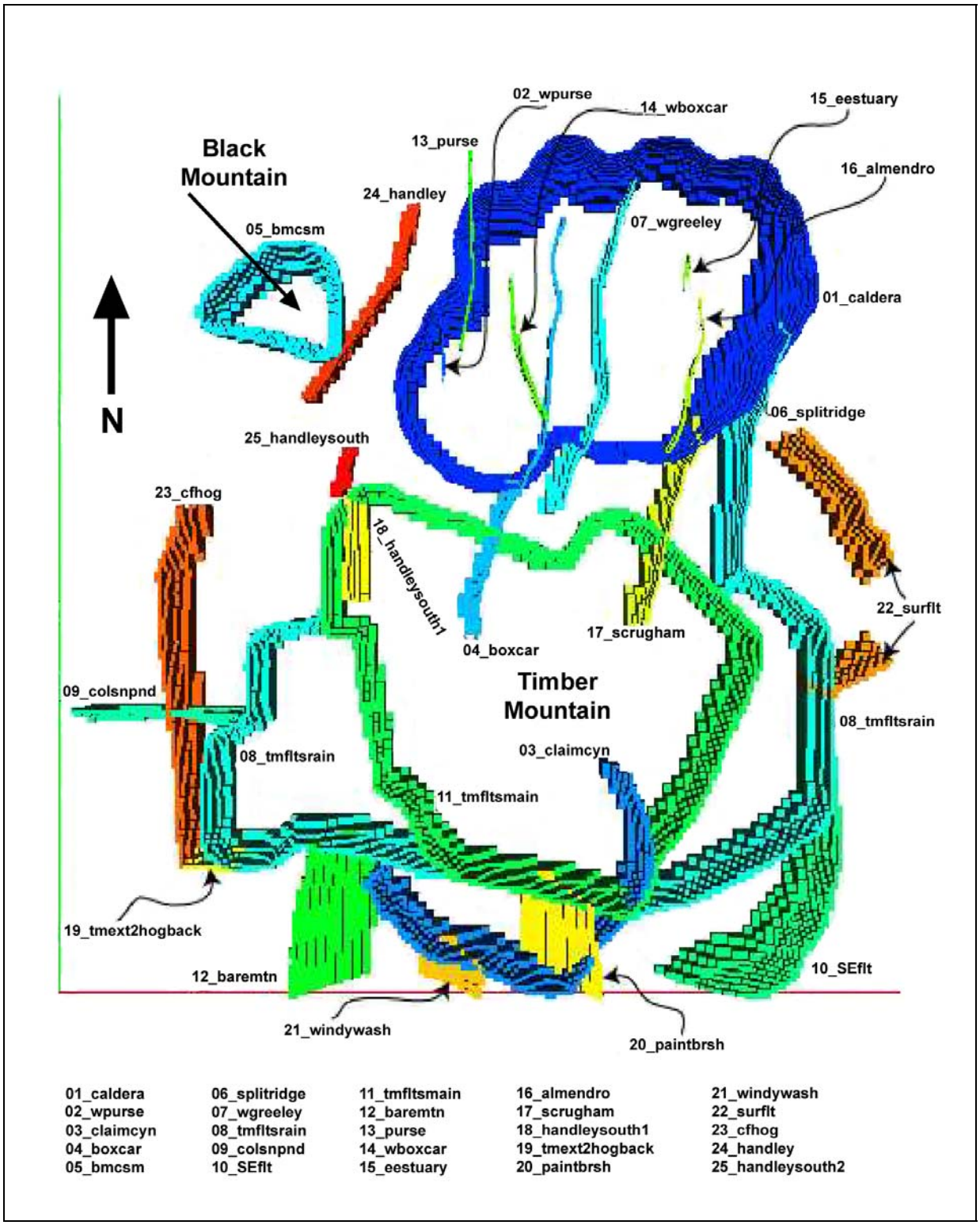

Figure 4-8
Fault Numbering Key - SCCC HFM

Uncontrolled When Printed

Table 4-2
Base HFM Fault Indices and Names

Fault ID	Name
01	Almendro
02	Bare Mountain
03	Black Mountain Caldera Structural Margin
04	Boxcar
05	Hogback
06	Claim Canyon Caldera Structural Margin
07	Colson Pond
08	East Greeley
09	East Estuary
10	East Thirsty Canyon Structural Zone
11	Handley
12	Handley South
13	Handley North
14	Moor Hen Meadow Structural Zone
15	North Timber Mountain Moat Structural Zone
16	Ribbon Cliff Structural Zone
17	Richey
18	Scrugham Peak
19	Silent Canyon Northern Structural Zone
20	Silent Canyon Structural Zone East
21	Silent Canyon Structural Zone West
22	YMP inferred/CP Thrust
23	Silent Canyon/West Purse
24	Purse North
25	Split Ridge
26	Southern Pahute Mesa Structural Zone
27	Gold Meadows Structural Zone/Big Burn Valley
28	Rainier Mesa Caldera Structural Margin
29	Ammonia Tanks Caldera Structural Margin
30	Hot Springs Lineament extension of Rainier Mesa Caldera Structural Margin
31	West Almendro
32	West Boxcar
33	West Greeley
34	West Estuary
35	Windy Wash/Claim Canyon 1
36	West Silent Canyon Structural Zone
37	Paintbrush Canyon
38	Fault 23 south of North Timber Mountain Moat Structural Zone
39	Fault 16 between faults 23 and 24
40	Extension of Purse Fault to northern edge of model
41	Purse Fault repair where fault 36 crosses

Uncontrolled When Printed

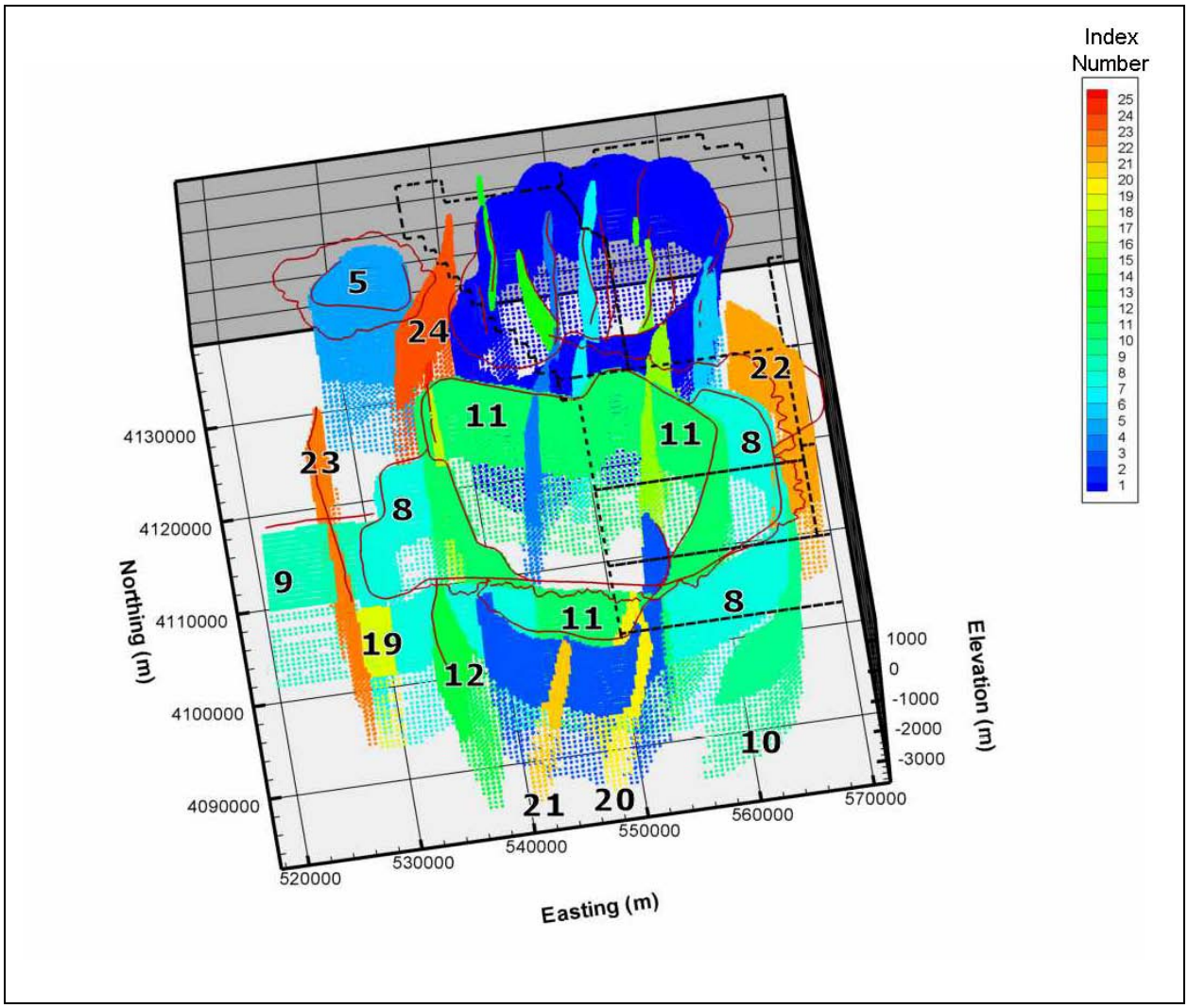

Figure 4-9
SCCC HFM Fault Structure Viewed from the Southwest

4.3.2 Discharge

The only internal discharge represented in the Pahute Mesa CAU model is Oasis Valley springs and ET outflow. Discharge from pumping wells is not included in the model. Spring and ET discharge are represented in a similar manner with FEHM as with the regional model with "drain" boundary conditions. In this condition, a head is set at the elevation of the point of discharge. If the model head at the node is above the specified elevation outflow representing spring or ET, spring discharge or ET loss flows occur. If head is below the set head, no flow of any kind occurs. This is different than a constant-head boundary condition, which will allow in or outflow; the boundary condition used to represent Oasis Valley only allows outflow. Nodes at the top of the model within the areas where

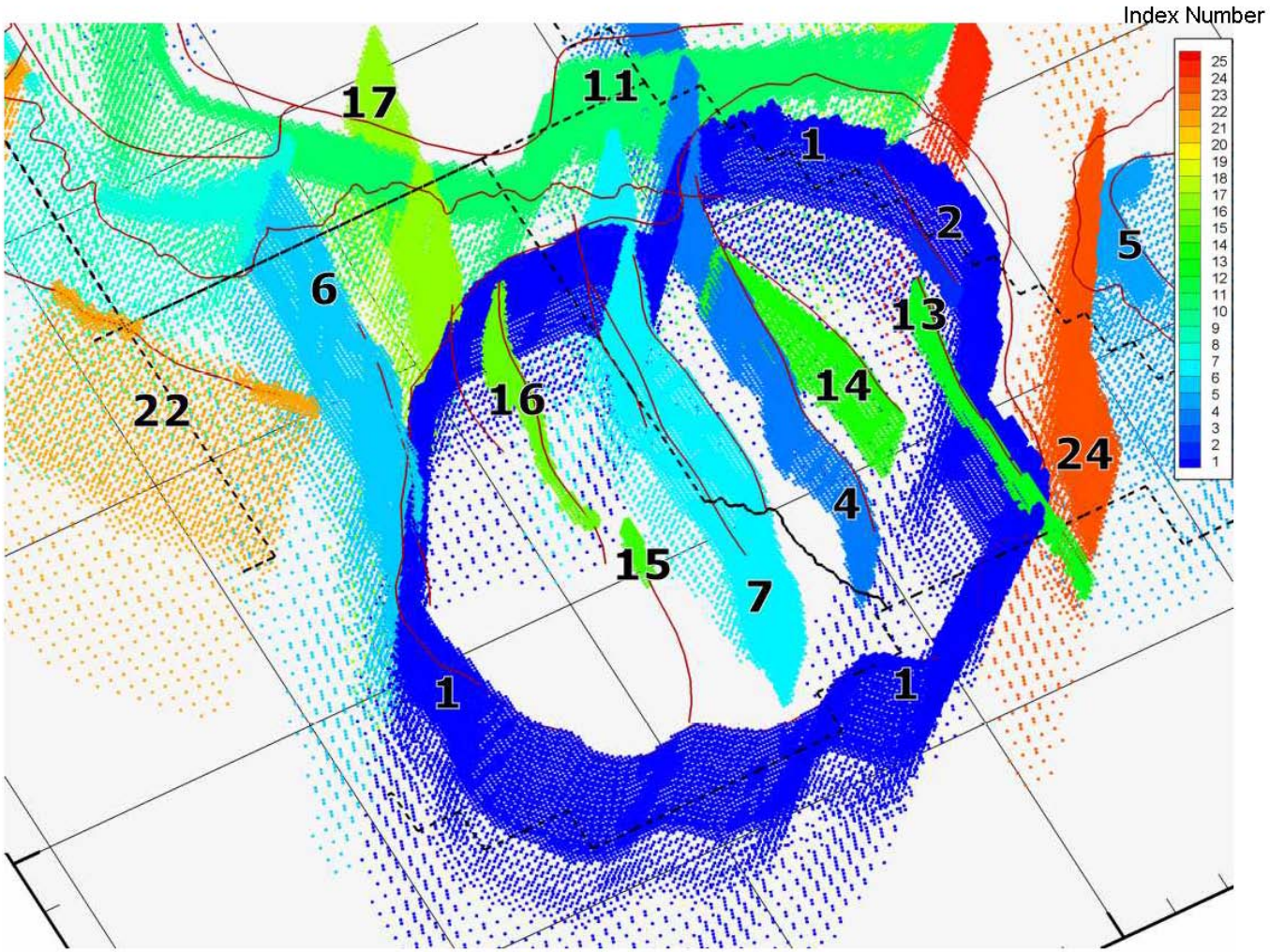

Figure 4-10
SCCC HFM Fault Structure Viewed from the Northeast

Uncontrolled When Printed

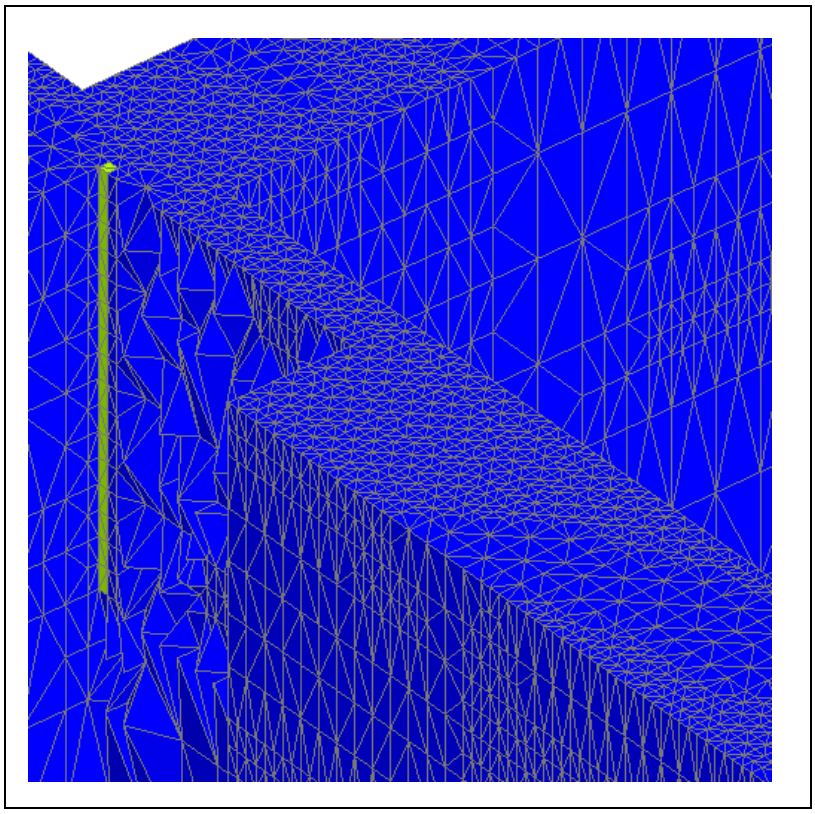

Figure 4-11
Mesh Detail Near Test Chimney

Table 4-3
SCCC HFM Fault Indices and Names
(Page 1 of 2)

Fault ID	Fault Name
01	Silent Canyon Caldera Margin
02	West Purse
03	Claim Canyon Caldera Structural Margin
04	Boxcar
05	Black Mountain Caldera Structural Margin
06	Split Ridge
07	West Greeley
08	Rainier Mesa Caldera Structural Margin
09	Colson Pond
10	YMP inferred/CP Thrust

Table 4-3
SCCC HFM Fault Indices and Names
(Page 2 of 2)

Fault ID	Fault Name
11	Ammonia Tanks Caldera Structural Margin
12	Bare Mountain
13	Purse
14	West Boxcar
15	East Estuary
16	Almendro
17	Scrugham Peak
18	Handley South
19	Hot Springs Lineament extension over to Hogback
20	Paintbrush Canyon
21	Windy Wash
22	Gold Meadows Structural Zone/Big Burn Valley
23	Hogback
24	Handley
25	Handley South

Laczniak et al. (2001) mapped ET were identified and drains assigned. In the case of springs, head was assigned at the estimated spring elevation. To represent ET, head equal to land surface elevation less 3 m was used to represent the maximum root depth from which plants could draw water (the effects of extinction depth are examined more in Section 6.2.4.1). Laczniak et al. (2001) estimated that 30 percent of Oasis Valley plant coverage was dense wetland vegetation (e.g., tall reedy and rushy marsh plants) where water was perennially at or very near land surface, 24 percent of plant coverage was dense meadow and forest with the water table from a few up to 20 ft (~1 to 6 m) below ground surface, and 14 percent dense to moderately dense grassland vegetation with the water table up to 5 ft (1.5 m) below ground surface; these 3 categories account for about 2/3 of the Oasis Valley discharge area. The water table in Oasis Valley is known to vary seasonally from ET (Reiner et al., 2002); thus, the depth of water table given above is a first approximation of the rooting depth, which ranges from 0 to 6 m. The UGTA regional model (DOE/NV, 1997) and USGS Death Valley regional flow model (DVRFM) (Faunt et al., 2004) both used values of 10 m. Figure 4-17 shows the discharge areas of Oasis Valley considered in the CAU model.

Uncontrolled When Printed

Table 4-4
Base and SCCC Mesh Statistics

	Base HFM	SCCC Alternative HFM
Number of Nodes	1,449,785	1,301,168
Number of Tetrahedral Elements	7,961,005	6,996,374
Number of Connections uncompressed matrix compressed matrix	 N/A 11,882,601	 18,315,432 10,706,526
Model Extents (UTM meters) xmin (West) xmax (East) xmax - xmin ymin (South) ymax (North) ymax - ymin zmin (Bottom) zmax (Top) zmax - zmin	 519,000 569,000 50,000 4,085,000 4,138,000 53,000 -3,500 1,500 5,000	 519,000 569,000 50,000 4,085,000 4,138,000 53,000 -3,500 1,500 5,000
Number of Hydrostratigraphic Units	45	40
Number of Faults	37	25
Number of Tests (Area 19)	36	36
Number of Tests (Area 20)	46	46
Number of Tests Inside Model	36	36
Number of Well Intervals	152	152

4.3.3 Boundary Heads

Initially, boundary heads from the UGTA regional model analysis described in SNJV (2004a) were interpolated onto the edge nodes of the FEHM CAU model. These heads represent a mass conservative calibrated solution to the groundwater flow equation from the UGTA regional model. During the calibration process these heads were reviewed, and in spots, revised based on further examination of measured heads and heads determined from the regional model. An additional factor that may cause slight adjustment is that the edge heads and head immediately inside the model may be different from different model resolution or properties. The beginning boundary head configuration is shown in Figure 4-18.

4.3.4 Lateral-Boundary Fluxes

Part of the CAU flow modeling strategy is to use the UGTA regional flow model (DOE/NV, 1997) as a mass conservative integrating model that allows evaluation of water-balance uncertainty around the

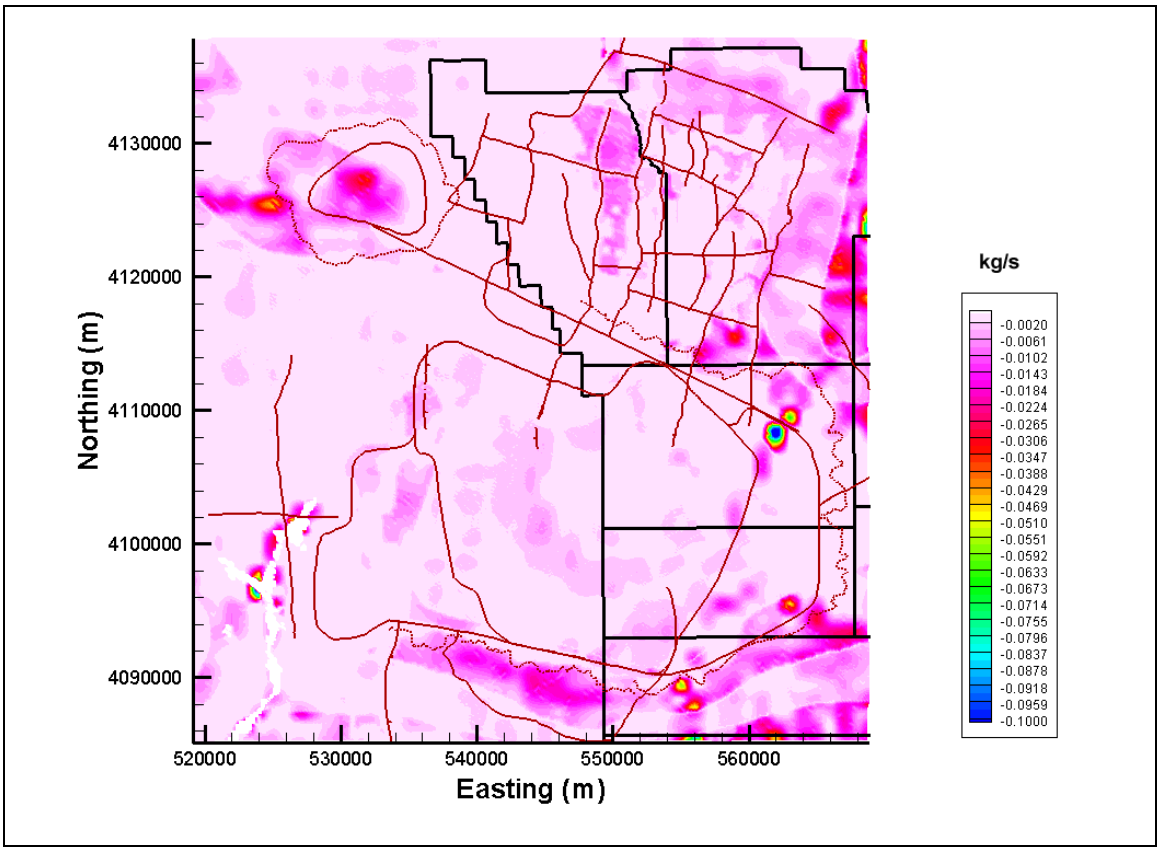

Figure 4-12
USGS Recharge Model (Hevesi et al., 2003), Redistribution Included

edges of the CAU model. In this analysis, the flows are not directly specified on all edges (to do so creates a numerically unstable problem, see Anderson and Woessner [1992]); head is specified and FEHM computes and reports the flows, which are used as calibration targets. Wolfsberg et al. (2002) used the same approach. Section 5.2 discusses these data in more detail.

4.4 Initial Conditions

Initial conditions are those applied at the start of a simulation. Theoretically, for steady-state flow, the initial conditions are not important. Practically, the iterative solvers employed in large numerical models gain efficiency if the starting conditions are consistent as possible with the properties and boundary conditions used in calibration. As described in the Pahute Mesa CAIP (DOE/NV, 1999), the initial conditions were determined from interpolation of the regional model results in the CAU domain onto the FEHM nodes. However, once converged steady-state model results were obtained, they became the new initial conditions for the continuation of model calibration.

Uncontrolled When Printed

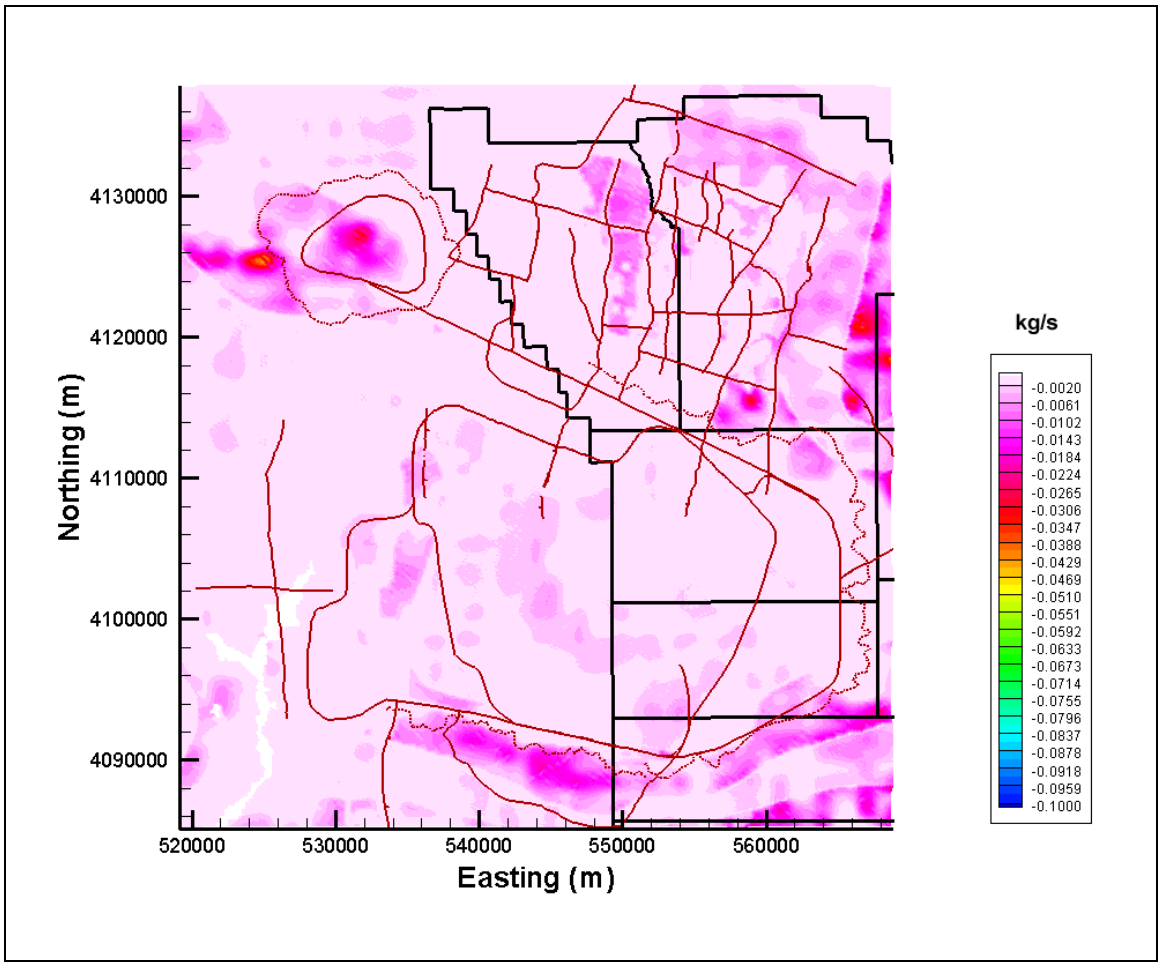

Figure 4-13
USGS Recharge Model (Hevesi et al., 2003), Redistribution Not Included

Los Alamos National Laboratory analyzed thermal data from the Pahute Mesa area and calibrated a thermal conduction model described in Appendix C of this report. Within the model domain, temperature varies enough that it should be considered in flow calculation. The FEHM code has the capability to allow specification of a thermal field without the need to simulate thermal transport. This feature was used in the CAU model to specify a fixed temperature distribution over the CAU model domain. Figure 4-19 shows a fence diagram of the calibrated temperature field.

Uncontrolled When Printed

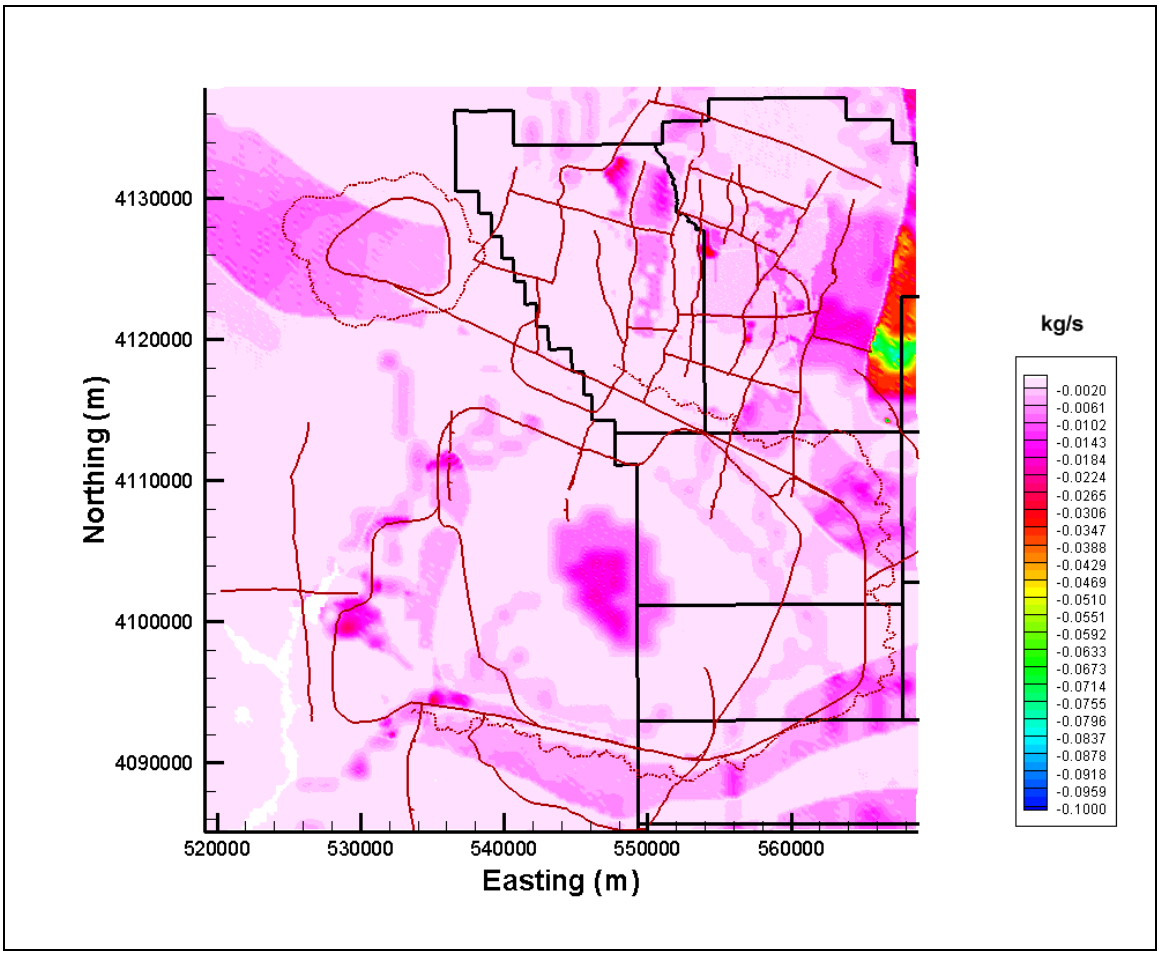

Figure 4-14
MME Recharge

Uncontrolled When Printed

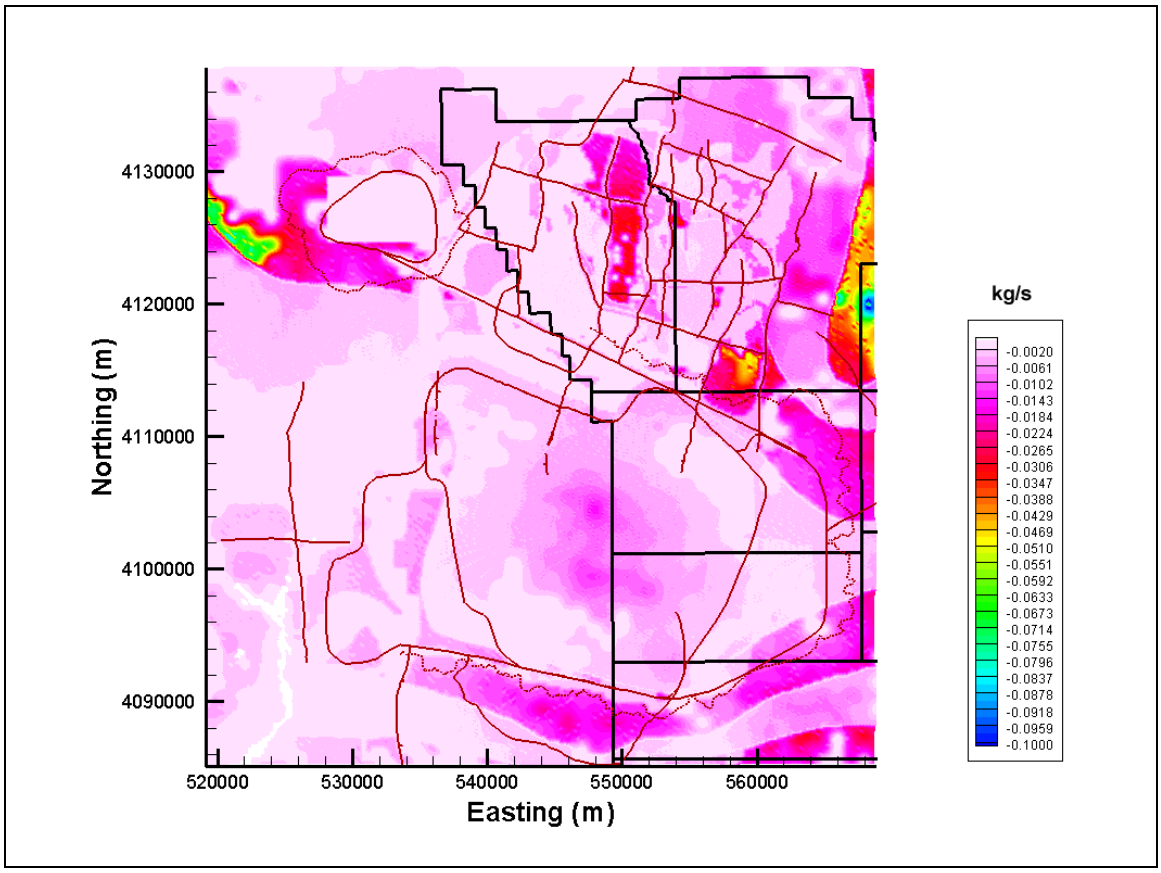

Figure 4-15
DRI Chloride Mass-Balance Recharge (Russell and Minor, 2002) with Alluvial Mask

Uncontrolled When Printed

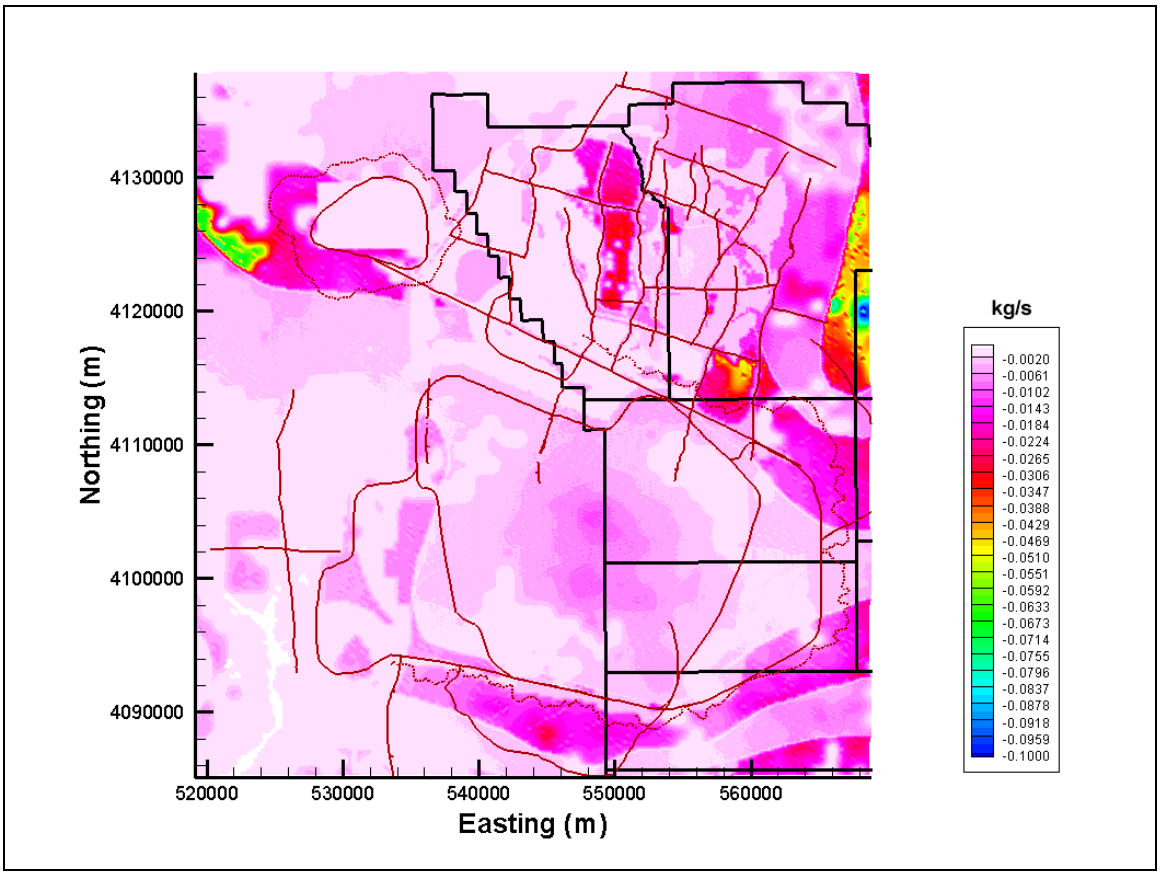

Figure 4-16
DRI Chloride Mass-Balance Recharge (Russell and Minor, 2002) with Alluvial Mask and Elevation Screen

Table 4-5
Mass Flows for USGS, MME, and DRI Recharge Maps

Recharge Model	Total Recharge Mass Rate (kg/s)
USGS - redistribution (USGSD)	318
USGS - no redistribution (USGSND)	233
Modified Maxey-Eakin (MME)	393
DRI - alluvial and no elevation screen (DRIA)	633
DRI - alluvial and elevation screen (DRIAE)	624

kg/s = Kilograms per second

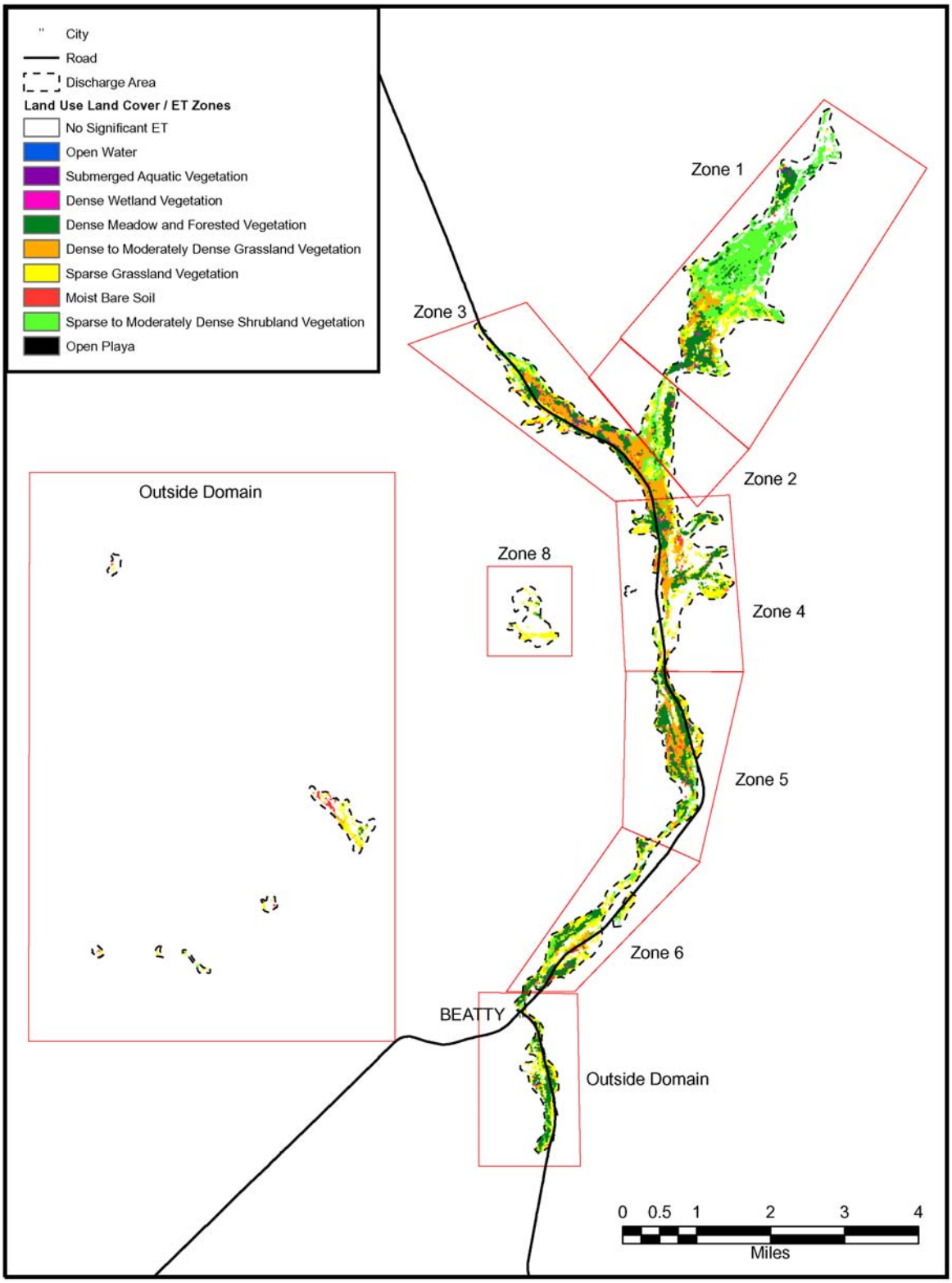

Figure 4-17
Oasis Valley Discharge Zones
(Source: Adapted from Laczniak et al., 2001)

Uncontrolled When Printed

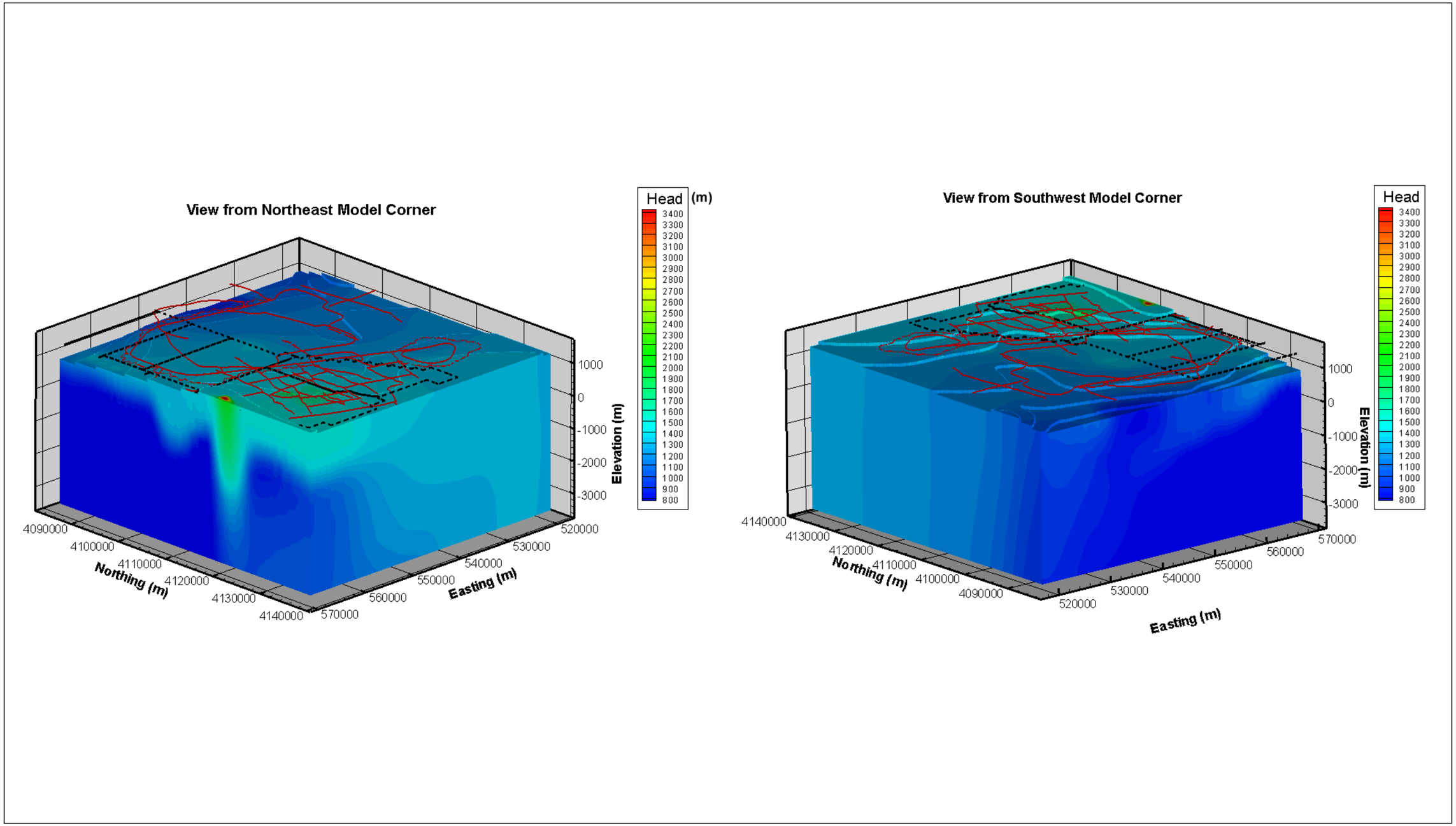

Figure 4-18
CAU Model Boundary Heads Modified from the UGTA Regional Model (SNJV, 2004a)

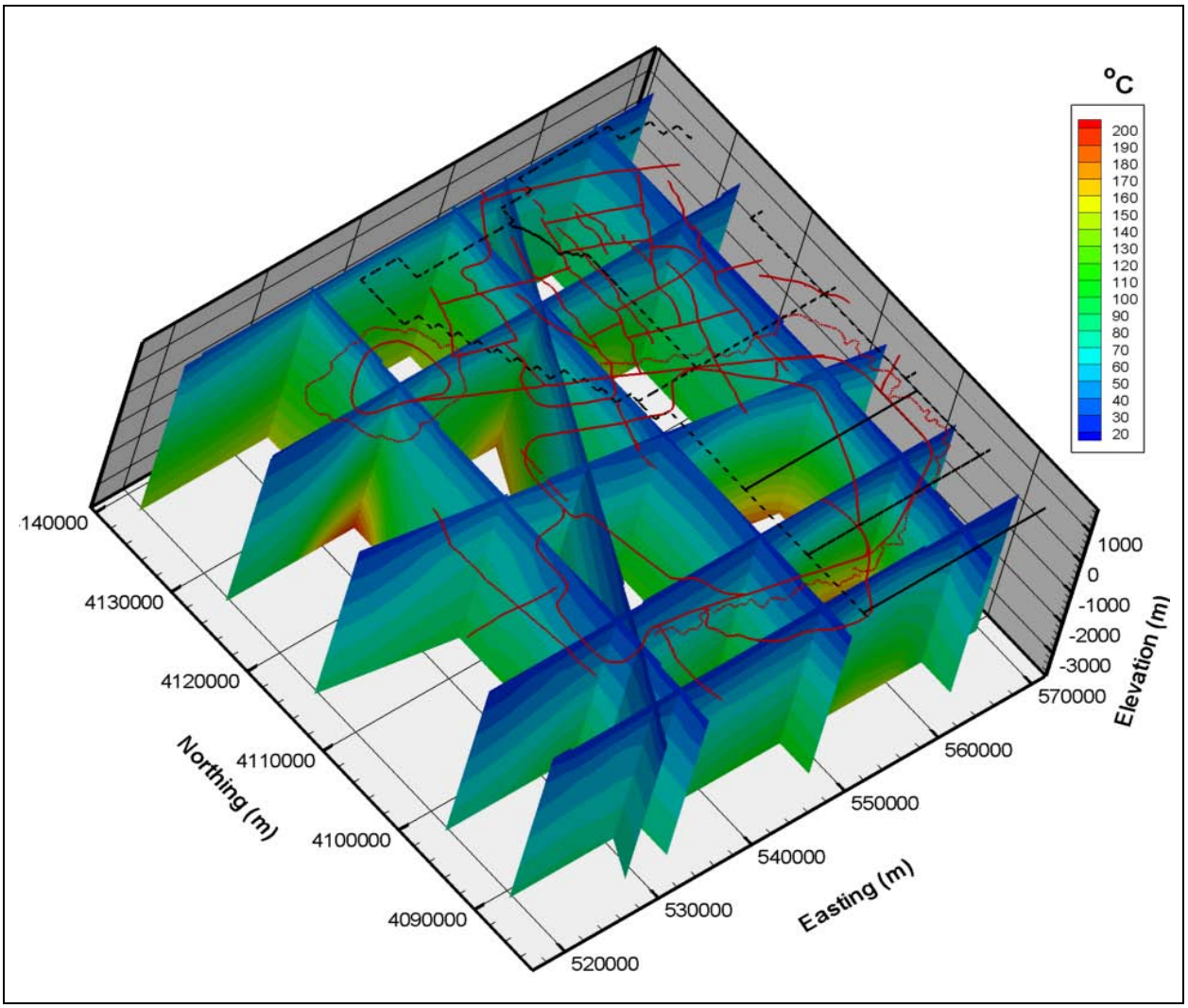

Figure 4-19
Calibrated Temperature Field

5.0 FLOW MODEL CALIBRATION

The Pahute Mesa CAIP (DOE/NV, 1999) and modeling approach/strategy (SNJV, 2004b) indicate that model calibration will be conducted after flow model construction. These documents describe model calibration as "the process of matching historical data" and "calibration consists of determining model parameter values such that simulated heads and fluxes are consistent with observed or target values." In addition, ASTM Standard Guide D 5490-93 (ASTM, 1993b) defines calibration as, "… the process of refining the model representation of the hydrogeologic framework, hydraulic properties, and boundary conditions to achieve a desired degree of correspondence between the model simulations and observations of the groundwater flow system." The purpose of the Pahute Mesa CAU-model calibration is to use observed head data, discharge estimates from Oasis Valley, boundary flow estimates from the regional model, and estimated hydraulic properties for HSUs to develop a numerical model representation of the groundwater flow system in the Pahute Mesa CAU area. This will be used to assess underground-test related radionuclide migration.

This section describes the flow model calibration approach, and the calibration results for the base HFM and the major alternative HFM, the SCCC. These HFMs, presented in Section 2.2.1, are described in detail by BN (2002). Other HFMs are considered in Section 6.3. In addition, the calibrations described in this section are with the MME recharge model; other recharge models are investigated in Section 6.4.

The flow model sensitivity and uncertainty analysis are presented in Section 6.0. Geochemical verification is presented in Section 7.0, and thermal sensitivity and verification is shown in Section 8.0.

The Pahute Mesa CAU flow model considered seven HFMs and five recharge models. In the interest of brevity, the following shorthand is used. The first part of the name is the HFM and the second is the water-balance condition. Two other modifications are applied only to the base model: SDA for selected HSU depth decay and anisotropy, and ADA for all HSU depth decay and anisotropy.

Uncontrolled When Printed

Examples of the naming conventions are as follows:

- BN-MME - Bechtel Nevada (or base) HFM with the MME recharge model and boundary flows.
- BN-DRIA - Bechtel Nevada (or base) HFM with the DRI alluvial recharge model and boundary flows.
- BN-USGSD - Bechtel Nevada (or base) HFM with the USGS redistribution recharge model and boundary flows.
- BN-USGSD - Bechtel Nevada (or base) HFM with the USGS no redistribution recharge model and boundary flows.

The other HFMs are:

- SCCC - Silent Canyon Caldera Complex
- PZUP - Raised Pre-Tertiary/Surface
- DRT - Deeply Rooted Belted Range Thrust Fault
- RIDGE - Basement Ridge
- TCL - Thirsty Canyon Lineament
- SEPZ - Contiguous Imbricate Thrust Sheet

Thus, SEPZ-MME is the contiguous southeast LCA HFM with the MME recharge model and boundary flows.

The five recharge models are:

- MME - Modified Maxey-Eakin
- USGSD - USGS recharge with redistribution
- USGSND - USGS recharge without redistribution
- DRIA - DRI recharge with alluvial mask
- DRIAE - DRI recharge with alluvial and elevation mask

5.1 Calibration Approach

The ASTM Standard Guide D 5981-96 (ASTM, 1996) (also Anderson and Woessner, 1992) describes a general protocol for model calibration. In this protocol, each cycle of parameter adjustment should begin with sensitivity and error analysis (Figure 5-1). The sensitive parameters to be adjusted should be considered in light of the data certainty. Conceptually, the process is not much different than if an automated parameter estimation technique is used (Poeter and Hill, 1997). The general protocol, as

Uncontrolled When Printed

used for the Pahute Mesa flow model, is shown in Figure 5-1. Notice that it is a process that iterates through model sensitivity and parameter adjustment. The Pahute Mesa CAIP (DOE/NV, 1999) states that the model calibration will be conducted by the trial-and-error method. The modeling approach/strategy (SNJV, 2004b) indicates that PEST (Watermark, 2004) parameter estimation software will be used. Both techniques have their strengths and weaknesses, and were used in calibrating the Pahute Mesa flow model.

Hill (1998) also presents a general model calibration procedure that has several components; the most relevant and how they were addressed in the Pahute Mesa flow model are shown in Table 5-1. In the trial-and-error approach the model is run, errors analyzed, adjustments made, and the cycle repeated. When this is improperly done, a shotgun type of approach results. Changes are made in an *ad hoc* manner without insight into the root cause of the model misfit. The trial-and-error method allows for more interpretive information to be considered, but can also be very tedious in that model datasets must be prepared and run by hand for analysis. Discrete sensitivity simulations to test model behavior are also often performed in a manual fashion. With a proper protocol (Figure 5-1), a trial-and-error calibration can yield reasonable and reliable results.

An alternative to trial-and-error calibration is to use an automated approach where the model response to parameter changes is systematically evaluated and the more important parameters that improve calibration identified. The PEST (Watermark, 2004) code was used for this purpose. The PEST code begins by changing each parameter to be considered by a certain amount and recording how the model calibration changes. The Levenberg-Marquardt procedure is used to compute parameters that improve the model agreement with the target data. The basic algorithm used by PEST has a long history of successful use in solving groundwater problems, and is also available in such codes as MODFLOW-2000 and UCODE. For more detail, refer to the PEST manual (Watermark, 2004).

Use of a parameter estimation code has several benefits, including using analyst time more effectively because less manual preparation and manipulation of datasets are required. In addition, a parameter estimation tool provides a framework that helps focus attention on analyzing model errors and their cause, and in the case of complicated models such as the Pahute Mesa CAU flow model, can greatly speed calibration. The PEST code also includes a variety of statistical analyses that help develop

Uncontrolled When Printed

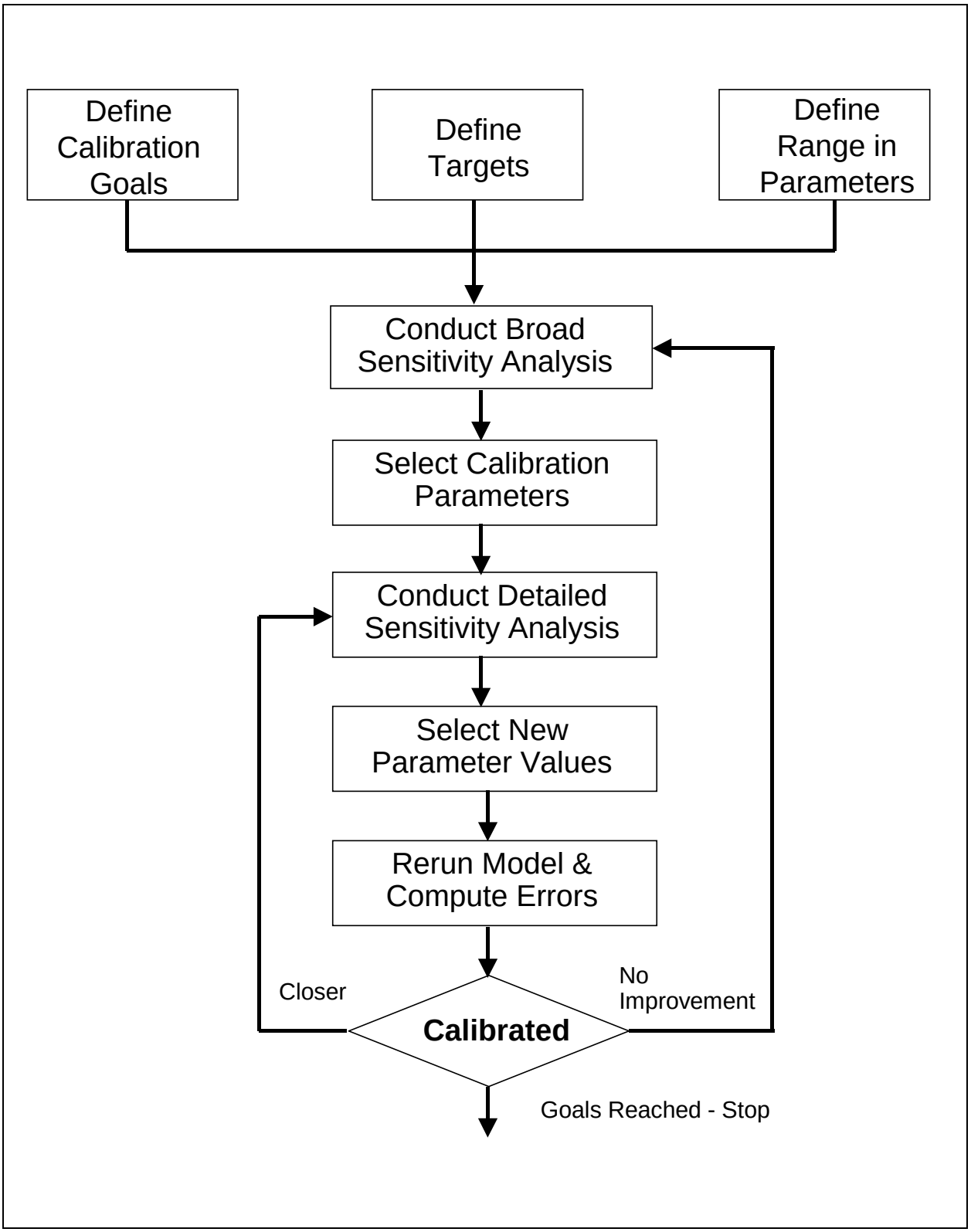

Figure 5-1
General Calibration Protocol

Uncontrolled When Printed

Table 5-1
Calibration Components and Implementation

Calibration Component[a]	Implementation in the Pahute Mesa CAU Flow Model
Apply the principle of parsimony	Hydrostratigraphic units or other geologic properties were not subdivided unless persistent model errors suggested it was necessary for model improvement, with some geologic rationale considered.
Include many kinds of data as observations	Well and spring head, regional water-balance considerations at the model edges, and Oasis Valley discharge were considered.
Assign weights that reflect measurement errors	Weights were developed from uncertainty estimates published in the Pahute Mesa hydrologic data document (SNJV, 2004a).
Evaluate model fit	Model fit was continually evaluated with residual post plots and other tools.
Evaluate optimized parameter values	The reasonableness of PEST revised model parameters was compared to estimated values. Review parameter correlations and fix selected correlated parameters.
Evaluate the potential for additional estimated parameters	Sensitivity analysis and post plots were used to identify locations where additional parameter adjustment was necessary.

[a]Hill, 1998

understanding of the model. These features include sensitivity and correlation coefficients, parameter confidence limits, and eigenvalue and eigenvector analysis. The sensitivity and correlation coefficients describe how much the model calibration changes relative to parameter change, and how parameters may influence one another. This is useful in testing the conceptual model as to what parameters are believed to control model behavior, and what parameters may act similarly on objective function. In addition, parameters that may be important to model calibration can be quantitatively identified and considered in more detail. The confidence limits and eigenvalue and eigenvector analysis are useful in understanding how well the observation data support the model parameters, and how many parameters should be considered for calibration. All these tools were used in calibrating the Pahute Mesa flow model.

The ASTM Standard Guide D 5490-93 (ASTM, 1993b) describes several approaches for evaluating the agreement between a flow model and modeled system. These procedures were used in calibrating

Uncontrolled When Printed

the Pahute Mesa flow model, and include qualitative and quantitative comparisons between model results and the following:

- Measured heads at wells and springs
- Water-balance information (recharge and discharge fluxes)
- Flow-direction information
- Estimated values of HFM hydraulic parameters from characterization data

The ASTM Standard Guide D 5490-93 recommends the use of quantitative measures for the agreement of hydraulic head and suggests quantitative measures for water-balance information if possible (ASTM, 1993b). For the Pahute Mesa CAU flow model, quantitative measures of the fit with head (wells and springs) data, Oasis Valley discharge, and lateral water balance were considered.

A variety of numeric and graphical tools are used to investigate flow model calibration. These include summary statistical measures such as the mean error (or residual) (ME), largest and smallest errors, standard deviation of the errors (SD), and sum of weighted squared errors. Error, or residual, is defined as follows:

$$r_i = H_i - h_i \tag{5-1}$$

where h_i is the computed head at the location where H_i was measured. Mean error, ME, is defined as follows:

$$ME = \Sigma w_i r_i / n w_i \tag{5-2}$$

The SD is defined as follows:

$$SD = \frac{\Sigma (r_i w_i)^2}{n} \tag{5-3}$$

Sum of weighted squared errors (also called phi after the Greek alphabet symbol used to denote it, as well as “goodness of fit”) is defined as (Watermark, 2004):

$$\Phi = \sum_{i=1}^{m} (w_i r_i)^2 \tag{5-4}$$

where Φ is the objective function (phi, or goodness of fit), *w* is the observation weight, *r* is the residual or difference between the simulated and measured values, and *n* is the number of observations of non-zero weight. If the weights assigned to calibration data change, all these measures will change even if the model results are the same. Thus, it is important to compare results using a consistent weighting scheme (see Section 5.2).

During calibration, it is desired to reduce the ME to zero; that is, there should be no bias in the ME. This will give a model that has no systematic (at least in the univariate statistical sense) bias. However, errors of –1 and +1 give the same ME as –50 and +50, but it is obvious a model with 50 ft of error is not as good as one with 1 ft. Consequently, the standard deviation is used to describe spread of the errors. The ME may be low, but if the spread is large, the model may be inadequate.

Statistical measures are useful for summarizing model behavior but do not readily give a sense for the spatial distribution of errors. To address this issue, the following graphical analyses are also used (see ASTM Standard Guide D 5490-93 [ASTM, 1993b] for more information):

- The *scattergram*, or cross plot, shows the observed data versus computed results plotted against each other, and is useful for identifying overall goodness and bias.
- Post plots of head residuals in plan view show the distribution of errors in the model. Recalling the ME example from above, it would be possible to have an ME of 0, with all the errors on one side of the domain at a +50 error and on the other with a –50 error, which is a vastly different result than if the errors are scattered randomly in space (the ideal case).
- Flow residuals are also examined using bar charts, although they can also be visualized with a scattergram.

The goal of model calibration (also called "parameter estimation," "solving the inverse problem," and "inversion") is to make the model agree with reality by adjusting, within their ranges of variation, model parameters. How this is approached can be critical. Freyberg (1988) presented a study in which students were given a model to calibrate. They had to calibrate the model and then make a prediction. The best-calibrated model actually made the worst predictions. This is because the best-calibrated model was fitted by tweaking hydraulic conductivity on a block-by-block basis, but the best predictive model chose to zone the hydraulic conductivity into a few homogenous regions. Minimizing the ME, standard deviation, and goodness of fit is not the sole objective of model calibration.

Uncontrolled When Printed

The reasonableness of the flow directions was also assessed qualitatively during the calibration phase via streamline particle tracking and quantitatively via geochemical analysis in Section 7.0. Finally, it is important to recognize that no matter the procedure, the goal of model calibration is a set of model parameters that best (or at least reasonably) represents the hydrogeologic system.

5.2 Calibration Data

Four types of information, or targets, were used for calibration of the Pahute Mesa flow model as follows:

- Hydraulic head from wells (see Appendix F)
- Estimated spring head in and near Oasis Valley (see Appendix F)
- Oasis Valley discharge derived from Laczniak et al. (2001)
- Edge flows estimated from regional model analysis presented in the Pahute Mesa hydrologic data document (SNJV, 2004a)

Because an automated procedure was used to aid calibration, multiplicative weighting factors were developed and assigned to data with different levels of accuracy and measurement units. The factors that PEST needs are the inverses of the measurement error standard deviations (Watermark, 2004). Thus, measurements with a larger standard deviation receive a smaller weight. The weights, which have reciprocal units of the target data, also transform the objective function contribution from different data types into dimensionless values that can be compared regardless of measurement units. However, an alternate empirical approach is also commonly used (e.g., Wolfsberg et al., 2002; DOE/ORD, 2004) in which the weights are assigned by considering accuracy along with judgment to give the desired contribution to the calibration for selected data.

The head calibration dataset was presented in Appendix E of the Pahute Mesa hydrologic data document (SNJV, 2004a) (see Plate 1). Along the east-central edge of the model, Wells Hagestad 1 (which may be perched), TW-1 (the upper two intervals may be perched), UE-12n #15A (which may be perched), and U-12s (which may be perched) were either outside the model boundary or just inside it (as well as perched), thus making them unsuitable for calibration because they were so close to the specified-head conditions at the edge of the model. Along the southern edge, Well Gexa 4 (also

Uncontrolled When Printed

suspected perched by the YMP [DOE/ORD, 2004]) was just inside the model boundary. These wells were used to check the model boundary head in these areas for reasonableness and were included in the calibration with a very low weight so the results could still be evaluated without unduly influencing the calibration.

As part of the hydraulic head dataset, the reference point elevation accuracy and the measurement uncertainty (as a standard deviation) were presented. Hill (1998) shows how to convert an estimated land surface error into a standard deviation. When the land surface elevation is estimated from USGS topographic maps, the formula is (contour interval/[2*1.65]). Reference point elevation accuracy of 6.096 m corresponds to locations estimated from USGS topographic maps with 40-ft (12-m) contour intervals.

The natural variability of rock permeability, which is not represented other than in a broad way in the Pahute Mesa flow model, creates variability in water levels. Gelhar (1986) shows how to use a solution by Naff (1978) to estimate the magnitude of this error. Appendix G of Wolfsberg et al. (2002) estimated correlation scales for the various types of volcanic rocks found on Pahute Mesa. These scales range from several tens of meters to a few hundred meters in the horizontal, to a few tens of meters in the vertical direction. Depending on the various assumptions required in the calculation, the standard deviation in head from heterogeneity could be as high as 2 m.

Simulated heads were not interpolated to the actual well location within an element, which gives up to 1 m of error when the gradient of Blankennagel and Weir (1973) and the smallest element size of 67.5 m is used. A value of 1 m was used to account for heterogeneity and interpolation error. Finally, all the standard deviations of reference point uncertainty, head value uncertainty, and heterogeneity were summed and the weight for PEST computed. Table 5-2 shows the weights used in model calibration for well and spring heads. Figure 5-2 shows a histogram of the weights used in model calibration for well and spring heads. The weights between 0 and 0.1 (none of which were actually zero) are mainly associated with wells and springs that had reference point elevation accuracy estimate from topographic maps with 6 or 3 m accuracy (40- or 20-ft contour interval) that result in low weights. Twelve of the lowest weights are from the wells described above that were located outside the model or just on its edge.

Uncontrolled When Printed

Table 5-2
Head and Spring Calibration Weights
(Page 1 of 6)

ID No.	Site Name	Weight	Comment
1	Beatty Wash Terrace Well	0.2	
2	Beatty Well No. 1	1.00×10^{-3}	Downweighted, just inside edge of mesh
3	Boiling Pot Road Well	0.2	ET Cycles but good
4	Coffer Dune Well	0.34	ET Cycles but good
5	Coffer Lower ET Well	0.32	ET Cycles but good
6	Coffer Middle ET Well	0.31	ET Cycles but good
7	Coffer Windmill Well	0.35	
8	ER-18-2	0.84	May still be rising
9	ER-19-1 #1 (deep)	1.00×10^{-3}	Downweighted, just inside edge of mesh; Fenelon (2000) suggests depressed below regional
10	ER-19-1 #2 (middle)	1.00×10^{-3}	Downweighted, just inside edge of mesh; large uncertainty from hydrograph
11	ER-19-1 #3 (shallow)	1.00×10^{-3}	Downweighted, just inside edge of mesh; Fenelon (2000) suggests elevated (perched?) above regional
12	ER-20-1	0.89	
13	ER-20-2-1	0.2	
14	ER-20-5 #1 (3-in. string)	0.72	
15	ER-20-6 #1 (3-in. string)	0.92	
16	ER-20-6 #2 (3-in. string)	0.95	
17	ER-20-6 #3 (3-in. string)	0.91	
18	ER-30-1	0.94	
19	ER-EC-1	0.83	
20	ER-EC-2A (498.3-681.5 m)	0.82	
21	ER-EC-2A (498.35-1,515.8 m)	0.78	
22	ER-EC-4 (290.2-1,062.8 m)	0.83	
23	ER-EC-4 (290.2-699.5 m)	0.83	
24	ER-EC-4 (Lower Interval)	0.84	
25	ER-EC-5	0.81	
26	ER-EC-6 (481.9-1,164.3 m)	0.83	
27	ER-EC-6 (481.9-1,524 m)	0.84	
28	ER-EC-7	0.78	
29	ER-EC-8	0.81	
30	ER-OV-01	0.83	
31	ER-OV-02	0.81	
32	ER-OV-03a	0.76	Declining trend (very small)
33	ER-OV-03a2	0.78	

Uncontrolled When Printed

Table 5-2
Head and Spring Calibration Weights
(Page 2 of 6)

ID No.	Site Name	Weight	Comment
34	ER-OV-03a3	0.76	Declining trend (very small)
35	ER-OV-03b	0.8	
36	ER-OV-03c	0.82	
37	ER-OV-03c2	0.82	
38	ER-OV-04a	0.77	ET Cycles but good
39	ER-OV-05	1.00×10^{-3}	Downweighted, just inside edge of mesh
40	ER-OV-06a	0.82	
41	ER-OV-06a2	0.82	
42	Gexa Well 4	1.00×10^{-3}	Downweighted, just inside edge of mesh; YMP also weighted low
43	Hagestad 1	2.00×10^{-3}	Downweighted, outside mesh; may be perched
44	Matheny Well	0.21	
45	Middle Oasis Valley ET Well	0.31	ET Cycles but good
46	Pioneer Road Seep Well	0.2	ET Cycles but good
47	PM-1 (2,356.408 m)	0.66	Hot water, so true water level may be lower
48	PM-2	0.67	
49	PM-3 (Upper Borehole)	0.67	Hydrograph declining
50	PM-3 (Lower Borehole)	0.67	
51	PM-3-1 (Piezometer 1)	0.67	Hydrograph still rising
52	PM-3-2 (Piezometer 2)	0.67	Hydrograph still rising
53	Springdale ET Deep Well	0.32	ET Cycles but good
54	Springdale ET Shallow Well	0.31	ET Cycles but good
55	Springdale Lower Well	0.18	ET Cycles but good
56	Springdale Upper Well	0.34	ET Cycles but good
57	Springdale Windmill Well	0.34	ET Cycles but good
58	TW-1 (1,125 m)	1.00×10^{-3}	Downweighted, edge of mesh
59	TW-1 (1,127-1,137 m)	1.00×10^{-3}	Downweighted, edge of mesh
60	TW-1 (170 m)	2.00×10^{-3}	Downweighted, edge of mesh; may be perched
61	TW-1 (492 m)	2.00×10^{-3}	Downweighted, edge of mesh; may be perched
62	TW-1 (560 m)	1.00×10^{-3}	Downweighted, edge of mesh
63	TW-1 (826 m)	1.00×10^{-3}	Downweighted, edge of mesh
64	TW-1 (839 m)	1.00×10^{-3}	Downweighted, edge of mesh
65	TW-1 (839-1,279 m)	1.00×10^{-3}	Downweighted, edge of mesh
66	U-12s (451.1 m)	2.00×10^{-3}	Downweighted, outside mesh; may be perched; fluctuating
67	U-19ab	2.00×10^{-3}	Fenelon (2000) indicates possibly perched
68	U-19ab 2	2.00×10^{-3}	Fenelon (2000) indicates possibly perched

Uncontrolled When Printed

Table 5-2
Head and Spring Calibration Weights
(Page 3 of 6)

ID No.	Site Name	Weight	Comment
69	U-19ad	0.98	Large uncertainty from hydrograph
70	U-19ae	0.69	
71	U-19ai	0.68	
72	U-19aj	0.52	
73	U-19aq	2.00×10^{-3}	Fenelon (2000) indicates possibly perched
74	U-19ar	0.18	
75	U-19aS (857 m)	0.98	
76	U-19au	0.86	
77	U-19au #1	0.68	
78	U-19ay	0.94	
79	U-19az	2.00×10^{-3}	Fenelon (2000) indicates possibly perched
80	U-19ba	2.00×10^{-3}	Fenelon (2000) indicates possibly perched
81	U-19bg #1	0.86	
82	U-19bh	2.00×10^{-3}	Fenelon (2000) indicates possibly perched
83	U-19bj	0.002	Declining trend may be perched
84	U-19bk	2.00×10^{-3}	Fenelon (2000) indicates possibly perched
85	U-19d #2	0.98	
86	U-19e	0.98	
87	U-19g	0.5	
88	U-19x	0.98	
89	U-20 WW (Open)	0.9	
90	U-20a	0.003	
91	U-20a #2 WW	0.84	
92	U-20ah	0.49	
93	U-20ai	0.59	
94	U-20ak	0.64	
95	U-20am	0.69	
96	U-20an	0.79	
97	U-20ao	2.00×10^{-3}	Perched
98	U-20ar #1	0.6	
99	U-20as	0.95	
100	U-20at #1	0.76	
101	U-20av	0.58	
102	U-20aw	0.89	Only about 4 m worth of saturated zone here
103	U-20ax	2.00×10^{-3}	Fenelon (2000) indicates possibly perched

Uncontrolled When Printed

Table 5-2
Head and Spring Calibration Weights
(Page 4 of 6)

ID No.	Site Name	Weight	Comment
104	U-20ay	0.003	
105	U-20az	0.98	
106	U-20bb (579.12 m)	0.003	
107	U-20bb (676.66 m)	0.52	
108	U-20bb #1	0.33	
109	U-20bc	0.003	Elevated compared to regional
110	U-20bd (689.15 m)	0.94	
111	U-20bd #1	0.86	
112	U-20bd #2	0.7	
113	U-20be	0.5	
114	U-20bf	0.5	
115	U-20bg	0.98	
116	U-20c	0.98	
117	U-20e	0.98	
118	U-20g	0.98	
119	U-20i	0.98	
120	U-20m	0.67	
121	U-20n PS #1DD-H (922 m)	0.98	Fenelon (2000) indicates impacted by pumping at U-20 WW
122	U-20y	0.56	
123	UE-12n #15A	2.00×10^{-3}	Downweighted, outside mesh; may be perched
124	UE-18r	0.61	
125	UE-18t	0.71	
126	UE-19b #1 WW	0.82	
127	UE-19c WW	0.67	
128	UE-19e WW	0.39	
129	UE-19fs	0.98	
130	UE-19gS	0.98	
131	UE-19gS WW	0.84	
132	UE-19h	0.89	
133	UE-19i	0.98	
134	UE-19z	0.2	
135	UE-20ab	0.52	
136	UE-20av	0.84	
137	UE-20bh #1	0.64	Fenelon (2000) indicates impacted by pumping at U-20 WW
138	UE-20c	0.003	

Uncontrolled When Printed

Table 5-2
Head and Spring Calibration Weights
(Page 5 of 6)

ID No.	Site Name	Weight	Comment
139	UE-20d	0.54	
140	UE-20e #1	0.98	
141	UE-20f (1,384.7 m)	0.93	
142	UE-20f (4,171 m)	0.45	
143	UE-20h WW	0.59	
144	UE-20j WW	1.67	
145	UE-20n #1 (1,005.84 m)	0.98	
146	UE-20n #1 (863.8 m)	0.98	Fenelon (2000) indicates impacted by pumping at U-20 WW
147	UE-20p	0.67	
148	UE-29a #1 HTH	2.00×10^{-3}	May be perched or local flow system
149	UE-29a #2 HTH	2.00×10^{-3}	May be perched or local flow system; YMP also weighted low
150	USW UZ-N91	0.44	Recharge seen in hydrograph
151	Ute Springs Drainage Well	0.19	ET Cycles but good
152	WW-8	0.98	Declining hydrograph trend
153	Spring	1	
154	Crystal Springs Area	2.00×10^{-3}	Downweighted; source water may be local or perched according to HDD
155	Revert Springs Channel	1.00×10^{-3}	Downweighted, just inside edge of mesh
156	Revert Springs Area	1.00×10^{-3}	Downweighted, just inside edge of mesh
157	Revert Springs Area	1.00×10^{-3}	Downweighted, just inside edge of mesh
158	Spring (Report R10)	1	
159	Spring	1	
160	Springdale Culvert	1	
161	Torrance Spring	1	
162	Ute Springs Area	1	
163	Spring	1	
164	Oasis Valley Upper Culvert Spring	1	
165	Hot Springs Area	1	
166	Hot Springs Pump House	1	
167	Hot Springs Bath House 1	1	
168	Hot Springs Bath House 2	1	
169	Hot Springs below Culvert 1	1	
170	Hot Springs Culvert 2	1	
171	Hot Springs above Culvert 2	1	
172	Ute Springs Area	1	

Uncontrolled When Printed

Table 5-2
Head and Spring Calibration Weights
(Page 6 of 6)

ID No.	Site Name	Weight	Comment
173	Spring	1	
174	Ute Springs Culvert	1	
175	Ute Springs	1	
176	Oleo Road Spring	0.004	Spring located in area of very high topographic gradient
177	Goss Spring - North	0.006	Locations uncertain
178	Goss Spring	0.006	Locations uncertain
179	Spring	0.006	Locations uncertain
180	Spring	1	

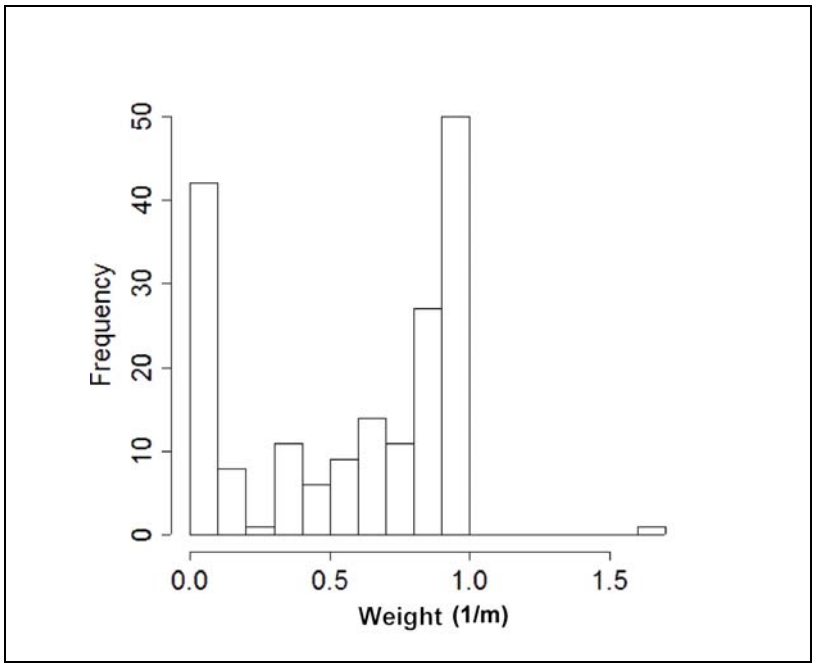

Figure 5-2
Histogram of Head Calibration Weights

The estimated spring head in the Oasis Valley area was also presented in the Pahute Mesa hydrologic data document (SNJV, 2004a). These data were assigned a unit weight in order to help emphasize Oasis Valley discharge, and in a few cases lower weights were assigned based on proximity to model edge and other factors (e.g., Oleo Road Spring was assigned a low weight because it lies in an area of high topographic gradient that made the model unable to match it). The location of three springs –

Uncontrolled When Printed

Goss Spring, Goss Spring-North, and Spring id 179 – had incorrect locations reported in the Pahute Mesa hydrologic data document (SNJV, 2004a). They were relocated as shown in Table 5-3.

Table 5-3
Corrected Spring Locations

Spring	Easting (UTM Zone 11, NAD 27) (m)	Northing (UTM Zone 11, NAD 27) (m)	Elevation (m)
Goss Spring	525419.43	4094275.13	1,139.34
Goss Spring-North	525289.20	4094402.54	1,139.34
Spring id 179	525460.21	4094286.46	1,139.35

Source: Watrus, 2004

NAD = North American Datum

Oasis Valley has long been known to be a groundwater discharge area. The UGTA regional model (DOE/NV, 1997) summarized the range in estimated discharge in this area. More recently, Laczniak et al. (2001) conducted an extensive field study to further refine the discharge estimate. Figure 4-17 shows the Laczniak et al. (2001) digital data overlaid on the southwestern part of the model domain, with seven zones (numbered 1-6, and 8) overlaid to define individual discharge segments. The CAU model does not completely encompass the discharge area studied by Laczniak et al. (2001). Table 5-4 summarizes the flow rates for each segment shown on Figure 4-17; the total is 227 kg/s. By comparison, the total mean Oasis Valley discharge estimated by Laczniak et al. (2001) is 242 kg/s.

Table 5-4
Oasis Valley Zone Discharge

Discharge Zone	Discharge (kg/s)
1	70.7
2	13.0
3	47.7
4	38.0
5	33.9
6	22.2
8	1.50

Oasis Valley discharge uncertainty was assessed by Laczniak et al. (2001). Using the reciprocal of the published Oasis Valley discharge standard deviation gives a weight of 0.0013 in measurement

Uncontrolled When Printed

units of acre-feet (ac-ft), or 0.034 in seconds per kilogram (s/kg) (the units used in FEHM). Laczniak et al. (2001) estimate the total mean discharge in Oasis Valley at 6,200 acre-feet per year (ac-ft/yr) (242 kg/s). With a weight of 0.034, a 50 percent error (3,100 ac-ft/yr or 121 kg/s) would result in a weighted error of only 16. This would be an equivalent well head error of only 4 m with a unit weight. Mathematically, Oasis Valley discharge is key to constraining the flow model because it is well known that a model with constant head boundaries calibrated only to head is not unique. To address a similar problem, Wolfsberg et al. (2002) used the flow estimated by Blankennagel and Weir (1973) (80 kg/s) to constrain their TYBO/BENHAM sub-CAU model, and assigned it a unit weight. This resulted in a strong contribution from flow to their model goodness of fit relative to the 22 wells used for head calibration, which were generally matched within a few meters. During calibration, a weight value of 2 s/kg was found to give good results in matching Oasis Valley discharge.

The UGTA regional model boundary flow analysis is summarized in Appendix F of the Pahute Mesa hydrologic data document (SNJV, 2004a). However, the CAU mesh is not aligned precisely with the UGTA regional model (DOE/NV, 1997); thus, some interpolation of the edge flows is necessary. Gable and Cherry (2001) developed a general procedure for interpolating MODFLOW (McDonald and Harbaugh, 1988) cell flows onto a piecewise linear surface. In the case of the Pahute Mesa CAU model, the surfaces are the planes that define the north, west, south, and east edge for which the UGTA regional model flow into or out of the CAU model is to be interpolated. The approach transforms the flows into an approximate Darcy velocity at each face of the MODFLOW cell. The velocity is interpolated onto the linear control surface, and flow is completed by integration of the velocity normal to the control surface. The interpolated edge flows are shown in Table 5-5. These flows were used as calibration targets that the CAU model was required to reasonably honor.

Model boundary flow uncertainty was derived in a discrete manner from the regional model by combining different combinations of HFM and recharge. An initial weighting procedure was attempted by considering the base HFM and MME recharge boundary flow as the mean, with results of the base HFM and DRI and USGS recharge defining the upper and lower 95 percent confidence limits. This gives approximately (considering only the northern edge for example) a weight of 0.027. With this weight, an error of 100 kg/s would give a squared weighted error of about 9 ([100*0.027]^2); as with the weights for Oasis Valley discharge, this seems an unreasonably small

Table 5-5
Interpolated Regional Model Boundary Flows

Case[a]	North[b] (kg/s)	South[c] (kg/s)	East[c] (kg/s)	West[a] (kg/s)	HFM	Recharge Model
g1ar1a	263.2	-324.6	-32.4	23.6	BN[d]	MME[e]
g1ar1b	291.6	-415.9	-40.9	56.5	BN	ME[f]
g1ar2	156.2	-296.0	-38.4	39.2	BN	USGSND[g]
g1ar3a	335.4	-547.4	-81.6	75.0	BN	DRIA[h]
g1ar3b	289.1	-524.7	-49.7	57.8	BN	DRIAE[i]
g1br1a	280.3	-418.6	-38.0	59.8	BN	MME
g2ar1a	305.1	-536.6	-66.4	64.0	SCCC[j]	MME
g2br1a	328.3	-547.5	-73.1	64.1	SCCC	MME
dvrfs[k]	350	-350	-8	50	-	-

[a]As defined in the Pahute Mesa hydrologic data document SNJV (2004a)
[b](-) = is into model
[c](+) = is out of model
[d]BN = Bechtel Nevada base model
[e]MME = Modified Maxey-Eakin
[f]ME = Maxey-Eakin
[g]USGSND = USGS no redistribution
[h]DRIA = DRI alluvial mask
[i]DRIAE = Alluvial and elevation masks
[j]SCCC = Silent Canyon Caldera Complex
[k]dvrfs = Not interpolated

contribution and was adjusted during calibration to a value of 0.5 for all boundaries. The contribution of each type of data is presented in Sections 5.6 and 5.7 and discussed in Section 5.8.

5.3 Boundary Head Adjustments

The starting point for the CAU-model specified-head boundary conditions was the UGTA regional model (DOE/NV, 1997) results interpolated onto the mesh edges as described in Section 4.3.3. Changes were made during calibration based on the following considerations:

- When the UGTA regional model (DOE/NV, 1997) was developed, the exact nature of the western boundary (just west of Oasis Valley) was unknown but was assumed to be a no flow, or streamline. More recent work by SNJV (2004a) and the USGS (Faunt et al., 2004) suggests that there is flow east from Sarcobatus Flat into Oasis Valley. For the CAU model, the boundary head west of Oasis Valley and south of northing 4,098,000 m, the boundary head was raised to create flow into Oasis Valley (Figure 5-3). The head along the northern edge west of about easting 550,000 m was adjusted to better approximate the head on the northern edge of the model.

Uncontrolled When Printed

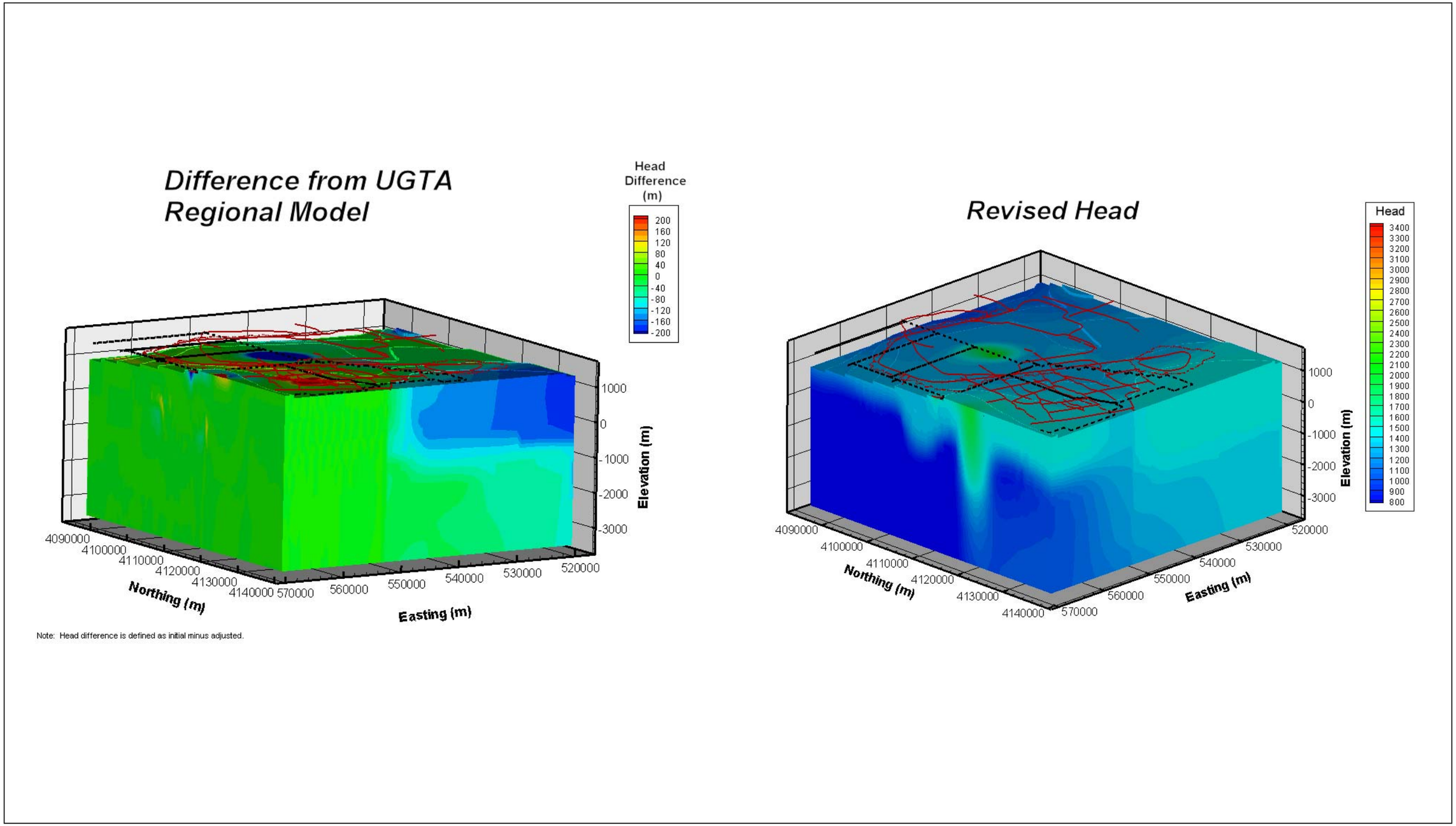

Figure 5-3
Calibrated CAU-Model Boundary Heads and Difference from UGTA Regional Model Viewed from the Northeast

- The UGTA regional model (DOE/NV, 1997) (and the recent DVRFM [Faunt et al., 2004]) has a persistent misfit at the Gold Flat 2 well just outside the north-central edge of the CAU-model domain of over 100 m with simulated head about 1,320 m. Just south of Gold Flat inside the CAU model are Wells UE-20p and PM-2, both of which have mean water levels of over 1,400 m. Thus, if the boundary head in the part of the model is used directly from the UGTA regional model (or DVRFM), there will be an immediate 100-m error that should not be corrected by parameter adjustment because the error is entirely a consequence of an inaccurate boundary condition assignment. Figure 5-3 shows the view of the head field used to calibrate the model and its change from the starting interpolated UGTA regional model head.

- The southern edge of the model east of Oasis Valley is coincident with an area of high-hydraulic gradient that is poorly understood. Zyvoloski et al. (2003) investigated several conceptual models of this area, and in general found that some type of low-permeability feature (possibly from hydrothermal alteration) was required to replicate this feature. The UGTA regional model (DOE/NV, 1997) performed only fairly in this area. Gexa 4, USW UZ-Na91, and UE-29a #1 and UE-29a #2 Hydrologic Test Holes (HTHs) are the only wells in this area selected for calibration, and it is unclear whether UE-29a taps an aquifer system or a local and possibly perched flow system. The water level at Gexa 4 was combined with regional model data and interpolated onto the southern CAU-model edge. The effects of the change can be seen in Figure 5-4 near easting of 535,000 m and at an elevation above 0 m.

- Well TW-1, excluding the upper two intervals, was used to revise the eastern boundary heads, which otherwise remained relatively unchanged from the UGTA regional model (DOE/NV, 1997) results seen in Figure 5-4.

- The interpolated and corrected heads on the northwest corner (both north and west faces) of the model created a local flow cell, where flow entered on the far west northern edge and then immediately departed on the far northwestern edge. This created an erroneous boundary flow estimate that was not in the UGTA regional model (DOE/NV, 1997), which had a no-flow boundary along its western edge. Thus, this flow was entirely an artifact of the constant-head specification on the western edge. Water-level maps were reviewed, and the western edge north of 4,103,000 m was specified as a no-flow boundary along what is reasonably believed to be a regional flow divide. The conversion of this boundary to no-flow and the effects of correcting the heads on the northwestern edge to better match PM-2 and UE-20p cause the changes seen in Figure 5-4. Also see Figure 3-4 in Section 3.0 for a water-level map that supports this interpretation.

Uncontrolled When Printed

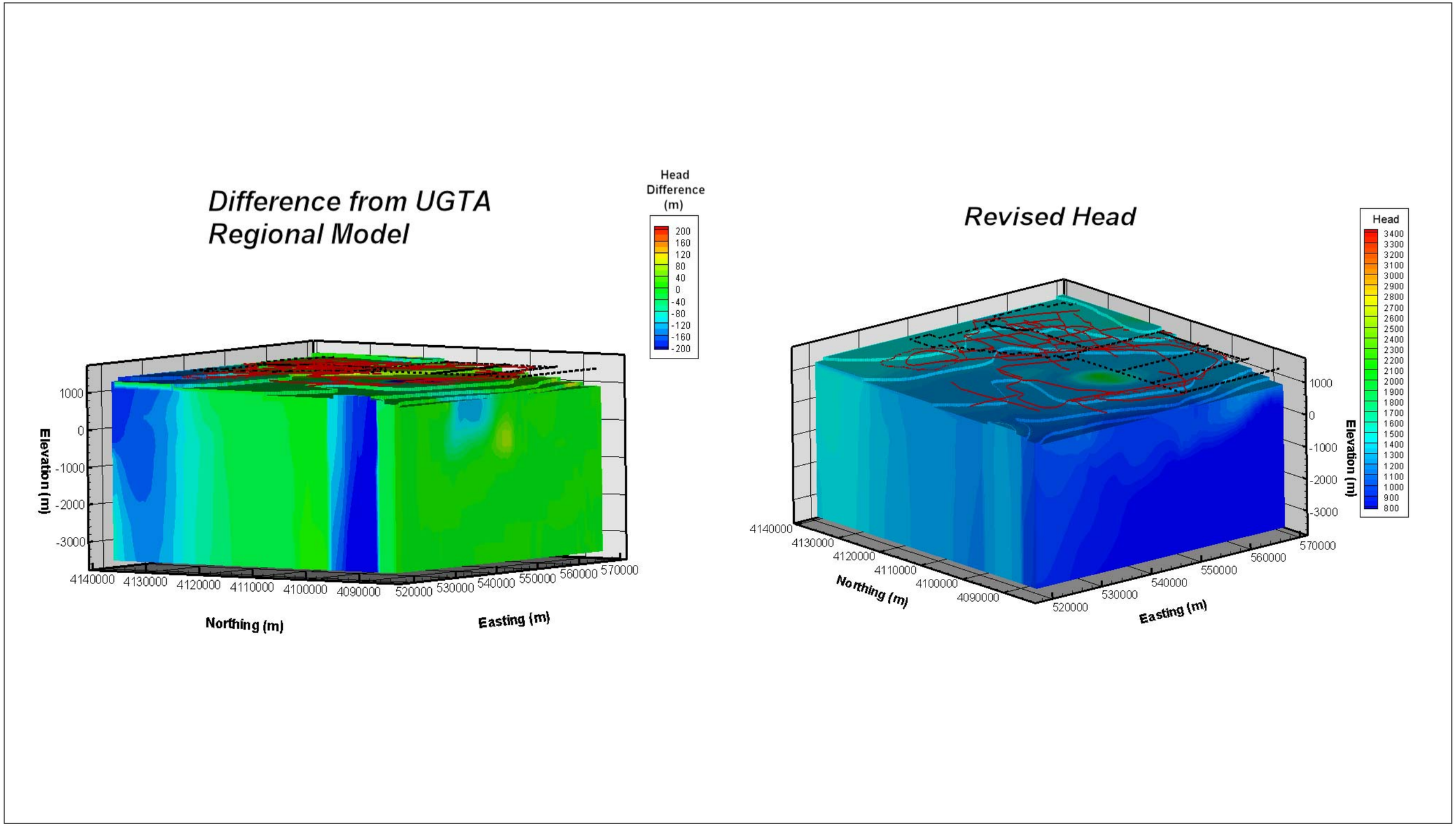

Figure 5-4
Calibrated CAU-Model Boundary Heads and Difference from UGTA Regional Model Viewed from the Southwest

Uncontrolled When Printed

5.4 Geologic Model Subdivision

During the calibration process, it was discovered that the flow model was particularly sensitive to the properties of two regionally extensive HSUs: the PBRCM and the TMCM. Both of these units exist over large areas of the model. In order to better address the geologic heterogeneity that almost certainly exists in these two large units, they were subdivided areally. In the case of the PBRCM, it was divided outside of Areas 19 and 20 as defined by the Silent Canyon Caldera bounding faults in the base model as shown in Figure 5-5. Figure 5-5 also shows faults and structure contours. Bechtel Nevada (2002) suggested subdivision of the TMCM into several hydrogeologic domains (Figure 5-6) that were adopted with the further subdivision of the Northern Timber Mountain and Ammonia Tanks subdomains into east and west sections at easting 560,000 m.

In addition, the UGTA regional model further subdivided the LCA, TCVA, and TMA (see Volume VI, DOE/NV, 1997). These divisions were propagated into the CAU model, as they were originally made for hydrogeologic reasons. Figure 5-7 shows the nodes as solid blue rectangles from the subdivision of the LCA along the southeastern corner of the model domain as derived from the UTGA regional model (DOE/NV, 1997). This fragment of LCA belongs to the larger subdivision that extended to the east and encompassed the eastern part of the NTS and low hydraulic gradient area in the UGTA regional model. Figure 5-8 shows the nodes from the subdivision of the TMA. Note that the node spacing is so dense that the nodes appear as a solid fill. Also note that the nodes are entirely at the top of the model domain. The UGTA regional model subdivided the TMA to allow for potential alteration effects within the Timber and Black Mountain calderas. Zone, or material, 36 is the TMA in the CAU model (top panel), which was further divided by Zone 6, which represents the area near Black Mountain, from the UGTA regional model (DOE/NV, 1997). Thus, Zones 6 and 36 give the entire extent of the TMA. The TMCM HSU replaced the other TMA zones and the division suggested in Figure 5-6. Figure 5-9 shows the nodes from the subdivision of the TCVA. The TCVA, like the TMA, also was divided to allow for alteration effects. Zone 44 is the TCVA in the CAU model (top panel), which was further subdivided by Zone 6, again representing the area near Black Mountain. Zones 6 and 44 give the extent of the TCVA in the CAU model.

Uncontrolled When Printed

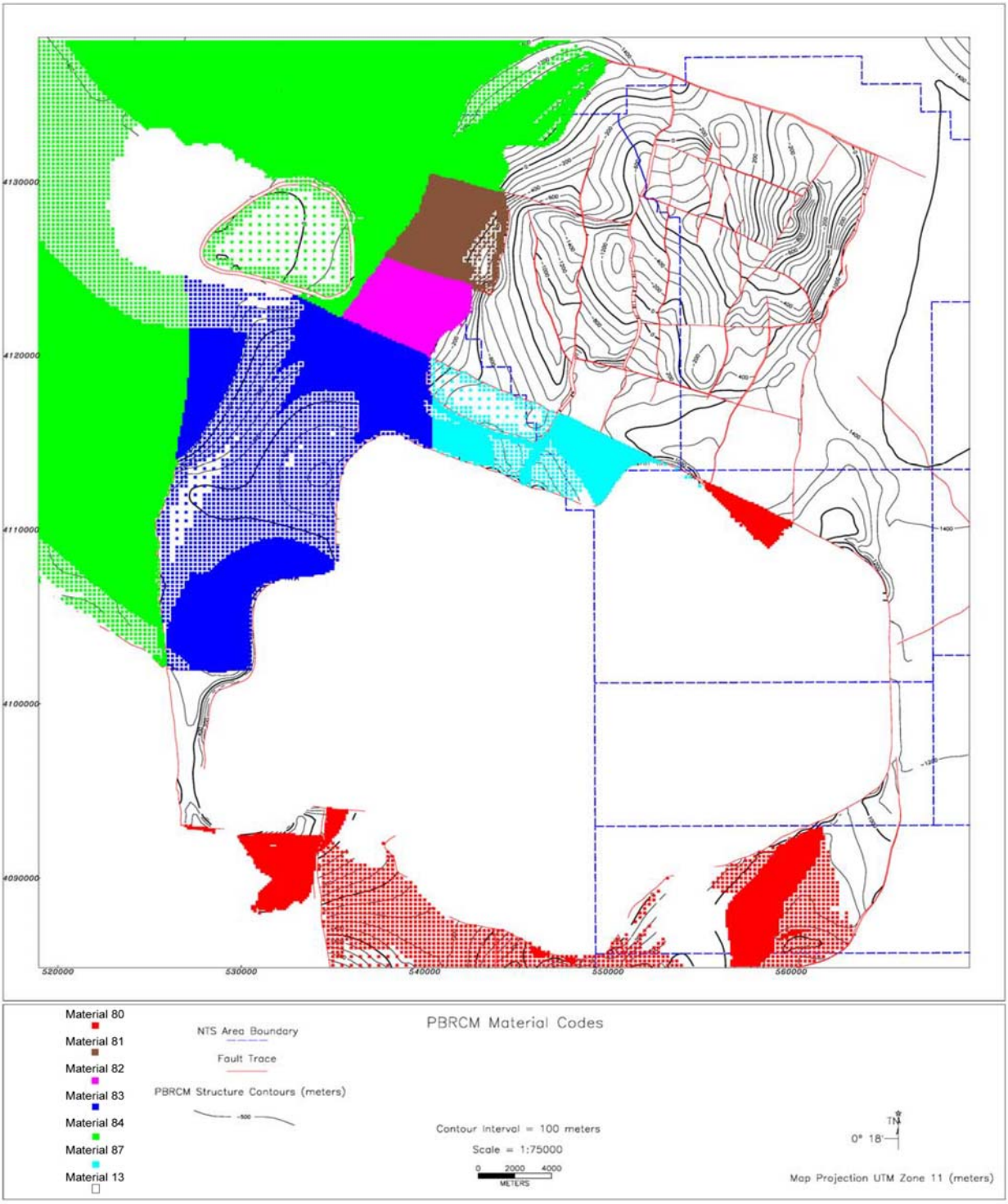

Figure 5-5
CAU-Model Pre-Belted Range Composite (PBRCM) Material Zones

Uncontrolled When Printed

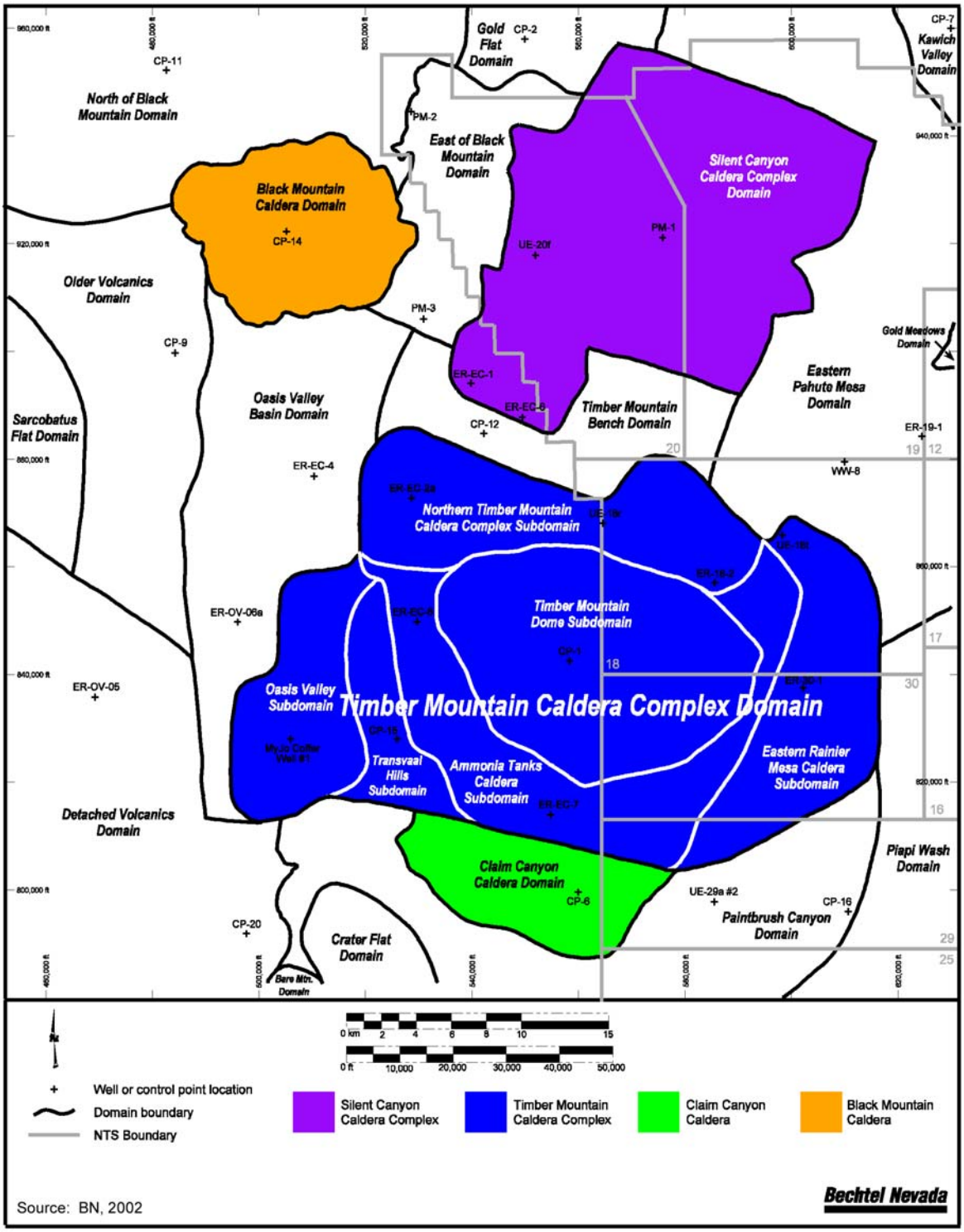

Figure 5-6
Map Showing Hydrogeologic Domains in the Pahute Mesa/Oasis Valley Model Area

Uncontrolled When Printed

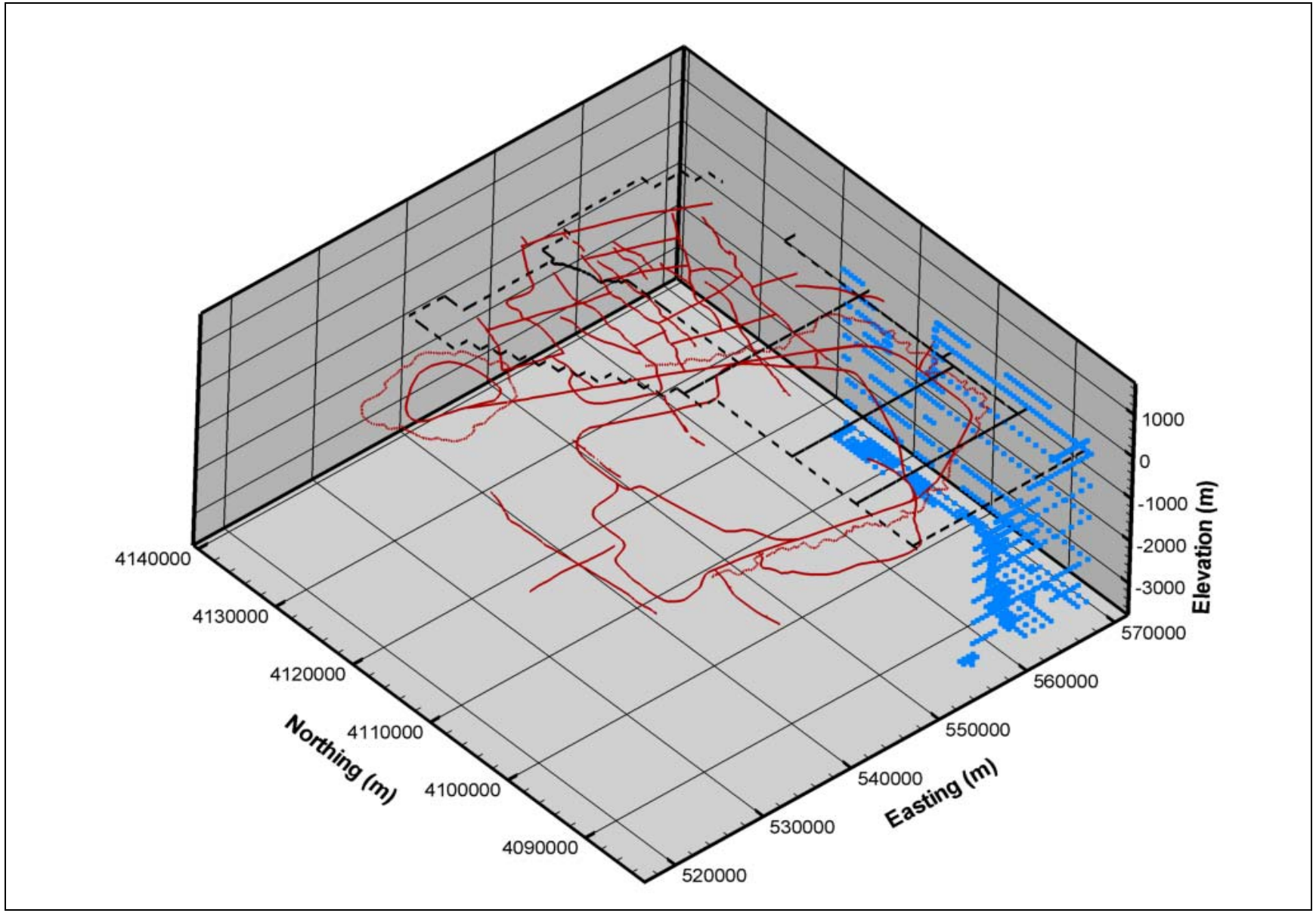

Figure 5-7
Map Showing LCA Nodes from UGTA Regional Model Zone 1

Uncontrolled When Printed

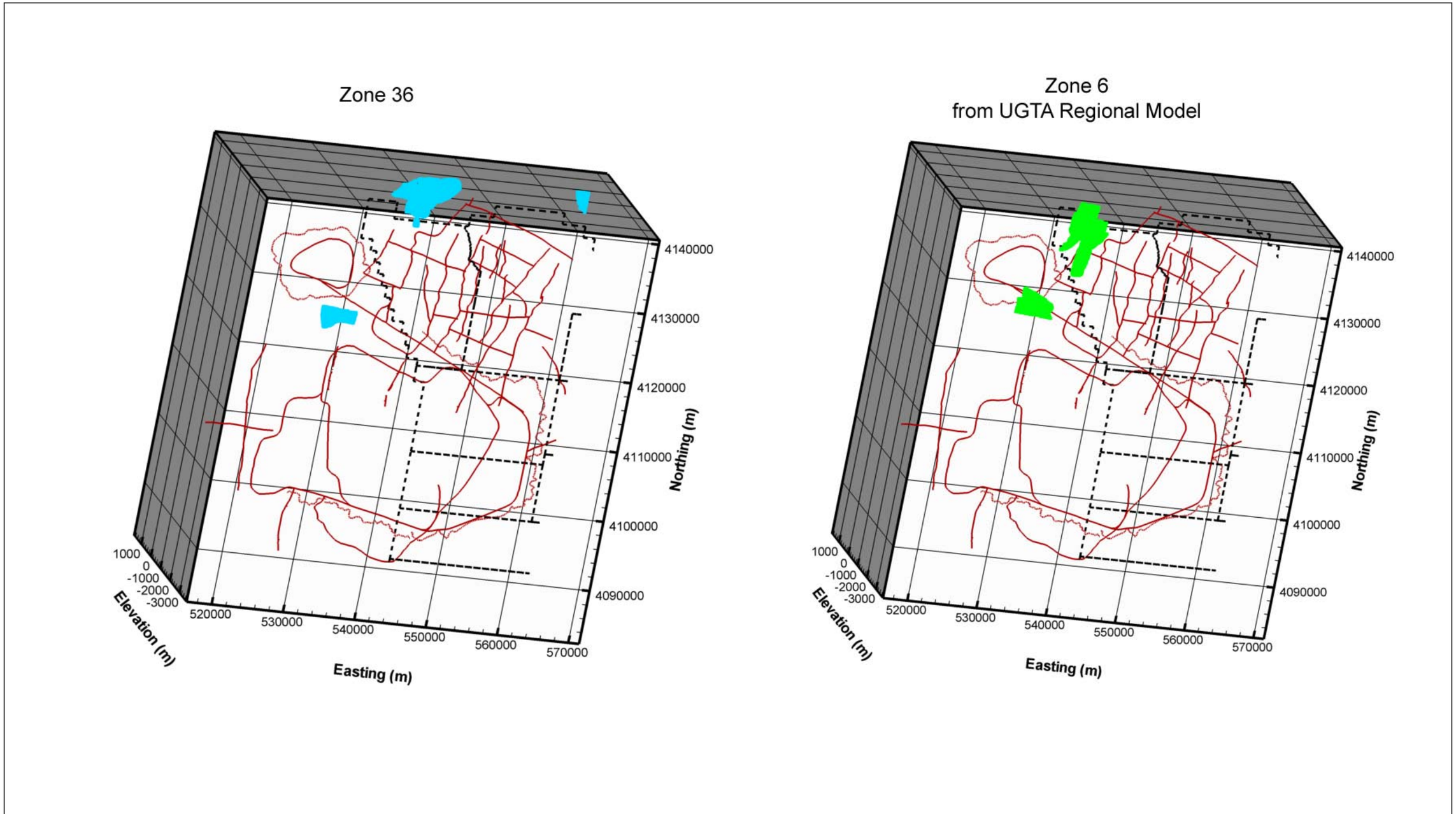

Figure 5-8
Map Showing TMA Nodes Following UGTA Regional Model TMA Subdivision

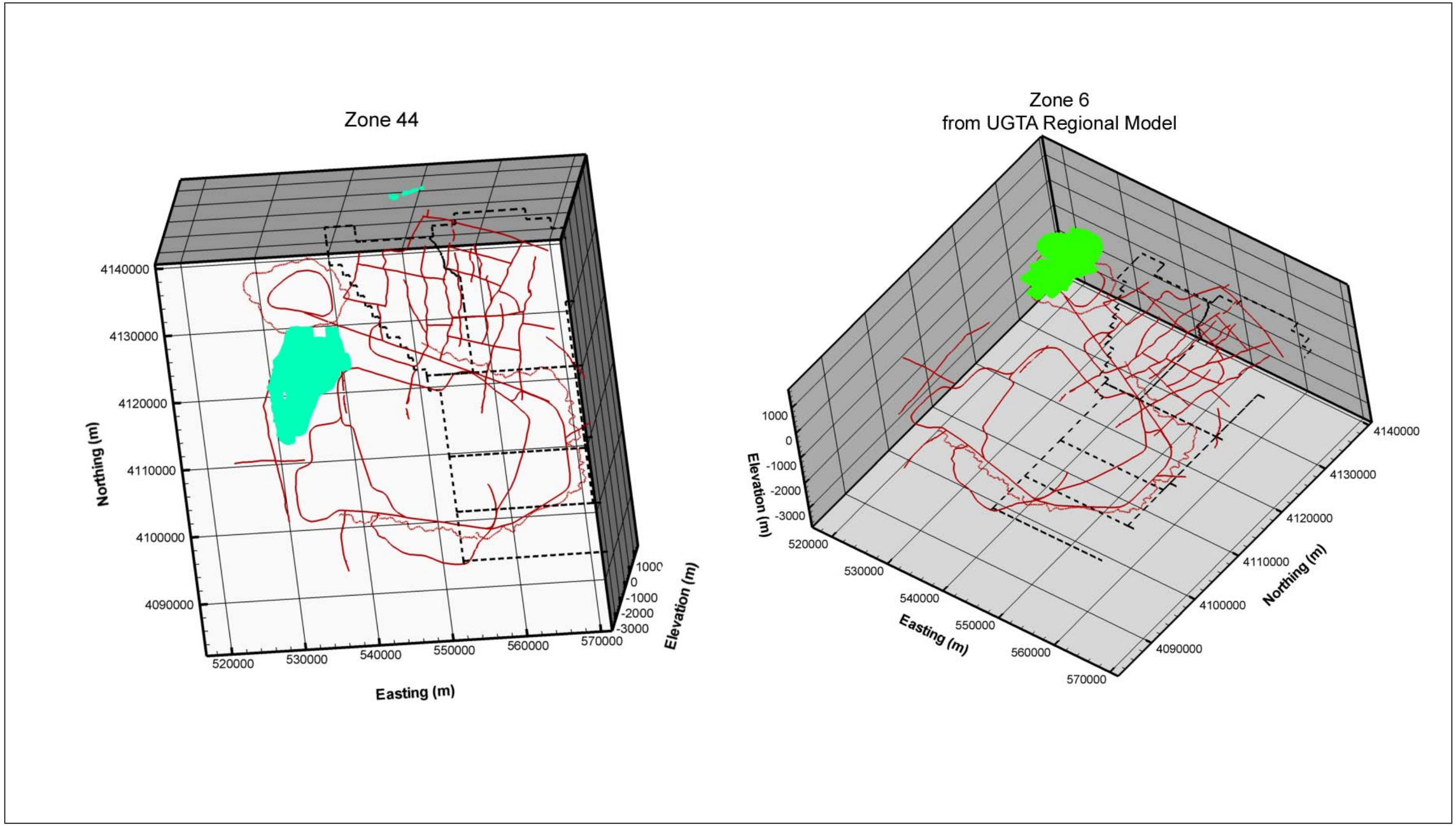

Figure 5-9
Map Showing TCA Subdivision from UGTA Regional Model Zone 52

Uncontrolled When Printed

5.5 Parameter Assignment

Each node in the FEHM mesh has an associated material property index that is used to assign hydraulic properties. Faults are also specified by material zones, and are specified after the HSUs are defined. However, the material properties associated with the HSU nodes remain assigned to the fault nodes pending another property assignment. The approach in parameterizing the faults was to assign a permeability factor that multiplies the existing fault node properties (still derived from an HSU). Thus, the difficulty that could be encountered in directly assigning a fault permeability that is reconciled with each HSU that it crosses is avoided. For instance, if a vertical fault crosses both aquifers and confining units (which most do), and a uniform fault permeability of 10^{-16} m^2 is assigned, the aquifer (with a permeability of 10^{-12} m^2) would see the fault as a barrier, but a confining unit with a permeability of 10^{-16} m^2 would see the fault as neutral. This approach tacitly assumes that a fault acts the same in each HSU that it encounters. Depth decay was computed in the depth-integrated manner described in the UGTA regional model (DOE/NV, 1997). Because FEHM determines its control volumes from node locations (unlike the block-centered code used in the regional model), which also may not necessarily be rectangles or squares, the bounding control volume coordinates were used in the depth-decay calculation. In the case of non-rectangular control volumes, the computed depth decay is approximate because the height of the control volume may not be constant. This was deemed a reasonable approximation in light of the overall uncertainty surrounding the depth-decay process.

5.6 Base Hydrostratigraphic Framework Model Flow Model Calibration

Bechtel Nevada (2002) presents a best estimate, or what will be referred to hereafter as the "base," HFM of Pahute Mesa and the surrounding area, as well as several alternative interpretations. The following sections document the evaluation of four different approaches (two in Section 5.6.2) to assigning model parameters in the base model. The same calibration data and model structure were used in each case; only the approach to assigning parameters was changed. These approaches include:

- No depth decay, no anisotropy
- Selected HSU depth decay
- Selected HSU depth decay and anisotropy
- All HSU depth decay and anisotropy

Uncontrolled When Printed

5.6.1 No-Depth-Decay, No-Anisotropy Case

The Pahute Mesa CAU model discretizes each HSU with multiple nodes in the horizontal and vertical dimensions. It was thought that this level of discretization might not require horizontal-to-vertical anisotropy because the arrangement of the HSUs would naturally produce the stratification of flow, and the approach described in this section was designed to test this hypothesis. In addition, the necessity of permeability depth decay was also tested by using a single permeability for each HSU estimated from characterization data as described in the Pahute Mesa hydrologic data document (SNJV, 2004a).

This case was not as extensively examined as the others described in Section 5.6 for reasons that are explained in the following text. It also was set aside before other changes were made to the model, but this section describes the process and results used in developing the Pahute Mesa CAU flow model.

Figures 5-10 through 5-13 show the observed (or estimated in the case of boundary flows) and unweighted simulated values for the calibration wells, springs, Oasis Valley discharge, and boundary flows, respectively. On Figures 5-10 and 5-11, the line of perfect agreement is shown, and ideally the data would plot exactly onto this line. Figure 5-13 compares the regional and CAU-model boundary flows. The scatter around the line of perfect agreement is generally random in Figure 5-10, although there are some large errors at around 1,450 m and a bias toward undersimulation above 1,300 m. Figure 5-14 shows a histogram of weighted observation well residuals. The bulk of the weighted errors are less than 20 m. The errors are approximately symmetrically distributed around zero, with a single large undersimulated (positive sign) PM-2, and single large oversimulated UE-19b #1 WW.

The Oasis Valley discharge and boundary flow components provide the water-balance constraint on the model. The total estimated Oasis Valley discharge, divided among seven zones numbered 1-6 and 8, is 227 kg/s. The simulated discharge, shown in Figure 5-12, is 128 kg/s. The model captures the northernmost two discharge zones well, but performs poorly for the rest of Oasis Valley. This suggests that the head in the southern part of Oasis Valley needs to rise in order to produce the observed discharge. The boundary flows, estimated from regional model analysis, do not trend the same way on the western edge, although the north, south, and east flows reasonably agree with the regional model.

Uncontrolled When Printed

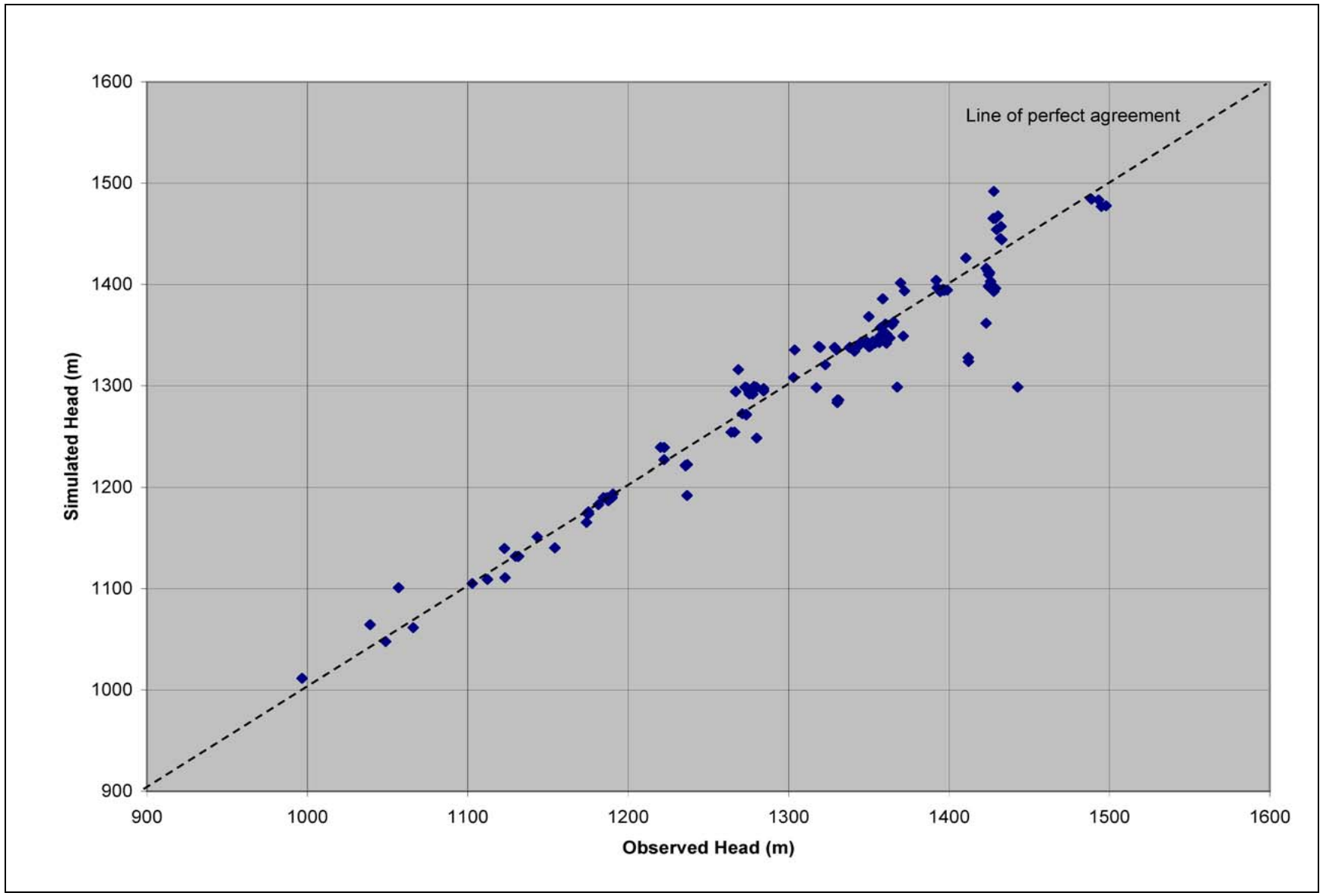

Figure 5-10
Observed Versus Simulated Well Head - Base HFM, No Depth Decay, No Anisotropy

Uncontrolled When Printed

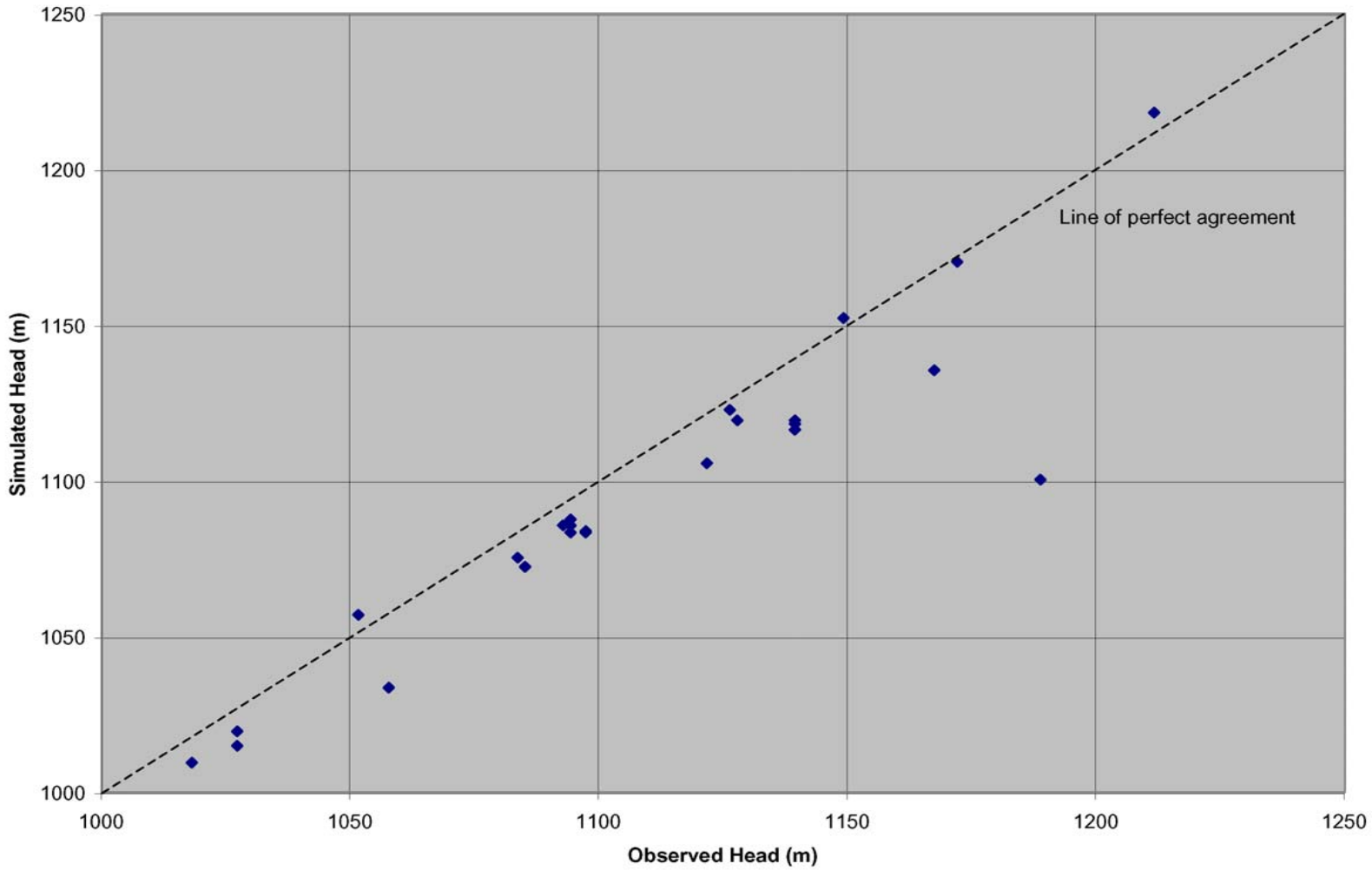

Figure 5-11
Observed Versus Simulated Spring Head - Base HFM, No Depth Decay, No Anisotropy

Uncontrolled When Printed

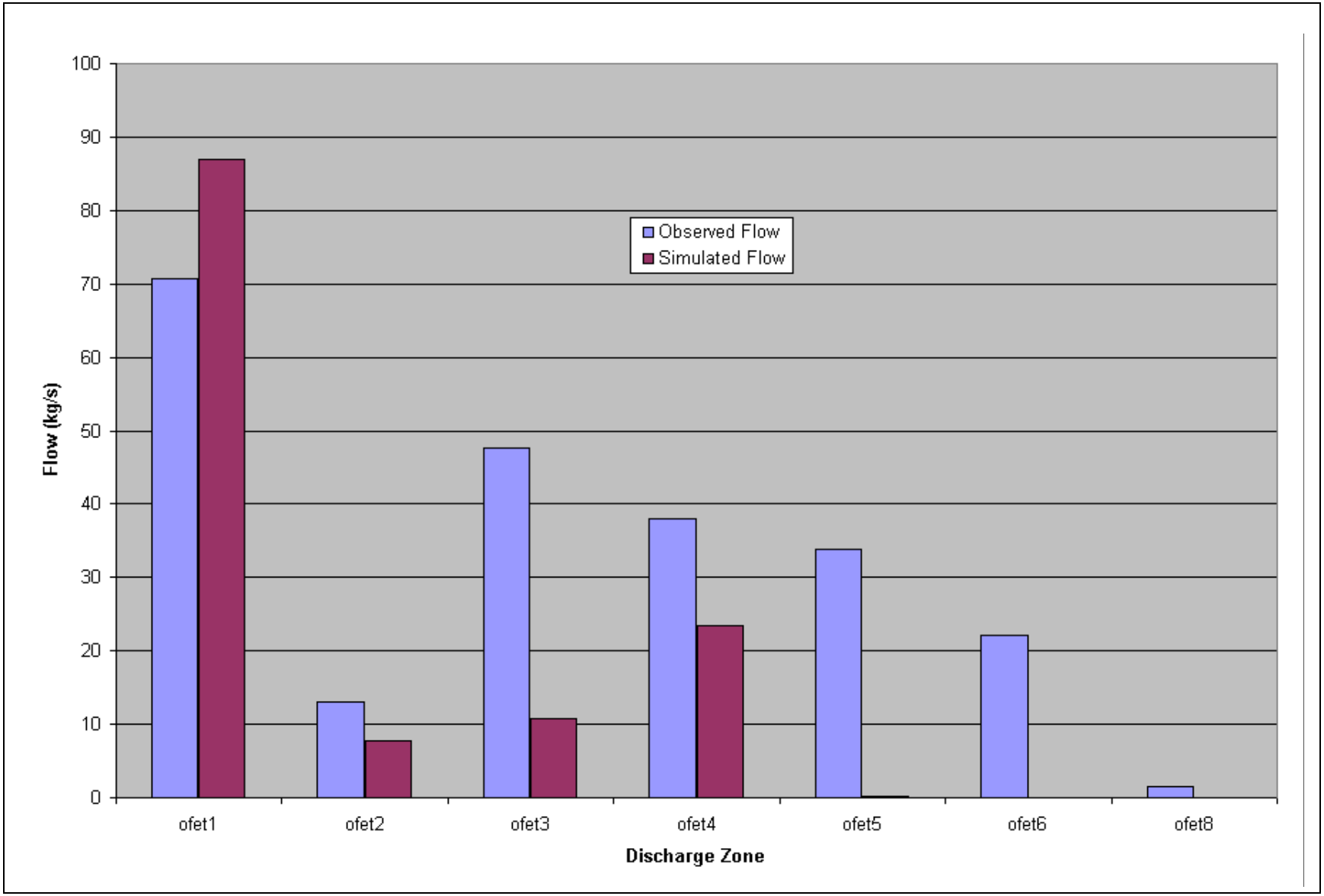

Figure 5-12
Observed Versus Simulated Oasis Valley Discharge - Base HFM, No Depth Decay, No Anisotropy

Uncontrolled When Printed

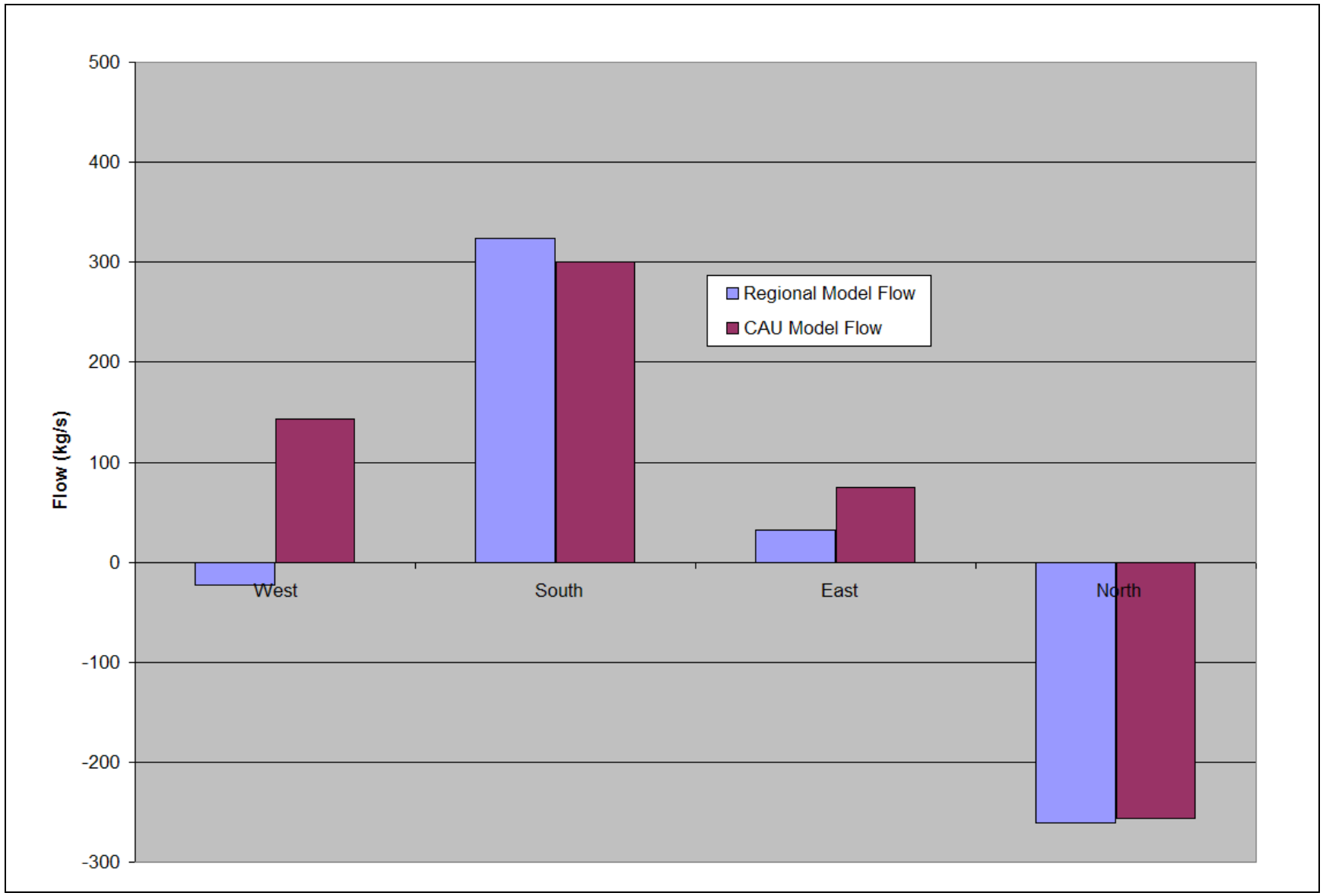

Figure 5-13
Estimated and Simulated Boundary Flows - Base HFM, No Depth Decay, No Anisotropy

Uncontrolled When Printed

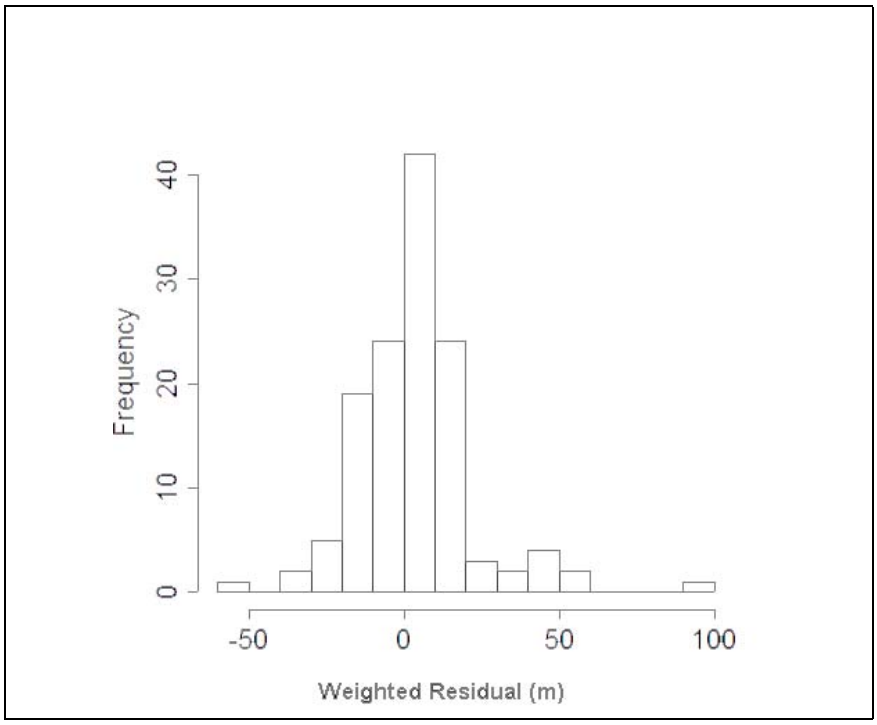

Figure 5-14
Histogram of Weighted Head Residuals - Base HFM, No Depth Decay, No Anisotropy

The weighted head and spring errors (or residuals), defined as observed minus simulated heads, are shown on Figure 5-15, color-coded by value and sign. Only locations with weights greater than 0.01 (m^{-1}) are shown in order not to bias the display (low weight observations will give an erroneously favorable impression because almost any error times the low weight will be low). There is a pattern of undersimulated wells west of the Purse Fault and in Oasis Valley. The low simulated water levels in Oasis Valley result in the undersimulation of observed discharge in the valley. There is an area of high bias in northeastern Area 19.

The quantitative measures of the model calibration are given by summary statistics shown in Table 5-6. There is a noticeable low bias in the spring heads, resulting in the undersimulation of Oasis Valley discharge. The standard deviation is wider than the other cases described in Section 5.6, reflecting the overall poorer fit of this case. Table 5-7 shows the contribution to model goodness of fit from each data type.

Uncontrolled When Printed

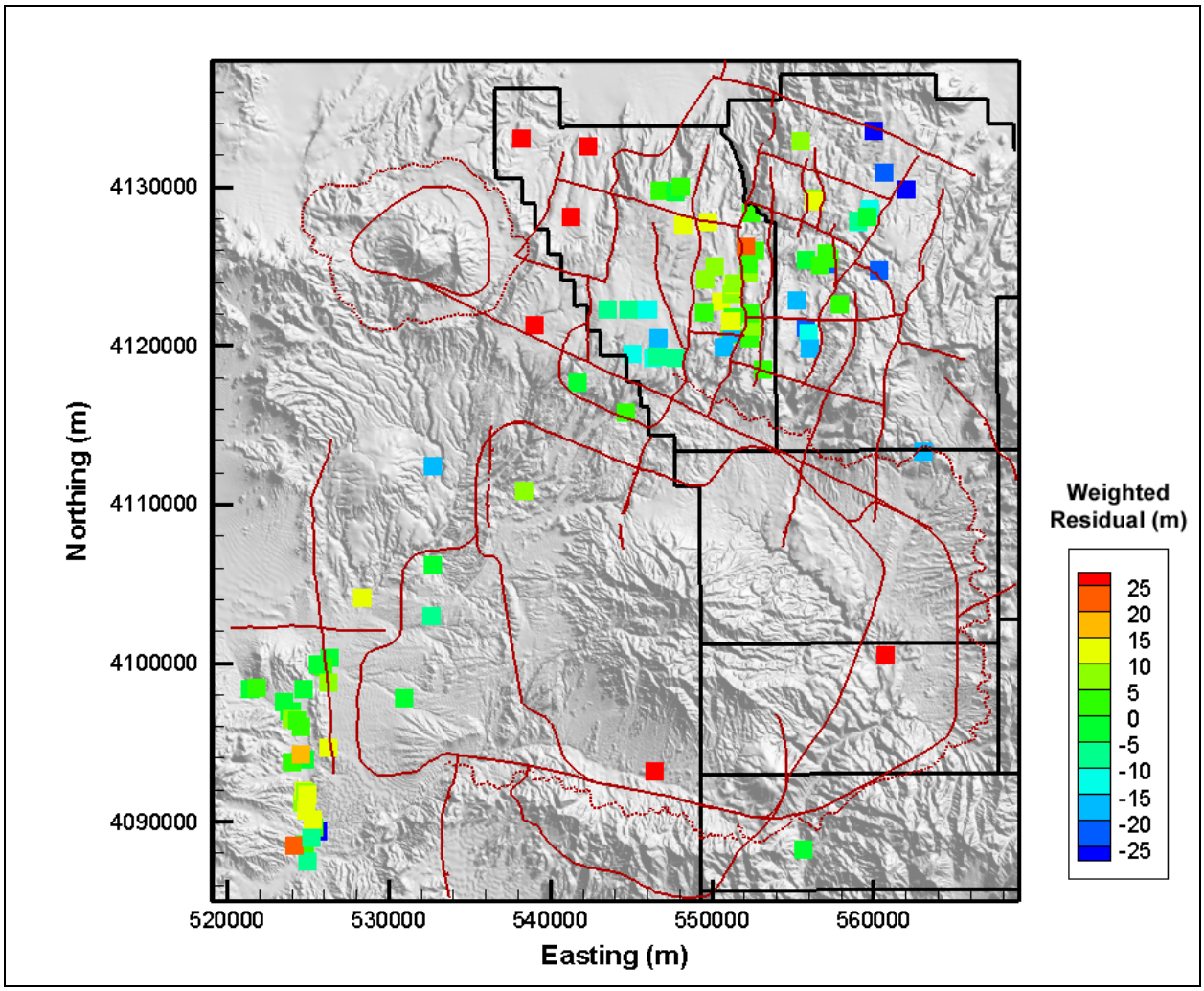

Figure 5-15
Post Plot of Weighted Well and Spring Head Residuals - Base HFM, No Depth Decay, No Anisotropy

Figure 5-16 shows the simulated water table for this model case. In the western part of Area 20, the influence of the Purse Fault is absent except along the northern part of the fault. Head in southern Area 20 is very similar to that on the other side of the Purse Fault, which is the incorrect representation and results in the low heads at PM-2, PM-3, UE-20j WW, U-20m, and UE-20p (the area of low bias in Figure 5-15). The misfit at PM-2 is particularly large and, as described in Section 5.3, is directly caused by regional model misfit just north of the CAU-model boundary. This result led to the revision of boundary head (also described in Section 5.3) on the northern CAU-model edge. A mound is not simulated under Timber Mountain; this interpretive feature was added after this case was no longer being investigated. If implemented, it may raise head and discharge in Oasis

Uncontrolled When Printed

Table 5-6
Calibration Summary Statistics - Base HFM, No Depth Decay, No Anisotropy

Calibration Data	Number of Data	Mean Weighted Error (m or kg/s)[a]	Maximum Weighted Residual	Minimum Weighted Residual	Error Standard Deviation (m or kg/s)
Well Head	152	1.6	96 (PM-2)	-52 (UE-19b #1 WW)	16
Spring Head	28	5.8	24 (Spring id 159)	-6.5 (Spring id 180)	9.2
Oasis Valley Discharge	7	28	74 (Zone 3)	-33 (Zone 1)	45
Boundary Flow	4	-15	50 (North)	-91 (West)	53

[a]Positive is undersimulation of target data, negative is oversimulation.

Table 5-7
Contribution to Model Goodness of Fit by Data Type for Base HFM Selected HSU Depth Decay and Anisotropy

Data Type	Value (-)	% of Total
Well Head	42,531	61
Spring Head	2,387	3
Oasis Valley Discharge	14,029	20
Boundary Flow	11,156	16
Total	70,103	100

Valley by diverting water to the west. Oasis Valley discharge is apparent, but not as pronounced as in other cases because it only is about half of the observed flow (the other cases capture the flow much better).

Particle tracking (Figure 5-17) from each of the NTS wells used in model calibration shows generally the same noted flow paths as shown by SNJV (2004a) and as shown in Appendix A of the Pahute Mesa hydrologic data document (SNJV, 2004a). However, very few of the particles discharge in Oasis Valley, and as previously noted, this model greatly undersimulates Oasis Valley discharge. The broad flow path through the Timber Mountain area is not known to exist. However, data do not exist to rule it out. The flow paths shown are consistent with the boundary conditions applied to the model. However, as a matter of first principles, an area of higher elevation and commensurate recharge should have higher hydraulic head underlying it. Thus, the flat potentiometric surface and associated flow paths through Timber Mountain shown in Figure 5-17 are not thought to be realistic. In southern Area 20, the flow paths look reasonable, but the heads are not correct along the Purse Fault. Finally,

Uncontrolled When Printed

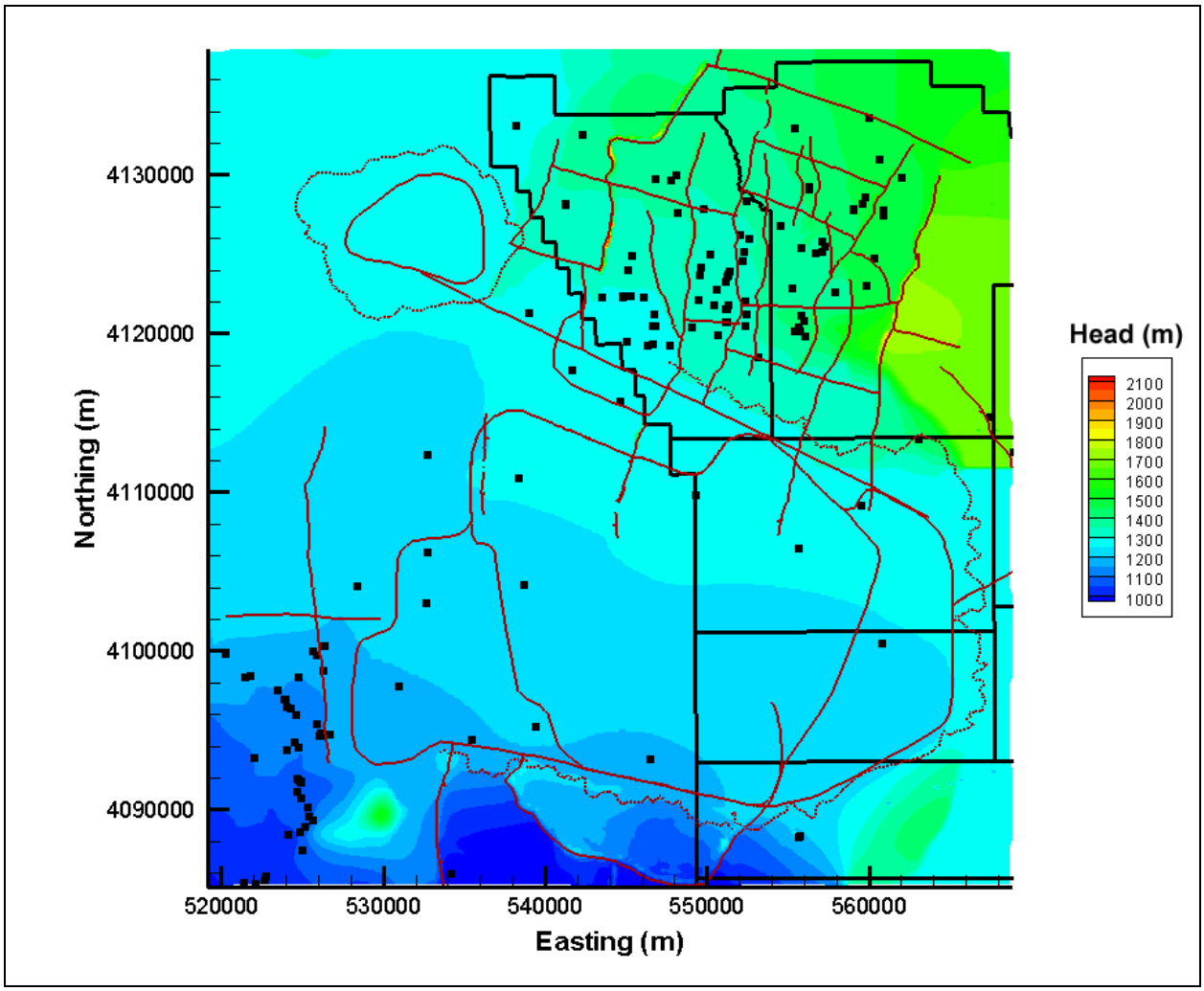

Figure 5-16
Simulated Water Table - Base HFM, No Depth Decay, No Anisotropy

a large number of flow paths exit the model deep (elevation of –1,000 m or more) in the LCA underlying Oasis Valley, which is unsupported by the analysis of SNJV (2004a). This was one of the key observations that lead to this parameterization of the base HFM not being investigated further.

This parameterization approach, no depth decay and no anisotropy, produced flow paths that were judged unrealistically deep and represented Oasis Valley discharge poorly. It also required systematically low permeabilities relative to the expected values and ranges as described in the Pahute Mesa hydrologic data document (SNJV, 2004a). Figure 5-18 shows the estimated versus calibrated permeabilities; the estimated standard deviation is published in SNJV (2004a), but for practical purposes can be considered to be one order of magnitude. Nearly all the values are multiple

Uncontrolled When Printed

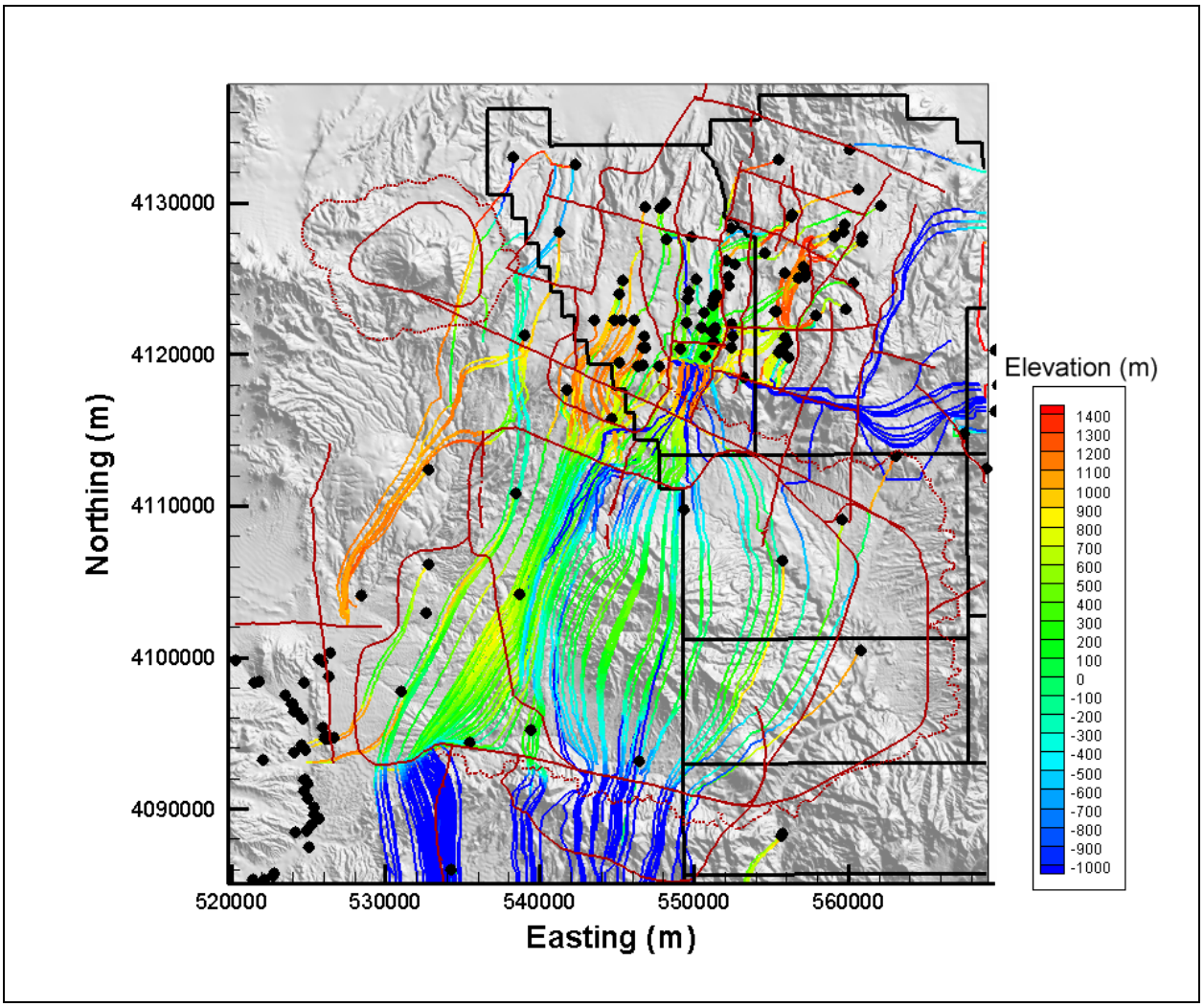

Figure 5-17
Particle Tracks - Base HFM, No Depth Decay, No Anisotropy

orders of magnitude lower than the estimated. However, not all these low values are significant. For instance, a single hydraulic test was used to assign permeability for all the ICUs. Because they are brittle, the intrusive units tend to be fractured at shallow depths, and it is probably sampling bias that gives the relatively high single value. Concepts of caldera formation of the ICUs is poorly understood, and their presence is inferred from first principles and gravity measurements (BN, 2002). Bechtel Nevada (2002) conceptualizes the ICUs as igneous intrusive masses, postulates that they behave as confining units, and indicates that at depth fractures are probably filled with secondary minerals from circulation of hot, mineral-rich waters associated with deep magma bodies. Thus, the low permeabilities of the ICUs are less important. However, model performance could only be

Uncontrolled When Printed

enhanced with systematically lower values of permeability throughout the model. Anisotropy could be introduced to constrain vertical flow, but in units where fracture flow predominates, the concept of horizontal-to-vertical anisotropy was judged to be inappropriate because, in general, overburden loading will tend to close low-angle fractures. Anisotropy could be applied to the more bedded units, but given the poor performance of this case, excessively low values were likely to be required and were not investigated.

Uncontrolled When Printed

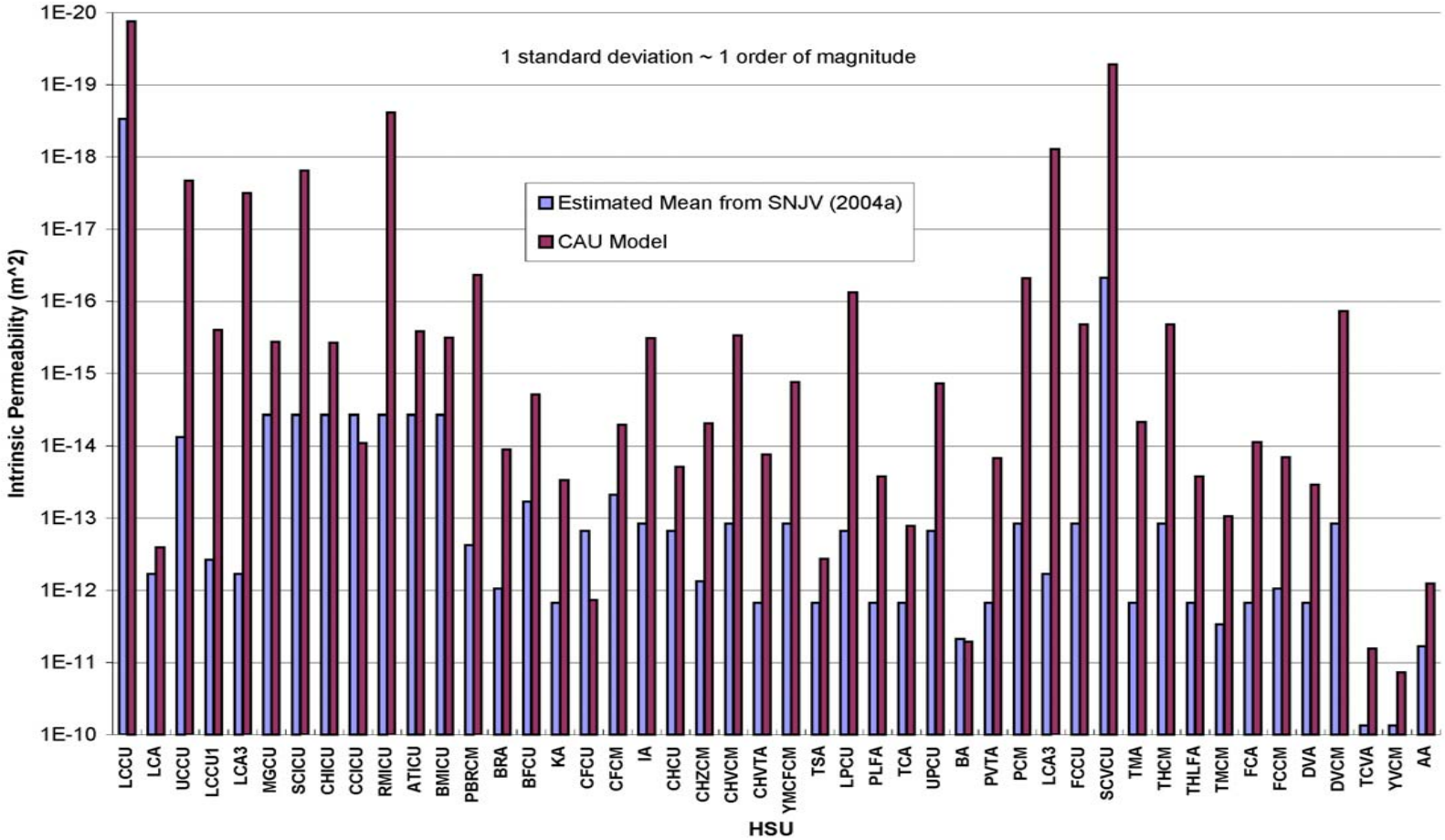

Figure 5-18
Hydrostratigraphic Unit Parameters - No Depth Decay, No Anisotropy
See Table 2-6 for HSU descriptions.

Uncontrolled When Printed

5.6.2 Selected HSU Depth Decay and Anisotropy (SDA)

The SDA parameterization approach began by assessing the effect of permeability depth decay only, and its effects were found to be quite pronounced in terms of not requiring consistently low permeabilities as in the case described in Section 5.6.1. The depth-decay-only case was used to establish the insight into the need for permeability depth decay and was not extensively investigated.

In the UGTA regional model (DOE/NV, 1997), depth decay and horizontal-to-vertical anisotropy were assigned to every HSU. An alternate parameterization of the base HFM was designed to test whether depth decay applied to regionally contiguous units existing at a wide variety of depths along with anisotropy in selected units could give a reasonable result. Table 5-8 shows the units selected for depth decay and anisotropy. The rationale for selectively applying depth decay is that units that are contiguous over the CAU and that exist over a great range of depths (such as the LCA and PBRCM) would have large variation in permeability, which is conceptually best addressed via depth decay rather than, for instance, subdividing HSUs by burial depth and assigning individual permeabilities based on depth. The depth-decay coefficients are the mean values presented in the UGTA regional model report (DOE/NV, 1997). The vertical-to-horizontal anisotropy value is derived from the YMP site-scale saturated zone model (DOE/ORD, 2004).

Horizontal-to-vertical anisotropy, typically associated with granular media, may not be a meaningful concept in fractured rock. Pawloski et al. (2001) did not use horizontal-to-vertical anisotropy in the analysis of the CHESHIRE HST. They showed that it was reasonable to have permeability along the main flow direction be the same through the vertical extent of fractured HSUs. The composite units in the CAU HFM model are, by definition, an amalgamation of HGUs that could not be extensively mapped. Thus, internally a layer-cake arrangement of massive fractured units with bedded tuffs, for example, would tend to impart horizontal-to-vertical anisotropy over the scale of a CAU-model element. If the geologic description were detailed enough, and if the computational mesh could accommodate such detail, such anisotropy would result naturally. However, as described in Section 5.6.1 it appears that the HFM model and FEHM mesh are not fine enough for this to occur.

Figures 5-19 through 5-22 show the observed (or otherwise estimated) and unweighted simulated values for wells, springs, Oasis Valley discharge, and boundary flows, respectively. On Figures 5-19 and 5-20, the line of perfect agreement is shown, and ideally the data would plot exactly onto this

Uncontrolled When Printed

Table 5-8
Hydrostratigraphic Units with Depth Decay and Anisotropy

HSU	Depth Decay λ	Anisotropy
TMCM	0.0026	0.1
YMCFCM	0.0026	N/A
LCA	0.001	N/A
PBRCM	0.0026	0.1
BRA	0.0026	N/A
PCM	0.0026	N/A
TCVA	0.0026	N/A
TMA	0.0026	N/A
CFCM	N/A	0.1
CHZCM, CHVCM, CHVTA	N/A	0.1
FCCM	N/A	0.1
YVCM	N/A	0.1
AA	N/A	0.1

See Table 2-6 for HSU descriptions.

line. However, in practice, there is always some model misfit. The scatter around the line of perfect agreement is generally random in Figure 5-19, until an observed head of 1,450 m is exceeded. At the very highest-observed observation well water levels, the model has a tendency towards undersimulation. The largest error is associated with the ER-19-1 deep completion. The remaining errors above 1,450 m are all in far eastern Area 19, where data become very sparse and uncertainty increases. Figure 5-23 shows a histogram of weighted observation well residuals. The bulk of the weighted errors (95 percent) are less than ±10 m. The errors are not symmetrically distributed around zero, with larger oversimulated (negative sign) wells. Total number of errors above +10 m and below –10 m appear to be about the same.

Uncontrolled When Printed

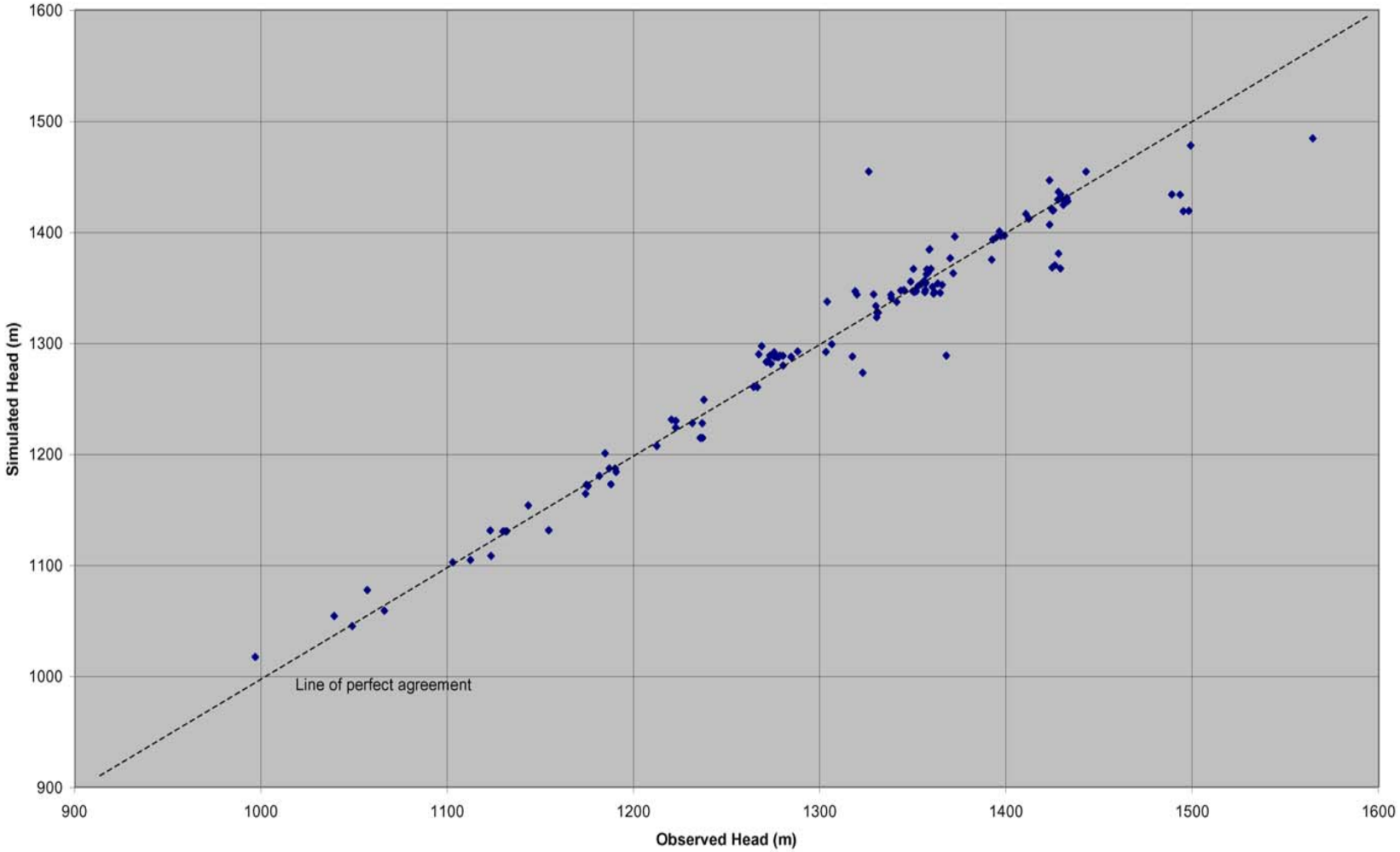

Figure 5-19
Observed Versus Simulated Well Head for BN-MME-SDA

Uncontrolled When Printed

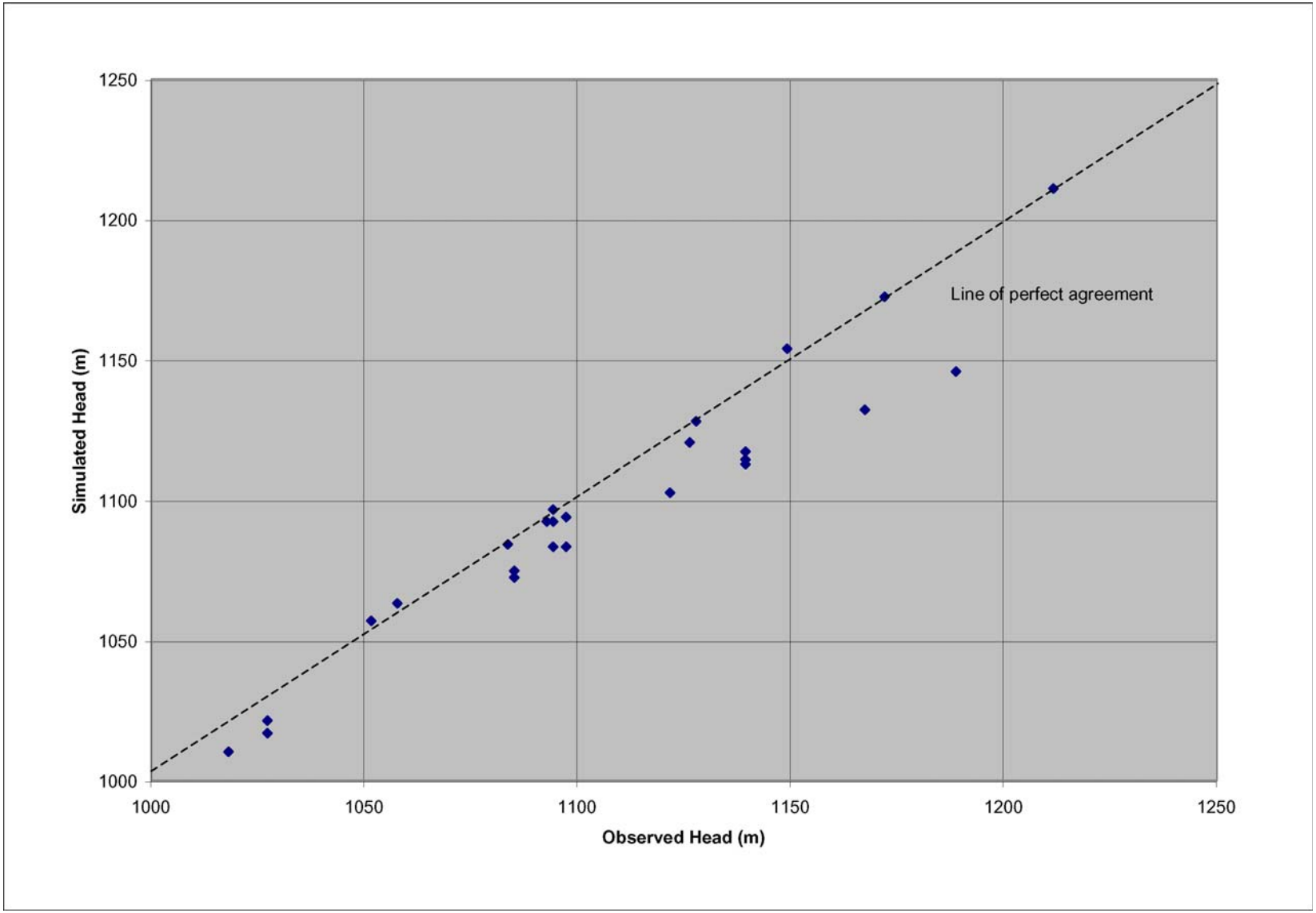

Figure 5-20
Observed Versus Simulated Spring Head for BN-MME-SDA

Uncontrolled When Printed

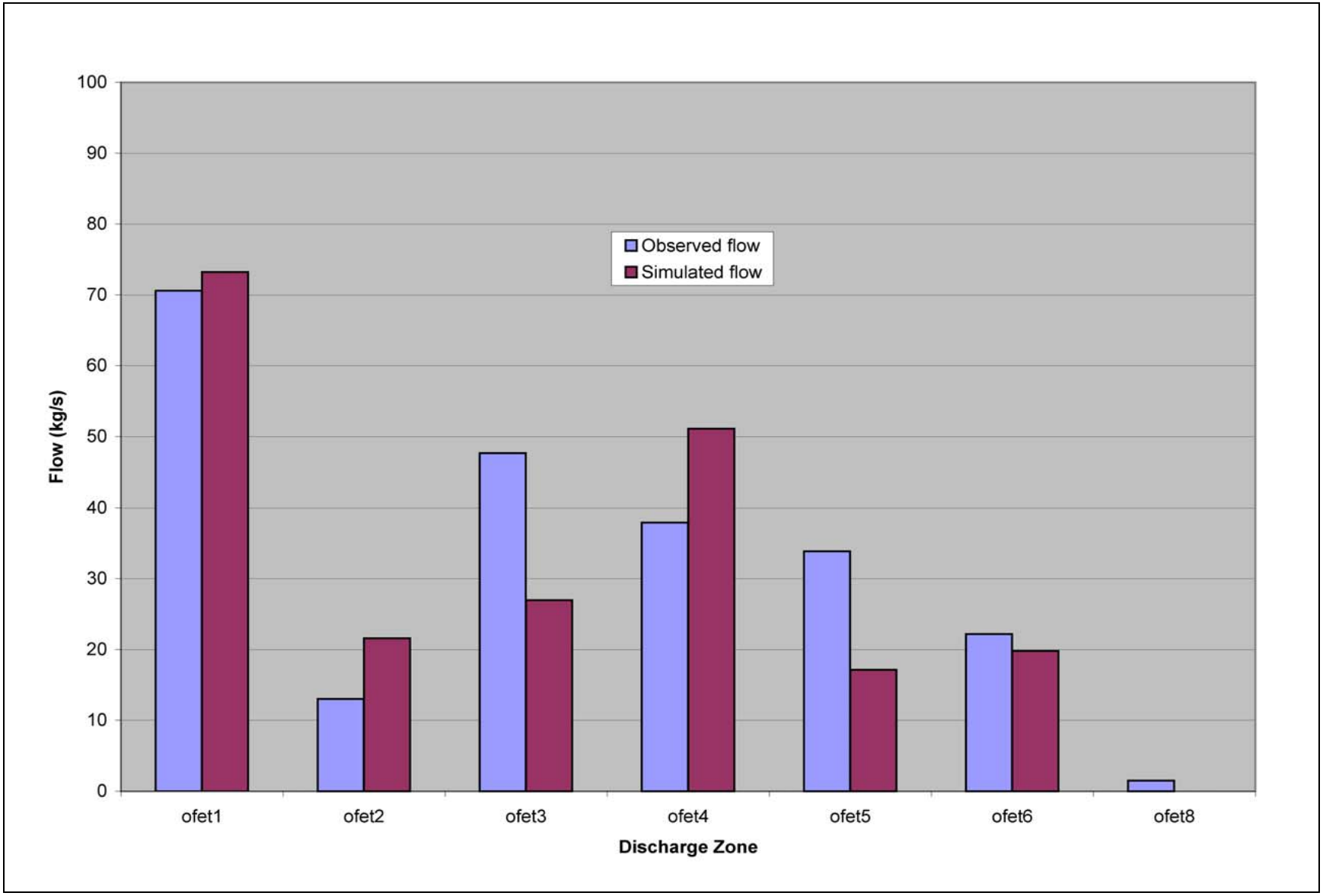

Figure 5-21
Observed Versus Simulated Oasis Valley Discharge for BN-MME-SDA

Uncontrolled When Printed

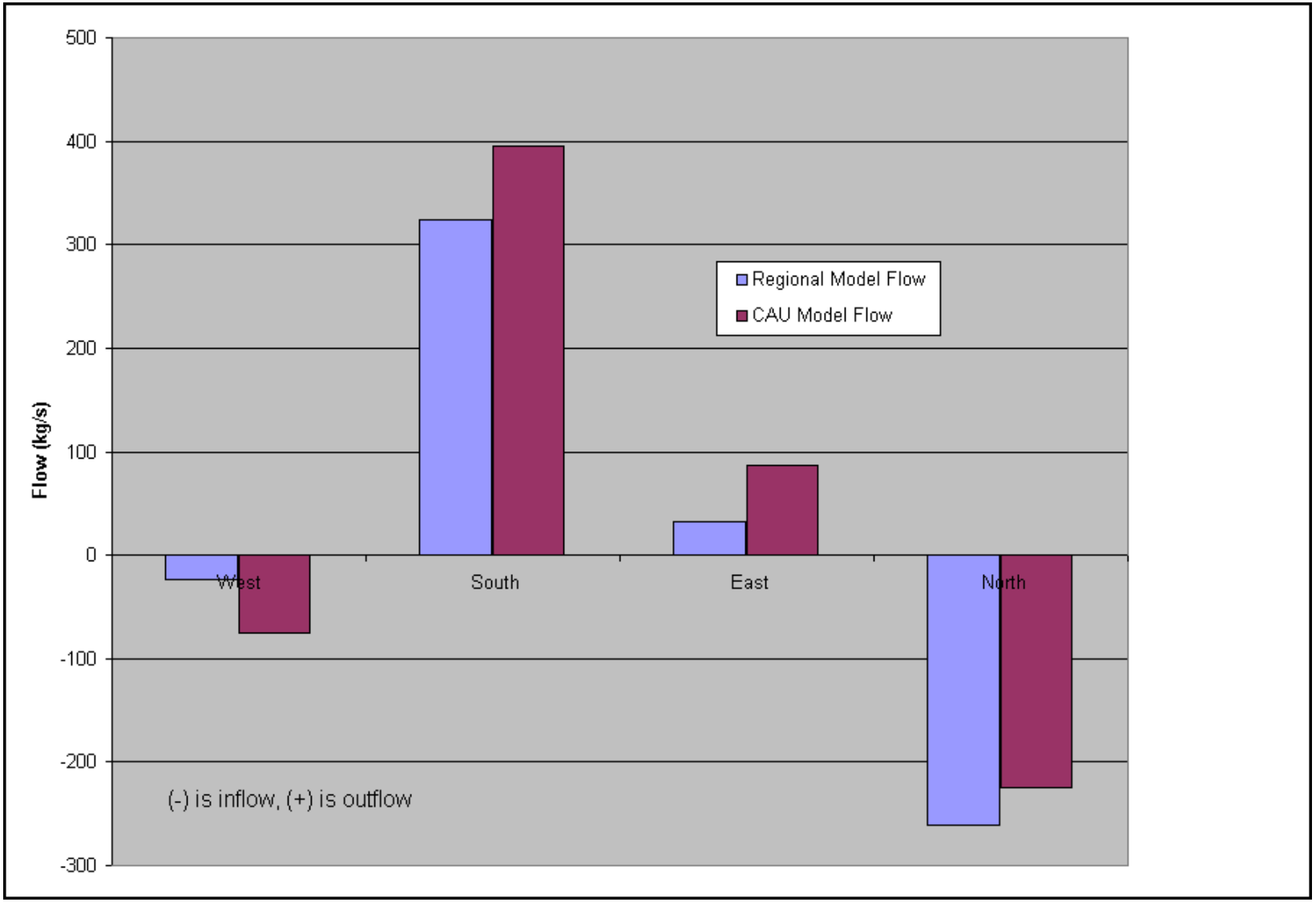

Figure 5-22
Estimated and Simulated Boundary Flow for BN-MME-SDA

Uncontrolled When Printed

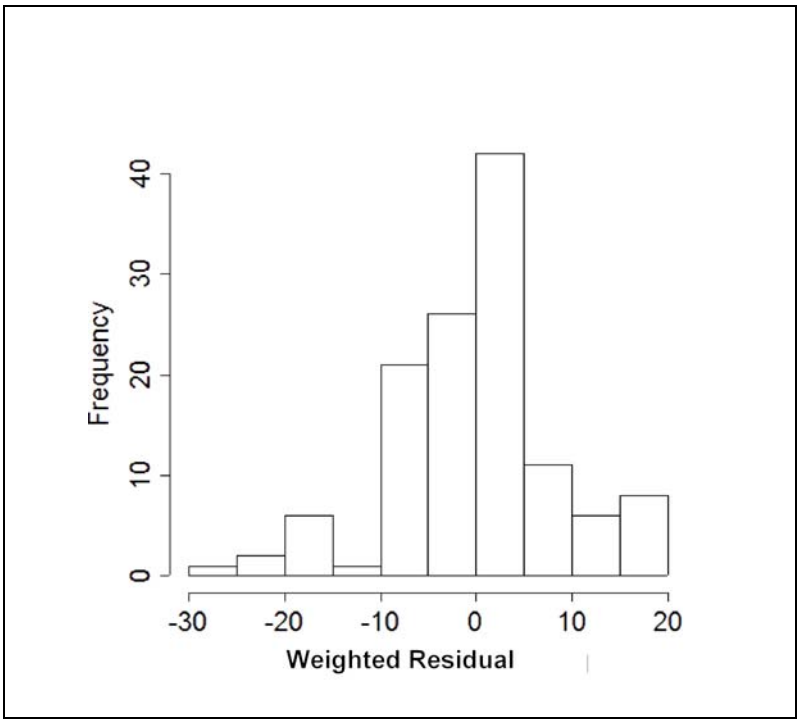

Figure 5-23
Histogram of Weighted Head Residuals for BN-MME-SDA

The weighted head and spring errors are shown on Figure 5-24, color coded by value and sign. The two lowest, or undersimulated, wells were ER-OV-06a and ER-OV-01. The single highest well was UE-20a #1 in northern Area 19. In general, the errors are randomly distributed, although there is a slight low bias in northern Area 20 at easting and northing of about 547,500 and 4,130,000 m, which includes wells U-20i, UE-20e #1, U-20e, and U-20ar #1.

The two springs with the largest errors are Goss Spring, which has an uncertain location, and Oleo Road Spring in an area of very high topographic gradient that the model is unlikely to represent in sufficient detail. Goss Spring was incorrectly located in the Pahute Mesa hydrologic data document (SNJV, 2004a), and locations were re-estimated based on USGS 1:24,000 maps. These two springs were assigned low weights because of their questionable representativeness. However, springs at similar and higher elevations were matched well, and this misfit appears to be a local issue.

The Oasis Valley discharge and UGTA regional model (DOE/NV, 1997) boundary flows provide the water-balance constraint on the model. The total estimated Oasis Valley discharge is 227 kg/s. The simulated discharge, shown in Figure 5-21, is 209 kg/s. The total error is within one standard

Uncontrolled When Printed

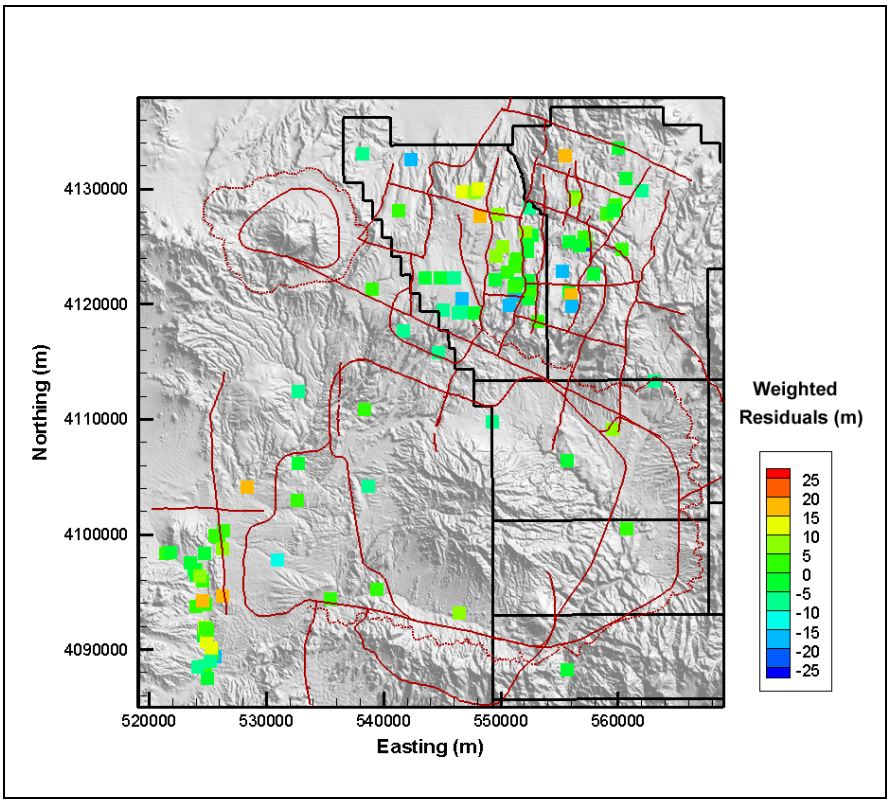

Figure 5-24
Post Plot of Weighted Well and Spring Head Residuals for BN-MME-SDA

deviation (30 kg/s) as reported by Laczniak et al. (2001). The model trends the same as the data with some scatter, showing that the general representation of Oasis Valley is correct. The northernmost (and closest to the NTS) zone is matched well. The boundary flows (Figure 5-22), estimated from regional model analysis, all trend the correct way (e.g., have the proper sign), with the largest relative misfit on the western edge.

The quantitative measures of the model calibration are given by summary statistics shown in Table 5-9. These statistics alone are not used to judge model calibration; they are used in conjunction with the graphical approaches shown previously. There is a slight dry bias in the spring heads, with a slight overprediction bias for the flows. The total model objective function was 16,651. Table 5-10 shows the contribution of each data type to the total model goodness of fit. The strongest contributors are observation well heads and Oasis Valley flow, which are also the two key pieces of calibration data.

Uncontrolled When Printed

Table 5-9
Calibration Summary Statistics for BN-MME-SDA

Calibration Data	Number of Data	Mean Weighted Error (m or kg/s)[a]	Maximum Weighted Residuals	Minimum Weighted Residual	Error Standard Deviation (m or kg/s)
Well Head	152	-0.46	18 (ER-OV-06a)	-27 (UE-20n #1)	7.4
Spring Head	28	2.7	19 (Torrance Spring)	-5.5 (Spring id 159)	6.7
Oasis Valley Discharge	7	4.8	41 (Zone 3)	-26 (Zone 4)	23
Boundary Flow	4	-13	26 (West)	-35 (South)	27

[a]Positive is undersimulation of target data, negative is oversimulation.

Table 5-10
Contribution to Model Goodness of Fit by Data Type for BN-MME-SDA

Data Type	Value (-)	% of Total
Well Head	8,487	51
Spring Head	1,283	8
Oasis Valley Discharge	3,883	23
Boundary Flow	2,997	18
Total	16,651	100

Figure 5-25 shows the simulated water table for this model case. In the western part of Area 20, the influence of the Purse Fault (Figure 4-7) is evident by nearly 100 m offset in water levels across it, with more subdued effects also present at West Boxcar Fault. Water flows from Areas 19 and 20 towards the southwest and Oasis Valley. A mound is simulated under Timber Mountain. It is unknown whether such a feature exists, but from first principles, a higher elevation area where recharge occurs should have a higher groundwater potential. This assumption tends to focus flow between the northern part of the Timber Mountain Caldera and the southern Silent Canyon Caldera. Ubiquitous discharge in Oasis Valley, including flow from Sarcobatus Flat to the west, is also evident by the simulated low trough-shaped potentiometric surface. Finally, flow occurs out across the southern boundary towards Yucca Mountain and Crater Flat.

Uncontrolled When Printed

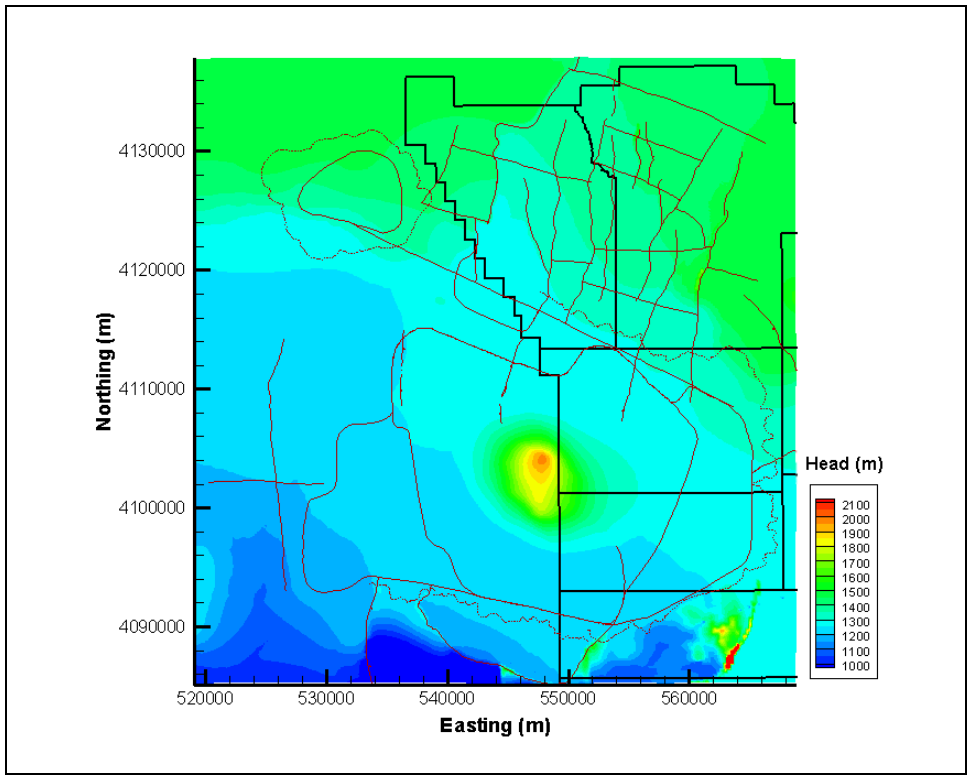

Figure 5-25
Simulated Water Table for BN-MME-SDA

Particle tracking from each of the NTS calibration wells was run until all particles discharged from the model or ceased to move (Figure 5-26). Because the flow field is steady state, porosity does not change the trajectories, and an arbitrary value of effective porosity can be used. In southern Area 20, where the influence of the Purse Fault on the calibration was pronounced, flow is west-southwest but quickly changes at the end of the Purse Fault to southeasterly and then hugs the western flank of Timber Mountain to the southwest because of the influence of the simulated recharge mound under Timber Mountain. Note that some of the wells shown do not have tracks leaving them; this is because the motion of the particle was so minor that it does not show a legible trace. This occurred at PM-2 and UE-20p in northern Area 20. The particle release points in PM-2 are nearly 1 km bmsl. The flow velocities are apparently simulated as being very low in this area of the model. There is only minor flow from Area 18, southern Area 19, and the Rainier Mesa area south down Fortymile Canyon. Particles that go to the west of Timber Mountain are all in the TMCM, and then move into the FCA in the lower part of Oasis Valley. Flow paths rise in elevation as flow converges into Oasis Valley. Moreover, they also rise near Bare Mountain due to the complex arrangement of rocks caused by the Bare Mountain Fault and the UCCU.

Uncontrolled When Printed

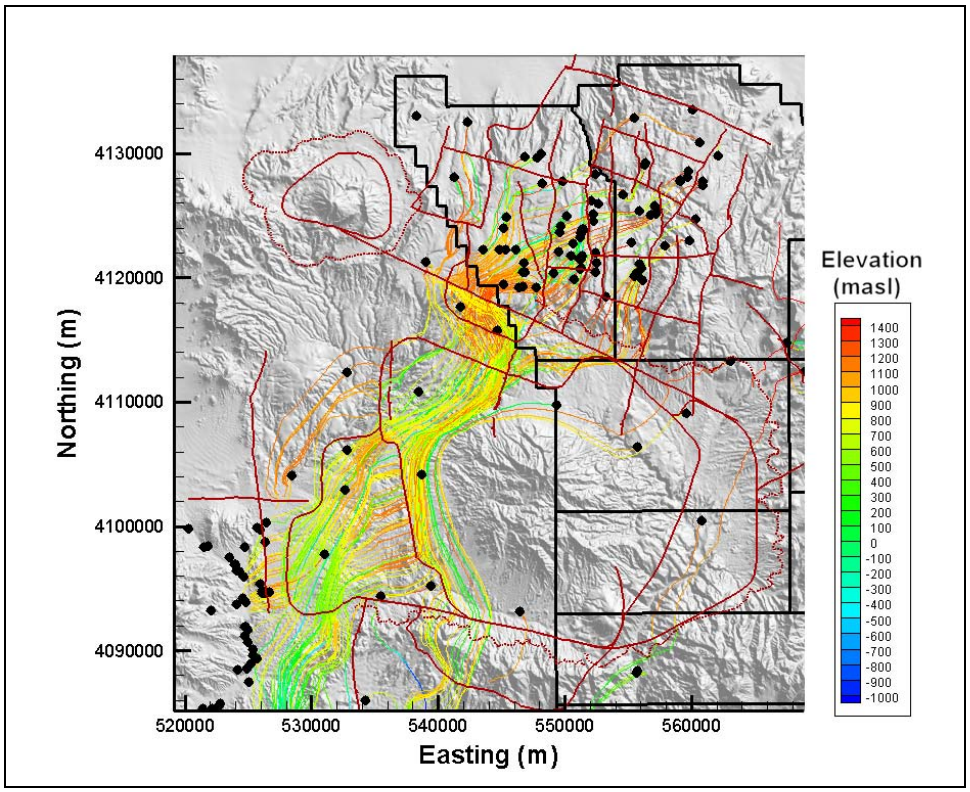

Figure 5-26
Particle Tracks for BN-MME-SDA

The properties used to parameterize this model are shown in Tables 5-11 and 5-12 for HSU and faults, respectively. The HSUs with depth decay are bolded in Table 5-11. The key to the fault locations is presented in Section 4.2.1

Table 5-11
Hydrostratigraphic Unit Parameters for BN-MME-SDA
(Page 1 of 3)

HSU	Log (k or k_0) (m^2)	Notes
LCCU	-18	k
LCA	**-14.20**	**k_0**
UCCU	-16.78	k
LCCU1	-12.43	k
LCA3	**-13.38**	**k_0**
MGCU	-18.38	k
SCICU	-18.38	k
CHICU	-18.38	k
CCICU	-18.38	k
RMICU	-18.38	k

Uncontrolled When Printed

Table 5-11
Hydrostratigraphic Unit Parameters for BN-MME-SDA
(Page 2 of 3)

HSU	Log (k or k_0) (m^2)	Notes
ATICU	-18.38	k
BMICU	-18.38	k
PBRCM	**-11.91**	**k_0**
BRA	**-11.51**	**k_0**
BCU	-13.67	k
KA	-11.78	k
CFCU	-12.60	k
CFCM	-15.07	k
IA	-13.56	k
CHCU	-14.61	k
CHZCM	-13.49	k
CHVCM	-13.39	k
CHVTA	-11.81	k
YMCFCM	**-14.54**	**k_0**
TSA	-10.09	k
LPCU	-13.04	k
PLFA	-11.78	k
TCA	-11.48	k
UPCU	-15.33	k
BA	-11.34	k
PVTA	-12.33	k
PCM	**-10.82**	**k_0**
LCA3a	**-14.03**	**k_0**
FCCU	-12.98	k
SCVCU	-16.28	k
TMA	**-14.55**	**k_0**
THCM	-12.88	k
THLFA	-11.78	k
TMCM	**-11.04**	**k_0**
FCA	-11.50	k
FCCM	-13.04	k
DVA	-12.71	k
DVCM	-13.23	k
TCVA	**-10.65**	**k_0**
YVCM	-10.08	k
AA	-13.50	k
LCA Zone 1	**-14.37**	**k_0**
TCVA Zone 6[a]	**-12.52**	**k_0**
TMA Zone 6[b]	**-12.18**	**k_0**

Uncontrolled When Printed

Table 5-11
Hydrostratigraphic Unit Parameters for BN-MME-SDA
(Page 3 of 3)

HSU	Log (k or k_0) (m^2)	Notes
PBRCM Zone 80[c]	**-10.42**	**k_0**
PBRCM Zone 81[c]	**-8.84**	**k_0**
PBRCM Zone 82[c]	**-11.30**	**k_0**
PBRCM Zone 83[c]	**-14**	**k_0**
PBRCM Zone 84[c]	**-11.49**	**k_0**
PBRCM Zone 87[c]	**-10.452**	**k_0**
TMCM-ERM[d]	**-11.26**	**k_0**
TMCM-ATCW[d]	**-10.05**	**k_0**
TMCM-ATCE[d]	**-11.05**	**k_0**
TMCM-THS[d]	**-11.94**	**k_0**
TMCM-OV[d]	**-10.76**	**k_0**
TMCM-TMD[d]	**-12.5**	**k_0**
TMCM-NTMW[d]	**-9.40**	**k_0**
TMCM-NTME[d]	**-10.19**	**k_0**
LPCU West of Purse Fault	-15.95	k
UPCU West of Purse Fault	-14.09	k
BRA West of Purse Fault	**-10.80**	**k_0**

See Table 2-6 for HSU descriptions.

k = Intrinsic permeability
k_0 = Reference permeability

[a]See Figure 5-8 for TCVA subdivisions.
[b]See Figure 5-9 for TMA subdivisions.
[c]See Figure 5-5 for PBRCM subdivisions.
[d]See Figure 5-8 for TMCM subdivisions.

Table 5-12
Fault Permeability Multiplier for BN-MME-SDA
(Page 1 of 2)

Fault ID	Name	Fault Permeability Multiplier
01	Almendro	0.32
02	Bare Mountain	0.1
03	Black Mountain Caldera Structural Margin	1
04	Boxcar	1.13
05	Hogback	1
06	Claim Canyon Caldera Structural Margin	0.1
07	Colson Pond	1
08	East Greeley	3.44
09	East Estuary	0.24
10	East Thirsty Canyon Structural Zone	1.28
11	Handley	1.34

Uncontrolled When Printed

Table 5-12
Fault Permeability Multiplier for BN-MME-SDA
(Page 2 of 2)

Fault ID	Name	Fault Permeability Multiplier
12	Handley South	9.32×10^{-2}
13	Handley North	0.1
14	Moor Hen Meadow Structural Zone	1
15	North Timber Mountain Moat Structural Zone	0.29
16	Ribbon Cliff Structural Zone	1.04
17	Richey	0.92
18	Scrugham Peak	0.26
19	Silent Canyon Northern Structural Zone	1
20	Silent Canyon Structural Zone East	1
21	Silent Canyon Structural Zone West	1
22	YMP inferred/CP Thrust	0.1
23	Silent Canyon/ West Purse	1.00×10^{-6}
24	Purse North	1.00×10^{-6}
25	Split Ridge	0.1
26	Southern Pahute Mesa Structural Zone	2.42
27	Gold Meadows Structural Zone/Big Burn Valley	0.86
28	Rainier Mesa Caldera Structural Margin	1
29	Ammonia Tanks Caldera Structural Margin	1
30	Hot Springs Lineament extension of Rainier Mesa Caldera Structural Margin	1
31	West Almendro	7.25×10^{-2}
32	West Boxcar	4.40×10^{-2}
33	West Greeley	2.31756
34	West Estuary	8.43×10^{-3}
35	Windy Wash/Claim Canyon 1	0.1
36	West Silent Canyon Structural Zone	2.558146
37	Paintbrush Canyon	0.1
38	Fault 23 south of North Timber Mountain Moat Structural Zone	1
39	Fault 16 between faults 23 and 24	1.00×10^{-6}
40	Extension of fault 24 to northern model edge	1.00×10^{-5}
41	Repair of fault 24 where crossed by fault 36	1.00×10^{-6}

Uncontrolled When Printed

5.6.3 All HSU Depth Decay and Anisotropy (ADA)

In the UGTA regional model (DOE/NV, 1997), depth decay and horizontal-to-vertical anisotropy were assigned to every HSU. Parameterization of the base HFM described in this section was designed to examine whether this approach would result in a reasonable calibration. Corrective action unit model calibration began with parameters developed from the regional model analysis performed to evaluate CAU-model boundary flows as presented in the Pahute Mesa hydrologic data document (SNJV, 2004a).

Figures 5-27 through 5-30 show the observed (or otherwise estimated) and unweighted simulated values for the calibration wells, springs, Oasis Valley discharge, and boundary flows, respectively. On Figures 5-27 and 5-28, the line of perfect agreement is shown, and ideally the data would plot exactly onto this line. However, in practice there is always some model misfit. The scatter around the line of perfect agreement is generally random in Figure 5-27, until an observed head of 1,450 m is exceeded. At the very highest-observed observation well water levels, the model has a tendency towards undersimulation. However, the highest water level (and the largest error) shown is associated with the ER-19-1 shallow completion, which may be perched (Fenelon, 2000). The remaining errors above 1,450 m are all in far eastern Area 19, where data became very sparse and uncertainty increases. Figure 5-31 shows a histogram of weighted observation well errors. There is a strong central tendency, with a few undersimulated wells (positive values) with errors greater than 20 m (WW-8 and ER-EC-7). The behavior of this parameterization with respect to WW-8 is investigated further in Section 6.2.

Uncontrolled When Printed

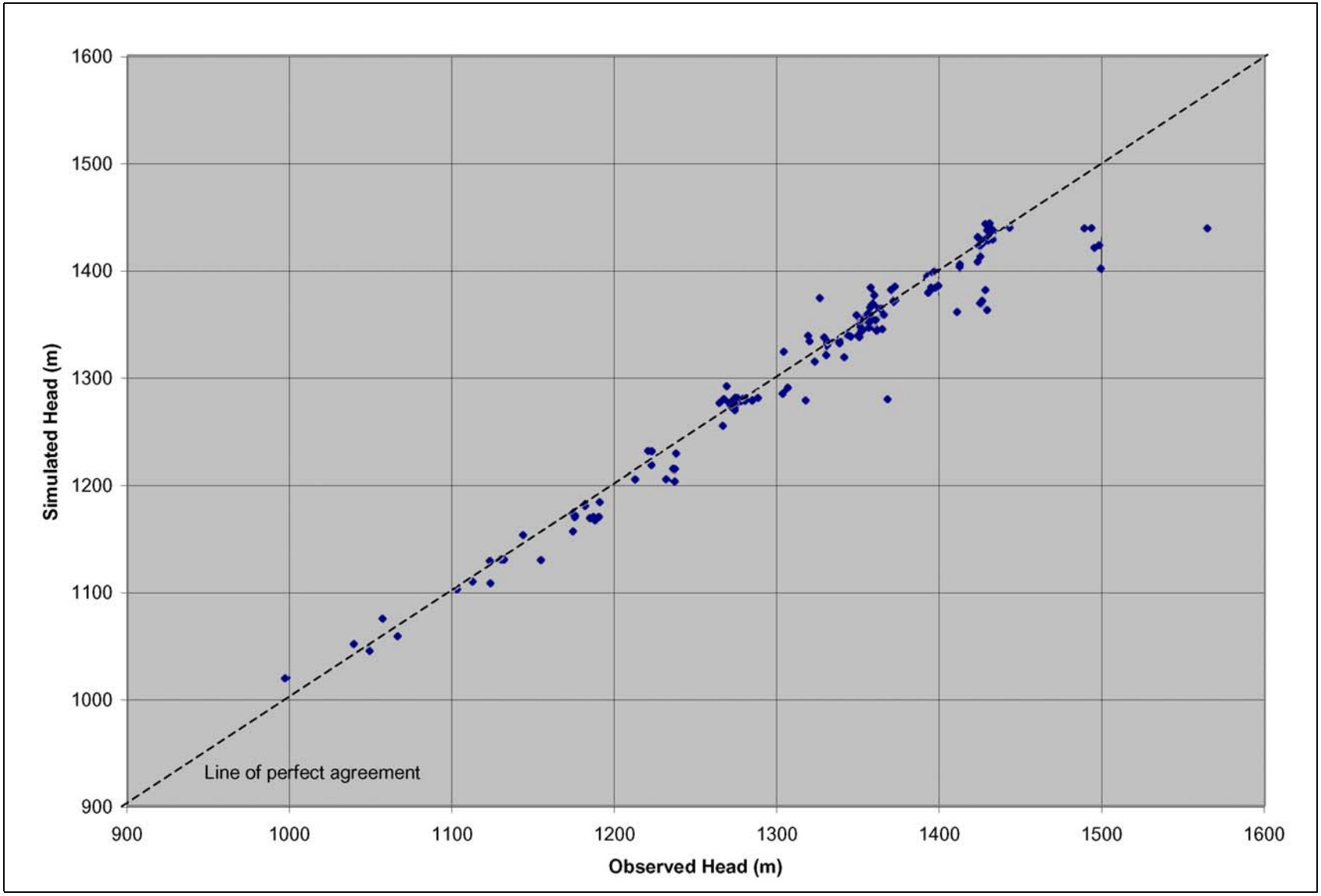

Figure 5-27
Observed Versus Simulated Well Head for BN-MME-ADA

Uncontrolled When Printed

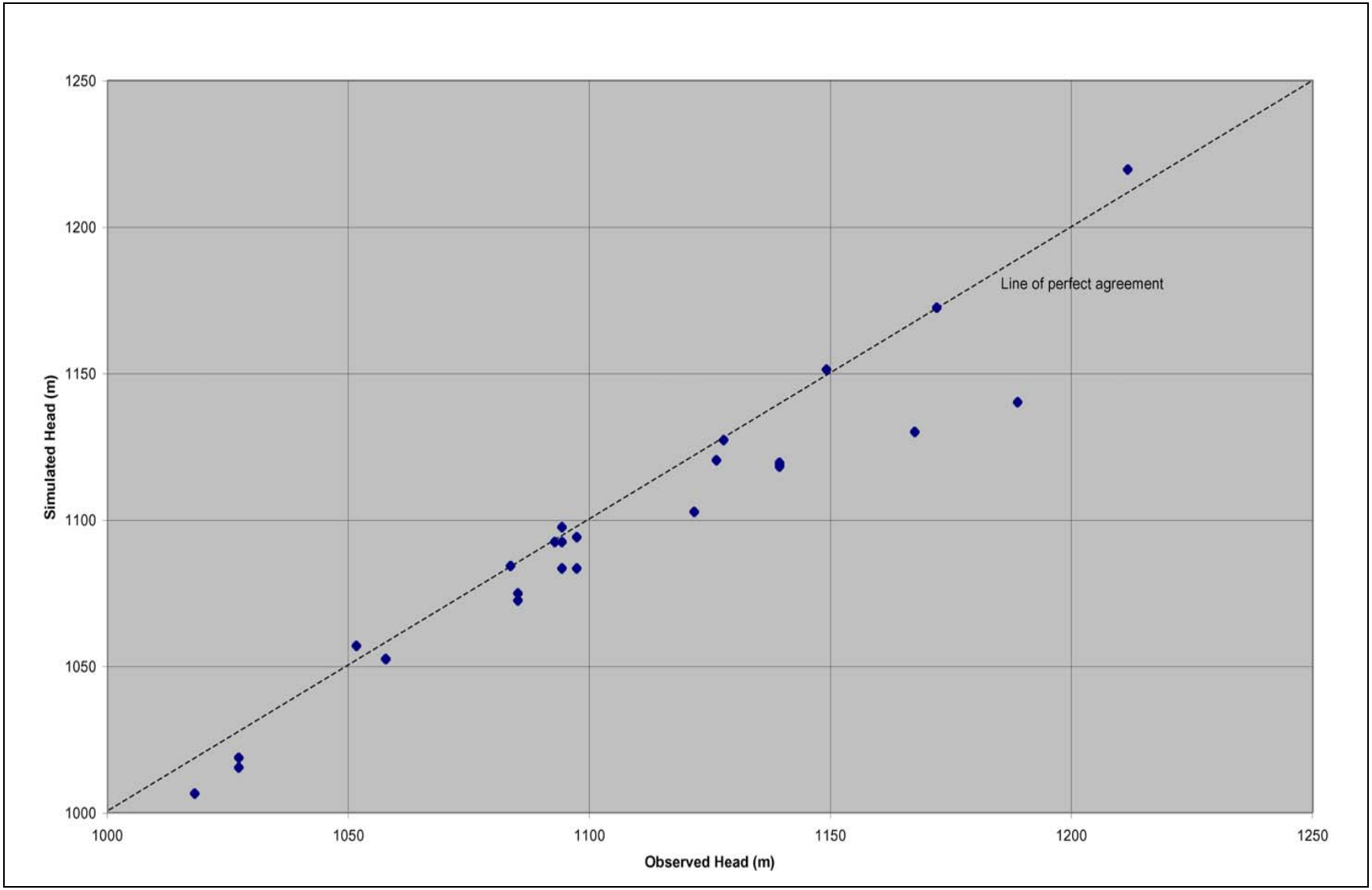

Figure 5-28
Observed Versus Simulated Spring Head for BN-MME-ADA

Uncontrolled When Printed

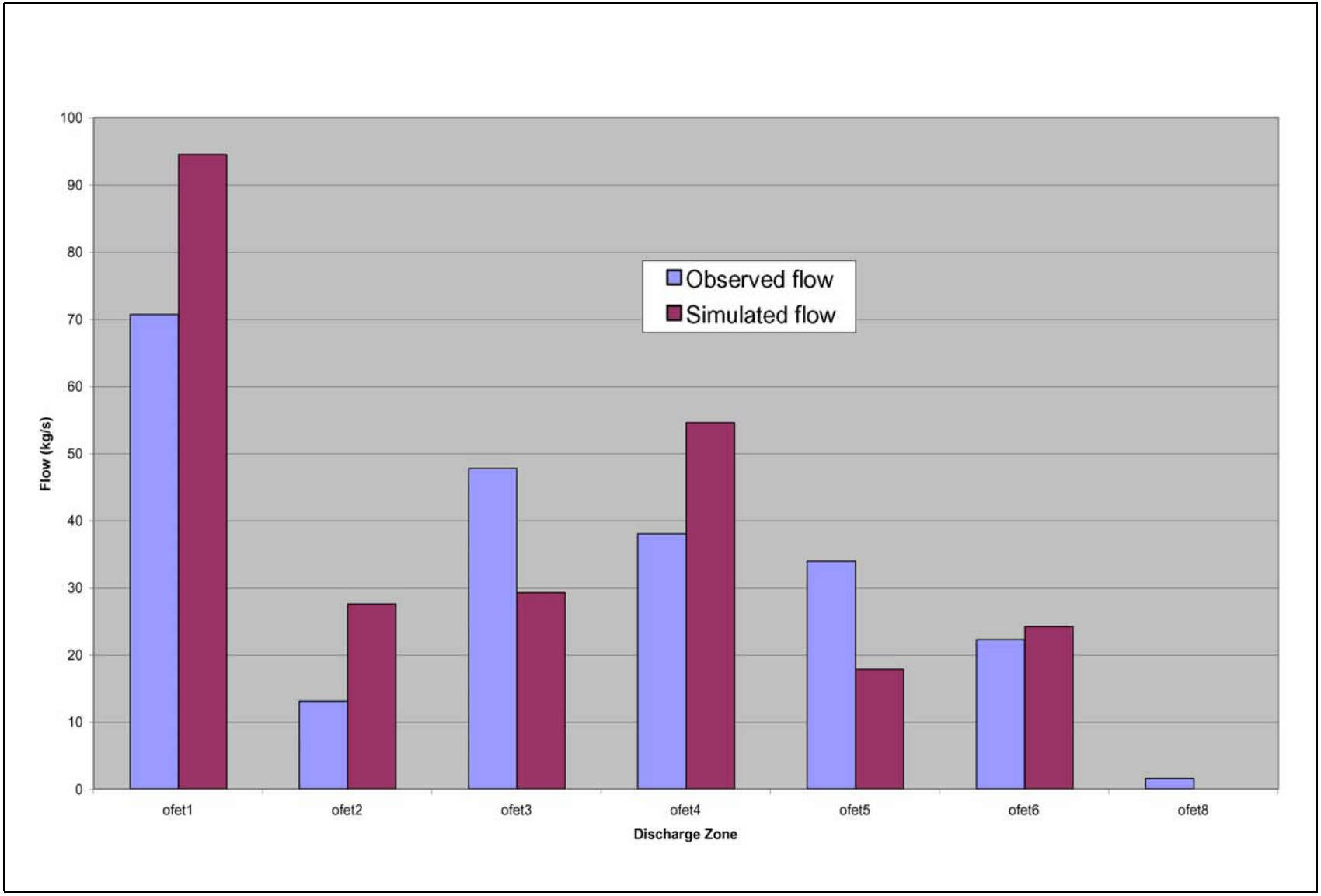

Figure 5-29
Observed and Simulated Oasis Valley Discharge for BN-MME-ADA

Uncontrolled When Printed

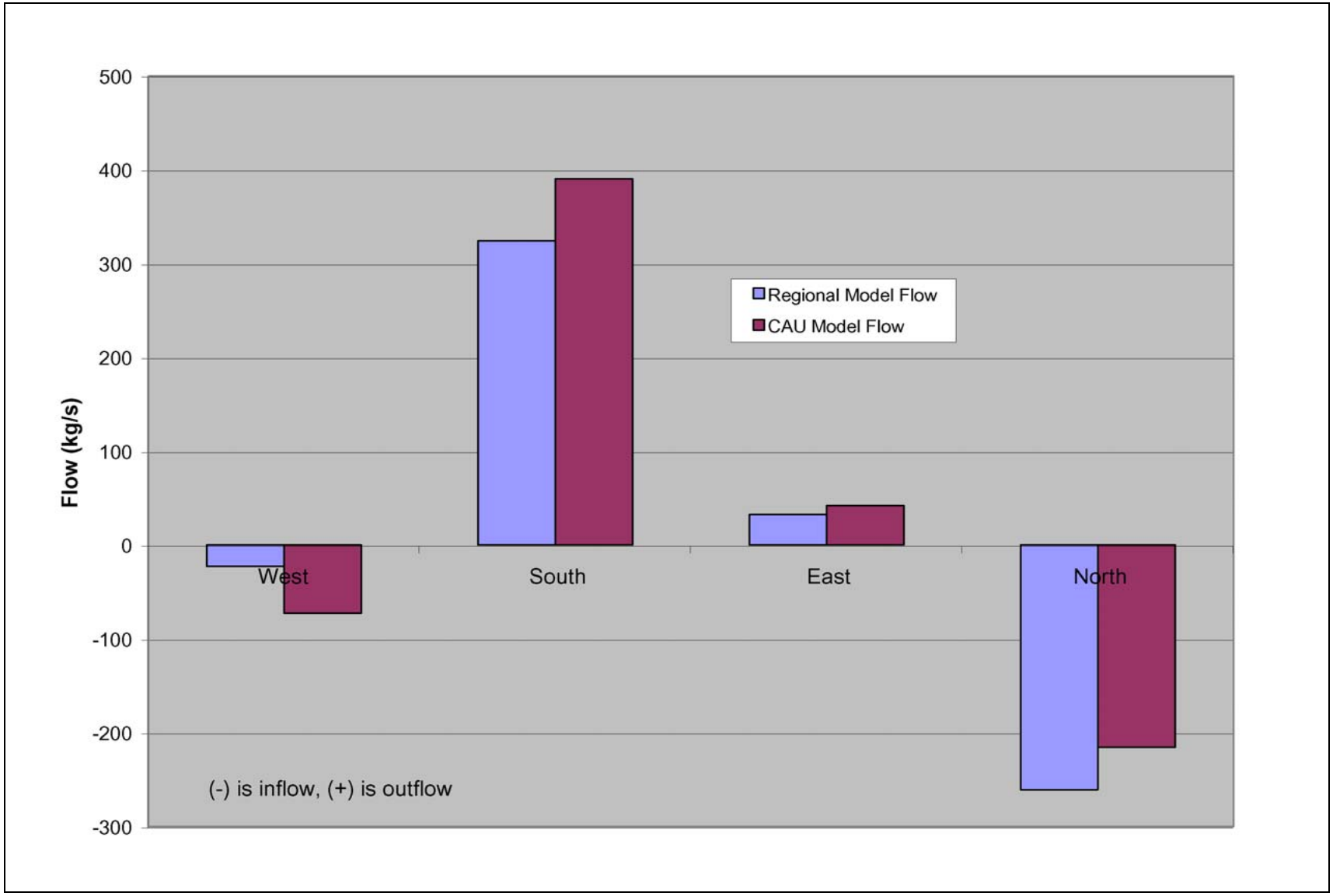

Figure 5-30
Estimated and Simulated Boundary Flows for BN-MME-ADA

Uncontrolled When Printed

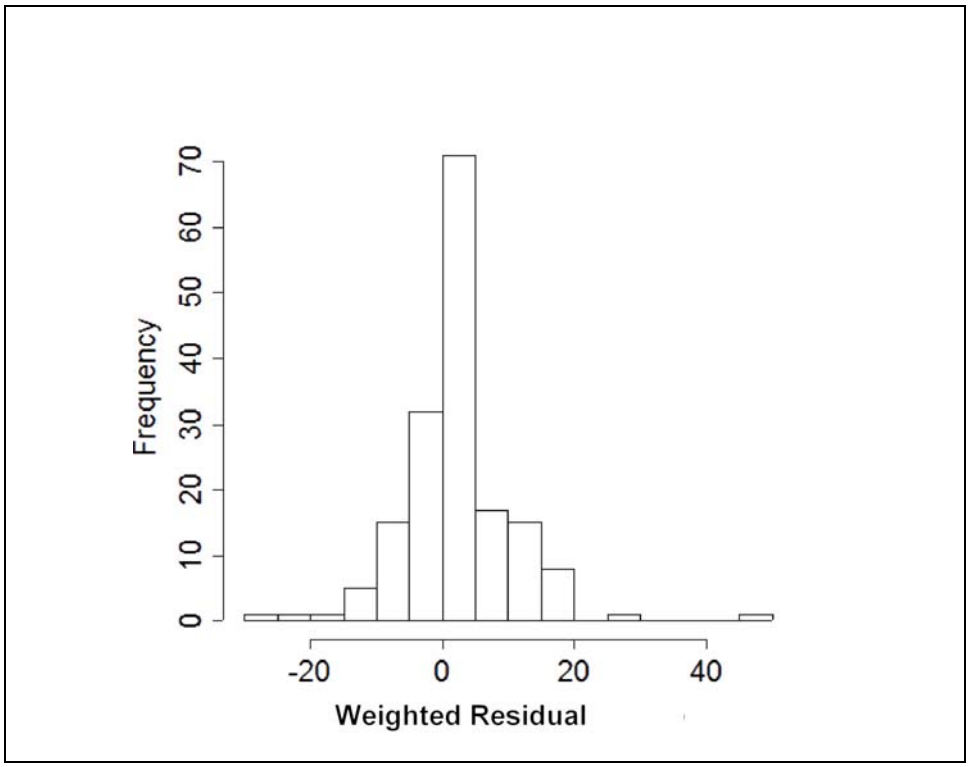

Figure 5-31
Histogram of Weighted Head Residuals for BN-MME-ADA

The weighted head and spring errors are shown on Figure 5-32, color coded by value and sign. The two lowest, or undersimulated, wells were WW-8 and ER-EC-7. The most oversimulated water level was U-20g in northern Area 19. Well U-20g has a target head of 1,357.27 m, while Well U-20aw approximately 2,100 m nearly due south has a target head of 1,371.43 m. Well U-20g is primarily in the BFCU, and thus its connection to the flow system may be marginal. In general, the errors are randomly distributed, although there is a slight low bias in northern Area 20.

The two springs with the largest errors are Goss Spring, which has an uncertain location, and Oleo Road Spring in an area of very high topographic gradient that the model is unlikely to represent in sufficient detail. Thus, these two springs were assigned low weights because of their questionable representativeness. However, springs at similar and higher elevations were matched well, and this misfit appears to be a local issue.

The total estimated Oasis Valley discharge is 227 kg/s. The simulated discharge, shown in Figure 5-29, is 247 kg/s. The total error is within one standard deviation (30 kg/s) as reported by Laczniak et al. (2001). With the exception of Zone 4, the model trends the same as the data with

Uncontrolled When Printed

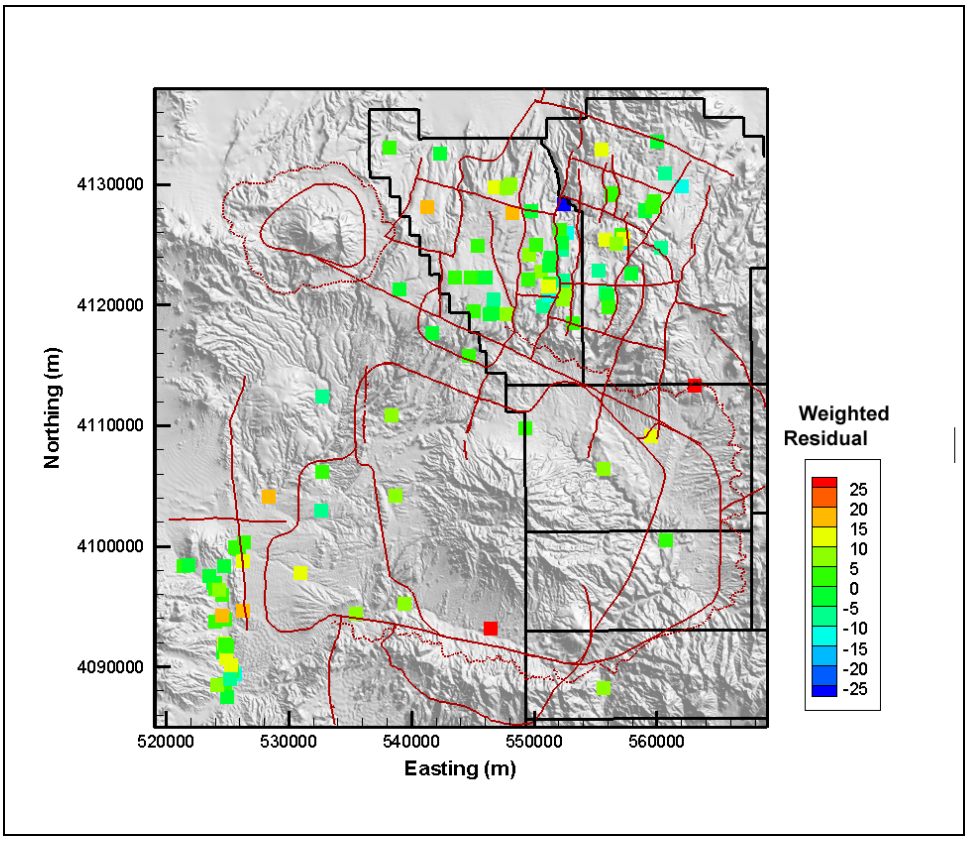

Figure 5-32
Post Plot of Weighted Well and Spring Head Residuals for BN-MME-ADA

some scatter, showing that the general representation of the area is correct. The northernmost zone accounts for 38 percent of the discharge versus 30 percent observed, which is important because this area is closest to the NTS. The boundary flows (Figure 5-30), estimated from regional model analysis, all trend the correct way (e.g., have the proper sign), with the largest relative misfit on the western edge.

The quantitative measures of the model calibration are given by the summary statistics shown in Table 5-13. These statistics alone are not used to judge model calibration; they are used in conjunction with the graphical approaches described previously. There is a slight low bias in the spring heads, with a slight overprediction bias for the flows. The total model objective function was 21,292. Table 5-14 shows the contribution of each data type to the total model goodness of fit. The strongest contributors are observation well heads and Oasis Valley flow, which are also the two key components of calibration data.

Uncontrolled When Printed

Table 5-13
Calibration Summary Statistics for BN-MME-ADA

Calibration Data	Number of Data	Mean Weighted Error (m or kg/s)[a]	Maximum Weighted Residual	Minimum Weighted Residual	Error Standard Deviation (m or kg/s)
Well Head	152	1.5	48 (WW-8)	-25 (U-20g)	8.5
Spring Head	28	2.9	19 (Torrance Spring)	-7.9 (Spring id 180)	6.9
Oasis Valley Discharge	7	-5.9	37 (Zone 3)	-47 (Zone 1)	30
Boundary Flow	4	-8.9	25 (West)	-33 (South)	23

[a]Positive is undersimulation of target data, negative is oversimulation.

Table 5-14
Contribution to Model Goodness of Fit by Data Type for BN-MME-ADA

Data Type	Value (-)	% of total
Well Head	11,060	52
Spring Head	1,331	6
Oasis Valley Discharge	6,638	31
Boundary Flow	2,263	11
Total	21,292	100

Flow paths were qualitatively assessed during calibration by inspecting the simulated water table configuration and tracking particles forward from NTS calibration well locations. Figures 5-33 and 5-34 show the simulated water table and travel paths for this model case. The water table shows higher heads on the eastern edge at a northing of about 4,120,000 m, which is coincident with Gold Meadows stock and the western edge of Rainier Mesa. In the western part of Area 20, the influence of the Purse Fault is evident by nearly 100 m offset in water levels across it, with more subdued effects also present at West Boxcar Fault. Water flows from Areas 19 and 20 towards the southwest and Oasis Valley. Ubiquitous discharge in Oasis Valley, including flow from Sarcobatus Flat to the

Uncontrolled When Printed

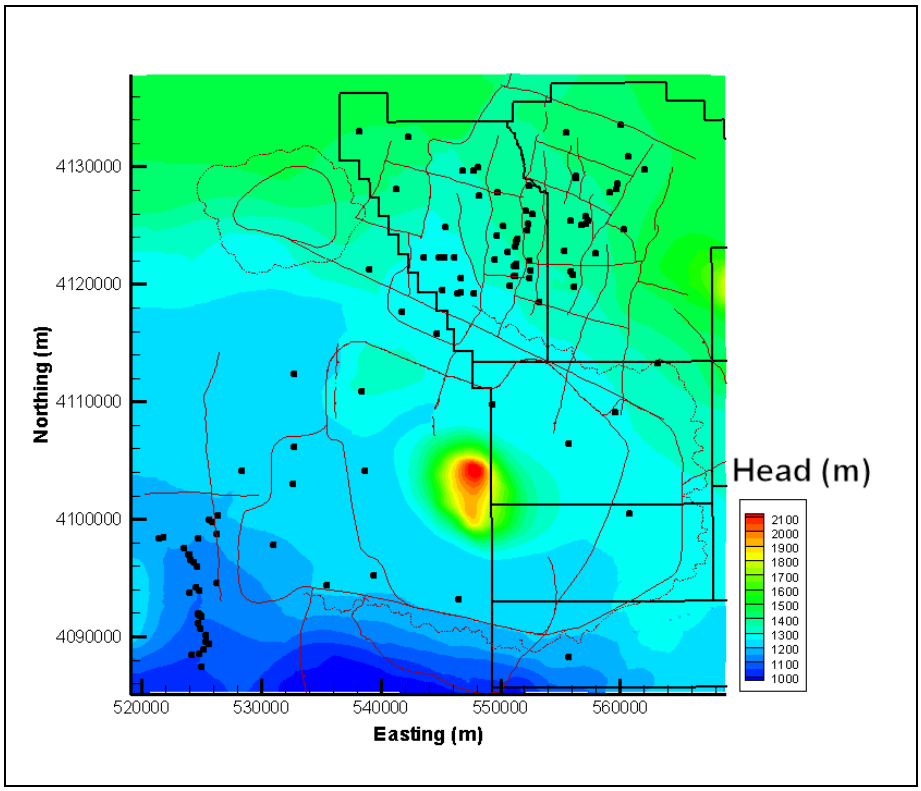

Figure 5-33
Simulated Water Table for BN-MME-ADA

west is also evident. The particle trajectories along the western side of Timber Mountain are influenced by either the contact between the TMCM and TMA, or the fault that defines the contact, and lie mainly within the TMCM.

Particle tracking shows the same generally noted flow paths as SNJV (2004a) with flow noticeably skirting the Purse Fault on the west from flow originating in northwestern Area 20. Like the selected HSU depth decay and anisotropy case, the flow paths become very complicated where the Purse Fault has been assumed to end near the Moat Fault. This case also shows flow along the western flank of Timber Mountain down into Oasis Valley and out to the south. Unlike the selected HSU depth-decay and anisotropy case, particles move from northwestern Area 20 down the western side of Purse Fault. Thus, this parameterization of the base HFM simulates a higher velocity in this area than the selected HSU depth-decay and anisotropy case. This model also has poorer agreement on the edge flows in the direction of oversimulation; thus, it is possible that in order to improve the agreement with the edge flows that permeability must decrease, and the effects are seen in the change in flow velocity in northern Area 20.

Uncontrolled When Printed

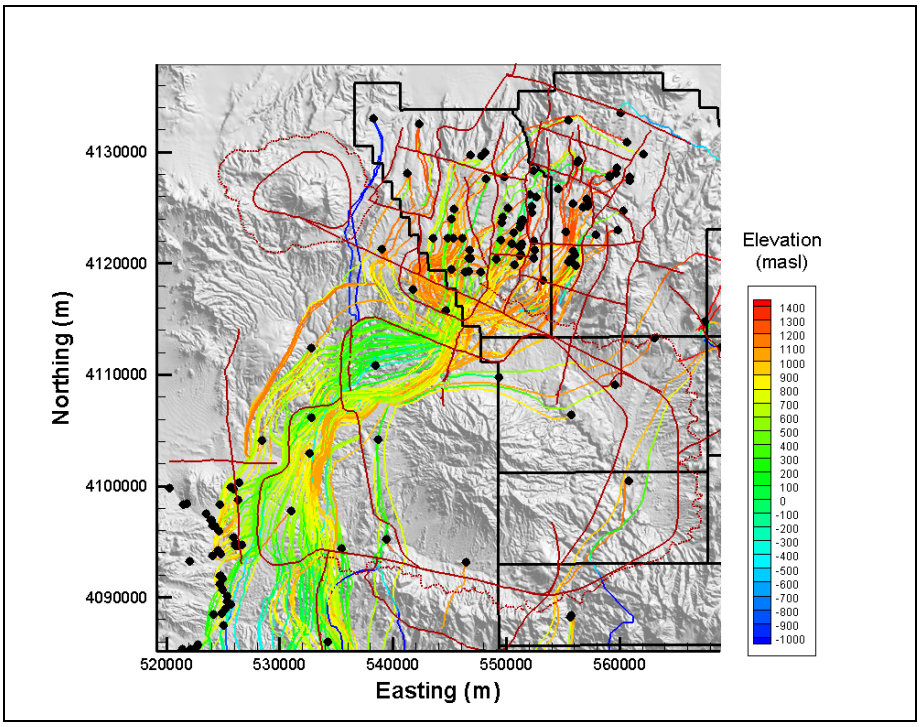

Figure 5-34
Particle Tracks for BN-MME-ADA

The properties used to parameterize this model are shown in Tables 5-15 and 5-16 for HSUs and faults, respectively.

Uncontrolled When Printed

Table 5-15
Hydrostratigraphic Unit Parameters for BN-MME-ADA
(Page 1 of 2)

HSU	Log (k or k_0) (m^2)	Horizontal/Vertical Permeability	Depth Decay λ	Notes
LCCU	-15	0.15	1.20×10^{-3}	Depth decay all parameters
LCA	-13	1.50×10^{-2}	1.00×10^{-3}	
UCCU	-13.93	2.00×10^{-2}	1.50×10^{-3}	
LCCU1	-12.72	2.00×10^{-2}	2.60×10^{-3}	
LCA3	-11	2.00×10^{-2}	1.00×10^{-3}	
MGCU	-12.93	0.5	1.50×10^{-3}	
SCICU	-9.81	0.5	1.50×10^{-3}	
CHICU	-9.81	0.5	1.50×10^{-3}	
CCICU	-11.81	0.5	1.50×10^{-3}	
RMICU	-12.81	0.5	1.50×10^{-3}	
ATICU	-11.81	0.5	1.50×10^{-3}	
BMICU	-10.81	0.5	1.50×10^{-3}	
PBRCM	-11.73	2.0×10^{-2}	2.60×10^{-3}	
BRA	-10.47	8.00×10^{-2}	2.60×10^{-3}	
BCU	-13.81	2.00×10^{-2}	2.60×10^{-3}	
KA	-10.71	8.00×10^{-2}	2.60×10^{-3}	
CFCU	-9.73	2.00×10^{-2}	2.60×10^{-3}	
CFCM	-10.03	2.00×10^{-2}	2.60×10^{-3}	
IA	-10.06	8.00×10^{-2}	2.60×10^{-3}	
CHCU	-12.71	2.00×10^{-2}	2.60×10^{-3}	
CHZCM	-11.49	2.00×10^{-2}	2.60×10^{-3}	
CHVCM	-11.14	2.00×10^{-2}	2.60×10^{-3}	
CHVTA	-12	8.00×10^{-2}	2.60×10^{-3}	
YMCFCM	-11.90	8.00×10^{-2}	2.60×10^{-3}	
TSA	-9.21	8.00×10^{-2}	2.60×10^{-3}	
LPCU	-12.93	2.00×10^{-2}	2.60×10^{-3}	
PLFA	-10.84	8.00×10^{-2}	2.60×10^{-3}	
TCA	-8.49	8.00×10^{-2}	2.60×10^{-3}	
UPCU	-11.99	2.00×10^{-2}	2.60×10^{-3}	
BA	-9.89	8.00×10^{-2}	2.60×10^{-3}	
PVTA	-10.41	8.00×10^{-2}	2.60×10^{-3}	
PCM	-11.35	2.00×10^{-2}	2.60×10^{-3}	
LCA3a	-12.06	2.00×10^{-2}	1.00×10^{-3}	
FCCU	-12.71	2.00×10^{-2}	2.60×10^{-3}	
SCVCU	-12.71	2.00×10^{-2}	2.60×10^{-3}	
TMA	-10.86	8.00×10^{-2}	2.60×10^{-3}	
THCM	-12.71	2.00×10^{-2}	2.60×10^{-3}	
THLFA	-10.71	8.00×10^{-2}	2.60×10^{-3}	
TMCM	-9.41	2.00×10^{-2}	2.60×10^{-3}	
FCA	-9	8.00×10^{-2}	2.60×10^{-3}	
FCCM	-13.37	2.00×10^{-2}	2.60×10^{-3}	
DVA	-11.75	2.00×10^{-2}	2.60×10^{-3}	

Uncontrolled When Printed

Table 5-15
Hydrostratigraphic Unit Parameters for BN-MME-ADA
(Page 2 of 2)

HSU	Log (k or k_0) (m^2)	Horizontal/Vertical Permeability	Depth Decay λ	Notes
DVCM	-12.40	2.00×10^{-2}	2.60×10^{-3}	Depth decay all parameters
TCVA	-10.52	8.00×10^{-2}	2.60×10^{-3}	
YVCM	-11.36	2.00×10^{-2}	2.60×10^{-3}	
AA	-12	0.22	3.70×10^{-3}	
LCA Zone 1	-9.89	1.50×10^{-2}	1.00×10^{-3}	
TCVA Zone 6[a]	-12.33	8.00×10^{-2}	2.60×10^{-3}	
TMAR Zone 6[b]	-12.80	8.00×10^{-2}	2.60×10^{-3}	
TMCM-ERM[c]	-11	2.00×10^{-2}	2.60×10^{-3}	
TMCM-ATC	-10.5	2.00×10^{-2}	2.60×10^{-3}	
TMCM-TH	-11.21	2.00×10^{-2}	2.60×10^{-3}	
TMCM-OV	-9.89	2.00×10^{-2}	2.60×10^{-3}	
TMCM-TM	-12.5	2.00×10^{-2}	2.60×10^{-3}	
TMCM-NTM	-9	2.00×10^{-2}	2.60×10^{-3}	
TMCM-ATCE	-10.80	2.00×10^{-2}	2.60×10^{-3}	
TMCM-NTME	-10.18	2.00×10^{-2}	2.60×10^{-3}	
UPCU West of Purse Fault	-11.36	2.00×10^{-2}	2.60×10^{-3}	
LPCU West of Purse Fault	-11.90	2.00×10^{-2}	2.60×10^{-3}	
BRA West of Purse Fault	-9	8.00×10^{-2}	2.60×10^{-3}	

See Table 2-6 for HSU descriptions.

[a]See Figure 5-8 for TCVA subdivisions.
[b]See Figure 5-9 for TMA subdivisions.
[c]See Figure 5-8 for TMCM subdivisions.

Uncontrolled When Printed

Table 5-16
Fault Permeability Multiplier for BN-MME-ADA

Fault ID	Fault Name	Fault Permeability Multiplier
01	Almendro	10
02	Bare Mountain	1
03	Black Mountain Caldera Structural Margin	1
04	Boxcar	7.00×10^{-2}
05	Hogback	1
06	Claim Canyon Caldera Structural Margin	1
07	Colson Pond	1
08	East Greeley	1
09	East Estuary	0.1
10	East Thirsty Canyon Structural Zone	1
11	Handley	5
12	Handley South	1
13	Handley North	1
14	Moor Hen Meadow Structural Zone	1
15	North Timber Mountain Moat Structural Zone	1
16	Ribbon Cliff Structural Zone	5
17	Richey	1
18	Scrugham Peak	1
19	Silent Canyon Northern Structural Zone	1
20	Silent Canyon Structural Zone East	1
21	Silent Canyon Structural Zone West	1
22	YMP inferred/CP Thrust	1
23	Silent Canyon/ West Purse	1.00×10^{-4}
24	Purse North	1.00×10^{-4}
25	Split Ridge	1
26	Southern Pahute Mesa Structural Zone	1
27	Gold Meadows Structural Zone/Big Burn Valley	1
28	Rainier Mesa Caldera Structural Margin	1
29	Ammonia Tanks Caldera Structural Margin	1
30	Hot Springs Lineament extension of Rainier Mesa Caldera Structural Margin	1
31	West Almendro	10
32	West Boxcar	7.00×10^{-2}
33	West Greeley	1
34	West Estuary	1.00×10^{-2}
35	Windy Wash/Claim Canyon 1	1
36	West Silent Canyon Structural Zone	5
37	Paintbrush Canyon	1
38	Fault 23 south of North Timber Mountain Moat Structural Zone	1
39	Fault 16 between faults 23 and 24	1.00×10^{-4}
40	Extension of Purse Fault to northern edge of model	1.00×10^{-5}
41	Purse Fault repair where fault 36 crosses	1.00×10^{-5}

Uncontrolled When Printed

5.7 Silent Canyon Caldera Complex Hydrostratigraphic Framework Model Flow Model Calibration

The major alternative model presented by BN (2002) is the SCCC. This model has fewer HSUs than the base HFM, and does not have as deep or extensive of a fault system. In particular, the Calico Hills formation is reduced from five separate HSUs to one that is several hundred meters thick. More details are given in BN (2002).

The calibration of the SCCC alternative began with the calibrated parameters from the selected HSU depth decay and anisotropy base HFM for both the HSUs (where still present) and faults (where still present). However, because of the lumped nature of the Calico Hills unit its anisotropy was increased to 50:1 because many dissimilar types of units were combined. In addition, the BA also incorporates the LPCU in the SCCC HFM. The BA was assigned anistropy of 20:1. The units selected to have permeability depth decay and anisotropy are the same as presented in Table 5-8 in Section 5.6.2. Figures 5-35 through 5-38 show the observed and unweighted simulated values for the calibration wells, springs, Oasis Valley discharge, and boundary flows, respectively. The scatter around the line of perfect agreement is generally random in Figure 5-35, although a large error occurs at 1,326 m associated with Well ER-19-1 (deep completion). Above an observed head of 1,450 m, there is a bias towards underprediction. However, the highest water level (and the largest error) shown is associated with the Well ER-19-1 shallow completion, which may be perched (Fenelon, 2000). Figure 5-39 shows a histogram of weighted observation well water levels. There is a strong central tendency with relatively even tails. Unlike the calibration cases for the base HFM, there are more large errors at both ends of the distribution, which qualitatively suggests that this calibration (and underlying model structure) is not as good as the others.

The weighted head and spring errors are shown on Figure 5-40, color coded by value and sign. The two lowest, or undersimulated, wells were WW-8 in the east-central part of the model and PM-3 (at coordinates of about 540,000 and 4,120,000 m). After these two wells, UE-18t was the next largest undersimulation to the southwest of WW-8.

Uncontrolled When Printed

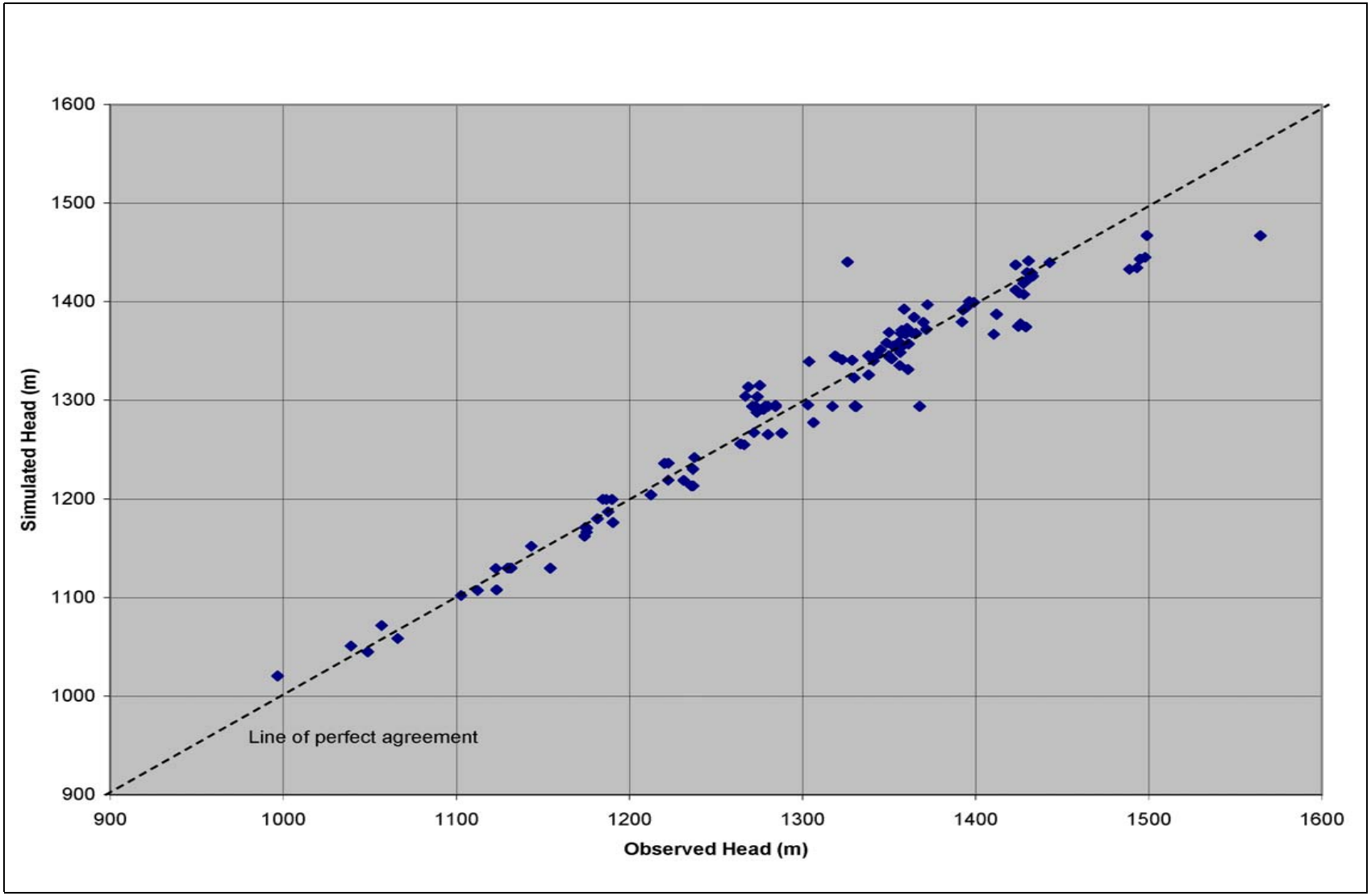

Figure 5-35
Observed Versus Simulated Well Head for SCCC-MME-SDA

Uncontrolled When Printed

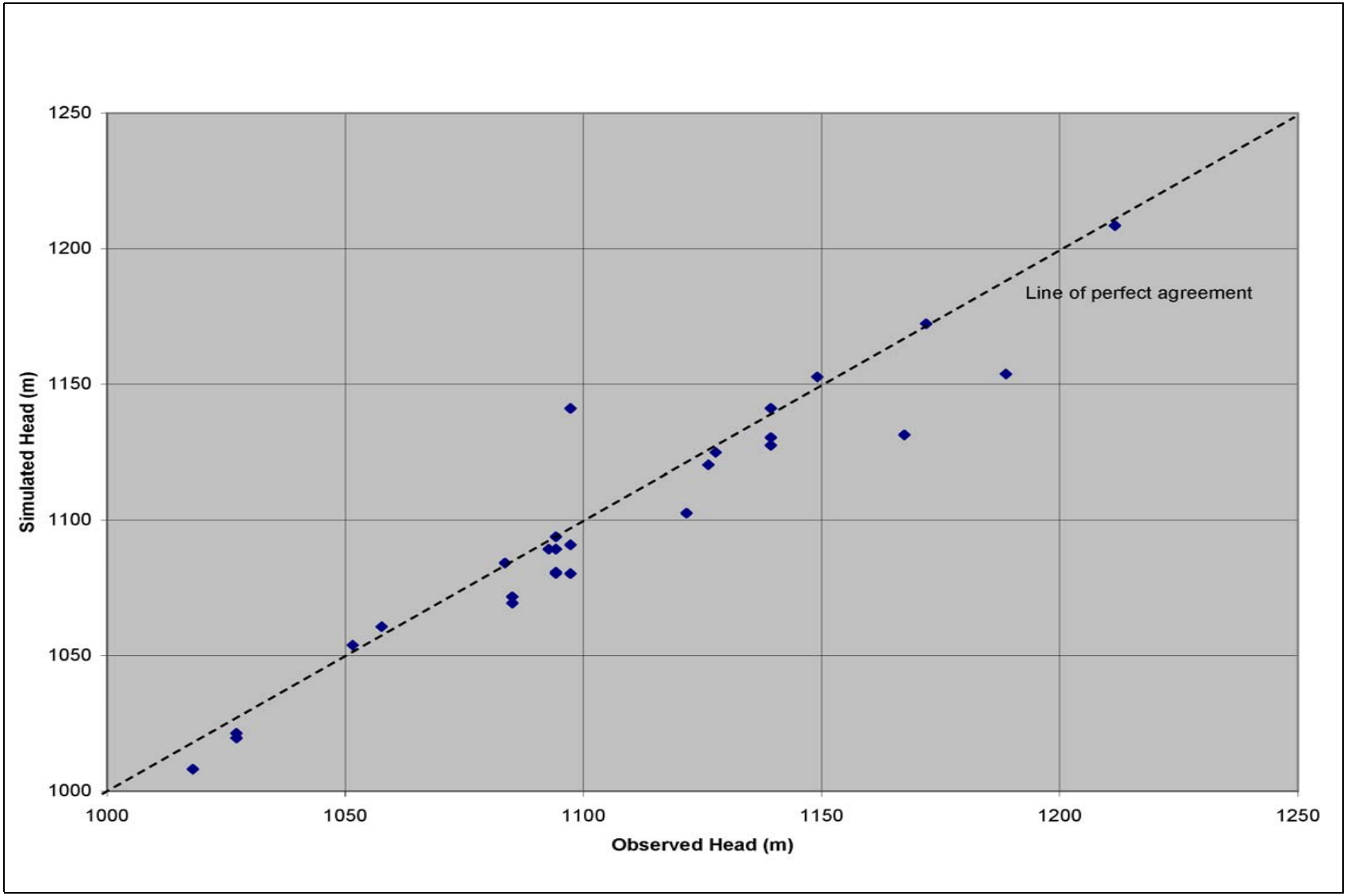

Figure 5-36
Observed Versus Simulated Spring Head for SCCC-MME-SDA

Uncontrolled When Printed

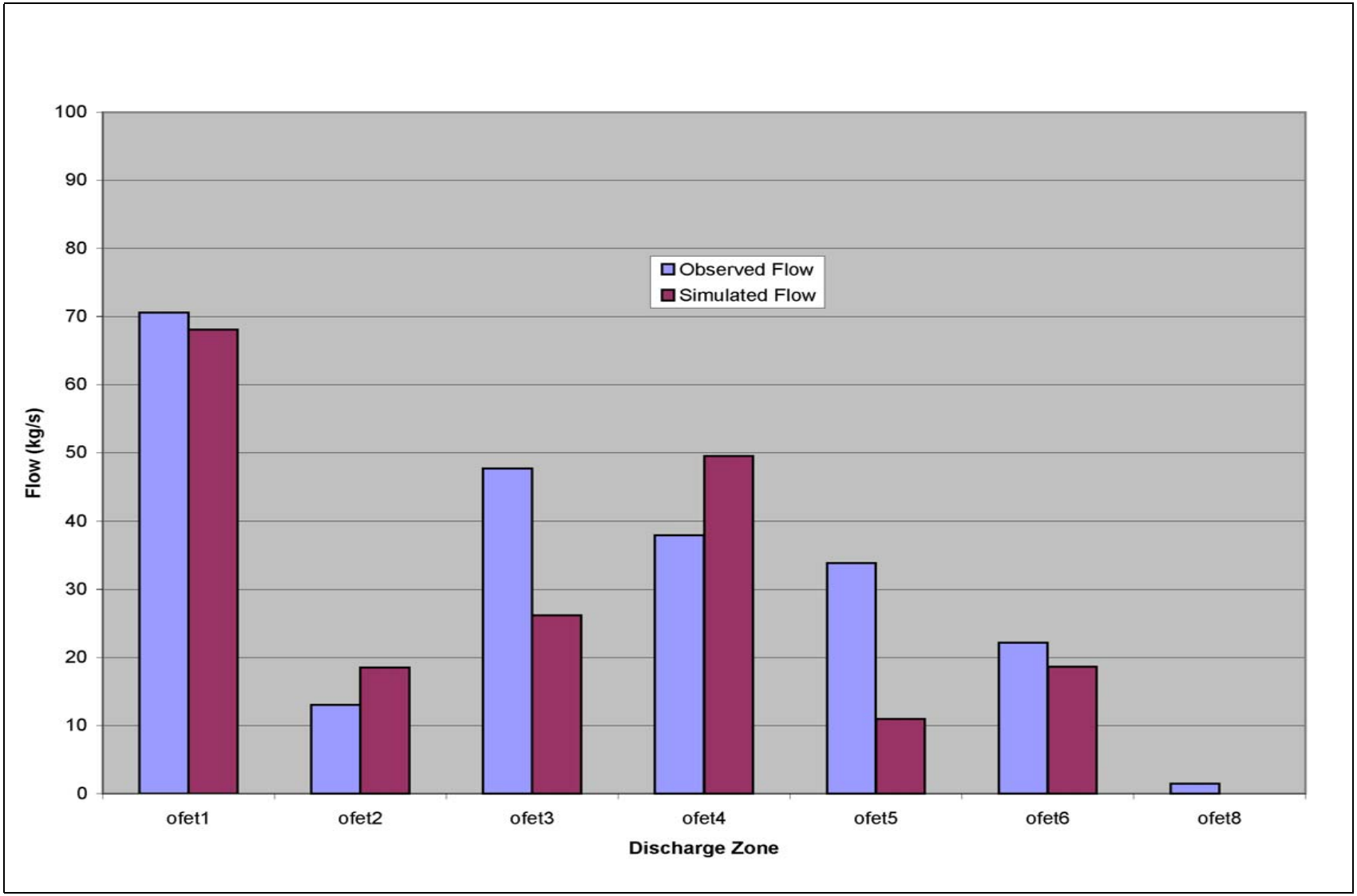

Figure 5-37
Observed Versus Simulated Oasis Valley Discharge for SCCC-MME-SDA

Uncontrolled When Printed

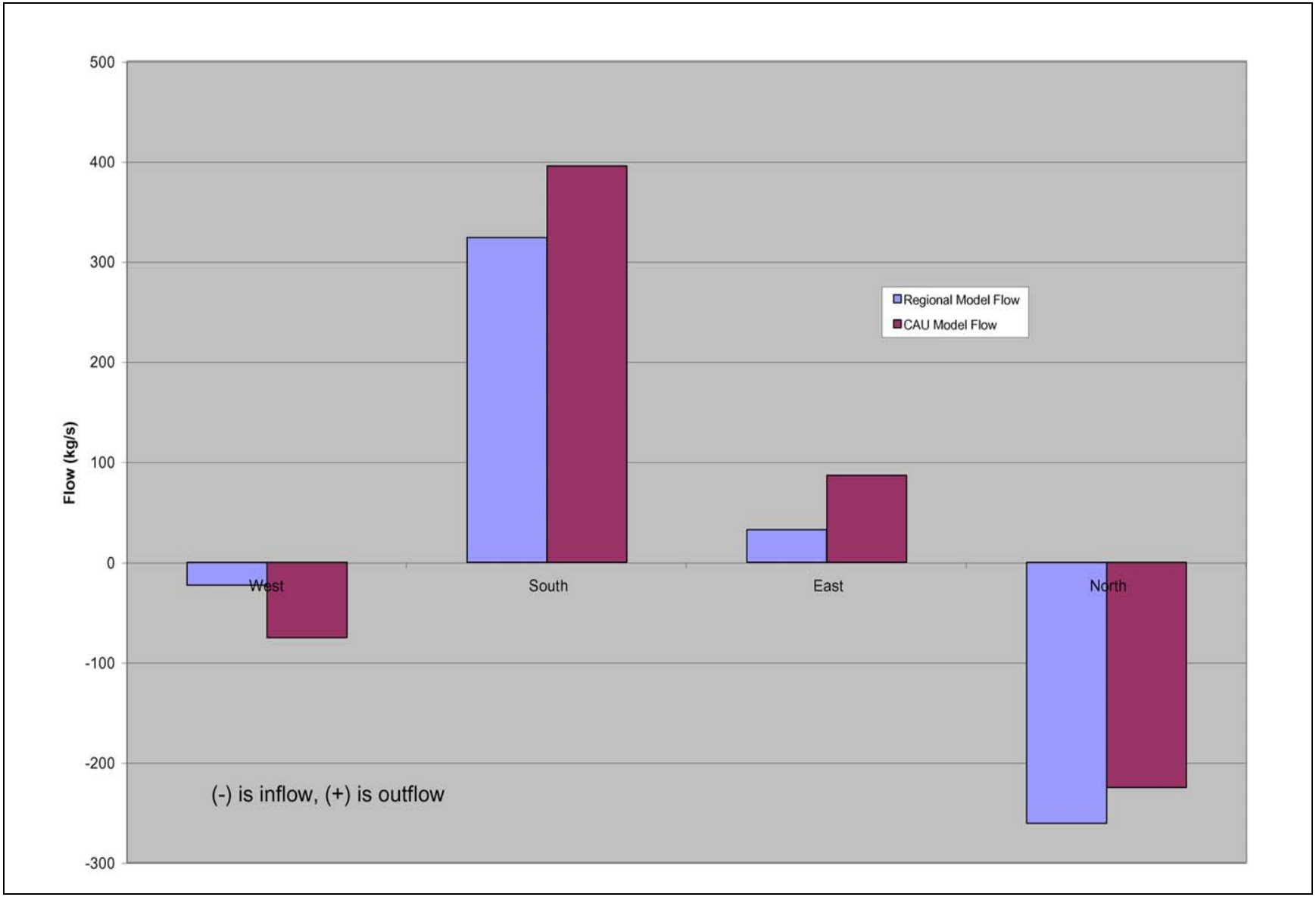

Figure 5-38
Estimated Versus Simulated Boundary Flows for SCCC-MME-SDA

Uncontrolled When Printed

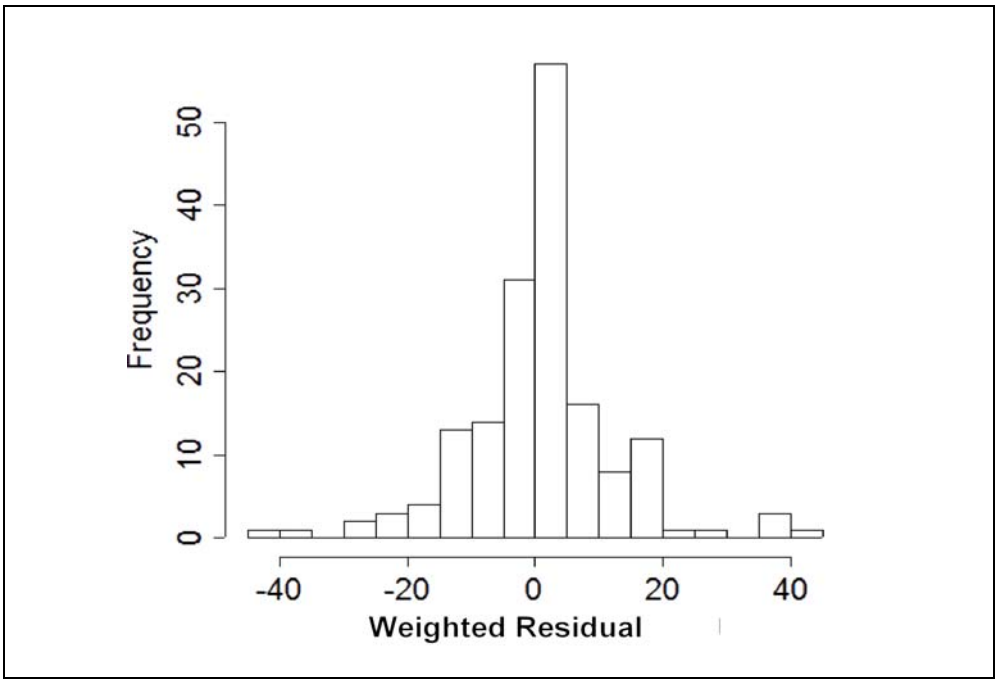

Figure 5-39
Histogram of Weighted Head Residuals for SCCC-MME-SDA

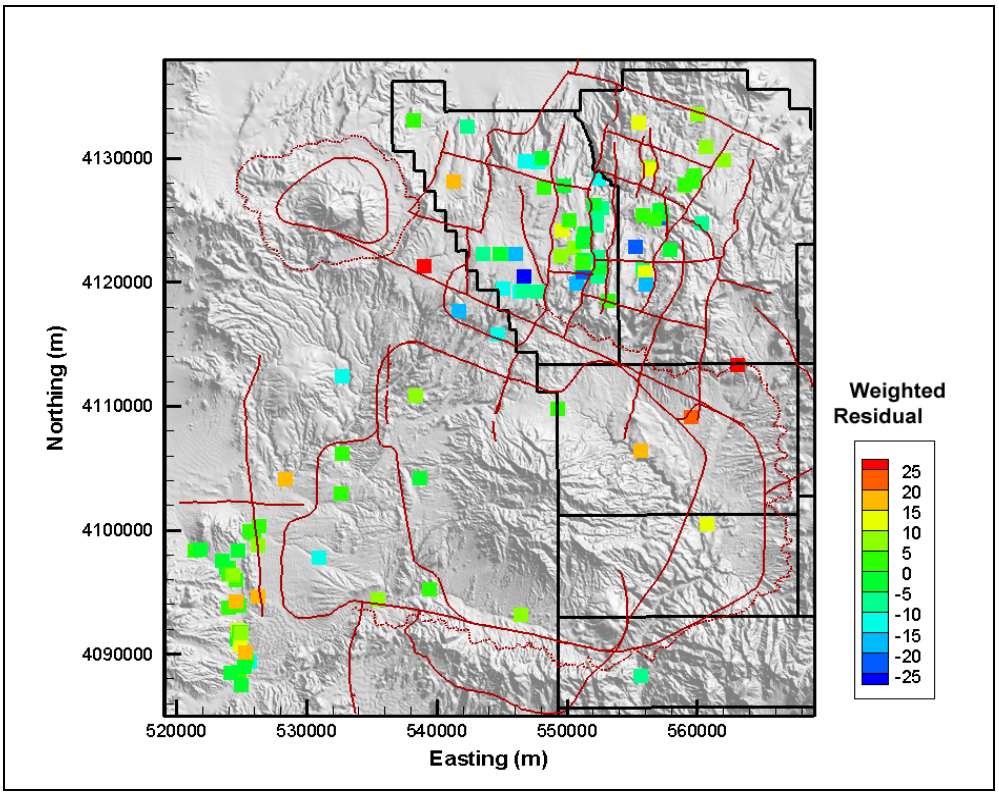

Figure 5-40
Post Plot of Weighted Well and Spring Head Residuals for SCCC-MME-SDA

Uncontrolled When Printed

The total estimated Oasis Valley discharge is 227 kg/s. The simulated discharge, shown in Figure 5-37, is 192 kg/s. The total error is nearly within one standard deviation (30 kg/s) as reported by Laczniak et al. (2001). As with the other flow models, with the exception of Zone 4 (Figure 4-17), the model trends the same as the data with some scatter, showing that the general representation of Oasis Valley is correct. The northernmost zone is in nearly perfect agreement with the data. The boundary flows (Figure 5-38), estimated from regional model analysis, all trend the correct way (e.g., have the proper sign), with the largest relative misfit on the eastern and western edges.

The quantitative measures of the model calibration are given by summary statistics shown in Table 5-17. Note that the ME for the well heads is better than some of the previous models for the base HFM, but that the standard deviation is nearly 50 percent larger than for depth decay and anisotropy applied to all HSUs case in Section 5.6.3. The low ME is a reflection of the even scatter of larger residuals towards both under and overprediction seen earlier in the weighted residual histogram. The total model goodness-of-fit statistic is 31,869, which is nearly double that of the selected depth-decay and anisotropy case in Section 5.6.2 and 150 percent of the all depth-decay and anisotropy case in Section 5.6.3. Table 5-18 shows the contribution of each data type to the total model goodness of fit.

Table 5-17
Calibration Summary Statistics for SCCC-MME-SDA

Calibration Data	Number of Data	Mean Weighted Error (m or kg/s)[a]	Maximum Weighted Residual	Minimum Weighted Residual	Error Standard Deviation (m or kg/s)
Well Head	152	0.34	43 (WW-8)	-39 (U-20c)	11
Spring Head	28	2.5	19 (Torrance Spring)	-43 (Spring id 163)	11
Oasis Valley Discharge	7	9.9	45 (Zone 5)	-23 (Zone 4)	25
Boundary Flow	4	-16	20 (West)	-43 (North)	30

[a]Positive is undersimulation of target data, negative is oversimulation.

Uncontrolled When Printed

Table 5-18
Contribution to Model Goodness of Fit by Data Type for SCCC-MME-SDA

Data Type	Value (-)	% of Total
Well Head	19,998	63
Spring Head	3,538	11
Oasis Valley Discharge	4,681	15
Boundary Flow	3,632	11
Total	31,849	100

Flow paths were qualitatively assessed during calibration by inspecting the simulated water table configuration and tracking particles forward from calibration well locations. Figures 5-41 and 5-42 show the simulated water table and travel paths, respectively, for this model case. As shown on these figures, water flows from Areas 19 and 20 towards the southwest and Oasis Valley as suggested by observed regional groundwater potentials and geochemical analysis. The effects of the West Boxcar Fault can be seen clearly. Observed heads at PM-3 are more than 100 m higher than those in southern Area 20, and it is the relatively shallow and disconnected Purse Fault in this alternative that allows groundwater from PM-3 and the eastern side of Black Mountain to spill into Area 20. This causes misfit at both PM-3 and the wells throughout southern Area 20. A slight mound is simulated under Timber Mountain. Discharge in Oasis Valley, including flow from Sarcobatus Flat to the west, is also evident. Unlike the other HFMs discussed in this section, the SCCC has more particle tracks going down Fortymile Canyon. The flow paths in southern Area 20 are nearly due south, in contrast to the base HFM models and the observed water-table surface. While the goodness of fit and qualitative assessment of the residuals suggest that this HFM does not perform as well as the base HFM, the broad characteristics of the flow system are still correct. This may be at least a partial consequence of specifying head around the edges of the CAU model.

The properties used to parameterize this model are shown in Tables 5-19 and 5-20 for HSU and faults, respectively.

Uncontrolled When Printed

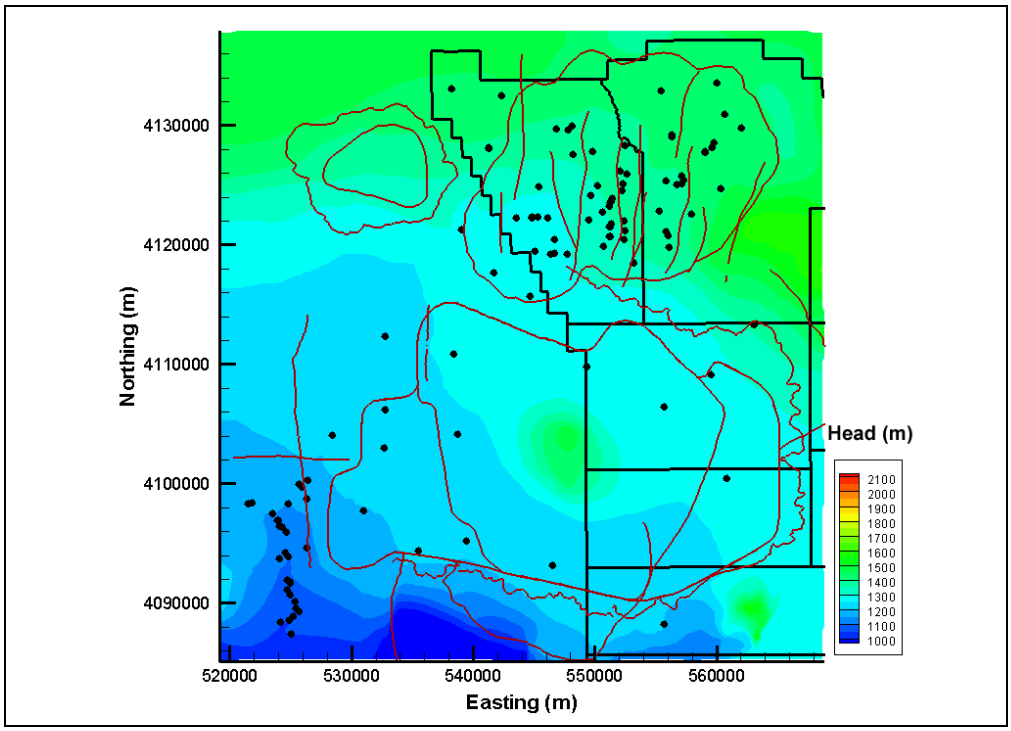

Figure 5-41
Simulated Water Table for SCCC-MME-SDA

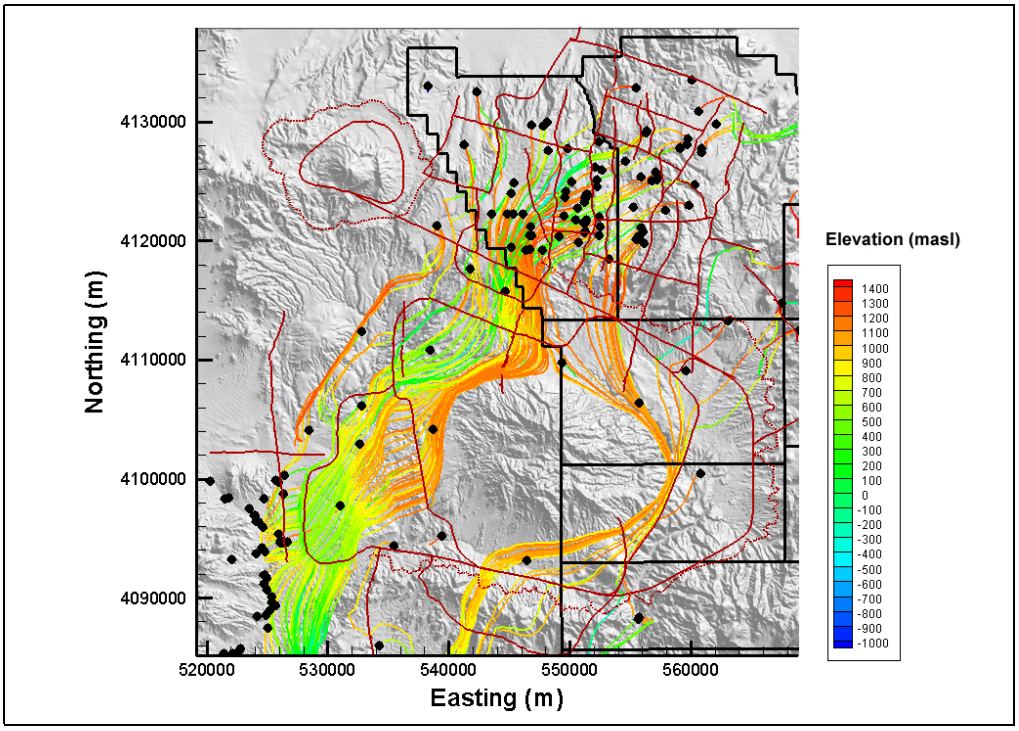

Figure 5-42
Particle Tracks for SCCC-MME-SDA

Uncontrolled When Printed

Table 5-19
Hydrostratigraphic Unit Parameters for SCCC-MME-SDA
(Page 1 of 2)

HSU	Log (k or k_0) (m^2)	Notes
LCCU	-18	k
LCA	**-13.78**	**k_0**
UCCU	-16.78	k
LCCU1	-12.99	k
LCA3a	**-13.04**	**k_0**
MGCU	-18.38	k
SCICU	-18.38	k
CHICU	-18.38	k
CCICU	-18.38	k
RMICU	-18.38	k
ATICU	-18.38	k
BMICU	-18.38	k
PBRCM	**-11.91**	**k_0**
BRA	**-11.51**	**k_0**
BCU	-13.67	k
KA	-11.78	k
CFCU	-12.73	k
IA	-13.56	k
CHCU	-13.83	k
YMCFCM	**-14.54**	**k_0**
TSA	-13.84	k
LPCU	-13.04	k
PLFA	-11.78	k
TCA	-11.48	k
UPCU	-15.33	k
BA	-12.57	k
PVTA	-12.90	k
PCM	**-11.08**	**k_0**
LCA	**-14.28**	**k_0**
FCCU	-12.98	k
SCVCU	-16.28	k
TMA	**-12.04**	**k_0**
THCM	-12.88	k
THLFA	-11.78	k
TMCM	**-11.04**	**k_0**
FCA	-11.50	k
FCCM	-13.48	k
DVA	-12.71	k
DVCM	-13.27	k

Table 5-19
Hydrostratigraphic Unit Parameters for SCCC-MME-SDA
(Page 2 of 2)

HSU	Log (k or k_0) (m^2)	Notes
TCVA	**-10.76**	**k_0**
YVCM	-10.08	k
AA	-13.50	k
LCA Zone 1	**-14.43**	**k_0**
TCVA[a] Zone 6	**-11.45**	**k_0**
TMA[b] Zone 6	**-15.16**	**k_0**
TMCM-ERM[b]	**-11.65**	**k_0**
TMCM-ATCW	**-9.74**	**k_0**
TMCM-ATCE	**-10.79**	**k_0**
TMCM-THS	**-11.93**	**k_0**
TMCM-OV	**-10.72**	**k_0**
TMCM-TMD	**-12.01**	**k_0**
TMCM-NTMW	**-9.31**	**k_0**
TMCM-NTME	**-9.93**	**k_0**
LPCU West of Purse Fault	-14.55	k
UPCU West of Purse Fault	-13.09	k
BRA West of Purse Fault	**-10.80**	**k_0**

See Table 2-6 for HSU descriptions.

[a]See Figure 5-7 for TCVA subdivisions.
[b]See Figure 5-8 for TMA and TMCM subdivision.

Table 5-20
Fault Permeability Multipliers for SCCC-MME-SDA
(Page 1 of 2)

Fault ID	Fault Name	Fault Permeability Multiplier
01	Silent Canyon Caldera Margin	1.3
02	West Purse	1.00×10^{-4}
03	Claim Canyon Caldera Structural Margin	1.1
04	Boxcar	1.07
05	Black Mountain Caldera Structural Margin	1
06	Split Ridge	1.1
07	West Greeley	2.32
08	Rainier Mesa Caldera Structural Margin	1
09	Colson Pond	1
10	YMP inferred/CP Thrust	0.1
11	Ammonia Tanks Caldera Structural Margin	1
12	Bare Mountain	0.1
13	Purse	1.00×10^{-5}

Uncontrolled When Printed

Table 5-20
Fault Permeability Multipliers for SCCC-MME-SDA
(Page 2 of 2)

Fault ID	Fault Name	Fault Permeability Multiplier
14	West Boxcar	3.69×10^{-2}
15	East Estuary	0.24
16	Almendro	0.32
17	Scrugham Peak	0.26
18	Handley South	1
19	Hot Springs Lineament extension over to Hogback	1
20	Paintbrush Canyon	0.1
21	Windy Wash	0.1
22	Gold Meadows Structural Zone/Big Burn Valley	0.86
23	Hogback	1
24	Handley	1.34
25	Handley South	1.1

CP = Control Point

5.8 Calibration Summary

During the Pahute Mesa CAU flow model calibration analysis, the base HFM was parameterized with four different strategies in order to test the impact of the concepts of permeability depth decay and anisotropy. In addition, an alternative HFM, the SCCC, was also calibrated. In all, a total of five calibration analyses with the MME recharge model were performed on two HFMs. Key behaviors and observations are summarized in this section.

The Pahute Mesa CAIP (DOE/NV, 1999) states that many ("often greater than 100") flow model simulations are necessary during the model calibration analysis. Flow model calibration, sensitivity, and uncertainty analysis was conducted jointly by SNJV and LANL on two separate computer systems. Los Alamos National Laboratory used its LAMBDA computer cluster comprised of 164 nodes each with two Intel Pentium processors (1 to 1.4 gigahertz [GHz] clock speed) and 4 gigabytes (GB) of random access memory (RAM). Stoller-Navarro Joint Venture began with six Intel Pentium 2 GHz workstations and finished the project with 28 computers, of which 20 were rack-mounted 3.4 GHz Xeon processors with 4 GB of RAM each. It is estimated that about 5,000 simulations were performed during the calibration phase of the Pahute Mesa CAU flow model. This level of computing power was necessary in order to calibrate the models to the state presented in this report;

Uncontrolled When Printed

the classic computing model of a single fast computer, even a workstation, would not have allowed the timely completion of the project.

5.8.1 Purse Fault Behavior

A striking difference between the base and SCCC HFMs is the area along the Purse Fault. Figure 5-43 (taken from Fenelon, 2000) shows groundwater levels in western Area 19, Area 20, and west of Area 20 along with a view of the BN-MME-SDA (Figure 5-44) and SCCC-MME-SDA results in the area (Figure 5-45). An area of "hydraulic discontinuity" exists coincident with the Purse Fault that shows about 100-m head difference across the fault with flow directed sub-parallel to the fault (e.g., the fault may act as an approximate no-flow barrier). In order to match the head in Wells PM-3, PM-2, UE-20p, UE-20j, and U-20m in the base HFM on the western side of the Purse Fault and wells in southwestern Area 20, the Purse Fault permeability had to be reduced by a factor (10,000) relative to the surrounding HSUs in order to maintain the 100 m or so difference between the two areas. The sensitivity of this is tested further in Section 6.2.

It is important to note that not just the single segment of the Purse Fault in the base HFM actually designated as the Purse Fault had to be adjusted. All of fault 24, part of fault 16 where it connected fault 24 and fault 23, fault 23 north of the Moat Fault (fault 15), and where fault 36 crossed fault 24 all had to be assigned a low permeability multiplier in order to reproduce the observed data. In contrast, the SCCC HFM does not have a Purse Fault geometry that allowed connection or goes as deep (the base HFM has faults projected to the bottom of the model). Thus, as described in Section 5.7, simulated head at Well PM-3 was too low and head in southwestern Area 20 too high because the fault did not separate the two areas sufficiently. The geology along the caldera margins is quite complex, and it is possible that with further geologic review the SCCC HFM could be modified to give a better calibration, although considerable effort was expended to calibrate this HFM. However, the SCCC does incorporate juxtaposition across the caldera margins and the low permeability nodes of the Black Mountain ICU, so the explanation would have to be an amplification of what has already been done. Whether or not the Purse Fault alone is the source of the observed discontinuity is unclear, but its configuration in the base HFM does allow the observed head to be reproduced, which juxtaposition alone does not. The UGTA regional model used lower permeability from between alteration between Black Mountain and the Purse Fault to try to generate the observed

Uncontrolled When Printed

differences. Hydraulic testing of PM-3 (DOE/NV, 1996) showed relatively low permeabilities in this area, but little other information is available.

The effects of the Boxcar Fault can also be seen in Figures 5-44 and 5-45, and both the BN-MME-SDA and SCCC-MME-SDA calibrations improved as its permeability multiplier decreased. Wolfsberg et al. (2002) also noted similar model performance as the West Boxcar and southern part of the main Boxcar Fault permeability decreased. Heads to the east of the fault are higher than those to the west and require some portion of the Boxcar faults to have a lower permeability. Thus, these results are consistent with the data and previous analysis.

Uncontrolled When Printed

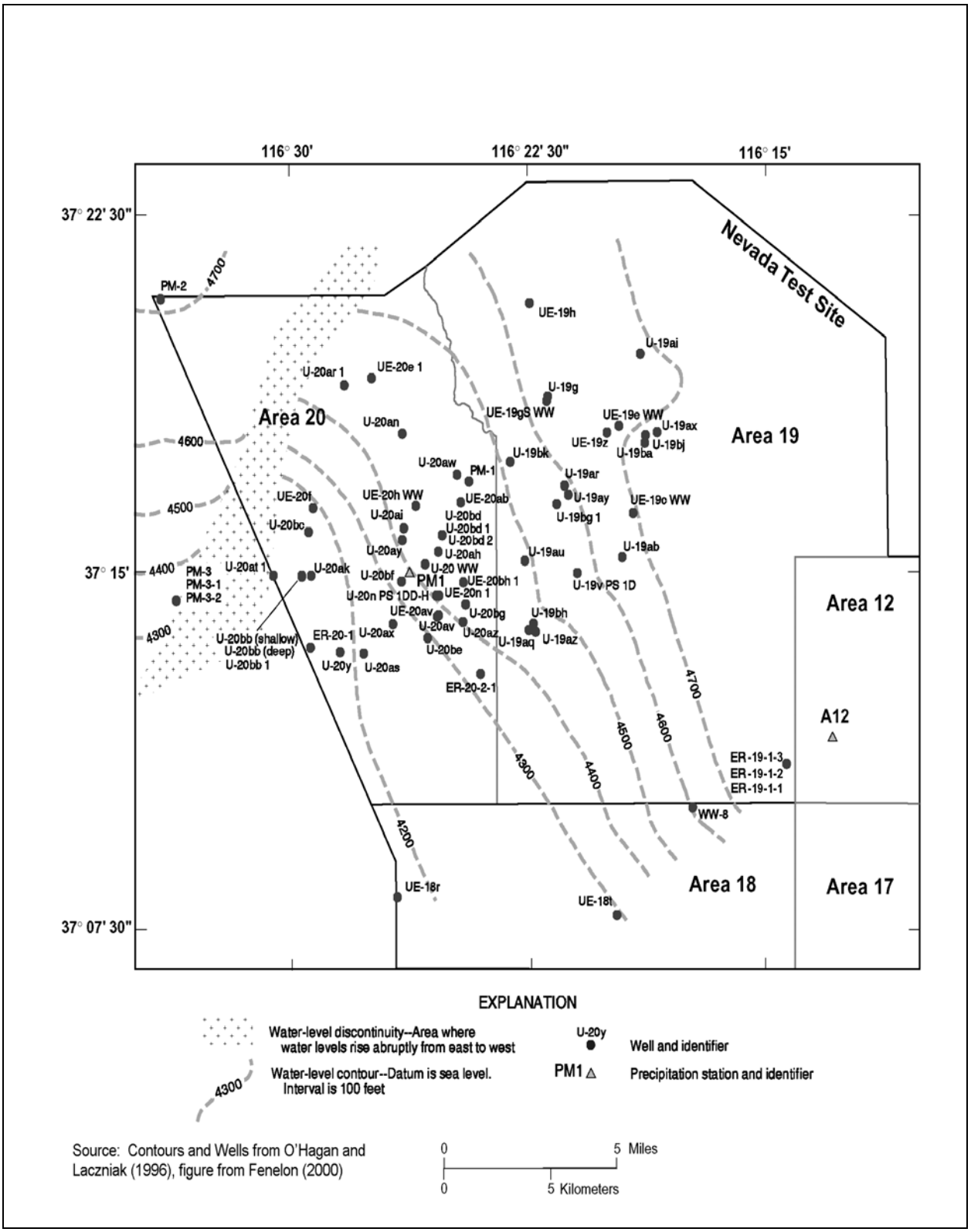

Figure 5-43
Groundwater Levels on Pahute Mesa and Vicinity

Uncontrolled When Printed

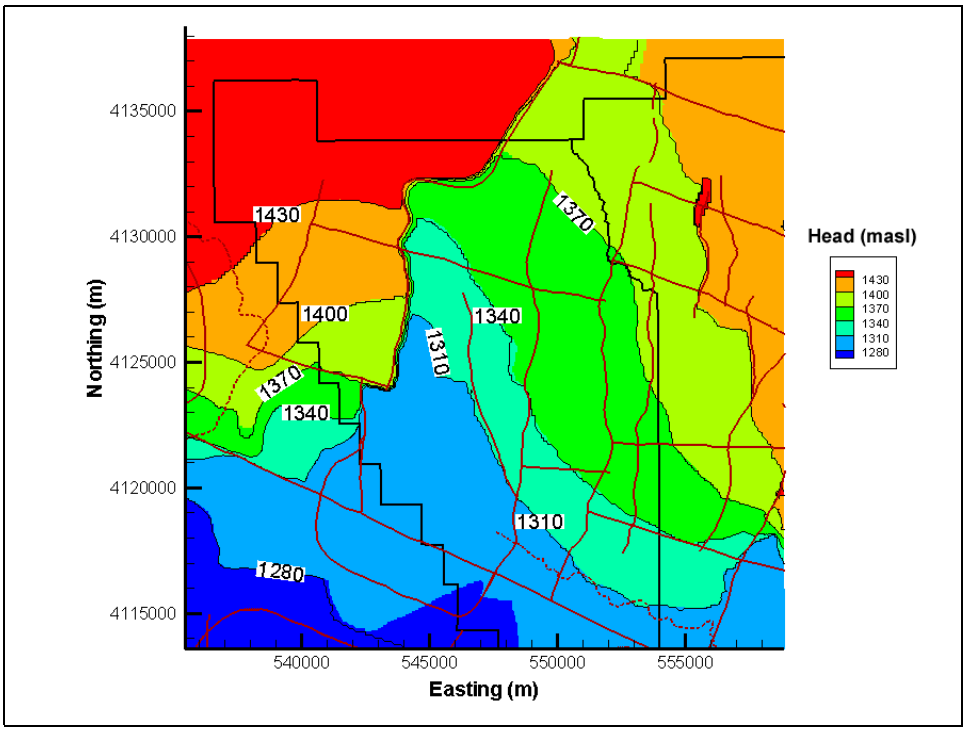

Figure 5-44
Simulated Heads Near the Purse Fault for BN-MME-SDA

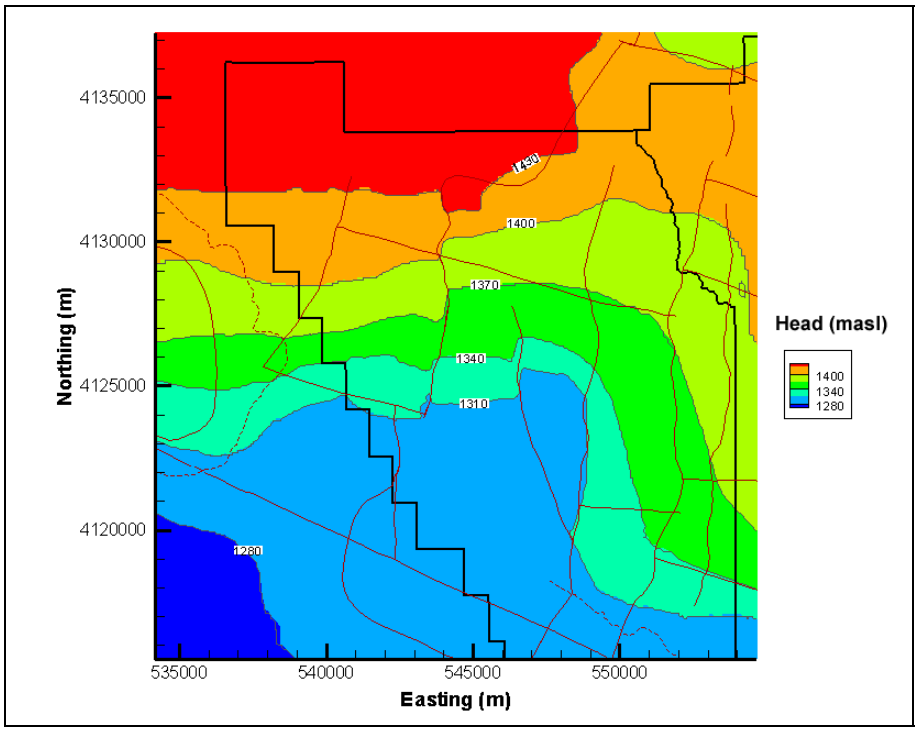

Figure 5-45
Simulated Heads Near the Purse Fault for SCCC-MME-SDA

Uncontrolled When Printed

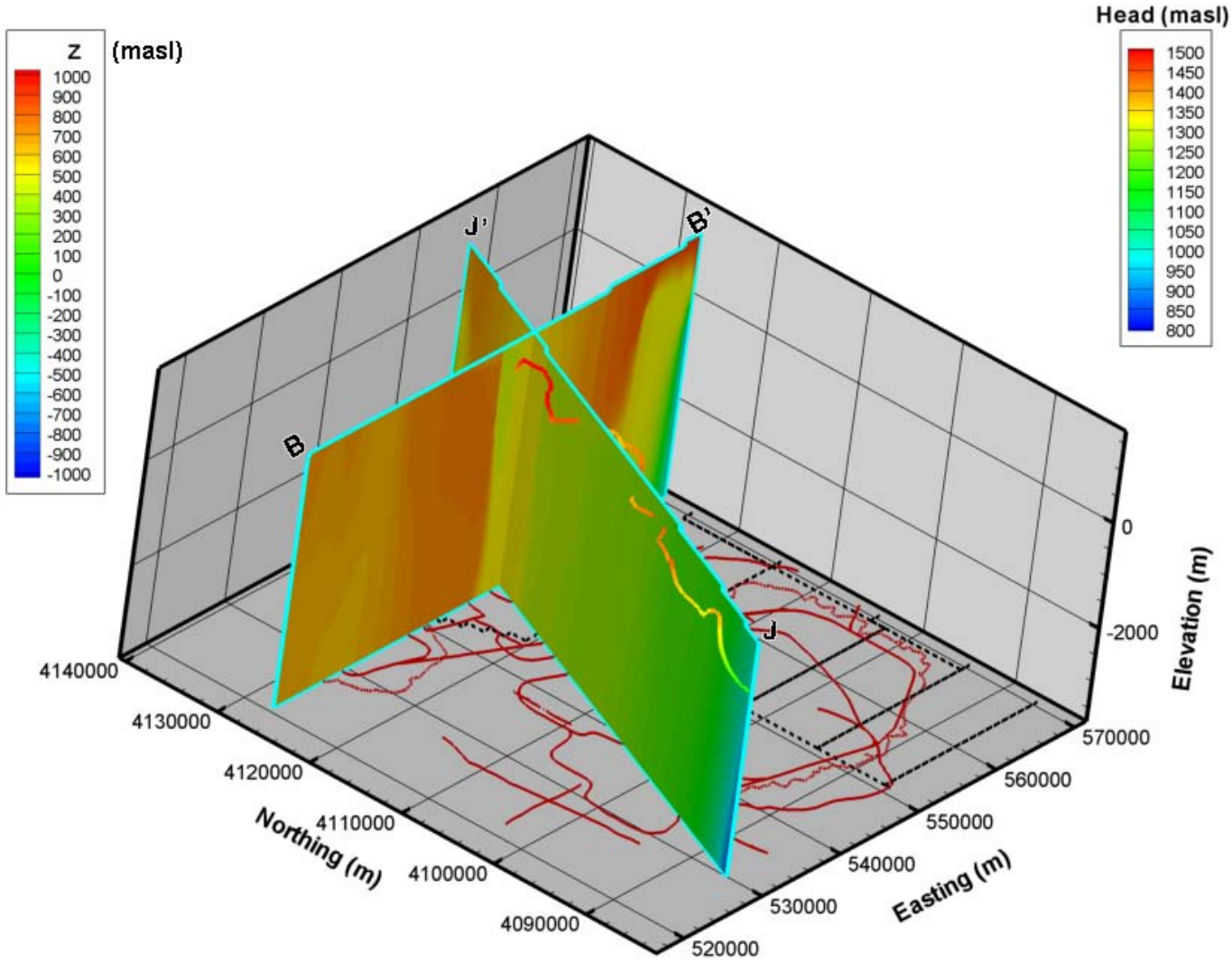

Figure 5-46
Simulated Head Along B-B' and J-J' with Simulated Flow Path for SCCC-MME-SDA

Uncontrolled When Printed

5.8.2 Head and Flow Path Comparison Along B-B' and J-J'

Figures 5-46 through 5-48 show head along geologic model cross-section planes B-B' and J-J', along the trajectory of a particle of water released in central Area 20, BN-MME-SDA, BN-MME-ADA, and SCCC-MME-SDA models. Figures 5-49 and 5-50 also show the permeability along B-B' and J-J' for the same cases. Along the eastern boundary, a lower head is specified in all cases, but its effects are quite different near the edge among the alternatives because of the variation in MGCU (Gold Meadows Stock) permeability. However, the effect dies out in similar locations in each alternative. Another striking difference along B-B' is the sharp gradient just west of where J-J' crosses B-B'. This feature is from the Purse Fault and is clear in base HFMs, but it is imperceptible in the SCCC HFM. The vertical gradient in the western part of B-B' is less for the selected HSU depth decay and anisotropy than the all HSU depth decay and anisotropy. This is a consequence of ubiquitously applying depth decay and anisotropy, which tends to continuously reduce permeability with depth and stratify flow.

Simulated head along J-J' is (Figures 5-46 through 5-48) broadly similar for all HFMs, with flow down to Oasis Valley with gentle horizontal and vertical gradients. At the southern end of the section, the head in the all HSU depth decay case is lower, reflecting the persistence of the specified head boundary condition caused by a higher LCA permeability.

Flow paths from central Area 20 for the three calibrated models have the same basic trajectory with discharge in the Oasis Valley area, but the detailed behavior of the trajectories are quite different (Figures 5-46 through 5-48). For instance, initially the particle rises in the selected HSU depth-decay case, but flows more horizontally in the all HSU depth-decay case. All the particles show a hook behind the plane of J-J' and then returning to the front of the J-J' plane from the influence of Timber Mountain. Thus, while the general model characteristics are similar in terms of calibration and boundary flows, the variability in flow paths resulting from alternative parameterization approaches and the major HFMs are noticeable, although not in disagreement with the data that show flow from Pahute Mesa to the south-southwest into Oasis Valley (SNJV, 2004a). Quantitative measures of flow-path goodness are discussed in Section 7.0.

Uncontrolled When Printed

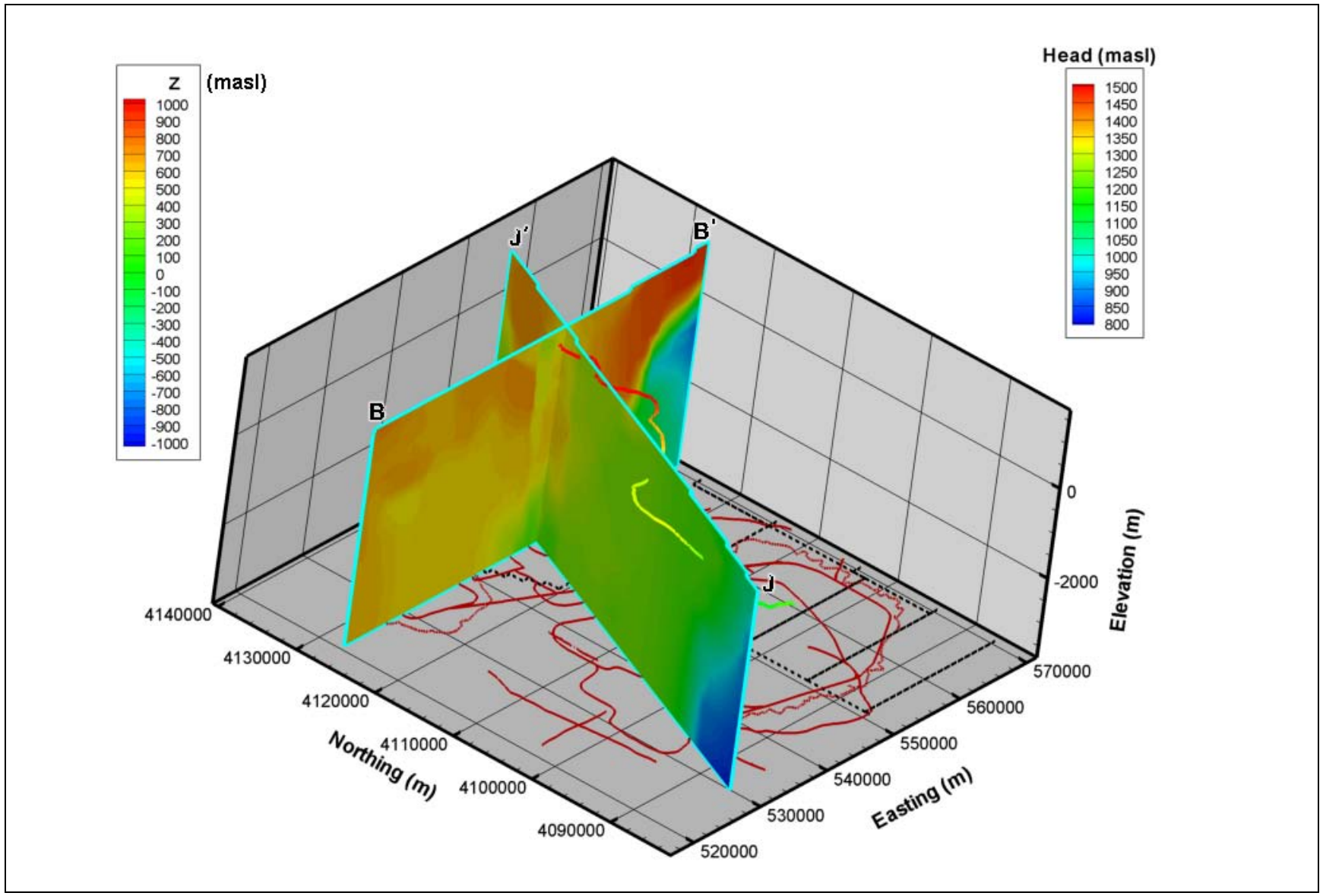

Figure 5-47
Simulated Head Along B-B' and J-J' with Simulated Flow Path for BN-MME-SDA

Uncontrolled When Printed

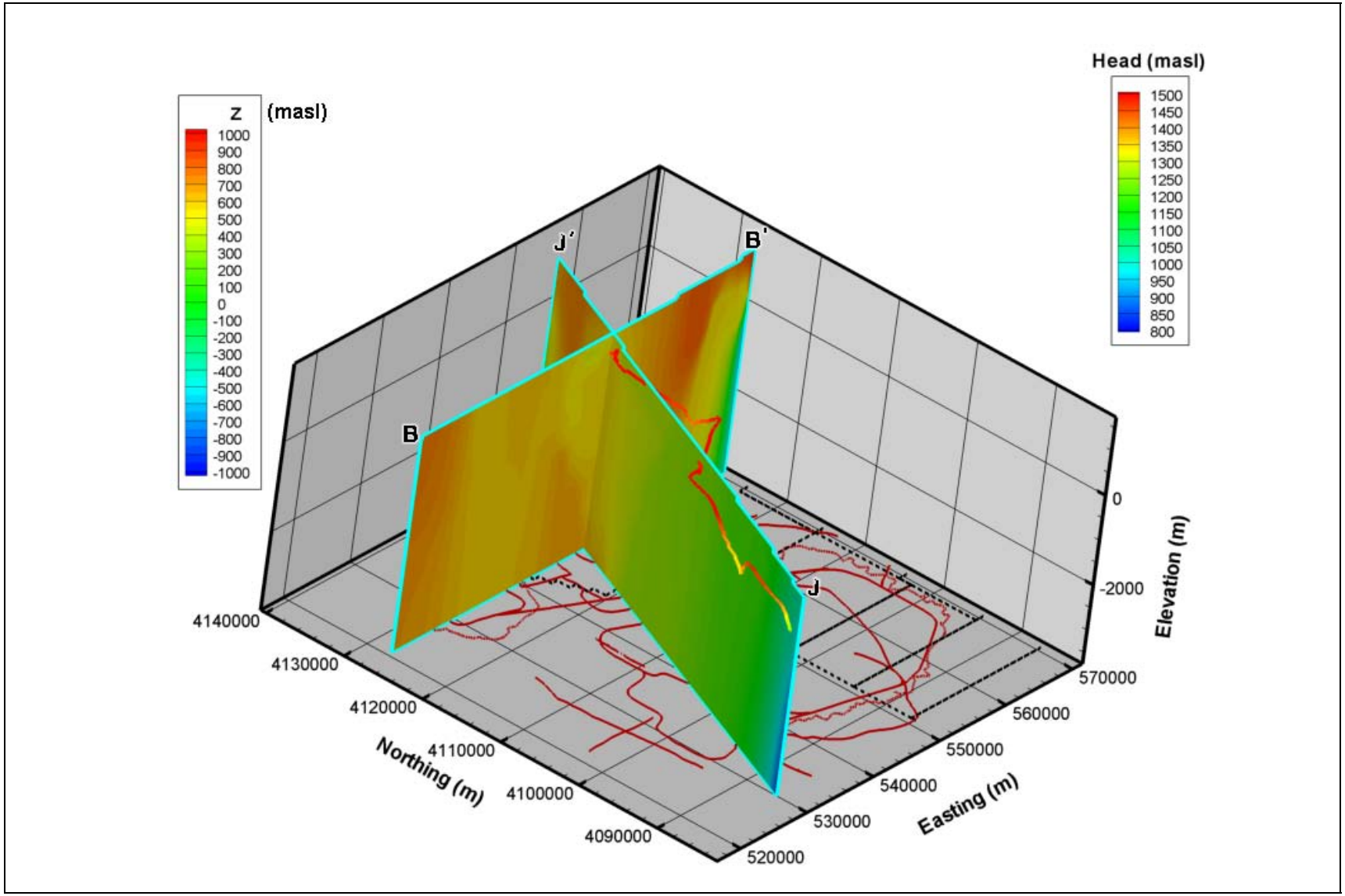

Figure 5-48
Simulated Head Along B-B' and J-J' with Simulated Flow Path for BN-MME-ADA

Uncontrolled When Printed

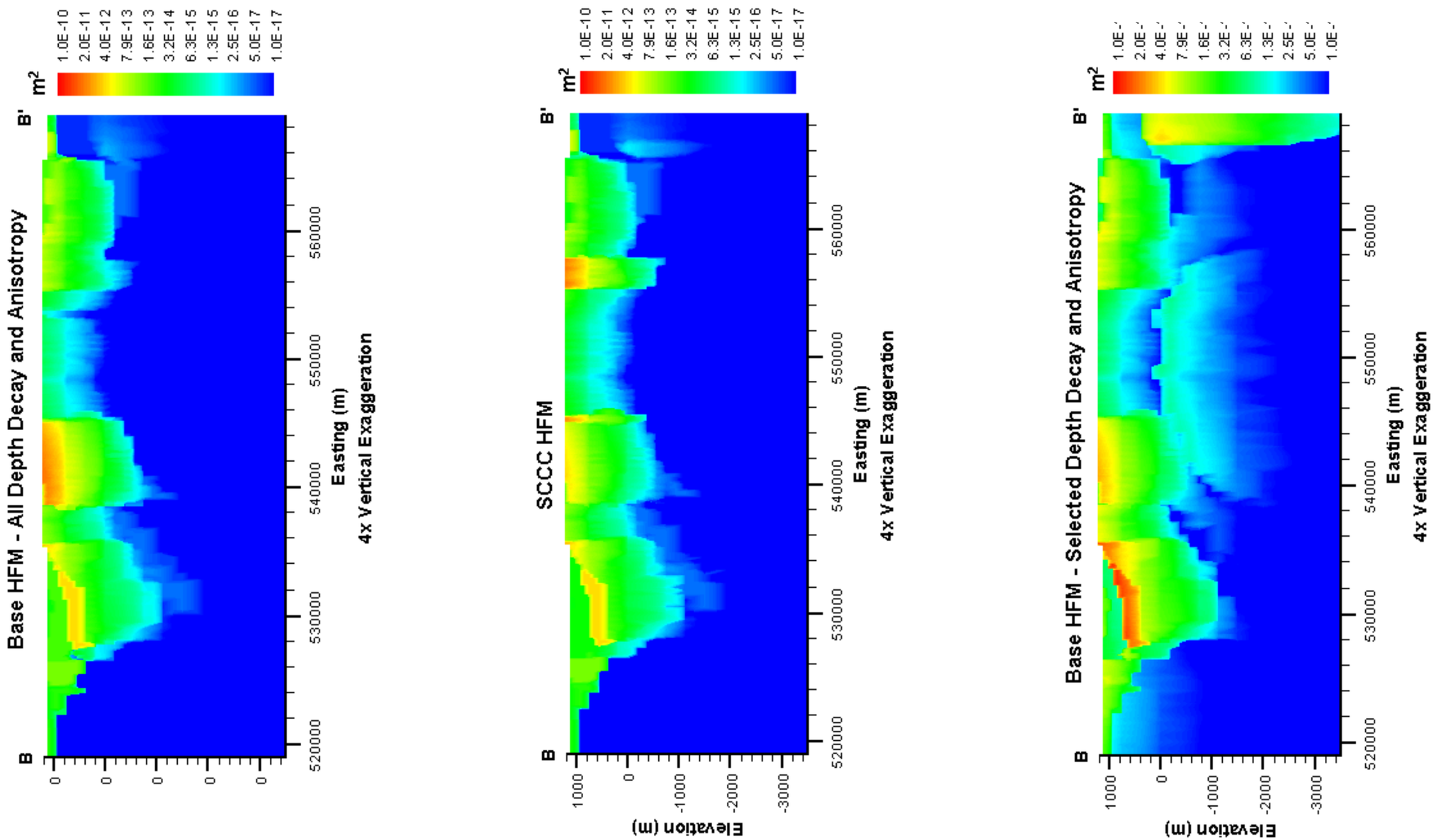

Figure 5-49
Permeability Along Section B-B'

Uncontrolled When Printed

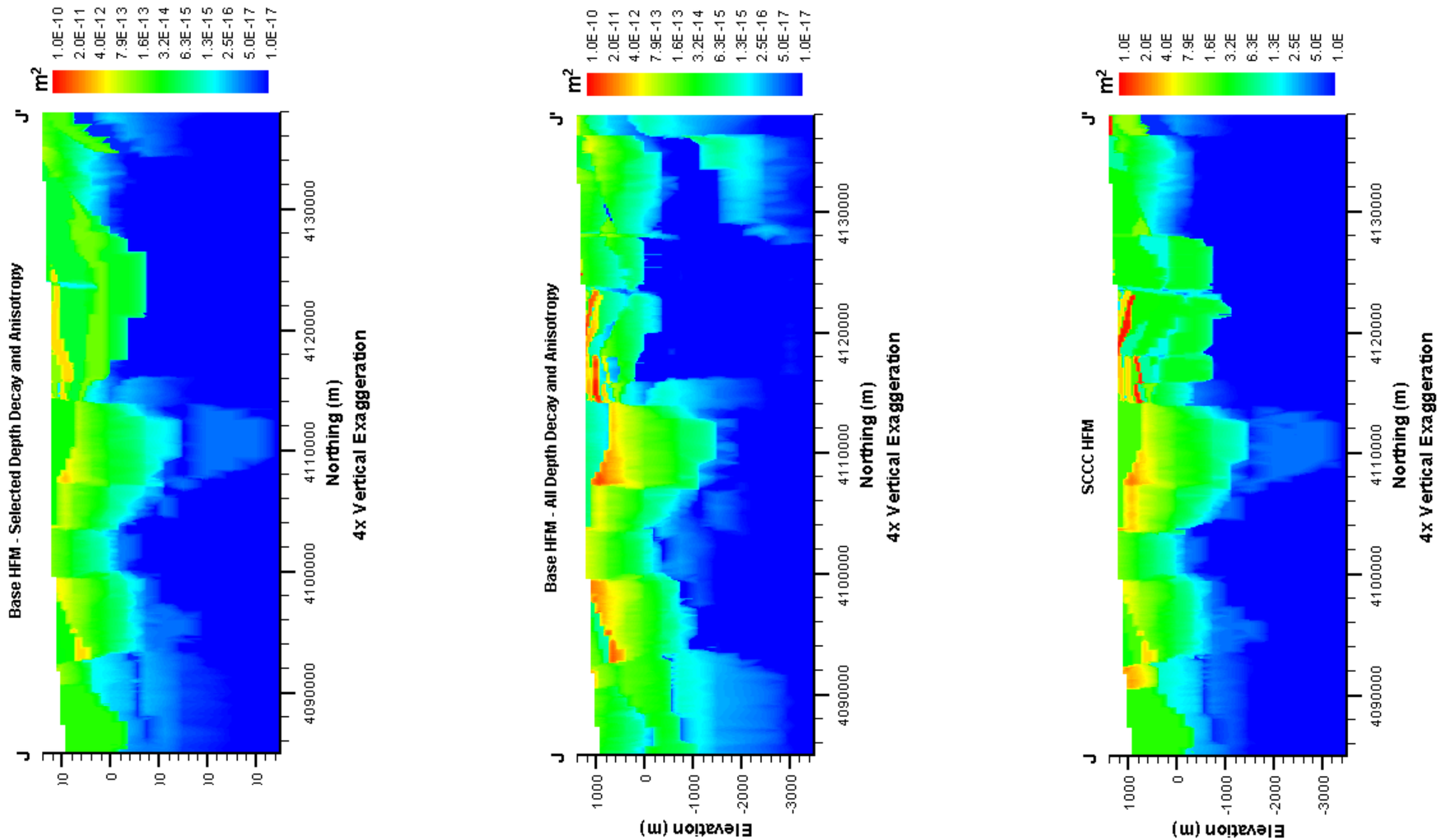

Figure 5-50
Permeability Along Section J-J'

5.8.3 Comparison of Model and Single-Well Test Permeabilities

The estimates of HSU permeability used to guide the calibration were developed from the interpretation of hydraulic tests. As a qualitative model check, permeability from the CAU-model nodes associated with each well test interval were extracted and arithmetically averaged in the case of a test zone with more than one associated node, and are shown in Figures 5-51 and 5-52 with the model-calibrated values. Also shown is the mean permeability estimated for the test HSU as given by SNJV (2004a). Wells ER-EC-1, ER-EC-4, UE-19e, UE-19h, UE-20f, and UE-20h had noisy test data, and the estimated permeability should be considered very uncertain. The model-calibrated permeabilities at the two observation wells from the BULLION FGE (IT, 1998a) (ER-20-6 #1 and ER-20-6 #2) are about an order of magnitude and a half lower than the test values and lower than the value estimated (1.13×10^{-13} m^2) from the model calibration by Wolfsberg et al. (2002) for the CHZCM. The CHZCM HSU has multiple rock types in it. Protho and Warren (2001) characterized an LFA embedded in it that is not accounted for in the model. The CHZCM, a zeolitized composite unit, would be considered to have low permeability and sparse fracturing. In the BULLION FGE (IT, 1998a) the geologic section clearly shows that the pumping test tested the embedded LFA. Thus, because this feature was not included in the CHZCM, which in the model is undifferentiated, it is not surprising that the model-calibrated value is lower. The model agreement with UE-19h has the largest scatter among the HFMs, but the test value is fairly uncertain. There is some observed scatter that appears to be related to the HFMs. For instance, at ER-EC-7, the SCCC HFM has a permeability an order of magnitude less than the base HFMs, which themselves are half an order of magnitude less than the estimated test value, but in good agreement with the estimated mean value. Similar results are also seen at Wells ER-EC-1 and ER-EC-6, and at ER-18-2 where the SCCC HFM is actually quite a bit lower than the other data. However, no general conclusions can be drawn from the permeability comparison about the goodness of the HFMs because at ER-EC-8, ER-EC-4, UE-19c, and UE-19gS, the BN-SDA and SCCC-SDA cases compare better to each other than the BN-ADA case (two different HFMs that were parameterized the same way).

It appears that some of the difference in model permeabilities is from the HFM; some is from the parameterization approach and some is also probably from the goodness of each calibration, which while similar are not identical. In general, because tested zones in fractured rock are those that typically have higher permeabilities while the model incorporates the entire thickness of rock, the

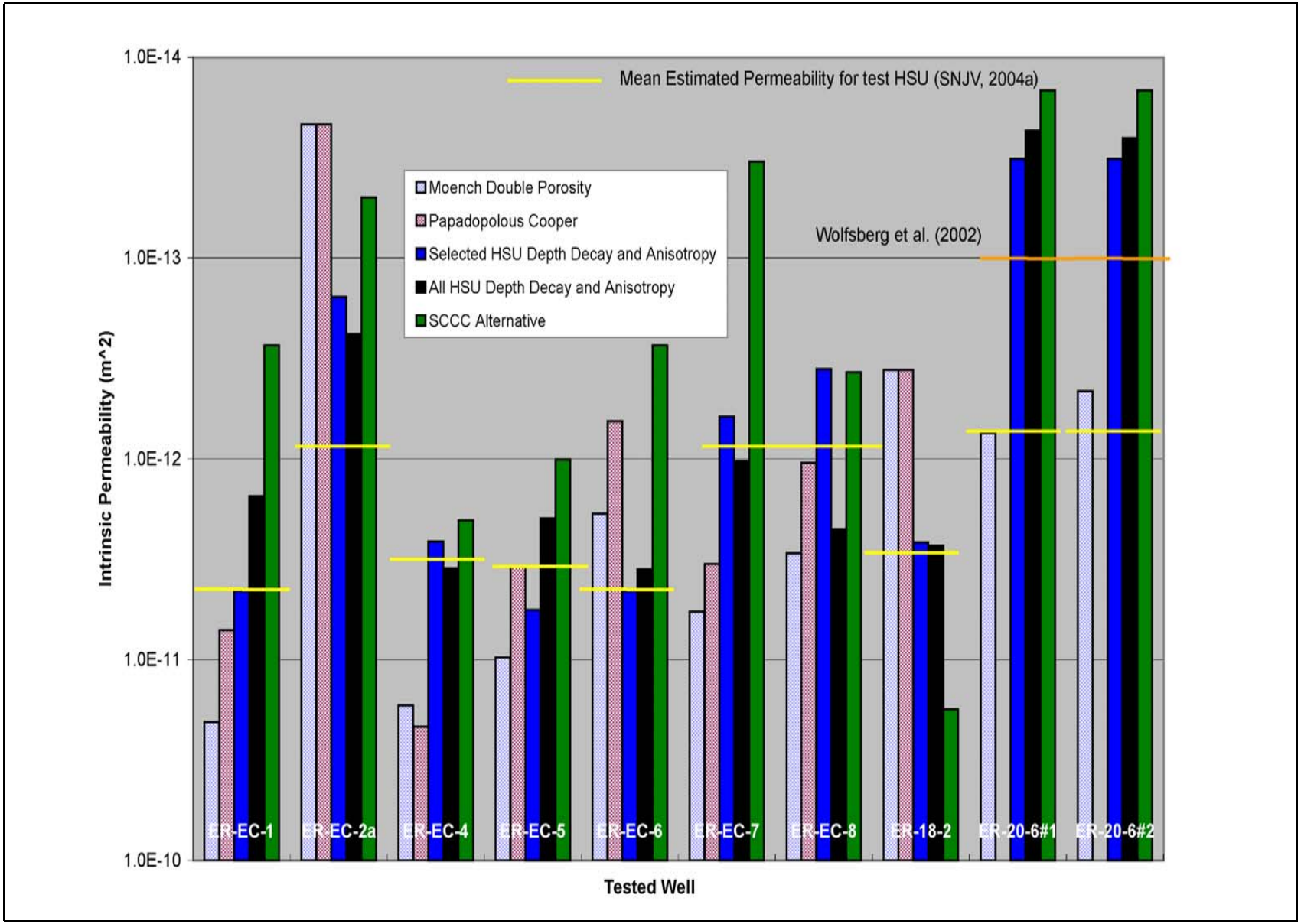

Figure 5-51
Comparison of Hydraulic Test and Model Permeability - Newer Well Data

Uncontrolled When Printed

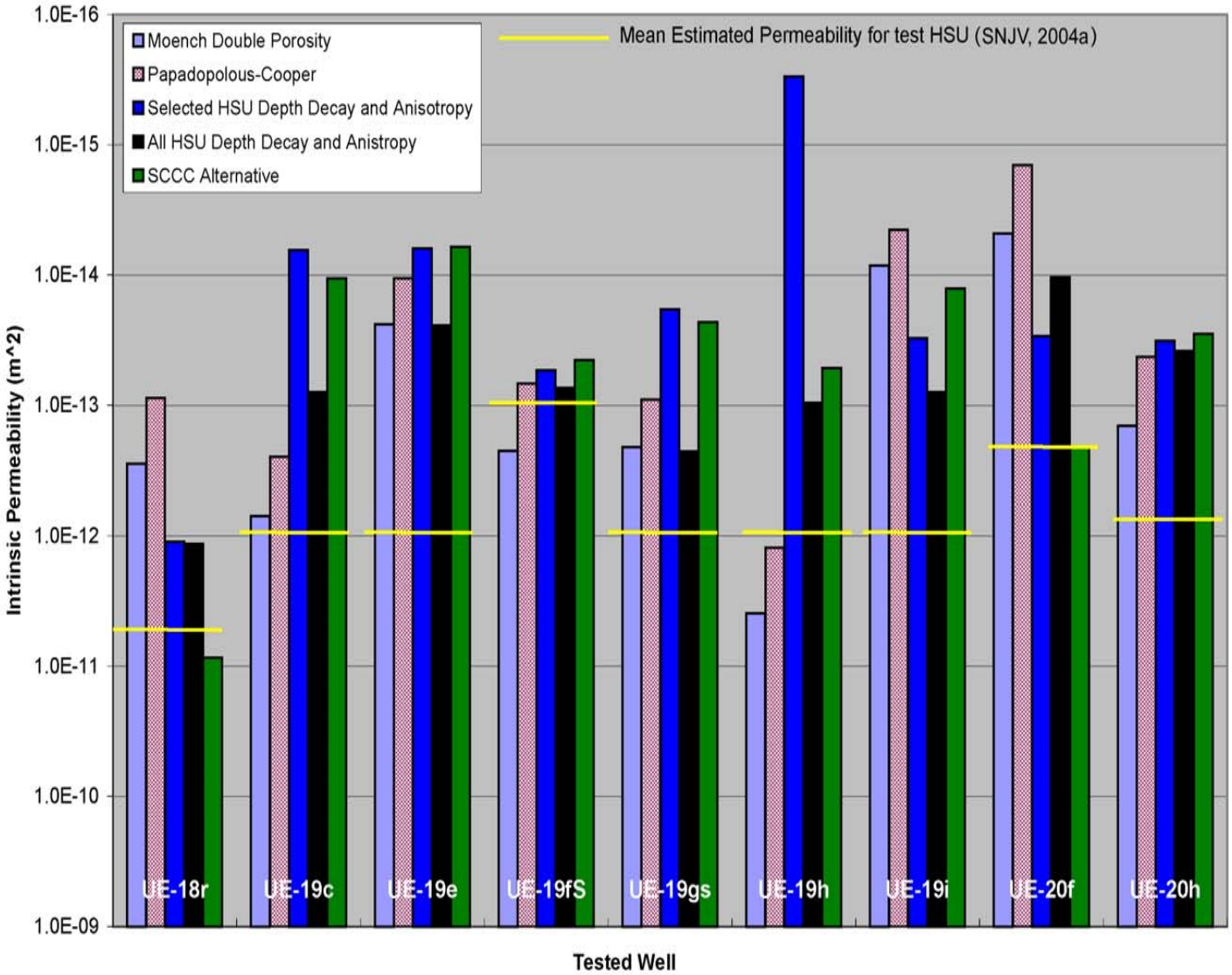

Figure 5-52
Comparison of Hydraulic Test and Model Permeability - Older Well Data

Uncontrolled When Printed

comparison could reasonably be expected to show the model biased low, which it is. In addition, it has been shown that effective properties of a porous medium, especially permeability, decrease with the scale of analysis (Neuman, 1990); the so-called "scale effect." With the exception of ER-20-6 #1 and ER-20-6 #2, all the tests were single- well, which would tend to have a relatively small sampling radius. Slug tests were not considered in this comparison because they are strongly affected by near-well mechanical disturbance (e.g., drilling) (Butler, 1997) and have an even smaller sample volume than single-well tests. Finally, the approach taken (and described in the Pahute Mesa CAIP [DOE/NV, 1999]) in parameterizing HSUs for the HFMs was to avoid specifying many small patches of different properties, but rather to use broad zones of constant parameters that were developed from characterization data. Any individual test describes only a small volume of the zone in which it lies; thus, some misfit must be tolerated because the data density does not allow anything but a broad description of HSU properties.

5.8.4 Comparison of Model and Estimated Permeabilities

As part of the modeling protocol described in Section 5.1, estimates of mean hydraulic properties and their uncertainty were made in the Pahute Mesa hydrologic data document (SNJV, 2004a) before beginning model calibration. These estimates were used as a guideline during calibration for determining whether a permeability adjustment was plausible. This section compares the model-calibrated permeabilities to estimated values for all HSUs. In the case of HSUs with depth decay, a single value has no meaning; thus, the evaluation is based on the range of permeabilities computed over the depth of the HSU versus the estimated range of uncertainty.

Figures 5-53 through 5-55 show the TMCM, TMA, PBRCM, YMCFCM, PCM, and LCA permeability ranges from depth decay versus the mean and estimated uncertainty at 95 percent (approximately two standard deviations) for the BN-MME-SDA, BN-MME-ADA, and SCCC-MME-SDA calibrated models. Reference permeability is shown at the top of each depth range; it does not exactly lie at the top (and is not expected to, because it would require all units at land surface), but at the scale used the slight offsets cannot be seen. For the TMCM, the model range spans the estimated uncertainty and more because no floor was used to limit depth decay; at greater depths, the TMCM permeability is unknown, but because permeability is related to fracture intensity (which tends to diminish with increasing overburden pressure), continued decline seems reasonable.

Recall that the ICUs underlay the calderas, and this rock is expected to be essentially impermeable. The TMA, which does not extend to as great a depth as TMCM, shows a lower limit on permeability due to the limit of its depth. The magnitude of the range is comparable to the range of uncertainty, with a shift to extend slightly outside the lower uncertainty limit for the BN-MME-SDA case. The PBRCM, which exists over most of the model at a wide variety of depths, has a permeability range that spans the uncertainty and goes to even lower values at great depths. Like the TMCM, the PBRCM is not well characterized over its full depth, and no floor on permeability was applied. The YMCFCM, which is not characterized at all, has similar ranges of uncertainty, although biased to the low side. The PCM, which occurs over a limited depth, shows a range of variability similar to the range of uncertainty.

Figures 5-56 through 5-58 mainly show the comparison of model and estimated permeabilities for the non-depth decayed HSUs, although for the case of the BN-MME-ADA, reference permeability was reported. The reference permeability cannot be directly compared to the permeability, but because of depth decay, the reference permeability should be higher than the mean permeability, and this qualitative assessment can be made from these figures. In Figure 5-56, KA, CHVTA, CHVCM, CFCU, and BFCU model-calibrated values are very similar to the estimated mean. The IA is about an order of magnitude lower than expected. In contrast, CHZCM, CFCM, and CHCU are toward the lower end of uncertainty (close to two orders of magnitude lower than the mean). Composite units are a mixture of HGUs, and because homogeneous parameters were used for these HSUs, it may be the heterogeneity of the HSU causing this variance. In Figure 5-57, THLFA, THCM, LPCU, TCA, PLFA, and FCCU all are close (less than half an order of magnitude variation) to the expected mean. The BA is close to the mean for BN-MME-SDA but an order of magnitude lower for SCCC-MME-SDA because it also includes the UPCU. The TSA has the greatest fluctuation among HFMs. The UPCU for BN-MME-SDA is about two orders of magnitude lower than the mean. In Figure 5-58, FCA, YVCM, DVCM, LCCU1, and PVTA are close (within a half an order of magnitude), while FCCM and DVA are about an order of magnitude lower than expected. The AA and UCCU are lower than even the lower limit by 2 and 1.5 orders of magnitude, respectively. The estimated mean permeability for the UCCU of 3.7×10^{-13} m^2 seems somewhat high, and is based on two data points (see Figure 5-22 in SNJV, 2004a). The two constant-rate tests used to estimate the mean UCCU permeability show a pronounced reduction in permeability with depth, which while not

Uncontrolled When Printed

particularly convincing with two data points do establish that considerable uncertainty exists in UCCC permeability.

The preceding comparisons suggest that the flow model has been reasonably parameterized with respect to the expected values of HSU permeability.

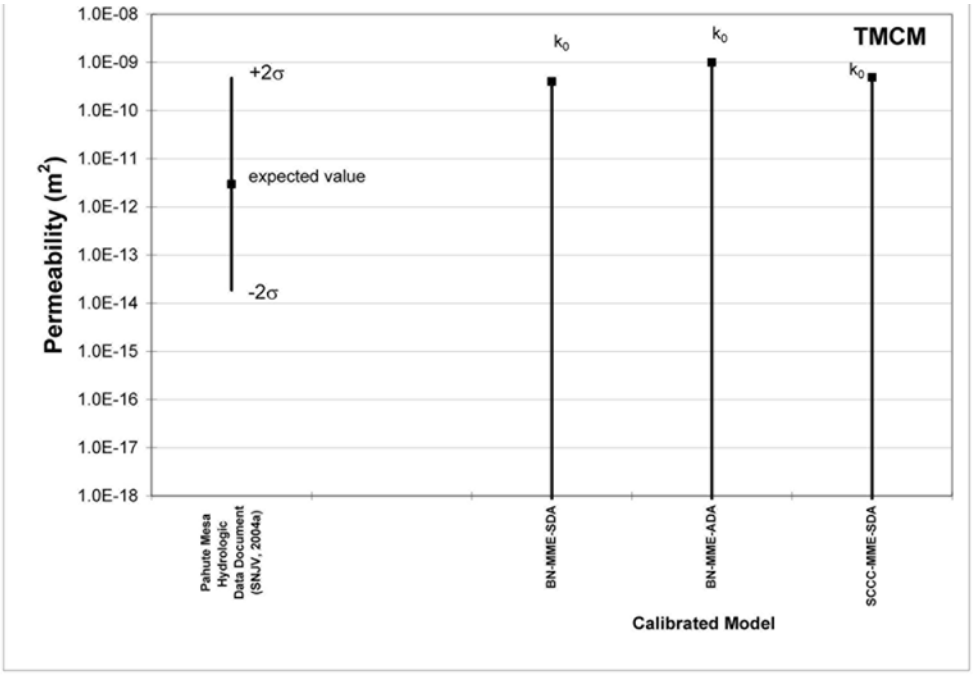

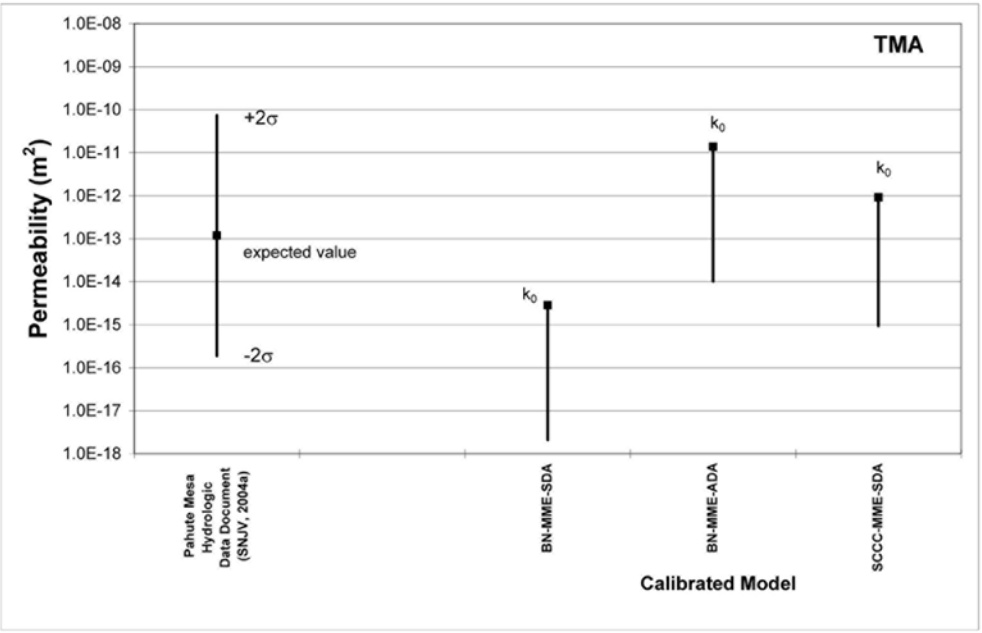

Figure 5-53
Comparison of Model and Permeabilities for TMCM and TMA

Uncontrolled When Printed

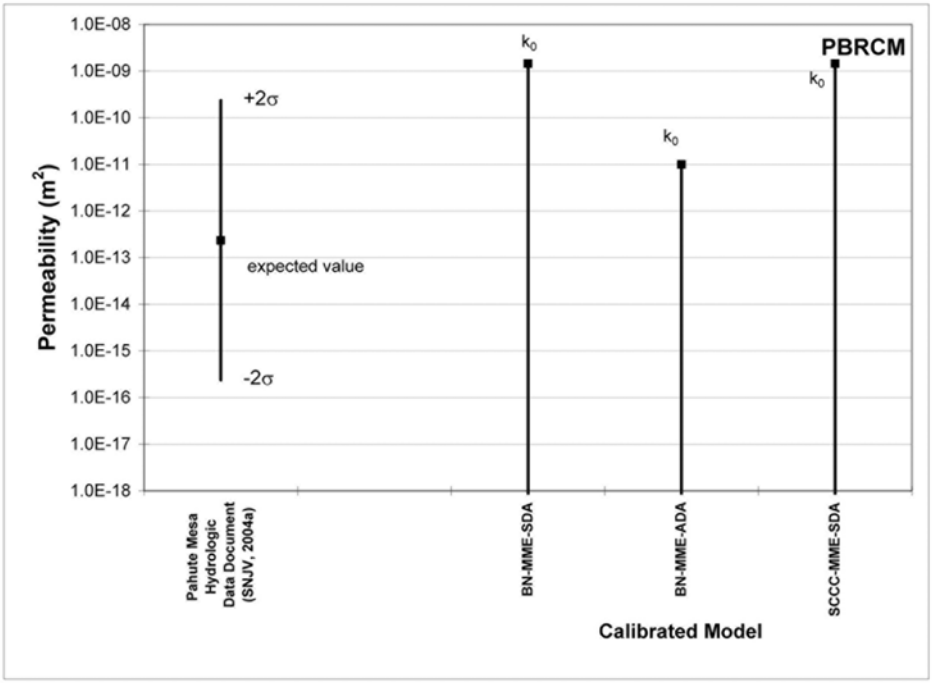

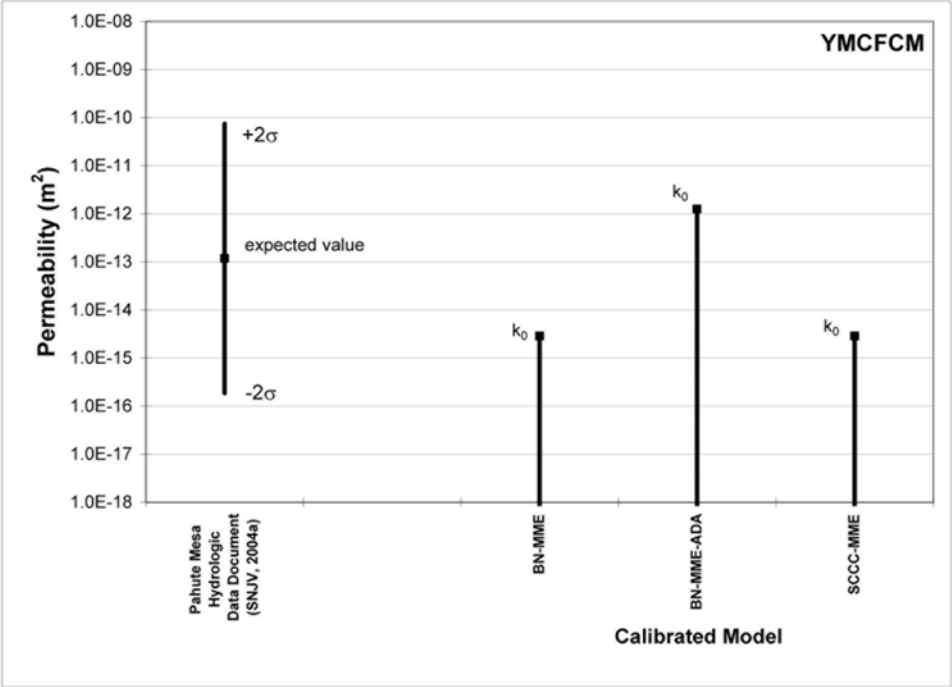

Figure 5-54
Comparison of Model and Estimated Permeabilities for PBRCM and YMCFCM

Uncontrolled When Printed

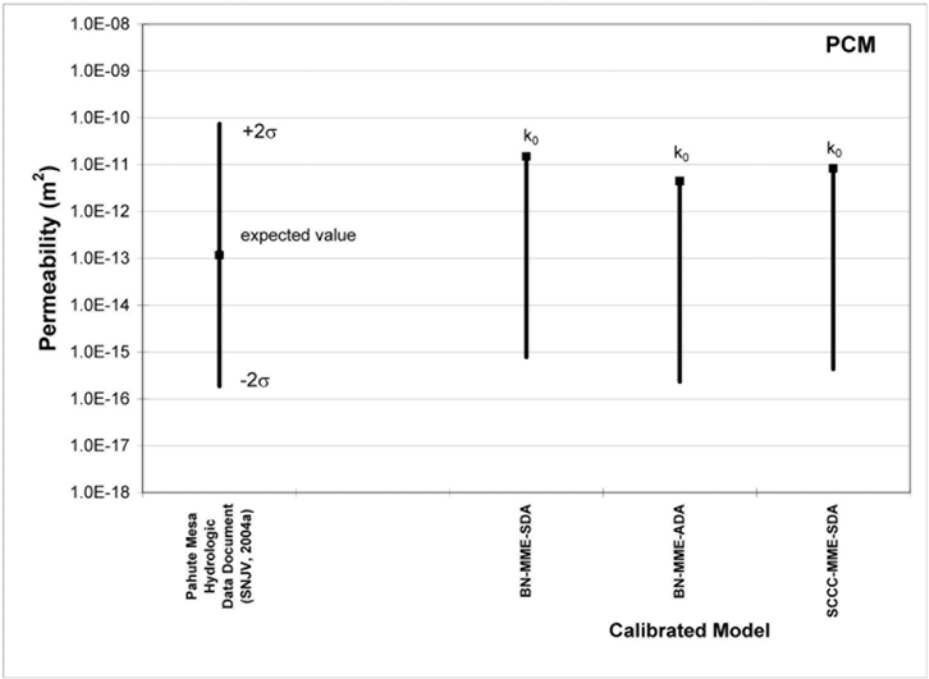

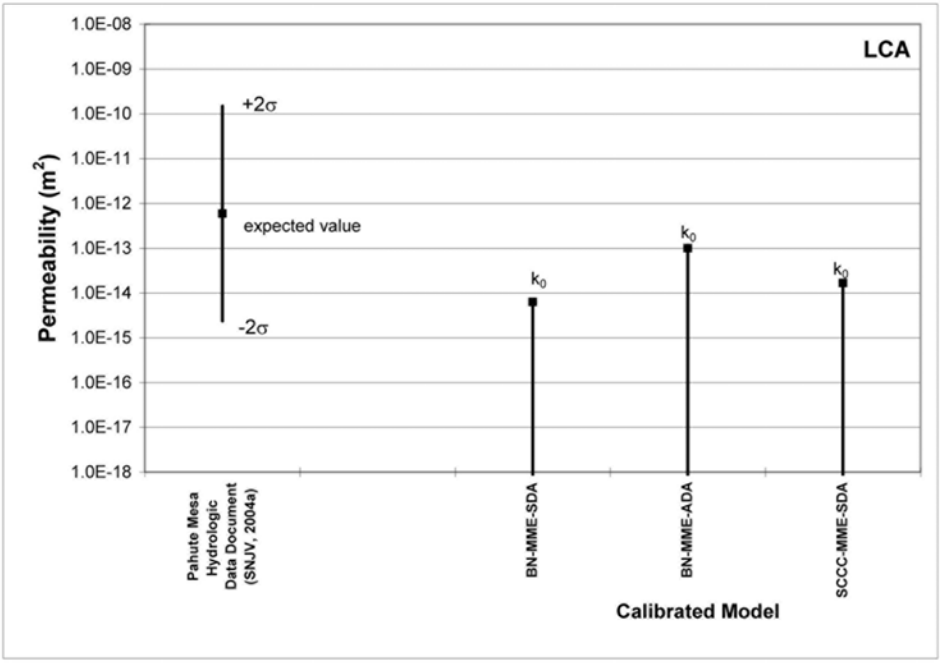

Figure 5-55
Comparison of Model and Estimated Permeabilities for PCM and LCA

Uncontrolled When Printed

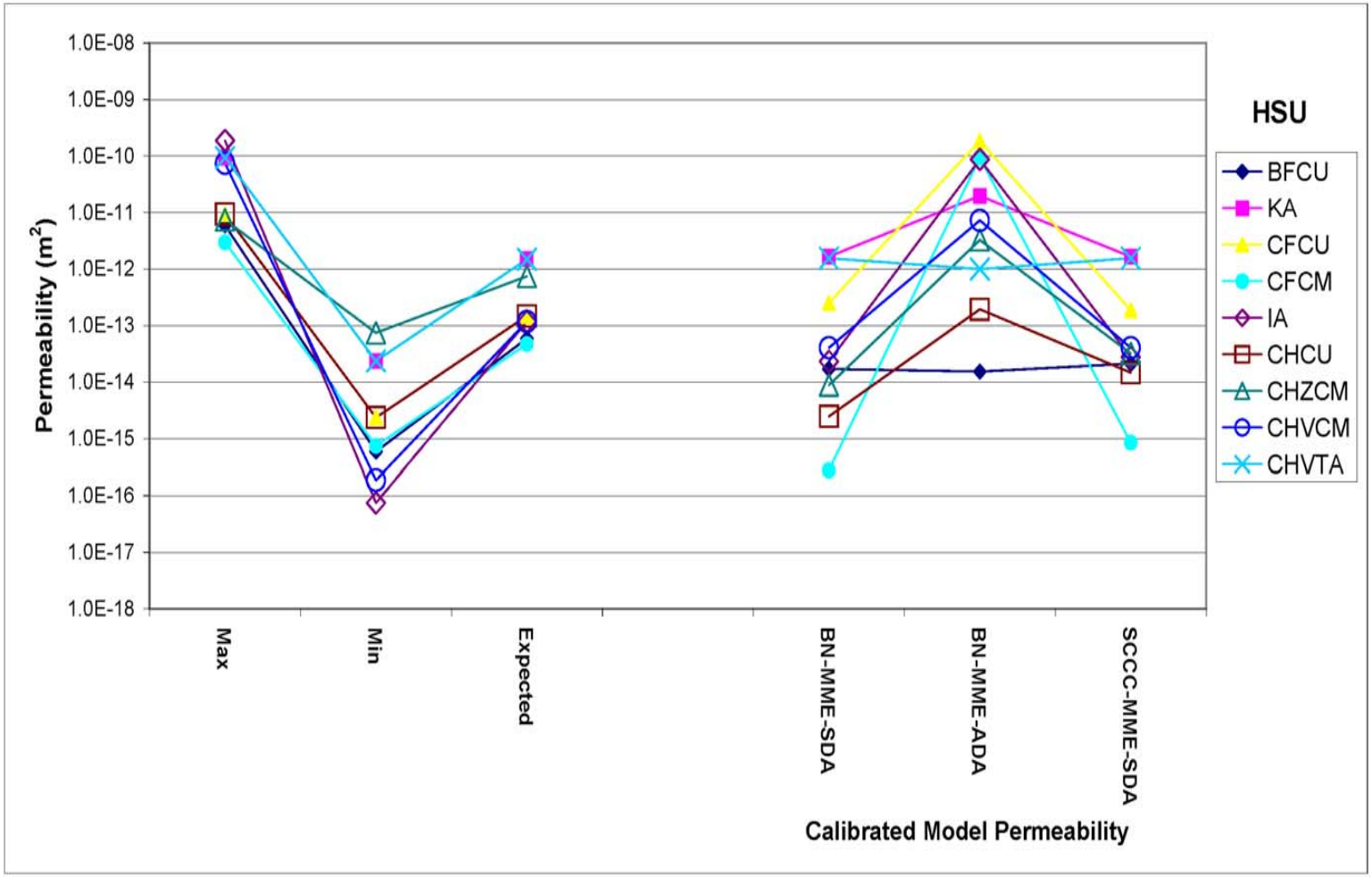

Figure 5-56
Comparison of Model and Estimated Permeabilities for BFCU, KA, CFCU, CFCM, IA, CHCU, CHZCM, CHVCM, and CHVTA

Uncontrolled When Printed

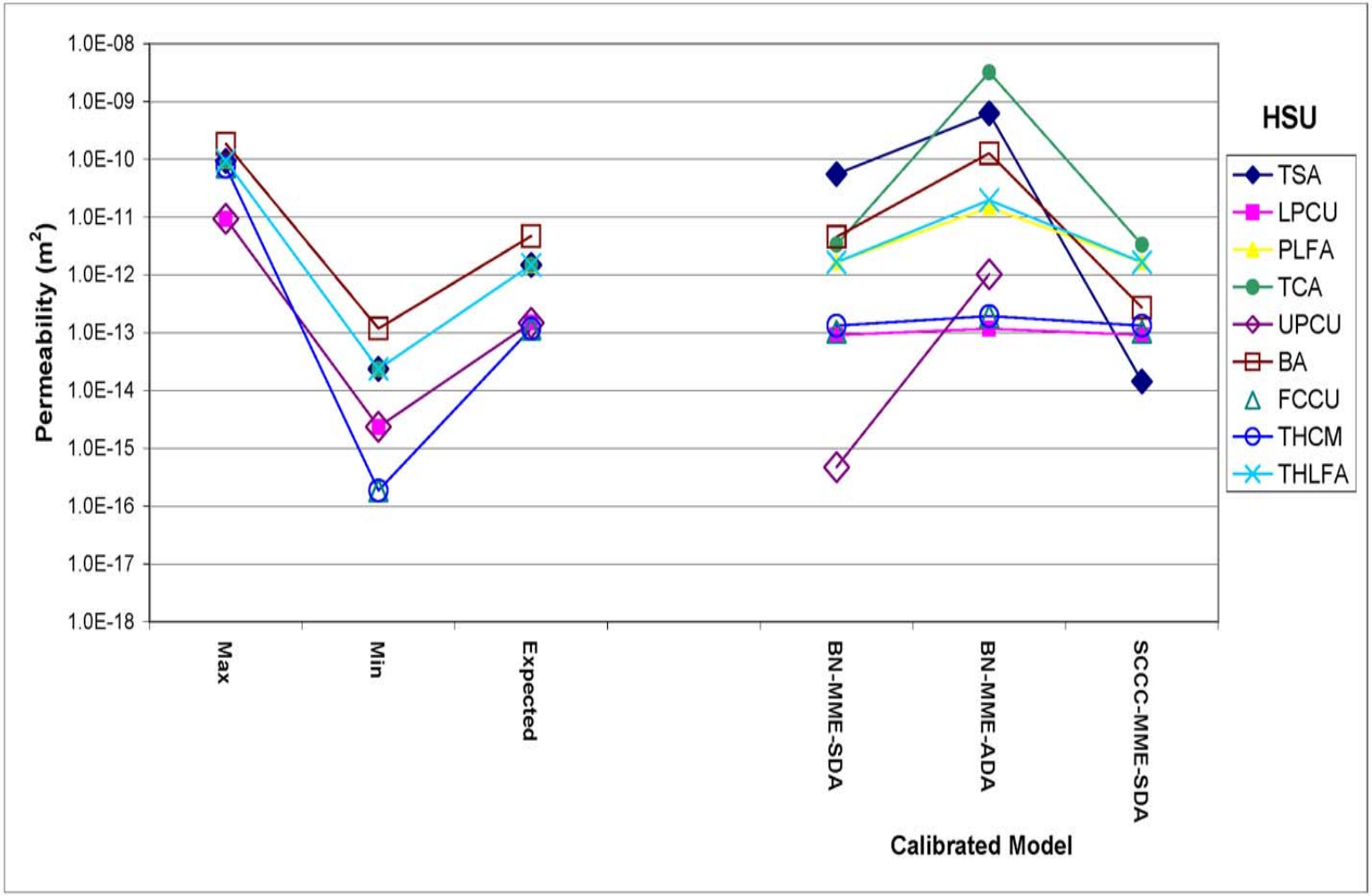

Figure 5-57
Comparison of Model and Estimated Permeabilities for TSA, LPCU, PLFA, TCA, UPCU, BA, FCCU, THCM, and THLFA

Uncontrolled When Printed

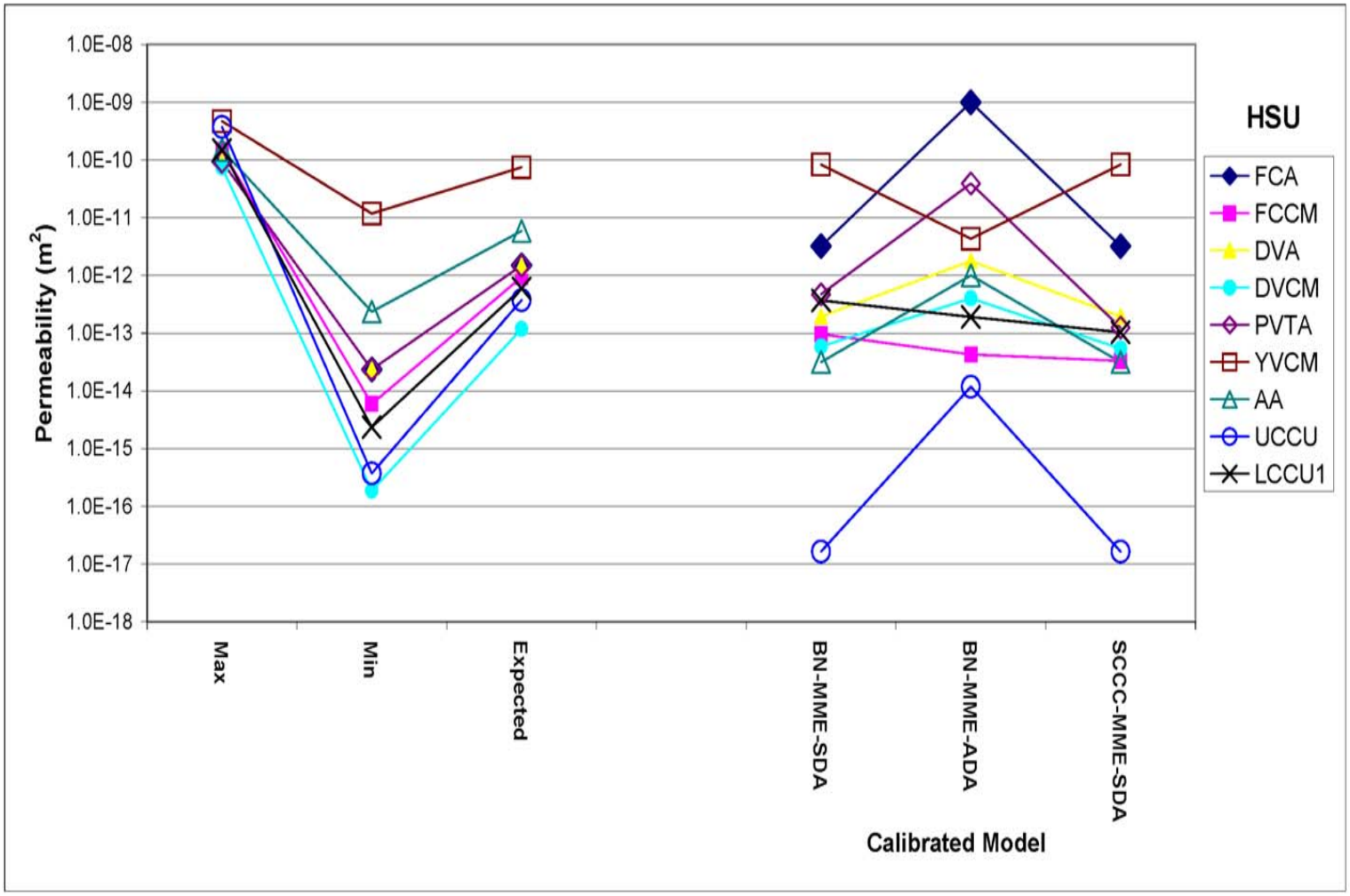

Figure 5-58
Comparison of Model and Estimated Permeabilities for FCA, FCCM, DVA, DVCM, PVTA, YVCM, AA, UCCU, and LCCU1

Uncontrolled When Printed

5.8.5 Water-Balance Summary

The water balance of the models is shown in Table 5-21. There is about a 0.4 percent discrepancy between the inflow and outflow relative to the inflow (e.g. -3/[-393+-75+-225]) for the first case in Table 5-1). This difference is from deactivating recharge along the low permeability faults at the top of the model to prevent the ridge-like features noted in Wolfsberg et al. (2002). Flow along the north, south, and eastern boundaries fluctuated more than that along the west because, as discussed previously, most of the western boundary was changed to no-flow based on the interpretation that it lays on a streamline.

Table 5-21
Water-Balance Components (kg/s)

Case	North[a]	South[b]	East	West	Oasis Valley	Recharge	Sum (kg/s)
Base HFM - Selected HSU depth decay and anisotropy	-225	395	86	-75	209	-393	-3
Base HFM - All HSU depth decay and anisotropy	-216	390	42	-73	246	-393	-3
SCCC HFM - Selected HSU depth decay and anisotropy	-174	334	104	-64	192	-393	-1

[a] (-) = is into model
[b] (+) = is out of model

An additional check on the CAU water balance is the comparison of flow along the northern edge of the Yucca Mountain saturated zone model, which lies entirely within the Pahute Mesa CAU flow model. The YMP saturated zone model (DOE/ORD, 2004) gives a value of 196 kg/s inflow. The calibrated models give values of 250, 300, and 218 kg/s for the BN-MME-SDA, BN-MME-ADA, and SCCC-MME-SDA cases, respectively. The DVRFM (Faunt et al., 2004) boundary flows were also estimated (see Table 5-5) for the Pahute Mesa CAU flow model boundaries and were found to be in reasonable agreement with estimates developed from the UGTA regional model (DOE/NV, 1997). Thus, the Pahute Mesa CAU model is in reasonable agreement with other independent water-balance analyses in the area.

Uncontrolled When Printed

5.8.6 Evaluation of Low-Weight Head Data

It is suspected that some of the wells in the calibration dataset for Pahute Mesa may be perched, or otherwise of questionable representativeness (Fenelon, 2000; SNJV, 2004a; DOE/ORD, 2004). As described in Section 5.2, weights were assigned to calibration data that generally reflected data accuracy using an approach suggested by Hill (1998). Because successful calibration hinges on the use of representative data, questionable data were assigned low (less than 0.01) weights as shown in Table 5-2. However, it is also important to check the consistency of model results with the suspect data. Figure 5-59 compares the estimated data and simulated results for all the head data (wells and springs) assigned low weights for the BN-MME-SDA, BN-MME-ADA, and SCCC-MME-SDA models. In general, the model and data trend from low to high properly.

The models agree quite well with the suspect values in Oasis Valley, probably because the overall constraint of wells, springs, and discharge has a very strong influence on all the results in the area. Gexa 4, whose companion Gexa 3 is perched, is located in an area of high hydraulic gradient from an unknown source and is also reasonably captured. The UE-29a #1 and UE-29a #2 HTHs were also quite consistent with the calibrated results, probably because Well USW UZ-N91 is located nearby and was reasonably matched. Well ER-19-1 deep was simulated 50 to 125 m too high, but was better represented by the all HSU depth-decay and anisotropy case because it has higher permeability for the Gold Meadows Stock, which allows the high head boundary to propagate further into the model. Well ER-19-1 shallow is thought to be perched (Fenelon, 2000), and is undersimulated by the model (which is a consistent representation). However, data in that area are sparse, and this cannot be proven conclusively. The TW-1 (492 m) may also be perched, and the model correctly represents such a condition, as it also does for UE-12n #15A. Hagestad 1 may also be perched and is outside the model boundary (it was projected to the nearest edge node for this comparison). There is a larger spread in and around the line of best fit in Figure 5-59 relative to the other calibration results, although some of this effect may simply be because the data in Figure 5-59 did not strongly participate in the calibration, although they were considered qualitatively. The qualitative behavior of high head in the east-central part of the model (near Rainier Mesa and Gold Meadows) is properly captured, and the fact that the water balance on the eastern boundary was reasonably matched (see Sections 5.3 and 5.4) suggests the model representation is acceptable in this area.

Uncontrolled When Printed

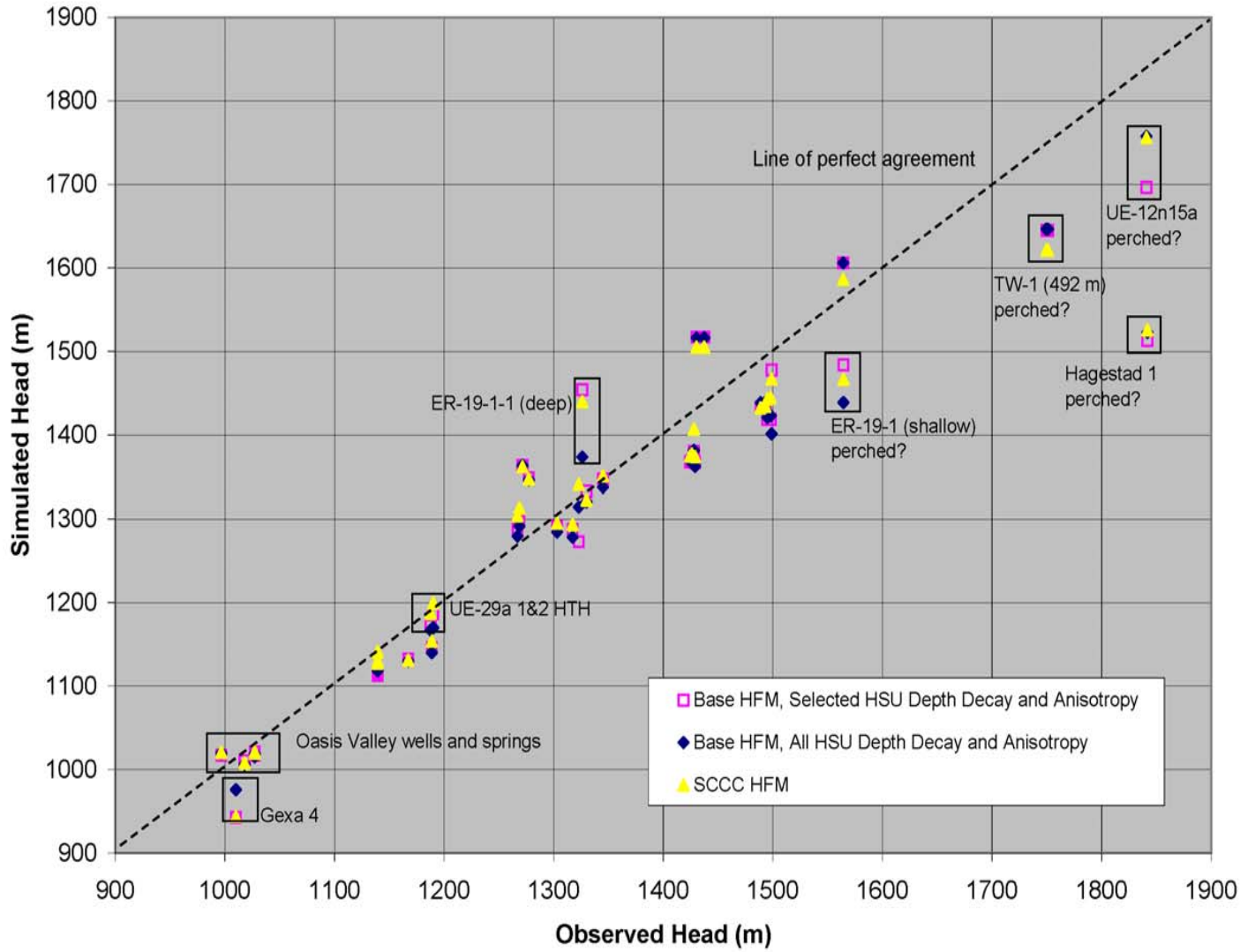

Figure 5-59
Observed Versus Simulated Low-Weight Head Data

Uncontrolled When Printed

5.8.7 Data Components of Calibration

Four categories of data, representing two types (head and flow), were used to calibrate the Pahute Mesa CAU flow model: observation well head, spring head, Oasis Valley ET discharge, and net model boundary flow. Weights, as discussed in Section 5.2, were developed from data accuracy and other qualitative considerations. Tables 5-7, 5-10, 5-14, and 5-18 show the contribution of each data type to the model goodness of fit. In all cases, observation well heads comprised the bulk (between about 50 to 60 percent) of the objective function, followed by Oasis Valley discharge (about 25 percent), estimated regional boundary flow (about 15 percent), and spring head (5 to 10 percent). Clearly, observation well data must be given strong consideration in model calibration because they define the direction and magnitude of the hydraulic gradient, which is directly related to the velocity field that will be used to simulate radionuclide transport. Oasis Valley discharge is the only internal flow constraint for the model, and as such is a major control on the effective permeability. Oasis Valley is also the nearest access point for radionuclides that might leave Pahute Mesa, and matching its discharge ensures that the potential for such migration is properly captured in the flow model. In addition, matching the spring data also helps ensure that the heads in Oasis Valley are reasonably matched, and that the combination of head and flow that results is plausible. All the calibrated models showed similar patterns of error in fitting Oasis Valley flow, and it may be possible to improve the discharge by more explicitly accounting for the rooting depths of the different plant communities in the discharge area. Finally, the regional model water balance is considered via the boundary flow targets, which clearly play some role in calibration.

There is no general rule as to what the share of the model objective function different data types should have, but it should be considered that the simulated Oasis Valley discharge is generally within one standard deviation of the mean value, which suggests that its weight was assigned appropriately. Faunt et al. (2004) presents a similar analysis for the DVRFM, and shows for that regional model the contribution from steady-state heads is 95 percent of the objective function, with the balance coming from flow targets. If well and spring head are considered together, head comprises about 70 percent of the objective function, a value comparable to that shown by Faunt et al. (2004).

Uncontrolled When Printed

5.8.8 Hydrostratigraphic Framework Model Assessment

Two HFMs, the base and SCCC alternative, were considered during model calibration. As noted in Section 5.8.1 the SCCC does not perform as well in matching observed heads along the Purse Fault, and, in general, does not calibrate as well as the base HFM as can be seen from comparing Tables 5-9 and 5-17.

The least weighted fitting squares (as embodied in PEST) is a special case of maximum likelihood estimation arising from the assumption that the errors are normally distributed (see Appendix A of Hill, 1998). The parameter set or model that reduces the value of the objective function is considered superior to those that give higher values because it improves the model fit according to the criterion embedded in the objective function itself. Thus, from purely the standpoint of flow model calibration goodness, the SCCC HFM is not as likely as the base BN HFM.

5.8.9 Model Limitations

The Pahute Mesa CAU flow model covers a plan area of approximately 2,000 km^2 and has a saturated thickness of nearly 5 km, for a total volume of about 10,000 km^3. A total of 191 calibration targets of head and flow were used in calibration. The overall density of the data versus the size of the model suggests that the calibration data are somewhat sparse. Not all of the uncertainty is likely to be important; for instance, it is almost certain that flow in the ICUs is very slow, if not nil, which has no effect on the shallower part of the flow system. However, many types of analysis such as head mapping and geochemistry tend to give a similar broad picture of flow from Pahute Mesa southwest to Oasis Valley, and while there may be further refinements in understanding if more data are collected the key point of migration to Oasis Valley is unlikely to change.

The CAU flow model was calibrated to estimated steady-state condition, and is not currently set up for transient flow analysis. The flow model also assumes regional steady state in the CAU area, and any future change in hydrologic conditions could affect this assumption.

Uncontrolled When Printed

6.0 FLOW MODEL SENSITIVITY AND UNCERTAINTY ANALYSIS

The Pahute Mesa CAIP (DOE/NV, 1999) requires and general modeling protocol (ASTM *Standard Guide for Conducting a Sensitivity Analysis for a Ground-Water Flow Model Application* [ASTM, 1994c]) recommends analysis of parameter sensitivity and conceptual model uncertainty. This section presents these analyses.

The Pahute Mesa CAU flow model has a large number of parameters that can be changed in order to calibrate the model to observations of hydraulic heads, spring heads, lateral boundary flows, and ET flows. Not all of these parameters have the same influence on the performance of the model. Therefore, it is necessary to identify those parameters to which the model outputs are most sensitive, and how they relate to the conceptual model. The results of sensitivity analyses are presented for three models described in Sections 5.6 and 5.7. These models are:

- Base HFM - selected HSU depth decay and anisotropy with MME recharge (BN-MME-SDA)
- Base HFM - all HSU depth decay and anisotropy with MME recharge (BN-MME-ADA)
- SCCC HFM - selected HSU depth decay and anisotropy with MME recharge (SCCC-MME-SDA)

While sensitivity analyses are formally presented in Section 6.2, such analyses were also carried out as an integral part of the calibration process.

In addition, alternative HFMs, recharge models, and boundary flows have been considered in the CAU flow model. Sections 6.3 through 6.5 describe the approach and results of the uncertainty analysis associated with these model alternatives.

Uncontrolled When Printed

6.1 Approach

6.1.1 Parameter Sensitivity Analysis

Both local and global sensitivity analysis techniques are used to identify and evaluate key parameters in the Pahute Mesa CAU groundwater model. The local sensitivity analysis techniques include PEST sensitivity analysis and perturbation analysis. The global sensitivity analysis techniques include classification tree analysis and entropy analysis.

6.1.1.1 Local Sensitivity Analysis

Two approaches to local parameter sensitivity analysis were implemented for the Pahute Mesa flow model. In the first approach, parameter sensitivity and correlations were evaluated using PEST (Watermark, 2004). The PEST code calculates a sensitivity coefficient for each parameter with respect to all weighted observations. This analysis is termed "local" because only slight changes are made that investigate parameter values near the base value. The second approach involves perturbing each of the parameters, one at a time, from a reference value and computing the corresponding change in the model output (Anderson and Woessner, 1990).

PEST Sensitivity Analysis

Sensitivity coefficients, computed as the change in output divided by the change in input, reflect the slope of the input-output relationship at a reference point. These sensitivities can be obtained quantitatively from the outputs of PEST (Watermark, 2004), a non-linear parameter estimation code. In the process of optimizing a nonlinear model, PEST calculates the Jacobian matrix. The Jacobian matrix relates the model-calculated observations to the model input parameters where any element of the Jacobian matrix, J_{ij}, describes the derivative of the *i*'th observation with respect to the *j*'th parameter. Based on the Jacobian matrix, PEST calculates the composite sensitivity of each parameter with respect to all weighted observations. The composite sensitivity of parameter *i* (s_i) is defined as:

$$s_i = \frac{\sqrt{(J^t Q J)_{ii}}}{m} \tag{6-1}$$

Uncontrolled When Printed

where J is the Jacobian matrix; J^t is the transpose of J; Q is the "cofactor matrix," an m-dimensional, square, diagonal matrix comprised of the squared observation weights; and m is the number of observations of non-zero weight (Watermark, 2004). In other words, the sensitivity coefficient for a given parameter is the weighted average of the derivatives of all the observations with respect to that parameter.

These composite sensitivity coefficients reflect the weighted slope of the input-output relationship at a reference point. In the case of the sensitivity analysis presented here, the reference point refers to the parameter values at calibration and the derivative is approximated by a forward finite-difference method with a 3 percent parameter increment. These sensitivity coefficients are therefore indicative of the parameter sensitivity in the vicinity of the calibration point and apply only to the parameter range over which the input-output relationship is linear.

The Jacobian matrix is also manipulated to derive the covariance matrix, which in turn can be used to estimate parameter correlations and confidence limits. The correlations and confidence limits are, themselves, subject to the same linearity assumption as sensitivity coefficients but still provide a useful semi-quantitative tool for understanding how model parameters interact and how the data support the model (Poeter and Hill, 1997).

To provide some estimate of the sensitivity of observations to all the adjustable parameters, PEST also calculates composite observation sensitivity. The composite observation sensitivity of observation j (s_i) is defined as:

$$s_j = \frac{\sqrt{Q(JJ^t)_{jj}}}{n} \tag{6-2}$$

where J and Q are the Jacobian and cofactor matrices, respectively, and n is the number of adjustable parameters (Watermark, 2004). While the observation sensitivities do not generally provide as much useful information in guiding model calibration as the parameter sensitivities, they may provide some insight into which observations are sensitive to many parameters.

To describe the degree to which parameters are correlated to one another, PEST computes the correlation coefficient matrix. The correlation coefficient matrix is a symmetric, n-dimensional,

square matrix, ρ_{ij}, where *n* is the number of adjustable parameters. Each element of the matrix ρ_{ij} represents the correlation between parameter *i* and parameter *j*. The diagonal elements of the correlation coefficient matrix are always equal to 1 because a parameter is perfectly correlated with itself. The off-diagonal elements range between -1 and 1 and, the closer the absolute value is to 1, the more highly (either directly or inversely) correlated the parameters are. Again, these values are subject to the assumption of linear model input-output response near the reference point.

Perturbation Analysis

In a perturbation analysis, individual model input parameters are systematically increased and decreased from reference values (in this case, calibrated values) while all other parameter values are held constant. The model is then run for each "perturbed" parameter case, and some summarized metric of the model output is calculated. This exercise provides information about the sensitivity of model outputs to changes in individual parameter values over the parameter range.

In contrast to the sensitivity coefficients, a perturbation analysis can provide information about the input-output relationship away from the reference point, and nonlinear input-output relationships can be identified. By varying input parameters over their range of uncertainty (i.e., multiple standard deviations away from the reference point), some insight into the corresponding uncertainty in model output can also be gained. However, because parameters are perturbed individually, synergistic effects between multiple input parameters on the model output are neglected.

Perturbation analysis corresponds to computing a cross section of the objective function (model goodness of fit) along the dimension of the variable under consideration. For instance, Figure 6-1 shows a sample objective function surface (from Hill, 1998) that involves transmissivity (T) and storativity (S).

If a profile of the objective function in Figure 6-1 is visualized at a fixed T of 0.12 with S varying, it would be relatively flat between S values of 0.00025 and 0.00075, rising gently to higher and lower S values. If a profile at fixed S (say 0.0050) is considered, it has a steep slope and narrow valley bottom at the calibration point. Perturbation analysis describes these types of responses for the Pahute Mesa CAU flow model.

Uncontrolled When Printed

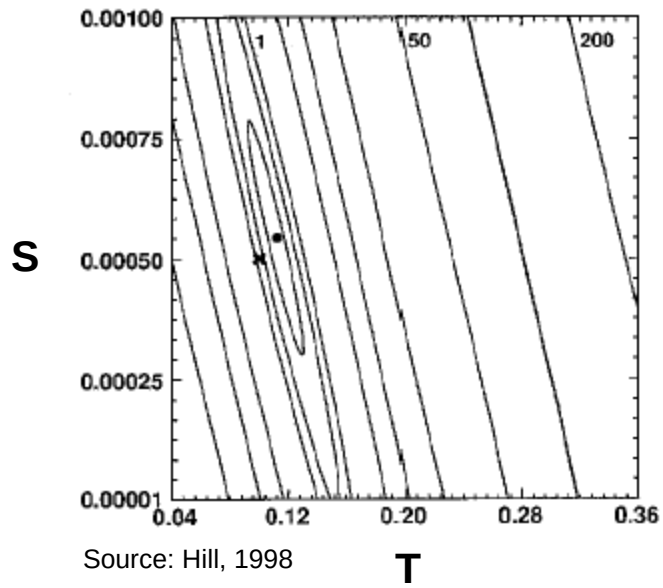

Source: Hill, 1998

Figure 6-1
Sample Objective Function for Perturbation Analysis

If the calibration data weights or the number or type of calibration data are changed, then the results from the perturbation analysis that follows will only generally still be applicable.

6.1.1.2 Global Sensitivity Analysis

Unless the functional relationship between the output and the input of interest is linear over the entire range of input values, local analyses only provide information regarding the relative sensitivities of input parameters valid in the vicinity of the reference point. As a result, global sensitivity analysis techniques are used for investigating input-output sensitivities that are valid over the entire range of possible parameter variations and not just at or near the reference point (Saltelli et al., 2000).

The starting point for global sensitivity analysis is the selection of a strategy for exploring the entire parameter space over which model calculations will be performed. The approach adopted is a Monte Carlo simulation based uncertainty analysis methodology using Latin Hypercube sampling (McKay et al., 1979). The values resulting from calibration are taken as the mean, and the log normal distribution and associated standard deviation from SNJV (2004a) are used with the code of Iman et al. (1980) to generate 1,000 uncorrelated samples, which are then run through FEHM. For fault

Uncontrolled When Printed

permeability multipliers, a log-uniform distribution was sampled that went about two orders of magnitude above and below the calibrated values. Classification tree and mutual information (entropy) analysis are used to analyze the sampling results.

Although several methods are available for global sensitivity analysis (e.g., Saltelli et al., 2000), analyzing input-output relationships for a non-monotonic output (i.e., quadratic objective function) requires special consideration. As shown by Mishra and Knowlton (2003), entropy (mutual information) analysis is particularly useful for determining the strength of input-output association for any general non-linear non-monotonic relationship, whereas commonly used sensitivity analysis techniques such as stepwise rank regression are known to fail under such conditions. A second issue is the determination of decision rules that identify which variables or combinations of variables lead to low values of the objective function (i.e., good fit) versus high values (i.e., bad fits). Classification tree analysis has been shown to be a useful tool for analyzing such categorical problems (Mishra et al., 2003).

For the global sensitivity analysis of the Pahute Mesa flow model, the goodness-of-fit criteria are evaluated for several types of calibration targets (also discussed in Section 5.2). These are as follow:

- WELL – groundwater elevation in observation wells
- SPRING – groundwater elevation in springs
- FLUX - boundary flow
- ETF – Oasis Valley ET flux
- PHI - total of above

These are the same components used to calibrate the flow model, including data values and weights.

Classification Tree Analysis

Classification tree analysis can provide useful insights into what variable or variables are most important in determining whether outputs fall in one particular category. Categories are generally based on meeting some acceptable threshold (e.g., pass versus fail, fit versus misfit). Traditional applications of classification trees have primarily been in medical decision making and data mining for social sciences. Mishra et al. (2003) describe an application of the methodology to a Monte Carlo simulation-based model for predicting performance of a potential nuclear waste repository.

Uncontrolled When Printed

The setting up of the Monte Carlo simulations is described in Section 6.2.3. The number of uncertain parameters is the same as that used in the perturbation analysis, and can be found in the first paragraph of Sections 6.2.2.1, 6.2.2.2 and 6.2.2.3. The code of Iman and Conover (1979) is used to ensure that no spurious correlation exists between any two arbitrary parameters during the Latin Hypercube Sampling process. The composition of the RMS objective function, used as the performance measure of interest for the sensitivity analyses, is also described in Section 6.2.3.

A binary decision tree is at the heart of classification tree analysis. The decision tree is generated by recursively finding the variable splits that best separate the output into groups where a single category dominates. The degree by which a single category dominates is called the split "purity." For each successive fork of the binary decision tree, the algorithm searches through the variables one by one to find the purest split within each variable. The splits are then compared among all the variables to find the best split for that fork. The process is repeated until all groups contain a single category, or a specified level of purity is reached for all groups. In general, the variables that are chosen by the algorithm for the first several splits are most important, with less important variables involved in the splitting near the terminal nodes of the tree.

The tree-building methodology used here is based on a probability model approach. Classifiers at each node are selected based on an overall maximum reduction in impurity, for all possible binary splits over all the input variables. The impurity at a given node A (I_A) is based on the Gini index (Breiman et al., 1984), which for the two class case reduces to:

$$I_A = 2\rho_{1A}\rho_{2A} \tag{6-3}$$

where ρ_{1A} and ρ_{2A} are the estimated probabilities of classes 1 and 2, respectively, at node A. The probabilities are estimated from the proportion where n is the number of observations in a class at a node by:

$$\rho_{1A} = \frac{n_{1A}}{n_A} \tag{6-4}$$

where ^{n}A is the total number of observations at node A, and $^{n}1A$ is the proportion belonging to class 1.

The decrease in impurity for a given split of node A into nodes L and R (left and right) is:

$$\Delta I = I_A - \rho_L I_L - \rho_R I_R \tag{6-5}$$

where ρ_L and ρ_R are the proportions of the cases that go to L and R, respectively.

The classification tree is built by successively taking the maximum reduction in purity over all the allowed splits of the branch to determine the next split. Termination occurs when the number of cases at a node drops below a set minimum, or when the maximum possible reduction in purity for splitting a particular node drops below a set minimum.

As an example, Figure 6-34 in Section 6.2.3.1 shows the results of a classification tree analysis to determine the decision rules separating the smallest and largest 10 percent values for the dependent variable PHI. Here, the category "low" refers to the smallest 10 percent PHI values and the category "high" refers to the largest 10 percent PHI values. In Figure 6-34, each node of the classification tree is labeled with the numbers of each category that have been assigned to that node, with the number of high values comprising the first and the number of low values comprising the second. For example, "68/0" indicates that 68 from the high category have cascaded to the node. Note that the "83 low" and "68 high" observations can be perfectly categorized with just two splits. Also, some judgment of the importance of the variables can be made from the structure of the tree itself. Here, variable LCCU thrust sheet (LCCU1) is the most important because it was chosen for the first split, followed by Detached Volcanics Composite (DVCM).

Tree-based models are attractive because: (a) they are adept at capturing non-additive behavior, (b) they can handle more general interactions between predictor variables, and (c) they are invariant to monotonic transformations of the input variables. These attributes make classification trees more suitable for input-output modeling as compared to regression analysis, which is restricted to a linear (or linearized) input-output relationship and where the functional form of the relationship has to be specified *a priori*.

Uncontrolled When Printed

Entropy Analysis

The information-theoretic concept of entropy is a useful metric for the characterization of uncertainty (or information) in the univariate case, and redundancy (or mutual information) in the multivariate case (Press et al., 1992). The concept of mutual information has been utilized to select key input variables in neural network based input-output modeling (Bonnlander and Weigand, 1994). Because mutual information is a natural measure of input variable relevance, it is also being used as an indicator of variable importance in many areas of science (Moddmeijer, 1989).

The following theoretical discussion is based on Press et al. (1992). Let the input variable x have I possible states (labeled by i), and the output variable y have J possible states (labeled by j). This information can be compactly organized in terms of a contingency table – a table whose rows are labeled by the values of the independent variable, x, and whose columns are labeled by the values of the dependent variable, y. The entries of the contingency table are non-negative integers giving the number of observed events for each combination of row and column.

The contingency table can also be visualized using a "bubble plot," where the entries of the contingency table are shown as bubbles of varying sizes. Here, the contingency table is organized such that the quintiles of the independent variable (input) increase from left to right, and that of the dependent variable (output) increase from top to bottom. The size of the bubble indicates how many observations fall in each quintile-quintile box. Bubble plots generated for this report are presented beginning in Section 6.2.3.1.

The probability of outcomes corresponding to both states x_i and y_j is $\rho_{ij} = N_{ij}/N$, where N_{ij} denote the number of events occurring when x takes its i-th value and y takes its j-th value. Let $N_{i.}$ denote the number of events for which x takes its i-th value regardless of the value of y; similarly, let $N_{.j}$ denote the number of events with the j-th value of y regardless of x. The probability of outcomes corresponding to state x_i alone is: $\rho_{i.} = N_i/N$, and the probability of outcomes corresponding to state y_j alone is: $\rho_{.j} = N_{.j}/N$. Then, the entropies of x and y are defined as:

$$H(x) = -\sum_i \rho_{i.} \ln \rho_{i.}; \; H(y) = -\sum_j \rho_{.j} \ln \rho_{.j} \tag{6-6}$$

and denote the average information in observing x (or y). Similarly, the joint entropy of x and y, denoting the average information in observing both x and y, is defined as:

$$H(x, y) = -\sum_i \rho_{ij} \text{In} \rho_{ij} \tag{6-7}$$

The mutual information between x and y, which measures the reduction in uncertainty of y due to knowledge of x (or vice versa), is defined as:

$$I(x, y) = H(x) + H(y) - H(x, y) = -\sum_i \sum_j \rho_{ij} \text{In}\left(\frac{\rho_{ij}}{\rho_{i.}\rho_{.j}}\right) \tag{6-8}$$

If x and y are completely independent, then $H(x,y) = H(x) + H(y)$, so $I(x,y) = 0$. On the other hand, if x and y are completely dependent, then $H(x,y) = 0.5[H(x) + H(y)]$, so $I(x,y) = 0.5[H(x) + H(y)]$.

The R-statistic has been proposed as a measure of association based on the concept of entropy or mutual information as follows (Granger and Lin, 1994):

$$R[x, y] = [1 - \exp\{-2I(x, y)\}]^{1/2} \tag{6-9}$$

R takes values in the range [0,1], with values increasing with I. R is zero if x and y are independent, and is unity if there is an exact non-linear relationship between x and y. It can also be shown that if x and y have a bivariate normal distribution with correlation ρ, then $R = |\rho|$ (Cover and Thomas, 1991).

The entropy-based measure R-statistic can thus be recognized as a very general tool for quantifying the strength of an association. It is applicable to both linear/non-linear and monotonic/non-monotonic relationships, whereas commonly used regression-based measures are restricted to linear and monotonic associations only.

6.1.2 Conceptual Model Uncertainty Analysis

There are seven HFMs for the Pahute Mesa CAU flow model, five recharge models, and five sets of lateral boundary flows. If all combinations were considered, this would result in 175 calibrated flow

Uncontrolled When Printed

models. However, as discussed further in Section 6.4.2, it is neither necessary nor reasonable to investigate all combinations. The approach taken was to use a given recharge model in the Pahute Mesa CAU flow model with the UGTA regional model (DOE/NV, 1997) boundary flows derived from the same recharge model in the UGTA regional model. Table 6-1 summarizes the combinations of HFM, recharge, and boundary flow uncertainties that were investigated.

Table 6-1
Recharge, Boundary, and HFM Uncertainty Matrix

Geology/Boundary	DRIA/ DRIA	DRIAE/ DRIAE	MME/ MME	USGSND/ USGSND	USGSD/ USGSND
BN[a]	X	X	X	X	X
SCCC	X		X		X
DRT	X		X		X
PZUP	X		X		X
TCL			X		
SEPZ			X		
RIDGE			X		

Note: Row header is recharge model/boundary flow, and column header is HFM.

[a]Only for selected HSU depth decay and anisotropy.

In general, the strategy is to discretely combine HFMs, recharge models, and lateral boundary flows in order to at least bound uncertainty associated with each model component. Thus, for the PZUP alternative HFM for the DRIA water balance, the DRIA recharge map is used as input, and the boundary flows estimated from the UGTA regional model (DOE/NV, 1997) with the DRIA recharge map were used as calibration constraints. In this way, the effects of the recharge model on regional-scale results are indirectly captured in the CAU-scale flow model.

6.2 Parameter Sensitivity Analysis

6.2.1 Local Parameter Sensitivity and Correlations

After the calibration of the Pahute Mesa flow model, local parameter sensitivity and correlations were evaluated using a PEST control file that was updated to reflect the calibrated parameter values. The PEST code was then run, calculating statistics and sensitivity coefficients for the calibrated parameter set. Sensitivity coefficients were ranked in descending order, and the 15 largest were plotted.

Uncontrolled When Printed

In PEST, the objective function, or PHI, is the sum of the squares of the weighted residuals:

$$\Phi = \sum_{i=1}^{m} (w_i r_i)^2 \tag{6-10}$$

where Φ is the objective function, w is the observation weight, r is the residual or difference between the simulated and measured values, and m is the number of observations of non-zero weight. For the Pahute Mesa flow model, PHI can be divided into four components representing different types of calibration target data. Head measurements at wells are described by the WELL component. The FLUX component represents lateral boundary flow estimates from the regional model. The heads and flows at discharge locations are represented by the SPRING and ETF components, respectively. It is important to note, this sensitivity analysis only addresses the model response with respect to the flow model calibration data; direct references cannot be drawn about transport prediction sensitivity.

The sensitivity of HSUs that are connected to the model boundaries is somewhat distorted by the arbitrary model boundaries required by the scale of the problem. For instance, if an HSU permeability increased the head remains unchanged at the model edge but the flow would increase. However, if the full regional context was maintained, the head could conceivably change rather than the flow.

For the objective function and the individual portions contributing to it, a simple difference (D) was used:

$$D = \Phi_{sens} - \Phi_{cal} \tag{6-11}$$

where Φ_{sens} is the sensitivity simulation objective function and Φ_{cal} is the calibrated simulation objective function.

6.2.1.1 Base HFM - Selected HSU Depth-Decay and Anisotropy (BN-MME-SDA) Model Parameter Sensitivity and Correlations

For this model, permeability, reference permeability (k_0), and fault permeability multiplier parameters were varied individually by HSU or fault, as appropriate. A single vertical anisotropy parameter was

Uncontrolled When Printed

used for HSUs for which anisotropy was assigned (see Table 5-7). A single depth-decay coefficient for the volcanic HSUs and another for carbonate HSUs was also used. This latter approach mimics in a broad way how these parameters were assigned during calibration. This resulted in approximately 100 parameters for which sensitivity coefficients (to all calibration data, hence "composite") were calculated.

The 15 largest sensitivity coefficients calculated by PEST are shown in Figure 6-2. This figure shows that the two depth-decay parameters have much greater sensitivity coefficients than any of the other parameters (note the log-scale used for the y-axis). This is not surprising because permeability in the model is an exponential function of the depth-decay coefficient. After depth decay, the next three most sensitive parameters are the permeability of the LCCU1, k_0 of the PCM, and the permeability of the DVCM. The permeability of the LCCU1 is completely unknown, and is estimated to be relatively high based on enhanced fracturing from being overthrust (SNJV, 2004a). The PCM lies along the southern edge of the model, and its sensitivity is derived from controlling head in the domain by throttling the sharp drop in head imposed along the southern boundary, and outflow along the southern boundary. The DVCM lies on the western edge of Oasis Valley and controls inflow from Sarcobatus Flat to the west; it is also located proximal to a large number of calibration targets in Oasis Valley. The DVA is nearly as sensitive as the DVCM, and it also lies in a critical location to control head and flow in central and southern Oasis Valley. The only fault to show much sensitivity is the Claim Canyon Caldera Structural Margin (fault 06; see Figure 4-5 for fault locations). Considering its location (see Figure 4-5), this is because it controls flow and head in much the same manner as the PCM by acting as a check on the southern outflow and controlling the influence of the southern boundary. The PBRCM permeability Zones 84 and 13 are the areas on the western side of the domain, and under Areas 19 and 20, respectively. The PBRCM Zone 84 is shown in Section 6.2.3.1 to control flow into northern Oasis Valley, and Zone 13 is interpreted as having sensitivity because of its large extent, presence in an area that includes a large part of the calibration data, and connection with the northern edge of the model, which very few HSUs have. The FCCM rings Timber Mountain and is another HSU with large areal extent. The CHZCM has 23 calibration targets in it exclusively, hence its sensitivity. Vertical anisotropy is relatively far down on the list of sensitive parameters. The TMCM-ERM subdivision (see Figure 5-6) and TCVA, two areally extensive HSUs, have mild sensitivity, finally followed by the BFCU.

Uncontrolled When Printed

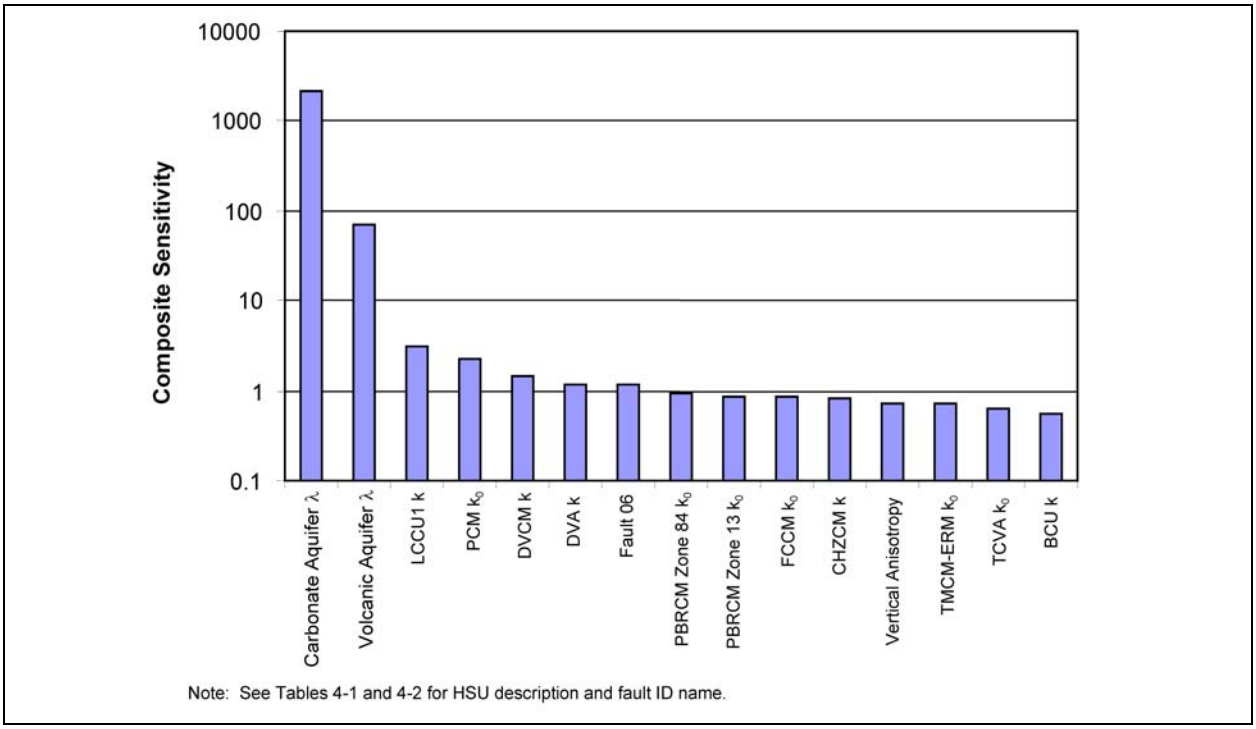

Figure 6-2
Largest Sensitivity Coefficients from PEST for BN-MME-SDA

Recall that the sensitivity coefficient relates to the weighted slope of the input-output relationship at the calibration point and, unlike perturbation or global sensitivity analyses, is independent of the range in uncertainty of a parameter. Because the depth-decay coefficients have a small range in uncertainty with respect to other parameters, they were perturbed over a smaller range and were not observed to have such pronounced sensitivity in the perturbation analysis or the global sensitivity analysis.

The 15 most sensitive observation targets to all the calibration data (hence "composite") calculated using PEST are depicted in Figure 6-3. This figure shows that the lateral boundary flux targets for the eastern and southern model boundaries are the most sensitive observations. This may indicate that many parameters impact the flow through the eastern and southern boundaries. Another interpretation is that relatively few, but broadly defined, HSUs influence flow on the east and south model edges. Considering the parameter sensitivities noted above the latter interpretation seems more likely, particularly with regard to the PCM and Claim Canyon Caldera Structural Margin. Following these two boundary fluxes, head observations in selected wells have very comparable observation sensitivity coefficients that are less than half the magnitude of those for the boundary

Uncontrolled When Printed

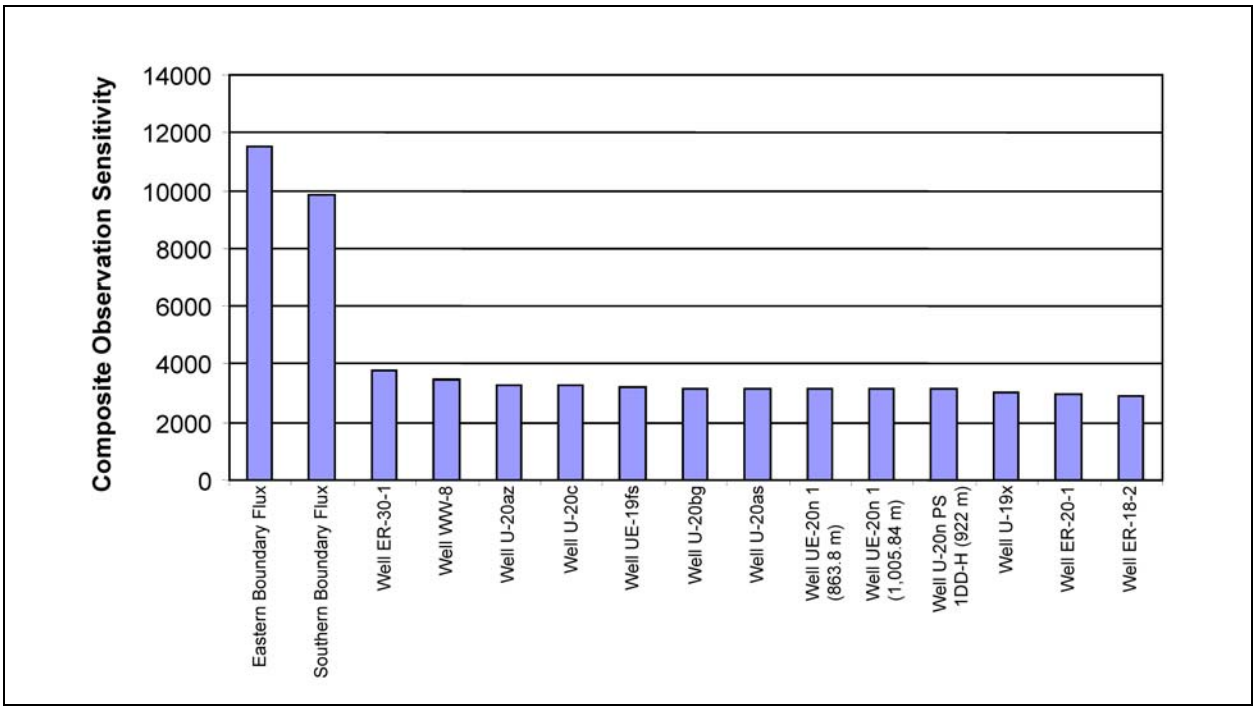

Figure 6-3
Composite Observation Sensitivity from PEST for BN-MME-SDA

fluxes. Well ER-30-1 is one of the few wells on eastern Timber Mountain, and WW-8 is located to the east of it. Both wells are located in a sparsely populated area of the model, with respect to calibration data, and are concluded to provide a great deal of useful calibration information in this area of the model. Most of the other sensitive observations are located throughout Areas 19 and 20, and do not appear to have any special significance other than they tend to have the high weights.

The 15 most highly correlated pairs of parameters (from the PEST correlation coefficient matrix) are shown in Figure 6-4. For context, Hill (1998) suggests a significant level of correlation is 0.90. This figure shows that the fault permeability multiplier for the Claim Canyon Caldera Structural Margin and the k_0 parameter for PCM are almost perfectly inversely correlated. The Claim Canyon Caldera Structural Margin also has strong correlation with carbonate depth decay. This supports the observation made previously in this section that the Claim Canyon Caldera Structural Margin acts to control the flow domain along the southern edge of the model. Its nearly perfect inverse correlation shows that the effect of decreasing the fault permeability multiplier can be offset, at least over the range of perturbation, by increasing PCM permeability. The control of the Claim Canyon Caldera Structural Margin on the southern boundary is also expressed by the correlation with LCA depth

Uncontrolled When Printed